中国五矿集团有限公司
CHINA MINMETALS CORPORATION

(Original in Chinese)

Environmental Impact Statement

Testing of Polymetallic Nodule Collector Vehicle in the Block A-5 of the Minmetals Contract Area

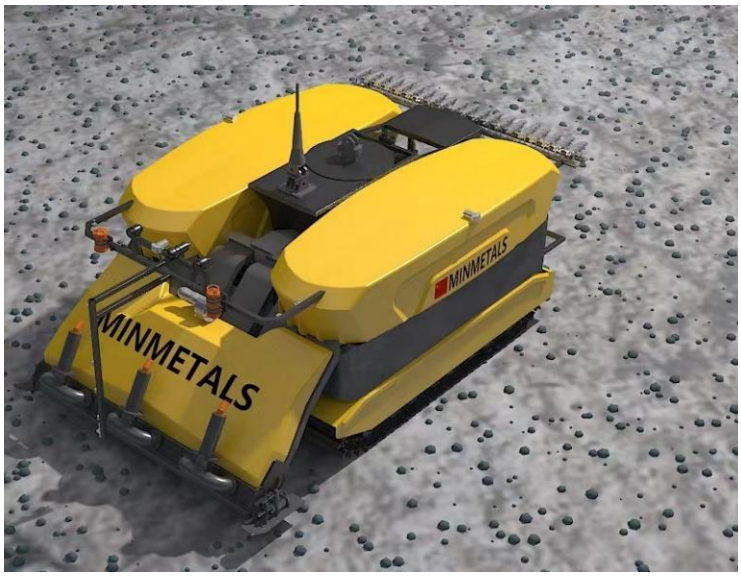

China Minmetals Corporation

October 2024

Table of Contents

Figures

Tables

Executive Summary

Project background

China Minmetals Corporation (Minmetals) plans to carry out testing of the polymetallic nodule collector vehicle in July-October of 2025 in the Block A-5 of the Minmetals Contract Area stipulated in the Contract between Minmetals and the International Seabed Authority (ISA). This Project will verify the collecting and traveling performance, reliability, and economy of the collector vehicle. The test results will be used for optimizing the design of the collector vehicle. Minmetals will carry out environmental monitoring alongside the testing. Data and samples will be collected during the testing to assess the scale of environmental impact caused therefrom. A technical system for monitoring and assessing the environmental impact of seabed mining will be established to provide technical and data support for the environmental impact assessment (EIA) of commercial mining.

Figure 1 Conceptual model of Minmetals' collector vehicle

Article 6 (B)(33)(b) of the "Recommendations for the guidance of contractors for the assessment of the possible environmental impacts arising from exploration for marine minerals in the Area" (ISBA/25/LTC/6/Rev.3), requires EIA prior to activities

such as testing of mining components, as well as the implementation of an environmental monitoring programme (EMP) during and after the activity (paragraphs 33 and 38). To meet such requirements, Minmetals has prepared this Environmental Impact Statement (EIS) and Environmental Management and Monitoring Plan (EMMP).

This EIS follows the Annex III "Environmental impact statement template for reporting an environmental impact assessment undertaken during exploration" of the "Recommendations for the guidance of contractors for the assessment of the possible environmental impacts arising from exploration for marine minerals in the Area" (ISBA/25/LTC/6/Rev.3), as well as refers to some of the requirements of Annex IV "Environmental Impact Statement" of the "Draft regulations on exploitation of mineral resources in the Area" (ISBA/25/C/WP.1) issued by the ISA.

Proposed target mining area (TMA)

As shown in Figure 3.1-1, a primary working area (PWA, approximately 4,590 km^2, with an exploration grid of 7 km × 7 km), is delineated in the western basin of the Block A-5. This test will be carried out in the detailed exploration area (DEA, approximately 500 km^2, with an exploration grid 3.5 km × 3.5 km). The DEA is the proposed target mining area (TMA). For EIA prior to, during and after the collector vehicle test, the Impact Reference Zone (IRZ) (6 km × 5 km) and Preservation Reference Zone (PRZ), have been delineated in the TMA. The delineation of the IRZ and PRZ is based on the similarity of topography, the geological characteristics of sediments, and environment baselines. An area about 0.6 km^2 (1 km × 0.6 km) is delineated in the IRZ as the collector test area (CTA).

According to the international test-mining results and the results simulated in this EIS (Annex 1), the maximum impact of the sediment plume in this test is 2.1 km horizontally and 124 m vertically, and no more than 1 km^2 area will have 0.1 mm redeposited sediment plume. Located 15 km upstream of IRZ, the PRZ will not suffer any environmental impact from the planned testing of collector vehicle. Based on the

study of environment baseline characteristics, we believe that PRZ and IRZ meet the ISA's requirements for environmental similarity.

Proposed test system

The collector vehicle to be tested is part of Minmetals' long-term plan for developing seabed mining technologies. In 1995, Minmetals developed a prototype collector vehicle (PCV) and completed relevant laboratory tests. In 2021, Minmetals successfully developed China's first engineering PCV, and completed the lake test for it. In 2016-2018, Minmetals has independently developed the Kunlong 500 collector vehicle, and then completed at-sea testing of it at the water depth of 514 m in the South China Sea in June 2018. Based on the R&D of Kunlong 500 collector vehicle, Minmetals has developed a collector system for water depth of 1,000 m, and completed a polymetallic nodule collector system test at water depth of 1,000 m in the South China Sea in June-July of 2021. On the basis of the above-mentioned R&D efforts, Minmetals has developed a new generation of seabed collector system, and will validate the key mining technologies in the TMA.

The seabed collector system to be tested consists of a collector vehicle, an acoustic positioning system, an umbilical cable and a surface support vessel (SSV). The collector vehicle collects nodules from the seabed; the acoustic positioning system provides positioning support for the collector vehicle; the umbilical cable provides power supply and communication with the collector vehicle; the SSV is a surface operation platform responsible for the monitoring and operation of at-sea testing of the collector vehicle.

The collector vehicle to be tested consists of traveling mechanism, collection mechanism, main structure, inspection and monitoring mechanism, underwater control system and hydraulic system. The collector vehicle is 9 m long, 5 m wide and 4 m high, weighing 40 t in air and 20 t under water, with a design power of 500 kW, a collector head width of 5 m, a maximum underwater traveling speed of 1 m/s and a production capacity of 125 t/h (with nodule abundance at 12 kg/m^2).

According to the proposed EMMP, an environmental monitoring vessel (EMV) will be used for environmental monitoring and assessment during the testing of the collector vehicle.

Proposed plan for collector vehicle test

The planned collector vehicle test includes two separate underwater operations. The first one is for testing of the collector vehicle's basic functions, including static test after equipment landing, inspection and monitoring test, temperature rise and noise test, straight-line traveling test, turning radius test, collecting performance test under different parameters, continuous nodule-collecting test, sampling operation, equipment status check before recovery, etc. (see Table 3.3-4 for details). The first underwater operation will last for 70 h, with an underwater traveling distance of 4,840 m and a disturbance area of 24,200 m^2.

The second one is for testing of the collector vehicle's basic performance (traveling and collecting), including static test after equipment landing, inspection and monitoring test, temperature rise and noise test, regional collecting and disturbing operations, sampling operation, equipment status check before recovery, etc. (see Table 3.3-5 for details). The second underwater operation will last for 60 h, with an underwater traveling distance of 15,160 m and a disturbance area of 75,800 m^2.

The total disturbance area is 0.1 km^2. The total wet weight of nodules collected is estimated to be about 1,300 t, and that lifted alongside with the collector vehicle to the surface platform to be no more than 10 t.

Environment baseline studies

Minmetals used R/V *XIANGYANGHONG LIUHAO,* R/V *XIANGYANGHONG SANHAO,* R/V *XIANGYANGHONG SHIHAO,* R/V *DAYANG YIHAO* and R/V *DAYANG HAO* in 2017, 2018, 2019, 2021, 2022 and 2023 survey cruises for 99 days, 61 days, 113 days, 104 days, 75 days and 85 days respectively, totaling 537 days. By the end of 2023, Minmetals has been carried out environmental survey projects at 316 stations and several survey lines in the Block A-5, including 200 m-depth conductivity,

temperature, and depth (CTD) measurement at eight stations, full-ocean-depth profiling CTD measurement at 13 stations, multicorer sampling at 25 stations, box corer sampling at 208 stations, gravity piston corer sampling at eight stations, plankton vertically towed net sampling at nine stations, multinet sampling at three stations, in-situ geotechnical properties test of sediments at 27 stations, mooring observation at four stations, baited trap lander observation at six stations, large volume in-situ filtration system (MULVFS) at two stations, hydrophone monitoring at three stations, and 13 seabed optical survey lines (including two autonomous underwater vehicle (AUV) survey lines). Based on the samples and data of the above-mentioned surveys, and combined with the collection of public environmental data, Minmetals have carried out environment baseline studies on the following aspects in the Block A-5:

Geological properties

The topography of the Block A-5 is complex, with sea knolls, sea knoll groups, seamounts and intermontane basin. Hereinto, the ocean basin zone accounts for 70.8 %. The results of near-bottom acoustic survey by AUV show that the TMA has a small relief, and there is no obvious steep slope. Both the IRZ and PRZ are located in the ocean basin zone, with gentle topography and an elevation difference of less than 20 m.

The nodule abundance in the TMA varies in the range of 0.59 - 25.92 kg/m^2, averaging 14.04 ± 4.69 kg/m^2. The shipboard photography coverage varies in the range of 2 - 85 %, averaging 43 ± 15 %. There is a sound positive correlation between shipboard photography coverage and nodule abundance (R^2=0.82), and most of the nodules in the TMA are exposed. The IRZ and PRZ have similar nodule abundance (10 -15 kg/m^2) and nickel equivalent grade (NEG), indicating that these two zones have similar resources.

The silt-grade content in the surface-layer sediment of the Block A-5 is the highest (approximately 53 % on average), followed by clay-grade content

(approximately 35 % on average). The sand-grade content is comparatively low. The concentrations of heavy metals (e.g. Cd, Cr, Ni, Cu, Zn and Pb) in sediments are unevenly distributed, generally low except for the northeast and southwest corners of the PWA. Total organic carbon (TOC) is low (<0.25 %) in the northeast and southwest corners of the PWA, while the TOC contents in other areas are between 0.25 % and 0.45 %. Survey results show that the IRZ and PRZ have similar particle sizes, heavy metal and organic carbon contents in sediments.

In the IRZ and PRZ, the concentrations of heavy metals in the pore water of sediments shallower than 0-30 cm are generally low, while the concentrations of heavy metals (e.g. Cr, Cd, Zn, Ni and Pb) are close to those of overlying water collected with box corer. These two zones have similar total nutrient concentrations in the pore water, as well as the same variation of nutrients with increasing depths. The total alkalinity in pore water in sediments shallower than 30 cm is basically stable at 2.4 mmol/L.

In shallower-than-10-cm sediments collected with multicorer in the Block A-5, the chlorophyll *a* (Chl *a*) content per unit wet weight is 0-0.0239 μg/g and that per unit dry weight is 0.0001 - 0.1058 μg/g. Under the influence of burial degradation, the Chl *a* content shows a gradual decline trend.

In-situ geotechnical properties test results show that penetration/shear strength of sediment at 1 m depth in the Block A-5 increase in a nonlinear or linear way with increasing depth.

Physical oceanography characteristics

The results of temperature and salinity profile observation show that the Block A-5 has a similar interannual variation trend in full-depth temperature profile. In different years, the vertical variation trends of temperature in the upper layer (no deeper than 200 m) are basically similar, but the thermocline positions are slightly different, with a variation of about 40 m. The deep-layer temperature variation trends are similar, with a variation of about 0.03 ℃. In the Block A-5, the interannual variation trends of full-depth salinity profile were similar in 2019, 2021 and 2022.

The analysis results of the measured flow of ship-mounted Acoustic Doppler Current Profiler (ADCP) show current speed and directions vary significantly in different years in this area. The current speeds observed during the 2017 and 2021 survey cruises were relatively high, exceeding 1 m/s locally, while those observed during the 2019 and 2022 survey cruises were usually less than 0.5 m/s. Equatorial countercurrent are dominant in the Block A-5.

The long-term monitoring results of deep-sea currents in this area obtained by using submerged buoys of mooring show that the annual average speeds of deep-sea currents (water depths of 5,150 m, 5,250 m and 5,350 m) are in the range of 4.56 - 4.83 cm/s, and the average direction is eastward. The seawater flow field in the middle layer (water depth of 1930 m) is dominated by eastward flow, with the speed in the range of 6 - 12 cm/s (averaging 7.34 cm/s).

The monitoring results of the turbidimeter mounted on the mooring show that most of the time, the turbidity of seawater in the bottom layer (20 m above the bottom) and near-bottom layer (100 m above the bottom) is critical to the detection limit of equipment, and the overall turbidity is below 0.4 FTU.

Chemical oceanography characteristics

The pH of seawater at full ocean depth in the Block A-5 presents obvious stratified distribution characteristics, and is the highest in the surface-layer water column. Between the surface and 100 m water depth, the pH decreases rapidly, reaching the lowest at approximately 300 m water depth. Then, the pH increases slowly with increasing depth, and tends to be stabilize at 7.6 - 7.8 below the water depth of 2,000 m.

The dissolved oxygen (DO) in seawater is the highest in the surface layer, and then decreases sharply to less than 3.0 mg/L at the depth of 100 - 200 mm at all stations, indicating the phenomenon of hypoxia. Below 1000 m, with the increasing depth, the DO content begins to rise slowly and returns to 4.0 - 6.0 mg/L in the bottom-layer seawater.

The concentrations of inorganic nitrogen (including ammonium, nitrate and nitrite), silicate and reactive phosphate in the Block A-5 are in the following descending order: silicate > inorganic nitrogen > reactive phosphate. There is a significant correlation between the content of particulate organic carbon (POC) and

the content of total suspended particulate matter (TSM) in the seawater column. The variation of POC content with depth may be related to the vertical distribution of Chl (mainly plankton) in the seawater, since the relatively strong plankton activity in the subsurface may produce higher POC content.

Biological environment characteristics

Boobies are the dominant seabirds in this region. There is no direct sighting record of whales or dolphins in the Block A-5 of the Contract Area. Assessments based on publicly available data indicate that the Block A-5 is far from Marine Mammal Protected Areas and areas where scientific evidence suggests protection is needed. The nearest major global migratory corridor for cetaceans to the western portion of the CCZ is the migratory corridor between the area around the Hawaiian Islands and the high-latitude offshore areas of the northeastern Pacific Ocean. This corridor is far from the Block A-5.

The Chl *a* concentration and primary production in the Block A-5 are lower than those in the eastern part of the Clarion-Clipperton Zone (CCZ), and the interannual variations of surface-layer Chl concentration are small among the IRZ and PRZ. In all seasons, the isoline of surface Chl *a* concentration is roughly zonal, so the IRZ and PRZ in the Block A-5 are highly consistent and comparable in the spatio-temporal variations of primary production.

The maximum value of the primary production profile is in the subsurface layer (water depth of 50 m). The integral primary production of water column shows that the average total primary production of water column at this station is 51.44 mg C m^{-2} h^{-1}. The vertical variation of Chl *a* concentration was consistent in both PRZ and IRZ, with maximum values at about 50 m, 0.2 mg/m^3 and 0.28 mg/m^3, respectively.

The average phytoplankton abundance in the surveyed area is 338 cells/L. The community is dominated by Bacillariophyta, followed by Dinoflagellate. The dominant phyla are Bacillariophyta (e.g. *Bacteriastrum hyalinum* var. *hyalinum* and *Coscinodiscus jonesianus*), and Dinoflagellate (e.g. *Ceratium teres*).

A total of 193 zooplankton species belonging to six phyla have been identified.

Copepoda is the dominant taxon, followed by Cnidaria, Ostracoda, Chaetognatha, Tunicata, etc. The biomass gradually decreases from the surface to deep sea.

Gammaproteobacteria is the dominant taxon of microbial community, with Burkholderiales and Pseudomonadales being the main orders. Nitrosopumilales is the dominant taxon of archaea. The community structure of microbes showed significant changes with depth, and was gradually steady over 10 cm depth. The dominant taxa of bacteria and archaea in this area are consistent with those in the German Contract Area located in the eastern part of the CCZ, suggesting that the microbial ecological functioning of the deep-sea sediments in the Clarion-Clipperton Zone is stable to some extent. The analysis of water and sediment microbial communities in the IRZ and PRZ suggests that the main drivers of spatial variation in microbial communities in the region are environmental changes along water and sediment depths, rather than changes in horizontal geographic gradients.

The results of meiofauna show that meiofauna communities in the IRZ and PRZ of the Block A-5 have similar compositions, with the dominant taxa being Nematoda (more than 90 %), followed by Harpacticoida and Polychaeta. The meiofauna abundance varies in the range of 50 - 66 ind./m^2, similar to the western CCZ but lower than the eastern CCZ. The taxa composition is closer to both the western and eastern parts of the CCZ.

The results of macrofauna show that macrofauna communities in the IRZ and PRZ of the Block A-5 have similar compositions, including Polychaeta, Ostracoda, Isopoda, Tanaidacea, etc. The dominant taxon is Polychaeta, with abundance exceeding 40%. The abundance of macrofauna varies in the range of 32 - 52 ind./m^2, which is lower than that in the eastern CCZ, but with similarity in community composition.

The results of megafauna show that the dominant groups include eight phyla: Protozoa, Porifera, Cnidaria, Echinodermata, Annelida, Mollusca, Arthropoda, Mollusca and Chordata. The average megafauna abundance is about 452.6 ind./ha,

and there is no significant difference in megafauna abundance between PRZ and IRZ (431.0 ind./ha vs 510.6 ind./ha). The species composition and community structure of megafauna in PRZ and IRZ are similar.

The average abundance of nodule fauna in the Block A-5 is 3.9 ind./m^2, mainly including Protozoa, Bryozoa, Cnidaria, Porifera and Annelida.

The scavenger groups are mainly *Coryphaenoides yaquinae*, Anarhichadidae, *Alicella Gammarus* and *Eurythenes* sp. in the PRZ and IRZ. Among them, *Coryphaenoides yaquinae* has high connectivity on a large scale indicated by molecular biology analyses.

Impact assessment

This Project may have the following impacts on the surrounding environment:

(1) The collector vehicle testing, including nodule removal, sediment removal and sediment disturbance, may change the original habitat. These changes may impact on the abundance and diversity of benthic microorganisms, meiofauna, macrofauna, megafauna and nodule fauna;

(2) Sediment redeposition may cause changes in the physical and chemical characteristics of bottom water columns and variations in the geological setting and chemical environment of the habitat, which in turn may create the burial effect and ecotoxicological effect on benthic fauna;

(3) The lighting of the collector vehicle, SSV/EMV and remotely operated vehicle (ROV) may have an impact on phototactic plankton and nekton;

(4) Noise from the collector vehicle and SSV/EMV may have an impact on surrounding organisms, especially large marine mammals (e.g. cetaceans);

(5) The internal combustion engines of SSV/EMV may discharge exhaust;

(6) Potential leakage of toxic substances (e.g. fuel oil, lubricating oil and hydraulic oil) from the collector vehicle, SSV/EMV and the ROV may lead to acute toxic effects on plankton; and

(7) Potential risks caused by natural disasters.

For the potential plume effects from this testing of the collector vehicle, we have built a numerical model of mining plume dispersal in the CTA to assess the spatio-temporal distribution characteristics of plume dispersal and redeposition caused by this Project. The simulation results show that plume with suspended sediment concentration higher than 10 mg/L are limited in the CTA. The dispersal direction of plume is controlled by the bottom-layer flow field, so the dispersal direction is northwest in July and east in September. The 0.1 mg/L plume contour reaches a horizontal extent of 2.1 km. The 0.1 mg/L isolines are taken as the vertical impact scope of plume, and the vertical impact reaches up to 124 m above the seafloor. The plume disappears within 3.5 days after the test-mining. The maximum thickness of redeposition caused by this test is 0.33 cm. The area with redeposition thickness greater than 1 mm is 0.06 - 0.12 km^2, and the area with redeposition thickness greater than 0.1 mm is 0.59 - 0.64 km^2.

The Block A-5 covers an area of 22,821 km^2, while this project only has a direct collection area of approximately 0.1 km^2. Since the area with direct disturbance accounts only 0.000438 % of the total area of the Block A-5, the potential impact is extremely small.

Mitigation measures

This Project will follow the best scientific knowledge and a feasible technical scheme to mitigate the potential environmental impact caused by the test, as well as adopt the impact mitigation measures throughout the test to minimize environmental impact. Specific measures are as follows:

(1) Further optimizing the design of the system and equipment of the collector vehicle, and adopting the topography-adaptive collection mechanism to avoid unnecessary and deeper sediment disturbance; adopting wide crawler belts and weight reduction design for the collector vehicle to avoid unnecessary and deeper sediment disturbance; installing sediment disturbance shielding and slowing device on the crawler belts to reduce the sediment disturbance intensity caused by the crawler belt.

(2) Selecting reasonable traveling mode and speed of the collector vehicle through numerical simulation to reduce the environmental impact; selecting the appropriate time of test-mining to reduce plume dispersal.

(3) Observing and monitoring the activities of large marine animals (e.g. turtles and whales) around the vessels during the cruise and test; adopting proactive collision avoidance measures to avoid damage to these organisms.

(4) Minimizing unnecessary lighting during the test.

(5) Taking avoidance/prevention measures to ensure the legal treatment of pollutants (e.g. ship garbage, domestic sewage, oily sewage, sewage containing toxic and harmful substances and waste gas) during the Project period, in strict accordance with the "Regulation on the Prevention and Control of Vessel-induced Pollution to the Marine Environment" (MARPOL) and the relevant provisions of the International Maritime Organization (IMO).

(6) Conducting environmental monitoring activities according to the formulated EMMP; immediately putting an end to the in-situ operation, if follow-up monitoring results show that the actual impact exceeds expectations, and then submitting a report to the ISA as per relevant requirements.

EMMP

Environmental impact analysis results show that the possible environmental impact of this Project is mainly on the seabed and the near-bottom-layer seawater. Therefore, this EMMP focuses on the monitoring of the bottom environment, benthic ecosystem and near-bottom-layer ecosystem.

To assess the environmental impact of this test, Minmetals will take four environmental monitoring measures:

(1) Installing on the collector vehicle an environmental monitoring and in-situ sampling system, including a small ROV for simultaneous environmental monitoring and assessing operational safety risk during the test;

(2) Deploying environmental monitoring arrays in and around the CTA;

(3) Using the EMV's shipboard equipment, the ROV and AUV to conduct monitoring, sampling and surveys;

(4) Deploying a set of near-bottom long-term environmental observation equipment in the CTA; and conducting annual return visit and sampling during the subsequent survey cruises to obtain the data on the recovery of the disturbed CTA.

The key environmental parameters of this EMP are:

(1) Temperature, salinity, DO, pH, turbidity and redox potential in the bottom layer;

(2) Particle concentration, turbidity, emission, dispersal trajectory, redeposition range and thickness of seabed sediment plume;

(3) Chemical elements such as nutrients (e.g. nitrate, carbonate, silicate), heavy metal elements (e.g. copper, zinc, lead, nickel, cadmium), organic pollutants and oil in bottom-layer seawater;

(4) Diversities, community structures and quantity variations of benthic communities.

To obtain the long-term observation data of natural variations in the environment after the test-mining, Minmetals will set up a long-term observation system in this area after the collector vehicle test and conduct interannual return visits. The said system can monitor environmental parameters (e.g. turbidity, ocean current, noise) and record near-bottom video over the long term.

This EIS briefly describes the layout scheme of monitoring system, sampling scheme, as well as the method for analysis of sediments and seawater. See the EMMP for details.

Report

Reporting unexpected accidents and disposal results to the ISA

Minmetals will strictly implement Regulation 33 of ISBA/19/C/17, which reads "any spill, accident or uncontrolled release into the marine environment will be notified to the ISA as an emergency within the specified reporting time". Minmetals will promptly report to the ISA's Secretary-General in writing, using the most effective means, any incident arising from activities which have caused, are causing or pose a threat of serious harm to the marine environment.

The report to the ISA will include the following:

—The event and all the important facts and circumstances known about the event at that time;

—Any and all actions taken to avoid or mitigate any adverse environmental impact;

—Any and all corrective measures that have been taken or may be taken to prevent similar incidents from happening again.

In addition, according to MARPOL OPRC-HNS 2000 Protocol, Minmetals will also notify any relevant third-party organizations as required.

Annual report

According to Regulation 32 of ISBA/19/C/17, the Contractor shall report annually in writing to the Secretary-General on the implementation and results of the EMP and shall submit data and information, taking into account all recommendations issued by the LTC. These reports will explain the compliance with the EMP and make recommendations for any corrective actions.

Minmetals will regularly disclose the monitoring and assessment results of this Project to the ISA according to the above-mentioned requirements.

Minmetals also plans to hold a public stakeholder event to report the results from the testing of the collector vehicle and environmental monitoring.

Stakeholder consultation

This report is released for public comment on 2nd April and 11th April, 2024 on the official website of Minmetals and ISA, respectively. As of the end of the public

announcement period (to 31 May, 2024), a total of 8 stakeholders' opinions on the environmental impact statement have been received. The current version of the EIS document has been updated in response to public comments provided as part of the stakeholder consultation process. The modifications mainly include biological baselines (microbial diversity, more detailed biological classification and identification results, annual variation characteristics of benthic communities, comparison results of IRZ and PRZ, statistical analysis of spatial differences in megafauna communities, heavy metal concentrations in organisms, etc), description of plume modeling method, and results of heavy metal toxicology tests. We appreciate all stakeholders' feedback, which greatly improved this report.

Conclusion

The information provided in this EIS supports the following conclusions. The impact of small-scale testing of the collector vehicle on the physico-chemical environment and ecosystems can be reduced to a non-significant level by adopting a specific design of the collector vehicle, implementing the EMP and proposed mitigation measures, and strict reporting and supervision procedures. The risk of "serious harm" to the marine environment caused by this Project in the Area is very low.

1 Introduction

1.1 Objective

Minmetals plans to carry out testing of the polymetallic nodule collector vehicle in July-October of 2025 in the Block A-5 of the Contract Area stipulated in the Contract between Minmetals and the ISA. This Project will verify the collecting and traveling performance, reliability, and economy of the collector vehicle. The test results will be used for optimizing the design of the collector vehicle. This Project mainly aims to achieve the following two objectives:

(1) Testing and improving the collector vehicle's technical performance: During the test, we will verify the collector vehicle's collecting function, traveling function, navigation and positioning function, launch and recovery function, environmental monitoring and sampling function as well as its operability, reliability and nodule-collecting efficiency, so as to provide data for the design of the collector system.

(2) Monitoring and assessing the environmental impact of the collector vehicle: We will carry out environmental monitoring through the whole process, covering the whole area (from point to line) and the whole space (from far field to near field). Data and samples collected will be used for assessing the environmental impact caused by the collector vehicle test, as well as providing information for the testing of the collector system and subsequent commercial mining.

1.2 Background

In 2017, Minmetals signed a 15-year Contract for Exploration for Polymetallic Nodules with the ISA. The Contract Area is located in the CCZ of the East Pacific Ocean and consists of eight blocks. The proposed TMA is located in the Block A-5 (Figure 1.2-1).

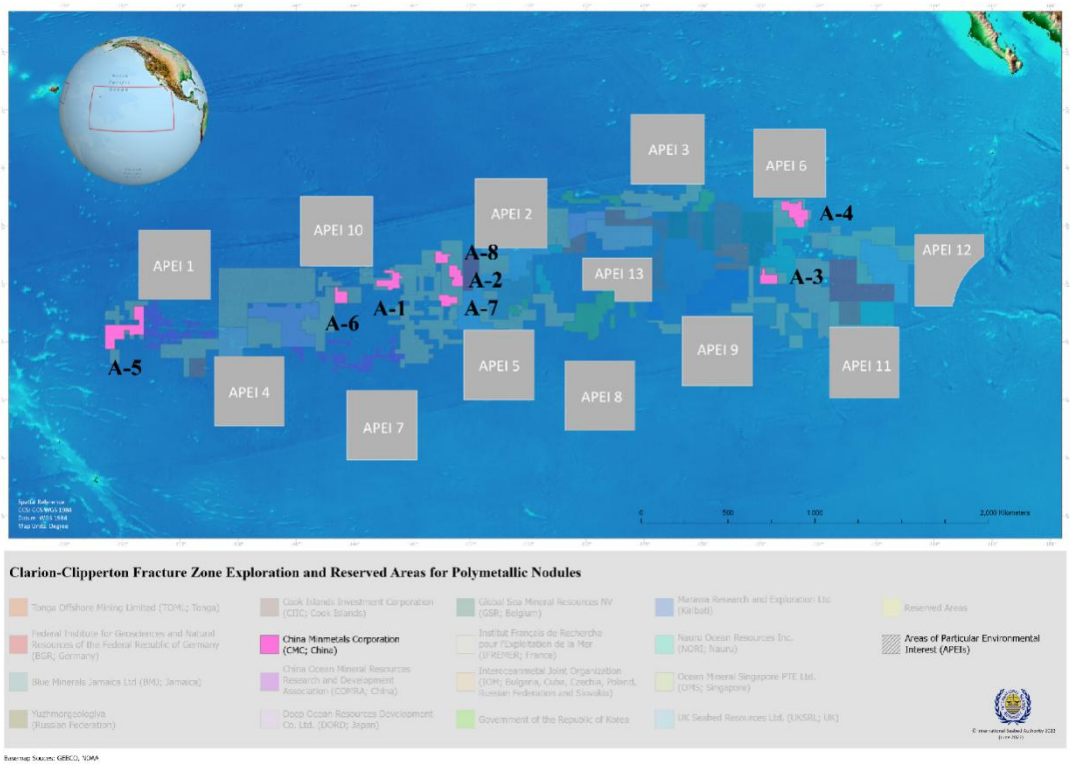

Figure 1.2-1 Schematic diagram for the distribution of eight blocks in the Contract Area

(From http://www.isa.org.jm)

After the signing of the Exploration Contract, Minmetals conducted six survey cruises in eight blocks delineated in the Contract. Since 2021, Minmetals has conducted resource and environmental surveys in PWA within the Block A-5 for three consecutive years.

The collector vehicle to be tested is part of Minmetals' long-term programme for developing seabed mining technologies. In 1995, Minmetals developed a prototype collector vehicle (PCV) and completed relevant laboratory tests. In 2021, Minmetals developed China's first engineering PCV, and completed the lake test for it. In 2016-2018, Minmetals has independently developed the Kunlong 500 collector vehicle, and then completed at-sea testing of it at the water depth of 514 m in the South China Sea in June 2018. Based on the R&D of Kunlong 500 collector vehicle, Minmetals has developed a collector system for water depth of 1,000 m, and completed a polymetallic nodule collector system test at water depth of 1,000 m in the South China Sea in June-July of 2021. On the basis of the above-mentioned R&D efforts,

Minmetals has developed a new generation of seabed collector system to validate key deep-sea mining technologies in the Contract Area.

1.3 Project feasibility

Technical feasibility: The collector vehicle to be tested has been optimized and designed on the basis of the previously developed small-scale PCV. The equipment has the characteristics of low disturbance, environmental friendliness, intelligence, safety and reliability.

Environmental feasibility: Similar to the Benthic Impact Experiments (BIE) conducted in the CCZ in the 1980s and 1990s (JET-BIE, IOM-BIE, NOAA-BIE), this test will bring a small spatio-temporal impact to the seabed environment. In compliance with the latest "Recommendations for the guidance of contractors for the assessment of possible environmental impacts arising from the exploration for marine minerals in the Area" (ISBA/25/LTC/6/Rev.3), Minmetals will formulate an EMP for prior to, during and following the test-mining as well as the entire region in all dimensions. So far, Minmetals has conducted resource exploration and environment baseline survey for six cruises, and obtained environmental data and samples from the CTA of the Block A-5, thus providing a basic support for this EIA.

Industrial feasibility: As human demands for new energy materials (e.g. cobalt, nickel and copper) are increasing, the existing land mineral resources are depleting, thus pushing up metal prices. Rich in polymetallic nodules, cobalt-rich crusts, polymetallic sulphides, rare earth-rich sediments and other resources, the international seabed area has high economic value and great development potential. The mineral resources in the Contract Areas belong to all mankind. It is in the interest of all mankind to exploit deep-sea mineral resources, which are an important continuation of land metal resources. Conducting deep-sea mineral resources exploration and environmental monitoring will not only make up for land mineral resources and promote the development of deep-sea exploration technologies and equipment capabilities, but also help promote the construction of global deep-sea governance

system as well as the fair, orderly and sustainable exploitation and utilization of deep-sea resources.

1.4 Project history

1.4.1 Overview of the Contract Area

The Contract Area is located in the CCZ (8-15 °N, 158-138 °W, Figure 1.2-1), and includes eight blocks with a total area of 72,745 km^2. Among them, the Block A-5 (22,821 km^2) is a polymetallic nodules reserved area submitted by the China Ocean Mineral Resource Research and Development Association (COMRA) to the ISA. Blocks A-1, A-2, A-6, A-7 and A-8 (totaling 31,049 km^2) are reserved areas submitted by Russia. Blocks A-3 and A-4 (totaling 18,875 km^2) are reserved areas submitted by the Interoceanmetal Joint Organization (OM).

The Block A-5 of the Contract Area is adjacent to the Block KW1 in the western part of the COMRA Contract Area. Japan's DORD Contract Area and the COMRA's eastern blocks are to the west and south of the Block A-6 of the Contract Area respectively. Russian Yuzhmorgeologiya Contract Area is to the south of the Block A-1 of the Contract Area. German BGR and British UKSRL Contract Areas are to the east of Minmetals' Blocks A-2, A-7 and A-8, respectively. There are many other Contract Areas, mainly including the NORI of Nauru, the TOML of Tonga, the BGR of Belgium and the MRE of Kiribati, around Minmetals' Blocks A-3 and A-4.

1.4.2 Historical fulfillment of exploration and environmental obligations in the Contract Area

In 2017, 2018, 2019, 2021, 2022 and 2023, Minmetals used R/V *XIANGYANGHONG LIUHAO, R/V XIANGYANGHONG SANHAO,* R/V *XIANGYANGHONG SHIHAO,* R/V *DAYANG YIHAO* and R/V *DAYANG HAO* respectively to conduct at-sea surveys in the Contract Area for 99 days, 61 days, 113 days, 104 days, 75 days and 85 days respectively, totaling 537 days. The main activities included multibeam bathymetric survey, geological sampling, deep-sea

video and photograph survey, AUV-based acoustic near-bottom survey, as well as sampling and monitoring for environment baseline survey.

Resource survey and studies: In terms of at-sea survey, as of the 2023 survey cruise, Minmetals has completed full-coverage multibeam sounding survey in eight blocks (approximately 72,700 km^2 of total area and 11,302 km of survey line) of the Contract Area; it has also conducted box corer sampling at 269 stations and gravity piston corer sampling at 11 stations, obtaining abundance and coverage data, as well as samples such as nodules and surface-layer sediments. We have completed 957.2 km of seabed optical survey line (including 109 km of AUV line), extracting coverage rate and other data. In the TMA of the Block A-5, we have completed 688 km of near-bottom acoustic survey line. See Table 1.4-1 for statistics of the main workloads of resource survey. **With respect to laboratory studies**, the topographic and geomorphological features of the Contract Area (characteristics of micro-topography and micro-geomorphology in some areas), the characteristics of nodule abundance, coverage and main metal elements content, the continuity characteristics and the mining environment conditions of nodules have been preliminary mastered, the delineation of nodule ore bodies in eight blocks of the Contract Area and the estimation of inferred resources have been completed, and the estimation of indicated resources and measured resources have been completed in the western primary working area (PWA) of the Block A-5.

Table 1.4-1 Information about resource survey in the Contract Area

Block	Area (km^2)	Box corer sampling		Optical	Multibeam	AUV acoustics
		Historic	2017-2023	2017-2023	2017-2023	2017-2023
A-1	8661	52	6	46.2	1065	
A-2	6935	36	6	38.9	993	
A-3	5747	21	8	39.5	1660	
A-4	13128	58	21	150.9	2351	
A-5	22821	29	208	552.5	3391	688
A-6	5346	13	8	41.1	644	

Block	Area (km^2)	Box corer sampling		Optical	Multibeam	AUV acoustics
		Historic	2017-2023	2017-2023	2017-2023	2017-2023
A-7	5537	35	4	36.4	662	
A-8	4570	33	8	51.1	536	
Total	72745	277	269	957.2	11302	688

Environmental survey and studies: In terms of at-sea survey, as of the 2023 survey cruise, Minmetals has surveyed environment baselines in eight blocks of the Contract Area to varying degrees, including 200 m depth seawater sampling for CTD measurement at 17 stations, full-ocean-depth profiling CTD measurement at 22 stations, multicorer sampling at 30 stations, box corer sampling at 35 stations (sharing of resources), plankton vertically towed net sampling at 16 stations, multinet sampling at five stations, in-situ testing for the geotechnical properties of sediments at 29 stations, mooring observation at five stations, baited trap lander observation at eight stations, MULVFS at three stations, and hydrophone monitoring at three stations. See Table 1.4-2 for the statistics of environmental survey. **With respect to laboratory studies**, basic environment baseline studies such as physical oceanography, chemical oceanography, biological community, sedimentation and sedimentary flux have been conducted in eight blocks of the Contract Area. A total of 727 species (including 86 species of culturable microbe) have been collected from the eight blocks of the Contract Area. These samples belong to 395 genera under 20 phyla, with Arthropoda species accounting for 15.5 % of the total species. Phytoplankton and zooplankton consist of ocean water species. Nematoda is the dominant taxon, accounting for more than 80 % of meiofauna. Crustacean is the most dominant taxon of macrofauna. Existing survey and analysis results show that the eight blocks have a large spatial span (approximately 4,000 km from east to west), and there are significant differences in geological setting. Environmental parameters (e.g. the characteristics of the upper-layer ocean current, the depths of mixed layer and thermocline, the Chl *a* concentration in seawater, and the values of DO, pH, biodiversity and its abundance) also vary among these blocks. For example, the Block A-5 (in the western part) has

significantly lower primary production and benthic density than other blocks in the eastern part, and has the water environment totally in consistency with the western block in the adjacent the COMRA Contract Area. Therefore, the Block A-5 can represent the overall environmental characteristics of the western part of the CCZ in the East Pacific Ocean.

In addition, we have deployed long-term observation systems in the PWA of the Block A-5 to gather long-time series environmental data. After further processing and analysis, these data will be used for studies on the natural variations of baselines and for EIA.

Table 1.4-2 Information about environmental survey in the Contract Area

Block	A-1	A-2	A-3	A-4	A-5	A-6	A-7	A-8	Total
200 m CTD survey (station)	1	1	1	2	8	1	1	2	17
Full-ocean-depth profiling CTD (station)	1	1	1	2	13	1	1	2	22
Multicorer sampling (station)	/	/	2	2	25	/	/	1	30
Box corer sampling (station)	2	/	4	4	22	2	/	1	35
Plankton vertically towed net sampling (station)	1	1	1	/	9	1	1	2	16
Geotechnical properties testing (station)	/	/	1	1	27	/	/	/	29
Mooring (station)	/	/	/	/	4	1	/	/	5
Sampling with baited trap lander (station)	/	/	1	/	6	/	/	1	8
MULVFS (station)	/	/	/	/	2	/	/	1	3
Multinet sampling (station)	/	/	1	/	3	/	/	1	5
Hydrophone monitoring (station)	/	/	/	/	3	/	/	/	3
Total	5	3	12	11	122	6	3	11	173

1.4.3 R&D and collector vehicle test and its components

Minmetals was one of the first companies in China to engage in technical studies

on deep-sea mineral resources exploitation, processing and utilization. We have conducted technological researches and equipment R&D in the fields of deep-sea exploration and mining. The collector vehicle to be tested is part of its long-term plan for developing seabed mining technologies. It is also one of the contents of the second five-year period (2022-2026) in Appendix I of the Exploration Contract. That is, Minmetals needs to organize the at-sea testing of the collector system's subsystems. Prior to this, Minmetals has conducted long-term studies in this regard, providing a solid technical foundation so for this test.

In the early stage of technology R&D, our collection technology has been successfully verified and tested in laboratories, deep-water lakes, offshore waters and deep seas under national jurisdiction (Figure 1.4-1). These test data and in-situ operation experience have improved the reliability of this test.

Figure 1.4-1 Development and testing of Minmetals' collector vehicle

First stage (1991-1995): Laboratory tests

The working principles of various collector vehicles, methods and mechanisms for separating slurry and crushing ore, traveling mechanism and other technological research have been conducted, and a PCV (Figure 1.4-2) has been successfully developed. The PCV has a nodule collection rate of over 80 % and a nodule-collecting capacity of 5 t/h. The laboratory tests of function and performance have been completed, and the feasibility of hydraulic collection technology has been verified.

Figure 1.4-2 Prototype of hydraulic collector vehicle

Second stage (1996-2001): Deep-water lake test

Entrusted by the COMRA, Minmetals has successfully developed China's first engineering PCV (Figure 1.4-3), and conducted the testing of partial collector system at the depth of 135 m in Fuxian Lake, Yunnan, China. With a nodule collection rate of more than 85 % and a nodule-collecting capacity of 30 t/h, the test-mining has collected 900 kg of simulated. This test has marked the debut of Chinese-developed seabed nodule mining technology, as well as accumulated valuable experience for subsequent mining test in shallow sea.

Figure 1.4-3 Engineering PCV for lake test

Third stage (2016-2021): At-sea tests at water depths of 500 m and 1,000 m

In 2016-2018, entrusted by the COMRA, Minmetals has independently developed the Kunlong 500 collector vehicle (Figure 1.4-4), and completed the 514 m depth at-sea test in the South China Sea in June 2018. The Kunlong 500 collector vehicle demonstrated a nodule-collecting capacity of 10 t/h, the longest traveling distance of 2,881 m and the positioning precision of 0.72 m. According to the planned route, the collector vehicle traveled a star-shaped route (120 m for each edge). The Kunlong 500 collector vehicle represents breakthroughs in the technology of travelling on muddy substrate, the adaptive collecting technology, as well as the integrated navigation and positioning and intelligent control technology. The success of this at-sea test indicates that the R&D of seabed collector system in China has been fully transferred from land trial to at-sea test.

Figure 1.4-4 At-sea (500 m water depth) testing of Kunlong 500 collector vehicle

Based on the R&D of Kunlong 500 collector vehicle, Minmetals has developed a collector system for water depth of 1,000 m (Figure 1.4-5), and completed a polymetallic nodule collector system test at water depth of 1,000 m in the South China Sea in June-July of 2021. The successful at-sea test has indicated the technological leap from shallow sea to deep sea, from unit testing to whole system testing for China's seabed nodule mining efforts. It has also laid a technical foundation for subsequent tests in the Contract Area.

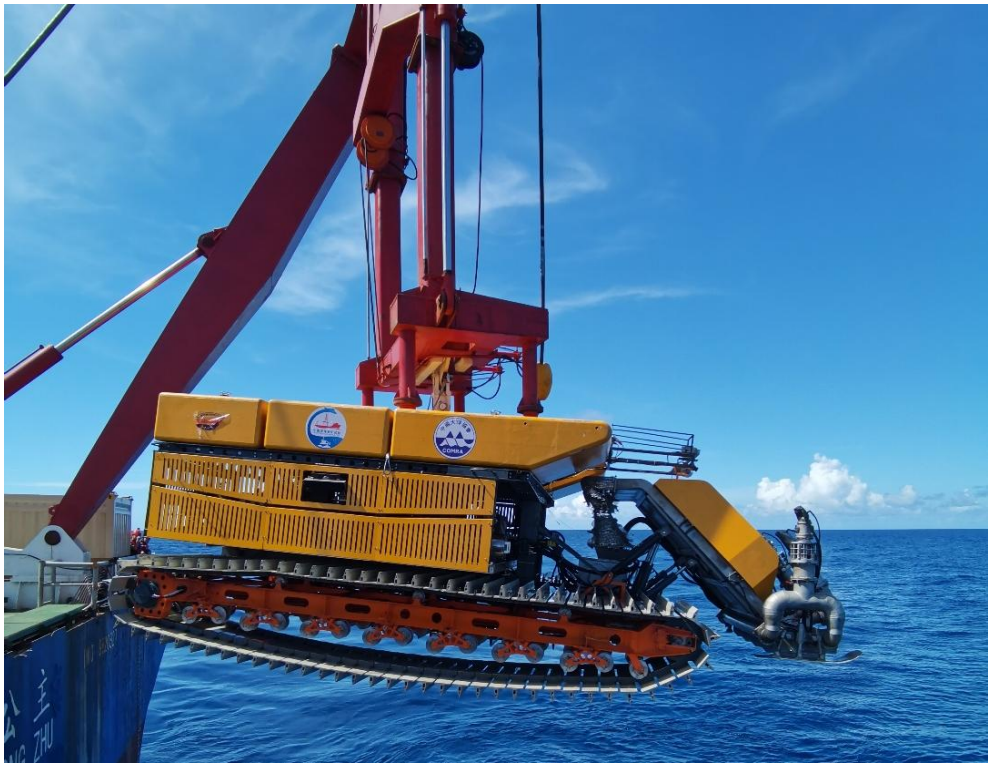

Figure 1.4-5 At-sea (1,000 m water depth) testing of the collector vehicle

Fourth stage (2021-present): Verification of key technologies in the Contract Area

With previous accumulation of mining technologies, Minmetals is committed to developing a safer, greener and smarter collector system with the basic principles of safety, reliability, low carbon, environmental friendliness and intelligence and high efficiency. In 2022, Minmetals started the design, R&D and testing project for a collector vehicle suitable for 5,000 m water depth. All the efforts have provided technical support for this collector vehicle test as well as the development and improvement of subsequent system test.

1.5 Information of the project proponent

1.5.1 Introduction to Minmetals

The project proponent, Minmetals, was established in 1950. As a large-scale enterprise with metal and minerals as its core business, Minmetals aims to become a world-class metal and mining enterprise group with global competitiveness. Minmetals has a "four beams and eight pillars" business system, consisting of metals and minerals, metallurgical construction, trade logistics and financial real estate, and

mineral development, metal materials, new energy materials, metallurgical engineering, capital construction, trade logistics, financial services and real estate development. By the end of 2023, Minmetals had total assets of over one trillion yuan and eight listed companies. It ranked 65th in the Fortune Global 500 list with a full-year operating revenue of approximately 940 billion yuan.

By the end of 2023, Minmetals had 14 established research and design institutions, 46 state-level R&D platforms such as State Key Laboratories, 30,000 scientific researchers, 52,000 valid patents, and more than 1,900 international and national standards. All these testify its outstanding scientific and technological innovation capabilities.

Minmetals proactively participates in sustainable development affairs at home and abroad. Examples include accelerating the integration of the United Nations Agenda for Sustainable Development in 2030 and Minmetals' social responsibility promotion model "Value Creation", creating a sustainable development model in the new era, and helping the United Nations achieve its 2030 Sustainable Development Goals.

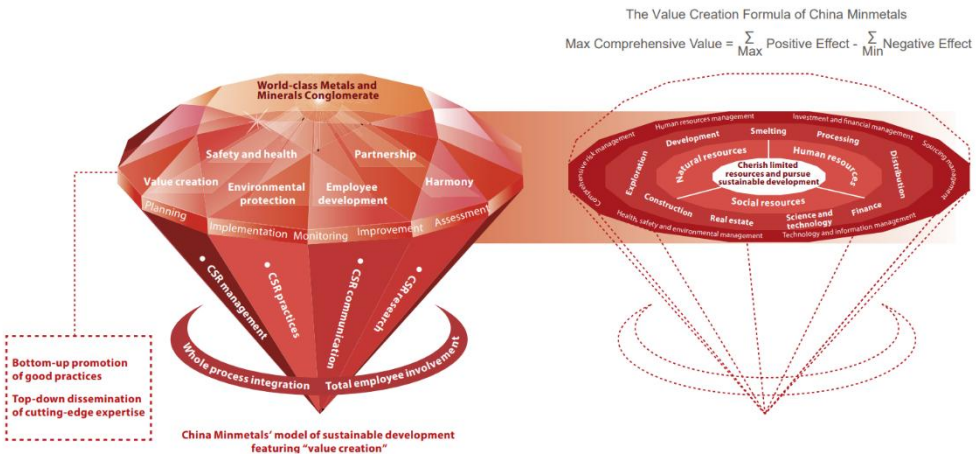

Figure 1.5-1 Minmetals' "Value Creation" social responsibility promotion model

In its annual sustainable development reports, Minmetals fully discloses its actions and achievements in value creation, innovation and development, safety and health, environmental protection, employee growth, partnership building and social

harmony. Regarding stakeholders as the most important resource for the company's sustainable development, and taking "cherishing stakeholders, striving to create unlimited value for stakeholders" as the main theme, Minmetals discloses the company's performance to stakeholders in an informative, true and objective manner. By doing so, Minmetals aims to achieve equal, comprehensive and in-depth communication, enhance mutual-trust and cooperation, and seek common progress and development with stakeholders.

Always prioritizing safe production and low-carbon environmental protection, Minmetals instills the concepts of safe development and green development into all fields and the whole process of corporation development. While facilitating the achievement of carbon peak and carbon neutrality and participating in the new development pattern of "dual circulation", Minmetals proactively expands footprints into the fields of new standards, new technologies, new energy, greening, digital intelligence, etc. It helps relevant industries become intelligent, efficient, green and low-carbon, creates a more optimized lifestyle, and contributes its part to the realization of high-quality and sustainable development worldwide.

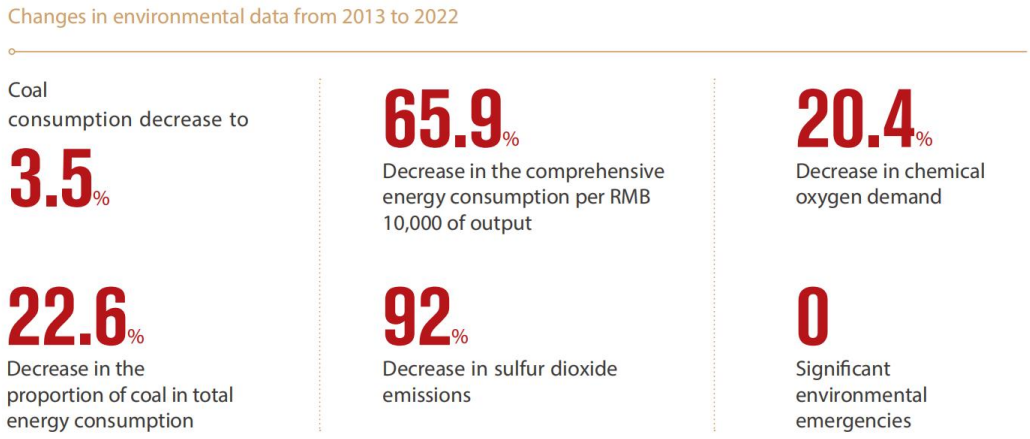

Figure 1.5-2 Comparison of the environmental data collected by Minmetals in 2013-2022

1.5.2 Basic information of Exploration Contract

Minmetals officially submitted to the ISA "An application for approval of a plan of work for exploration in the Area" on August 8, 2014, and sent a delegation to

Jamaica to complete the application defense organized by the ISA's LTC on February 18, 2015. In accordance with legal procedures, the 21st Council of the ISA discussed and approved the application for exploration rights of polymetallic nodules reserved areas in the Area submitted by Minmetals on the morning of July 20, 2015. Minmetals signed a 15-year Exploration Contract with the ISA on May 12, 2017, officially obtaining the exclusive exploration rights for 72,745 km^2 of nodule mines. By the end of 2023, Minmetals had fulfilled its contract for seven years, submitting six annual reports and one stage report. Survey data were also submitted with these annual reports.

1.5.3 This Project's organizational framework

1.5.3.1 Preparation of EIS

This EIS was jointly prepared by Minmetals, the Ministry of Natural Resources and other relevant research institutes. The personnel responsible for relevant chapters are as follows.

Chapter 1 Introduction (by Liu Yuwei, Sun Dong and Chen Shiping);

Chapter 2 Policies, Legal and Administrative Backgrounds (by Jiang Yuhuan);

Chapter 3 Description of Proposed Exploitation Activities (by Cheng Yangrui and Li Jun, Hao Xiangli and Li Zhenggang);

Chapter 4 Description of Existing Physicochemical Environment (by Li Zhenggang, Yang Chenghao, Li Weiwen, Xu Dong, Li Xiaohu, Zhang Weiyan and Lin Shiquan);

Chapter 5 Description of Existing Biological Environment (by Sun Dong, Lu Bo, Lin Shiquan and Zhang Wenqian);

Chapter 6 Description of Existing Socioeconomic Environment (by Sun Dong)

Chapter 7 Assessment of Impacts on the Physicochemical Environment and Proposed Mitigation Measures (by Yang Chenghao, Wang Jun, Sun Dong and Cheng Yangrui);

Chapter 8 Assessment of Impacts on the Biological Environment and Proposed

Mitigation Measures (by Sun Dong and Lu Bo);

Chapter 9 Natural Hazards and Accidental Events (by Li Manhong, Li Jun, Shuang Zhi and Ding Han);

Chapter 10 Environmental Management, Monitoring and Reporting (by Liu Yuwei, Chen Shiping, Sun Dong, Yang Chenghao and Zhang Wenqian);

Chapter 11 Product Stewardship (by Sun Dong)

Chapter 12 Consultation (by Liu Yuwei)

Chapter 13 Terminology and Abbreviation (by Sun Dong, Li Zhenggang and Lu Bo)

Chapter 14 Study Teams (by Liu Yuwei and Zhang Wenqian)

Annex 1 Study Report on Modeling Sediment Plume Caused by Bottom-layer Disturbance (by Wang Jun)

Annex 2 Survey Methods and Quality Assessment for Environment Baseline Studies (by Lin Shiquan)

The preparation of EIS is headed by Sun Dong and Liu Yuwei, with Sun Dong, Liu Yuwei and Zhang Wenqian in charge of whole edition and typing work, and Mao Guiting in charge of the final review.

1.5.3.2 Test team

This Project's test team consists of members from 12 enterprises, research institutes and universities. The specific tasks are as follows:

1) Overall design, integration and at-sea testing of collecting equipment

Changsha Research Institute of Mining and Metallurgy Co., Ltd. (CRIMM) of Minmetals

2) Key technologies and equipment for traveling and nodule collection

Changsha Institute of Mining Research Co., Ltd. (CIMR) of Minmetals, the CRIMM of Minmetals, Dalian University of Technology and Central South University

3) Positioning and navigation, power transmission and intelligent control technologies and equipment

Harbin Engineering University, the CRIMM of Minmetals, CRRC SMD (Shanghai) Ltd. and Central South University.

4) Development of launch and recovery system (LARS) and support with at-sea test vessel.

China Ship Design & Research Center, Shanghai Minghe Shipping Co., Ltd. and the CRIMM of Minmetals.

5) Environmental disturbance monitoring and impact assessment

The Second Institute of Oceanography of the Ministry of Natural Resources (SIOMNR), the Third Institute of Oceanography of the Ministry of Natural Resources (TIOMNR), the Ocean University of China, the Institute of Oceanology, Chinese Academy of Sciences (IOCAS), the CRIMM of Minmetals.

2 Policies, Legal and Administrative Backgrounds

2.1 Relevant international legislation, policies, procedures and standard

2.1.1 International legislation, policies, procedures and codes

2.1.1.1 Relevant provisions of the United Nations Convention on the Law of the Sea (UNCLOS)

The 1982 United Nations Convention on the Law of the Sea (UNCLOS) is the international framework convention regulating activities in the oceans and seas. Article 1 of the UNCLOS defines "activities in the Area" as all activities of exploration for, and exploitation of, the resources of the Area; Article 133 defines "resources" as all solid, liquid or gaseous mineral resources in situ in the Area at or beneath the seabed, including polymetallic nodules; Article 209 provides the obligations of States to adopt laws and regulations to prevent, reduce and control pollution of the marine environment from activities in the Area. China ratified and became a party to the UNCLOS in 1996, and is also a party to the 1994 Agreement relating to the Implementation of Part XI of the United Nations Convention on the Law of the Sea of December 10, 1982 (the "Implementation Agreement"). The nodule exploration activities involved in this EIA will be conducted in the Area defined in Article 1 of the UNCLOS, that is, at or beneath the seabed and ocean bottom and its subsoil beyond the limits of national jurisdiction (Article 1 (1) (1) of the UNCLOS). Therefore, this Project will be governed by the UNCLOS and the Implementation Agreement, and comply with the requirements of international law related to the implementation of activities and the environment.

2.1.1.2 The ISA's related rules, regulations, standard

As an international organization established according to the UNCLOS, the ISA is responsible for organizing, regulating and controlling activities in the Area.

According to the relevant provisions of Part XI of the UNCLOS and its Implementation Agreement (1994), the ISA has the duty to adopt appropriate rules, regulations and procedures to ensure the effective protection of the marine environment from the possible harmful effects of related activities (Article 145 of the UNCLOS). The ISA is composed of the European Union and 169 member states. China is one of the member States with permanent representation and has been a member of the ISA Council since 1996, becoming a member of the ISA Council's A Group in 2004 and continuing to this day.

2.1.1.3 The ISA Mining Code

The ISA Mining Code consists of a series of rules, regulations and procedures issued within the general legal framework established by the UNCLOS (e.g. Part XI) and the 1994 Implementation Agreement to regulate the prospecting, exploration and exploitation of marine resources in the Area.

2.1.1.3.1 Regulations on nodule exploration

Up to now, the ISA has issued three exploration regulations, including the "Regulations on Prospecting and Exploration for Polymetallic Nodules in the Area" (ISBA/19/C/17, Annex) adopted in 2000 and revised in 2013. The most relevant contents for this Project include:

The Part V (Protection and preservation of the marine environment) involves:

(1) Applying a precautionary approach and best environmental practices, and take necessary measures to prevent, reduce and control pollution and other hazards to the marine environment arising from activities in the Area as far as reasonably possible (Regulation 31);

(2) Proposal on the establishment of the IRZs and PRZs (Regulation 31);

(3) Gathering environment baseline data and establishing baseline (Regulation 32);

(4) Formulation of EMP and monitoring requirements for the environmental

impact of activities (Regulation 32);

(5) Reporting any incident arising from activities which have caused, are causing or pose a threat of serious harm to the marine environment, and take necessary measures to prevent, contain and minimize serious harm or the threat of serious harm to the marine environment arising out of activities in the Area (Regulation 33);

(6) Taking all measures necessary to ensure that the activities are conducted so as not to cause serious harm to the marine environment under the jurisdiction or sovereignty of coastal States (Regulation 34);

(7) Reporting and protecting any human remains and objects and sites of an archaeological or historical nature (Regulation 35).

The above-mentioned requirements cover the Contractor's obligations to the ISA in respect of exploration activities in the Area stipulated in the Contract. The preparation of this EIS and other specified documents related to the collector vehicle test of this Project meets the above-mentioned requirements. At the same time, the Contractor can provide with a guarantee of its financial and technical capabilities to comply with emergency orders to assure that the council can take such emergency measures (Regulation 33 (8)).

Sections 5 to 7 of Annex IV to the Regulations (Standard Clauses for Exploration Contracts) explain in detail the above matters involved in Part V, and specifically stipulate that:

5.2 Prior to the commencement of exploration activities, the Contractor shall submit to the ISA:

(a) An impact assessment of the potential impacts on the marine environment of the proposed activities;

(b) A proposal for an EMP to determine the potential impact on the marine environment of the proposed activities; and

(c) Data that could be used to establish an environment baseline against which to

assess the impact of proposed activities.

2.1.1.3.2 Draft mining regulations, standards and codes

The "Draft regulations on exploitation of mineral resources in the Area" and the drafts of relevant environmental standards and codes are in the process of consultation and revision. The proposals and related discussions in the draft regulations and codes on the contents of the environmental impact report prepared for the exploitation stage, the determination of environment baseline data, and the preparation of EMMPs provide the Contractor with useful information related to the obligations that may need to be fulfilled in the subsequent exploitation stage. Bearing in mind the relationship between the test-mining activities in the exploration stage and the subsequent commercial mining activities, we referred as appropriate the contents of draft exploitation regulations and related codes that are in line with the requirements of the Regulations on Prospecting and have guiding significance in the preparation stage of this EIS. In this way, we will more effectively fulfill the relevant requirements stipulated in the Exploration Contract during the implementation of this Project. We believe that a comprehensive understanding of the latest legislative background will also be conducive to improving the design and implementation of test-mining activities in the exploration stage as well as to more effectively carrying out studies, monitoring, assessment and management related to the status quo of and impact on the existing environment.

2.1.1.3.3 Recommendations on EIA

In 2002, the ISA's LTC issued the "Recommendations for the guidance of the Contractors for the assessment of the possible environmental impacts arising from exploration for polymetallic nodules in the Area" (ISBA/7/LTC/1/Rev.1), which was revised in 2010 (contained in ISBA/16/LTC/7). In March 2013, the LTC issued a set of consolidated environmental guidelines "Recommendations for the guidance of contractors for the assessment of the possible environmental impacts arising from exploration for marine minerals in the Area" (ISBA/19/LTC/8), and then three

revisions in March and June 2020 (ISBA/25/LTC/6/Rev.1 and ISBA/25/LTC/6/Rev.1/Corr.1), July 2022 (ISBA/25/LTC/6/Rev.2) and August 2023 (ISBA/25/LTC/6/Rev.3). The Recommendations determines the exploration activities that need prior EIA, the form and content of the EIA, and provides relevant guidelines on baseline studies, monitoring and reporting.

The most relevant contents in the Recommendations (ISBA/25/LTC/6/Rev.3) are as follows:

(1) Activities requiring EIA during exploration

Section VI (B)(33) states: The following activities require prior EIA, as well as an EMP to be conducted during and after the specific activity, in accordance with the recommendations contained in paragraphs 33 and 38. It is important to note that these baselines, monitoring and impact assessment studies are likely to be the primary inputs to the EIA for commercial mining. The activities include:

(a) Use of sediment disturbance systems that create artificial disturbances and plumes on the sea floor;

(b) Testing of mining components;

(c) Test-mining;

(d) Testing of discharge systems and equipment;

(e) Drilling activities using on-board drilling rigs;

(f) Sampling with epibenthic sled, dredge or trawl, or similar technique, in nodule fields, that exceeds 10,000 m^2;

(g) Taking of large samples to test land base processes.

Therefore, the PCV (1/4 the scale of a full-size commercial system, including testing its traveling, collecting, obstacle avoidance and other functions) to be tested needs an EIA and an EMMP as the main basis for the EIA for subsequent commercial mining activities.

(2) Related procedure steps

Section VI (B)(34) states: The EIS and data mentioned in Paragraph 38 of the

Recommendations shall be submitted by the Contractor to the Secretary-General not later than one year before the start of the activity.

Section VI (E) outlines the process for reviewing the EIS on the testing of mining components.

Accordingly, this EIS will be submitted with relevant documents and materials in accordance with the above-mentioned timetable and procedural steps.

(3) Relevant requirements for environment baseline data

Sections III and IV of the Recommendations specify in detail the requirements for environment baseline studies, baseline data collection, data collection and analysis, reporting and archiving procedures. The explanatory commentary in Annex I also provides additional information on baseline data requirements.

Sections VI (C) and VI (D) respectively define the information and measurement to be provided by contractors performing an activity that requires EIA during exploration, and the observations and measurements to be made after undertaking an activity that requires an EIA during exploration.

Baseline data are essential in monitoring variations resulting from these activities and predicting the impacts of commercial mining activities. Since 2017, we have formulated the sampling strategy of environment baseline survey through the design and planning of geographic information system, conducted long-term data collection, obtained and recorded sufficient information on the natural conditions of PCV before testing from the exploration zone, and collected other data related to sea surface, middle ocean layer, near-bottom layer and seabed communities, so as to establish baseline data for EIA. Therefore, this EIS meets the relevant requirements of the above-mentioned recommendations.

(4) EIS template

Annex III of the Recommendations provides a template for the EIS. It is also noted that a more detailed template for preparing the EIS is contained in the "Draft regulations for exploitation of mineral resources in the Area" (ISBA/25/C/WP.1).

Therefore, this EIS is mainly arranged according to the contents of the Environmental Impact Report in the Recommendations, and seeks to obtain some more specific operational guidelines from Annex IV (Environmental Impact Statement) of the draft mining regulations for the contents that are consistent or consistent with the exploration regulations and recommendations and the basic requirements related to the test-mining activities of this Project.

(5) Relevant progress of stakeholder consultation

Article VI. (E)(41)(a) of the Recommendations clearly states that "In its submission, the contractor is to include information on the stakeholder consultation conducted, as reflected in annex I to the present recommendations", and Annex I provides the best available technology and methodological guidance for implementing the relevant recommendations of the consultation process, including the consultation time, methods and progress, and the handling of relevant concerns of stakeholders. The above-mentioned guiding recommendations were fully taken into account in the stakeholder consultation process for the activities in this EIS (see Chapter 12 of this EIS), and the sponsoring State presided over the public consultation process. The output of stakeholder consultation is helpful to the compilation of the final mining EIA report and has a positive effect on the Contractor's better performance of environmental obligations.

2.1.1.4 Relevant environmental management policies of the ISA

The preparation and implementation of the regional environmental management plan (REMP) are part of the ISA's policy framework for environmental management (ISBA/24/C/3, para. 7). The REMP at the regional level is one of the appropriate and necessary measures to ensure the effective protection of the marine environment in the Area from the possible harmful effects of activities in the Area in accordance with Article 145 of the UNCLOS. Although the REMPs are not binding legal instruments and, therefore, do not impose legal obligations on contractors (ISBA/25/C/4, para. 7), it can still provide guidance for the design of environmental management objectives

and measures for activities in the Area. The REMP developed by the LTC for the CCZ, where the Contract Area (this Project) is located, was approved by the ISA Council in 2012 (according to ISBA/17/LTC/7). The main point of this REMP (ISBA/17/LTC/7) is to designate nine Areas of particular environmental interest (APEI) (according to ISBA/18/C/22) where exploration or mining activities should not be conducted. Four new APEIs were added in 2021 (according to ISBA/26/C/58). The REMP sets out the vision, goals and strategic objectives of environmental management in the region, including better understanding of the regional environmental conditions, promoting the development of seabed mineral resources in an environmentally responsible way, and maintaining regional biodiversity and ecosystem structure and function.

Therefore, the Contractor of this Project has considered the objectives in the above-mentioned EMMP before applying for the relevant Exploration Contract, and throughout the preparation and completion of the environmental management and REMP. The relevant tasks conducted to complete this EIS are conducive to the implementation of the above-mentioned objectives/measures, and will also provide data support for the determination and implementation of further cooperative actions in the future.

2.1.2 Other relevant international conventions and agreements

In addition to the provisions on seabed mining in Part XI, Part XII of the UNCLOS stipulates the general obligations for the protection and preservation of the marine environment and the requirements for measures to prevent, reduce and control the pollution of the marine environment, which are applicable to "pollution from installations and devices used in exploration or exploitation of the natural resources of the seabed and subsoil" (Article 194 (3)(c). Article 143 of the UNCLOS stipulates the promotion of marine scientific research and the publication and dissemination of research and analysis results in the Area. The research work and related data output of this Project are in line with these provisions.

Table 2.1-1 provides other international conventions and agreements related to maritime affairs, environment and maritime safety. Among which:

- **The conventions of the IMO on environmental protection and maritime**

safety are applicable to the operation activities of the vessels in this Project. Each vessel used for activities in the Area holds valid certificates issued in accordance with these international rules and standards (in accordance with standard clause 15.1 of the Contract in Annex IV of the exploration regulations), which meets the requirements of environmental rules and measures of relevant instruments.

Table 2.1-1 Relevant international conventions and agreements

Conventions and agreements	Notes to relevant contents
Maritime navigation	
International Convention for the Prevention of Pollution from Ships (MARPOL 73/78) and its annexes	The Convention stipulates the environmental rules and measures applicable to vessels, aiming at preventing vessels from polluting the marine environment by discharging harmful substances or waste liquid containing such substances.
International Convention for the Control and Management of Ships' Ballast Water and Sediments, 2004 (BWM Convention)	The BWM Convention puts forward specific technical requirements for the discharge control of ballast water and sediments from vessels, so as to prevent, reduce and finally eliminate the harm of ballast water discharge to the marine environment and public safety.
International Convention on the Control of Harmful Anti-fouling Systems on Ships (AFS), 2001	The AFS stipulates the control measures of the anti-fouling bottom system of vessels to reduce or eliminate the adverse effects of the anti-fouling bottom system on the marine environment and human health.
Convention on the Prevention of Marine Pollution by Dumping of Wastes and Other Matter, 1972, and its 1996 Protocol	The Convention and Protocol stipulate the marine dumping permit system, aiming at protecting the marine environment from dumping activities. Article 1(4)(3) provides that: The provisions of this Protocol do not include the disposal or storage of wastes or other substances directly produced by or related to the exploration, development and related at-sea processing of seabed mineral resources.
Maritime safety	
International Convention for the Safety of Life at Sea (SOLAS),	The Convention makes detailed provisions on ship construction, number of passengers and safety facilities, so as

1974	to improve the safety of life at sea.
Labour	
Maritime Labour Convention (MLC), 2006, International Labour Organization	The MLC specifies the minimum requirements for seafarers' employment, employment conditions, standards of living facilities on board, occupational health and safety protection, etc., and defines the rights of seafarers and the obligations of member states. The current requirements of the International Labour Organization, such as crew training and protection of labour rights and interests, are applicable to seafarers at sea.
Biodiversity	
Convention on Biological Diversity (CBD), 1992	Articles 3 and 4 of the CBD clarify that all countries have the responsibility to ensure that activities and processes under their jurisdiction or control do not cause damage to the environment in areas beyond national jurisdiction. Article 14 sets out the requirements for the notification obligation in the case of impact assessment and minimization of adverse effects, as well as in the case of serious danger or damage. The related objectives of marine biodiversity protection in the "Kunming-Montreal Global Biodiversity Framework" reached in 2022 and the description of EBSAs-related work under the framework of the Convention have global scientific reference significance. The Agreement under the United Nations Convention on the Law of the Sea on the Conservation and Sustainable Use of Marine Biological Diversity of Areas beyond National Jurisdiction (BBNJ Agreement) was adopted on 19 June 2023. This report has fully considered the important concerns of the BBNJ Agreement and will reasonable regard the conservation and use of biodiversity in the activity area based on the actual circumstances of the event.
Climate	
1992 United Nations Framework Convention on Climate Change (UNFCCC) and its Kyoto	The UNFCCC system provides measures to control greenhouse gas (GHG) emissions and provides guidelines and

Protocol and Paris Agreement	framework for solving global climate change problems.
Vienna Convention for the Protection of the Ozone Layer (1985) and Montreal Protocol (1987)	The Convention defines the principle of international cooperation in protecting the ozone layer, and the Protocol defines the framework of global international cooperation in protecting the ozone layer. It provides guidelines for global ozone-depleting substance management and ozone layer protection.

2.1.3 Other applicable standards, principles and policies

2.1.3.1 Other relevant policies and recommendations of the ISA

The ISA implements a data management strategy. The DeepData database launched by the ISA in 2019 is the global repository of all deep seabed related data submitted by contractors and collected in the Area during their exploration activities. The sharing of knowledge gained by contractors from marine scientific research in the Area is the content of this management tool. In this Project, the data types, collection frequency and analytical techniques collected according to the ISA related standards and recommendations follow the best available methods, and use internationally recognized or popular operating procedures and laboratories. The ISA's "Recommendations for the guidance of contractors on the content, format and structure of annual reports" (ISBA/21/LTC/15) provides guidance for contractors to submit reports and digital data.

The ISA supports the United Nations Decade of Ocean Science for Sustainable Development. The goal of "the Ocean Decade" is the core of the ISA's mission, that is, to promote and encourage marine scientific research in the Area and to promote the participation of developing countries in deep-sea exploration and research programs. The EIA-associated work of this Project is relevant to the strategic research priorities defined in the "Action plan of the International Seabed Authority in support of the United Nations Decade of Ocean Science for Sustainable Development" (ISBA/26/A/4), especially the scientific research work related to the environmental impact of this test-mining. The expected short-term and long-term outputs will help to enhance the scientific knowledge about the regional natural conditions and variations, and support the relevant short-term strategic plans or high-level action plans of the ISA.

2.1.3.2 Relevant standards, principles and codes of other institutions or industries

This EIS takes into account internationally recognized standards or industry best practice guidelines applicable to the EIA and management of marine mining (Table 2.1-2), and will fully consider the reference value of these standards, principles and codes in this Project and subsequent mining activities, and seek specific guidance in the absence of more detailed the ISA operation guidelines.

Table 2.1-2 Other relevant standards, principles and codes

Standards, principles and codes	Notes to relevant contents
Equator Principles	The application of social and environmental assessment and management related principles contained in the Equator Principles in this Project and subsequent activities will help to achieve the purpose of protecting society and environment.
The International Organization for Standardization (ISO)'s "Environmental management systems" (ISO 14001)	The Contractor will make a REMP for mining activities in the project area with reference to the principles of ISO 1400133, and submit it according to the time nodes and relevant requirements specified by the ISA.
The International Marine Minerals Society (IMMS)'s "Code for Environmental Management of Marine Mining" (2001, revised in 2011)	The Code provides a framework and benchmark for contractors to formulate and implement environmental programs and stakeholder participation, and provides complementary best practice guidance for studies and exploration activities related to this Project.
The International Finance Corporation (IFC)'s "Performance Standards on Environmental and Social Sustainability"	Provision of guidance on sustainability related standards for identifying risks and their impacts, managing environmental and social risks throughout the project cycle.

2.2 National legislation, procedures, standards and codes

2.2.1 National legislation and procedures related to seabed mining and environment

In February 2016, China promulgated the "Law of the People's Republic of China on the Exploration for and Exploitation of Resources in the Deep Seabed Area" (hereinafter referred to as the "Deep Seabed Law"). The purpose of this law is to "standardize the exploration and exploitation activities of resources in the deep seabed area, promote deep-sea scientific and technological research and resource survey, protect the marine environment, promote the sustainable utilization of resources in the deep seabed area and safeguard the common interests of mankind" (Article 1), which is applicable to "citizens, legal persons or other organizations in People's Republic of China that are engaged in resource exploration, exploitation and related environmental protection, scientific and technological research and resource survey activities in the deep seabed area" (Article 2). According to Article 5, the State Oceanic Administration (currently the Ministry of Natural Resources) is responsible for the supervision and management of exploration and exploitation of resources, as well as survey activities in the deep seabed area, and other relevant departments of the State Council are responsible for related management according to the functions prescribed by the State Council. The State Oceanic Administration of China, which is directly under the Ministry of Natural Resources of the People's Republic of China, is responsible for approving matters related to the exploration and exploitation of resources in deep seabed regions.

2.2.1.1 System for administration of exploration activities

The "Deep Seabed Law" defines exploration as: Use and testing of collecting systems and equipment, processing facilities and transportation systems and the conducting of studies of the environmental, technical, economic, commercial and other appropriate factors that must be taken into account in exploitation (Article 27

(1)).

This Project belongs to the exploration activities to which this law applies, and this law clearly stipulates the legal obligations directly related to the contractor's exploration operations:

—The obligations under the exploration and exploitation contracts shall be fulfilled, the personal safety of the personnel engaged in exploration and exploitation operations shall be guaranteed, and the marine environment shall be protected (Article 9).

—Cultural relics and laying in the exploration and exploitation areas shall be protected (Article 9).

—The exploration and exploitation operations shall also abide by the laws and administrative regulations of the People's Republic of China concerning safety in production and labor protection (Article 9).

—Emergency response plans shall be initiated and measures shall be taken when accidents with serious harm to the marine environment occur or may occur (Article 11).

Therefore, the Contractor will fulfill the Contract obligations in strict accordance with the law, abide by the applicable operation-related requirements mentioned above, under the supervision of the competent national authorities.

2.2.1.2 Environmental protection system

Chapter III of the "Deep Seabed Law" specifically stipulates the environmental obligations of prospectors to prevent, reduce and control pollution and other hazards caused by activities to the marine environment, and to take necessary measures to protect and preserve rare or fragile ecosystems. The following specific requirements are directly related:

—In accordance with the requirements of the Contract, survey and study the marine conditions in the exploration and exploitation areas, determine the environment baselines, and assess the possible impact of the activities on the marine

environment;

—Formulate and implement an EMP, monitor the impact of activities on the marine environment in the project area, ensure the normal operation of monitoring equipment, and keep original monitoring records so as to provide a basis for inspection.

The above-mentioned requirements are consistent with the requirements of the ISA related rules, regulations and procedures, and the activities conducted and planned in this Project will strictly comply with the relevant regulations.

2.2.1.3 Scientific research and data management

The Chapter IV of the "Deep Seabed Law" makes special provisions on scientific and technology Research, resource investigation and capacity building, and clarifies the relevant contents of strengthening the collection and sharing of deep-sea scientific and technological research data, which is related to the relevant activities of this Project. Among them, Article 18 provides requirements for the submission, registration, storage and utilization of relevant data and physical samples obtained by the Contractor through exploration and exploitation activities. In 2017, the former State Oceanic Administration issued normative documents—"Interim Measures for Administration of Samples in Exploration and Exploitation of Resources in Deep Seabed Areas" and "Interim Measures for Administration of Materials in Exploration and Exploitation of Resources in Deep Seabed Areas" (in the process of studying and revising to meet the variations required by the new ISA regulations), which provided specific guidance for the reporting and management of samples and data obtained from related activities of this Project. The international exchange of deep-sea data obtained from this Project will be conducted under the unified management of the national competent authorities and in accordance with the relevant requirements and procedures of the ISA.

2.2.1.4 Relevant national standards and codes

In addition to complying with the obligations and management procedures of the

relevant laws and supporting normative documents of the "Deep Seabed Law", a series of relevant standards and codes will also be applied or considered during the implementation of this Project.

Table 2.2-1 below lists the national standards and codes that provide technical methods and work codes for this Project's activities.

Table 2.2-1Relevant standards and codes

Standards and guidelines	Notes to relevant contents
"Specification for oceanic polymetallic nodules exploration" (GB/T 35571-2017)	Provision of normative guidance for resource exploration.
"Classification code of ocean sample management" (GB/T 42330-2023)	Provision of reference for the information and standardized management standards of the obtained ocean samples.
"Terminology for oceanic resources survey" (GB/T 34908-2017)	Provision of normative guidance for the standard terminology of resource survey.
"The technology specification for the pre-treatment of deep-sea microorganism samples" (GB/T 30744-2014)	Provision of technical guidance for deep-sea microbial sample treatment.
"Chemical analysis methods for marine polymetallic nodules" (GB/T 20259-2006)	Provision of guidelines for nodule-related chemical analysis methods.
National standard "Specifications for oceanographic survey" Parts 1-11 (GB/T 12763-2007)	Provision of guidelines for on marine hydrology, meteorology, chemistry, sound and light, ecology, geology and geophysics, biology, seabed topography and geomorphology, marine engineering geological survey, and survey data exchange.
"Code of practice for international seabed area and high seas environmental survey—Part 1: General" (GB/T 42629.1-2023)	Provision of methods and guidelines for environmental survey and assessment in the high seas and international seabed areas
"Code of practice for international seabed area and high seas environmental survey—Part 2: Marine chemical survey" (GB/T 42629.2-2023)	Provision of methods and guidelines for chemical oceanography survey and assessment in the high seas and

	international seabed areas
"Code of practice for international seabed area and high seas environmental survey—Part 3: Marine biological survey" (GB/T 42629.3-2023)	Provision of methods and guidelines for the survey and assessment of marine organisms in the high seas and International Seabed Aeas
"Code of practice for international seabed area and high seas environmental survey—Part 4: Physical features survey of marine sediments" (GB/T 42629.4-2023)	Provision of methods and guidelines for the survey and assessment of marine sediment physical features

2.2.2 Other relevant national legislation, policies and regulations

In addition to the above-mentioned national laws, procedures and technical codes related to seabed mining activities and their environmental protection, other national laws and policies related to maritime navigation, pollution prevention and control of vessels and operational activities, marine traffic safety, safety in production and labor protection also provide the Contractor with normative guidance on related work, and the relevant legal provisions mainly observed or referred to include:

The "Marine Environmental Protection Law of the People's Republic of China" (2023 Revision, 2024 in effect) is the "basic law" on the protection of marine ecology and environment, which is applicable to the sea areas under the jurisdiction of China. Although the "Marine Environmental Protection Law of the People's Republic of China" is applicable to the waters under the jurisdiction of China, it is the basic law of marine environmental protection in China after all, and the concepts, systems and methods of marine protected areas can provide reference for Minmetals in carrying out related work in international waters. Article 9 stipulates that all entities and individuals have the obligation to protect the marine environment. Article 124 provides that: if the international treaties related to marine environmental protection concluded or acceded to by People's Republic of China have different provisions from this Law, the provisions of the international treaties shall prevail, except the provisions on which the People's Republic of China has made reservation. Therefore,

the Contractor of this Project will follow the relevant legal guidance of this Law and the provisions of environment-associated international treaties during the implementation of the related activities involved in this EIS, so as to ensure that the implementation of related activities in the high seas and the Area will not cause pollution or potential risks to the sea areas under national jurisdiction, and will be supervised by relevant state departments and institutions.

The "Regulation on the Prevention and Control of Vessel-induced Pollution to the Marine Environment" (2018, Revision) is a regulation formulated according to the Marine Environmental Protection Law, and Article 10 thereof stipulates: "The structure, equipment and instruments of a vessel shall conform to the relevant technical requirements of the state for preventing and controlling the vessel-induced pollution to the marine environment and the requirements of the international treaties concluded or acceded to by the People's Republic of China. The vessels shall, in accordance with the laws, administrative regulations, provisions of the transport administrative department under the State Council and the requirements of the international treaties concluded or acceded to by the People's Republic of China, obtain and carry on board corresponding certificates and documents relating to the prevention and control of vessel-induced pollution to the marine environment." Article 73 provides that: If the international treaties concluded or acceded to by the People's Republic of China have provided for the prevention and control of the pollution caused by vessels and the relevant operations to the marine environment, such provisions shall prevail, except the provisions on which the People's Republic of China has made reservation." Therefore, the vessels and related equipment used in the exploration and follow-up activities of this Project meet the relevant national qualification requirements, and we will conduct relevant operation activities in a manner consistent with the above provisions and relevant international treaties as appropriate as possible.

The "Maritime Traffic Safety Law of the People's Republic of China" (Revised

in 2021) is applicable to navigation, berthing, operation and other activities related to marine traffic safety in the waters under the jurisdiction of China. This law stipulates the requirements of relevant national laws, administrative regulations, standards and technical specifications that China-registered vessels and other important marine equipment, components and materials must abide by, including ship inspection, safety management, maritime labor qualification licensing, early warning of overseas emergencies and emergency response. As stipulated in Article 86, "If a vessel of Chinese nationality has a marine traffic accident outside the sea areas under the jurisdiction of the People's Republic of China, the accident shall be promptly reported to the maritime administrative agency and investigated." Therefore, the qualification of operating vessels, maritime labor certificate, maritime safety management and guarantee in this Project "conform to relevant national laws and regulations, mandatory standards and applicable international treaties."

In addition, China has issued a series of other regulations, rules, and standards to prevent and control pollution caused by maritime activities, including the "Administrative Regulation on the Prevention and Treatment of the Pollution and Damage to the Marine Environment by Marine Engineering Construction Projects", "China Maritime Oil Spill Emergency Plan", "Regulations of the People's Republic of China Governing Survey of Ships and Offshore Installations", "Implementation Measures for the Regulations on the Management of Marine Dumping of the People's Republic of China", and "Technical specification for assessment of sea water, marine sediment and marine biological quality".

2.3 Stakeholder consultation

This report is released for public comment on 2nd April and 11th April, 2024 on the official website of Minmetals and ISA, respectively. Deadline for comments was by the end of May, 2024.

Figure 2.4-1 Screenshot of EIS report for stakeholder consultation in the website

A total of 8 stakeholders' comments on this EIS have been received as of the end of the stakeholder consultation period (see Chapter 12). The current version of the EIS has been updated in response to public comments provided as part of the stakeholder consultation process. The modifications mainly include biological baselines (microbial diversity, more detailed biological classification and identification results, annual variation characteristics of benthic communities, comparison results of IRZ and PRZ, statistical analysis of spatial differences in megafauna communities, heavy metal concentrations in organisms, etc), description of plume modeling method, and results of heavy metal toxicology tests. We appreciate all stakeholders' feedback, which greatly improved this report.

2.4 Domestic procedures for this activities

This EIS is one of the materials that should be submitted to the national competent authorities for review, as required by the relevant domestic procedures for the management of exploration and Deep Seabed Law in the sponsoring State mentioned in 2.1.2.1. Therefore, Minmetals has publicly released EIS, EMMP and other materials in accordance with relevant regulations on April 2, 2024, and start the stakeholder consultation process. Minmetals modified this report according to the consultation opinions, and then submitted it to the China Ocean Affairs Administration (COAA). COAA commissioned a third party (Marine Consultation Center of the Ministry of Natural Resources) to conduct an EIS review on August 30, 2024, and provided suggestions for modification/ supplementation. Minmetals further revised this report according to the review opinions, and submitted the final report to COAA for filing.

3 Description of Proposed Exploitation Activities

3.1 Definition of project area

3.1.1 Location

This collector vehicle test will be conducted in the Block A-5, which has relatively flat topography, high nodule abundance and strong continuity. It is currently the block with the highest degree of resource and environmental surveys. The western basin of the Block A-5 is a PWA (yellow polygon in Figure 3.1-1, with an area of approximately 4,590 km^2), and its resource exploration grid reaches 7 km × 7 km (also called general exploration area, or GEA), in which, an exploration grid of 3.5 km × 3.5 km is adopted (called DEA, with an area of approximately 500 km^2). Considering the topography, nodule abundance and environmental survey, the DEA is preliminarily regarded as TMA (Figure 3.1-1).

The IRZ is delineated in the TMA (Figure 3.1-1), with an area of approximately 30 km^2 (with a range of 6 km × 5 km), and one CTA (approximately 0.6 km^2, 1 km × 0.6 km, Figure 3.1-2) has been preliminary delineated in it. See Table 3.1-1 for the information of topography slope, nodule abundance and geotechnical properties of sediments. The PRZ is delineated at 15 km upstream of the IRZ and has an area (approximately 20 km^2) and geological properties similar to those of the IRZ.

According to the international test-mining results, the boundary of 0.1 mm sediment thickness caused by sediment plume is about 5 km. According to simulation results in this EIS (Annex I), the boundary of 0.1 mm sediment thickness caused by sediment plume does not exceed 1 km^2. Therefore, the distance of 15 km between PRZ and IRZ set in this Project can ensure that the collector vehicle test will not impact the sediment environment of PRZ. Based on the study of environment baseline characteristics, we believe that PRZ and IRZ meet the ISA's requirements for environmental similarity.

In addition, the ESRZ has been delineated in the eastern part of the Block A-5,

with an area of about 400 km^2. This area is far away from the PWA in the Block A-5, and will not be impacted by subsequent detailed exploration activities, test-mining activities or future commercial exploitation activities. This means that the deep-sea environment and biodiversity will be preserved in a more effectively manner.

See Table 3.1-2 for the corner coordinates of the PWA, IRZ, PRZ and ESRZ in the Contract Area.

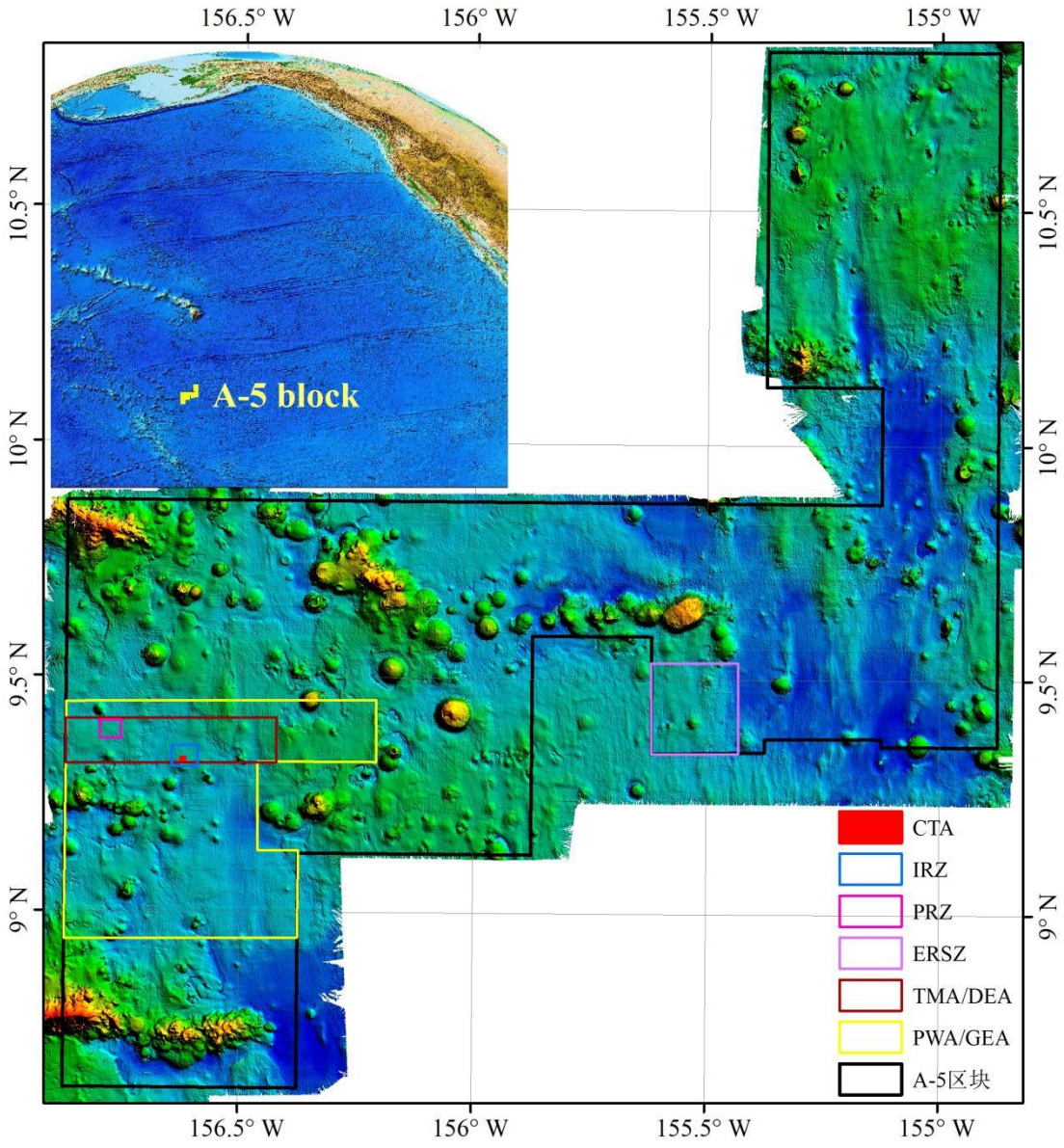

Figure 3.1-1 Locations of the PWA, TMA, IRZ, PRZ and ESRZ in the Block A-5 of the Contract Area

(PWA=primary working area, TMA=target mining area, IRZ=impact reference zone, PRZ=preservation reference zone, CTA=collector test area)

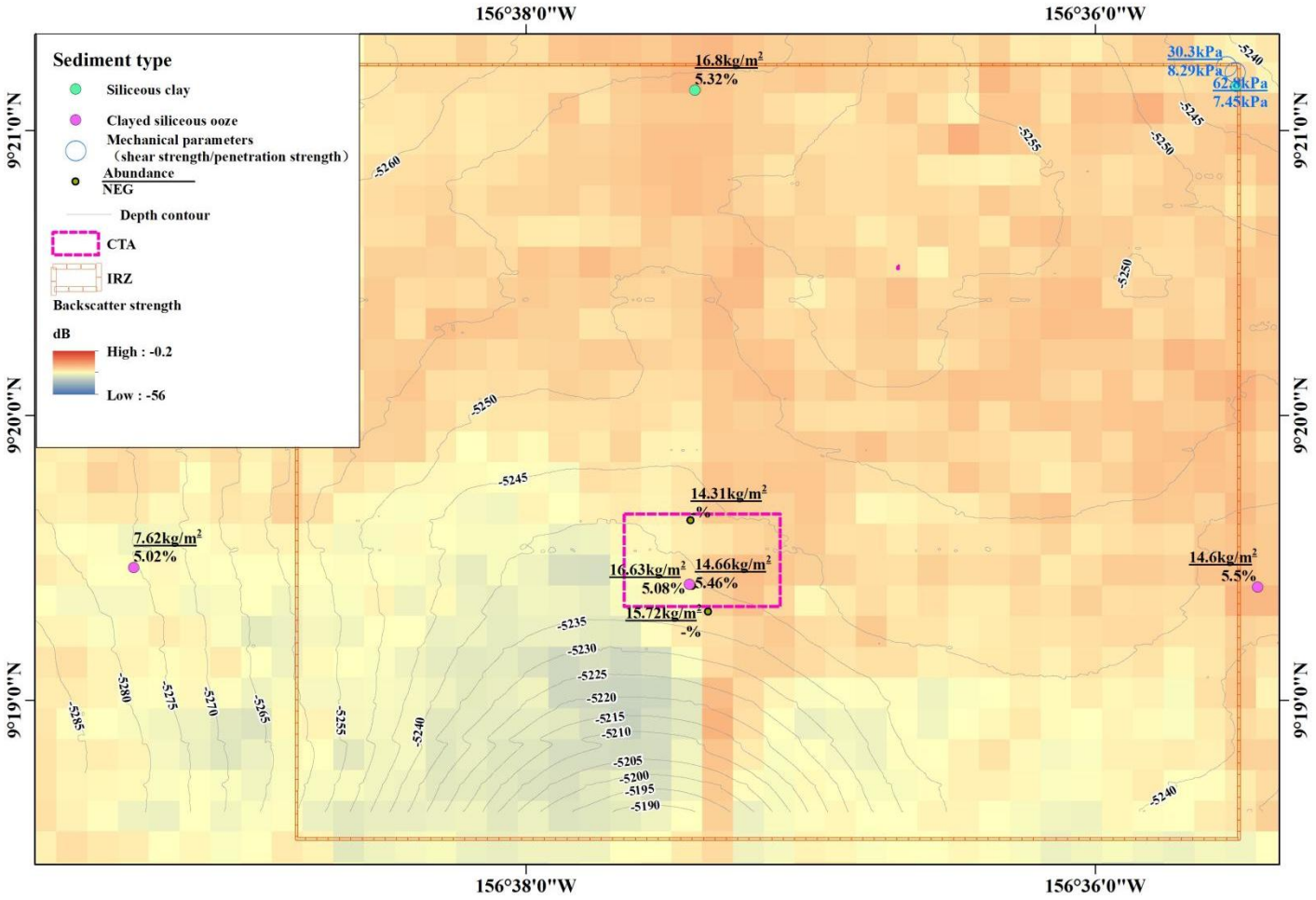

Figure 3.1-2 Location of the CTA in the Block A-5

Table 3.1-1Characteristics of the CTA's parameters

Collector test area (CTA)	
Area (km^2)	0.6
Length (km)	1.0 (East-West)
Width (km)	0.6 (North-South)
Number of stations	3
Abundance (kg/m^2)	15.20
NEG(%)	5.26
Water depth (m)	-5247~-5237
Slope (°)	0.40~1.34
Backscatter strength (dB)	-25.95~-22.99
Sediment type	Clay siliceous ooze
Clay (<4 μm) content (%)	36.16

Table 3.1-2 Corner coordinates of the PWA, IRZ, PRZ and ESRZ in the Contract Area

Corner	Longitude (°)	Latitude (°)	Region name
Point 1	-156.42200	9.31870	TMA/ DEA
Point 2	-156.87300	9.31407	
Point 3	-156.87399	9.40904	
Point 4	-156.42300	9.41371	
Point 1	-156.20900	9.32000	PWA/ GEA
Point 2	-156.46300	9.32000	
Point 3	-156.46100	9.13100	
Point 4	-156.37399	9.13200	
Point 5	-156.37500	8.94500	
Point 6	-156.87500	8.94000	
Point 7	-156.87399	9.44500	
Point 8	-156.20900	9.45200	
Point 1	-156.59158	9.30857	IRZ
Point 2	-156.64675	9.30857	
Point 3	-156.64675	9.35385	
Point 4	-156.59158	9.35385	
Point 1	-156.75600	9.40535	PRZ
Point 2	-156.75600	9.36756	
Point 3	-156.80177	9.36756	
Point 4	-156.80177	9.40535	
Point 1	-155.61752	9.53553	ESRZ
Point 2	-155.43893	9.53669	

Point 3	-155.43774	9.34547	
Point 4	-155.61623	9.34433	

3.1.2 Related activities

This test does not involve auxiliary activities and required infrastructure outside the CTA.

3.2 Mineral resources

In the PWA of the Block A-5 of the Contract Area, an exploration grid of 7 km × 7 km is adopted, meeting the requirement for the estimation of indicated resources. An in the TMA of the PWA, an exploration grid of 3.5 km × 3.5 km is adopted, meeting the requirement for the estimation of measured resources.

The ore bodies are delineated by indexes such as abundance ≥5 kg/m^2, NEG ≥4.46 % and slope ≤5°. Resources in the TMA of the Block A-5 are estimated by polygon method (Thiessen Polygon block formed on the basis of survey station is used as the resource estimation unit). Results show that the Block A-5 has approximately 500 km^2 of measured resources and approximately 5.14 million metric tons of dry nodules. See Table 3.2-1 for the total metal amount of Cu, Co, Ni and NEG. This area is suitable for the collector vehicle test.

Table 3.2-1 Estimates for measured resources in the TMA of the Block A-5

Ore body area (km^2)	Wet nodules (10 kt)	Dry nodules (10 kt)	Mn resources (10 kt)	Cu resources (10 kt)	Co resources (10 kt)	Ni resources (10 kt)	NEG resources (10 kt)
505.76	734.02	513.82	128.15	3.71	1.46	5.02	27.09

NEG=0.13×Mn%+0.42×Cu%+2.64×Co%+Ni%

3.3 Project composition

3.3.1 Project scale

This test is scheduled in July-October of 2025. The PWA of the collector vehicle on the seabed is 0.6 km^2 (1,000 m long, 600 m wide) (Figure 3.3-6). The plan for collector vehicle test involves two separate underwater tests. The disturbed area during the first underwater operation is 24,200 m^2. The disturbed area by traveling and nodule-collecting activities during the second underwater operation is 75,800 m^2. The total disturbance area is 0.1 km^2. In the whole test, the total wet weight of nodules to be collected in the operation is estimated to be 13 kg/m^2 ×0.1 km^2 =1,300 t.

Based on the data in Section 3.3 of this EIS, we estimated the impact of this test on the physicochemical and biological environments in the deep sea, and assessed its potential environmental impact in Chapters 7 and 8. The maximum impact range of plume caused by this test-mining is 2.1 km horizontally and 124 m vertically. The plume disappears within 1-1.5 days after the test-mining. The range of sediment plume redeposition with thickness greater than 0.1 mm in this test is no more than 1 km^2.

3.3.2 Test system and programme

（1） Systematic composition

The seabed collector system to be tested consists of a collector vehicle, an acoustic positioning system, an umbilical cable and a surface support vessel (SSV). The collector vehicle collects nodules from the seabed; the acoustic positioning system provides positioning support for the collector vehicle; the umbilical cable provides power supply and communication with the collector vehicle; the SSV is a surface operation platform responsible for the monitoring and operation of at-sea collector vehicle test. (Figure 3.3-1).

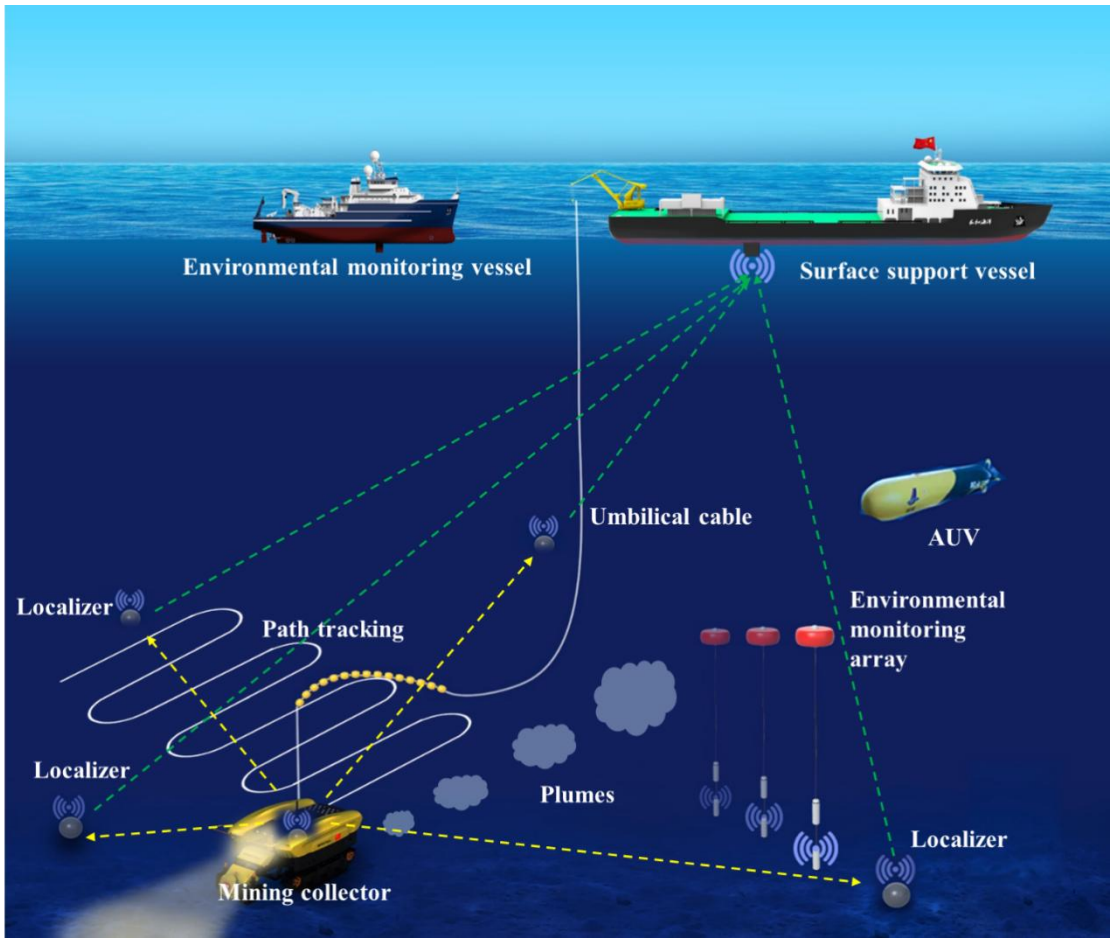

Figure 3.3-1 Systematic composition of this collector vehicle test

1） collector vehicle

The collector vehicle is the core equipment of the underwater operation of the seabed collector system. Its main function is to collect nodules on the seabed and provide disturbance source for environmental impact monitoring as an operating mechanism. The collector vehicle consists of traveling mechanism, collection mechanism, main structure, inspection and monitoring mechanism, underwater control system and hydraulic system (Figure 3.3-2). See relevant technical parameters in Table 3.3-1. All key parts of the collector vehicle have been fully tested and verified in the laboratory. The collection mechanism, traveling mechanism, hydraulic system, control system and main structure passed the laboratory test and lake test (135 m water depth), as well as the 500 m water depth at-sea test in 2018 and 1,300 m water depth at-sea test in 2021. These tests have fully verified the reliability of related

key technologies and equipment. The operation function of the inspection and monitoring mechanism is based on the current ROV technology. Related technologies can fully meet the needs of this Project.

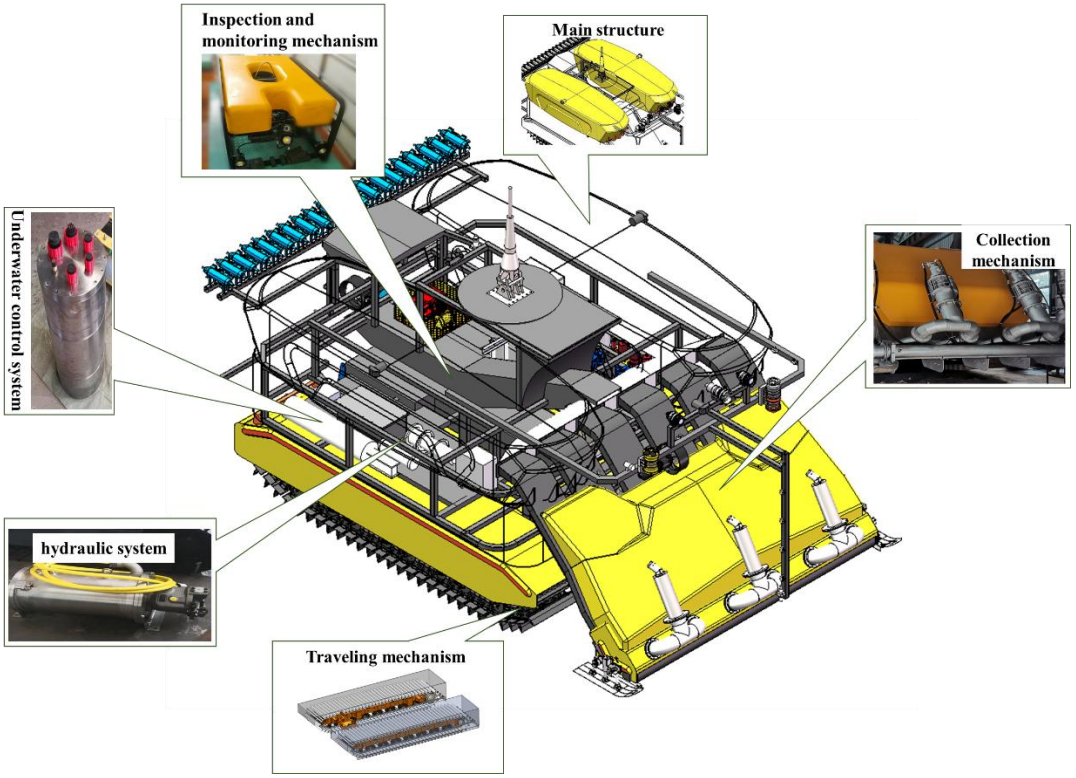

Figure 3.3-2 Overall structural design and systematic composition of the collector vehicle

During mining operation, the traveling mechanism (crawler belts) provides a stable moving platform for the whole collector vehicle and carries out the operation according to the predetermined path. The collection mechanism will put the collected nodules in the bin at the rear of the vehicle body after desliming and crushing (Figure 3.3-3).

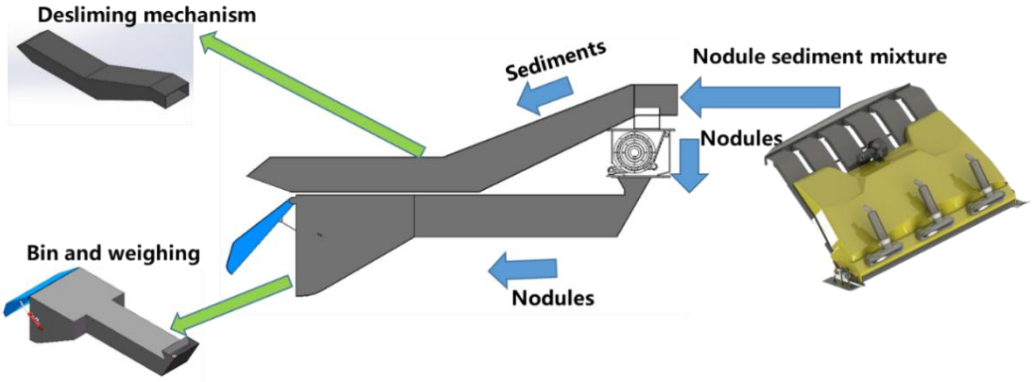

Figure 3.3-3 Basic design and collection process of nodule-collecting system

Table 3.3-1 Relevant technical parameters of the collector vehicle

S.N.	Item	Parameters	Remarks
1	Adaptive water depth	6,000 m	Design water depth
2	Production capacity	125 t/h	Abundance of 12 kg/m^2
3	Power	500 kW	
4	Traveling speed	1 m/s	Maximum
5	collection depth	5 m	
6	Collection depth	50 mm-120 mm	
7	Overall dimensions	9 m×5 m×4 m	Length × width × height
8	Weight in air	40 t	
9	Weight in water	20 t	

2） Acoustic positioning system

During the at-sea test, the long baseline acoustic positioning system will be used to provide position information for the collector vehicle. Before the collector vehicle is launched, the long baseline beacon will be deployed near the underwater operation area, and the collector vehicle will be launched after the deployment.

3） Umbilical cable

The umbilical cable is made of nonmetallic armored cable, which can bear the weight load of the collector vehicle during the launch and recovery. After the collector vehicle is laid on the seabed, the umbilical cable provides power and communication for the collector vehicle through power cables and optical fibers inside it.

4） SSV

The SSV acts like an operation platform to provide control, energy and logistics for the entire at-sea test.

This at-sea test plans to use R/V *ZHANG JIAN* (Figure 3.3-4) as the SSV for the collector vehicle. R/V *ZHANG JIAN* is a multi-disciplinary, multi-functional and multi-technique modern marine scientific comprehensive research vessel jointly built by Taihe Ocean Science and Technology Group and Shanghai Rainbowfish Ocean Technology Co., Ltd. It meets the requirements for this collector vehicle test.

Figure 3.3-4 R/V *ZHANG JIAN* multi-purpose survey vessel

The specific parameters of R/V *ZHANG JIAN* are shown in Table 3.3-2:

Table 3.3-2 Parameters of R/V *ZHANG JIAN*

Indicator	Parameters
Vessel length	97.55 m
Vessel width	17.80 m
Moulded depth	8.40 m
Draft	5.70 m
Power positioning	DP-1
Tonnage	4,800 t
Design maximum speed	14 kn
Design economic speed	12 kn
Design wind resistance	Magnitude 10
Travel range	15,000 nautical miles
Vessel's complement	60 people (20 crew members, 40 survey personnel)
Region	Unlimited sailing zone
Self-sufficient capability	More than 60 days

According to the plan, R/V *DAYANG HAO* (Figure 3.3-5) or another research vessel will be used as the EMV during this test. R/V *DAYANG HAO* will be used as the SSV for the launch and recovery of environmental survey equipment during this test.

Figure 3.3-5 R/V *DAYANG HAO*

The specific parameters of R/V *DAYANG HAO* are shown in Table 3.3-3:

Table 3.3-3 Parameters of R/V *DAYANG HAO*

Indicator	Parameters
Total length	98 m
Molded width	17 m
Design draft	5.4 m
Design displacement	4,780 t
Vessel's complement	60 people (including 22 crew members)
Travel range	14,000 nautical miles/12 kn
Self-sufficient capability	60 days
Maximum speed	16 kn
Propulsion mode	All electric propulsion
Noise criteria	As per DNV Silent-R
Total laboratory area	>360 m^2
Rear deck working area	>400 m^2
Class notation	CSA SPS/Research ShipPSPC, Ice Class B3, COMF (NOISE) 3, COMF (VIB) 3 CSM AUT-0, OMBO, DP-1, Loading Computer (I, D), Lifting Appliance, Clean, FTP, BWMP, BWMS, GPR

（2） At-sea test process

The entire at-sea test will be divided into two parts, with the first underwater operation lasting 70 h and the second underwater operation lasting 60 h. The first underwater operation mainly tests the basic functions and performance of the collector vehicle. The second underwater operation mainly tests its collecting and traveling capacities, during which environmental disturbance experiments also will be carried out to provide data for environmental impact studies. The second underwater operation path is planned as in Figure 3.3-6. Environmental monitoring will comprehensively cover the whole cycle of the entire test.

1） The first underwater testing of the collector vehicle

The first underwater testing of the collector vehicle mainly includes static test after equipment landing, inspection and monitoring test, temperature rise and noise test, straight-line traveling test, turning radius test, collecting performance test under different parameters, continuous nodule-collecting test, sampling operation, equipment status check before recovery, etc. (see Table 3.3-4 for details).

Table 3.3-4 Contents of first underwater testing of the collector vehicle

S.N.	Project content	Duration (min)		Nodules in the bin (kg)	Traveling distance (m)
		Single-time	Cumulative		
a	Static test after equipment landing	240	240	-	-
b	Inspection and monitoring test	300	300	-	-
c	Temperature rise and noise test	300	300	-	-
d	Straight-line traveling test	70	700	-	1,000
e	Turning radius test	40	800	-	1,000
f	Collecting performance test under different parameters	30	900	0	300
g	Continuous nodule-collecting operation test	30	300	8100	2540
h	Sampling operation	480	480	-	0
i	Equipment status check before recovery	180	180	-	-
	Total	-	4200	8100	4840

a. Static test after equipment landing (240 min)

Turn on all monitoring components (acoustic positioning, water depth sensor, turbidimeter, ADCP, camera, lamp, pressure sensor, flow sensor, water leakage sensor, voltage, current and temperature sensor, etc.) after the equipment landing.

Obtain and record the position, depth, turbidity, current, image, pressure, flow, water leakage, voltage, current, temperature and other information after landing. Record once every 5 min for a total of 240 min.

b. Inspection and monitoring test (300 min)

After completing the static test of the equipment, check the condition of the inspection and monitoring mechanism, operate it to detect the collector vehicle body and surrounding environment. For collector vehicle subsidence, plume dispersal, etc., test once every 20 min for a total of 300 min.

c. Temperature rise and noise test (300 min)

Start the hydraulic pump station and load it, and record the information such as system temperature and noise. Record once every 10 min for a total of 300 min.

d. Straight-line traveling test (700 min)

Input parameters for different straight-line traveling to test the straight-line traveling performance of the collector vehicle. During the test, modify and optimize the input parameters, so as to obtain the relationship between input and output parameters that can travel in a straight line in deep-sea environment.

The traveling speeds are 0.1 m/s, 0.2 m/s, 0.3 m/s, 0.4 m/s, 0.5 m/s, 0.6 m/s, 0.7 m/s, 0.8 m/s, 0.9 m/s and 1.0 m/s, totaling 10 groups of data. The test distance is 20 m for each group of data. Each group is tested five times, with an average estimated duration of 10 min. After each traveling, the inspection and monitoring mechanism will be used for operation test for 20 min. It is estimated that the cumulative traveling distance is 1,000 m and the total duration is 700 min.

e. Turning radius test (800 min)

Give different traveling parameters for two crawler belts to test the turning radiuses under different parameters. During the test, let the collector vehicle drive in a straight line for 20 m before turning, then continue traveling in a straight line for 20 m after turning, and measure the turning radius. It is estimated that there will be 20 tests, each lasting 20 min. After each test, the inspection and monitoring mechanism will be used to detect the operation situation. Each operation lasts 20 min. The total traveling distance will be 1,000 m and the total test duration will be 800 min.

f. Collecting performance test under different parameters (900 min)

The collecting capacity under different collection parameters will be tested at different traveling speeds. The traveling speeds are 0.1 m/s, 0.2 m/s, 0.3 m/s, 0.4 m/s, 0.5 m/s, 0.6 m/s, 0.7 m/s, 0.8 m/s, 0.9 m/s, 1.0 m/s.

There will be three groups of collection parameters. After the test, the weight of collected nodules will first be measured by the weighing sensor, and then unloaded. After that the area will be inspected by the inspection and monitoring mechanism. The collected nodules will total approximately 16,200 kg.

It is estimated that 30 groups of data will be tested, with a distance of 10 m and duration of 10 min for a single collection test, 20 min for each single inspection and monitoring test. The total traveling distance will be 300 m and the total test duration will be 900 min.

g. Continuous nodule-collecting operation test (300 min)

After obtaining the optimal traveling and nodule-collecting activities parameters, the state of the whole system will be tested and the continuous nodule-collecting operation parameters will be set. The straight-line traveling distance for continuous operation is 150 m. After the straight-line traveling is completed, the collector vehicle will turn 180 degrees to the adjacent path, and the collected nodules will be unloaded on the turning path during the turning process. Then, the next straight-line operation will be conducted. During the test, collecting operations will be conducted in 10 straight-line segments. The nodules collected in the last straight-line segment, totaling 8,100 kg, will be left in the bin.

Set the turning radius at the depth of 15 m, the turning speed at 0.3 m/s and the turning path at approximately 104 m, then the turning duration is 347 s. The traveling speed in the straight-line segment is 0.6 m/s, so the traveling duration is 250 s. It is estimated that it will take 597 s (approximately 10 min), to complete traveling a straight-line segment and turning. After completing a straight-line segment and turning operation, the results will be inspected by the inspection and monitoring mechanism. Each inspection will take 20 min. It will take 300 min to complete all

continuous nodule-collecting operation tests.

h. Sampling operation (480 min)

Inspection and observation, fixed-point sampling, etc. in the post-mining area are expected to take 480 min in total.

i. Equipment status check before recovery (180 min)

After all operations are completed, the equipment status inspection will be conducted, which is expected to last for 180 min.

j. Aggregate parameters of underwater operation

Traveling distance: 1,000+1,000+300+10×(150+104)=4,840 m.

Traveling area: 4,840×5=24,200 m^2.

2） Second underwater testing of the collector vehicle

The second underwater testing of the collector vehicle mainly includes static test after equipment landing, inspection and monitoring test, temperature rise and noise test, regional collecting and disturbing operations, sampling operation, equipment status check before recovery, etc. See Table 3.3-5 for details.

Table 3.3-5 Contents of second underwater testing of the collector vehicle

S.N.	Project content	Duration (min)		Nodules in the bin (kg)	Traveling distance (m)
		Single-time	Cumulative		
a	Static test after equipment landing	120	120	-	-
b	Inspection and monitoring test	120	120	-	-
c	Temperature rise and noise test	120	120	-	-
d	Regional collecting and disturbing operations	2203	2203	8100	15160
	Path spacing: 0 m	842	842	-	5080

	Path spacing: 15 m	454	454	-	3276
	Path spacing: 25 m	473	473	-	3960
	Path spacing: 50 m	434	434	8100	2844
e	Sampling operation	720	720	-	-
f	Equipment status check before recovery	300	300	-	-
	Total	-	3583	8100	15160

a. Static test after equipment landing (120 min)

Turn on all monitoring components (acoustic positioning, water depth sensor, turbidimeter, ADCP, camera, lamp, pressure sensor, flow sensor, water leakage sensor, voltage, current and temperature sensor, etc.) after the equipment landing.

Obtain and record the position, depth, turbidity, current, image, pressure, flow, water leakage, voltage, current, temperature and other information after landing. Record once every 5 min for a total of 120 min.

b. Inspection and monitoring test (120 min)

After completing the static test of the equipment, check the condition of the inspection and monitoring mechanism, operate it to detect the collector vehicle body and surrounding environment. The collector vehicle subsidence and plume dispersal will be tested once every 20 min for a total of 120 min.

c. Temperature rise and noise test (120 min)

Start the hydraulic pump station and load it, and record the information such as system temperature and noise. Record once every 10 min for a total of 120 min.

d. Regional collecting and disturbing operations (2,203 min)

We will conduct continuous nodule-collecting and disturbing operations in the CTA. The straight-line traveling distance for continuous operation is 150 m. After the straight-line traveling is completed, the collector vehicle will turn 180 degrees to the adjacent path, and the collected nodules are unloaded on the turning path during the

turning process, and then the next straight-line operation will be conducted. During the operation, different path spacings and traveling speeds will be set to test the mining technologies and methods.

The collecting path spacing will be 0 m, 15 m, 25 m and 50 m respectively, and the traveling speeds will be 0.2 m/s, 0.4 m/s, 0.6 m/s, 0.8 m/s and 1.0 m/s respectively.

While traveling and nodule-collecting activities at different path spacing, the collector vehicle will travel at 0.2 m/s in the 1st-2nd straight-line segments, 0.4 m/s in the 3rd-4th straight-line segments, 0.6 m/s in the 5th-6th straight-line segments, 0.8 m/s in the 7th-8th straight-line segments, and 1.0 m/s in the 9th-10th straight-line segments. The turning radius is 15 m with the spacing of 0 m, 10 m with the spacing of 15 m, 15 m with the spacing of 25 m and 27.5 m with the spacing of 50 m, respectively.

- **Path spacing: 0 m (842 min)**

The turning path length is 104 m; the straight path is 150 m; and there are 20 straight-line segments. The distance between two 10 straight-line segments is 50 m.

With the traveling speed of 0.2 m/s, the traveling duration is: 2×(104+150)/0.2=2,540 s

With the traveling speed of 0.4 m/s, and the turning speed of 0.3 m/s, the traveling duration is: 2×104/0.3+2×150/0.4 =1,444 s

With the traveling speed of 0.6 m/s, and the turning speed of 0.3 m/s, the traveling duration is: 2×104/0.3+2×150/0.6 =1,194 s

With the traveling speed of 0.8 m/s, and the turning speed of 0.3 m/s, the traveling duration is: 2×104/0.3+2×150/0.8 =1,068 s

With the traveling speed of 1.0 m/s, and the turning speed of 0.3 m/s, the traveling duration is: 2×(104+150)/1.0=994s

Inspection and monitoring check: 60 min

Cumulative duration: 2×((2,540+1,444+1,194+1,068+994)/60+5×60)=842 min

Cumulative traveling distance: 20×150+20×104=5,080 m

- **Path spacing: 15 m (454 min)**

The turning path length is 32 m; the straight path is 150 m; and there are 18 straight-line segments.

With the traveling speed of 0.2 m/s in five straight-line segments, the traveling duration is: 5×(32+150)/0.2=4,550 s

With the traveling speed of 0.4 m/s in four straight-line segments, and the turning speed of 0.3 m/s, the traveling duration is: 4×32/0.3+ 4×150/0.4=1,927 s

With the traveling speed of 0.6 m/s in three straight-line segments, and the turning speed of 0.3 m/s, the traveling duration is: 3×32/0.3+ 3×150/0.6=1,070 s

With the traveling speed of 0.8 m/s in three straight-line segments, and the turning speed of 0.3 m/s, the traveling duration is: 3×32/0.3+ 3×150/0.8=883 s

With the traveling speed of 1.0 m/s in three straight-line segments, and the turning speed of 0.3 m/s, the traveling duration is: 3×32/0.3+ 3×150/1=770 s

Inspection and monitoring check: 60 min

Cumulative duration: (4,550+1,927+1,070+883+770)/60+5×60=454 min.

Cumulative traveling distance: 18×150+18×32=3,276 m

- **Path spacing: 25 m (473 min)**

The turning path length is 48 m; the straight path is 150 m; and there are 20 straight-line segments.

With the traveling speed of 0.2 m/s in four straight-line segments, the traveling duration is: 4×(48+150)/0.2=3,960 s

With the traveling speed of 0.4 m/s in four straight-line segments, and the turning speed of 0.3 m/s, the traveling duration is: 4×48/0.3+ 4×150/0.4=2,140 s

With the traveling speed of 0.6 m/s in four straight-line segments, and the turning speed of 0.3 m/s, the traveling duration is: 4×48/0.3+ 4×150/0.6=1,640 s

With the traveling speed of 0.8 m/s in four straight-line segments, and the turning speed of 0.3 m/s, the traveling duration is: 4×48/0.3+ 4×150/0.8=1,390 s

With the traveling speed of 1.0 m/s in four straight-line segments, and the turning speed of 0.3 m/s, the traveling duration is: 4×48/0.3+ 4×150/1=1,240 s

Inspection and monitoring check: 60 min

Cumulative duration: (3,960+2,140+1,640+1,390+1240)/60+5×60=473 min

Cumulative traveling distance: 20×(150+48)=3,960 m

- **Path spacing: 50 m (434 min)**

The turning path length is 87 m; the straight path is 150 m; and there are 12 straight-line segments.

With the traveling speed of 0.2 m/s in four straight-line segments, the traveling duration is: 4×(87+150)/0.2=4,740 s

With the traveling speed of 0.4 m/s in two straight-line segments, and the turning speed of 0.3 m/s, the traveling duration is: 2×87/0.3+ 2×150/0.4=1,330 s

With the traveling speed of 0.6 m/s in two straight-line segments, and the turning speed of 0.3 m/s, the traveling duration is: 2×87/0.3+ 2×150/0.6=1,080 s

With the traveling speed of 0.8 m/s in two straight-line segments, and the turning speed of 0.3 m/s, the traveling duration is: 2×87/0.3+ 2×150/0.8=955 s

With the traveling speed of 1.0 m/s in two straight-line segments, and the turning speed of 0.3 m/s, the traveling duration is: 2×87/0.3+ 2×150/1=880 s

Inspection and monitoring check: 60 min

Cumulative duration: (4,740+1,330+1,080+955+880)/60+5×60=434 min

Cumulative traveling distance: 12×(150+87)=2,844 m

- **Total operation duration**

Total operation duration: 842+454+473+434=2,203 min≈37 h

- **Operation zone**

Operation length: 5,080+3,276+3,960+2,844=15,160 m

Collection area: 15,160×5=75,800 m^2

e. Sampling operation (720 min)

Inspection and observation, fixed-point sampling, etc. in the post-mining area are expected to take 12 h.

f. Equipment status check before recovery (300 min)

After all operations are completed, the equipment status inspection will be conducted, which is expected to last for 5 h.

（3） Test disturbance region

Area dimensions: 0.6 km^2 (1,000 m long, 600 m wide).

Area of disturbance by traveling and nodule-collecting activities: 24,200 m^2 (first underwater operation) +75,800 m^2 (second underwater operation) = 0.1 km^2.

Total weight of wet nodules involved in operation: 13 $kg/m^2 \times 0.1\ km^2$=1,300 t.

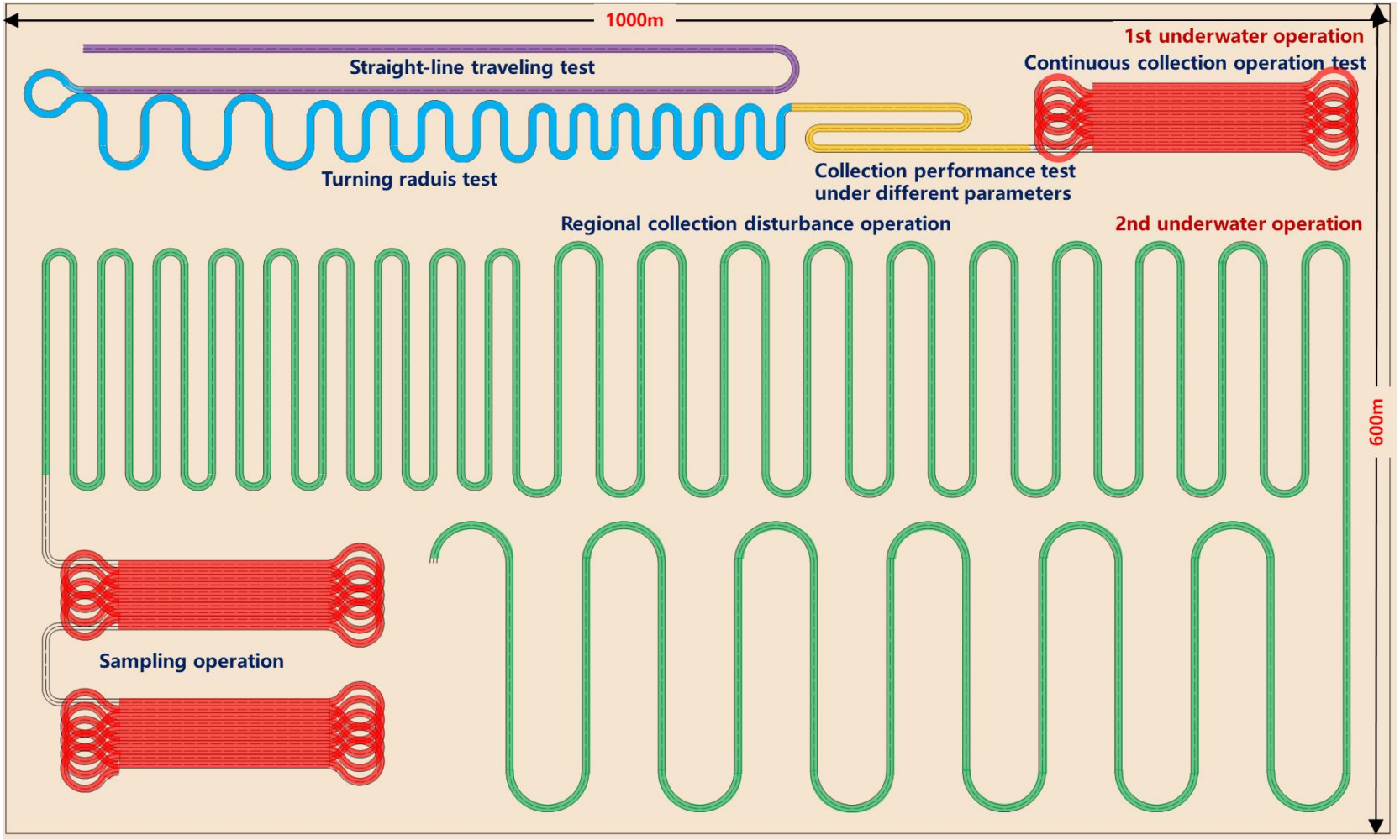

Figure 3.3-6 Planned underwater operation paths for the collector vehicle test

3.3.3 Transshipment

This test only includes the testing of the collector vehicle, and does not involve the pipeline lifting of minerals and surface transportation.

3.3.4 In-situ treatment

This test does not involve deck treatment of minerals.

3.3.5 Support equipment

The main support equipment used in this test includes a deep-water ROV and an AUV for operation at 6,000 m water depth. The ROV and AUV are mainly responsible for obtaining environmental monitoring data and samples.

(1) ROV *HAILONG-IV*

ROV *HAILONG-IV* is a 6,000 m deep-sea ROV system developed by Shanghai Jiao Tong University. It is electrically driven and has strong underwater maneuverability and operation ability. It is equipped with seven-function manipulator, high-definition camera, camera and LED underwater lighting, good underwater fine observation ability, inertial navigation system and automatic underwater hovering and line patrol control system. All these have greatly improved the navigation and positioning precision and operation efficiency of ROV. ROV *HAILONG-IV* can also be equipped with high-definition high-speed optical detection equipment.

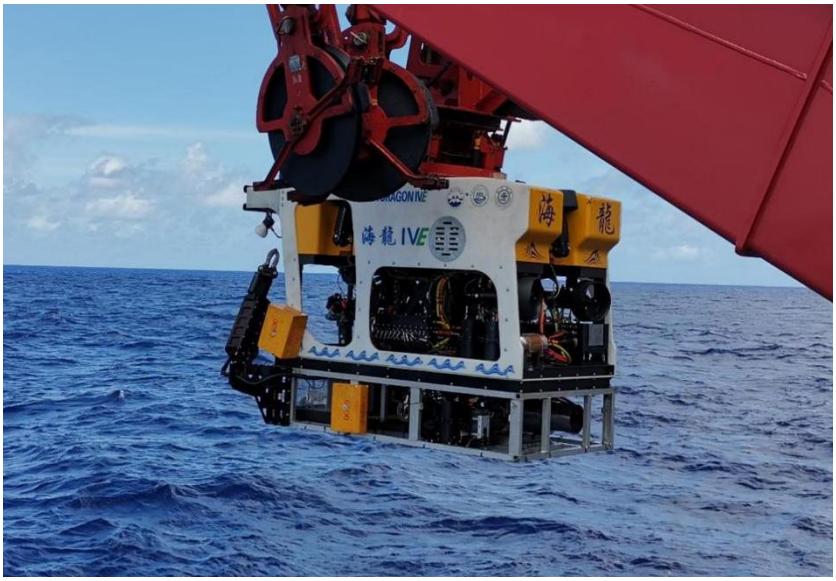

Figure 3.3-7 ROV *HAILONG-IV*

(2) AUV *QIANLONG-IV*

AUV *QIANLONG-IV* is a 6,000 m deep-sea AUV system developed by Shenyang Institute of Automation, Chinese Academy of Sciences (SIACAS). It is equipped with an inertial navigation system, a high-definition camera, a camera and LED underwater lighting, and carries a deep-water multibeam system, a shallow stratum profile detection system, etc. All these have given it long endurance and near-bottom optical, acoustic and hydrological environment detection capabilities.

Figure 3.3-8 AUV *QIANLONG-IV*

4 Description of Existing Physico-chemical Environment

4.1 Key information

This Chapter mainly describes the physico-chemical environment conditions of the Contract Area, and reviews Minmetals' collector vehicle test and survey of physico-chemical environment in the Block A-5.

Firstly, according to the information obtained from publicly available data, it summarizes the region's geological setting, the physical and chemical oceanography backgrounds of the CCZ (where the Contract Area is located), and then explains the overall environmental background conditions of the Contract Area.

Secondly, it introduces the at-sea survey and physico-chemical environment tasks completed by the Minmetals since the signing of the Contract. These tasks are also the main source of analysis data in this EIS.

Thirdly, it analyzes the meteorological characteristics, geological characteristics, physical oceanography characteristics, chemical oceanography characteristics, natural disasters, noise and light in the Block A-5, according to the findings of previous survey cruises. The above-mentioned analysis results provide a basis for the impact assessment in Chapter 7.

4.2 Overview of the region

4.2.1 Geological setting of the region

(1) Structural characteristics

The Block A-5 is located to the west of the CCZ in the East Pacific Ocean. The CCZ is located in the East Pacific Basin. With its north-south boundary named after two transform faults: the Clarion-Clipperton Fracture Zone and the Clarion Fracture Zone, the CCZ belongs to an intermediate body of the Pacific Plate. The structural characteristics of the CCZ are closely related to the history of plate evolution in the Pacific region, which was formed by seabed expansion from late Mesozoic to

Cenozoic. A large number of bathymetric survey data show that the water depth in the CCZ is approximately 5,000 m on average (Figure 4.2-1), and tends to decrease gradually from west to east. The seabed topography in the area varies greatly, showing the characteristics of alternating arrangement of seabed plains, seamounts, sea knolls, submarine rises, depressions, ditches and troughs.

The fault structures in the CCZ mainly include the Clarion-Clipperton Fracture Zone (Figure 4.2-1). These fault zones are NE-trending and mainly formed during the Cenozoic Pacific Plate expansion. There are also secondary or smaller transform faults the above-mentioned huge fault zones. Especially in the western part of the CCZ, the number and scale of faults are obviously stronger than those in the east due to regional uplift. As a channel or place for volcanic activity the western part of the CCZ has formed a large-scale volcanic chain and intermontane basin structure.

According to the differences of geophysical characteristics and tectonic framework, the CCZ can be divided into three structural units: western, central and eastern parts, with 145°W and 125°W longitudes as boundaries. The basement oceanic crust is mainly composed of oceanic tholeiite. The western basement was formed in the Late Cretaceous (approximately 100-70 Ma). The low positive gravity background of gravity anomaly in the area shows high density mantle anomaly and seabed uplift, with the Block A-5 of the Contract Area located in this unit. The central basement was formed in the Eocene-Oligocene (approximately 70-40 Ma ago), with the Blocks A-1, A-2, A-6, A-7 and A-8 of the Contract Area located in this structural unit. The eastern basement was formed in Oligocene-Pliocene (approximately 40-5 Ma ago), a relatively young oceanic crust area, with the Blocks A-3 and A-4 of the Contract Area located in this structural unit (Figure 4.2-1).

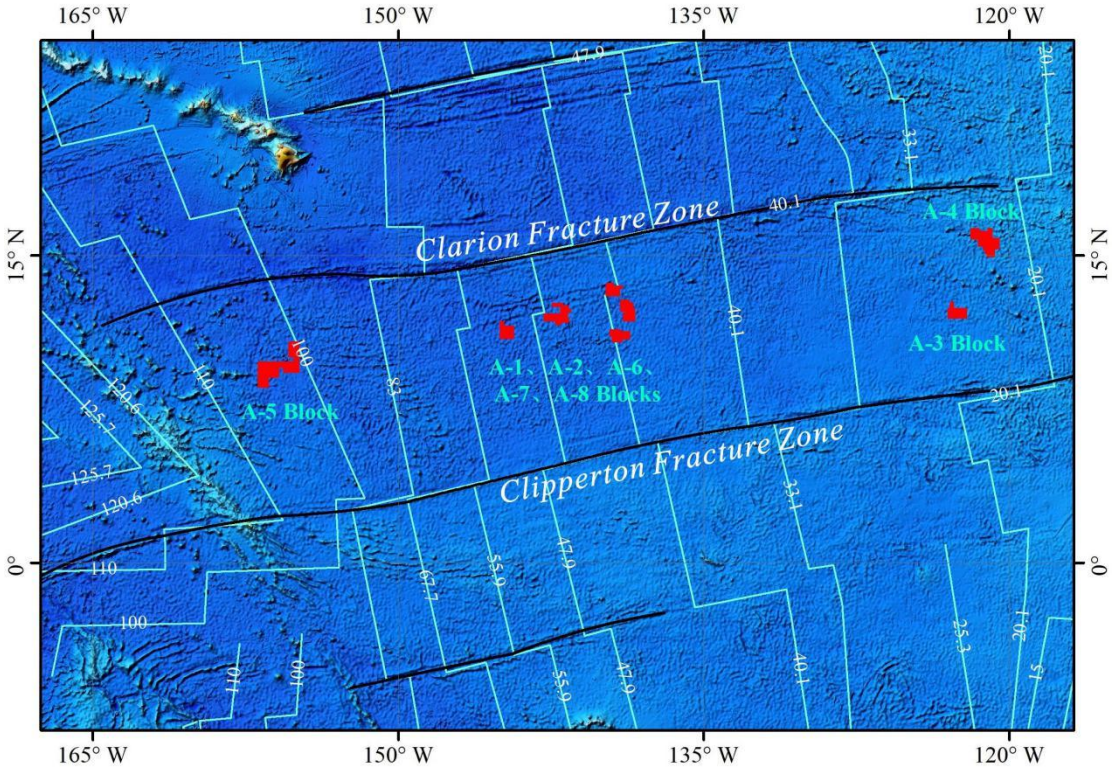

Figure 4.2-1 Distribution of geological and magnetic stripes in the Pacific Region

(Pacific crustal isochron age data from Müller et al. (2016))

(2) Sedimentary characteristics

The equatorial region of the East Pacific Ocean has high primary production, and its sediment type is mainly calcareous ooze. The seamount area has a water depth shallower than the carbonate compensation depth (CCD: ~4,500 m), so its sediment type is also mainly calcareous ooze. The main types of sediments in the CCZ are deep-sea clay, radiolarian ooze and siliceous clay. Except for radiolarian ooze in the northeastern part of the Block A-5, which is in the western part of the Contract Area, deep-sea clay is dominant in other blocks (Figure 4.2-2).

The sediment thickness is mainly affected by the deposition time and deposition rate. The calcareous ooze area has a higher deposition rate and a larger sediment thickness. It can be seen from the isolines map of sediment thickness distribution in the East Pacific Ocean (Figure 4.2-3) that the sediment thickness in the seamount area is the largest (up to 800 m), followed by that in equatorial high primary production zone (up to 500 m). Impacted by the formation time of oceanic crust, the thickness of

sediments in the CCZ gradually increases from east to west (Dutkiewicz et al., 2017). The Blocks A-3 and A-4 in the eastern part of the Contract Area are close to the ocean ridge and have a young crust, so their sediment thicknesses are less than 100 m. The sediment thicknesses in the central blocks of the Contract Area are in the range of 100-200 m. The Block A-5 located in the westernmost part of the CCZ is older (~100 Ma), so its sediment thicknesses are the largest (200-300 m) (Figure 4.2-3).

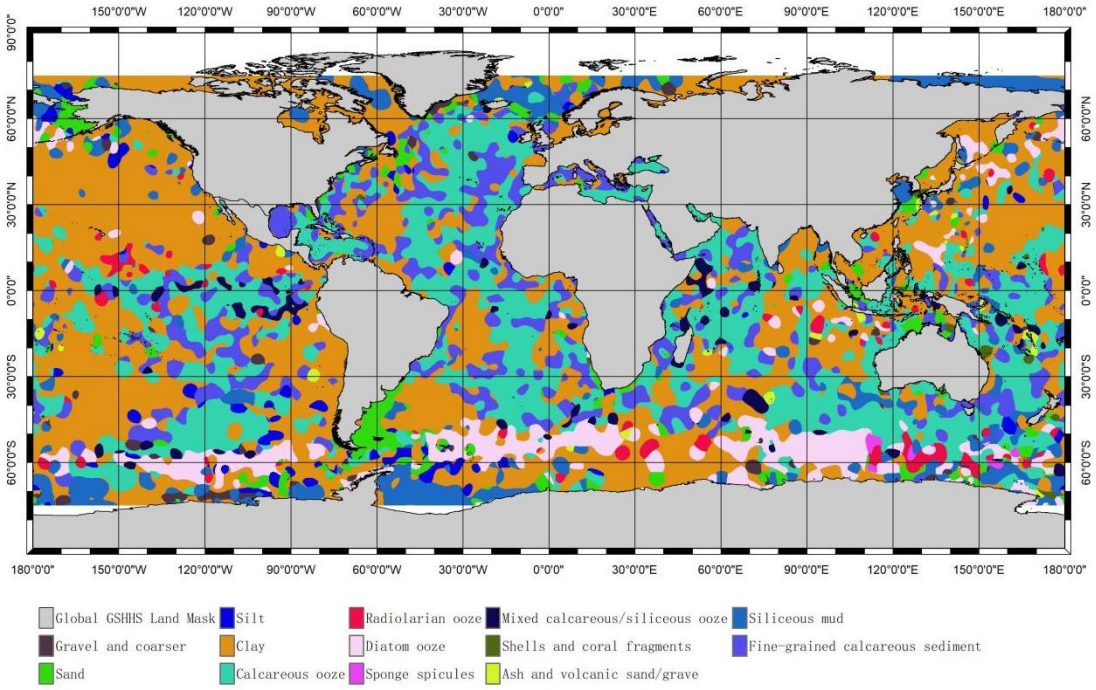

Figure 4.2-2 Distribution of sediment types in the CCZ of East Pacific Ocean

(Sediment type data from Dutkiewicz et al. (2015))

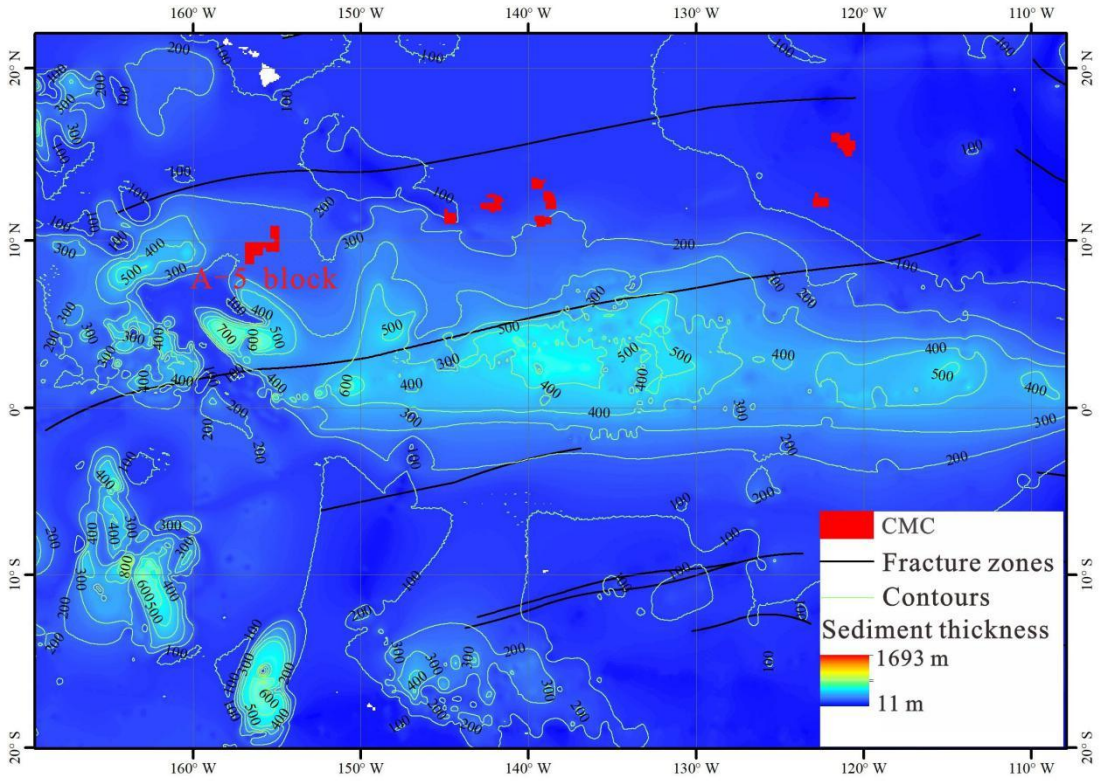

Figure 4.2-3 Isolines of sediment thickness distribution in the CCZ of East Pacific Ocean

(Sediment thickness data from Straume et al. (2019))

(3) Metallogenic characteristics of nodules

Publicly available data show that most of existing survey stations are distributed in the low latitudes of the northern and southern hemispheres, and relatively small amounts of nodules are distributed near the equator and in the middle and high latitudes (Figure 4.2-4). The distribution of seabed nodules in the world has typical zonality in geographical latitudes. Most of the nodule metallogenic belts are mainly distributed in the low latitudes north and south of the equator. For example, the nodule metallogenic belt in the CCZ of the East Pacific Ocean lies in 5°N - 15°N, that in the Central Indian Ocean basin lies in 10°S - 20°S, and that in the Cook Islands-Penrhyn Basin lies in 5°S - 35°S. It can be seen from the Pacific nodule occurrence probability prediction map (Figure 4.2-4) that the areas with high nodule occurrence probability are mainly distributed in the basin zones on the north and south sides of the equator. The high probability areas in the northern hemisphere are mainly the CCZ and the central and western Pacific basins. The high probability area in the southern

hemisphere is mainly the Penrhyn Basin. They are consistent with the findings of historical survey cruises.

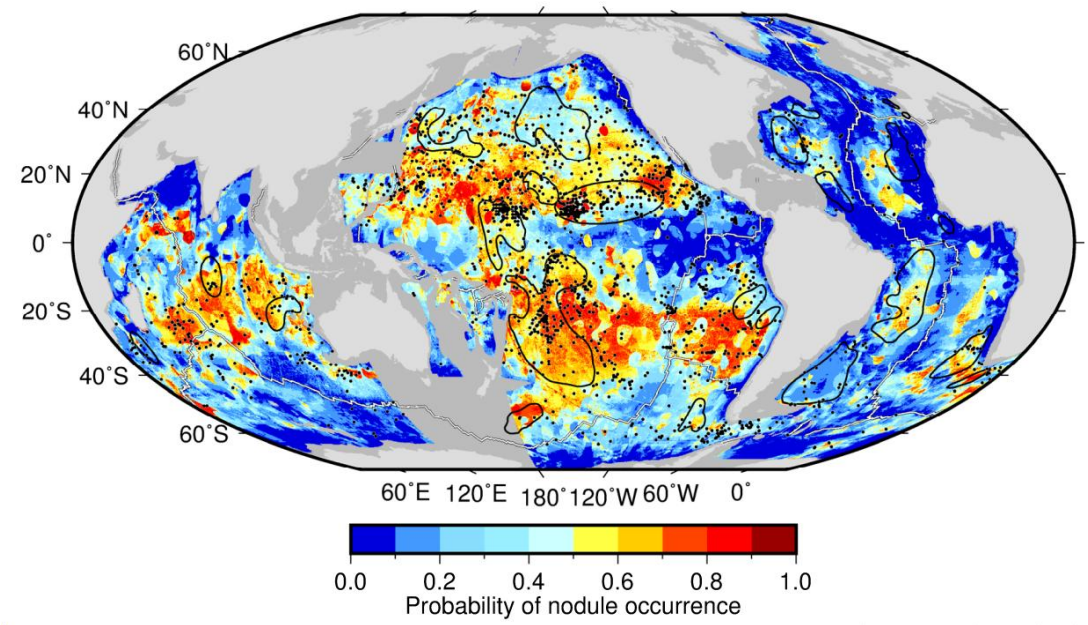

Figure 4.2-4 Distribution of nodule occurrence frequencies in the Pacific Ocean

(Nodule occurrence probability data from Dutkiewicz et al. (2020))

4.2.2 Physical oceanography background of the region

The CCZ is located in the middle of the Pacific Ocean, the southern end of the northeast trade-wind zone and the northern part of the Intertropical Convergence Zone (ITCZ). The climate is divided into two seasons: winter and summer. During the winter, the CCZ is mainly controlled by the northeast trade wind at the southern end of the subtropical high. Northeast gales trade wind surges are prevalent, with stable wind directions and wind forces. Magnitude 5 winds have the highest frequency, accounting for 41.1 %, with the maximum wind speed >15 m/s, and the maximum wave height above >5 m. The weather conditions and sea visibility are good, showing the climatic characteristics of trade-wind zone. During the summer, due to the seasonal northward jump of the ITCZ, the northeast wind in the exploration zone decreases, but there will be tropical storms in July-September, with the maximum wind speed >50 m/s, which are frequently affected by tropical depression and tropical cyclones. It is the characteristic of tropical maritime climate, with high temperature,

high humidity and much precipitation.

The Contract Area is located in the tropical marine area in the central and East Pacific Ocean, and the surface-layer ocean currents are mainly distributed in North Equatorial Current (NEC), North Equatorial Counter Current (NECC), South Equatorial Current (SEC) and its branch, New Guinea Coastal Current (NGCC). Under the surface-layer ocean currents, there are three kinds of currents: North Equatorial Undercurrent (NEUC), North Equatorial Subsurface Current (NESC) and Equatorial Undercurrent (EUC) (Figure 4.2-5). The sea area is a Pacific warm pool area. The surface-layer water temperature exceeds 28°C, which has a significant impact on the East Asian monsoon and atmospheric circulation (Hu et al., 2011).

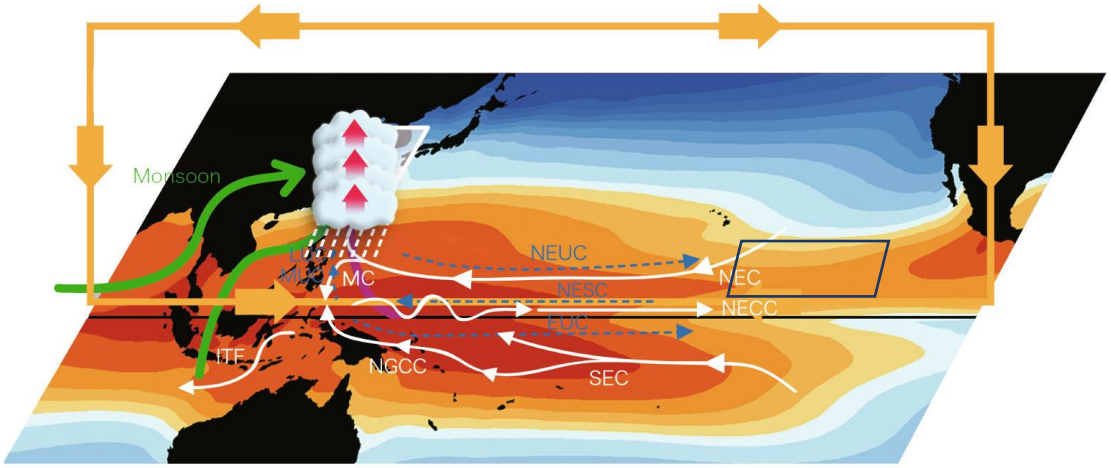

Figure 4.2-5 Distribution of tropical Pacific currents and their climate impacts

(Blue solid line box indicates the schematic position of the CCZ, Hu et al., 2011)

North/South Equatorial Current (NEC/SEC), New Guinea Coastal Current (NGCC), Mindanao Current (MC), North Equatorial Countercurrent (NECC), Indonesian Throughflow (ITF), Mindanao Undercurrent (MUC), Luzon Undercurrent (LUC), North Equatorial Undercurrent (NEUC), New Guinea Coastal Undercurrent (NGCUC), North Equatorial Subsurface Current (NESC) and Equatorial Undercurrent (EUC).

By the temperature and salinity of deep-layer seawater, the world's deep-layer seawater mainly comes from two types of water columns: the North Atlantic Deep Water (NADW) with high salinity (2.5 °C and 35 psu), and the AABW with low temperature and salinity (1 °C and 34.6 psu) but high density formed in the Weddell Sea. The deep-layer seawater in the Pacific Ocean comes from the Antarctic circumpolar current, and its flows are divided into upper lower deep branch of the Pacific Meridional Overturning Circulation (U-PMOC) and the lower deep branch of

the Pacific Meridional Overturning Circulation (L-PMOC). In the northeast Pacific basin, especially in the CCZ, the structure of deep-layer and near-bottom-layer seawater is determined by the inflow of the AABW and its accumulation and redistribution in the basin, because there is no channel for seawater to flow out, and the CCZ is located in an area where the AABW extends steadily to the northeast.

Entrusted by the COMRA, the SIOMNR conducted observation on the variations of the flow field within 600 m above the bottom in the eastern and western parts of the COMRA Contract Area in 1997-1999. The heights of the current meters above the bottom were set to 8 m, 200 m and 600 m for the first observation. The second observation was concentrated in the near-bottom layer, so the observation horizons were adjusted to 5 m, 15 m and 50 m (Liang, 2004). At stations (10˚02'N and 154˚03'W in the western zone this region is adjacent to the Block A-5), two sets of near-bottom submerged buoys were launched to obtain long-term ocean current observation data of 8 m, 50 m and 600 m above the bottom. Observation results show that the duration of low-frequency flow within 600 m above the bottom is 25-120 days, of which the low-frequency vibration is the main component with a duration of approximately 51 days. The topography has obvious impact on the low frequency flow within 50 m above the bottom.

In 1997-1998, the ocean currents of 8 m and 200 m above the bottom were observed in the western zone (Zhang, 1999). In 2019-2021, the measured current results of 20 m, 100 m, 200 m above the bottom and 2,010 m below the sea surface were obtained in the Block A-5 of the Contract Area (Minmetals Annual Report 2021). On September 20, 2022, a set of near-bottom mooring launched in October 2021 was successfully recovered, and the observed data of current speeds at the depths of 8 m and 100 m above the bottom were obtained.

These observation results show that currents in the near-bottom layer in this region are characterized by low average speed and high variability in speed and direction. Study findings show that the main variations of deep seabed current are related to inertia and tidal oscillation, just like the variations of meteorological scale. Ni Jianyu et al. (2002) classified the bottom-layer ocean currents in the CCZ into three hydrodynamic conditions according to the current speeds and variations:

(1) Quiet period: It is characterized by minimum ocean current speed (0-3 cm/s), moderate to low variability and low tidal activity. In fact, the bottom-layer ocean current even has an "inactive" period. When the bottom-layer ocean current is inactive,

the minimum current speed is only approximately 1.2 cm/s. At the depth of 200 m above the bottom, the "inactive" period of ocean current lasts one day minimally and six days maximally, while the interval of "inactive" periods is one day at the shortest, and 186 days at the longest. At the depth of 8 m above the bottom, the "inactive" period of ocean current lasts one day minimally and eight days maximally, while the interval of "inactive" periods is one day at the shortest, and 89 days at the longest.

(2) Mesoscale inertial tidal cycle: It is characterized by the variation of ocean current speed (0 to 5-6 cm/s) and the corresponding increase rate.

(3) Active period: At first, it was associated with the sharp increase of ocean current speed. This increase in ocean current speed can maintain a relatively stable period, the average flow current speed within 24 h can reach 8 cm/s or higher, and the average value in a specific hour can reach 13-15 cm/s. These events are called "undersea storms". Such variation is usually regular and lasts for 1-6 weeks, which is consistent with the timescale of typical hydrological and meteorological variations on the sea surface (Aller, 1997; Xie, 2022). Another feature that accompanies the deep undersea sea storm is that the ocean current directions also vary significantly.

4.2.3 Chemical oceanography background of the region

The CCZ is located at the junction of the NEC and the NECC. The nutrients in the CCZ can be supplemented by the equatorial high-nutrient brine brought by the north equatorial current. The nutrients in the upper-layer seawater are higher than those in the general oligotrophic sea area and higher in the eastern part than in the western part. Chemical elements (e.g. nutrients) in the upper-layer seawater in this region have certain annual and spatial variation characteristics, and the expression forms of different elements vary as well. The nutrient loss layer is affected by global climate events, such as El Niño. The westward propagation of subsurface SST anomaly near 10 °N is an important part of the El Niño-Southern Oscillation (ENSO) event. The annual nitrate and phosphate concentrations of La Niña increase significantly, and the loss layer moves down. It is the opposite in El Niño years. It was also found that the nitrate concentration increases abruptly at the junction of the NEC and the NECC in La Niña years. However, this phenomenon disappears in El Niño

years. The N/P/Si ratios of surface-layer seawater have obvious spatio-temporal fluctuations, and the ratio greatly deviates from the Redfield ratio. The analysis of nutrients and DO in deep- and bottom-layer seawater shows that the interannual variations of nutrients and DO echo ENSO events, and the variation law is opposite to that of upper-layer seawater.

The distribution law of DO in seawater in this region accords with the typical characteristics of ocean water columns, and the DO in the surface layer is the highest in the full water column, reaching saturation or even supersaturation. With the increasing water depth, the illumination intensity weakens, the photosynthesis weakens, but the respiration strengthens. The organic matters produced by biological physiological processes and death are continuously decomposed, consuming a lot of oxygen. The DO concentration below 100 m decreases continuously and the organic matter decomposition is the strongest in the water-depth layer of 140-800 m, thus making the DO in seawater the lowest, which is an anoxic layer with an oxygen concentration of 45-80 μmol/L. And then, the DO concentration starts to increase again due to the supplement of the bottom high-oxygen water, and tends to stable at the depth of 4000 m.

4.3 Studies completed

Minmetals has conducted six survey cruises in 2017-2023 of the "Exploration Contract" period, as well as physico-chemical environment baseline surveys in the Contract Area and its adjacent waters (Table 4.3-1). We have gained a preliminary understanding of the basic environmental conditions in the Contract Area, constructed the environment baselines in the Contract Area, and submitted the environment baseline study reports and basic data.

Table 4.3-1 Survey cruises in the Contract Area

Survey	S.N.	Start time	Surveyed blocks	Research vessel
2017 survey cruise	DY47	2017.08.29—2017.11.30	A-1, A-2, A-5, A-6, A-7, A-8	R/V *XIANGYANGHONG LIUHAO*
2018 survey cruise	DY50	2018.08.31—2018.10.19	A-1, A-2, A-6, A-7, A-8	R/V *XIANGYANGHONG SANHAO*
2019 survey cruise	DY54	2019.07.20—2019.12.29	A-3, A-4, A-5	R/V *XIANGYANGHONG SHIHAO*
2021 survey cruise	DY70	2021.09.30—2022.01.18	A-5	R/V *DAYANG YIHAO*
2022 survey cruise	DY73	2022.08.11—2023.11.23	A-5	R/V *DAYANG HAO*
2023 survey cruise	DY79	2023.08.09—2023.12.18	A-5	R/V *DAYANG YIHAO*

By 2023, Minmetals has carried out the physico-chemical environment survey projects at about 316 stations and several survey lines in the Block A-5 of the Contract Area. They mainly include the completion of 13 seabed photography survey lines (including two AUV optical survey lines), box corer sampling at 208 stations, multicorer sampling at 25 stations, gravity piston corer sampling at eight stations, in-situ geotechnical properties testing at 27 stations, 200 m CTD survey at eight stations, full-ocean-depth profiling CTD survey at 13 stations, mooring observation at four stations (launch and recovery at one station, successful recovery at three stations), MULVFS at two stations and hydrophone monitoring at three stations. On this basis, we have conducted testing of environment baseline data, including physical oceanography structure (temperature and salinity, ocean current), chemical oceanography characteristics (DO, pH, nutrients), sediment chemistry (pore water and sediment chemistry, etc.) and sedimentary flux, as well as established geological,

physical and chemical data sets.

4.3.1 CTD profile observation and sampling stations

Minmetals has been conducting exploration and survey cruises since 2017. During the 2017, 2018, 2019, 2021, 2022 and 2023 survey cruises in the TMA of the Block A-5, we have conducted CTD determination (including water sampling) 13 times for entire water column, and eight times in the water layer above 200 m depth. See Table 4.3-2 for information of the CTD survey stations.

Table 4.3-2 Statistics of CTD observation stations

S.N.	Station name	Year	Longitude (°W)	Latitude (°N)	Sampling Depth (m)	Region Location
1	DY47I-A5-CTD02	2017	155°54'54"	9°46'8.40"	5302	-
2	DY50I-A5-S06-CTD10	2018	156°24'3.60"	9°29'56.40"	5189	-
3	DY50I-A5-S06-CTD11	2018	156°25'1.20"	9°30'0.00"	200	-
4	DY54IV-A5-CTD01-Q	2019	156°46'12.00"	9°23'56.40"	5185	PRZ
5	DY54IV-A5-CTD01(200m)	2019	156°46'12.00"	9°23'56.40"	200	PRZ
6	DY54IV-A5-CTD02-Q	2019	155°33'28.80"	9°27'21.60"	5183	-
7	DY54IV-A5-CTD02(200m)	2019	155°33'28.80"	9°27'3.60"	200	-
8	DY70I-A5-CTD01-Q	2021	156°37'25.80"	9°19'24.73"	5239	IRZ
9	DY70I-A5-CTD02-200m	2021	156°46'11.53"	9°23'47.86"	200	PRZ
10	DY70I-A5-CTD02-Q	2021	156°46'6.77"	9°24'41.72"	5272	-
11	DY70I-A5-CTD03-Q	2021	156°37'27.74"	9°19'32.98"	5240	IRZ
12	DY73I-A5-CTD01-Q	2022	156°46'10.65"	9°23'48.34"	5245	PRZ
13	DY73I-A5-CTD02-Q	2022	156°37'25.10"	9°19'23.75"	5246	IRZ
14	DY79I-A5-CTD01-Q	2023	156°46'10.31"	9°23'50.02"	5244	PRZ
15	DY79I-A5-CTD02-200	2023	156°46'10.27"	9°23'50.00"	200	PRZ
16	DY79I-A5-CTD03-200	2023	156°41'41.17"	9°21'9.46"	200	IRZ
17	DY79I-A5-CTD04-200	2023	156°37'24.02"	9°19'23.01"	200	IRZ
18	DY79I-A5-CTD05-Q	2023	156°37'14.57"	9°19'58.83"	5253	IRZ
19	DY79I-A5-CTD06-Q	2023	156°41'40.91"	9°21'12.24"	5278	IRZ
20	DY79I-A5-CTD07-Q	2023	155°31'15.48"	9°31'46.01"	5289	-
21	DY79I-A5-CTD08-200	2023	155°30'51.57"	9°31'33.85"	200	-

4.3.2 Fixed-point mooring observation stations

Since the 2019 survey cruise, Minmetals has successfully recovered one set of mooring in each of the 2021, 2022 and 2023 survey cruises. Another set of mooring has been launched during the 2023 survey cruise, which is to be recovered. See Table 4.3-3 for the information of three recovered mooring and Figures 4.3-1 ~ 4.3-3 for the structural diagrams of mooring.

Table 4.3-3 Information of mooring stations in the Block A-5 during the 2019 survey cruise

Station	Year	Longitude (°W)	Latitude (°N)	Water depth (m)	Region Location
DY70II-A5-MX01	2021	156°44'51.06"	9°25'51.18"	5272	-
DY73I-A5-MX02	2022	156°37'32.11"	9°19'22.15"	5242	IRZ
DY79I-A5-MX01	2023	156°38'23.22"	9°17'50.11"	5246	-

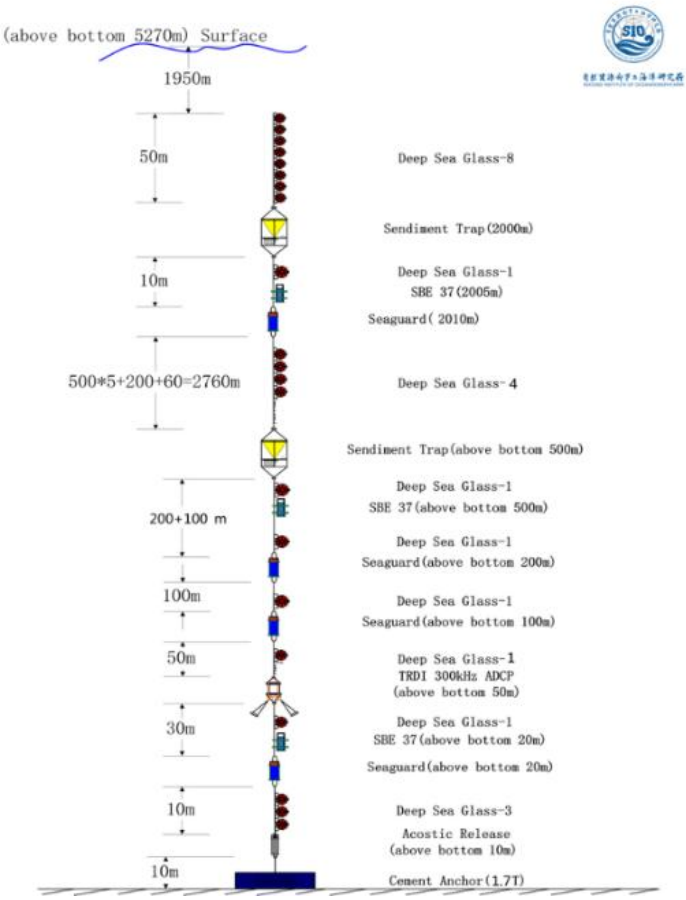

Figure 4.3-1 Structural diagram for mooring recovered at DY70II-A5-MX01 during the 2021 survey cruise

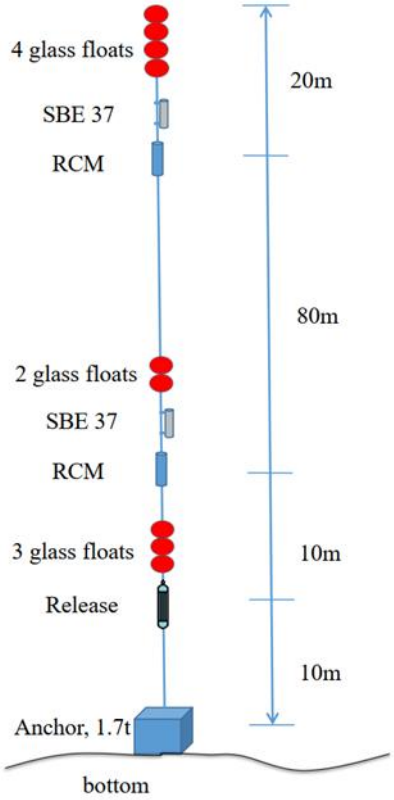

Figure 4.3-2 Structural diagram for DY73I-A5-MX02 mooring recovered during the 2022 survey cruise

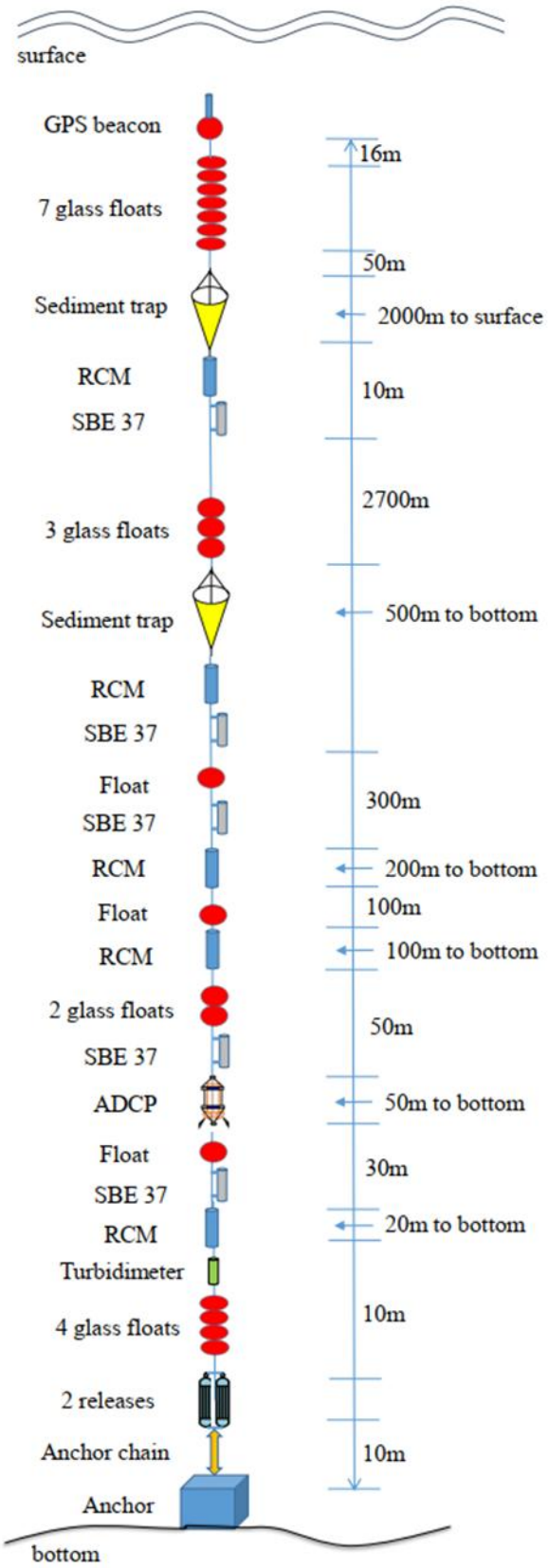

Figure 4.3-3 Structural diagram for mooring recovered at DY79I-A5-MX01 station during the 2023 survey cruise

4.3.3 Nodule resource survey stations

We have surveyed nodule abundance and coverage with box corer at 109 stations in the PWA and 50 stations in the TMA of the Block A-5. See Figure 4.3-4 for the distribution of stations.

4.3.4 Sediment survey stations

We have sampled sediments in the Block A-5 with box corer, gravity piston corer and multicorer. Surface-layer sediments at different depths were sampled with box corer sampling at 109 stations; while columnar sediments at various depths were obtained with gravity piston corer at four stations and multicorer at nine stations. See Figure 4.3-4 for the distribution of stations.

4.3.5 In-situ geotechnical properties survey stations

The physical properties of sediments within 1 m depth range in the Block A-5 were measured by geotechnical in-situ tester. See Figure 4.3-4 for the distribution of stations.

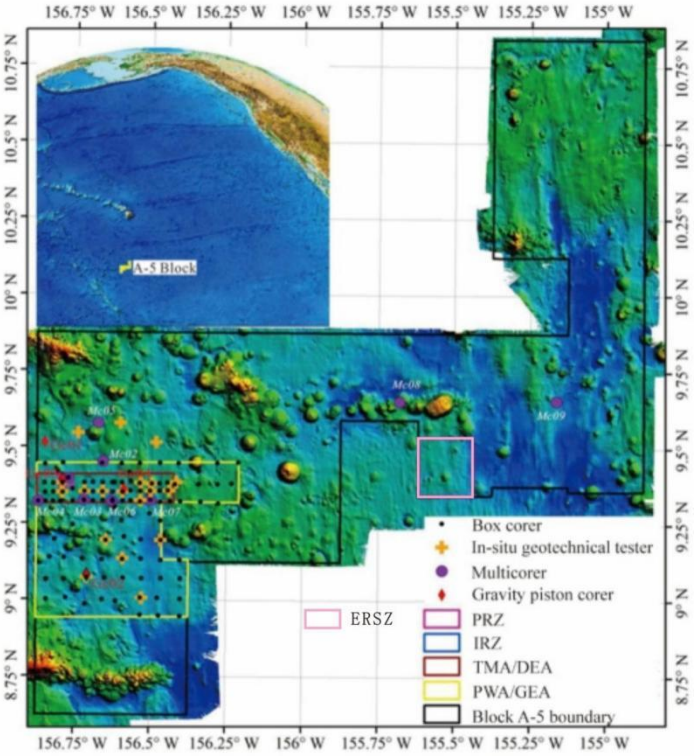

Figure 4.3-4 Distribution of box corer, gravity piston corer and multicorer sampling stations in the Block A-5

4.4 Meteorology and air quality

4.4.1 Meteorology

We used ECWMF ERA5 grid data (https://cds.climate.copernicus) to analyze the monthly average wind speeds in the Block A-5 in 2013-2023. We selected three levels (p=1,000 hpa, p=950 hpa and p=900 hpa) for analysis. The corresponding altitudes are approximately 100 m, 500 m and 1,000 m (refer to https://www.mide.com/air-pressure-at-altitude-calculator for the conversion formula of pressure grade and altitude grade, assuming the sea surface temperature is 30 °C).

Results show that the monthly average wind speeds in this region are the lowest (>4 m/s) in August-October every year. Comparatively speaking, the monthly average wind speeds in spring (March-April) are the highest, exceeding 10 m/s (Figure 4.4-1). The wind field in this region also has a significant diurnal pattern. The sea surface wind speed in the afternoon (12pm-03pm) and midnight (00am-02am) is less than 7 m/s, but it has a time window with great uncertainty (STD = 0.27). On the sea level, the highest wind speed will appear stably in the morning and evening of every day. Among the three heights, the wind with p=950 hpa is the strongest (Figure 4.4-1).

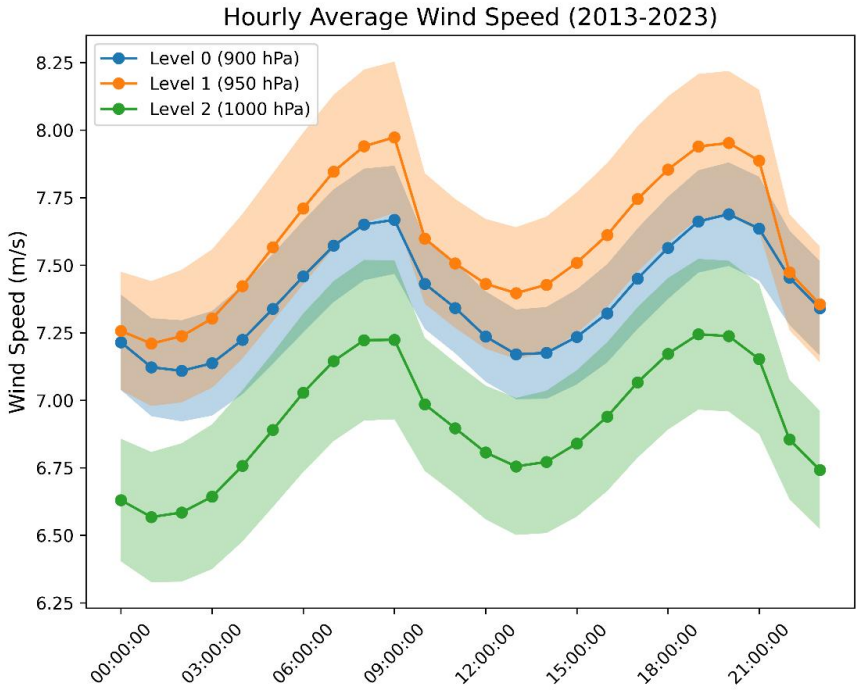

Figure 4.4-1 Diurnal variations of average wind speed in the Block A-5

(p=1,000 hpa, p=950 hpa and p=900 hpa correspond to altitudes of about 100 m, 500 m and 1,000 m, respectively).

We used ECWMF ERA5 grid data (https://cds.climate.copernicus) to analyze the monthly average wind field (p=900 hpa) in the Block A-5 in 2013-2023. Results show that the overall wind field in this region is relatively stable in the spatial sense, but with significant seasonal variations. The average wind directions in all months are shown in Table 4.4-1 and Figures 4.4-2 and 4.4-3. As can be seen from the figure, from July to October every year, the wind force in the Block A-5 is small, which is suitable for the collector vehicle test.

Table 4.4-1 Average wind directions in all months in the Block A-5

Month	Average wind direction
January	Southeast
February	Northwest
March	South
April	East
May	Southwest
June	West
July	Southwest
August	Northeast
September	North
October	East
November	West
December	Southeast

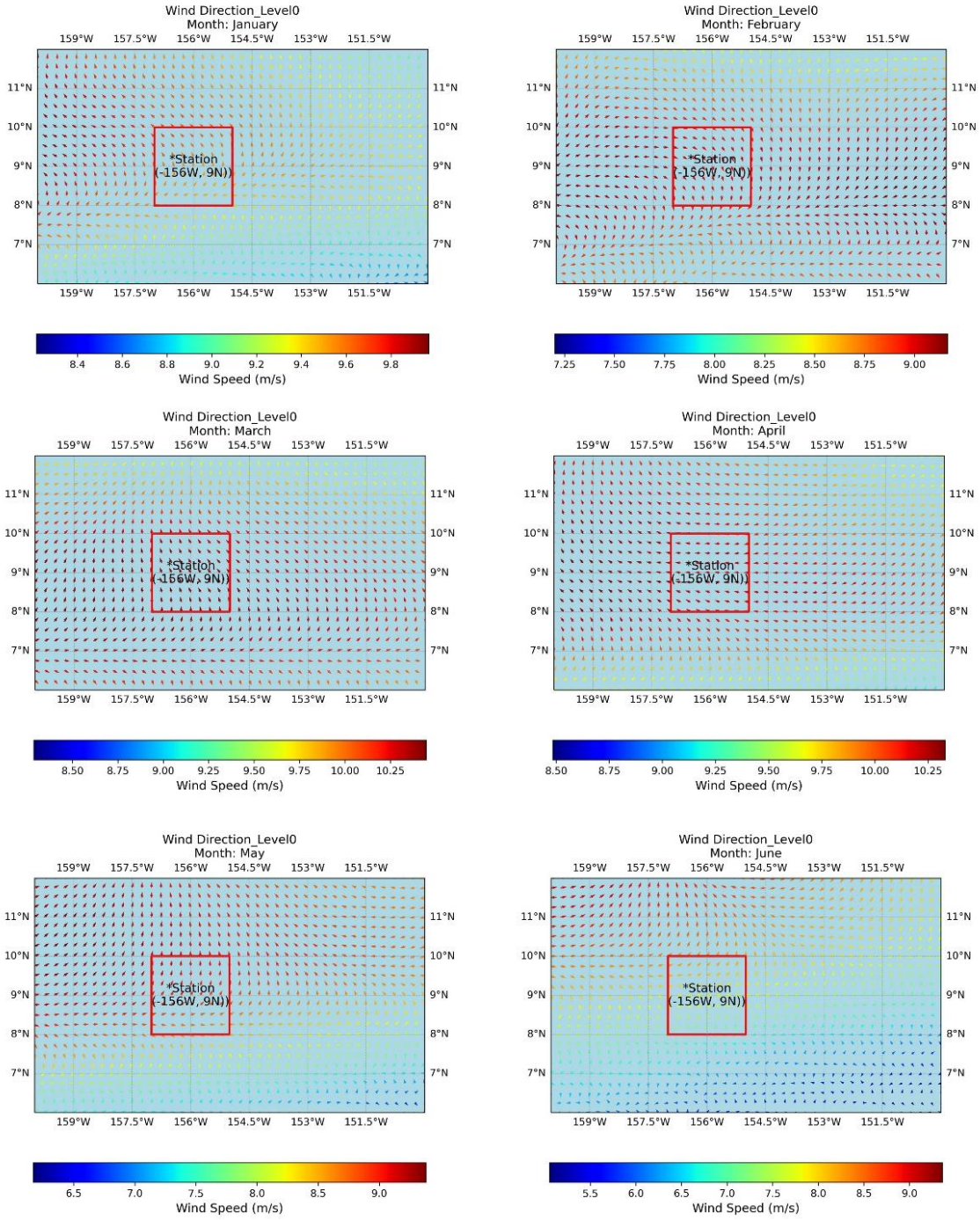

Figure 4.4-2 Vector wind fields in the Block A-5 in all months (2012-2023)

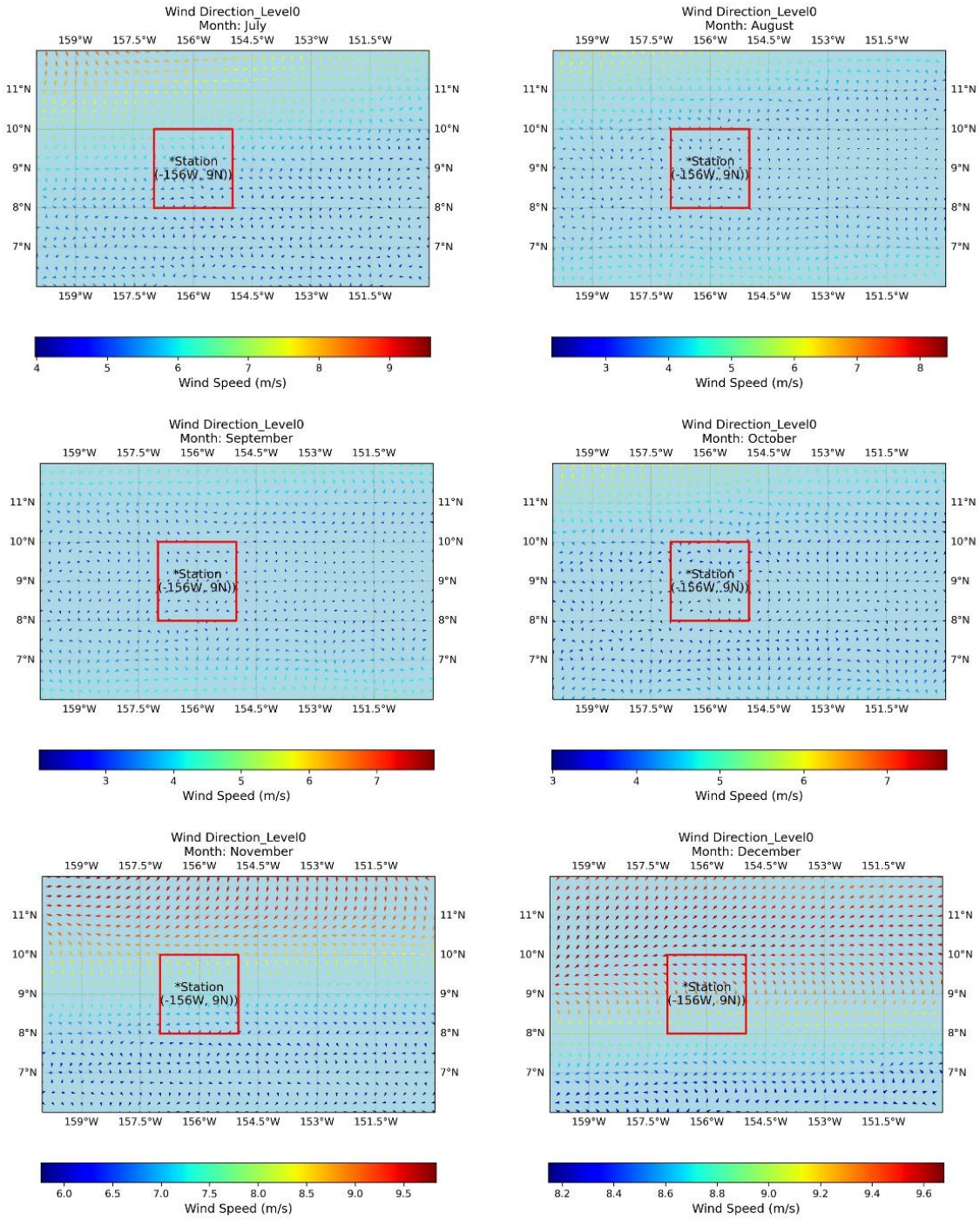

Figure 4.4-3 Vector wind fields in the Block A-5 in all months (2012-2023) (continued)

4.4.2 Air quality

We used the EDGAR grid data (https://edgar.jrc.ec.europa.eu/dataset_ap61#p2) to analyze the annual contents of nitrogen oxides and sulfur dioxide in the Block A-5 in 2015-2018. Results show that commercial vessels (especially those using high-

sulfur fuel) crossing the Pacific emit nitrogen oxides and sulfur dioxide from their engines. These emissions cause air pollution and will affect the air quality on the ocean (Figures 4.4-4 and 4.4-5). Generally speaking, the Block A-5 is located far away from the mainland and the busy maritime shipping area in the North Pacific Ocean. Therefore, although shipping is the main source of nitrogen oxides and sulfur dioxide pollutants in the Block A-5, the emission concentration of these two pollutants in this region is very low, with nitrogen oxides at approximately 2 e^{-13} kg m^2 s^{-1}, while the emission rate of sulfur dioxide is even lower at approximately 5 e^{-14} kg m^2 s^{-1}.

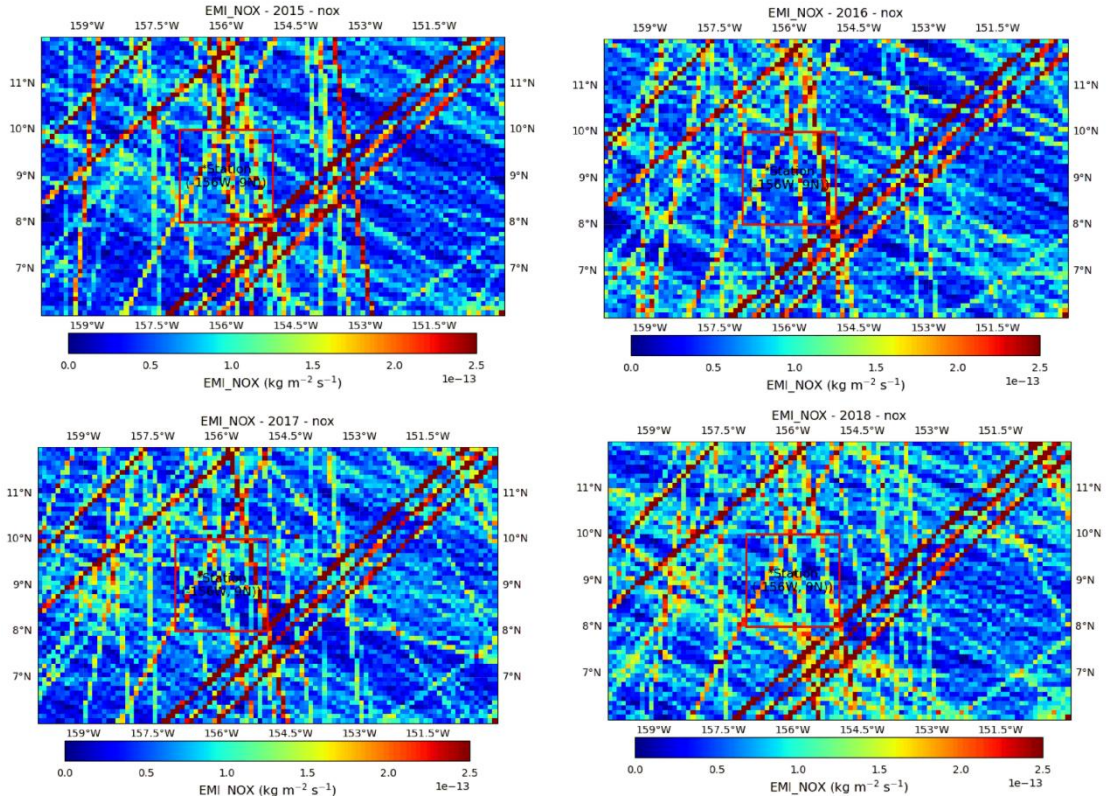

Figure 4.4-4 Atmospheric nitrogen oxide emissions in the Block A-5 (2015-2018)

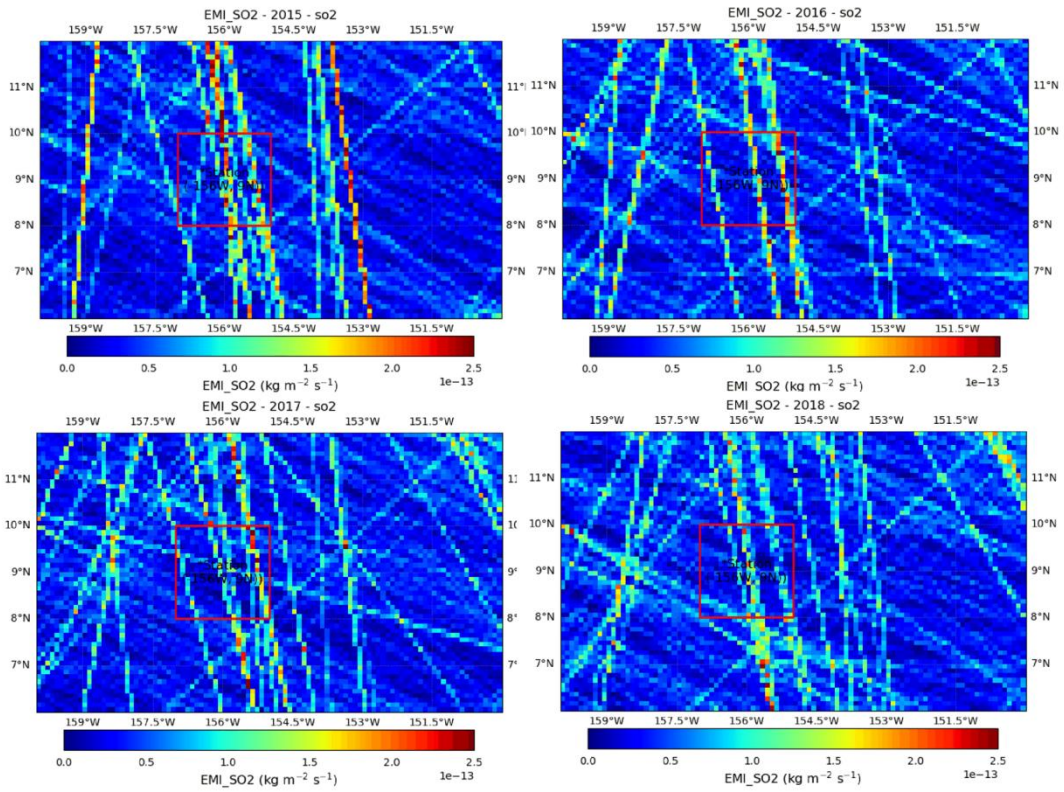

Figure 4.4-5 Atmospheric sulfur dioxide emissions in the Block A-5 (2015-2018)

4.5 Geological properties

4.5.1 Topographic characteristics

The Block A-5 is predominated with topographies of sea knolls, sea knoll groups, intermontane basins and seamounts (Figure 4.5-1). There is one sea knoll chain in the nearly east-west direction in the central and southern parts of the Block, respectively. In the western part of the Block, there are a group of scattered sea knolls, and intermontane basins with flat topography on both sides the group of sea knolls. The northwestern part of the Block is relatively flat, and dominated with hills, with sea knolls sporadically distributed over there.

Based on the BPI and slope values of topography relief, we classified the topography of the Block A-5 by using the iterative self-organizing clustering analysis (ISODATA) (Figure 4.5-2). Relief BPI is an important parameter for describing the rugged topography. A value of 0 indicates an absolutely flat area, while positive and negative values indicate that the topography is convex upward and concave

downward, respectively. The larger the value, the greater the rugged topography is. Slope value is an important parameter for describing the steepness of topography. BPI values can be used to effectively distinguish flat topography, slope topography, depressed seafloor depression shape and steep seamount topography. ISODATA classification results show that most areas in the Block A-5 are flat ocean basin zones (accounting for 70.8 %), followed by foothill slope areas (accounting for 14.0 %). The area of steep uplift seamounts accounts for 9.8 %, while the area of seafloor depressions (mainly formed by seamount gravity ballast) accounts for approximately 5.3 %. Compared with the whole Block A-5, the PWA has the flat ocean basin zone accounting for a larger proportion (79.9 %), the steep uplift seamount accounting for 6.6 %, and seafloor depressions accounting for a much smaller proportion (2.8 %).

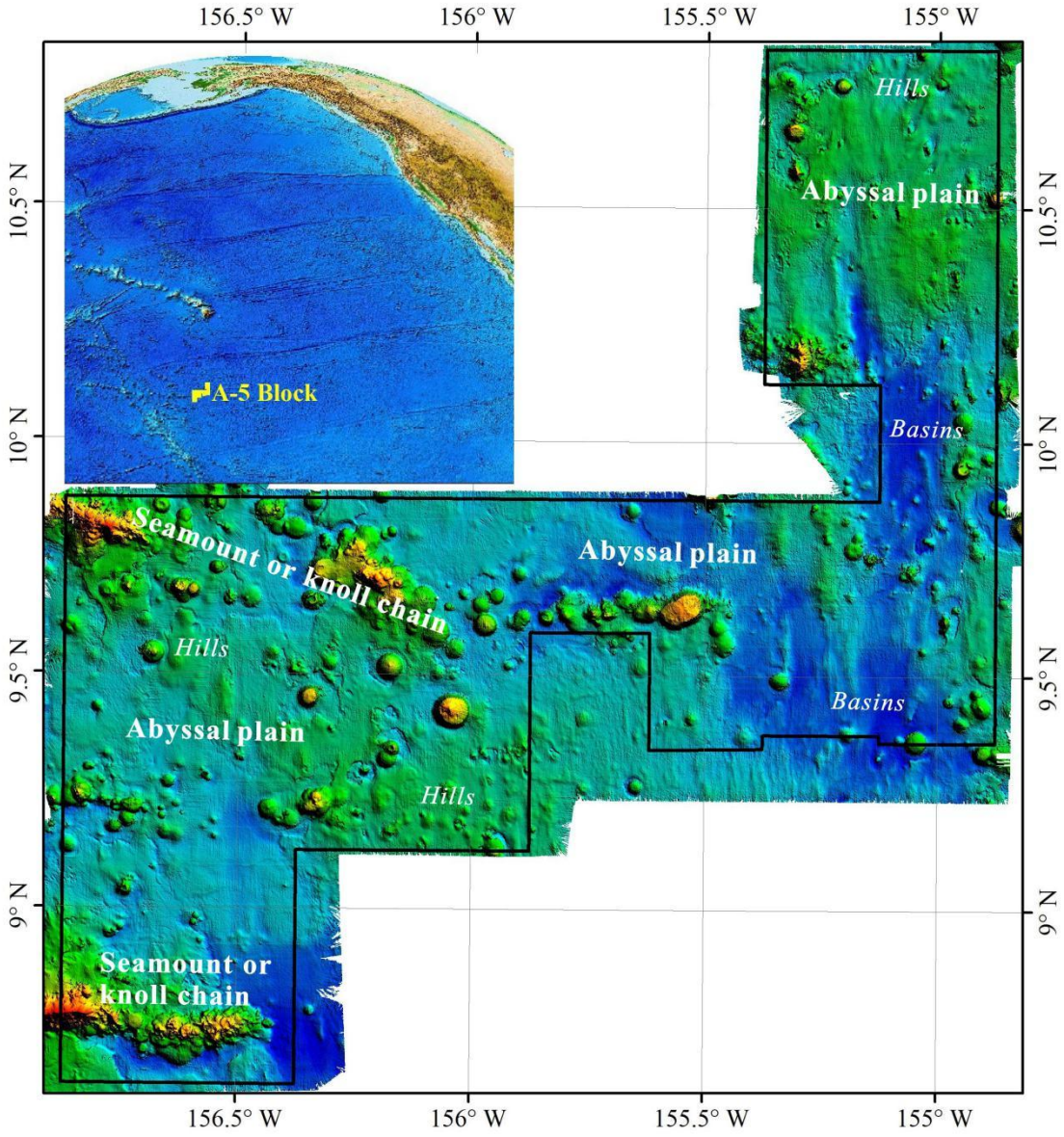

Figure 4.5-1 Topographic and geomorphological features of the Block A-5

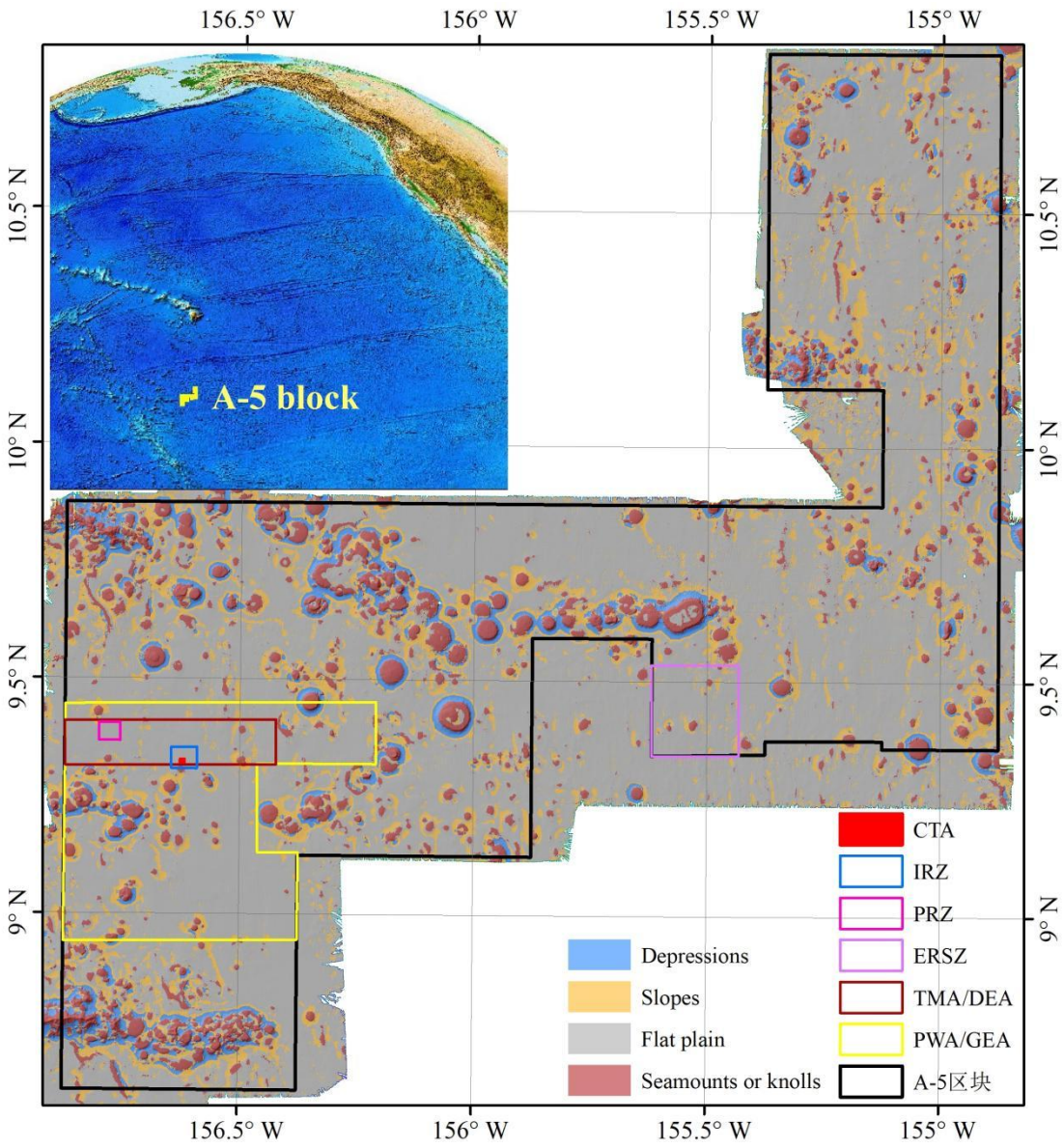

Figure 4.5-2 Classification of topographies in the Block A-5

Minmetals has conducted near-bottom acoustic survey with AUV in the TMA of the Block A-5, and obtained high-resolution (2 m grid) seabed topography (Figure 4.5-3).

The water depth of AUV survey area was 5,290-5,130 m, and the overall relief was small. The east and west sides of the survey area are seabed highlands, and the middle part is a small depression spreading in the north-south direction. There is a conical sea knoll in the southwest of the western highland, with a net height of about 100 m, which is the highest point in the whole region. There are two sea knolls in the eastern highland, the tops of which are relatively gentle, and the net heights are all

below 100 m. The contact zone between the seabed highland and the ocean basin is of flat topography, with no obvious scarp landform, but there are some small deep pits (Figure 4.5-3).

The IRZ (blue box) and PRZ (pink box in the western part of the Block A-5) are located in the AUV survey area. They are located on the highlands in the eastern and western highlands of AUV survey area, respectively. The overall topography is relatively flat, without small protrusions or deep pits, and the water depth varies less than 20 m. To sum up, the IRZ and PRZ have highly similar topographies.

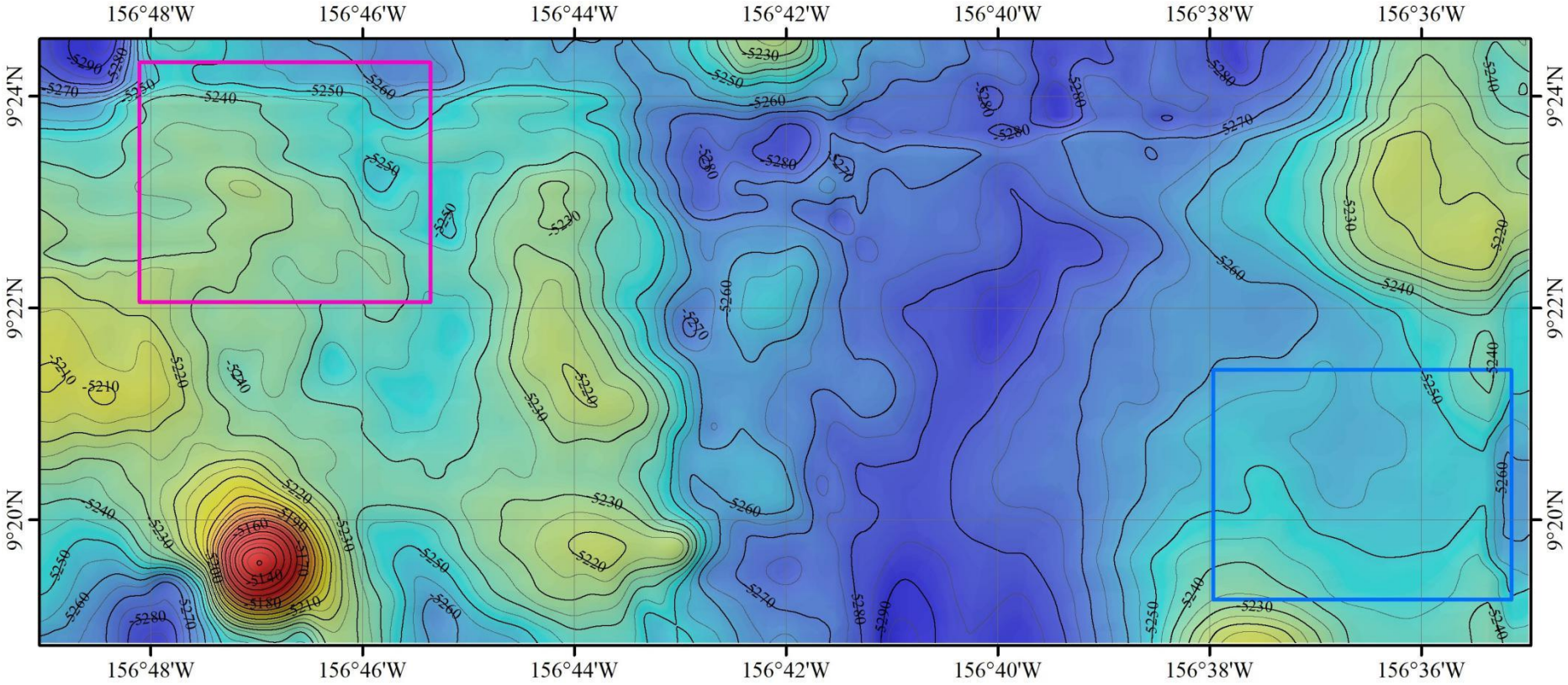

Figure 4.5-3 Topographic map of AUV testing depth in the TMA of the Block A-5

(Blue and pink boxes refer to IRZ and PRZ, respectively)

4.5.2 Nodule characteristics

The nodule abundance at 50 box corer sampling stations in the TMA of the Block A-5 is in the range of 0.5-25.92 kg/m^2, averaging 14.04±4.69 kg/m^2. The nodule abundance has the characteristics of negative skewness distribution, with the peak value being 15-16 kg/m^2, which is close to the average value (Figure 4.5-4). The shipboard photography coverage of 50 box corer sampling stations varies in the range of 2-85 %, averaging 43.34±15.0924 %. Shipboard photography coverage has the characteristics of negative skewness distribution, with the peak value being 40-45 %, which is close to the average value (Figure 4.5-5). There is a sound positive correlation between shipboard photography coverage and nodule abundance (Figure 4.5-6), and the correlation coefficient R^2 is as high as 0.82, which indicates that the particle size distribution of nodules in this area is generally uniform.

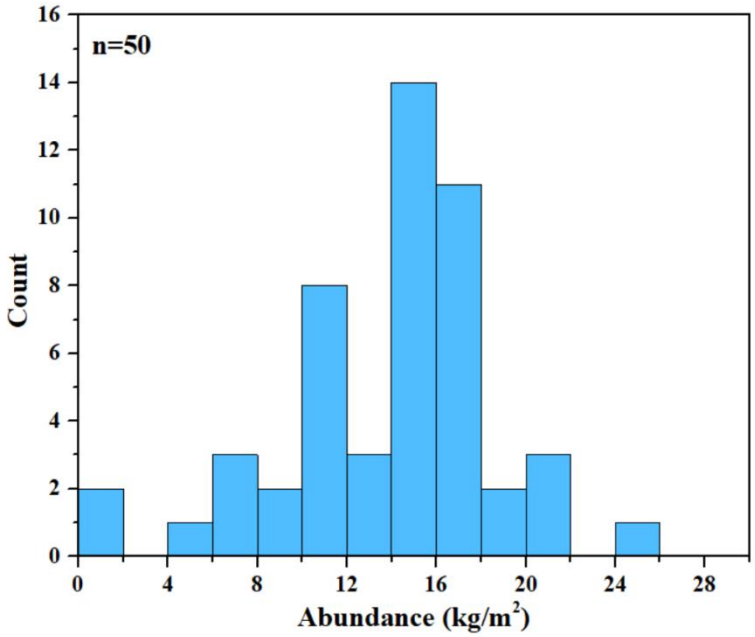

Figure 4.5-4 Distribution of nodule abundance frequencies at box corer stations in the TMA of the Block A-5

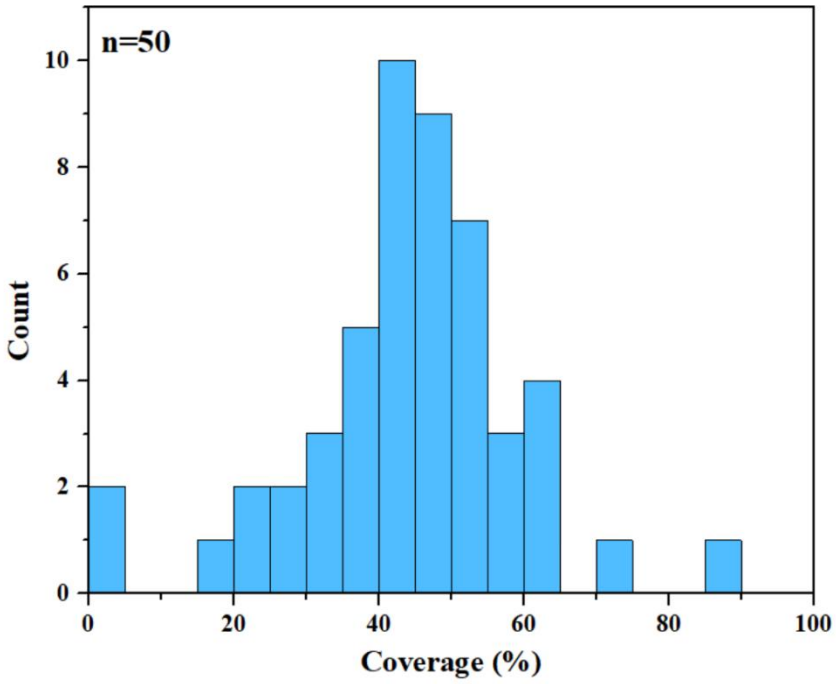

Figure 4.5-5 Distribution of shipboard photography coverage for nodules in the TMA of the Block A-5

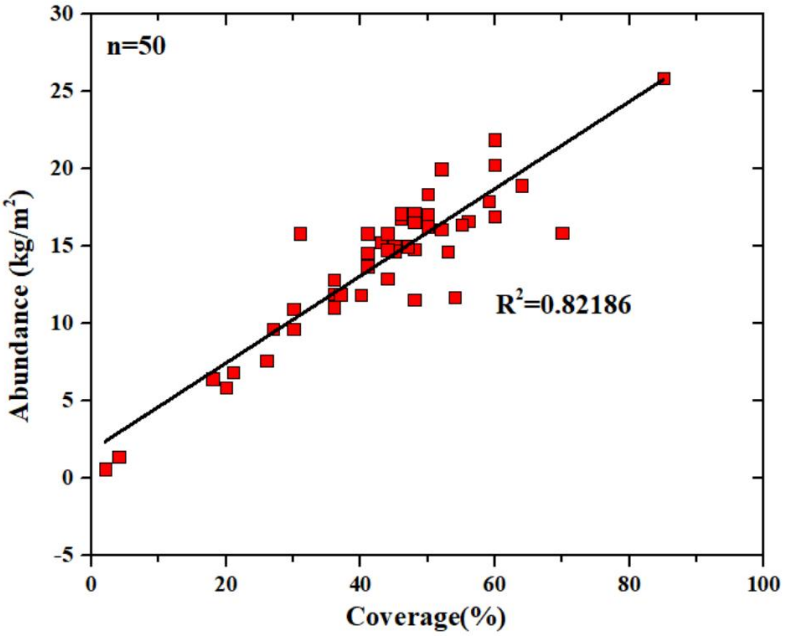

Figure 4.5-6 Relationship of nodule abundance and shipboard photography coverage at box corer stations in the TMA of the Block A-5

Using the inverse distance weighted interpolation method, we conducted spatial interpolation for the nodule abundance and NEG in the TMA of the Block A-5, and obtained their spatial distribution characteristics (Figures 4.5-7 and 4.5-8). Results show that the areas with high nodule abundance (>15 kg/m^2) in the TMA are mainly

distributed in the west, while the nodule abundance of most areas in the middle and east is 10-15 kg/m^2. The nodule abundance of the IRZ and PRZ is also in this range. The nodule NEG is high in the east and west but low in the middle, while the low value areas are mainly located near the IRZ and PRZ. Generally speaking, the nodule abundance and NEG of the IRZ and PRZ are similar.

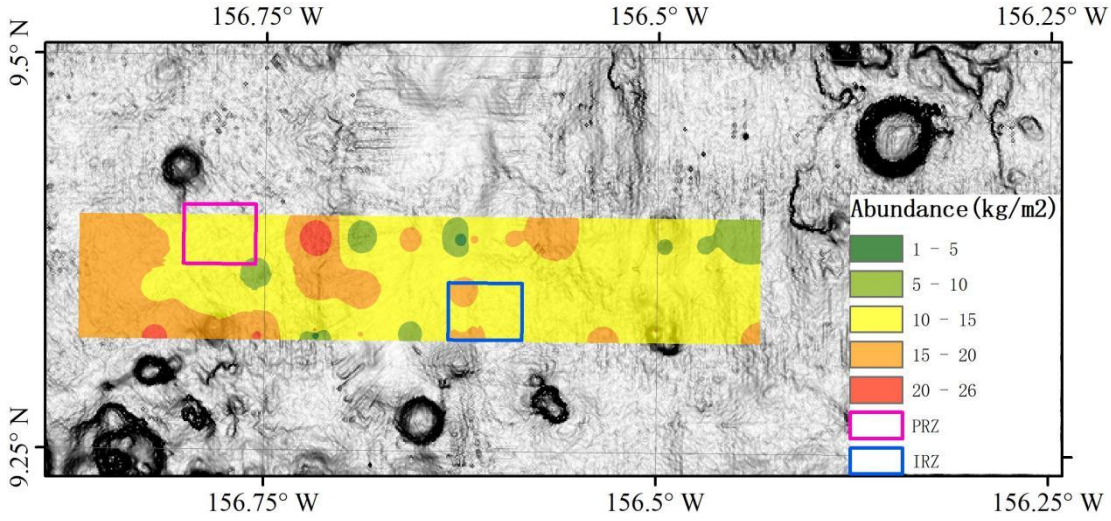

Figure 4.5-7 Isolines of nodule abundance in the TMA of the Block A-5

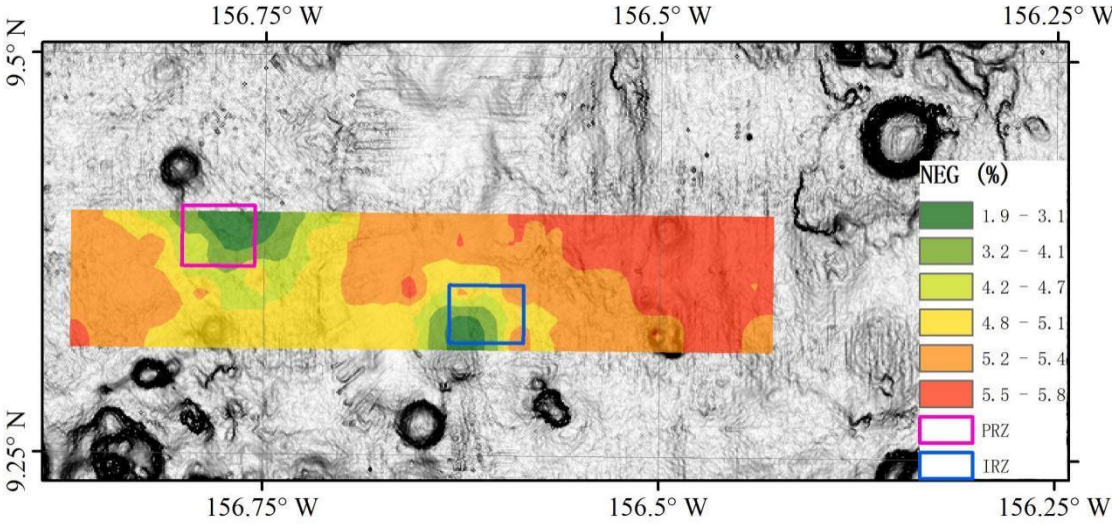

Figure 4.5-8 Isolines of nodule NEG in the TMA of the Block A-5

NEG=0.13×Mn%+0.42×Cu%+2.64×Co%+Ni%

Besides, nodule coverage in the TMA of the Block A-5 is relatively high. The results of near-bottom optical observation using AUV show that the nodule coverage rate is mainly 40-70 %, which is consistent with the results of box corer sampling (Figure 4.5-9). This indicates that nodules in the TMA are mainly exposed. There are

three kinds of spacing for AUV optical survey lines: 400 m, 200 m and 50 m. The length of a single survey line is usually less than 8 km, and the nodule coverage rate varies greatly within this distance; the nodule continuity perpendicular to the survey line is usually less than 2 km. This means that the distribution of nodules in the TMA is uneven on a small scale, and nodule with different coverage rates are distributed in sheet form.

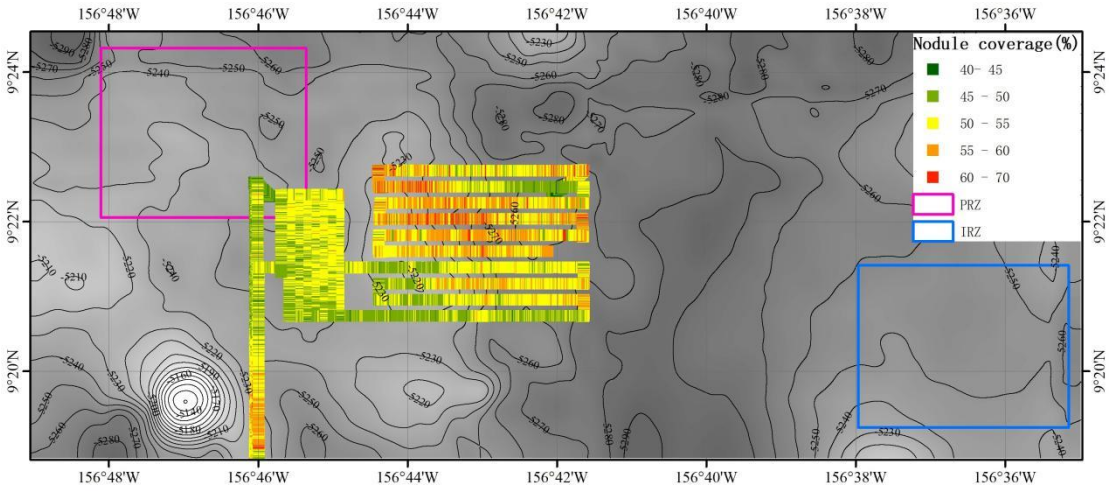

Figure 4.5-9 Distribution characteristics of AUV optically surveyed nodule coverage in the TMA of the Block A-5

4.5.3 Sedimentary characteristics

4.5.3.1 Sedimentary characteristics

In this section, the grain size, heavy metal concentration and organic matter of surface-layer sediment samples obtained with box corer at 109 stations and columnar sediment samples collected at two stations (DY70II-A5-GC02 and DY70I-A5-GC03) in the PWA of the Block A-5 are analyzed (see Figure 4.3-4).

(1) Particle size characteristics of sediment

According to the Folk classification standard, the surface-layer sediments in the Block A-5 are classified by particle size, with the particle sizes D=3.9 μm and 63 μm as the boundary values of clay, silt and sand. The silt-grade content of sediments in this zone is the highest, averaging approximately 53 %. Next comes the clay-grade content, which averages approximately 35 %. The sand-grade content is relatively low,

averaging approximately 15 %. According to the frequency distribution curve, there are two different peak states of particle size distribution in the Block A-5: single peak and double peak. Most samples have two peaks of ~3 μm and ~60 μm, while a few samples have a single peak with a particle size of 10-20 μm (Figure 4.5-10). Since the Block A-5 is far from the continent, most of the sand- and silt-grade particles are of biological origin, mainly radiolarians and Bacillariophyta. Some fish tooth fossils and iron-manganese oxide particles also contributed to the content variation of coarse components.

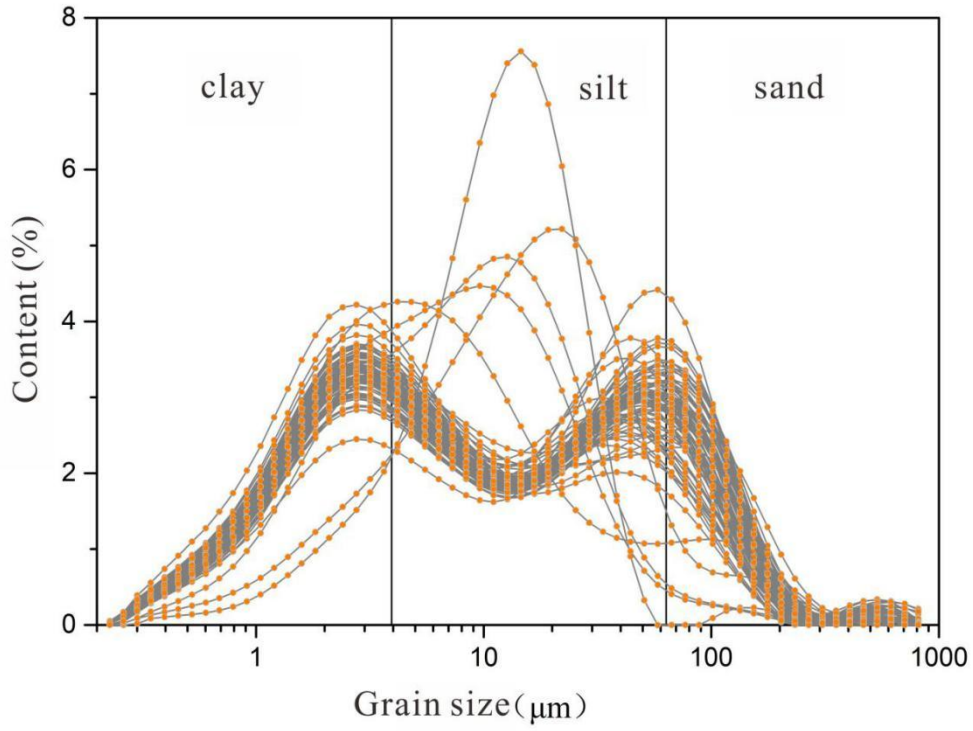

Figure 4.5-10 Sediment contents by particle size in the PWA of the Block A-5 (%)

The spatial distribution characteristics of average particle size (Mz_Φ, Φ=-log2D) and median particle size (Md_μm) of surface-layer sediments (Figure 4.5-11) show that sediment particles near the central sea knoll chain in the PWA are the finest, with a relatively high proportion of clay-grade components and poor sorting performance (δ >2). However, in the basin zone on both sides of the sea knoll chain, the particles are coarser, the proportion of silt-grade components is higher, and the sorting performance is worse (δ=2.2-2.5). This reflects that the biodetritus content in sediments is lower near the sea knoll chain than in the basins on both sides.

There are great differences in the historical sedimentary environment between the northern and southern basins of the central sea knoll chain. Columnar sediments collected at DY70I-A5-GC02 station in the southern basin are mainly composed of silt-grade and sand-grade components, with only a small amount of lay-grade components. Columnar sediments collected at DY70I-A5-GC03 in the northern basin are mainly silt- and clay-grade components, with only a small amount of sand-grade components (Figure 4.5-12). Vertically, the component contents of columnar sediment collected at DY70I-A5-GC02 station vary greatly with the increasing depth, and there is not an obvious trend. The contents of silt- and clay-grade components in columnar sediments collected at DY70I-A5-GC03 station gradually increase, while those of sand-grade components gradually decreases with the increasing depth.

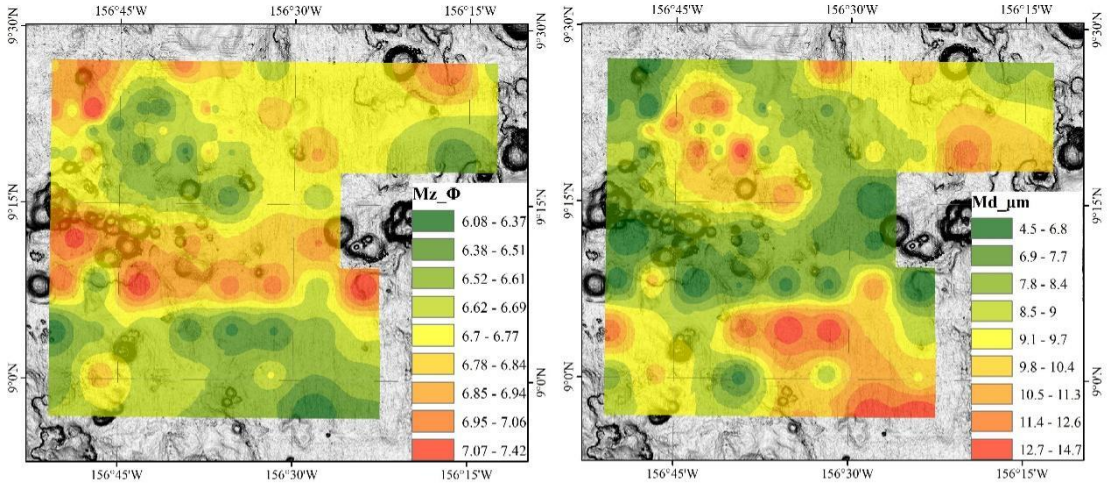

Figure 4.5-11 Spatial distribution of sediments of different particle sizes in the PWA of the Block A-5

The bottom map is a gray-scale topographic map.

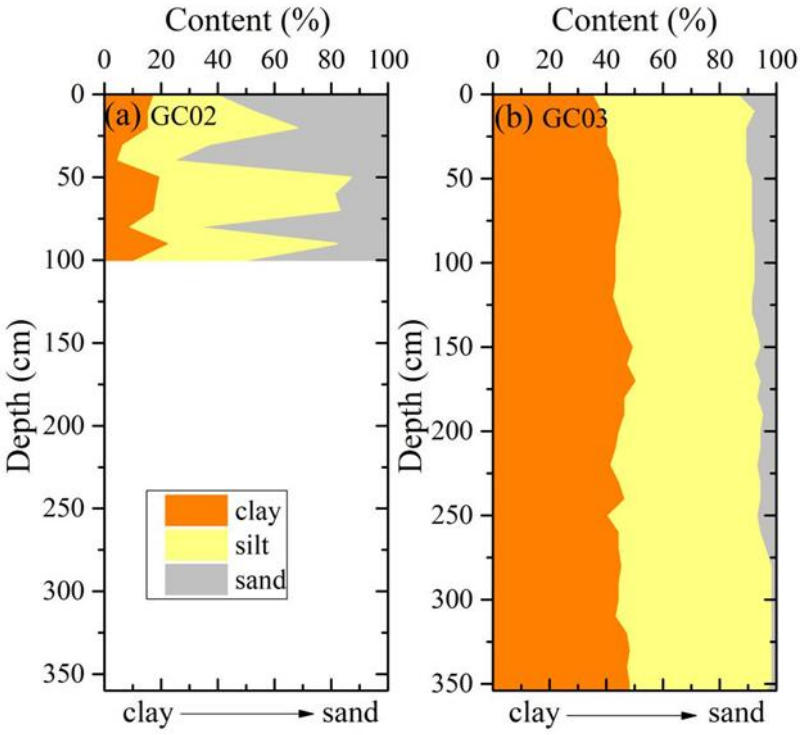

Figure 4.5-12 Vertical variation in the fractional components of columnar sediment in the Block A-5

（2）Heavy metal concentration in sediment

The distribution of heavy metals (e.g. Cd, Cr, Ni, Cu, Zn and Pb) in the surface-layer sediments of the PWA in the Block A-5 is uneven (Figure 4.5-13), and the coefficients of variation (standard deviation/average) are 0.2, 0.18, 0.23, 0.13, 0.13 and 0.06 respectively. In terms of spatial distribution, high Cd concentration is mainly distributed in the central basin in the north and the southeast of the southern basin in the PWA. Ni, Cu, Zn and Pb have strong similarity, that is, the concentrations of heavy metals are high in the northeast and southwest corners of the PWA, but generally low in other blocks. However, the distribution characteristics of Cr are just the opposite to those of Ni, Cu, Zn and Pb. The Cr are high in most parts of the PWA, except in the northeast and southwest corners. Compared with the spatial distribution of sediment heavy metals in the NORI-D region, the distribution of Ni, Cu and Zn is also similar. However, the distribution of Cr and Pb as well as other heavy metals has no obvious regularity (NORI 2022).

The heavy metal concentrations of columnar sediments in the northern and southern basins of the PWA vary greatly. The concentrations of heavy metals (e.g. Ni, Cd, Cu, Zn and Pb) in the columnar sediments collected at DY70I-A5-GC02 station in the southern basin are higher than those in the columnar sediments collected at the DY70I-A5-GC03 station in the northern basin. However, the Cr is lower in the former than in the latter (Figure 4.5-14). The concentrations of heavy metals in columnar sediments collected at DY70I-A5-GC03 station vary slightly, while those in the columnar sediments collected at DY70I-A5-GC02 station tend to decrease gradually with the increasing depth (except at the surface layer and 100 cm depth layer). The vertical variations of heavy metal concentrations in sediments at 0-1 cm, 1-5 cm and 5-10 cm depths were investigated in the NORI-D region. Results showed that the maximum concentrations of Cr, Ni, Cu, Zn and Pb all appeared at 0-1 cm depth. Comparatively speaking, the sampling depths of sediments in the Block A-5 are deeper and the variations are more complicated (NORI 2022).

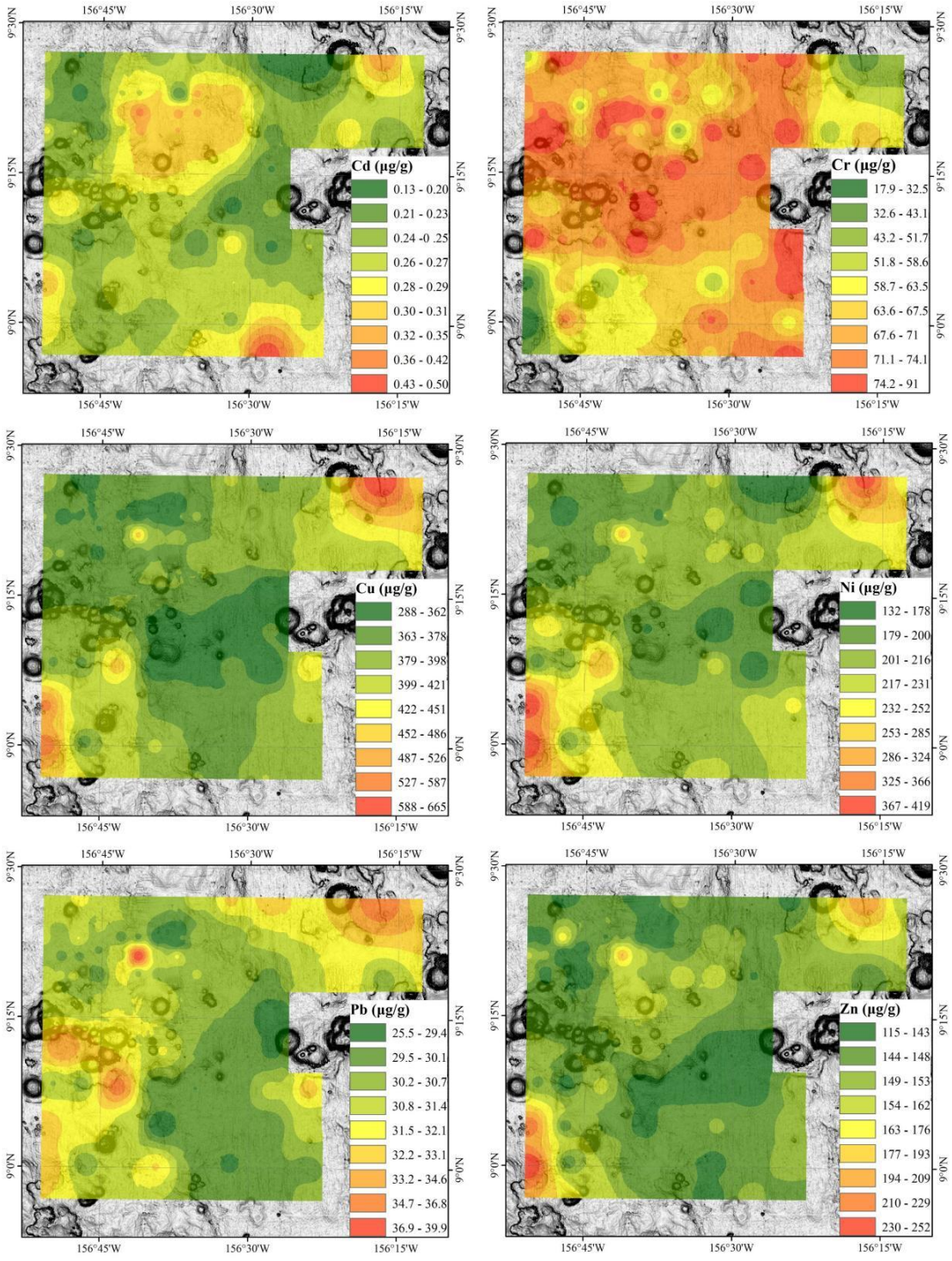

Figure 4.5-13 Distribution of heavy metal concentrations in the sediments in the PWA of the Block A-5

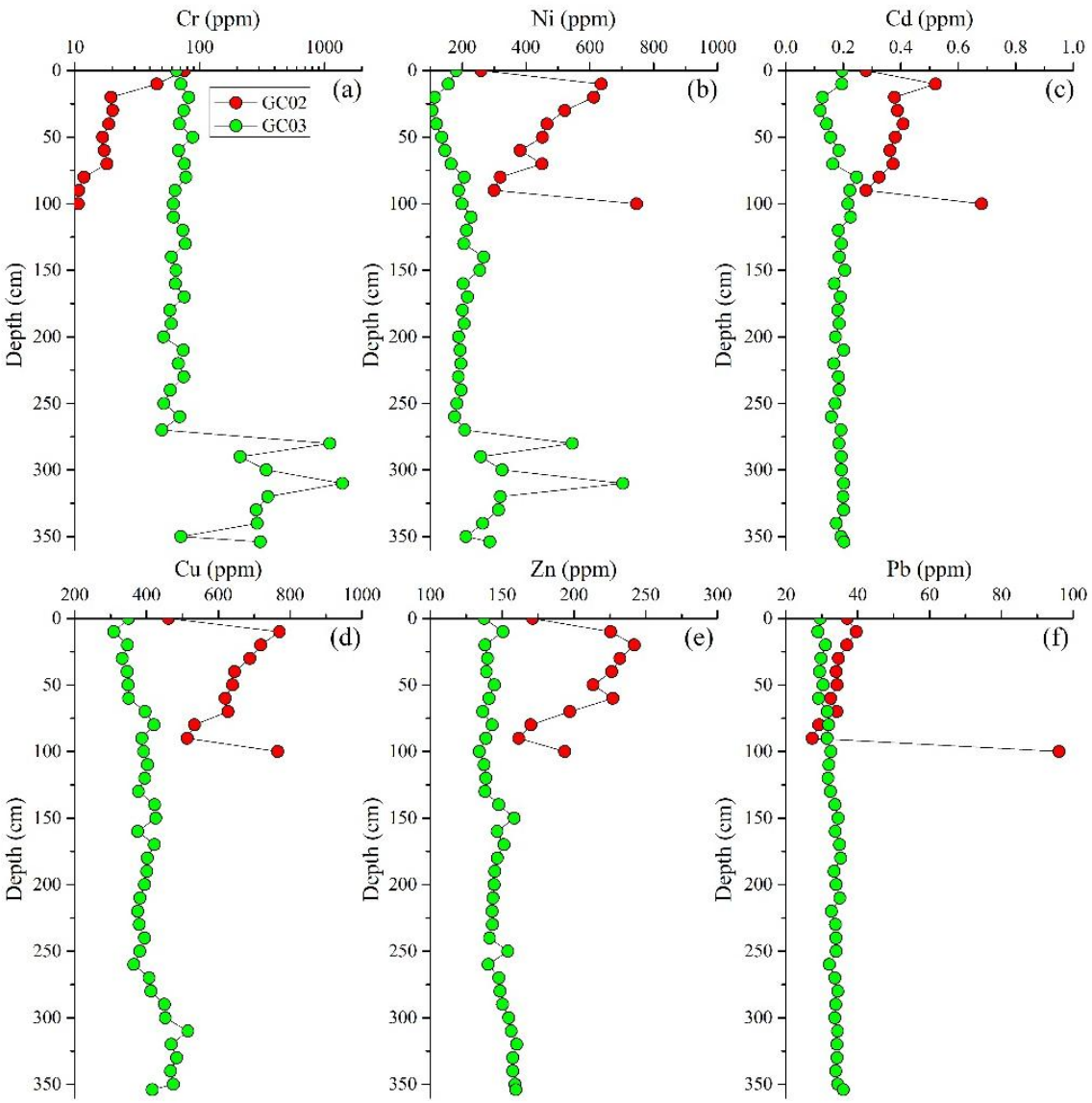

Figure 4.5-14 Vertical variation of heavy metal elements in columnar sediments in the PWA of the Block A-5

（3）TOC and total nitrogen (TN) in sediments

The distribution of TOC contents is uneven in the GEA (Figure 4.5-15). The organic carbon content is less than 0.25 % in the northeast and southwest corners of the Block, 0.25-0.35 % near the central sea knoll chain; and 0.35-0.45 % in the northern and southern basins of the sea knoll chain.

The TOC and TN in columnar samples collected at DY70I-A5-GC02 station are between 0.13-0.31 % and 0.02-0.08 %, which are higher than those (0.16-0.38 % and 0.06-0.09 %) in columnar samples collected at DY70I-A5-GO03 station.Besides, the

TOC and TN contents tend to decrease gradually with the increasing depth (Figure 4.5-16).

The TOC content in the surface-layer sediments (0-30 cm) in the NORI-D region decreases with increasing depth. The TOC content is 0.1-0.7 %, which is consistent with the variation trend of the profile in the Block A-5, but the variation range is larger and the decline is faster (NORI 2022).

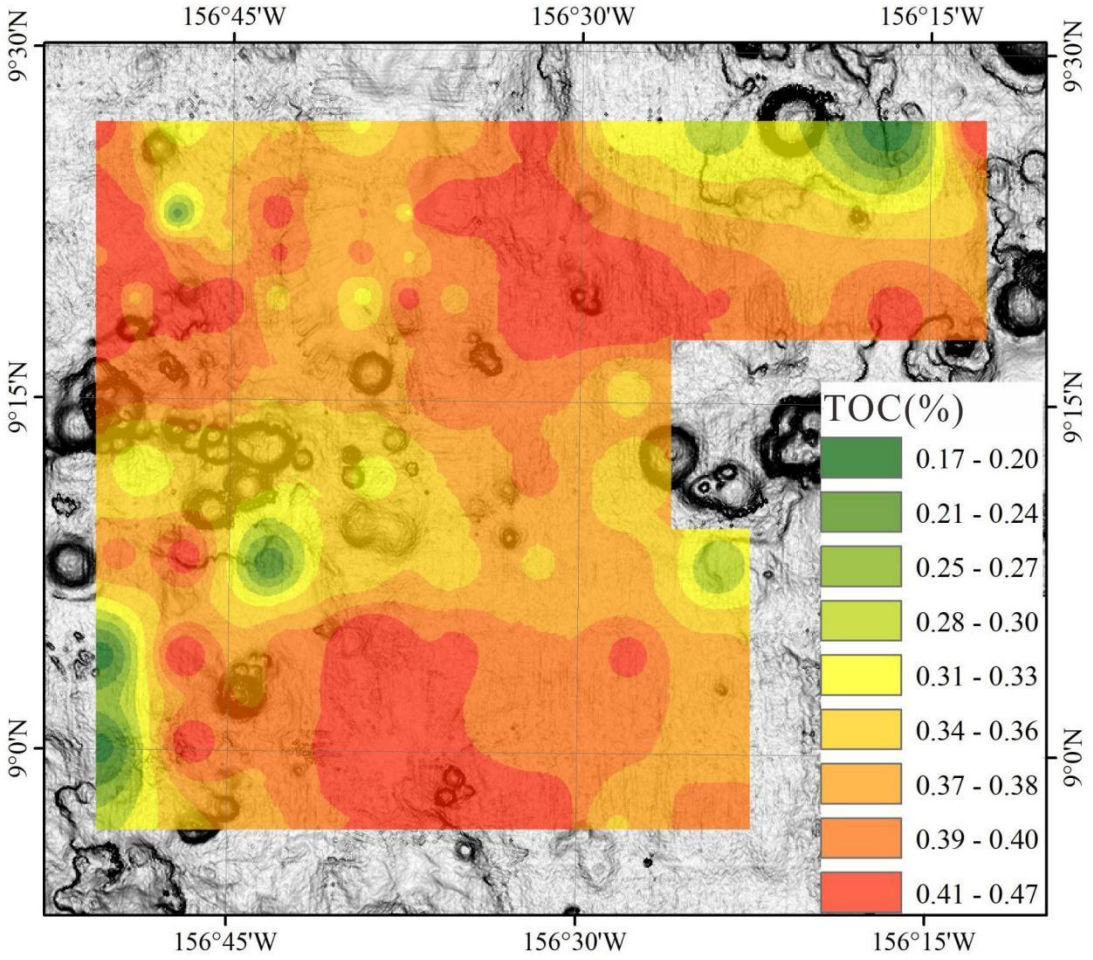

Figure 4.5-15 Distribution of organic carbon contents in the surface-layer sediment in the PWA of the Block A-5

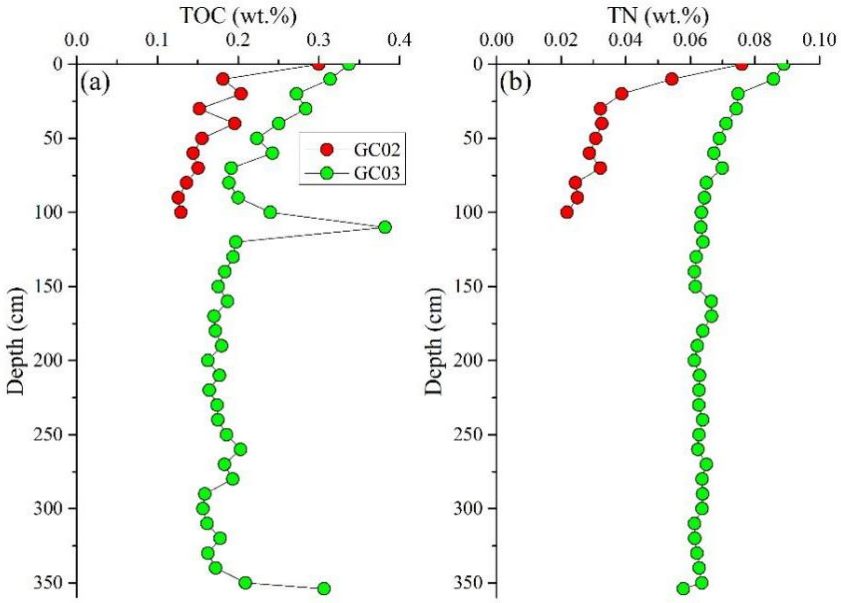

Figure 4.5-16 Vertical variation of organic matters in the columnar sediments in the PWA of the Block A-5

（4）Sediment Chl *a*

During the 2022 survey cruise, we have carried out the sampling observation of sediment Chl *a* at nine stations in the Block A-5 of East Pacific Ocean (Figure 4.3-4), obtaining 90 samples of layered sediment Chl *a*.

According to the requirements of the regulations, the Chl *a* concentration per unit wet weight sediment (Chl concentration 1) and the Chl *a* concentration per unit dry weight sediment (Chl concentration 2) can be calculated, with the unit being μg/g. In this survey, the moisture contents of sediment samples from 90 layers at nine stations are in the range of 58.14-87.32 %, averaging 74.04±4.65 %. The moisture contents of the upper-layer core samples are significantly higher than those of the lower-layer core samples. The moisture contents of the surface-layer sediment samples are the highest, averaging 82.59 % (Table 4.5-1).

The measured Chl *a* concentrations per unit wet weight sediment are in the range of 0-0.0239 μg/g, averaging 0.0042±0.0043 μg/g. The measured Chl *a* concentrations per unit dry weight sediment are in the range of 0.0001-0.1058 μg/g, averaging 0.0183±0.0217 μg/g. Among them, the average Chl concentrations in all sampling

layers at DY73I-A5-MC08 and DY73I-A5-MC01 stations are significantly higher than those at other stations (Tables 4.5-2 and 4.5-3).

Comparison of the average Chl *a* concentrations per unit wet weight and those per unit dry weight of samples collected from different sampling layers at relevant stations shows that both the wet weight and dry weight Chl *a* concentrations are the highest in surface-layer sediments; with the increasing depth, the Chl *a* concentration shows a gradual downward trend (Table 4.5-1). This is mainly because Chl *a* concentration in lower-layer sediments gradually decreases after a longer period of burial degradation.

The vertical distribution of Chl *a* concentrations per unit dry weight sediment at relevant stations also shows the above-mentioned vertical distribution characteristics (Figure 4.5-17). Except DY73I-A5-MC08, other stations have the highest Chl *a* concentrations in surface-layer sediments and relatively low Chl *a* concentrations in lower-layer sediments.

The concentration of Chl *a* in the NORI-D region varies greatly in the spatial sense, ranging from undetectable to 132.7 mg/kg (NORI 2022).

Table 4.5-1 Average Chl *a* concentrations and moisture contents in sediment core samples collected from the Block A-5

Sampling layer (cm)	Chl *a* concentration 1 (Wet weight) μg/g	Chl *a* concentration 2 (Dry weight) μg/g	Moisture content of sediment %
0-1	0.0096±0.0043	0.0547±0.0245	82.59±3.24
1-2	0.0063±0.0046	0.0293±0.0217	78.21±3.33
2-3	0.0060±0.0066	0.0241±0.0254	75.52±1.87
3-4	0.0039±0.0029	0.0145±0.0094	73.79±2.06
4-5	0.0033±0.0024	0.0116±0.0090	71.79±1.73
5-6	0.0019±0.0010	0.0068±0.0036	72.15±2.26
6-7	0.0015±0.0028	0.0052±0.0120	71.69±2.16

7-8	0.0019±0.0018	0.0064±0.0067	70.75±2.24
8-9	0.0022±0.0033	0.0075±0.0119	69.77±4.45
9-10	0.0017±0.0014	0.0060±0.0052	70.61±1.69
Total average	0.0042±0.0043	0.0183±0.0217	74.04±4.65

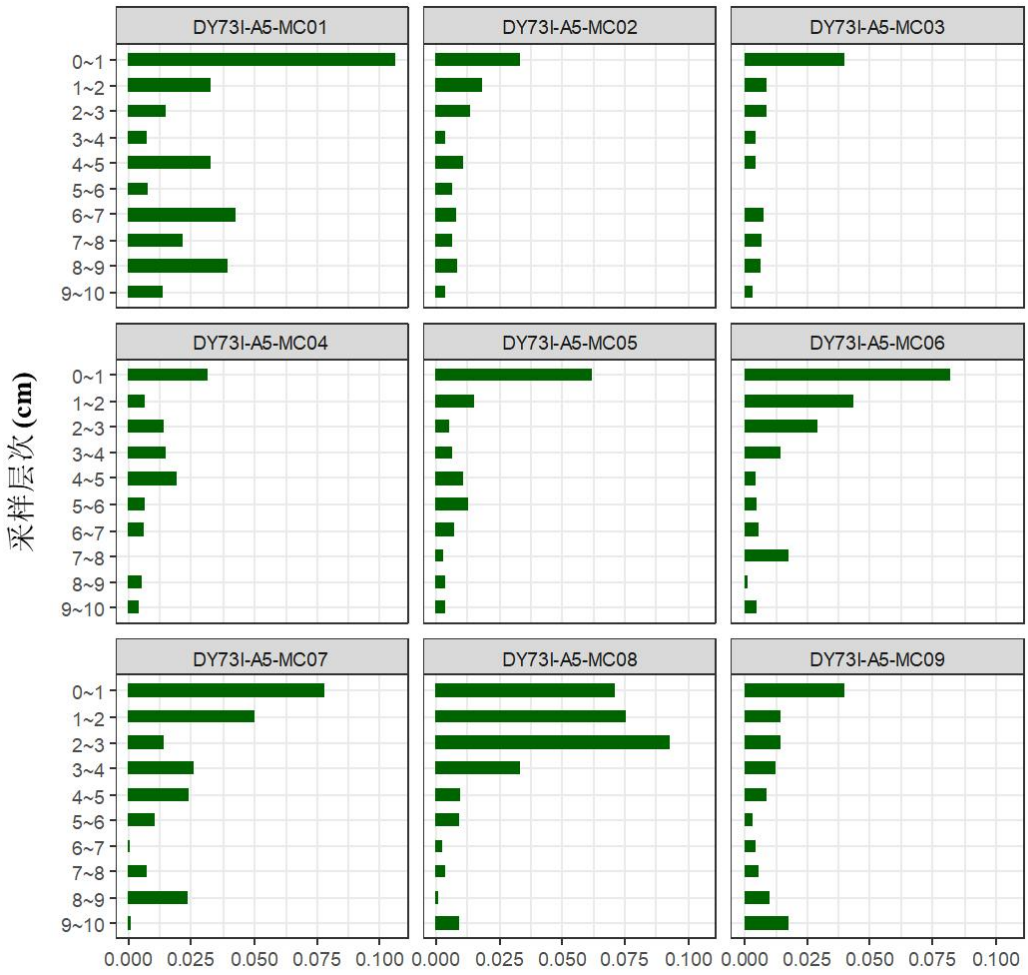

Figure 4.5-17 Vertical distribution of Chl *a* concentrations per unit dry weight sediment at relevant stations in the Block A-5 (μg/g)

Table 4.5-2 Determination results of Chl *a* concentrations per unit wet weight sediment in the Block A-5 (μg/g)

Sampling layer (cm)	MC01	MC02	MC03	MC04	MC05	MC06	MC07	MC08	MC09
0-1	0.0162	0.0051	0.0055	0.0069	0.0079	0.0134	0.0142	0.0162	0.0073
1-2	0.0057	0.0029	0.0023	0.0014	0.0040	0.0091	0.0120	0.0156	0.0032
2-3	0.0032	0.0033	0.0021	0.0037	0.0013	0.0066	0.0039	0.0239	0.0031
3-4	0.0017	0.0008	0.0012	0.0036	0.0017	0.0037	0.0071	0.0101	0.0032
4-5	0.0087	0.0030	0.0013	0.0053	0.0031	0.0011	0.0071	0.0028	0.0028
5-6	0.0019	0.0017	0.0000	0.0018	0.0037	0.0015	0.0031	0.0027	0.0010
6-7	0.0101	0.0025	0.0021	0.0015	0.0020	0.0017	0.0002	0.0006	0.0012
7-8	0.0056	0.0022	0.0018	0.0000	0.0008	0.0051	0.0021	0.0010	0.0018
8-9	0.0109	0.0025	0.0017	0.0016	0.0016	0.0005	0.0069	0.0003	0.0026
9-10	0.0037	0.0010	0.0011	0.0012	0.0010	0.0015	0.0003	0.0029	0.0049
Average	0.0068	0.0025	0.0019	0.0027	0.0027	0.0044	0.0057	0.0076	0.0031

Table 4.5-3 Determined Chl *a* concentrations per unit dry weight sediment in the Block A-5 (μg/g)

Sampling layer (cm)	MC01	MC02	MC03	MC04	MC05	MC06	MC07	MC08	MC09
0-1	0.1058	0.0331	0.0398	0.0314	0.0620	0.0822	0.0783	0.0710	0.0400
1-2	0.0329	0.0186	0.0090	0.0070	0.0156	0.0439	0.0502	0.0758	0.0143
2-3	0.0148	0.0135	0.0088	0.0141	0.0052	0.0297	0.0145	0.0927	0.0143
3-4	0.0073	0.0034	0.0046	0.0149	0.0069	0.0144	0.0257	0.0332	0.0127
4-5	0.0329	0.0108	0.0046	0.0191	0.0111	0.0044	0.0242	0.0097	0.0090
5-6	0.0082	0.0068	0.0002	0.0065	0.0131	0.0054	0.0106	0.0088	0.0034
6-7	0.0426	0.0078	0.0076	0.0060	0.0071	0.0061	0.0008	0.0022	0.0044
7-8	0.0217	0.0065	0.0069	0.0001	0.0029	0.0177	0.0076	0.0033	0.0061
8-9	0.0398	0.0082	0.0063	0.0054	0.0038	0.0018	0.0233	0.0009	0.0103

9-10	0.0137	0.0034	0.0036	0.0044	0.0034	0.0049	0.0011	0.0092	0.0176
Average	0.0320	0.0112	0.0091	0.0109	0.0131	0.0211	0.0236	0.0307	0.0132

4.5.3.2 Chemical properties of sediment pore water

for the sediments (approximately shallower than 31 cm) collected with multicorer in PRZ (D73I-A5-MC02) and IRZ (D73I-A5-MC06) in the Block A-5 during the 2022 survey cruise, we have analyzed their heavy metal and nutrient concentrations and total alkalinity in the bottom-layer seawater/sediment pore water. See Figure 4.3-4 for the distribution of stations. The sediment pore water was collected with a Rhizon head and a syringe, and the amount of pore water collected from sediment samples shallower than 5 cm was 15-25 mL.

(1) The concentration of heavy metal in pore water

The concentration of heavy metal in pore water was sampled at 5 cm intervals and analyzed by inductively coupled plasma mass spectrometry. See Figure 4.5-18 for test results.

Among the nine heavy metals analyzed, Zn and V are the highest while Pb is the lowest. The overlying water collected at two stations have generally similar heavy metal concentrations, with DY73I-A5-MC02 station featuring slightly higher and the concentrations of Cr, Co, Ni and Cd and slightly lower concentrations of V, Cu, Zn, As and Pb.

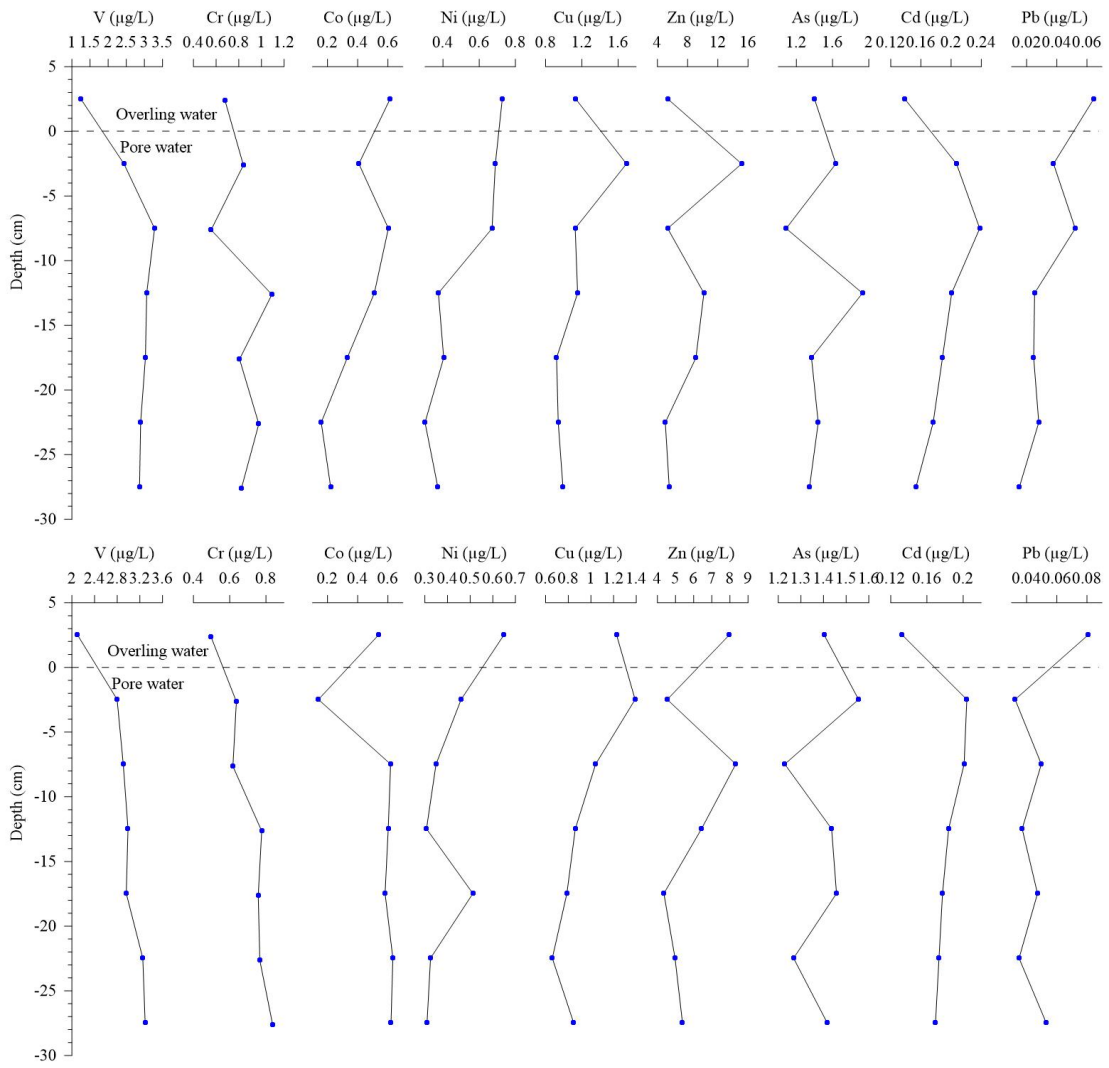

Figure 4.5-18 Vertical distribution of heavy metal concentrations in the overlying water and pore water of sediments in the PWA of the Block A-5

(Upper: D73I-A5-MC02, lower: D73I-A5-MC06)

At DY73I-A5-MC02 station, heavy metals can be divided into three categories according to the variation of depth profile. The first category (represented by V, Cr and Cd) has significantly lower concentrations in overlying water than in pore water. The second category (represented by Co, Ni and Pb) has significantly higher concentrations in overlying water than in pore water. The third category (represented by Cu, Zn and As) have the highest concentrations in the upper part (0-15 cm layer) of pore water.

At DY73I-A5-MC06 station, heavy metals can also be divided into three categories according to the variation of depth profile. DY73I-A5-MC02 station has a

similar classification, except that the highest concentration of Co appears in the deep-layer pore water instead of the overlying water.

(2) Nutrients in pore water

The concentrations of nutrients (silicate, reactive phosphate, nitrite and nitrate) in pore water were sampled at 5 cm intervals and analyzed by spectrophotometry. See Table 4.5-4 and Figure 4.5-19 for test results.

Table 4.5-4 Test results of nutrient concentrations in the overlying water and pore water of sediments in the PWA of the Block A-5

Station No.	Sample No.	Layer	Silicate (μmol/L)	Reactive phosphate (μmol/L)	Nitrite (μmol/L)	Nitrate (μmol/L)
DY73I-A5-MC02	M02-0	Overlying water	213.09	1.58	0.14	40.95
	M02-1	0-5cm	296.92	1.25	0.13	41.39
	M02-2	5-10cm	333.33	1.38	0.12	39.78
	M02-3	10-15cm	373.76	1.61	0.15	38.74
	M02-4	15-20cm	393.31	1.22	0.14	38.92
	M02-5	20-25cm	409.91	1.67	0.10	38.92
	M02-6	25-30cm	440.10	1.81	0.10	37.06
DY73I-A5-MC06	M06-0	Overlying water	199.22	1.53	0.13	43.75
	M06-1	0-5cm	307.69	1.22	0.12	44.53
	M06-2	5-10cm	346.00	1.19	0.18	45.44
	M06-3	10-15cm	373.27	1.34	0.25	43.86
	M06-4	15-20cm	398.92	1.54	0.22	42.17
	M06-5	20-25cm	419.52	1.22	0.16	41.10
	M06-6	25-30cm	440.61	1.79	0.22	36.58

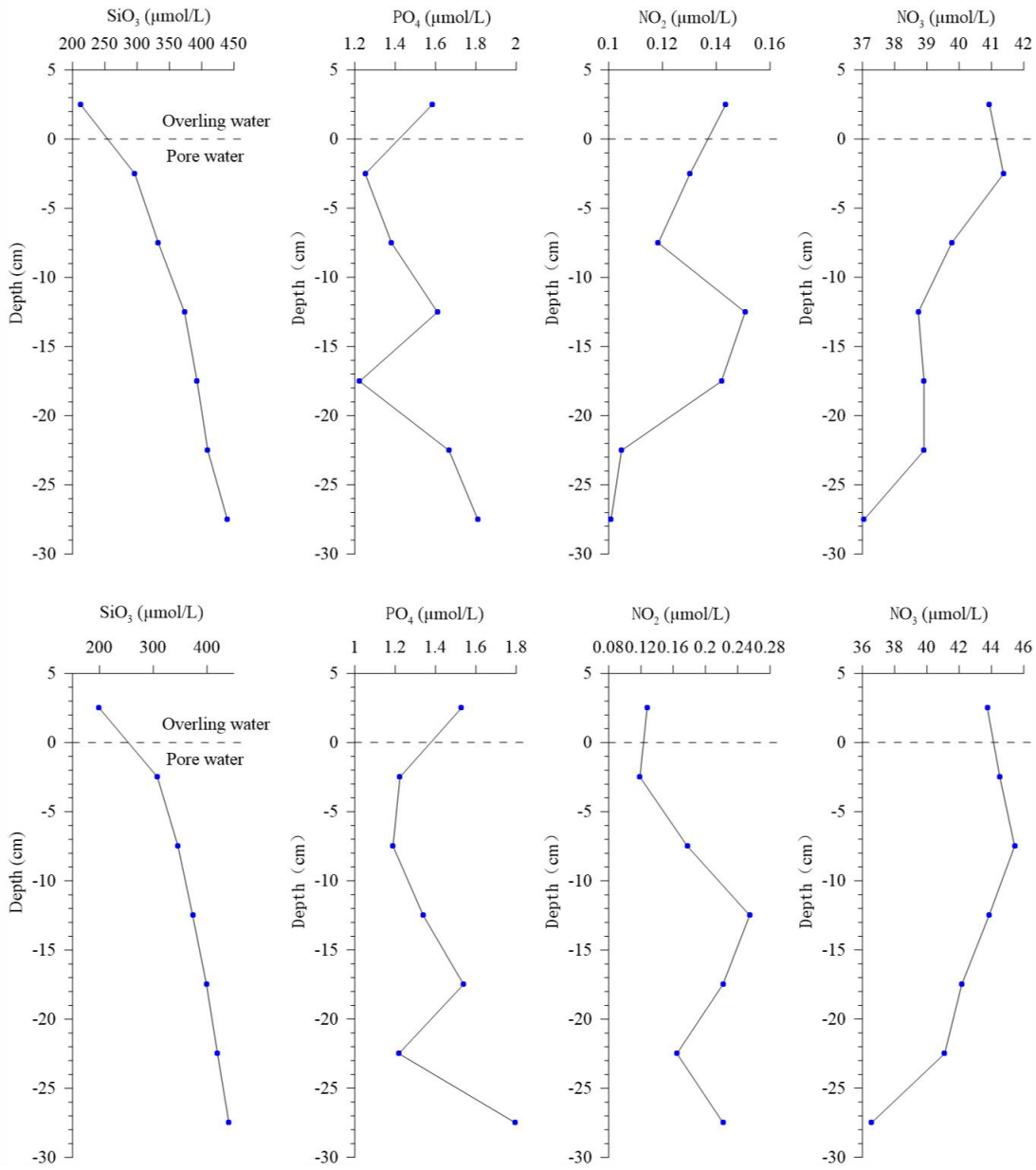

Figure 4.5-19 Vertical distribution of nutrient concentrations in the overlying water and pore water of sediment

(Upper: D73I-A5-MC02, lower: D73I-A5-MC06)

The concentrations of silicate, reactive phosphate, nitrite and nitrate in the pore water of sediment at DY73I-A5-MC02 station are 296.92-440.10 μmol/L (averaging 374.56 μmol/L), 1.22-1.81 μmol/L (averaging 1.49μmol/L), 0.10-0.15 μmol/L (averaging 0.12 μmol/L) and 37.06-41.39 μmol/L (averaging 39.14 μmol/L) respectively. The concentration of silicate is higher in sediment pore water than in overlying water, while the concentrations of reactive phosphate, nitrite and nitrate in sediment pore water are generally close to or slightly lower than those in overlying

water. With increasing depth, the concentrations of silicate and reactive phosphate in the pore water of sediments gradually increase, reaching the maximum at the bottom (25-30 cm layer), but the concentrations of nitrite and nitrate show an opposite trend. The concentration of silicate in sediment pore water increases with depth, which is mainly related to the unsaturated dissolution of silicate. The distribution of nitrite and nitrate concentrations at different depths is mainly related to the mineralization and degradation of organic matter and redox conditions.

The concentrations of silicate, reactive phosphate, nitrite and nitrate in the pore water of sediment at DY73I-A5-MC06 station are 307.69-440.61 μmol/L (averaging 381.00 μmol/L), 1.19-1.79 μmol/L (averaging 1.38 μmol/L), 0.12-0.25 μmol/L (averaging 0.19 μmol/L) and 36.58-45.44 μmol/L (averaging 42.28 μmol/L) respectively. The concentration of silicate is higher in sediment pore water than in overlying water, while the concentrations of reactive phosphate, nitrite and nitrate in sediment pore water do not have such a pattern. With increasing depth, the concentrations of silicate and reactive phosphate in the pore water of sediments gradually increase, reaching the maximum at the bottom (25-30 cm layer), but the nitrate concentration has an opposite trend, and the variation trend of nitrite concentration is not obvious.

At the two stations for surveying sediment pore water, the total nutrient concentrations in pore water are close, and the nutrient variation trends of with depth are also similar. The survey results show that the variation trends of nutrients in sediment pore water in the IRZ and PRZ are basically the same.

The silicate and nitrate concentrations in sediment pore water in the Block A-5 are similar to those in the NORI-D region (NORI 2022), but the survey results of nitrite and reactive phosphate are lower in the Block A-5 than in the NORI-D region.

(3) Total alkalinity in pore water

The total alkalinity in pore water in 0-15 cm and 15-30 cm layers in sediments collected with multicorer was analyzed by potentiometric titration. The total alkalinity

in pore water in the 0-15 cm and 15-30 cm layers of DY73I-A5-MC02 station is 2.410 mmol/L. The total alkalinity in pore water in the 0-15 cm and 15-30 cm layers of DY73I-A5-MC06 station are 2.401 mmol/L and 2.406 mmol/L, respectively. This result shows that IRZ and PRZ have very close total alkalinity, and the total alkalinity varies little in the range of 0-30 cm. The survey results of pore water alkalinity in the NORI-D region are similar to those in the Block A-5. The alkalinity range is 2.8±0.2 mM, and basically remains the same in the depth of 0-22 cm (NORI 2022).

4.5.3.3 Geotechnical properties

We carried out in-situ geotechnical properties tests in the Block A-5 during Minmetals' 2021, 2022 and 2023 survey cruises, obtaining 51 sets of in-situ test data of penetration strength and 35 sets of in-situ test data of shear strength. See Figure 4.3-4 for the distribution of stations.

The penetration depth is in the range of 0-900 mm. The penetration strength data were recorded every 50 mm, and the statistical data of penetration strength in different depths of the Block A-5 are shown in Figure 4.5-20. The average variation rate of penetration strength corresponding to the first 300 mm penetration depth is lower than that corresponding to the last 300 mm penetration depth, which may because that with increasing depth, the penetration strength of seabed sediments increases more obviously and the sediments are harder.

Shear strength was measured for 150 mm, 300 mm, 450 mm and 600 mm layers. The maximum shear strength and the average value after sediment shear failure were statistically analyzed (Figure 4.5-21). Results show that the average values of maximum shear stress and residual shear stress of all data groups have little difference from the median line. From the maximum shear stress analysis of means at different depths, there is a good linear relationship between the maximum shear stress and the shear depth (straight line state). According to the analysis of residual shear stress after sediment failure at different depths, there is a certain linear relationship between residual shear stress and measured depth, but its overall variation range is small.

Comparison between the maximum shear strength of the same layer and the residual shear stress after sediment failure shows that the residual shear stress of the sediment decreases sharply after sediment failure, and the difference between them increases with increasing depth.

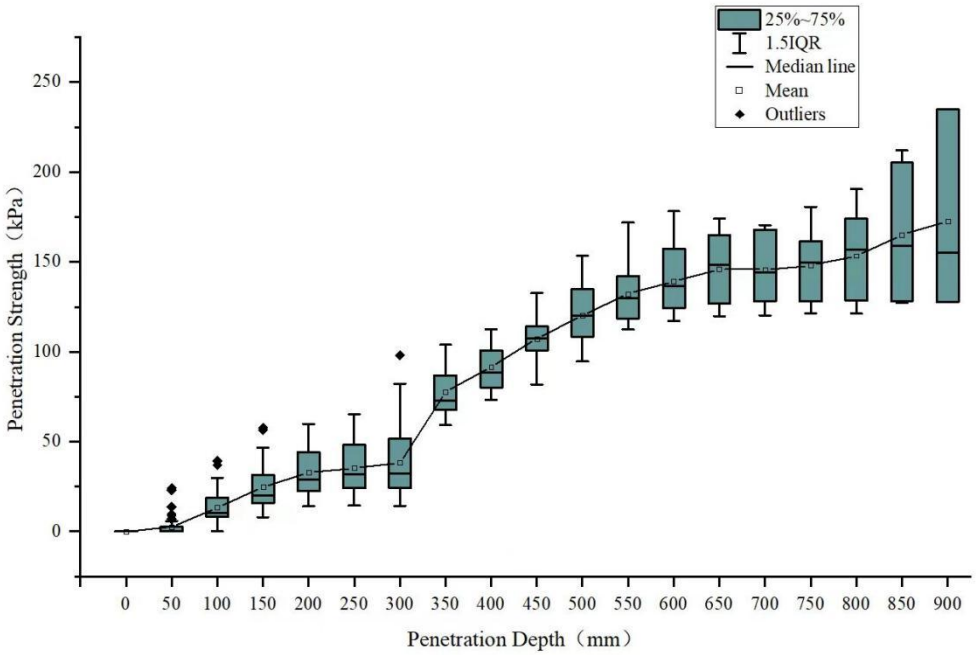

Figure 4.5-20 Statistical analysis of penetration strength in the Block A-5 of the Contract Area

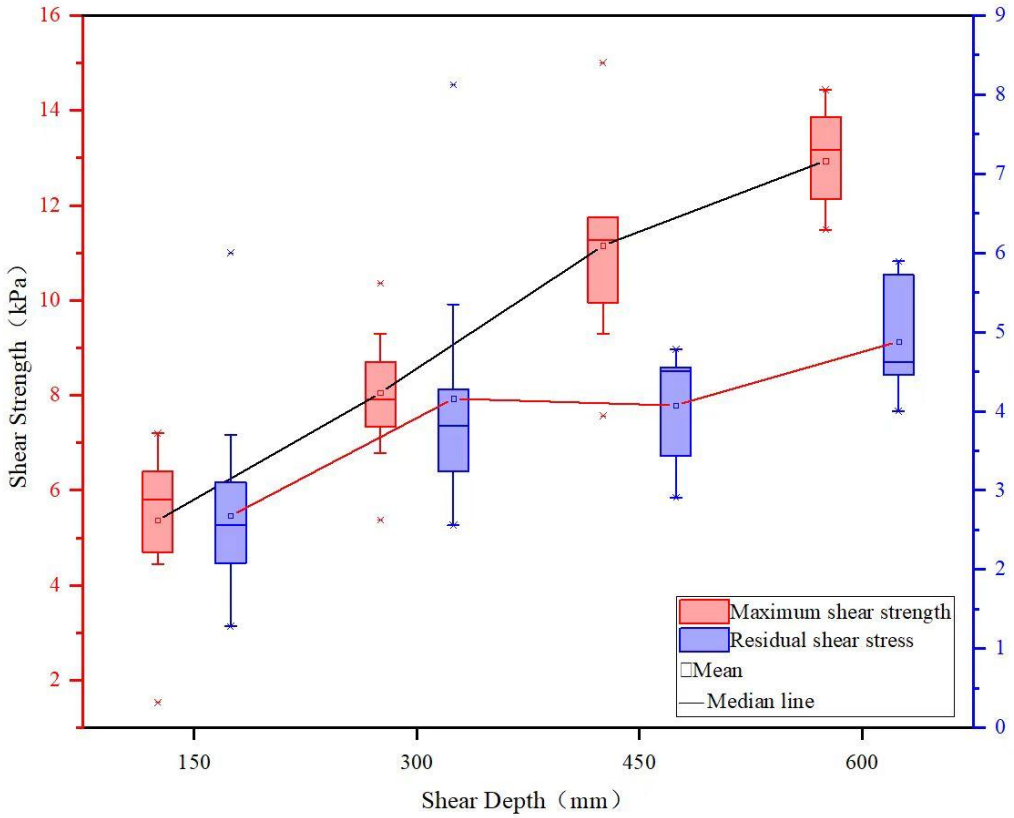

Figure 4.5-21 Statistical analysis of shear strength in the Block A-5 of the Contract Area

4.5.3.4 Bioturbation

During Minmetals' 2022 survey cruise, we have measured the ^{210}Pb specific activity and ^{226}Ra specific activity of samples collected with gravity piston corer sampling at DY73II-A5-GC01 and DY73II-A5-GC04 stations with gamma ray spectrometer, as well as calculated the ^{210}Pbex specific activity from the difference between them. The ^{210}Pb test results were used to assess the bioturbation. See Figure 4.3-4 for the distribution of stations.

In the vertical distribution profile of $^{210}Pb_{ex}$ in columnar sediments collected at DY73II-A5-GC01 station (Table 4.5-5 and Figure 4.5-22), the curve of $^{210}Pb_{ex}$ varies in an "S" shape from the surface layer to the 20 cm layer, and does not show a trend of attenuation with depth, which may be due to the influence of bioturbation on sediments, and the modern ^{210}Pb signal adsorbed by surface-layer sediments is mixed into the lower sediments. Below the depth of 20 cm, the fluctuation of ^{210}Pbex is small, but there is still 575.6 Bq/kg of ^{210}Pbex in 27 cm layer, which may reflect that there is

still ^{210}Pb that is not completely decayed. This may indicate that the maximum depth of bioturbation at DY73-A5-GC01 station can reach 27 cm.

Table 4.5-5 Data of gamma ray spectrometer for columnar sediments collected at DY73II-A5-GC01 station

S.N.	Sample No.	Sample depth cm	^{210}Pb specific activity Bq/kg		^{226}Ra specific activity Bq/kg		^{210}Pb$_{ex}$ specific activity Bq/kg	
			Measured value	U(k=2)	Measured value	U(k=2)	Measured value	Relative error
1	DY73II-A5-GC01	1	1,842.5	43.1	954.4	31.1	888.1	74.2
2	DY73II-A5-GC01	3	1,923.5	29.7	829.5	22.1	1,094.0	51.8
3	DY73II-A5-GC01	5	1,915.2	26.8	734.0	16.8	1,181.2	43.6
4	DY73II-A5-GC01	7	1,754.0	28.4	1,022.7	24.2	731.3	52.6
5	DY73II-A5-GC01	9	1,813.5	28.7	978.2	23.6	835.3	52.3
6	DY73II-A5-GC01	11	1,607.5	59.7	839.4	43.2	768.1	102.9
7	DY73II-A5-GC01	13	1,584.7	27.1	1,009.7	23.7	575.0	50.8
8	DY73II-A5-GC01	15	1,647.8	27.3	805.2	21.9	842.6	49.2
9	DY73II-A5-GC01	17	1,707.7	27.4	625.8	19.9	1,081.9	47.3
10	DY73II-A5-GC01	19	1,607.1	24.2	704.2	15.6	902.9	39.8
11	DY73II-A5-GC01	21	1,411.6	27.1	758.3	19.7	653.3	46.8
12	DY73II-A5-GC01	23	1,349.4	22.3	664.4	15.3	685.0	37.6
13	DY73II-A5-GC01	25	1,209.5	25.9	578.3	16.9	631.2	42.8
14	DY73II-A5-GC01	27	951.4	31.9	375.8	20.6	575.6	52.5

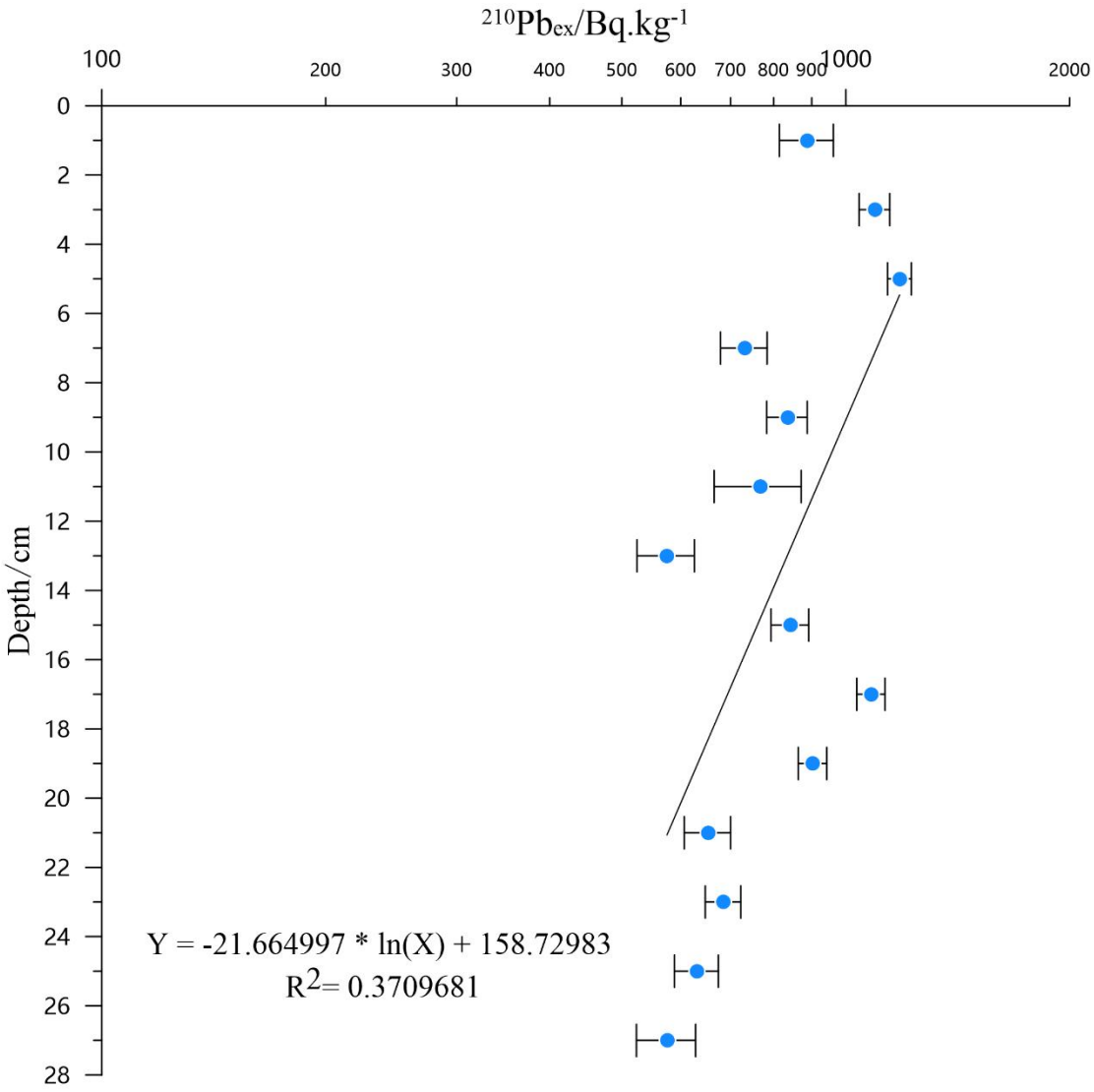

Figure 4.5-22 Distribution of $^{210}Pb_{ex}$ with depth in columnar sediments collected at DY73II-A5-GC01 station

The vertical distribution profile of $^{210}Pb_{ex}$ in columnar sediments collected at DY73II-A5-GC04 station (Table 4.5-6 and Figure 4.5-23) shows that the $^{210}Pb_{ex}$ in all layers of the 3-17 cm section is higher than that in the topmost layer (1 cm layer), and the $^{210}Pb_{ex}$ does not decrease with the depth, which reflects the disturbance of biological activities to the sediments. The $^{210}Pb_{ex}$ in the 19-27 cm section tends to decrease with depth, and is still close to 400 Bq/kg in the 25 cm layer. This indicates that biological activities can transmit the ^{210}Pb signal in the sediment surface to the depth of 25 cm, meaning that the depth of bioturbation in the sediment of DY73II-A5-GC04 station can reach 25 cm.

Table 4.5-6 Data of gamma ray spectrometer for columnar sediments collected at DY73II-A5-GC04 station

S.N.	Sample No.	Sample depth (cm)	^{210}Pb specific activity Bq/kg		^{226}Ra specific activity Bq/kg		^{210}Pb$_{ex}$ specific activity Bq/kg	
			Measured value	U(k=2)	Measured value (295.2 keV)	U(k=2)	Measured value	Relative error
1	DY73II-A5-GC04	1	1,523.8	34.0	823.9	21.6	699.9	55.6
2	DY73II-A5-GC04	3	1,791.9	25.3	691.9	17.2	1,100.0	42.5
3	DY73II-A5-GC04	5	1,738.7	25.1	822.8	18.4	915.9	43.5
4	DY73II-A5-GC04	7	1,723.3	26.9	654.1	18.1	1,069.2	45.0
5	DY73II-A5-GC04	9	1,702.9	26.6	711.9	18.6	991.0	45.2
6	DY73II-A5-GC04	11	1,910.2	47.8	680.0	31.6	1,230.2	79.4
7	DY73II-A5-GC04	13	1,836.1	26.2	826.1	19.0	1,010.0	45.2
8	DY73II-A5-GC04	15	1,748.7	26.0	891.7	19.7	857.0	45.7
9	DY73II-A5-GC04	17	1,591.2	22.7	587.2	15.0	1,004.0	37.7
10	DY73II-A5-GC04	19	1,206.6	19.0	669.0	14.3	537.6	33.3
11	DY73II-A5-GC04	21	1,064.1	43.6	535.0	32.8	529.1	76.4
12	DY73II-A5-GC04	23	937.3	18.8	434.6	13.8	502.7	32.6
13	DY73II-A5-GC04	25	714.7	17.1	318.1	12.2	396.6	29.3
14	DY73II-A5-GC04	27	646.1	17.1	379.1	13.1	267.0	30.2

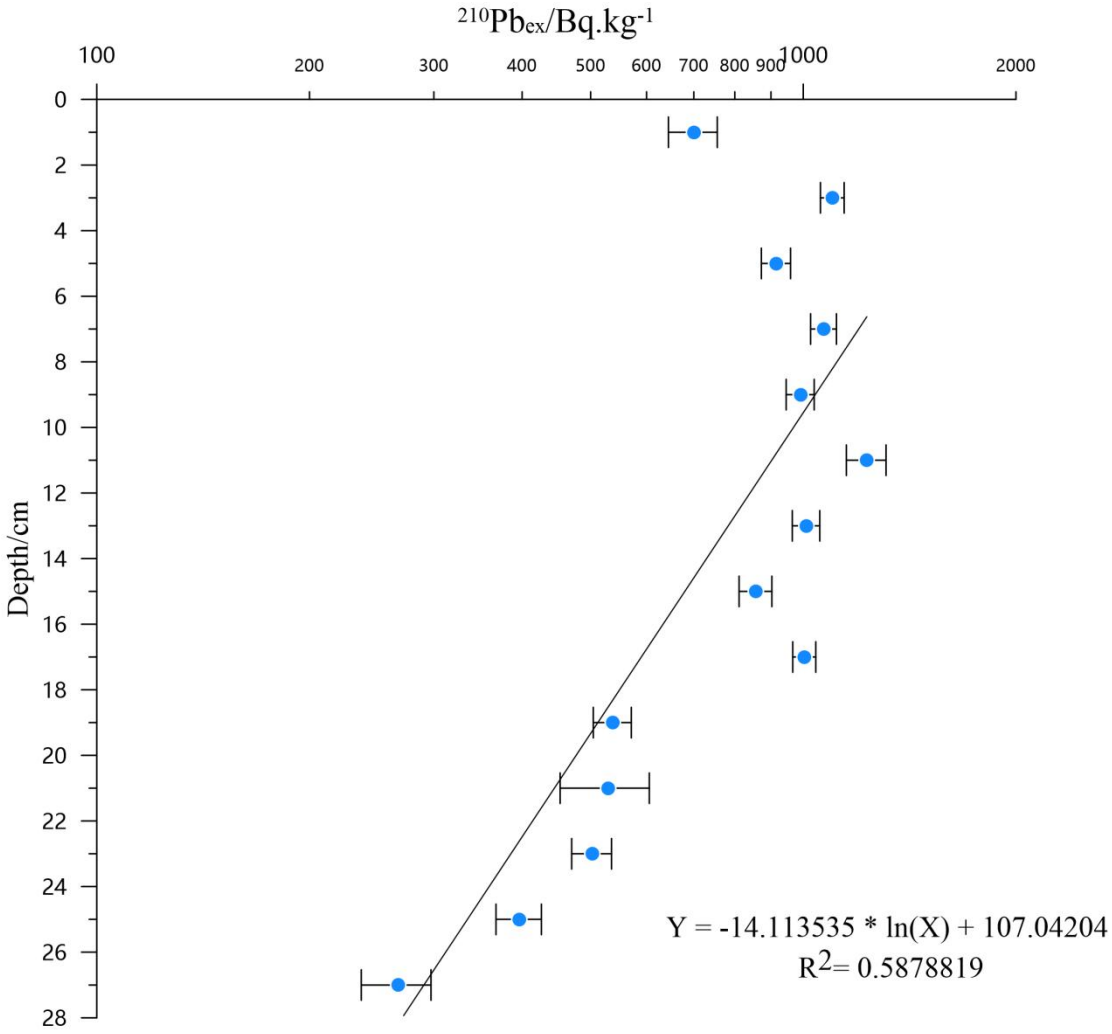

Figure 4.5-23 Distribution of $^{210}Pb_{ex}$ with depth in columnar sediments collected at DY73II-A5-GC04 station

The variation of ^{210}Pb profile in the NORI-D region is similar to that in the Block A-5, but NORI-D region has a higher specific activity of ^{210}Pb in the surface layer of sediments (NORI 2022).

4.6 Physical oceanography characteristics

4.6.1 Tidal current characteristics

The tides in the CCZ are mixed semi-diurnal tides, and the phenomenon of tidal inequality is obvious. During Minmetals' 2021 survey cruise, we have successfully recovered a set of anchors launched in the Block A-5 during the 2019 survey cruises, and obtained the ocean current speeds at the depths of 1,930 m, 5,150 m, 5,250 m and 5,350 m. The results of spectral analysis (95 % confidence interval) show that there is

an obvious tidal cycle in the seawater flow field at the mooring observation point (Figure 4.6-1), and both the deep-layer and middle-layer seawater flow fields are semi-diurnal tides.

Harmonic analysis of the flow field (Table 4.6-1, in which the negative value of the short axis indicates clockwise and the positive value indicates counterclockwise) shows that the main tidal constituent at the mooring observation point is M2, followed by K1. In terms of rotation direction, main tidal constituents (except O1 and H1, which rotate counterclockwise) rotate clockwise. According to the formula for judging tidal current type, the F value is 0.51, so the tidal current type of this station is mixed tide.

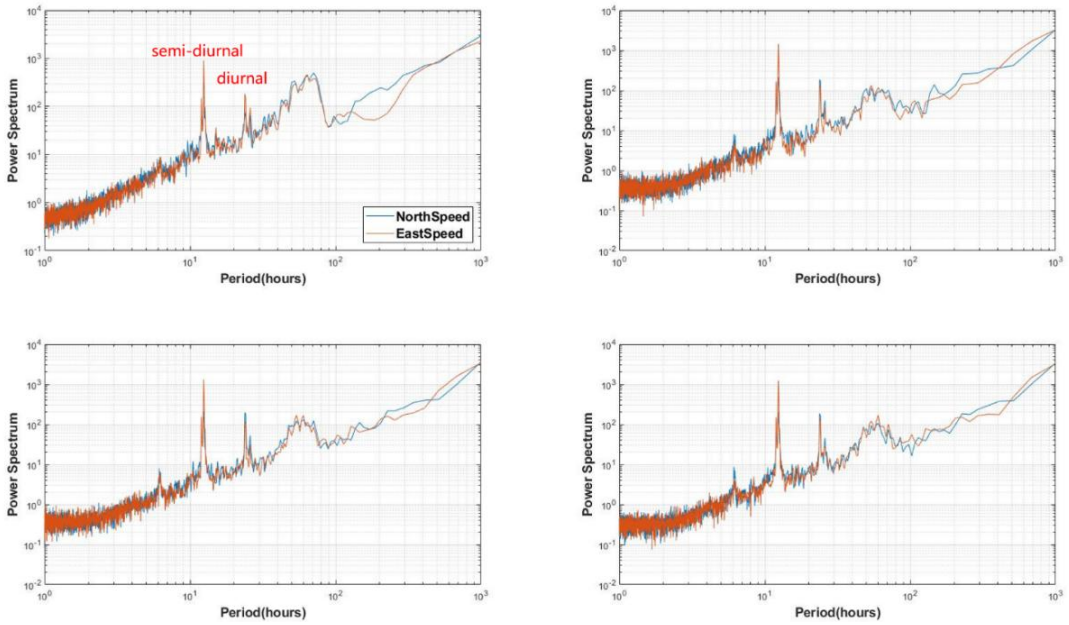

Figure 4.6-1 Distribution of seawater flow field tidal cycles at DY70II-A5-MX01 mooring observation point

Table 4.6-1 Main tidal information of mooring observation points

Tidal constituent	Frequency (cph)	Long axis (cm/s)	Short axis (cm/s)	Inclination (°)	Phase (°)
*M2	0.08051	1.354	-0.413	6.23	296.89
*K1	0.04178	0.684	-0.093	48.46	175.71
*S2	0.08333	0.465	-0.214	16.60	308.15
*N2	0.07900	0.275	-0.086	23.04	281.18

*H2	0.08063	0.246	-0.149	178.98	255.55
*O1	0.03873	0.243	0.125	59.75	156.44
*H1	0.08040	0.220	0.033	107.13	252.80
*S1	0.04167	0.208	-0.056	100.09	119.08

4.6.2 Characteristics of temperature and salinity profiles

Based on 10 vertical observation CTD profiles obtained by Minmetals in the Block A-5 in 2017-2022, we analyzedthe temporal variation characteristics of vertical hydrological profiles in the Block A-5. See Figure 4.6-2 for the distribution of CTD observation stations.

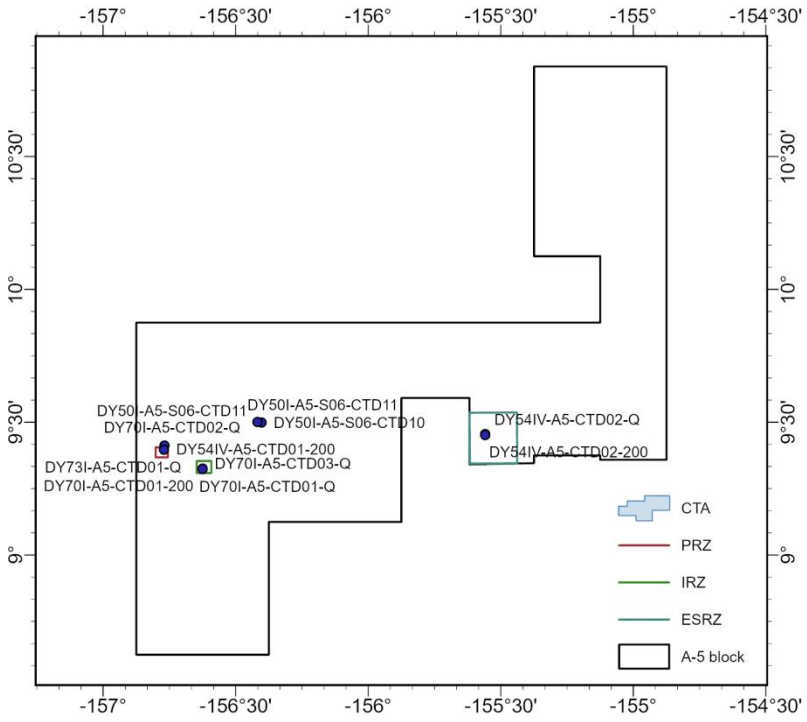

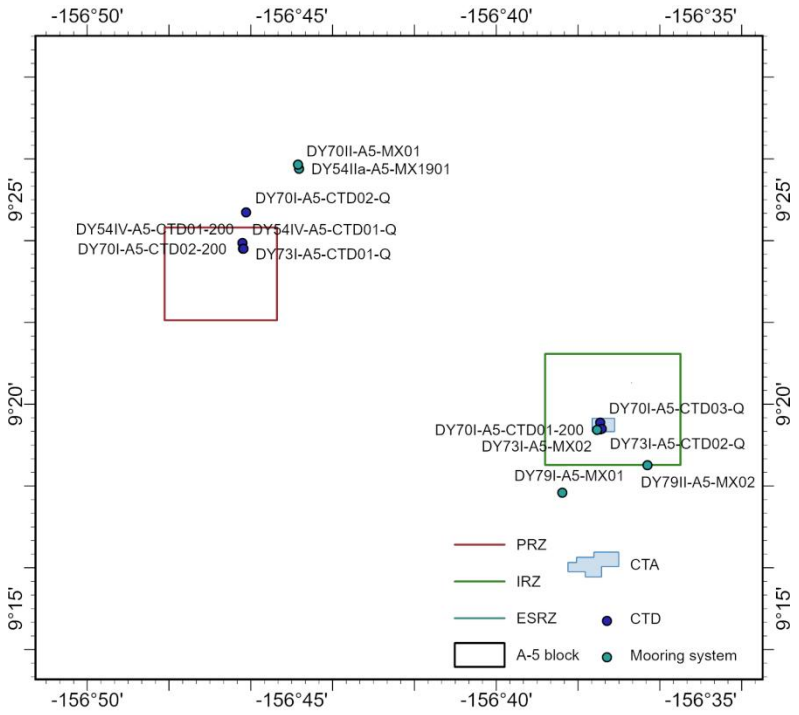

Figure 4.6-2 Schematic diagram for CTD and submerged buoys of mooring observation stations in the Block A-5

The vertical variation trend of full-depth temperature profile is similar. It is relatively high (about 28.5℃) in the surface layer, and has a strong thermocline at approximate 40 m depth. With increasing depth, and the temperature rapidly decreases to below 12℃ within the range of 100 m depth, and the downward temperature continues to decrease but the rate becomes smaller, showing a slow gradual variation state. From 4,000 m downward, the temperature tends to stabilize (Figure 4.6-3). In different years, the vertical variation trends of temperature in the upper layer (no deeper than 200 m) are basically similar, but the thermocline positions are slightly different, with a variation of about 40 m. The deep-layer temperature variation trends are similar, with a variation of about 0.03 ℃. The temperature was slightly higher in 2021 and 2022 than in 2019. The above-mentioned differences may be due to the comprehensive influence of climate change, observation period variation and other factors.

Three vertical variation results of the full-depth temperature profile in the NORI-D region are basically consistent with those in the Block A-5. The temperature drops

rapidly from about 29℃ to 15℃ in the first 100 m of surface layer, and then drops to 2℃ in the subsequent 2,000 m seawater. After that the water column remains relatively stable and maintains a low temperature (NORI 2022).

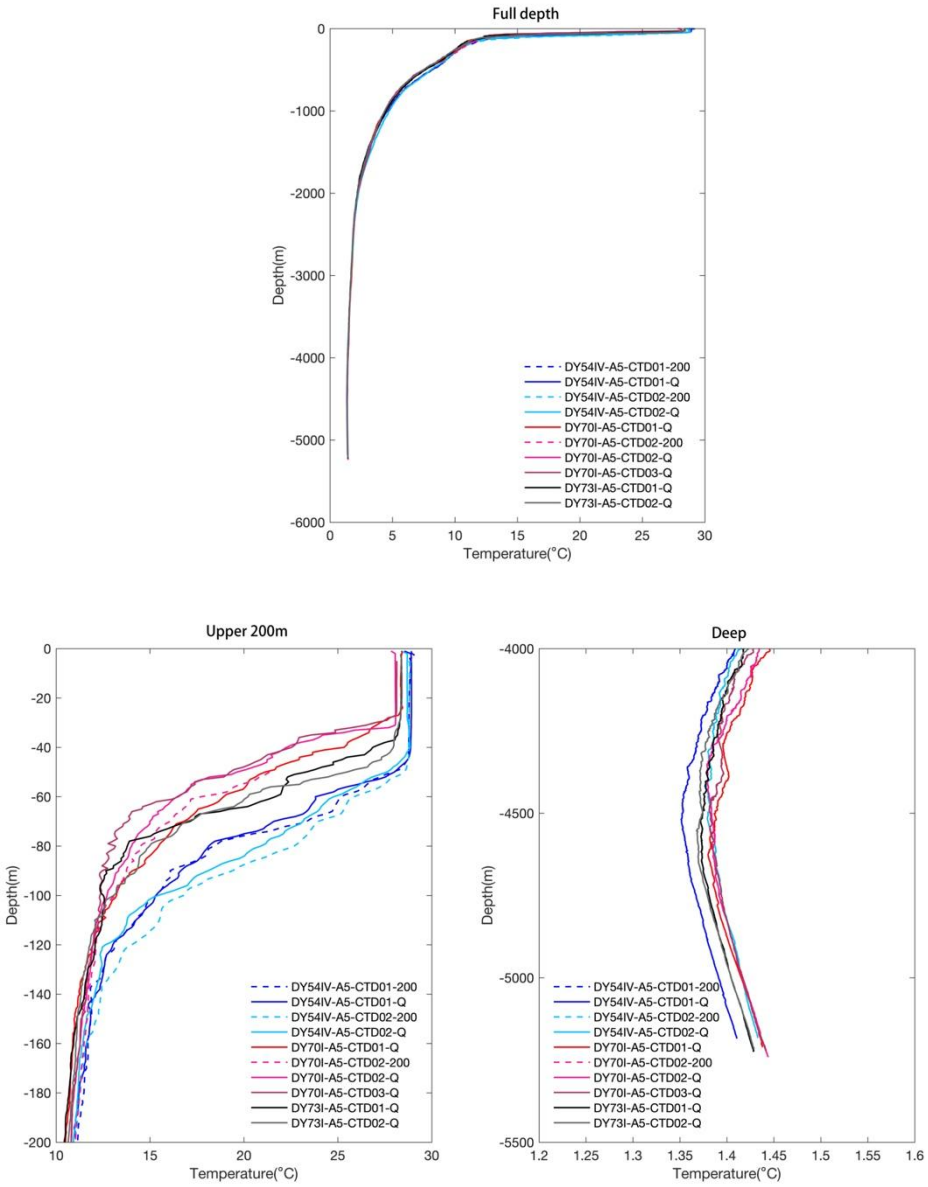

Figure 4.6-3 Variations of CTD temperature with depth in 2017-2022

The variation trend of full-depth salinity profile is similar, relatively high and stable in the surface layer, begins to decrease in the thermocline, and reaches the lowest and stable value in the deep layer. In 2019, 2021 and 2022, the salinity of the upper layer (200 m) increased with increasing depth at 0-50 m. At the water depth of 60-200 m, the variation trend in 2019 was opposite to that in 2021. The salinity

decreased with increasing depth at 60-70 m, and then increased to a stable level after reaching the minimum at 70 m in 2021. The salinity increased with increasing depth, reaching the maximum at 70 m, then decreased with increasing depth, and then gradually increased to a stable level after reaching another minimum at 120 m in 2019. The general variation trend of salinity in deep layer is similar, which tends to be stable after increasing with the depth, but the extreme value decreased in 2021 and increased obviously in 2022 (Figure 4.6-4). Such variations may be the result of many factors, including atmospheric precipitation and evaporation, fresh water input, ocean circulation, material transport and geological activities.

The water column salinity in NORI-D region ranges from 33.5 psu in the surface layer to 34.5 psu in the near-bottom layer. The halocline is within top 100 m in the surface layer of the water column, and the maximum salinity occurs at about 100 m depth. The salinity variation range (33.7-34.8 psu) and vertical profile variations in the Block A-5 and NORI-D region are basically the same (NORI 2022).

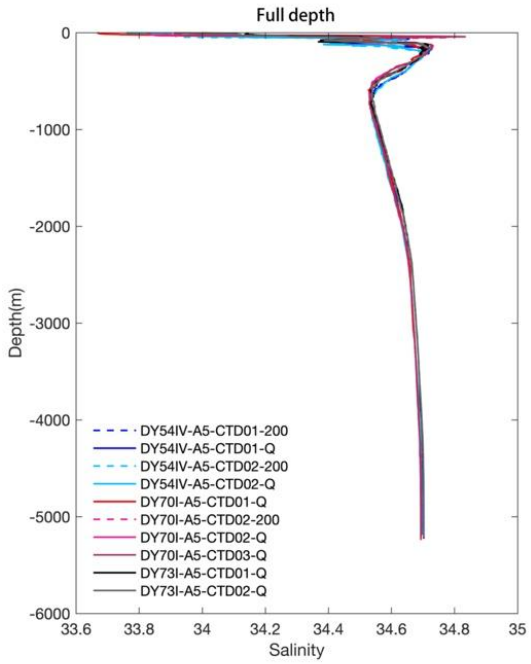

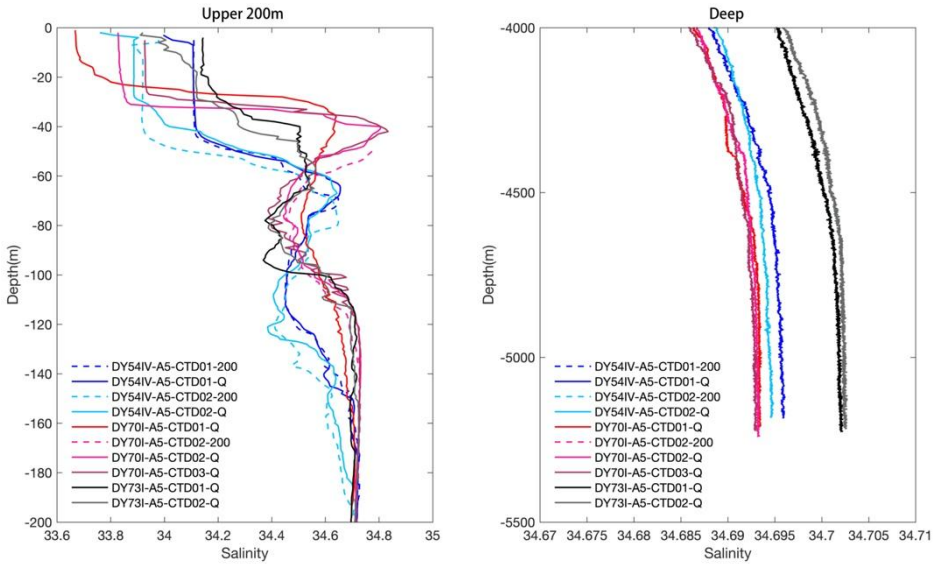

Figure 4.6-4 Variations of CTD salinity with depth in 2017-2022

4.6.3 Ocean current characteristics

Based on the ship-mounted ADCP observation data obtained by Minmetals during the 2017-2022 survey cruises in the Block A-5, we comparatively analyzed the time variation characteristics of the upper-layer ocean current in the Block A-5 (Figures 4.6-5 ~ 4.6-8). Results show that the current speed and direction vary significantly in different years in this area. The current speeds observed during the 2017 and 2021 survey cruises were relatively high, exceeding 1 m/s locally, while those observed during the 2019 and 2022 survey cruises were usually less than 0.5 m/s. As far as the current direction is concerned, there is obvious equatorial countercurrent in the southwestern part of the operation zone in 2017 and 2019, and in the southern part of the operation zone in 2021 and 2022. This indicates equatorial countercurrent are dominant in this sea area. In different years, the phenomenon of alternating northbound current and southbound current has also been observed in different positions in the whole survey area. We infer that it may have been influenced by mesoscale vortex and significant weather processes.

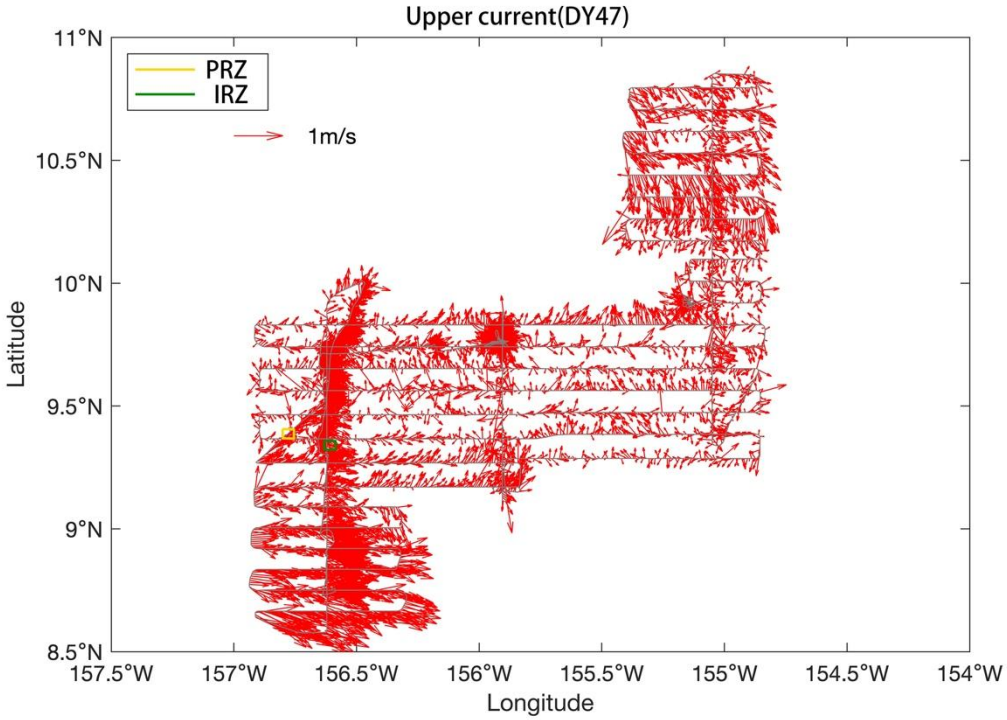

Figure 4.6-5 Ocean currents in the Block A-5 during the 2017 survey cruise

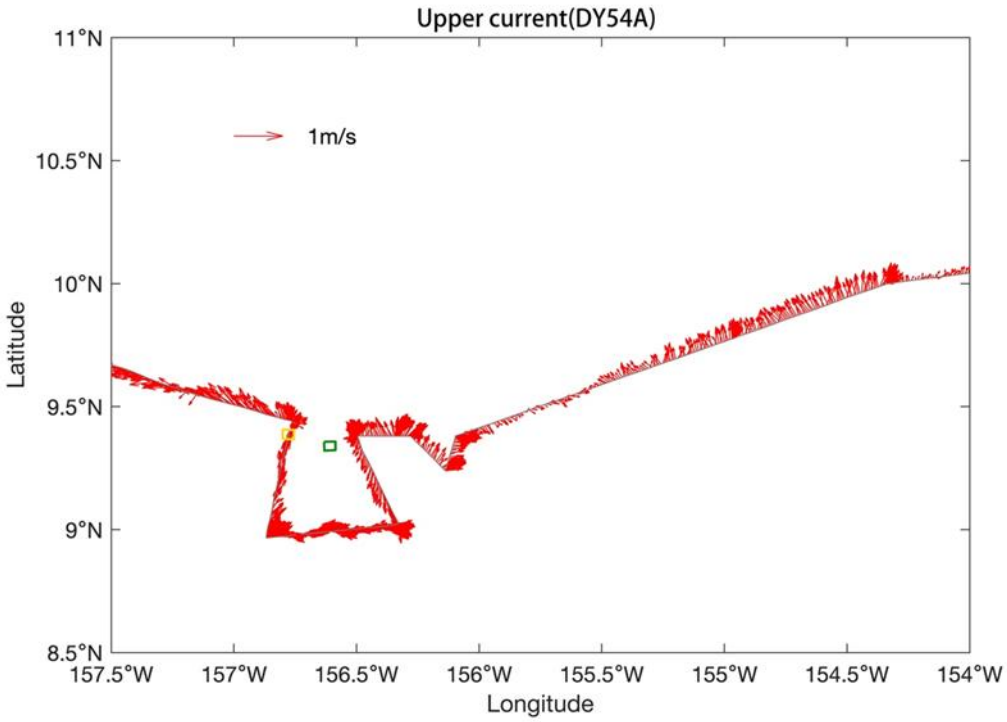

Figure 4.6-6 Ocean currents in the Block A-5 during the 2019 survey cruise

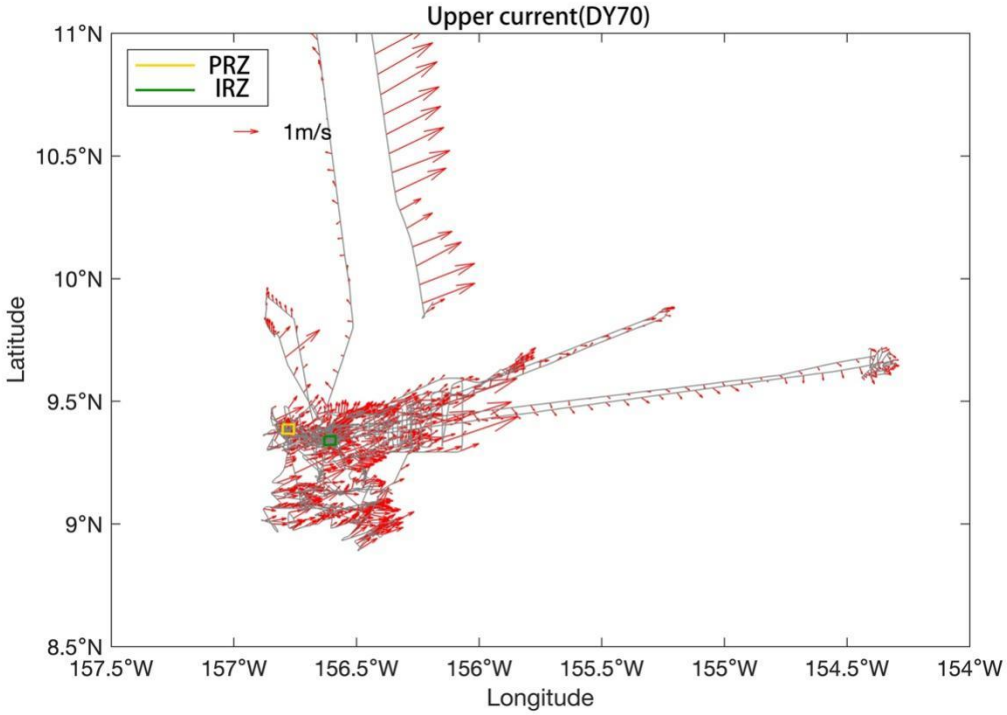

Figure 4.6-7 Ocean currents in the Block A-5 during the 2021 survey cruise

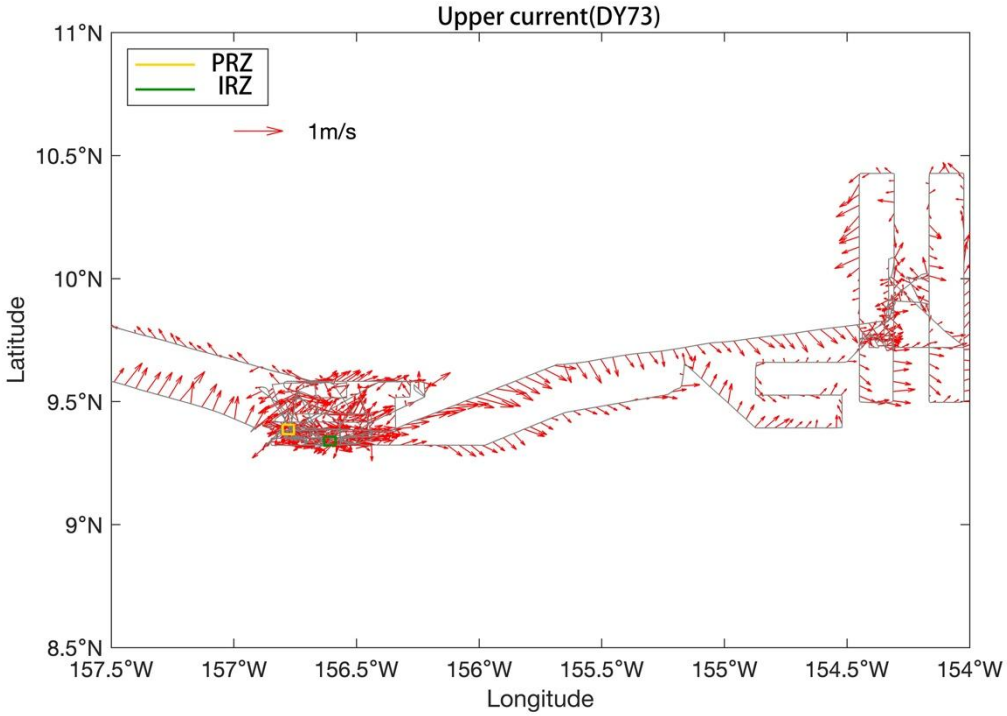

Figure 4.6-8 Ocean currents in the Block A-5 during the 2022 survey cruise

4.6.4 Long-term observation characteristics

4.6.4.1 Temperature

During Minmetals' 2021 survey cruise, we have successfully recovered a set of long mooring (DY70II-A5-MX01), and three CTDs were set at the depth of 20 m, 500 m and 1,925 m above the bottom respectively. The observation lengths are shown in the following Table 4.6-2.

Table 4.6-2 Information of CTD carried by the mooring

Equipment name	Water depth of equipment	Start and stop of effective measurement	Measurement duration (days)
CTD (037-20416)	5256 m	August 13, 2019 to December 25, 2021	865
CTD (037-20415)	4782 m	August 13, 2019 to December 25, 2021	865
CTD (037-20414)	1925 m	August 13, 2019 to December 25, 2021	865

The statistical results of seawater temperature at a depth of 1925m in the survey area from August to September are shown in Table 4.6-3. The average temperature of seawater in this layer in August was 2.3022 ℃, and the average temperature was 2.2768 ℃ (Table 4.6-3).

Table 4.6-3 Statistical of water temperature at 1925 m depth (August-September 2019)

Period	Temperature maximum	Temperature minimun	Average	Standard deviation
August, 2019	2.3795	2.2154	2.3022	0.0273
September, 2019	2.3616	2.1937	2.2768	0.0345

In the distribution of temperature-depth at 20 m above the bottom (Figure 4.6-9, above), the blue solid line is the pressure record of SBE37, and the red solid line is the salinity record. It can be seen that after the mooring lands, the sinking block gradually collapses. The pressure record shows that the early collapse is relatively fast,

approximately 2 m, and the later collapse can be basically ignored. During the whole observation period, the recorded pressure was in the range of 5349.1-5352.8 dbar, and the impact of tidal cycle on the bottom pressure was approximately 1 dbar. The characteristics of bottom-layer water are consistent, and the impact of tidal current on the height of equipment above the bottom can be ignored. In the temperature variation cycle, tidal current is not a significant factor, and the temperature varies in the range of 1.4148-1.4514 °C, averaging 1.4307 °C. The temperature baseline is relatively stable, and there are some aperiodic fluctuations. Data recorded by the mooring in the NORI-D region show that the near-bottom temperature is always stable at about 1.5℃. Therefore, the near-bottom temperature variation in the Block A-5 is similar to that in the NORI-D region (NORI 2022).

On the temperature-depth distribution map at the depth of 500 m above the bottom (Figure 4.6-9 below), the recorded pressure is in the range of 4861.7-4870.0 dbar, and the variation range is eight times that at the depth of 20 m above the bottom. In addition to the tidal cycle, there are some accidental events, which cause the pressure value to continue to be high. Part of the depth change may be related to the mooring tilt caused by the enhanced flow current speed. The equipment variation is 8 m at the depth of 500 m, and the corresponding mooring tilt angle is 10.3°. Combined with the bottom-layer ocean current speed distribution (Figure 4.6-11) and the temperature-depth observation record of SBE37 at 500 m above the bottom, the three pressure increases during February-March, July and September-October in 2020 all correspond to the bottom-layer ocean current speed increase synchronously.

The temperature at the depth of 500 m above the bottom ranges from 1.3600 °C to 1.4004 °C, averaging 1.3809 °C, which is slightly lower than the temperature at the depth of 20 m above the bottom, and the change is basically synchronous with that at the depth of 20 m above the bottom, but the temperature variations at the depth of 20 m and 500 m above the bottom do not reflect the variation of pressure records. In February and March 2020, due to the increase of flow current speed, the submerged

buoy system inclines and the pressure increases. However, corresponding temperature records do not always increase with the increasing depth. The temperature increases in the middle and late September of 2019 and August-September of 2020 correspond to decreases in pressure records. The two pressure increases in July and August 2020 did not correspond to the temperature increases. The impact factors of bottom temperature variation include not only the mooring tilt caused by the increase of current speed, but also the impact of the upper-layer ocean and variations in the nature of bottom-layer water columns. The temperature variations at 20 m and 500 m above the bottom recorded in the NORI-D region are basically synchronous and basically stable. Therefore, the temperature variations of the Block A-5 and NORI-D region at 500 m above the bottom are consistent (NORI 2022).

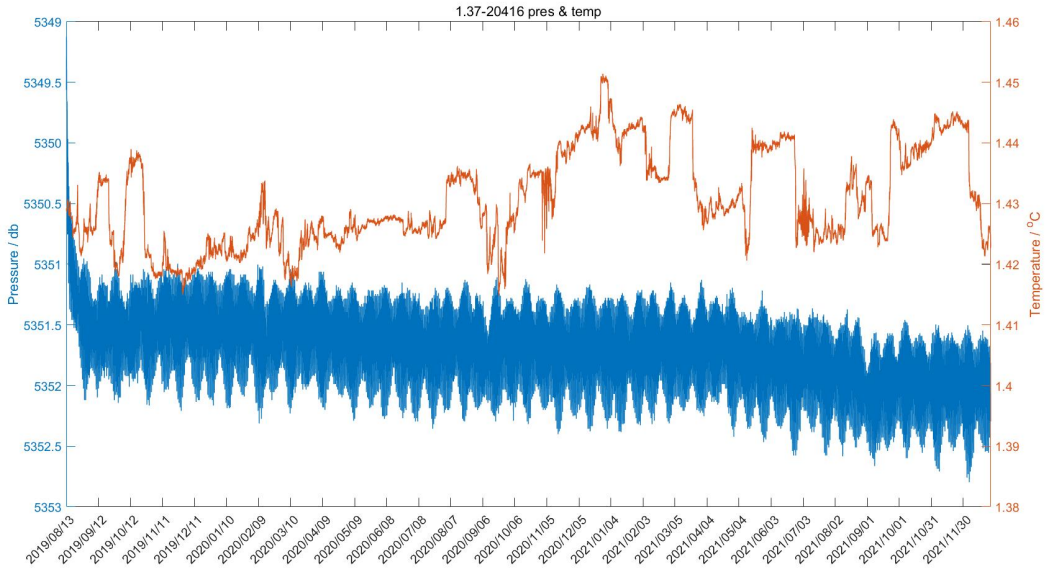

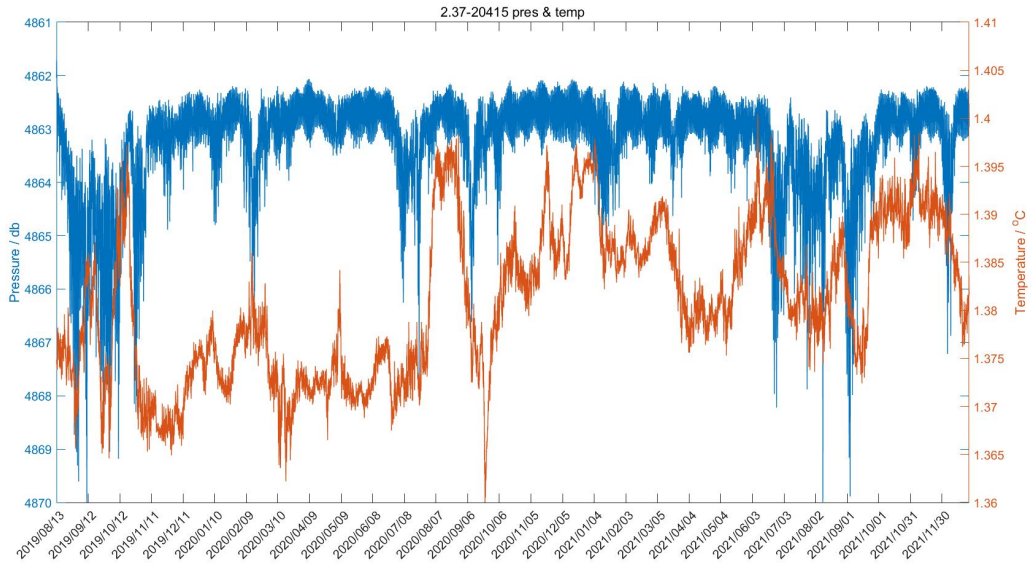

Figure 4.6-9 Characteristics of bottom-layer seawater temperature in the Block A-5

(Upper: 20 m; lower: 500 m above the bottom)

4.6.4.2 Salinity

The statistical results of seawater salinity at a depth of 1925m in the survey area from August to September are shown in Table 4.6-4. The average salinity of the seawater in this layer in August is 34.6350, and the average salinity in September is 34.6378.

Table 4.6-4 Statistical of water salinity at 1925 m depth (August-September 2019)

Period	Maximum	Minimum	Average	Standard deviation
August, 2019	34.6427	34.6202	34.6350	0.0024
September, 2019	34.6472	34.6282	34.6378	0.0026

The distribution of bottom-layer salinity is shown in Figure 4.6-10. The blue solid line is the pressure record of SBE37, and the red solid line is the salinity record. At 20 m above the bottom, the salinity is 34.7033 psu maximally and 34.6950 psu minimally, averaging 34.7000 psu. The temperature and salinity profile indicate that the water column originated from the L-PMOC in the Antarctic region.

At the depth of 500 m above the bottom, the salinity is 34.6975 psu maximally

and 34.6868 psu minimally, averaging 34.6934 psu.

In the NORI-D region, the salinity recorded by the mooring at 248 m, 1,999 m, 3,828 m and 4,325 m depth is stable at 34.7 psu. Therefore, the salinity values in the Block A-5 are basically the same as those in the NORI-D region at 20 m and 500 m above the bottom. After the mooring was put into use, the salinity in near-bottom-layer and at the depth of 500 m above the bottom gradually increased by 0.004 psu until December 2019. The overall trend of salinity variation at the depth of 500 m above the bottom is similar to that at the depth of 20 m above the bottom, and the salinity at the depth of 500 m above the bottom gradually decreases after 2020 (NORI 2022).

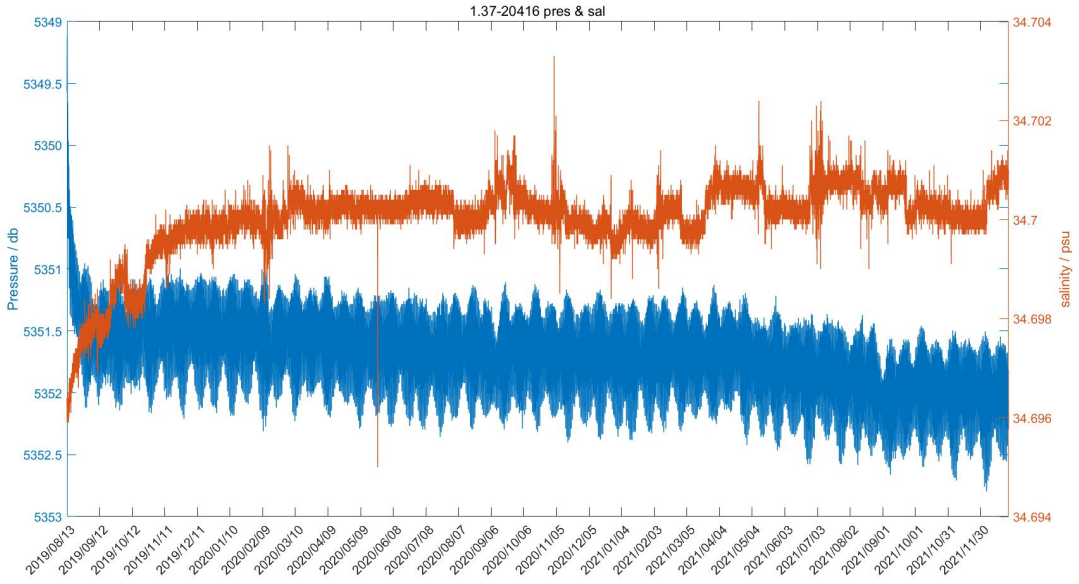

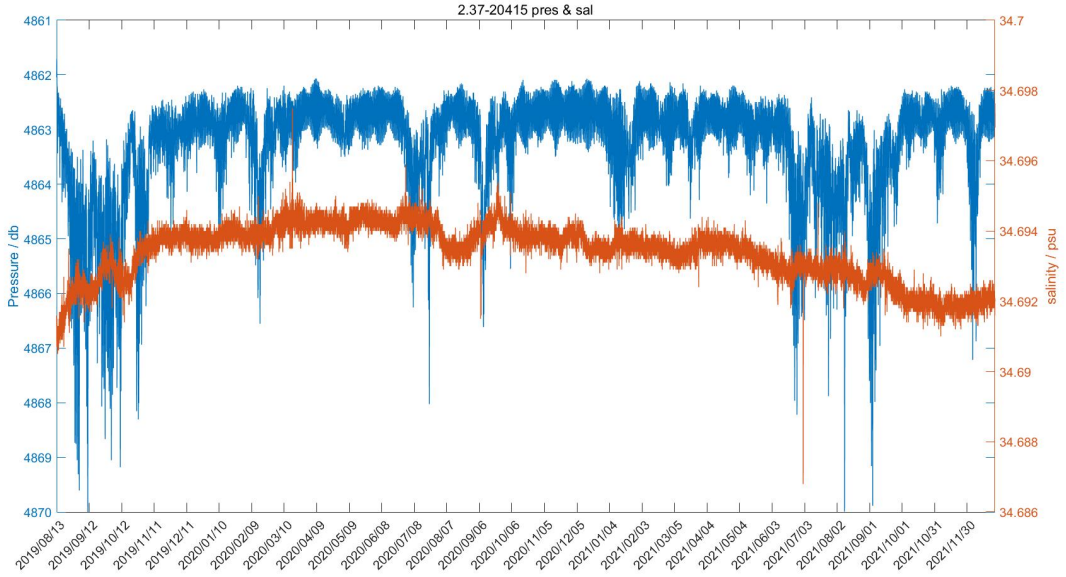

Figure 4.6-10 Characteristics of bottom-layer seawater salinity in the Block A-5

(Upper: 20 m; lower: 500 m above the bottom)

4.6.4.3 Turbidity

The mooring recovered in 2021 was equipped with four current meters. Those at the depths of 20 m, 100 m and 200 m above the bottom were all equipped with turbidity sensors. See Figure 4.6-11 for the turbidity observation values at the depths of 20 m, 100 m and 100 m above the bottom. There are significant abnormal variations in the bottom turbidity of the Block A-5. These abnormal values do not seem to have a direct corresponding relationship with the current speed of the near-bottom-layer ocean current. They are not caused by resuspension, but should be transported from the outside. For example, in September 2019, the turbidity anomaly exceeded 4.0 FTU. From December 2021 to March 2022, the bottom-layer ocean current speeds were relatively low. During this period, the turbidity tended to increase slowly, with the turbidity reaching 1.4 FTU maximally. Discontinuous abnormal values may come from biological interference. Besides, the turbidity is extremely low, and the background values are in the range of 0.2-0.4 FTU.

The extreme current speed at the depth of 100 m above the bottom is synchronous with the current speed at the depth of 20 m above the bottom, and there is no corresponding positive correlation between the current speed and the turbidity.

Most of the time, the turbidity of seawater is close to the detection limit of equipment, and individual discontinuous abnormal observed values may be due to organisms passing through the sensor, and the overall turbidity is below 0.4 FTU. Turbidity is stable within the background value range.

The EIS of The Metals Company (TMC) describes the background turbidity recorded by mooring in the IRZ and PRZ. The turbidity at 3.5 m above the bottom in the IRZ is 0.5-0.84 FTU, averaging 0.67 FTU. The turbidity at 12.5 m above the bottom is 0.46-0.72 FTU, averaging 0.57 FTU. The turbidity at 3.4 m above the bottom in the PRZ is 0.15-0.84 FTU, averaging 0.3 FTU. The turbidity at 9.6 m above the bottom is 0.42-3.7 FTU, averaging 0.54 FTU. The turbidity content in the near-bottom layer of the Block A-5 is basically consistent with that in the NORI-D region (NORI 2022).

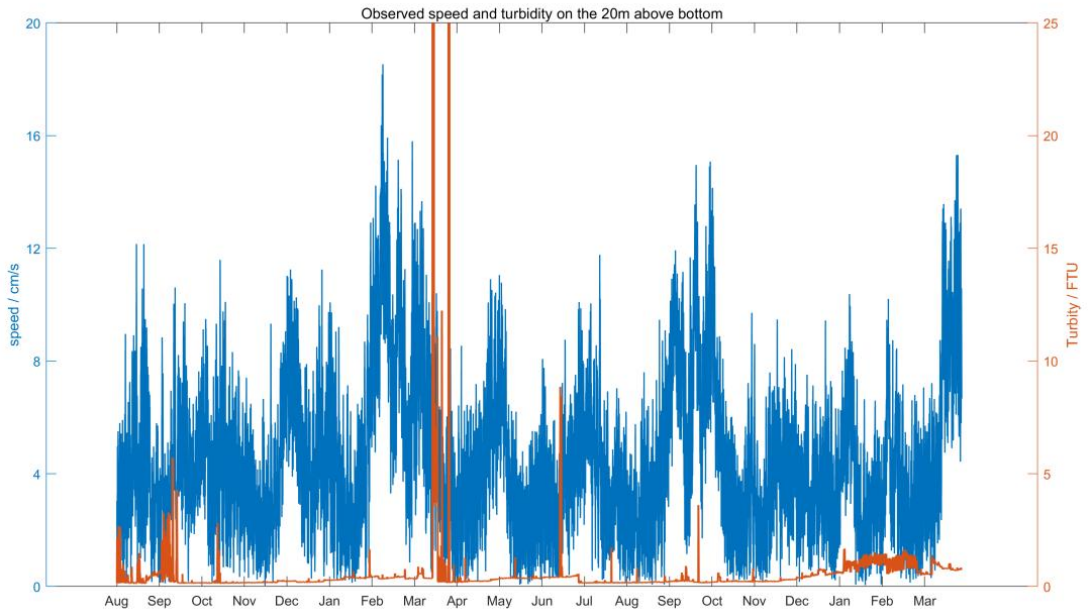

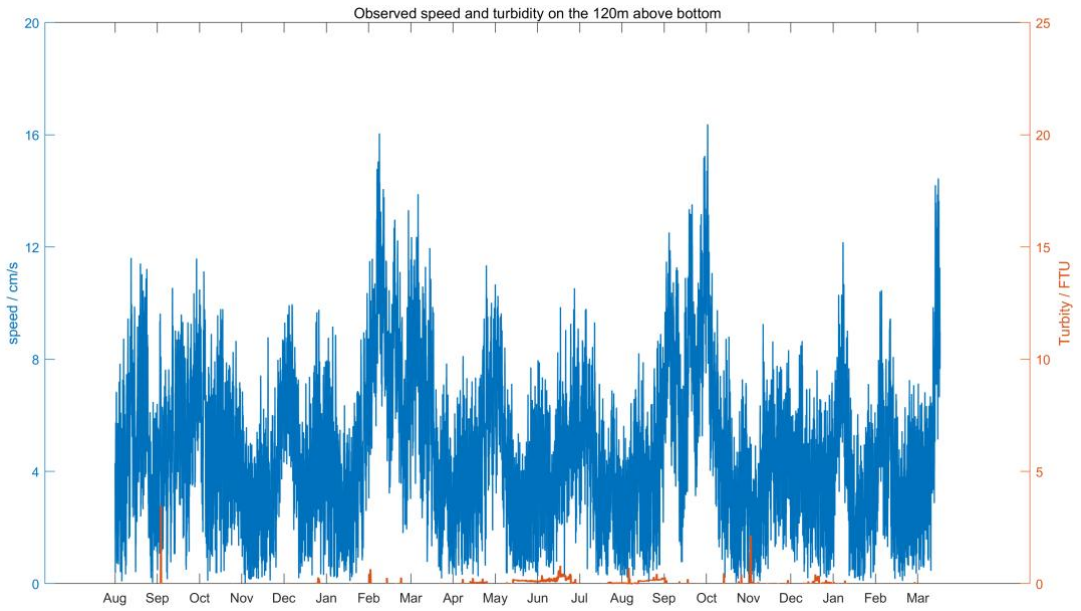

Figure 4.6-11 Relationship between current speed and turbidity at the depth of 20 m (upper) and 100 m (lower) above the bottom in the Block A-5

(DY70II-A5-MX01 station)

4.6.4.4 Ocean current

See Table 4.6-5 for the measurements of four single-point current meters on the mooring recovered in 2021. By the depth of current meter, we can divide them into middle layer (1,930 m) and deep layer (5,150 m, 5,250 m, 5,350 m) according to their relative positions. To visually see the variations of current speed and direction over time, we use the Nightingale Rose Chart of tidal current to visually analyze the data. As shown in Figure 4.6-12, the near-bottom-layer ocean current speed is changeable, the most concentrated current speed direction is southeast, followed by northwest, and the probability of current speed greater than 8 cm/s is also the highest in these two directions. The extreme current speed occurred in February 2020 and the direction was southeast. Before February 2020, the extreme current speed was relatively small, and the direction was mainly towards southeast. Since February 2022, the extreme current speed has increased, and the direction was mainly towards north (Figure 4.6-13).

As shown in Figures 4.6-12 and 4.6-13, the extreme current speed at the depth of 100 m above the bottom is synchronous with the current speed at the depth of 20 m

above the bottom, and the distribution is very similar on the Nightingale Rose Chart. Statistics on the occurrence of monthly extreme current speeds show that most of them also occur synchronously. Except in August-September of 2020 and February 2021, the extreme current speed at the depth of 20 m above the bottom is higher than that of 100 m above the bottom, and the current speed is slightly strengthened at the bottom.

Table 4.6-5 Information of current meters carried by the mooring

Equipment name	Water depth of equipment	Start and stop of effective measurement	Measurement Duration (days)
Single-point current meter (314)	1,930 m	August 13, 2019 to October 21, 2021	800
Single-point current meter (1,016)	5,150 m	August 13, 2019 to April 12, 2021	608
Single-point current meter (1,018)	5,250 m	August 13, 2019 to April 12, 2021	608
Single-point current meter (1,049)	5,350 m	August 13, 2019 to April 12, 2021	608

The seawater flow field in the middle layer (1,930 m) of the mooring point is dominated by the eastward flow, and the current speed is concentrated at 6-12 cm/s, and the maximum current speed can exceed 20 cm/s. In the deep layer, with the increasing depth of the current meter, the current speed and direction of seawater vary to a certain extent. The current speed gradually weakens with the increasing depth, the ratio of 9 cm/s current speed decreases, but the direction of seawater varies very little. Overall, ocean current speeds in the deep layers (5,150 m, 5,250 m and 5,350 m) are low at no more than 9 cm/s, and the currents are mainly from northwest to southeast (Figures 4.6-12 and 4.6-13).

Annual average analysis results (Table 4.6-6) show that the annual average current speed at ~2,000 m water depth is 7.34 cm/s, and the current direction is easterly. The annual average current speed of deep-layer ocean currents (5,150 m,

5,250 m and 5,350 m) is 4.56-4.83 cm/s, and the average current direction is easterly.

The average annual current speed in the NORI-D region is lower than that in the Block A-5 at a water depth of about 2,000 m and near the bottom. TMC's study report shows that the average annual current speed is 2.6±1.4 cm/s at the depth of ~2,000 m, the highest average current speed is recorded in July, with the lowest average current speed recorded in September-November and the current direction being southwestward. The average annual current speed at the water depth of ~4,321 m is 2.6±1.6 cm/s, with the highest average current speed recorded in June, the lowest average current speed recorded in October and the current direction being northwestward (NORI 2022).

Table 4.6-6 Statistics of annual average ocean current speeds and directions at different depths

Equipment S.N.	Water depth of equipment (m)	Annual average absolute current speed (cm/s)	Annual average vector current speed (cm/s)	Annual average current direction (°)
Single-point current meter (314)	1930	7.34	3.95	83.4
Single-point current meter (1,016)	5150	4.82	0.89	84.9
Single-point current meter (1,018)	5250	4.83	0.78	75.4
Single-point current meter (1,049)	5350	4.56	0.96	93.7

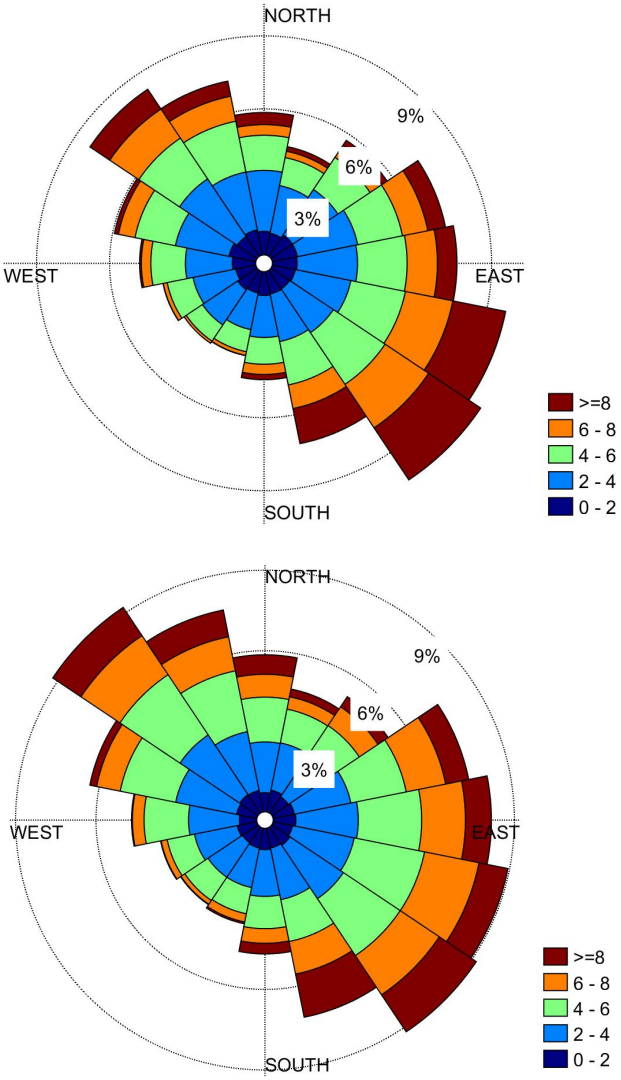

Figure 4.6-12 Nightingale Rose Chart for average annual flow field characteristics observed with single-point current meters in the Block A-5

(Upper: 5,350 m; lower: 5,250 m)

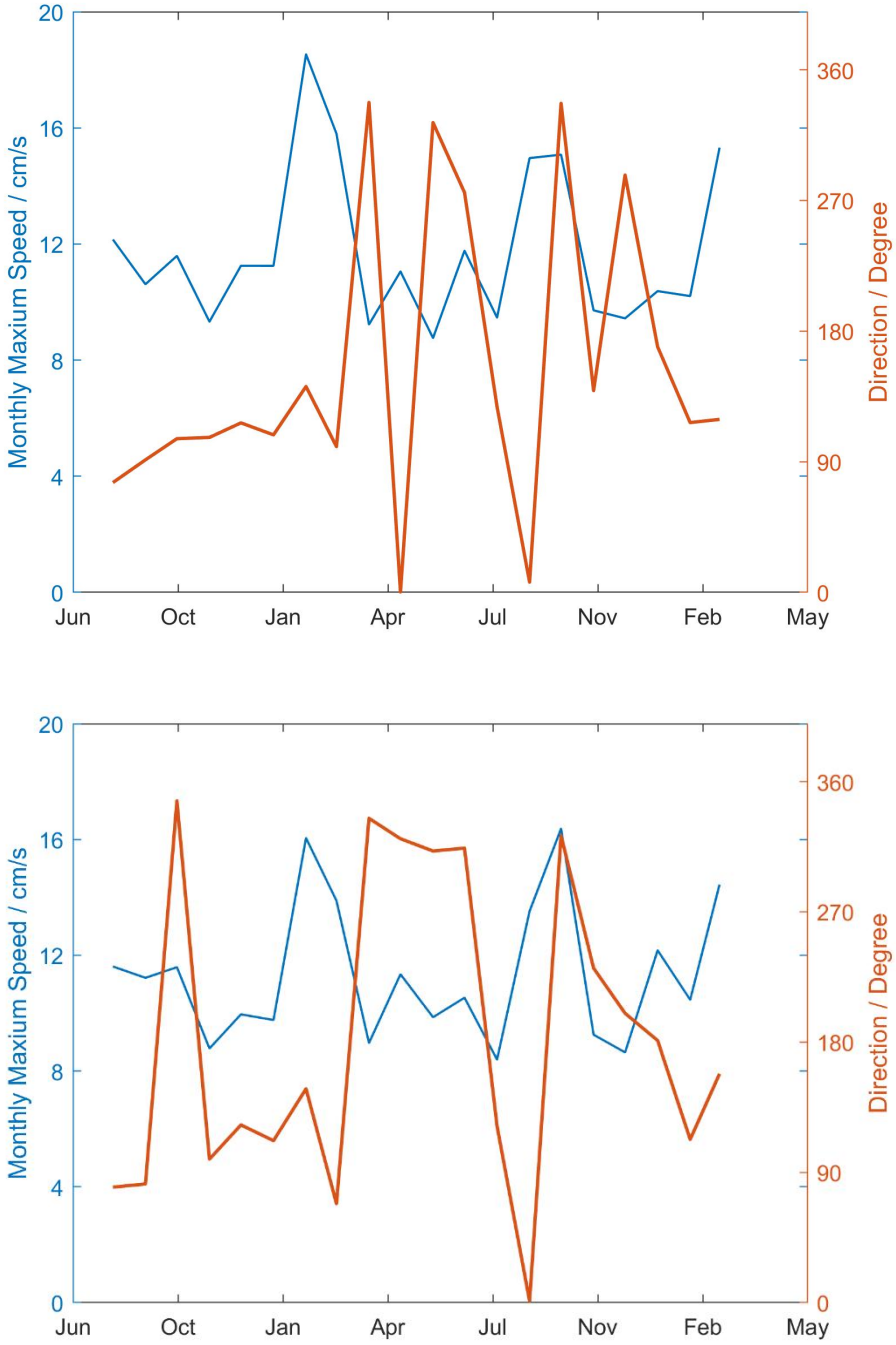

Figure 4.6-13 Extreme current speeds and directions at the near-bottom layer of the Block A-5

(Upper: 5,350 m; lower: 5,250 m)

Water depth: 5,350 m. The Nightingale Rose Chart for the distribution of monthly current speeds and directions at the 5,350 m depth layer is shown in Figure 4.6-14. See Table 4.6-7 for monthly average maximum current speeds and corresponding current directions of all observed water-depth layers at mooring point

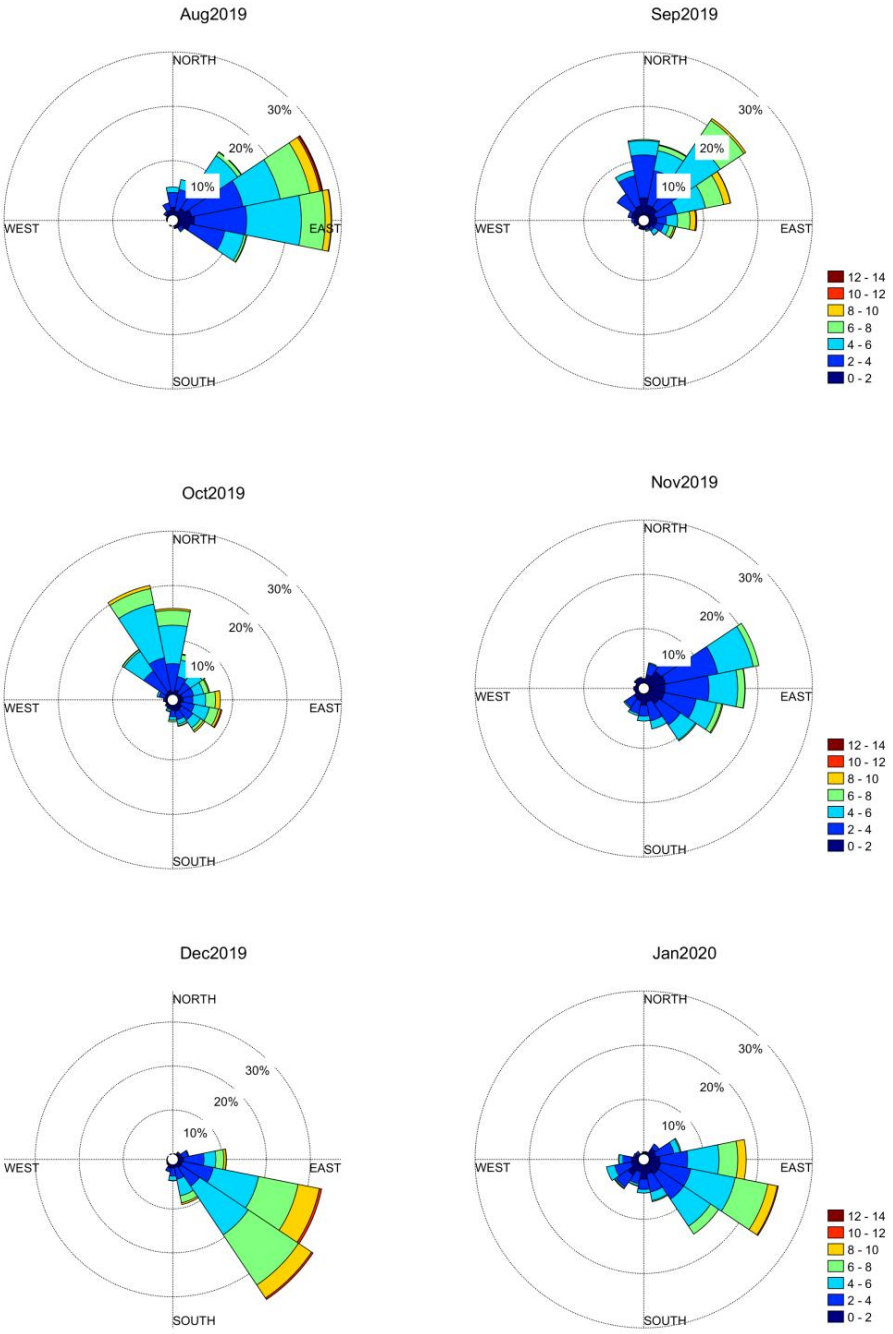

Figure 4.6-14 Monthly current speeds and directions at 5,350 m depth layer

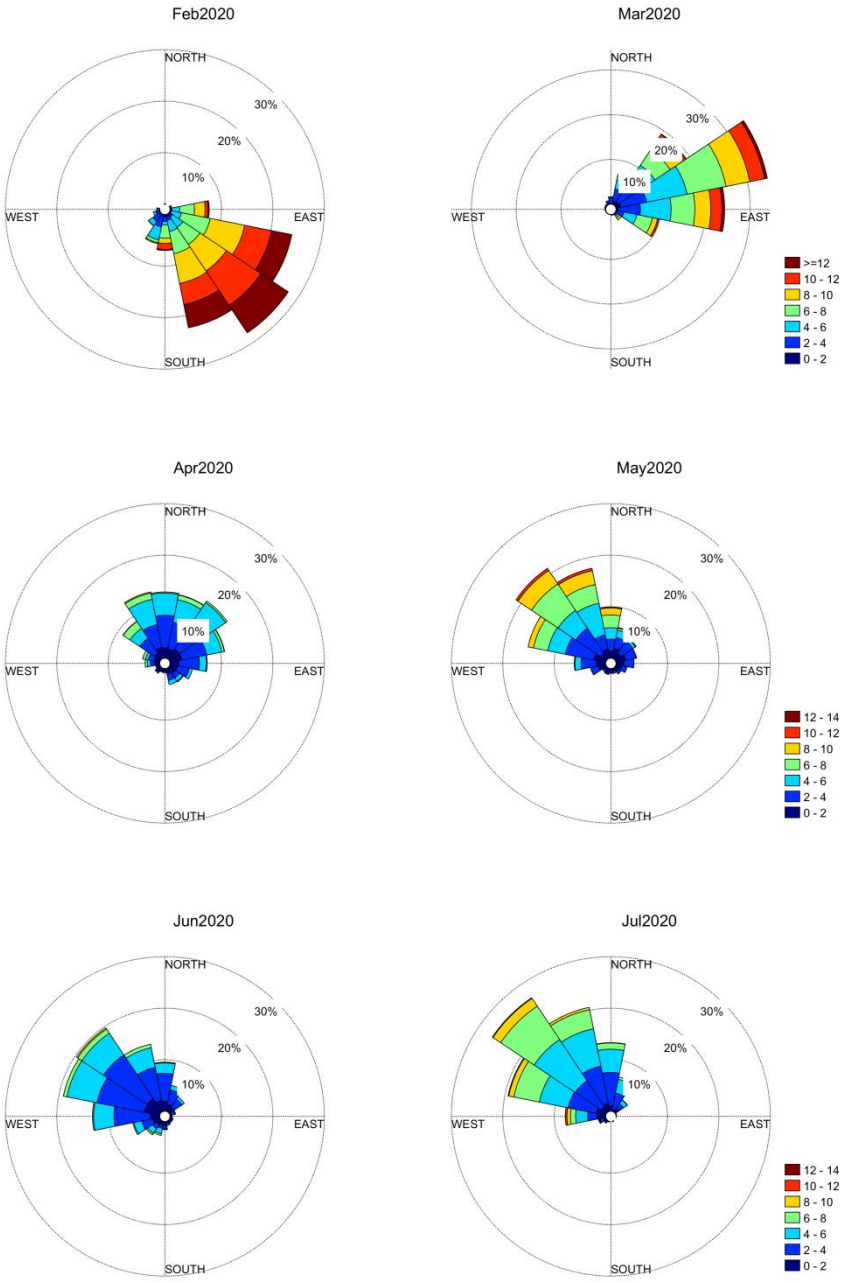

Figure 4.6-14 Monthly current speeds and directions at 5,350 m depth layer (continued)

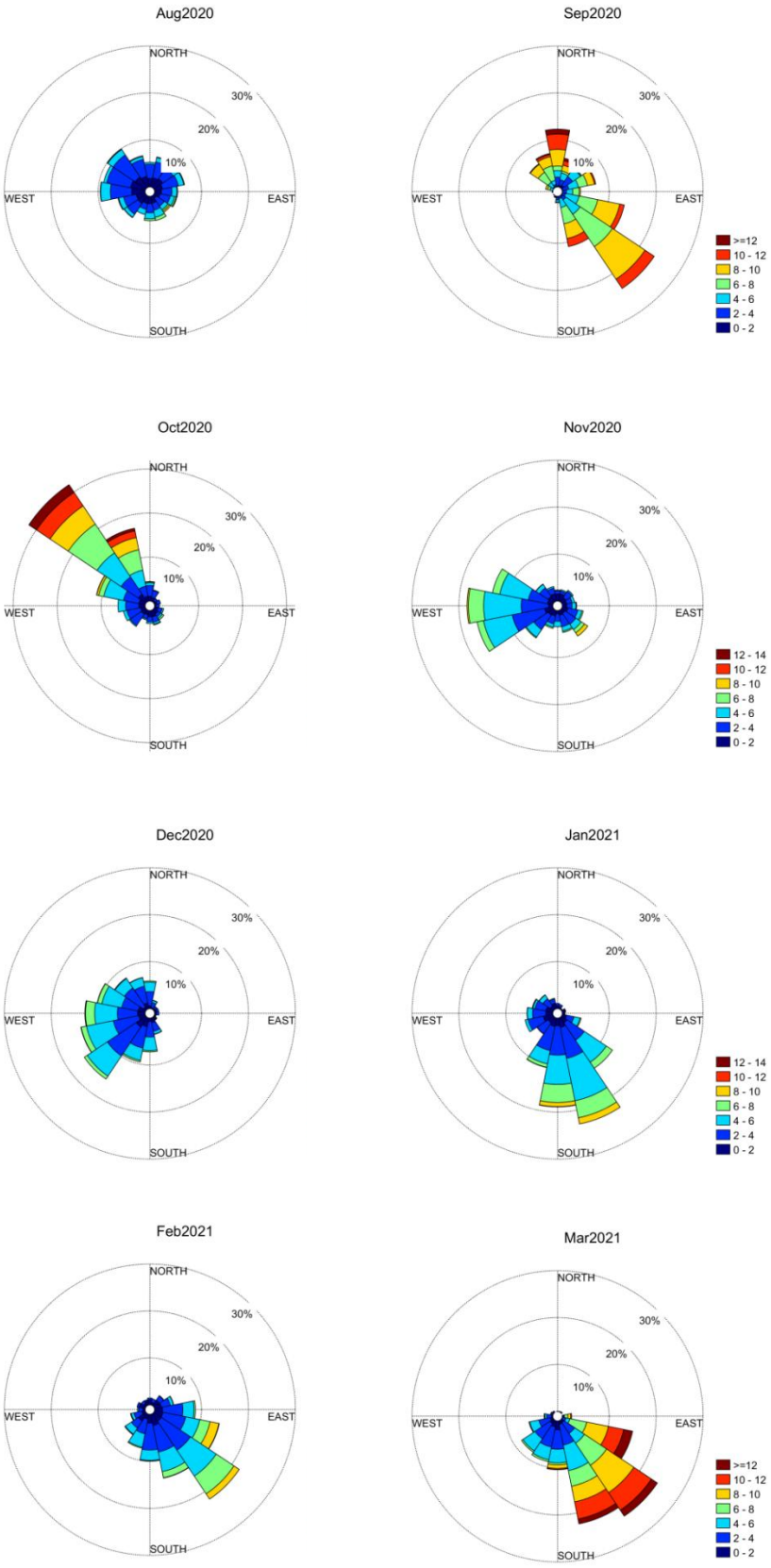

Figure 4.6-14 Monthly current speeds and directions at 5,350 m depth layer (continued)

Table 4.6-7 Monthly average maximum current speeds and corresponding current directions of all observed water-depth layers at mooring point

Current meter S.N.	Water depth (m)	August 2019		September 2019		October 2019		November 2019		December 2019		January 2020	
		Maximum current speed (cm/s)	Current direction (°)	Maximum current speed (cm/s)	Current direction (°)	Maximum current speed (cm/s)	Current direction (°)	Maximum current speed (cm/s)	Current direction (°)	Maximum current speed (cm/s)	Current direction (°)	Maximum current speed (cm/s)	Current direction (°)
314	1930	16.451	79.674	18.045	93.959	16.877	90.786	19.419	99.705	16.850	71.602	19.481	100.149
1016	5150	4.488	79.355	3.256	50.401	1.297	92.726	2.316	83.903	3.167	158.404	1.704	124.233
1018	5250	11.611	79.766	11.220	81.930	11.587	346.697	8.779	99.127	9.958	122.744	9.763	111.871
1049	5350	12.154	75.636	10.613	91.278	11.591	105.864	9.324	106.747	11.25	116.755	11.248	108.503
		February 2020		**March 2020**		**April 2020**		**May 2020**		**June 2020**		**July 2020**	
Current meter S.N.	**Water depth (m)**	**Maximum current speed (cm/s)**	**Current direction (°)**	**Maximum current speed (cm/s)**	**Current direction (°)**	**Maximum current speed (cm/s)**	**Current direction (°)**	**Maximum current speed (cm/s)**	**Current direction (°)**	**Maximum current speed (cm/s)**	**Current direction (°)**	**Maximum current speed (cm/s)**	**Current direction (°)**
314	1930	14.950	140.652	11.040	56.609	11.307	125.991	14.987	14.765	15.023	62.421	19.695	44.894
1016	5150	3.783	145.235	5.361	78.011	0.784	61.860	-1.695	356.671	-2.601	318.745	-2.452	325.065
1018	5250	16.051	147.727	13.884	68.334	8.969	334.610	11.344	320.500	9.859	312.014	10.533	314.010
1049	5350	18.534	141.818	15.801	100.402	9.227	337.519	11.053	0.21	8.76	323.645	11.769	275.427
Current	**Water**	**August 2020**		**September 2020**		**October 2020**		**November 2020**		**December 2020**		**January 2021**	

meter S.N.	depth (m)	Maximum current speed (cm/s)	Current direction (°)	Maximum current speed (cm/s)	Current direction (°)	Maximum current speed (cm/s)	Current direction (°)	Maximum current speed (cm/s)	Current direction (°)	Maximum current speed (cm/s)	Current direction (°)	Maximum current speed (cm/s)	Current direction (°)
314	1930	13.510	44.238	21.047	120.856	14.722	142.537	13.492	140.864	13.341	283.765	16.451	252.118
1016	5150	-0.356	21.516	2.454	148.725	-2.937	326.278	-2.062	269.635	-2.437	199.942	0.532	179.435
1018	5250	8.395	121.995	13.521	1.026	16.374	322.661	9.254	231.070	8.643	199.862	12.171	181.074
1049	5350	9.464	127.935	14.959	7.003	15.078	336.909	9.714	138.955	9.438	287.507	10.377	169.166

		February 2021		March 2021	
Current meter S.N.	Water depth (m)	Maximum current speed (cm/s)	Current direction (°)	Maximum current speed (cm/s)	Current direction (°)
314	1930	13.852	256.528	16.069	241.104
1016	5150	1.354	139.804	2.250	152.857
1018	5250	10.462	112.723	14.444	158.072
1049	5350	10.205	116.969	15.319	119.17

4.7 Chemical oceanography characteristics

Minmetals has surveyed the baseline characteristics of chemical oceanography in the Block A-5. The data in this section mainly came from Minmetals' 2019, 2021 and 2022 survey cruises. CTD water sampler was used to collect seawater samples through full ocean depth during these survey cruises. The chemical survey items of seawater mainly include pH, DO, nitrate (NO_3^-), silicate (SiO_3^{2-}), reactive phosphate (PO_4^{3-}), nitrite (NO_2^-), ammonium (NH_4^+), TSM and POC.

Among them, there are four CTD sampling stations located in the PRZ of the Block A-5 and three CTD sampling stations located in the IRZ of the Block A-5 (Figure 4.7-1).

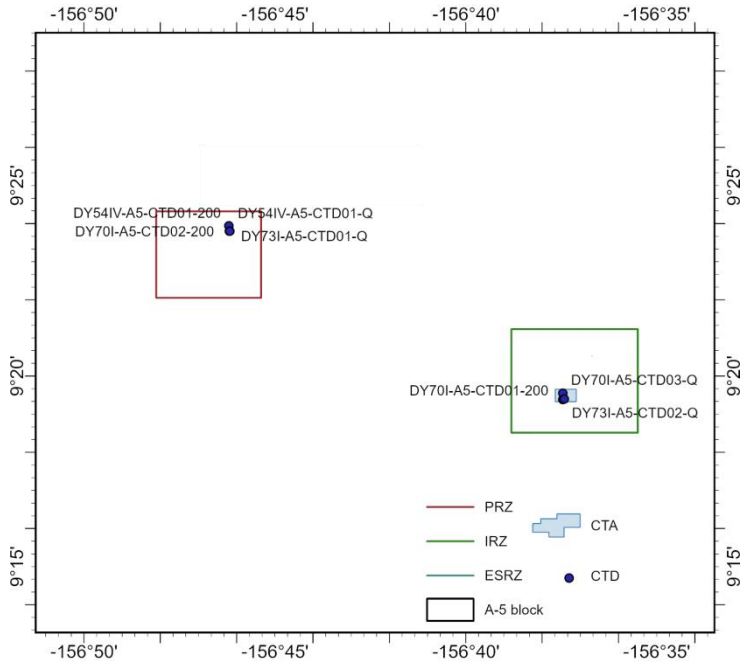

Figure 4.7-1 Distribution of CTD sampling stations during previous survey cruises and the locations of the IRZ and PRZ in the Block A-5

4.7.1 pH

The variation range of pH at the CTD survey stations in the IRZ and PRZ of the Block A-5 is 7.55-8.37, averaging 7.78 (Figure 4.7-2a). The entire-water-column pH of seawater shows obvious stratified distribution characteristics, and the pH is the highest in the surface-layer water, with thermocline occurring at about 100 m below

surface, the pH generally reaching the lowest in the water layer of 300 m. With the increasing depth, the pH rises slowly, and stabilizes at 7.6-7.8 from 2,000 m to water depth to the bottom.

In the eastern part of the CCZ, the pH in the NORI-D region ranges from 7.61 to 8.04 (NORI 2022), similar to that in the Block A-5. On the variation characteristics of pH profile, the Block A-5 and NORI-D region are basically the same, but the water layer with minimum pH in the Block A-5 is higher than that in the NORI-D region.

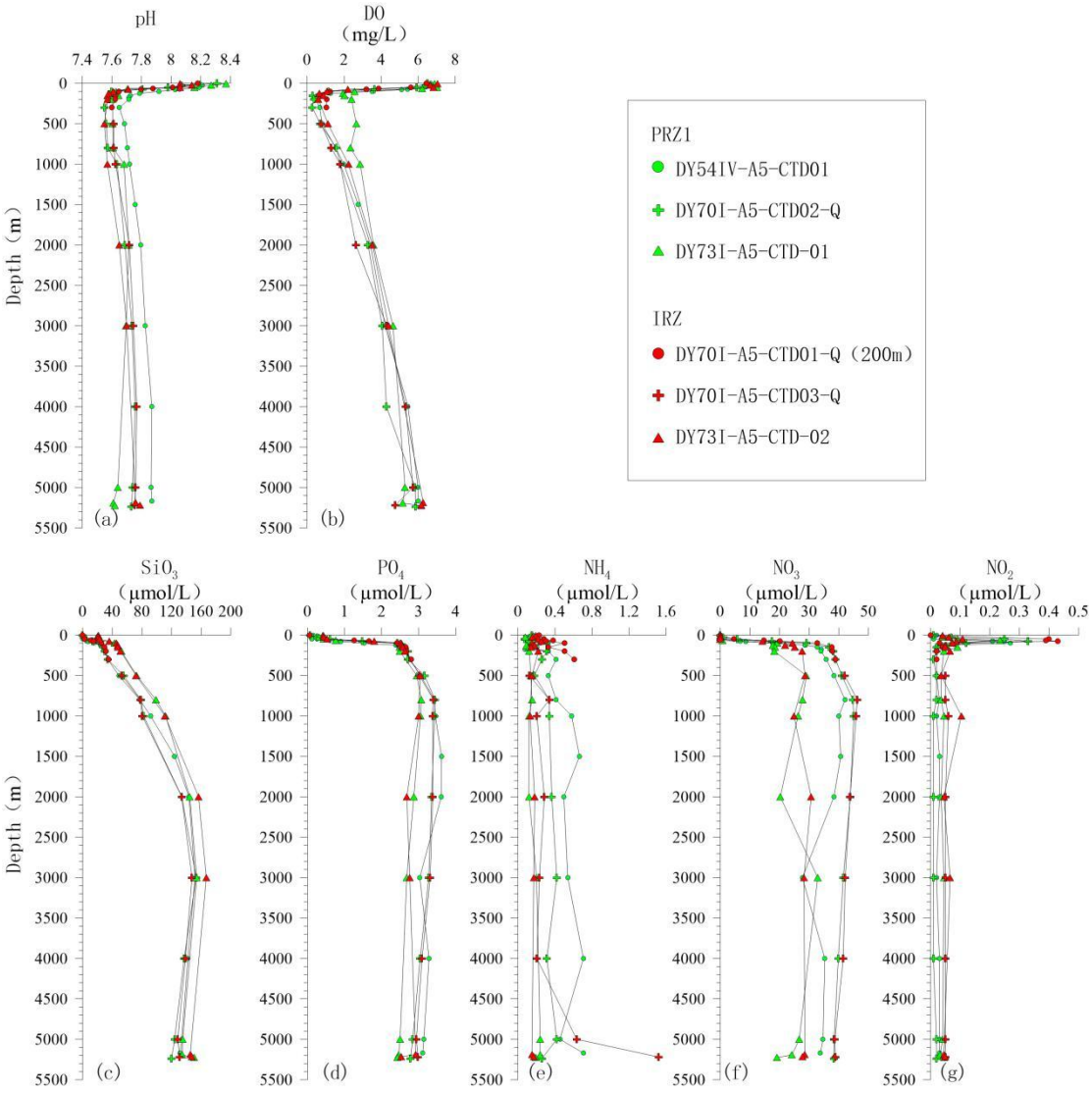

Figure 4.7-2 Vertical distribution characteristics of seawater pH, DO and nutrients in the Block A-5

4.7.2 DO

The DO measurement results with CTD in the IRZ and PRZ of the Block A-5 are

shown in Figure 4.7-2b. The DO concentration is in the range of 0.29-7.04 mg/L, averaging 3.53 mg/L. The variation trend of DO in water column is similar to that of pH, showing obvious stratified distribution. The highest value appears in the surface layer, and the DO in the surface layer is high due to the photosynthesis of a large number of phytoplankton and the mixing of surface layer. With increasing depth, the DO in the water column decreases sharply, and a thermocline appears between 50 m and 100 m, while the DO at different stations between 100 m and 1,000 m continue to decrease to less than 2.0 mg/L, showing the typical minimum DO layer characteristics in the Pacific Ocean and a significant phenomenon of anoxia. Below 1,000 m, with the increasing depth, the DO begins to rise slowly and returns to 4.0-6.0 mg/L in the bottom-layer seawater.

The range of DO in the NORI-D region is 0-7.6 mg/L, and the DO is the highest in the surface layer, and then rapidly decreases within 100 m. It is less than 2 mg/L in the water at the depth of 80-1,500 m, and gradually increases to 4.5 mg/L from the water depth of 1,500 m to the near-bottom layer. The variation of DO profile in the Block A-5 is basically consistent with that in the NORI-D region, but the layer with minimum DO concentrations is shallower in the Block A-5 than in the NORI-D region. However, the DO in the near-bottom layer of the Block A-5 is higher than that in the near-bottom layer of NORI-D region (NORI 2022).

4.7.3 Nutrients

The nutrient measurement results in the Block A-5 are shown in Figure 4.7-2.

NH_4^+ concentrations are low in the range of 0.07-1.52 μmol/L, averaging 0.28 μmol/L. The variation of NH_4^+ in the water column is unstable, showing great fluctuations above 1,000 m water depth. The variations are relatively small between 1,000 m and 5,000 m water depths, with differences between stations. The near-bottom-layer NH_4^+ vary slightly larger between stations.

NO_2^- concentrations vary in the range of 0.00-0.43 μmol/L, averaging 0.07 μmol/L. It is very low in the surface layer and generally reaches the maximum value

at around 75 m water depth, and then decreases rapidly. Below the depth of 100 m, it remains relatively stable, with no obvious variation trend.

NO_3^- concentrations vary in the range of 0.00-46.22 μmol/L, averaging 25.83 μmol/L. It is very low in the surface layer and gradually increases from the surface layer to the water depth of 800 m. It generally reaches the maximum at about 800 m water depth, and then slowly decreases.

PO_4^{3-} concentrations vary in the range of 0.06-3.62 μmol/L, averaging 2.30 μmol/L. PO_4^{3-} is similar to NO_3^- in terms of vertical distribution characteristics. Its concentration in the surface layer is very low, and gradually decreases downward, reaching the maximum at approximately 800 m water depth, and then slowly decreases with the increasing depth.

The SiO_3^{2-} is in the range of 0.00-166.89 μmol/L, averaging 68.79 μmol/L. It is very low in the surface layer and gradually increases with the increasing depth, reaching the maximum at approximately 3,000 m water depth, and then slowly decreases with the increasing depth.

To sum up, the variations of nutrient concentration profiles in the PRZ and IRZ of the Block A-5 are basically similar.

The concentrations of NO_3^-, NO_2^-, $PO_4^{3-}$and SiO_3^{2-}in NORI-D Contract Area in the eastern part of the CCZ all have the lowest values at 0-50 m water depth. Eutrophic water appears at 50-100 m. At the water depth of 950-1,500 m, most of the nutrient concentrations have the highest values at the bottom of minimum DO layer, while the concentration of SiO_3^{2-} reaches the maximum at the sampling depth of 2,500-3,000 m. The concentration profiles of PO_4^{3-} and SiO_3^{2-} in the Block A-5 are basically consistent with those in the NORI-D region (NORI 2022).

4.7.4 TSM

The TSM data in this section are from the CTD survey results of Minmetals' 2021 survey cruise.

The TSM content measurement results in the Block A-5 are shown in Figure 4.7-

3. At DY70I-A5-CTD01&03 and DY70I-A5-CTD02 stations, the TSM contents are in the range of 0.08-1.71 mg/L and 0.14-2.05 mg/L, averaging 0.89 mg/L and 0.90 mg/L respectively. The vertical variation trends of TSM content at these two stations are similar, and the TSM content in the upper layer above the water depth of 300 m is relatively high. In the layer of 300-4,000 m water depth, the TSM content is low and varies little. However, the TSM content reaches the maximum below the water depth of 5,000 m, which may be caused by the resuspension of bottom-layer sediments.

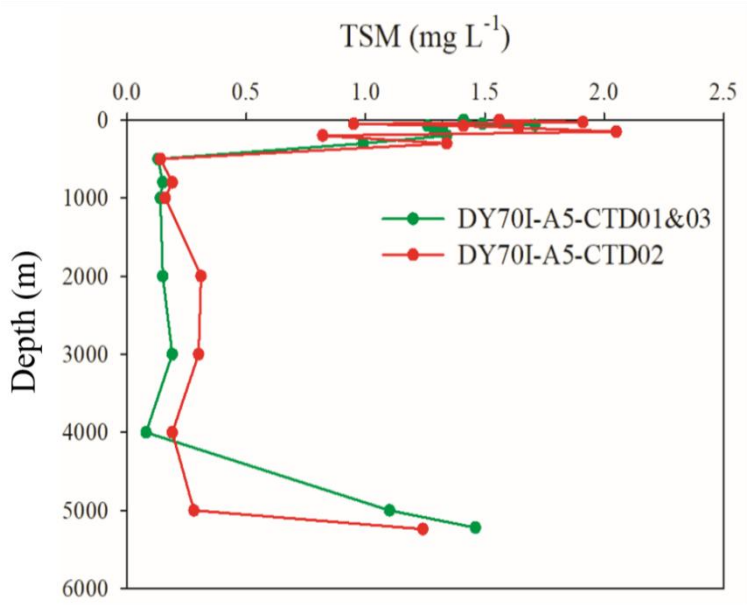

Figure 4.7-3 Distribution characteristics of seawater TSM content in the Block A-5

4.7.5 POC

The measured results of POC in the Block A-5 are shown in Figure 4.7-4. The POC contents at DY70I-A5-CTD01-Q&03-Q and DY70I-A5-CTD02-Q stations are in the range of 0.006-0.045 mg/L and 0.008-0.043 mg/L, averaging 0.019 mg/L and 0.022 mg/L, respectively. The POC content is relatively high in the surface layer above the water depth of 300 m, then gradually decreases with the increasing water depth, and reaches a stable level at the water depth of 2,000 m. Below 2,000 m, the POC content stabilizes at a low level.

The POC content in the NORI-D region in the eastern part of the CCZ is relatively high in the 0-50 m water layer. It shows an exponential decline with

increasing depth (NORI 2022), which is generally consistent with the POC content profile variation characteristics in the Block A-5.

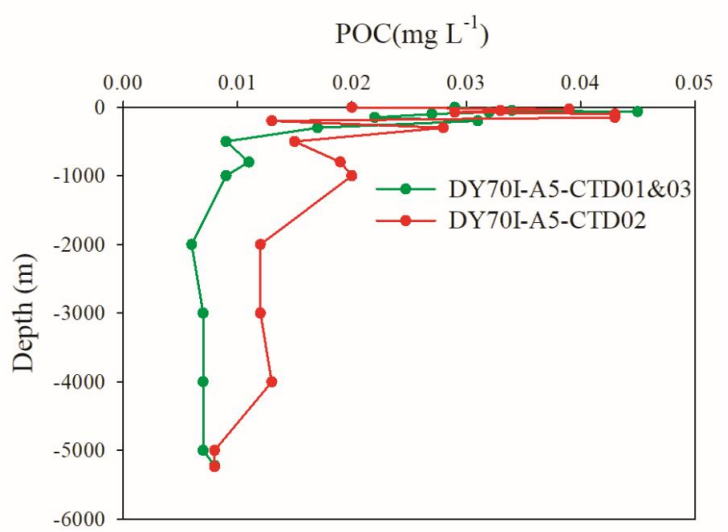

Figure 4.7-4 Distribution characteristics of seawater POC content in the Block A-5

4.7.6 Dissolved inorganic carbon (DIC) and TOC

The DIC measurement results in the Block A-5 are shown in Figure 4.7-5. At DY50I-A5-S06-CTD10 station, the DIC content is in the range of 1,979.2 - 2,416.4 μmol/L, averaging 2,293.9 μmol/L. In the water column above 100 m depth in the surface layer, the DIC content increases rapidly with the increasing water depth. From 100 m to 2,500 m, the DIC content increases slowly to the maximum with the increasing water depth. Below 2,500 m, the DIC content decreases slowly with the increasing water depth.

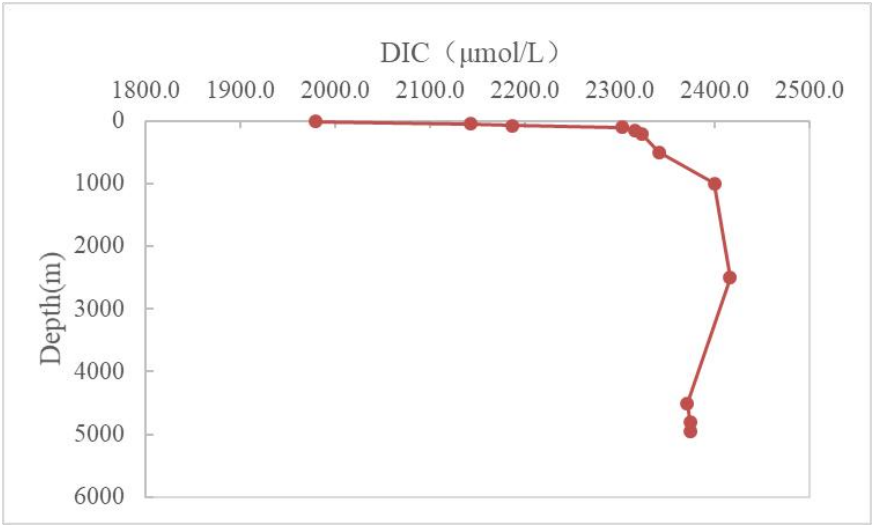

Figure 4.7-5 Distribution characteristics of seawater DIC content in the Block A-5

The TOC measurement results in the Block A-5 are shown in Figure 4.7-6. At DY50I-A5-S06-CTD10 station, the TOC content is in the range of 0.56-1.13 mg/L, averaging 0.71 mg/L. In the water column above 1,000 m depth in the surface layer, the TOC content decreases rapidly with the increasing water depth. From 1,000 m to 4,800 m, the TOC content fluctuates greatly with the increasing water depth, and the lowest value (only 0.56 mg/L) appears at 1,000 m and 4,800 m. Below 4,800 m, the TOC content increases rapidly with the increasing water depth.

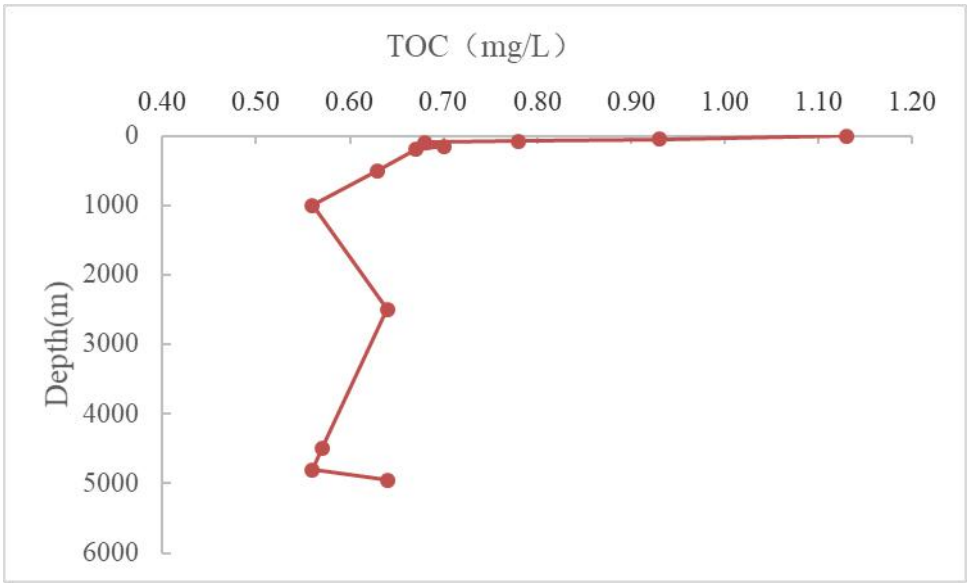

Figure 4.7-6 Distribution characteristics of seawater TOC content distribution in the Block A-5

4.7.7 Characteristics of sedimentary flux

Figure 4.7-7a shows the flux variations of settled particle samples captured at the water depth of 2,000 m at DY70II-A5-MX01 mooring station between August 2019 and August 2020. Results show that between August 2019 and August 2020, the average flux of particles in the water column captured by the sediment trap at the depth of 2,000 m was 6.98 mg m^{-2} d^{-1}. There were obvious differences in the fluxes of settled particle samples captured in this layer of water on the seasonal scale. The relatively high fluxes appear in March-June of 2020 and the relatively low fluxes appear between August 2019 and February 2020.

Figure 4.7-7b shows the flux variations of settled particle samples captured at the water depth of approximately 4,685 m at DY70II-A5-MX01 mooring station between August 2019 and August 2020. Results show that from August 2019 to August 2020, the annual average total flux of settled particles captured by the sediment trap in the water depth of 4,685 m is 4.37 mg m^{-2} d^{-1}. Compared with the upper layer (2,000 m water depth), the total flux of settled particles in this layer is relatively low. There are also obvious differences in the flux of settled particles in this layer on the seasonal scale. The relatively high fluxes appear in the first half of 2020 and the relatively low fluxes appear in the second half of 2019. The peak periods of the fluxes of settled particle samples captured by the sediment trap at the depths of 2,000 m and 4,685 m between August 2019 and August 2020 were very similar, and both had their respective peaks in April-May of 2020.

In the NORI-D region in the eastern part of the CCZ, the total flux of settled particles in the 2,000 m water layer is 20-88 mg m^{-2} d^{-1}, and the total flux of settled particles in the water layer at 500 m above the bottom is 4-68 mg m^{-2} d^{-1}, with the maximum values appearing in early April 2021 (NORI 2022), which is consistent with the month when high flux appears in the Block A-5. Generally speaking, the total fluxes of settled particles at two water depths in the NORI-D region are greater than those in the Block A-5.

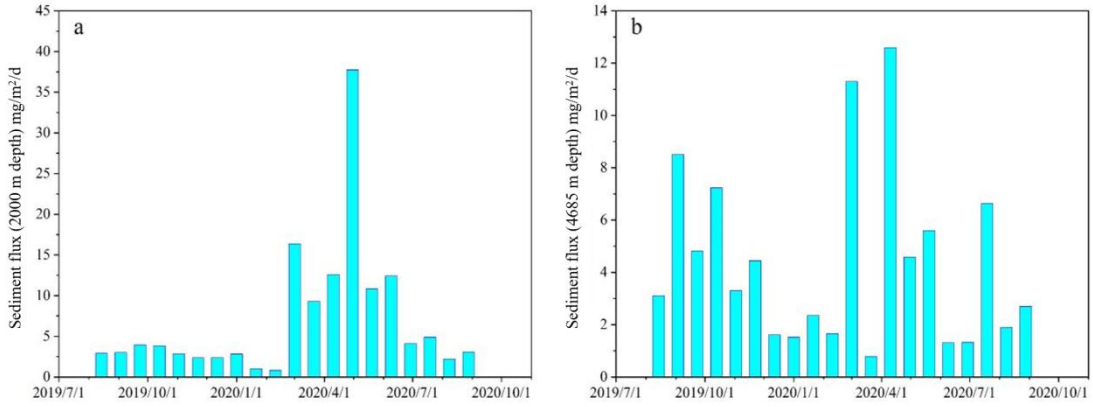

Figure 4.7-7 Variations in the fluxes of settled particle samples captured at DY70II-A5-MX01 station (August 2019 to August 2020)

a: Upper layer (2,000 m water depth); b: Upper layer (4,685 m water depth)

4.8 Natural disasters

See 10.1 and 10.2 for details.

4.9 Noise and light

Ambient noise in the ocean is usually classified according to its sources, which may include natural processes, such as wind-driven waves, rainfall, seismic activity and marine organisms. The main sources of ocean noise are different in frequency and time. The ocean noise in infrasound frequency band (1-20 Hz) is produced by the interaction between seismic activity and ground surface. The noise of 20-200 Hz in the deep sea is mainly generated by merchant vessels. The noise level is high in regions with heavy marine traffic. Wind-driven surface waves are the main source of noise in the frequency band of 200 Hz-20 kHz (Figure 4.9-1). These and other artificial sources (e.g. military sonar and seismic survey) constitute the total ocean noise (Hildebrand, 2009). These artificial noises are now considered to have a wide range of potential impacts on marine organisms (Hawkins et al., 2020).

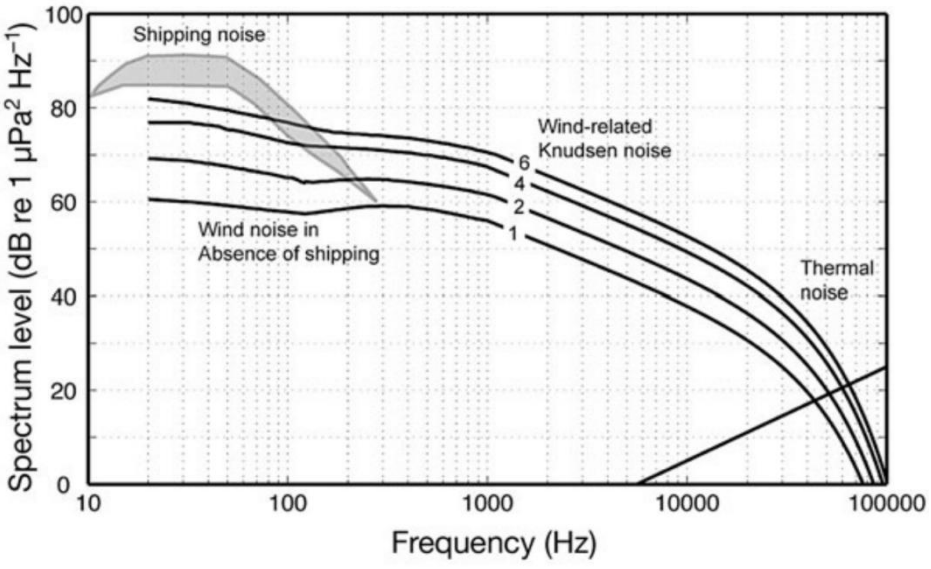

Figure 4.9-1 Generalized ocean ambient noise spectral levels for a deep-water site with the receiver located at 1,000 m depth

(Generalized ocean ambient noise spectral levels for a deep-water site with the receiver located at 1,000 m depth)(Hildebrand, 2009)

The underwater noise data collected in the western part of the CCZ are extremely

scarce. In the COMRA Contract Area, which is adjacent to the Block A-5, Niu et al. (2021) conducted long-term monitoring of the ocean noise baselines with hydrophones deployed 300 m underwater (Figures 4.9-2 ~ 4.9-4). Monitoring results show that the low-frequency high noise levels produced by distant vessels and whales are 70-100 dB (<100 Hz) and 64-93 dB (100-200 Hz) respectively. The noise level at high frequencies (>200 Hz) is low in the range of 53-75 dB, and is usually dominated by wind. The noise level in winter at this frequency is approximately 5 dB higher than that in summer, which is consistent with the seasonal wind speed variations. The underwater noise data in the eastern part of the CCZ mainly come from the NORI-D Contract Area. The shallow-layer (200-1,000 m) and deep-layer (near the bottom) underwater noises are recorded with hydrophones mounted on long mooring. Survey results show that the root mean square sound pressure level of shallow layer is 95-118 dB re 1 μPa, averaging 106 dB re 1 μPa. The range of shallow peak sound pressure level is 108-125 dB re 1 μPa. The deep-layer root mean square sound pressure level is 89-112 dB re 1 μPa, averaging 100 dB re 1 μPa. The range of peak sound pressure level in deep layer is 102-118 dB re 1 μPa, averaging 111 dB re 1 μPa (NORI 2022).

The maximum range of low-frequency noise (<50 Hz) generated by earthquake is 80-94 dB/Hz. Due to the noise of distant vessels and the sound of whales, the frequencies in all months are mainly below 100 Hz. The frequency spectrum with wind and waves as the main frequencies (>200 Hz) is low (<65 dB/1 μPa^2/Hz). In the frequency range of 50-300 Hz, the monthly variations are large (approximately 13 dB re 1 μPa2/Hz at 200 Hz), while in the frequency ranges below 50 Hz and above 300 Hz, the monthly variations are small (approximately 6 dB re 1 μPa2/Hz at 40 Hz and 500 Hz). The basic frequency of the sound made by *Balaenoptera physalus* is lower than 1 kHz. The sounds of two different kinds of whales have been recorded in this study. The pulse generated by *Balaenoptera physalus* in the frequency range of 20-30 Hz leads to an increase in noise (5-8 dB), which can be seen in the average frequency spectrum of most months. The signal produced by *Balaenoptera musculus* is obvious

during September-December and April-May, and the ambient noise level increases by approximately 2 dB in the range of 44-48 Hz. Due to the vocalization of fish, the noise spectrum level of 200 Hz to 500 Hz increases to approximately 10 dB/1 μPa2/Hz in May-July.

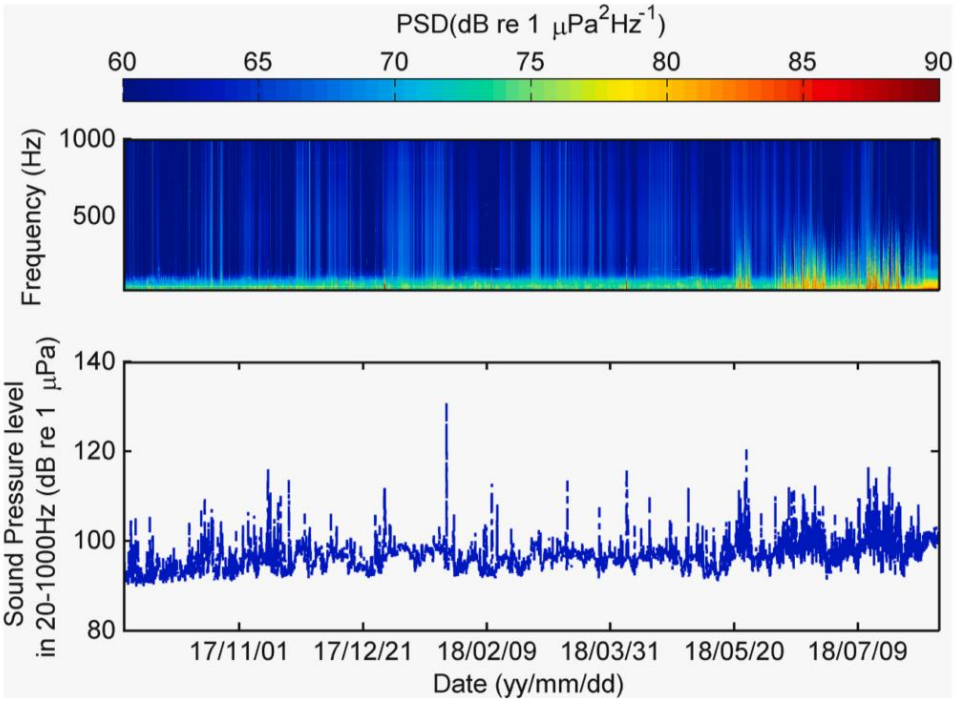

Figure 4.9-2 PSD and SPL in 20-1,000 Hz of acoustic data acquired with an autonomous hydrophone installed at the depth of 300 m

(PSD and SPL in 20–1,000 Hz of acoustic data acquired with an autonomous acoustic recorder installed at depth of 300 m)(Niu et al., 2021)

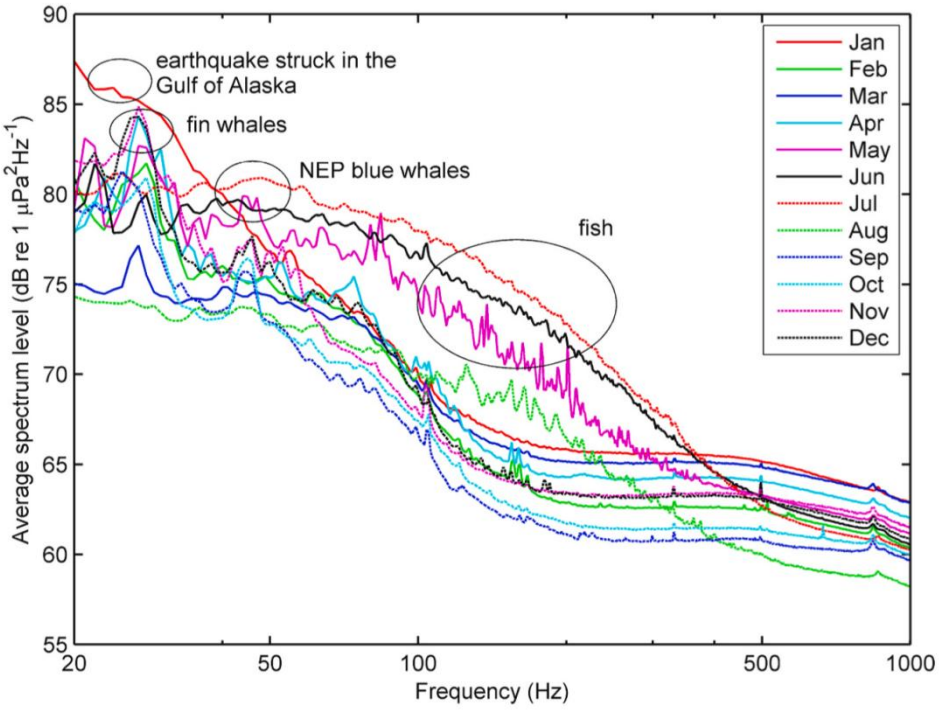

Figure 4.9-3 Monthly average sound pressure spectrum levels recorded with hydrophone monitoring at the depth of 300 mm (20-1,000 Hz)

(Different line types and colors indicate different months; the circled areas respectively indicate the frequency bands representing seismic activity, the calls of Balaenoptera physalus and Balaenoptera musculus, and other fish.)

(Average monthly sound pressure spectrum levels from 20 Hz to 1,000 Hz. Different line types and colors indicate individual months. Circled areas indicate frequency bands representative of seismicity, fin whale calls, northeast Pacific (NEP) blue whale calls, and fish, respectively, with an autonomous acoustic recorder installed at depth of 300 m)(Niu et al., 2021)

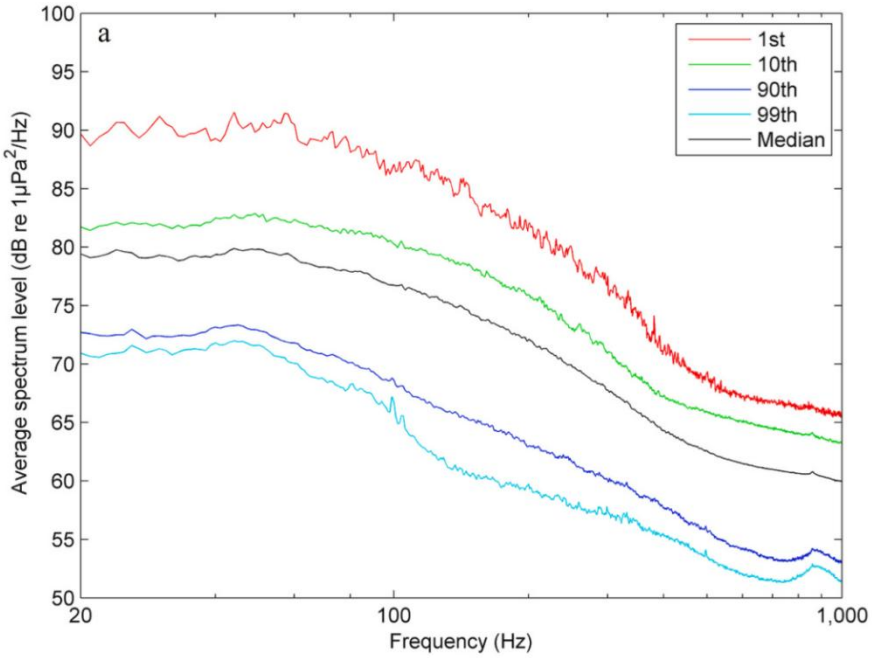

Figure 4.9-4 Percentile frequency distribution of sound pressure spectrum recorded with hydrophones at the depth of 300 m in July

(Different colors indicate different percentiles) (Niu et al., 2021)

During the survey of environment baselines, we installed hydrophones on the submerged buoys of mooring in the Block A-5 to monitor the noise level there. The deep-sea submerged buoys of mooring with hydrophones have not yet been recovered.

In this test, we will measure the noise generated by the mechanical parts of the collector vehicle and the noise generated during the traveling and nodule-collecting activities in detail.

The Block A-5 is far away from human habitation, and there is generally no artificial lighting in the upper layer of ocean. Only some vessels pass by occasionally. In this test, we will measure the collector vehicle's illuminance light attenuation during the seabed test.

4.10 Summary of existing physicochemical environment

The topography of the Block A-5 is generally flat, with sea knolls, sea knoll groups, seamounts and intermontane basin. Hereinto, the ocean basin zone accounts for 70.8 %. The results of near-bottom acoustic survey by AUV show that the TMA has a small relief, and there is no obvious steep slope. Both the IRZ and PRZ are located in the ocean basin zone, with gentle topography and an elevation difference of less than 20 m.

The nodule abundance in the TMA varies in the range of 0.59 - 25.92 kg/m^2, averaging 14.04±4.69 kg/m^2. The shipboard photography coverage varies in the range of 2 % - 85 %, averaging 43±15 %. There is a sound positive correlation between shipboard photography coverage and nodule abundance (R^2=0.82), and most of the nodules in the TMA are exposed. The IRZ and PRZ have similar nodule abundance (10 -15 kg/m^2) and nickel equivalent grade (NEG), indicating that these two zones have similar resources.

The silt-grade content in the surface-layer sediment of the Block A-5 is the

highest (approximately 53 % on average), followed by clay-grade content (approximately 35 % on average). The sand-grade content is comparatively low. The contents of heavy metals (e.g. Cd, Cr, Ni, Cu, Zn and Pb) in sediments are unevenly distributed, generally low except for the northeast and southwest corners of the PWA. Total organic carbon (TOC) is low (<0.25 %) in the northeast and southwest corners of the PWA, while the TOC contents in other areas are in the range of 0.25-0.45 %. Survey results show that the IRZ and PRZ have similar particle sizes, heavy metal and organic carbon contents in sediments.

In the IRZ and PRZ, the contents of heavy metals in the pore water of sediments shallower than 0-30 cm are generally low, while the contents of heavy metals (e.g. Cr, Cd, Zn, Ni and Pb) are close to those of overlying water collected with box corer. These two zones have similar total nutrient contents in the pore water, as well as the same variation of nutrients with increasing depths. The total alkalinity in pore water in sediments shallower than 30 cm is basically stable at 2.4 mmol/L.

In shallower-than-10-cm sediments collected with multicorer in the Block A-5, the chlorophyll *a* (Chl *a*) concentration per unit wet weight is 0-0.0239 μg/g and that per unit dry weight is 0.0001-0.1058 μg/g. Under the influence of burial degradation, the Chl *a* concentration shows a gradual decline trend, with the Chl concentration in the surface-layer sediments (shallower than 3 cm) accounting for more than 80 %.

In-situ geotechnical properties test results show that penetration/shear strength of sediment at 1 m depth in the Block A-5 increase in a nonlinear or linear way with increasing depth.

The results of temperature and salinity profile observation show that the Block A-5 has a similar interannual variation trend in full-depth temperature profile. In different years, the vertical variation trends of temperature in the upper layer (no deeper than 200 m) are basically similar, but the thermocline positions are slightly different, with a variation of about 40 m. The deep-layer temperature variation trends are similar, with a variation of about 0.03℃. In the Block A-5, the interannual variation trends of full-depth salinity profile were similar in 2019, 2021 and 2022.

The analysis results of the measured flow of ship-mounted Acoustic Doppler

Current Profiler (ADCP) show current speed and directions vary significantly in different years in this area. The current speeds observed during the 2017 and 2021 survey cruises were relatively high, exceeding 1 m/s locally, while those observed during the 2019 and 2022 survey cruises were usually less than 0.5 m/s. Equatorial countercurrents are dominant in the Block A-5.

The long-term monitoring results of deep-sea currents in this area obtained by using submerged buoys of mooring show that the annual average speeds of deep-sea currents (water depths of 5,150 m, 5,250 m and 5,350 m) are in the range of 4.56 - 4.83 cm/s, and the average direction is eastward. The seawater flow field in the middle layer (water depth of 1930 m) is dominated by eastward flow, with the speed in the range of 6 - 12 cm/s (averaging 7.34 cm/s).

The monitoring results of the turbidimeter mounted on the mooring show that most of the time, the turbidity of seawater in the bottom layer (20 m above the bottom) and near-bottom layer (100 m above the bottom) is critical to the detection limit of equipment, and the overall turbidity is below 0.4 FTU.

The pH of seawater at full ocean depth in the Block A-5 presents obvious stratified distribution characteristics, and is the highest in the surface-layer water column. Between the surface and 100 m water depth, the pH decreases rapidly, reaching the lowest at approximately 300 m water depth. Then, the pH increases slowly with increasing depth, and tends to be stabilize at 7.6 - 7.8 below the water depth of 2,000 m.

The dissolved oxygen (DO) in seawater is the highest in the surface layer, and then decreases sharply to less than 3.0 mg/L at the depth of 100 – 200 mm at all stations, indicating the phenomenon of hypoxia. Below 1000 m, with the increasing depth, the DO begins to rise slowly back to 4.0-6.0 mg/L in the bottom-layer seawater.

The concentrations of inorganic nitrogen (including ammonium, nitrate and nitrite), silicate and reactive phosphate in the Block A-5 are in the following descending order: silicate > inorganic nitrogen > reactive phosphate. There is a significant correlation between the concentration of particulate organic carbon (POC) and the content of total suspended particulate matter (TSM) in the seawater column. The variation of POC content with depth may be related to the vertical distribution of Chl (mainly plankton) in the seawater, since the relatively strong plankton activity in

the subsurface may produce higher POC content.

4.11 References

Liang Chujin. Internal mixing and near-bottom low-frequency fluctuation in China's p olymetallic nodule pioneer areas [D]. Gradual School of the University of Chines e Academy of Sciences (IOCAS), 2005.

Ni Jianyu, Zhou Huaiyang, Peng Xiaotong, Liang Chujin. Deep-sea environments in China's polymetallic nodule pioneer areas [J]. Marine Geology & Quaternary Ge ology, 2002,(01):43-47.

Zhang Guozhen, Zeng Ruijian, Zhang Xuehua. Mooring observation of bottom-layer ocean currents in China's pioneering areas in the East Pacific Ocean [J]. Marine Geology & Quaternary Geology, 1999,(03):118-123.

Aller, J. Y. (1997). "Benthic community response to temporal and spatial gradients in physical disturbance within a deep-sea western boundary region." Deep Sea Rese arch Part I: Oceanographic Research Papers 44(1): 39-69.

Dutkiewicz, A., Müller, R. D., O'Callaghan, S., & Jónasson, H.. Census of seafloor se diments in the world's ocean.Geology, G36883-1.doi: 10.1130/G36883.1 (2015).

Dutkiewicz, A., Müller, R. D., Wang, X., O'Callaghan, S., Cannon, J., &Wright, N. M. Predicting sediment thickness on vanished ocean crust since 200 Ma. Geochemi stry, Geophysics, Geosystems, 18, 4586–4603 (2017).

Dutkiewicz, A., et al.."Environmental predictors of deep-sea polymetallic nodule occu rrence in the global ocean." Geology 48: 293-297 (2020).

International Seabed Authority (ISA). A geological model of polymetallic nodule depo sits in the Clarion-Clipperton Fracture Zone. Technical Study 6, Kingston, p. 211 (2010).

Hawkins, Anthony D. "The Potential Impact of Offshore Wind Farms on Fishes and In vertebrates." Advances in Oceanography & Marine Biology (2020): n. pag.

Hildebrand, J. A. (2009). "Anthropogenic and natural sources of ambient noise in the ocean." Marine Ecology Progress Series 395: 5-20.

Macdonald, K.C., Fox, P.J., Alexander, R.T., Pockalny, R., Gente, P. Volcanic growth f aults and the origin of Pacific abyssal hills. Nature, 380, 125-129 (1996).

Müller, R. D., Seton, M., Zahirovic, S., et al. Ocean basin evolution and global-scale p late reorganization events since Pangea breakup, Annual Review of Earth and Pla netary Science, 44, 107-138 (2016).

NORI. 2022. Collector Test Study – Environmental Impact Statement – Testing of polymetallic collector system components in the NORI-D contract area, Clarion Clipperton Zone, Pacific Ocean. Jamaica.

Straume, E.O., Gaina, C., Medvedev, S., Hochmuth, K., Gohl, K., Whittaker, J. M., et al.. GlobSed: Updated total sediment thickness in the world's oceans. Geochemistry, Geophysics, Geosystems, 20. DOI: 10.1029/2018GC008115 (2019).

5 Description of Existing Biological Environment

5.1 Key information

This Chapter mainly describes the existing biological environment characteristics of the Contract Area. In general, regional biological environment analysis based on available data indicate that the region is characterized by low biomass and high diversity.

Minmetals has conducted biodiversity surveys on primary production, Chl *a*, microorganisms, phytoplankton, zooplankton, meiofauna, macrofauna, megafauna and scavengers in the Block A-5. This Chapter introduces the survey results of biological environment baselines, including the quantitative distribution and diversity characteristics of different fauna in the surface, middle and bottom layers of marine environment. It is considered that the biological environment of the IRZ is similar to that of the PRZ, especially the bottom biological characteristics, and has similarity with other blocks within the CCZ, especially the western part of the CCZ.

5.2 Overview of the region

According to the biogeography on a global scale, there are three biogeographic provinces on upper-layer biological communities in the CCZ of the East Pacific Ocean: The North Central Pacific Province, the Equatorial Pacific Province and the Eastern Tropical Pacific Province (Figure 5.2-1). By benthic community, there are mainly two biogeographic provinces in the CCZ of East Pacific Ocean, namely North Central Pacific Province and Equatorial Pacific Province (Figure 5.2-2). However, there is no relevant study on biogeographic provinces at the CCZ scale.

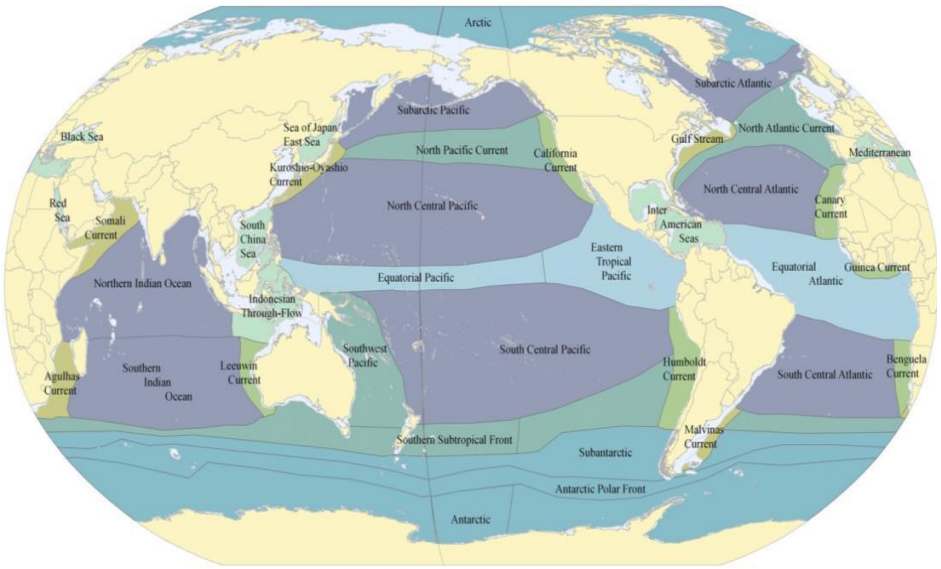

Figure 5.2-1 Biogeographic provinces of upper-layer biological communities on the global scale (Spalding et al., 2012)

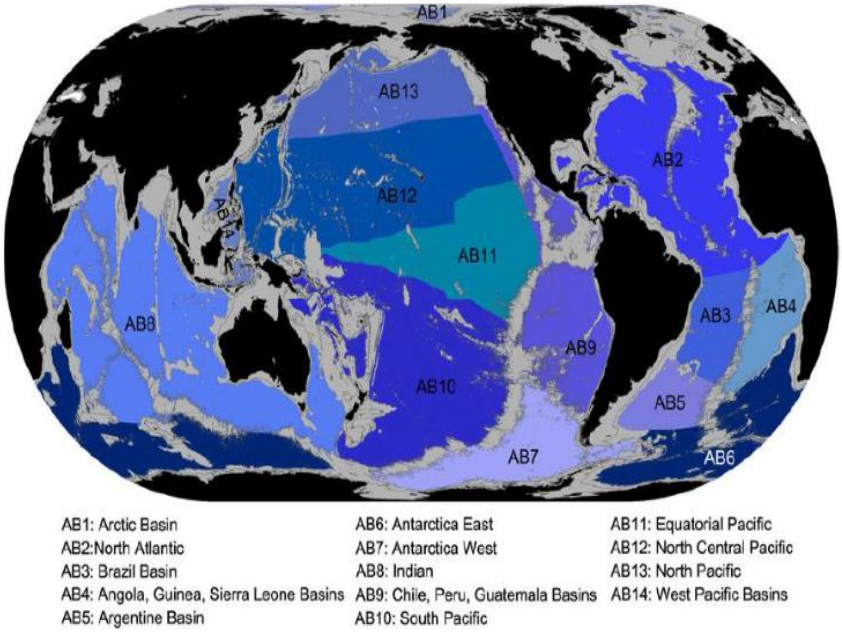

Figure 5.2-2 Biogeographic provinces of abyssal bottom biological communities on a global scale (Watling et al., 2013)

The study results of Kaplan Project and CeDAMar Project show that the biological environmental parameters in the CCZ feature obvious latitudinal and meridional gradient variations, which are generally high in the east, low in the west, high in the south and low in the north, including the distribution of chlorophyll concentration and primary production in the upper layer of ocean and the POC flux on floor. The findings of relevant studies show that the POC flux varies widely among

blocks in the range of 0.8-2.9 g C_{org} $m^{-2}y^{-1}$ (Figure 5.2-3). The primary production varies from north to south and from east to west, and the higher primary production occurs in the eastern and southern parts near the equatorial upwelling (Figure 5.2-4).

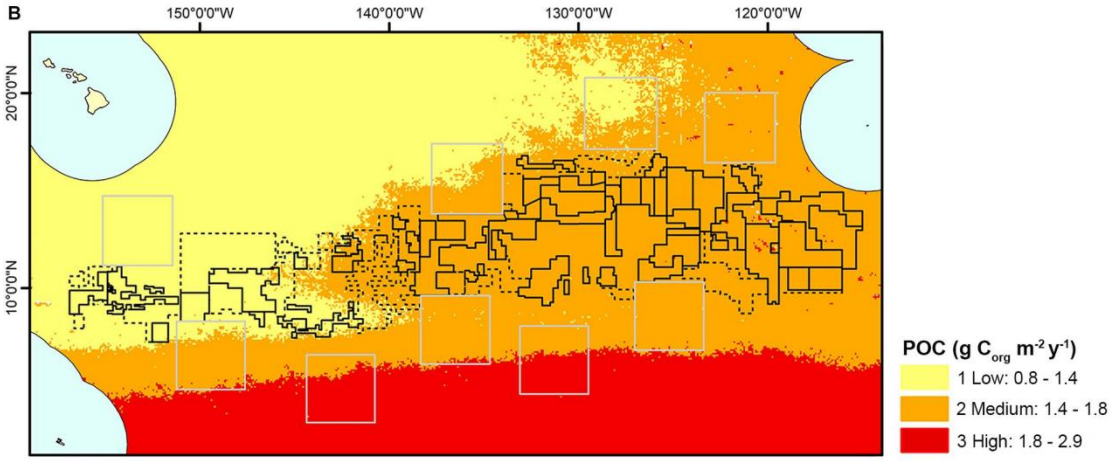

Figure 5.2-3 Distribution of POC fluxes in the CCZ (McQuaid et al., 2020)

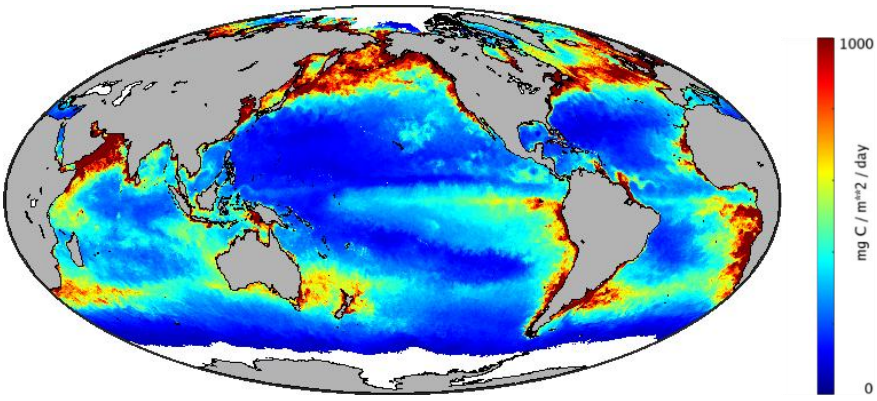

Figure 5.2-4 Distribution of primary production in global ocean

(Source: www.sites.science.oregonstate.edu/ocean.productivity/index.php)

The findings of studies on 12-24 samples collected with box corer during the joint survey cruise of Britain and other European Union countries in the UK1 Contract Area show that species with only 1-2 individuals account for 60 % of all species in the region, and rare species hold a key position in the region. The results of molecular and morphological studies show that 90 % of macrofauna in the region are new species, and the number of new species increases continuously alongside sampling intensity. Rabone et al. found that 92 % of the species identified in the CCZ were new species, and only 436 among 5,578 recorded species were named species (Rabone et al., 2023). Generally speaking, the region is characterized by low biomass and high diversity.

5.3 Studies completed

By the end of 2023, Minmetals has carried out about 122 environmental-related survey projects in the Block A-5 of the Contract Area, mainly including 13 seabed photography survey lines (including two optical survey lines by AUV), box corer sampling at 22 stations, multicorer sampling at 25 stations, full-ocean-depth profiling CTD measurement at 13 stations, 200 m depth CTD measurement at eight stations, plankton multinet sampling at three stations, plankton vertically towed net sampling at nine stations and baited trap lander observation at six stations. On this basis, we have conducted biodiversity testing and analysis of primary production, Chl *a*, microorganisms, phytoplankton, zooplankton, meiofauna, macrofauna, megafauna and scavengers.

5.4 Biological environment characteristics

5.4.1 Surface layer

5.4.1.1 Seabirds, turtles and marine mammals

No systematic and detailed survey and distribution assessment of seabirds and marine mammals have been conducted in the Block A-5 during previous cruises. Only general observation and photograph recording have been conducted during these survey cruises. Generally speaking, distribution of these species (e.g. the densities of phytoplankton, zooplankton, small nekton and fish) may reflect the abundance of prey. Therefore, the densities of seabirds and marine mammals can be deduced from the primary production of the upper-layer ocean. Due to the strong spatial gradient, primary production is significantly higher in the eastern part than in the western part of the CCZ (e.g. Block A-5). So, the densities of seabirds and marine mammals may have a similar spatial distribution trend.

During Minmetals' 2022 survey cruise, we have observed six species of seabirds in the Block A-5. Boobies are the dominant species, while most other species only appear occasionally.

There was no record of direct sighting of whales or dolphins during our cruises in the Block A-5 of the Contract Area.

In the NORI-D Contract Area in the eastern part of the CCZ, 323 biological observations were recorded through the observation of PelagOS project and three survey cruises. Results show that birds are the main species, followed by fish, marine mammals and reptiles (NORI 2022). All kinds of boobies are the most commonly recorded birds, which is similar to that in the Block A-5.

Due to the lack of direct records of cetaceans from our cruise observations, we searched for data on globally important marine mammal areas in the oceans given by the IUCN MARINE MAMMAL PROTECTED AREAS TASK FORCE. This database is maintained on an on-going basis by a number of global organizations, including the International Committee on Marine Mammal Protected Areas (ICMMPA), the International Union for Conservation of Nature's (IUCN) World Commission on Protected Areas (WCPA), and the IUCN Species Survival Commission (SSC). The assessment results associated with this database indicate that the Block A-5 is far from marine mammal protected areas ("Important Marine Mammal Areas" in the figure below) and areas where there is scientific evidence that they are worthy of protection ("Areas of Interest" in the figure below) (Figure 5.4-1).

The "Whale Superhighway" report, published by the World Wide Fund for Nature (WWF) in collaboration with dozens of research organizations around the world, also provides a clear picture of the main migration corridors for cetaceans around the world, with the closest corridor to the western part of the CCZ being the migration pathway between the area around the Hawaiian Islands and the high-latitude offshore areas of the north-eastern Pacific Ocean. This pathway is far from the Minmetals Block A-5 , which is located south of the Hawaiian Islands (Figure 5.4-2).

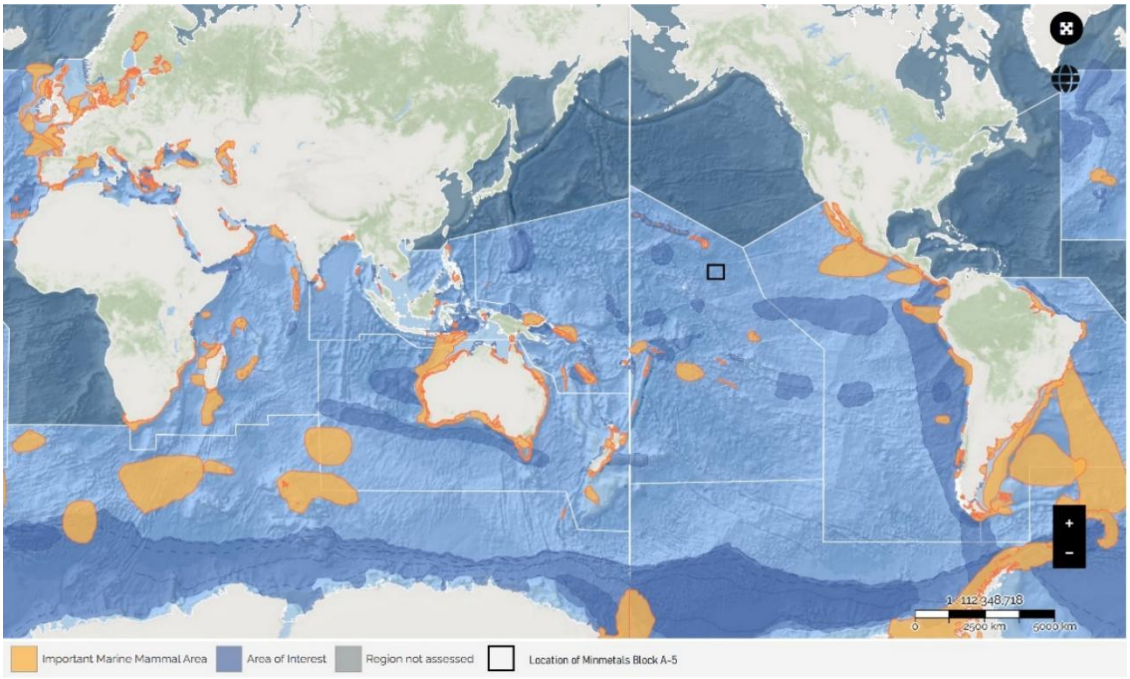

Figure 5.4-1 Important Marine Mammal Areas in global ocean (marinemammalhabitat.org)

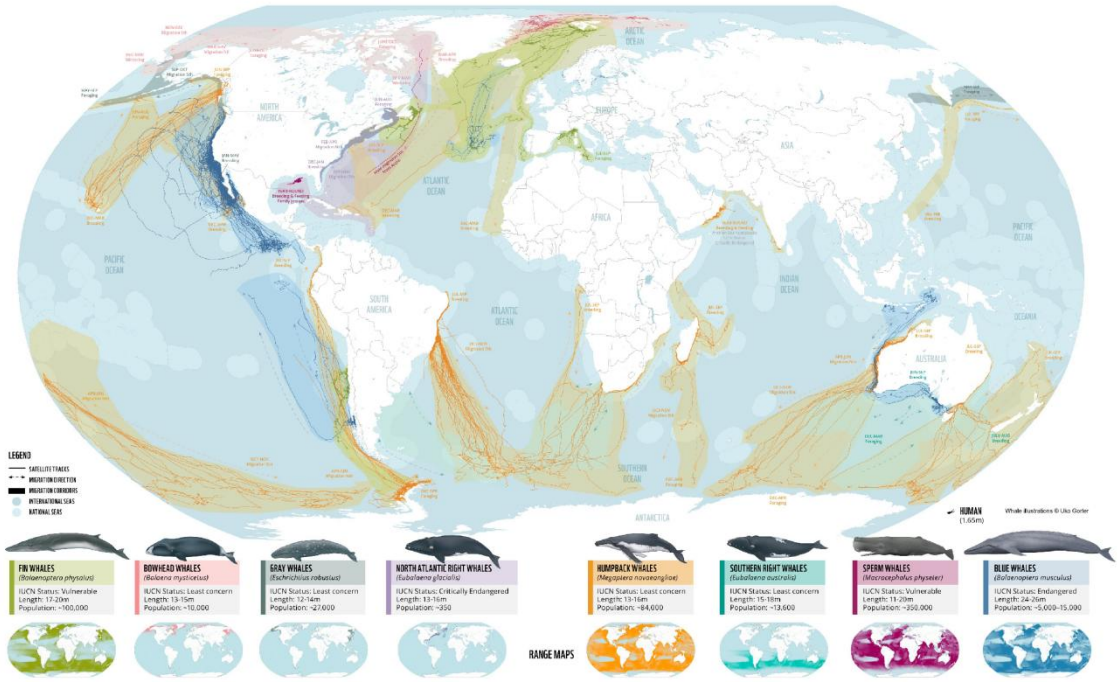

Figure 5.4-2 Main migration corridors for cetaceans around the world (wwfwhales.org)

Due to the lack of direct records of turtles from our cruise observations, we searched for data on two main species of sea turtles in east Pacific Ocean, named as Leatherback Turtles (*Dermochelys coriacea*) and Loggerhead Turtle (*Caretta caretta*).

The Pacific leatherback Turtle is one of flagship species for marine conservation. This species has therefore received considerable attention in terms of monitoring and conservation. The leatherback turtles in eastern Pacific Ocean tended to move within a migratory corridor to foraging grounds in the southeast Pacific, and their concentrated areas overlap with high concentrations of chlorophyll (Figure 5.4-3).

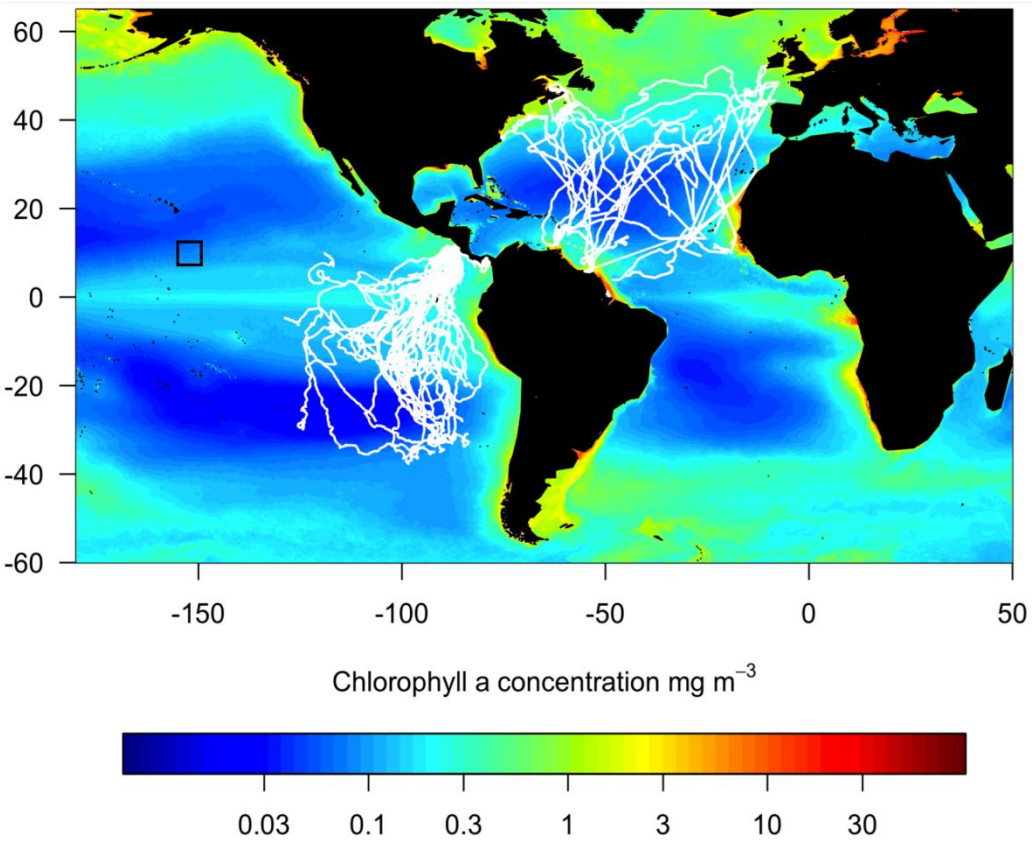

Figure 5.4-3 Leatherback turtle satellite tracks in the eastern Pacific Ocean and North Atlantic (Bailey et al. 2012)

The loggerhead turtles are circumglobal, nesting in tropical to sub-tropical regions and migrating into temperate regions. In the Pacific Ocean, their distribution area is mainly concentrated in the North Pacific Transitional Zone and the Southwest Pacific, with almost no record of distribution in the tropical Pacific region (Figure 5.4-4).

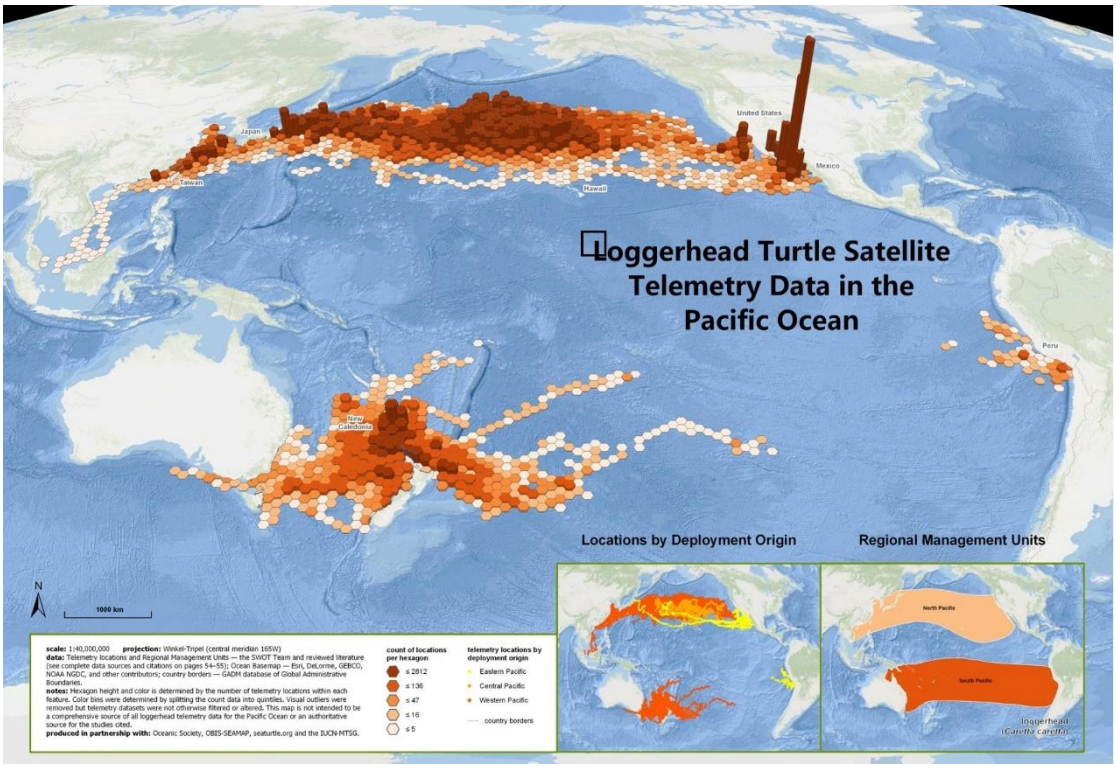

Figure 5.4-4 Loggerhead turtle satellite tracks in the Pacific Ocean (seaturtlestatus.org)

5.4.1.2 Chl *a* and primary production

(1) Remote-sensing observation of chlorophyll a

The western part of the CCZ, where the CTA is located, belongs to an oligotrophic sea area. Due to the obvious east-west primary production gradient in the CCZ, the surface-layer Chl concentration here is lower than that in the NORI-D region in the eastern part of the CCZ (NORI 2022). Based on the 1997-2019 satellite remote-sensing data (Figure 5.4-5), the annual average surface-layer Chl *a* concentration in the Block A-5 is 0.08±0.03 μg/L. The annual variations of Chl *a* concentration in the Block A-5 are low, reaching maximally 0.10±0.04 μg/L in April-June and minimally 0.07±0.02 μg/L in September-December every year.

Based on the 1997-2019 satellite remote-sensing data, we estimated the interannual variations of Chl *a* concentration in the surface layer of the IRZ, PRZ and ESRZ in the Block A-5 (Figure 5.4-5). The annual average Chl *a* concentration in the surface layer of the IRZ is 0.08±0.03 μg/L, reaching maximally 0.09±0.05 μg/L in

April-June and minimally 0.06±0.02 μg/L in October. The annual average Chl *a* concentration in the surface layer of PRZ is 0.08±0.03 μg/L, reaching maximally 0.09±0.05 μg/L in April-May and minimally 0.06±0.01 μg/L in October-November. The annual average Chl *a* concentration in the surface layer of ESRZ is 0.08±0.03 μg/L, reaching maximally 0.10±0.05 μg/L in April-June and minimally 0.07±0.02 μg/L in September-December. There is no significant difference in Chl *a* concentration between the IRZ, PRZ and ESRZ, and the interannual variation law is consistent.

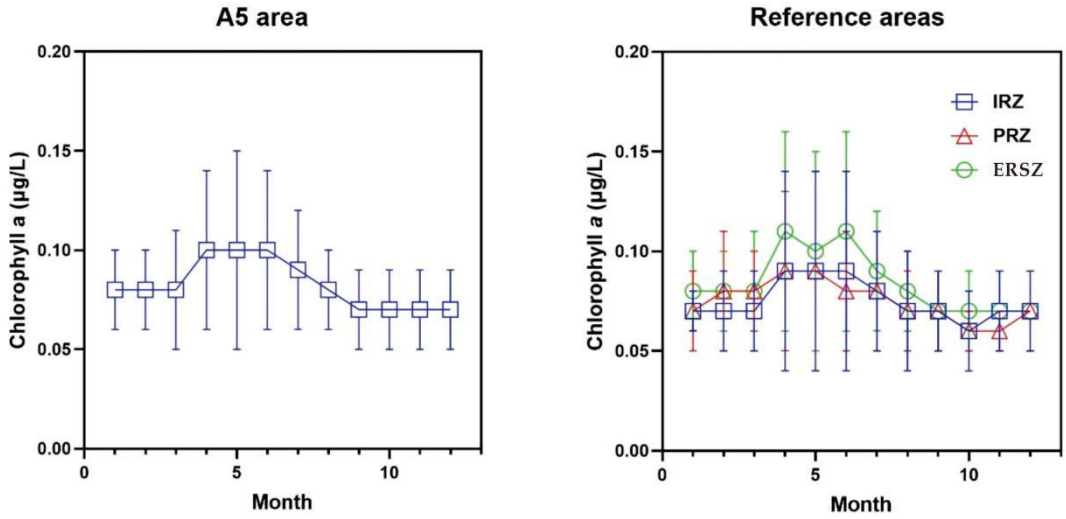

Figure 5.4-5 Annual variations of surface-layer Chl in the Block A-5 (1997-2019) and surface-layer Chl in the IRZ, PRZ and ESRZ of the Block A-5 (1997-2019)

Based on the 1997-2019 satellite remote-sensing data, we estimated the interannual variation of the spatial pattern of surface-layer Chl *a* concentration in the Block A-5 and its adjacent areas (Figure 5.4-6). Generally speaking, the surface-layer Chl *a* in this region presents a spatial gradient gradually decreasing from southeast to northwest, which reflects the large-scale spatial gradient of surface primary production mainly driven by equatorial currents to the north of the Eastern Tropical Pacific. The surface Chl *a* concentration is relatively high in March-June, which makes the isoline of 0.1 μg/L Chl *a* concentration broadly moves northward to the Block A-5, while in other seasons, the isoline of 0.1 μg/L moves southward to the

south of the Block A-5. In all seasons, the isolines of surface Chl *a* concentration are roughly zonal, so the IRZ, PRZ and ESRZ in the Block A-5 are highly consistent and comparable in the spatio-temporal variations of primary production.

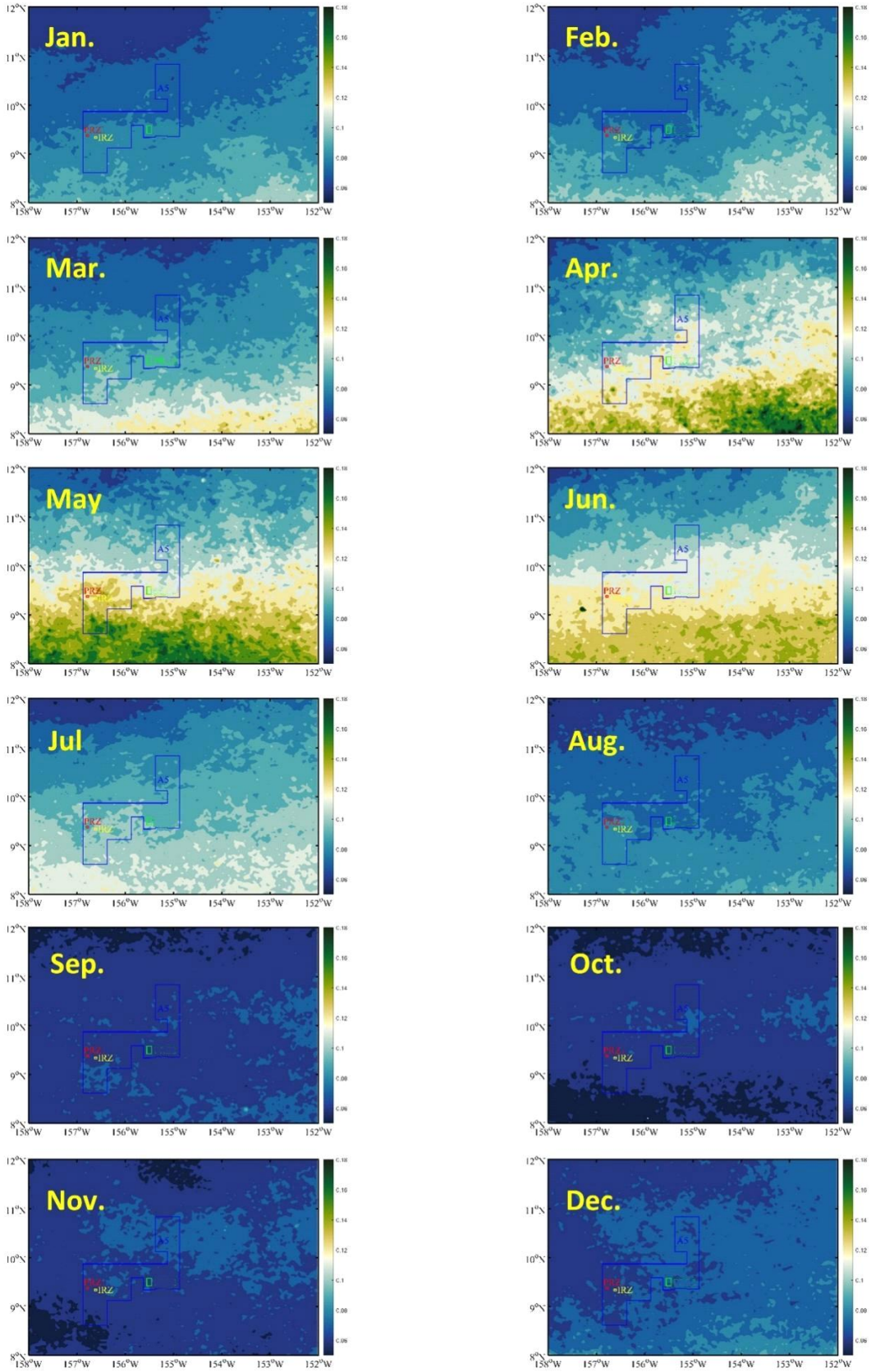

Figure 5.4-6 Annual variations in the spatial pattern of surface-layer Chl *a* concentration in the Block A-5 and its adjacent areas (1997-2019)

(2) Primary production

During Minmetals' 2018 survey cruise, we have conducted CTD sampling at DY50I-A5-S06-CTD11 station of the Block A-5 and DY50II-A8-S03-CTD01 station of the Block A-8, as well as determined the primary production, Chl *a* and other photosynthetic pigments concentration.

The distribution of primary production profiles at these two stations is shown in Figure 5.4-7. There is a similar pattern in the distribution of primary production profiles at these two stations. The maximum value appears in the subsurface of both stations. The primary production of DY50I-A5-S06-CTD11 station is 1.07 mgC m^{-3} h^{-1} at depth of 50 m, while that of DY50II-A8-S03-CTD01 station is 2.52 mgC m^{-3} h^{-1} at the same depth. It can be seen that the concentration values of primary production are higher in all the water depth layers of DY50II-A8-S03-CTD01 station than those of DY50I-A5-S06-CTD11 station. As shown in Figure 5.4-8, the integral primary production in water column is 51.44 mgC m^{-3} h^{-1} at DY50I-A5-S06-CTD11 station and 112.27 mgC m^{-3} h^{-1} at DY50II-A8-S03-CTD01 station. That infers the primary production of the Block A-8 is approximately 2.2 times that of the Block A-5. This may because that the Block A-8 is closer to the upwelling zone of the East Pacific Ocean and has higher nutrients concentration.

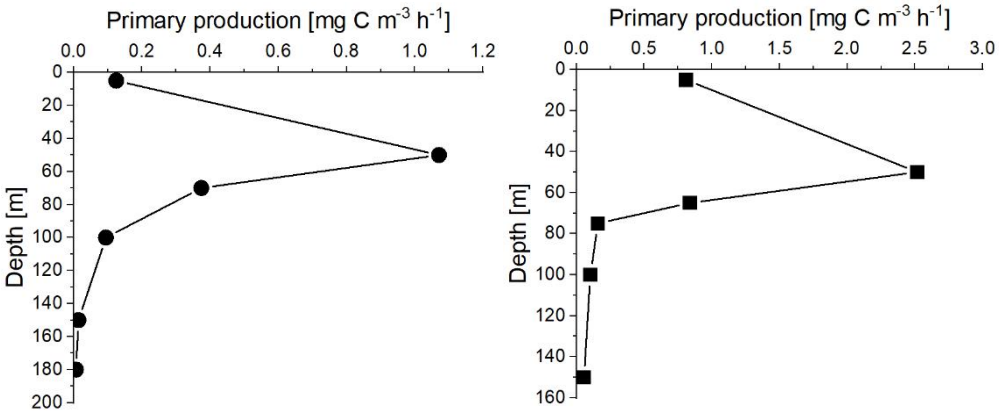

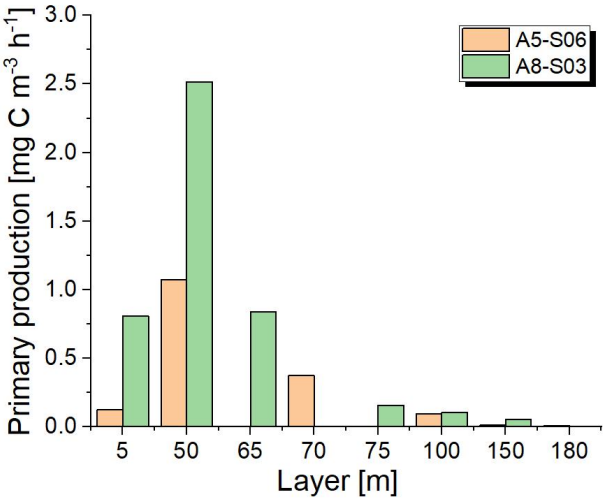

Figure 5.4-7 Distribution of primary production profiles at DY50I-A5-S06-CTD11 station (upper left) in the Block A-5 and DY50II-A8-S03-CTD01 station (upper right) in the Block A-8; comparison of primary production at all water-depth layers of these two stations (lower)

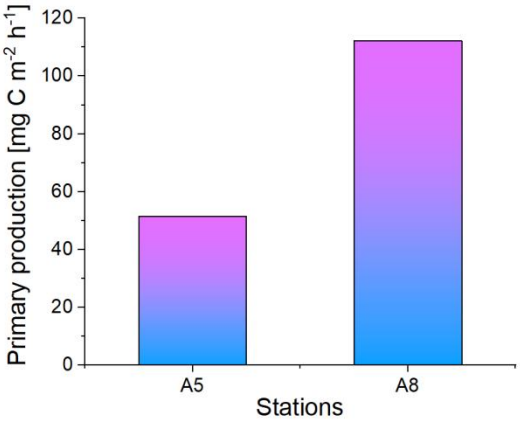

Figure 5.4-8 Comparison of integral primary production in water columns at two stations in the Blocks A-5 and A-8

(3) Chl *a* and photosynthetic pigments

During Minmetals' 2022 survey cruise, we have determined Chl *a* concentration comes from the DY73I-A5-CTD-01 and DY73I-A5-CTD-02 stations of the Block A-5. The former is located in the delineated PRZ and the latter is located in the IRZ. See Figure 5.4-9 for the distribution of Chl *a* profiles at these two stations. Results show that the vertical variation of Chl *a* at these two stations is consistent. The maximum values appear at about 50 m water depth in the subsurface layer, being 0.2 mg/m^3 at DY73I-A5-CTD-01 station and 0.28 mg/m^3 at DY73I-A5-CTD-02 station, and then gradually decrease with increasing depth. The vertical variations at these two stations

are basically the same, indicating that the IRZ and PRZ have similar Chl *a* concentration.

In the TMC-CSA project, the maximum Chl *a* concentration (0.1-0.8 mg/m^3) in the NORI-D region appears at 40-50 m water depth in the surface layer. In the TMC-UOH project, the maximum Chl *a* concentration (1.5-2 mg/m^3) in the NORI-D region appears between 50 m and 100 m water depths (NORI 2022). Results show that the Chl *a* concentration in the Block A-5 is less than that measured in the NORI-D region, basically conforming to the variation characteristics of primary production in the CCZ.

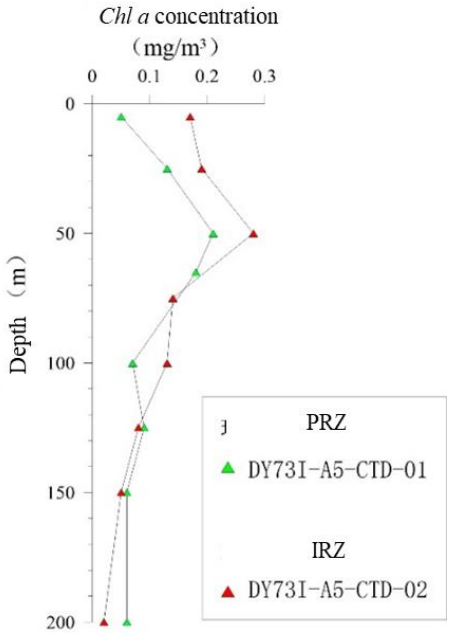

Figure 5.4-9 The profiles of Chl *a* concentration at the DY73I-A5-CTD-01 and DY73I-A5-CTD-02 stations within the Block A-5

During Minmetals' 2018 survey cruise, we have sampled and determined phytoplankton photosynthetic pigments at DY50I-A5-S06-CTD11 station in the Block A-5 and DY50II-A8-S03-CTD01 station in the Block A-8. The profiles of main phytoplankton photosynthetic pigments at these two stations are shown in Figures 5.4-10 and 5.4-11. The main photosynthetic pigments at these two stations are composed of Dv-Chl *a*, Mv-Chl *a*, zeaxanthin, 19'hex-fucoxanthin, diadinoxanthin, Chl $_{c2}$ and Chl $_{c3}$, while the maximum pigment concentration layer depth is consistent with the maximum Chl layer depth, generally appears in the depth range of 50-100 m. The zeaxanthin and Dv-Chl *a* concentrations (84.45 ng/L and 112.61 ng/L) are relatively

high at the depth of 75 mm at DY50I-A5-S06-CTD11 station; the Mv-Chl *a* concentration is also relatively high at 62.82 ng/L; while the concentrations of other photosynthetic pigments are lower than 20 ng/L. It is slightly different at DY50II-A8-S03-CTD01 station. All the photosynthetic pigments reached peak value at Chl *a* maximum value layer, except for zeaxanthin, maximum layer depth of which was shallower; Dv-Chl *a* concentration exhibit a bimodal distribution pattern; and 19'hex-fucoxanthin was much higher. Comparison of the integral concentration values of photosynthetic pigments in the water columns of these two stations infers that the main phytoplankton groups at these two stations are ultra-micro prokaryotes such as *Prorocentrum* and *Synechococcus*; the biomass of Dinoflagellate type 8 is higher in the Block A-8, but lower in the Block A-5 (Figure 5.4-12).

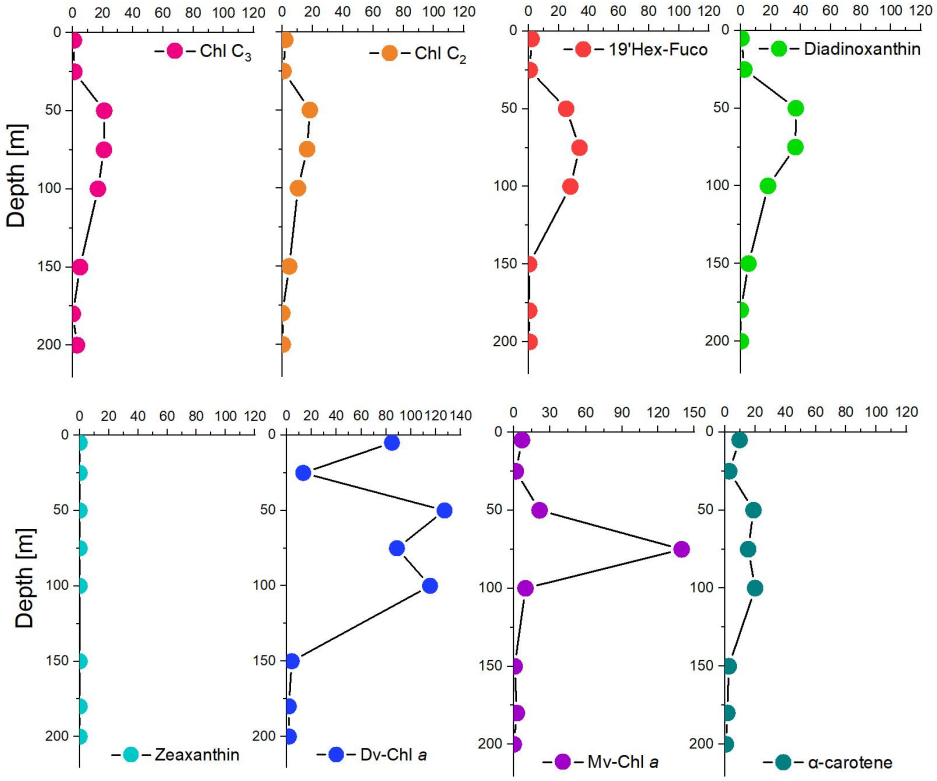

Figure 5.4-10 Distribution of main photosynthetic pigment concentration profiles at the DY50Ⅰ-A5-S06-CTD11 station of the Block A-5 (Unit: ng/L)

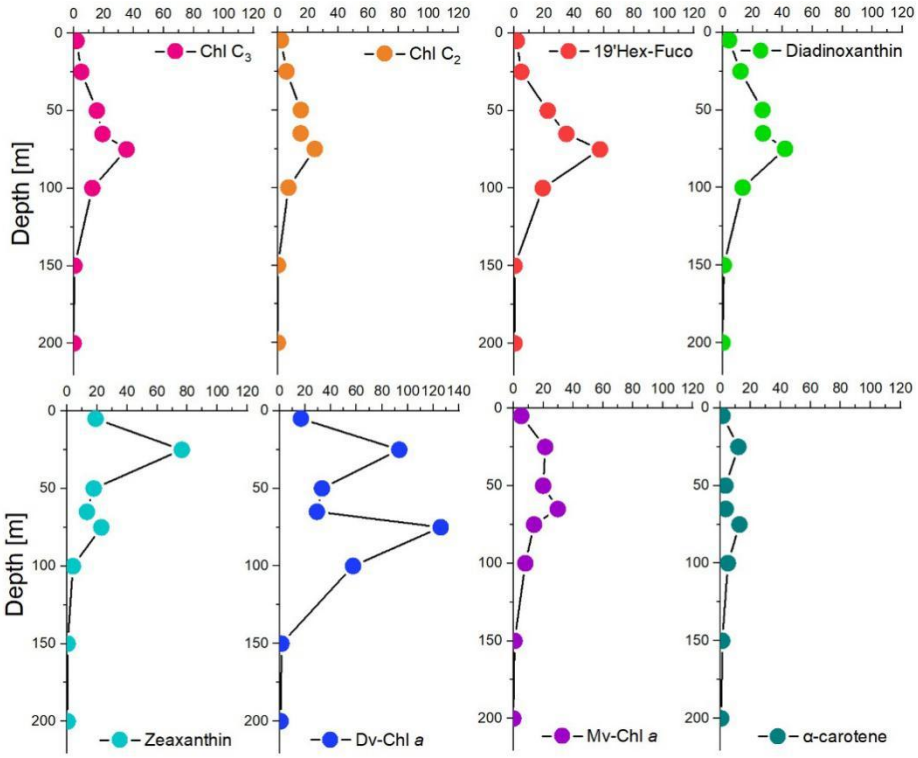

Figure 5.4-11 Distribution of main photosynthetic pigment concentration profiles at the DY50II-A8-S03-CTD01 station of the Block A-8 (Unit: ng/L)

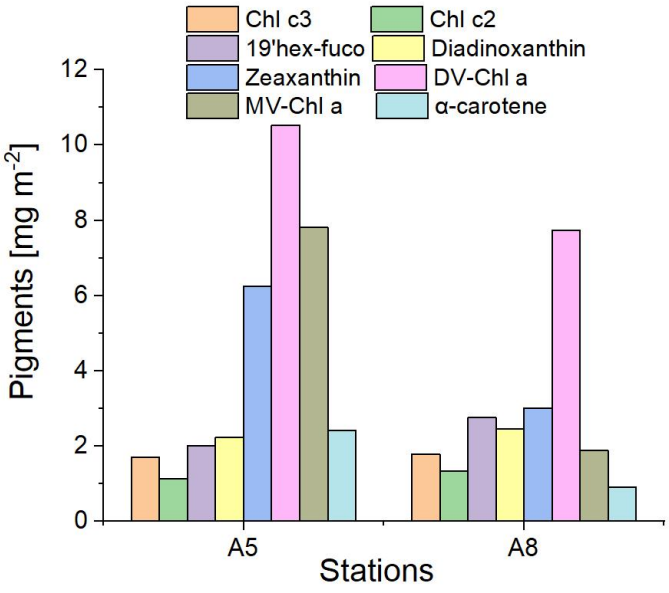

Figure 5.4-12 Comparison of integral pigment concentration in the water columns at two survey stations in the Blocks A-5 and A-8

5.4.1.3 Microorganisms

(1) Methods

During Minmetals' 2023 survey cruise (DY79), seawater samples were collected at two stations each in the IRZ, PRZ and ESRZ in the A-5 block. A Sea-Bird conductivity-temperature-depth (CTD) sampler (SBE 911 plus, Seabird Co., Ltd., Sunnyvale, CA, United States) was used to collect seawater from seven different depths (5 m, 50 m, DCM, 150m, 200 m, 1000 m, and bottom water) at each station. Approximately 4 L of seawater was filtered on board through a 0.22-μm pore-sized membrane (47-mm diameter polycarbonate, Millipore, Bedford, MA, United States). The filters were then frozen at −80◦C ultra low temperature freezer.

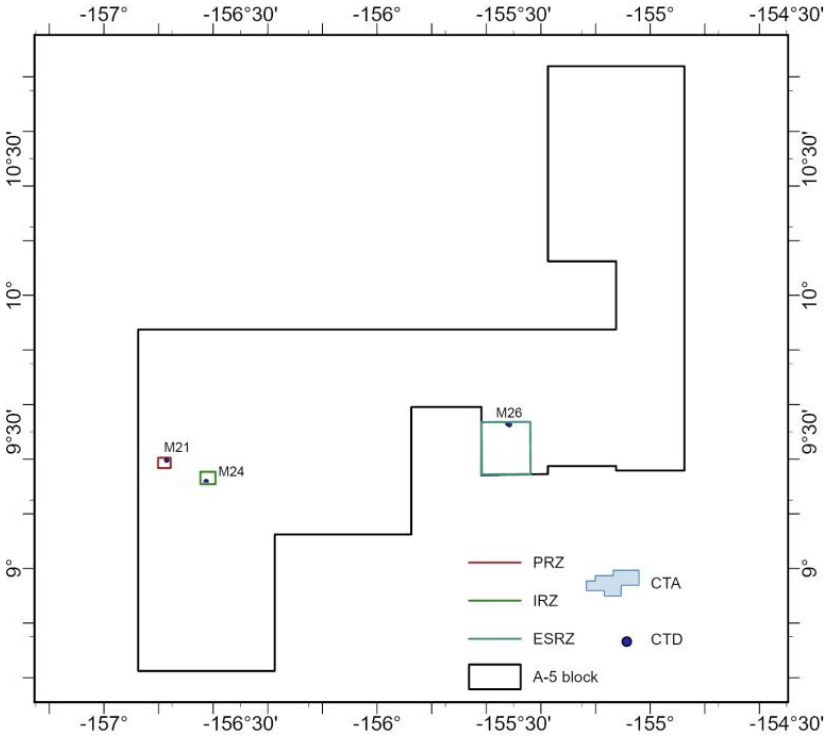

Figure 5.4-13 Location of water column sampling sites (black circles) in the A-5 (Minmetals' 2023 survey cruise)

Genomic DNA was extracted using the Powerwater® kit according to the manufacturer's protocols. The DNA quantity and quality were determined using a NanoDrop Spectrophotometer (NanoDrop Technologies Inc., Wilmington, DE, USA). The primer 341F/806R was used for archaeal 16S rRNA gene amplification. Polymerase chain reaction (PCR) Polymerase chain reaction (PCR) was conducted in

a 20-μL reaction system, and the parameters were 3 min at 95 °C, followed by 29 cycles at 95 °C for 30 s, 55 °C for 30 s, and 72°C for 45 s, ended with a final extension step at 72 °C for 10 min. Sequencing was performed by Shanghai Majorbio Bio-pharm Technology Company Ltd (Shanghai, China). DNA sequences were quality-filtered on the free online platform of Majorbio Cloud Platform (https://cloud.majorbio.com/) using QIIME v2 with the defined criteria. Amplicon Sequence Variants (ASVs) were clustered with 100% similarity and chimeric sequences were identified and removed. A representative sequence of each ASV was selected for taxonomic assignments. ASV taxonomy was assigned by RDP classifier against the SILVA database (http://www.arb-silva.de/).

The ASV table for subsequent comparative analysis was rarefied to the same sequencing depth. The alpha diversity, including richness, shannon diversity, shannoneven and phylogenetic diversity, was quantified using MOTHUR. The dissimilarity of beta diversity was estimated based on Bray-Curtis distances between each sample, and visualized by non-metric multidimensional scaling (NMDS). Multiple group differences were determined by the kruskal-wallis test with rstatix, where an adjusted $p < 0.05$ was considered significant.

(2) Microbial community composition

A total of 10,060 ASVs were identified in samples from this study area, spanning 38 phyla, 89 classes, 219 orders, 347 families, and 605 genera. The dominant bacterial phyla in this study area were Proteobacteria, Cyanobacteria, Actinobacteriota, SAR324_cladeMarine_group_B, Marinimicrobia_SAR406_clade, Chloroflexi, Bacteroidota, Verrucomicrobiota, Nitrospinota, Gemmatimonadota, Bdellovibrionota, and WPS-2, with Proteobacteria being the most abundant (Figure 5.4-14).

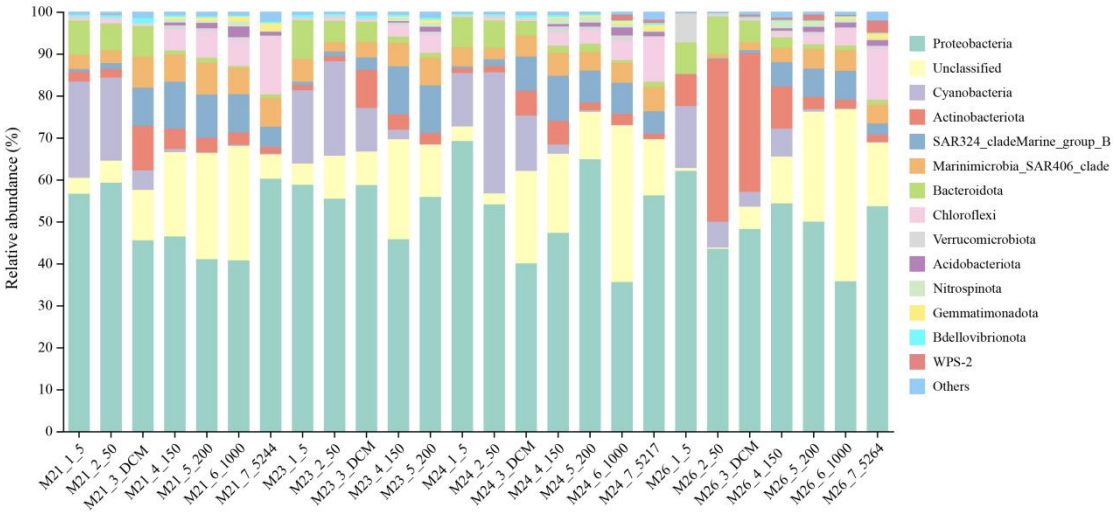

Figure 5.4-14 Relative abundance of dominant bacteria in each sample at the phyla level

Further, this study compared the bacterial composition at the phylum level across different water layers. It was found that Proteobacteria had the highest abundance at 5 m layer and reached its lowest abundance at 1000 m layer. Cyanobacteria dominated the photic zone (5m-150m) but were not detected below 200 m layer. Marinimicrobia_SAR406_clade remained relatively stable across all water layers. The largest proportion of unidentified species was detected at 1000 m layer (Figure 5.4-15).

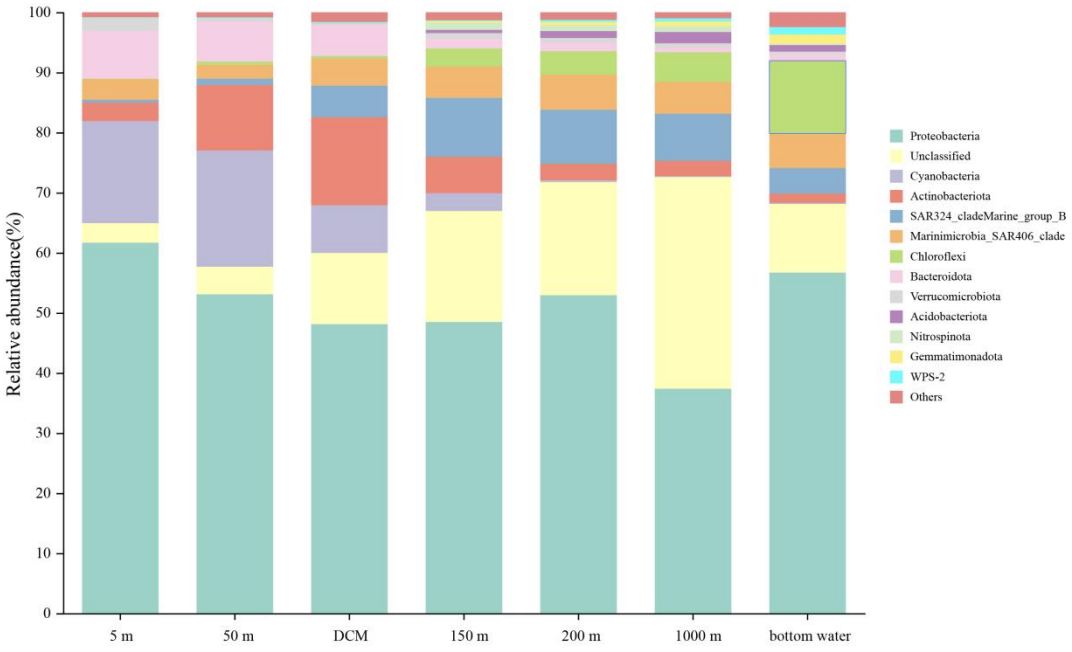

Figure 5.4-15 Relative abundance of dominant bacteria in each layer at the phyla level

This study divided the water layer into the epipelagic (0-200m), 1000m and

bottom layer by depth. At the phylum level, the abundance of bacterial phyla at sites M21, M24 and M26 was compared. The results showed that the relative abundance of Actinobacteriota was higher in the 0-200 m at site M26, while the relative abundance of Cyanobacteria was lower (Figure 5.4-16).

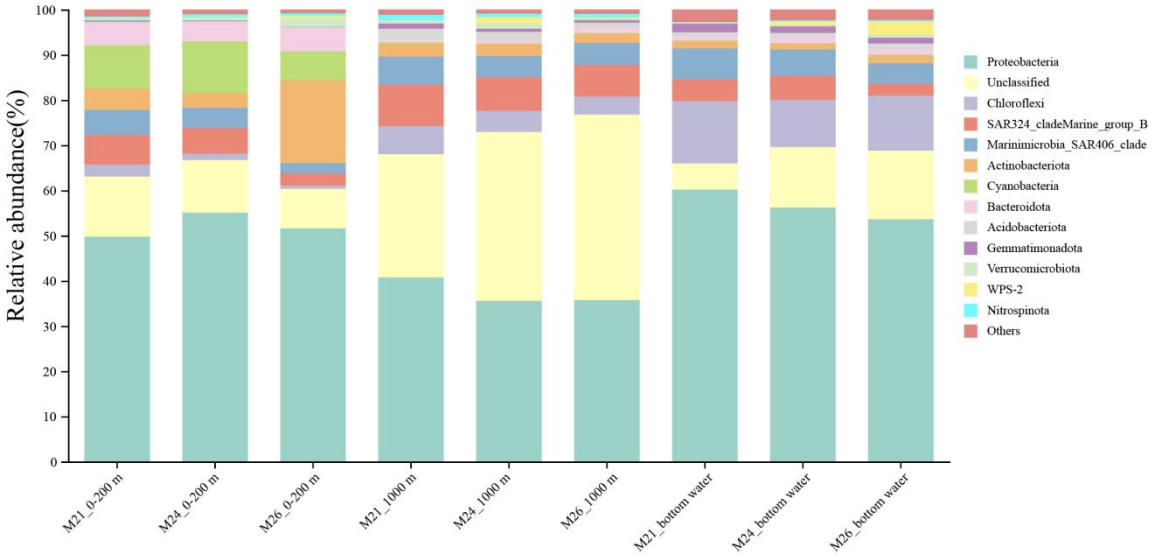

Figure 5.4-16 Relative abundance of dominant bacteria in different zones of M21, M24 and M26 at the phyla level.

This study analyzed the alpha diversity of microbial communities across different water layers. The results showed significant differences in alpha diversity between these layers ($P<0.5$). Both richness and phylogenetic diversity displayed similar variation patterns, being lowest in the surface layer and increasing with depth. Shannon diversity and evenness also exhibited similar trends, both being lowest at 50 m layer and highest at 200 m layer. These findings indicate that the diversity of microbial communities in this study area was significantly influenced by the depth of the water layer (Figure 5.4-17).

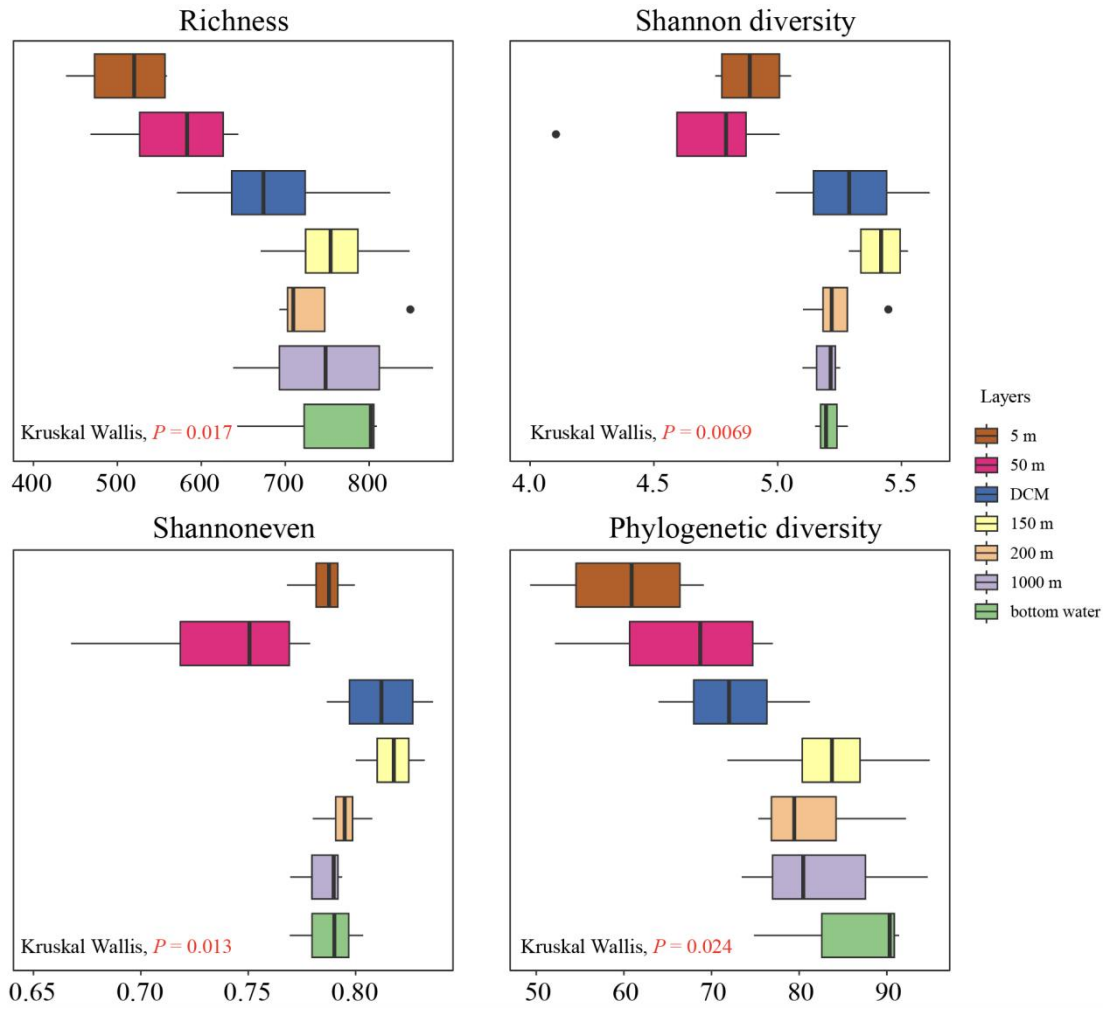

Figure 5.4-17 Alpha diversity of bacterial community in each layer

(3) Biomarkers

In this study, biomarkers were identified for different water layers in order to more effectively develop a comparative study for changes in microbial communities before and after mining. The LEfSe (Linear discriminant analysis Effect Size) analysis was used to identify the biomarkers of microbial communities in different water layers at five levels: phylum, order, order, family, and genus, respectively, and the biomarkers in different water layers were identified by the multi-group difference comparison strategy, in which the species with the LDA value of more than 4 and the P less than 0.01 were used as the biomarkers in different water layers (Figure 5.4-18) A total of 56 annotated species were identified as biomarkers in the seven water layers with seven known phyla, four known orders of bacteria, 15 known orders of bacteria,

17 known families of bacteria, and 12 known genera of bacteria. 15 biomarkers were found in the 5m layer, 13 biomarkers in the 50m layer, 8 biomarkers in the DCM layer, 2 biomarkers in the 150m layer, and 6 biomarkers in the 200m layer and 10 biomarkers in the near bottom layer.

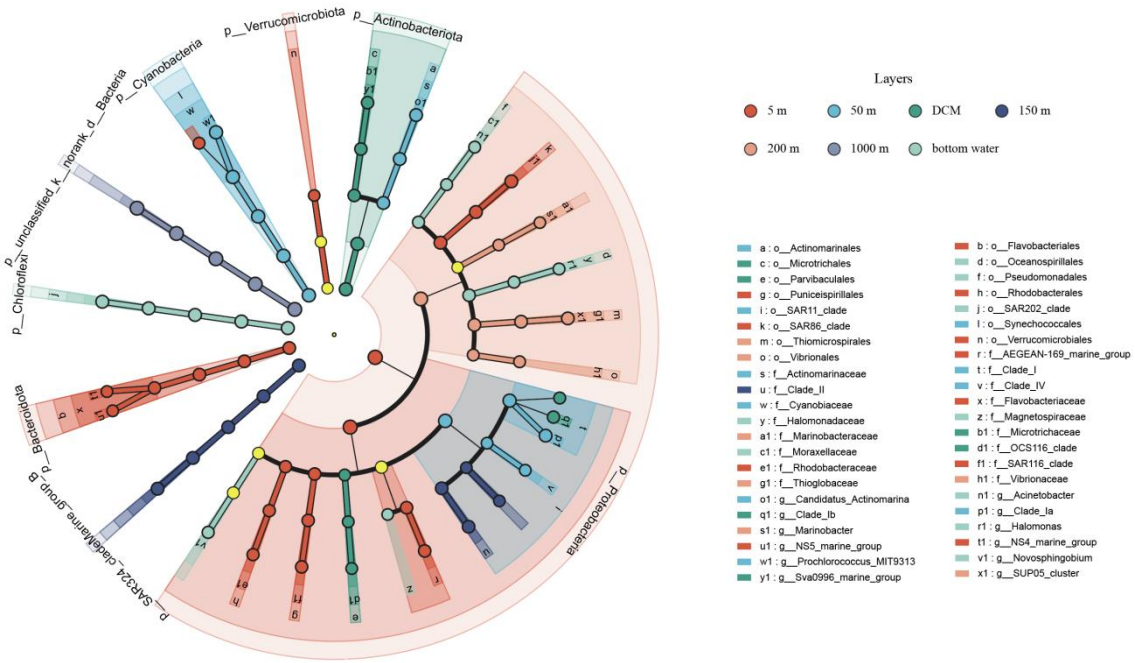

Figure 5.4-18 Biomakers of bacterial community in each layer.

(4) Comparison of the IRZ and PRZ

This study divided the water layers by depth into the epipelagic (0-200m), 1000m layer and bottom water layer. and compared the alpha diversity of sites M21 (PRZ), M24(IRZ) and M26(ESRZ). The results showed that the three sites were similar in terms of richness, Shannon diversity index, evenness index and phylogenetic diversity index, with only the microbial community in the 1000 m layer of water at site M24 having higher richness and phylogenetic diversity (Figure 5.4-19).

Further analysis of beta diversity of microbial communities in the region was conducted. The NMDS analysis revealed that microbial communities within the same water layer clustered together, with samples from adjacent water layers being more similar to each other (Figure 5.4-20). This suggests that the main driver of spatial variation in microbial communities in the region is environmental variation along the

water depth, rather than variation across a horizontal geographic gradient.

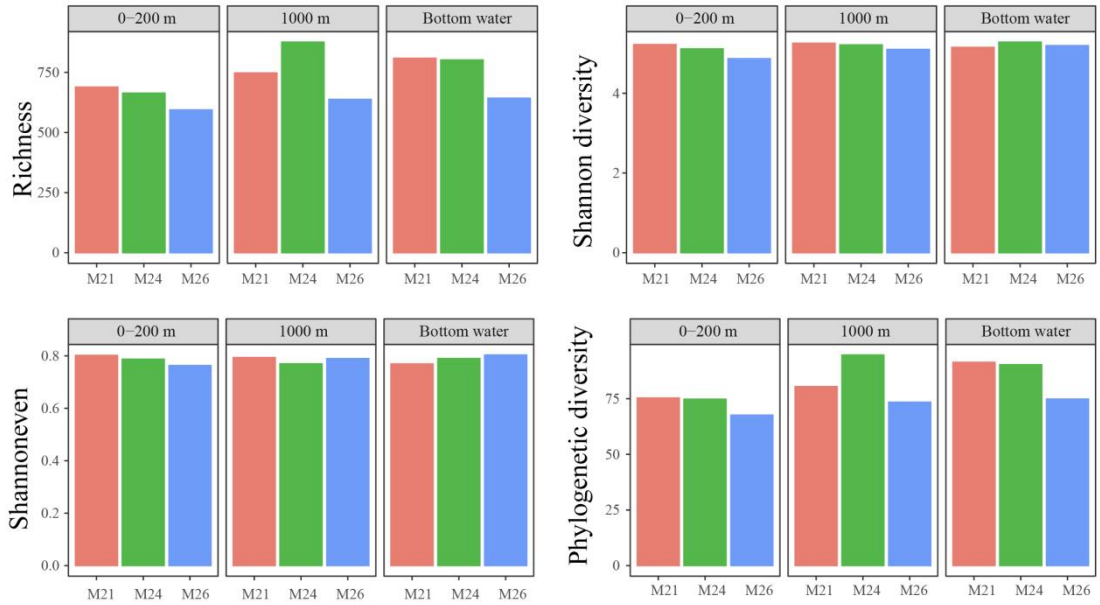

Figure 5.4-19 Alpha diversity of bacterial community in different zones of M21 (PRZ), M24(IRZ) and M26(ESRZ).

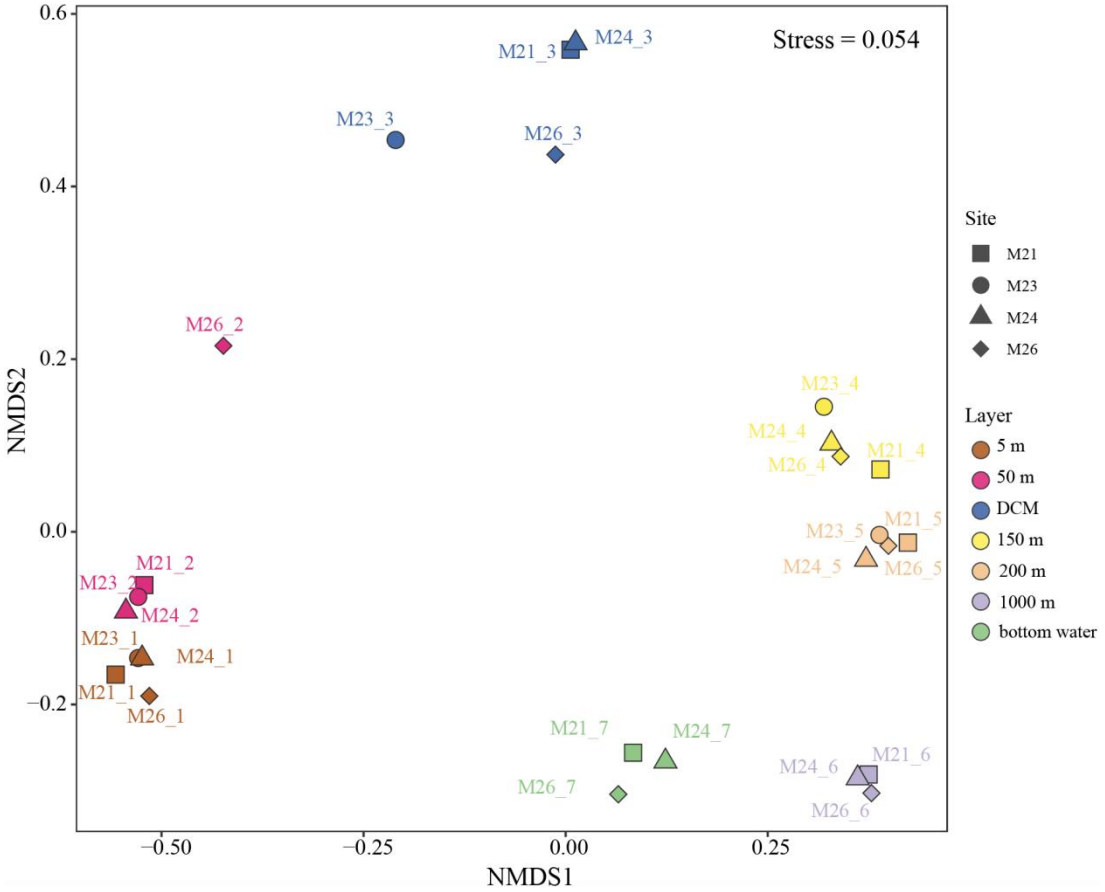

Figure 5.4-20 Beta diversity of bacterial community in each layer.

5.4.1.4 Phytoplankton

(1) Composition of phytoplankton community

During Minmetals' 2021 survey cruise, we conducted phytoplankton net (20 μm mesh) sampling at four stations in the Block A-5. A total of 59 phytoplankton species were identified to belong to two phyla, three classes, 11 orders, 19 families and 26 genera. Among them, there were 21 species of Dinoflagellate and 38 species of Bacillariophyta.

Among those four stations, DY70I-A5-BP01 station has the most phytoplankton species (27) (Figure 5.4-21), while DY70I-A5-BP02 station has the least number of species (14).

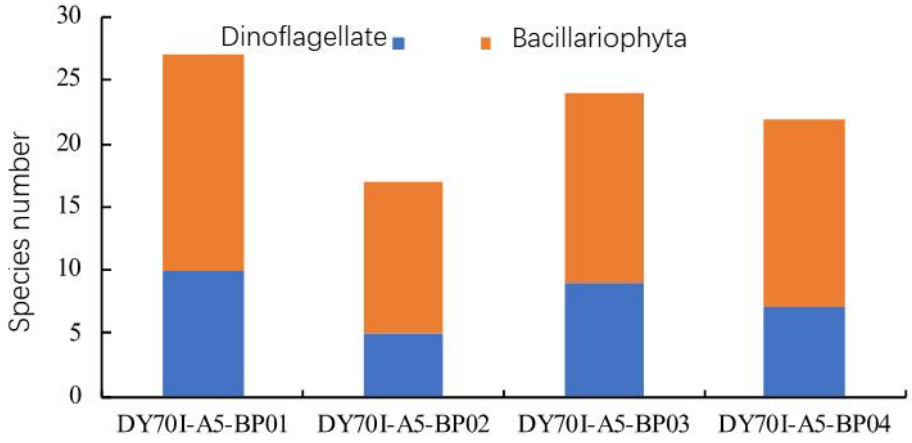

Figure 5.4-21 Numbers of phytoplankton species at survey stations

(2) Distribution of phytoplankton abundance

The average abundance of phytoplankton in the surveyed area is 338.0 cells/L, of which the average abundance of Bacillariophyta accounts for 73 % and Dinoflagellate accounts for 27 % (Figure 5.4-22). Abundance varies slightly at those four survey stations, in the range of 256.7-441.8 cells/L (Figure 5.4-23).

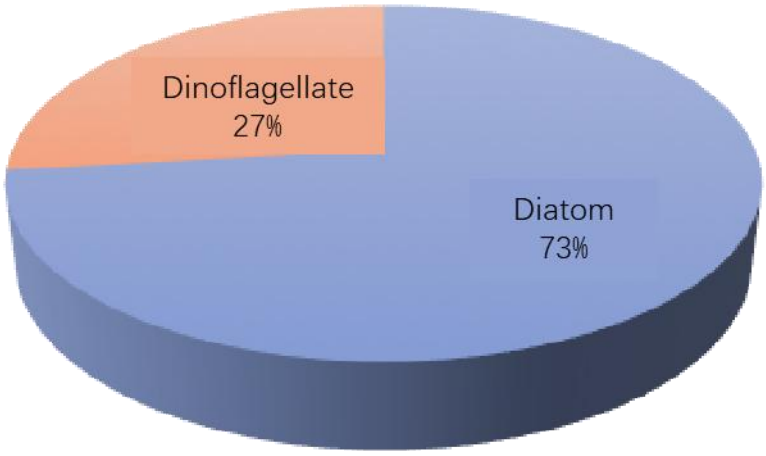

Figure 5.4-22 Phytoplankton community structure in the Block A-5

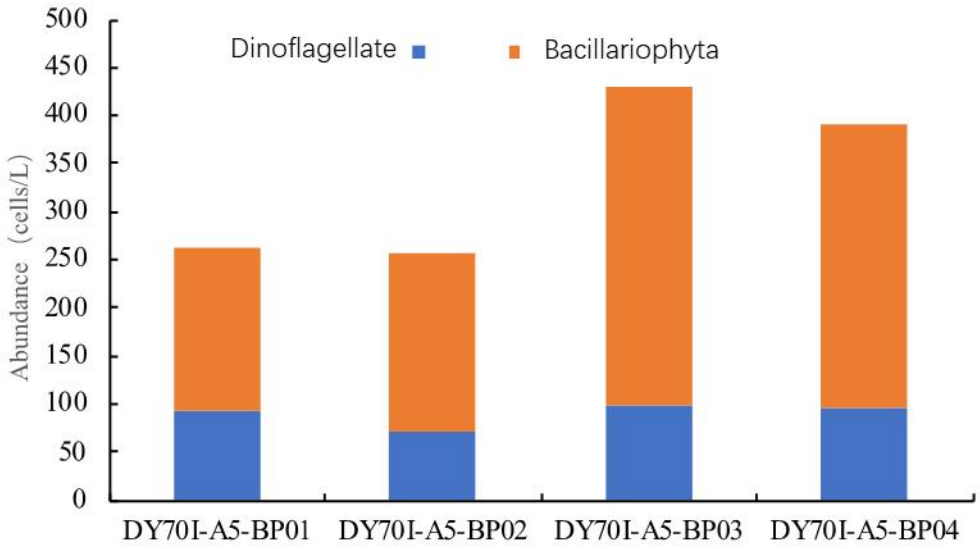

Figure 5.4-23 Phytoplankton abundance at survey stations

(3) Analysis of the diversity of phytoplankton species

Analysis of the above-mentioned survey results shows that the dominant species of phytoplankton in the Block A-5 are mainly Bacillariophyta species such as *Bacteriastrum hyalinum*, *Coscinodiscus jonesianus*, and Dinoflagellate species such as *Ceratium teres*. From Table 5.4-1, it can be seen that there are six species with dominance exceeding 0.02, including *Bacteriastrum hyalinum* var. *hyalinum*, *Coscinodiscus jonesianus*, *Ceratium horridum* var. *claviger*, *Ceratium teres*, *Chaetoceros compressus* and Fragilariopsis doliolus.

Table 5.4-1 Dominant species of phytoplankton and their dominance in the Block A-5

Latin name	Occurrence frequency (%)	Y
Bacteriastrum hyalinum var. *hyalinum*	50	0.095
Coscinodiscus jonesianus	75	0.028
Ceratium horridum var. *claviger*	75	0.027
Ceratium teres	50	0.022
Chaetoceros compressus	75	0.022
Fragilariopsis doliolus	75	0.021

5.4.1.5 Zooplankton

We have conducted vertically towing sampling (0-200 m) at nine stations and vertically stratified sampling with a multinet sampler (0-1,000 m) at three stations in the Block A-5 of the Contract Area.

(1) Zooplankton community structure

A total of 193 species of zooplankton have been identified, belonging to six phyla. In addition, 11 species of zooplankton larvae have been recorded. The zooplankton community consists of Copepoda, Cnidaria, Ostracoda, Amphipoda, Chaetognatha, Tunicata, Euphausiacea, Mollusca, Polychaeta and other groups. Among them, Copepoda is the dominant taxon, including 121 species and accounting for 59.3 % of the total species. Next in the lineup are Cnidaria (19 species), Ostracoda (11 species), Chaetognatha (nine species) and Tunicata (10 species) respectively. Other groups account for less than 4 % of the total species diversity (Table 5.4-2 and Figure 5.4-24).

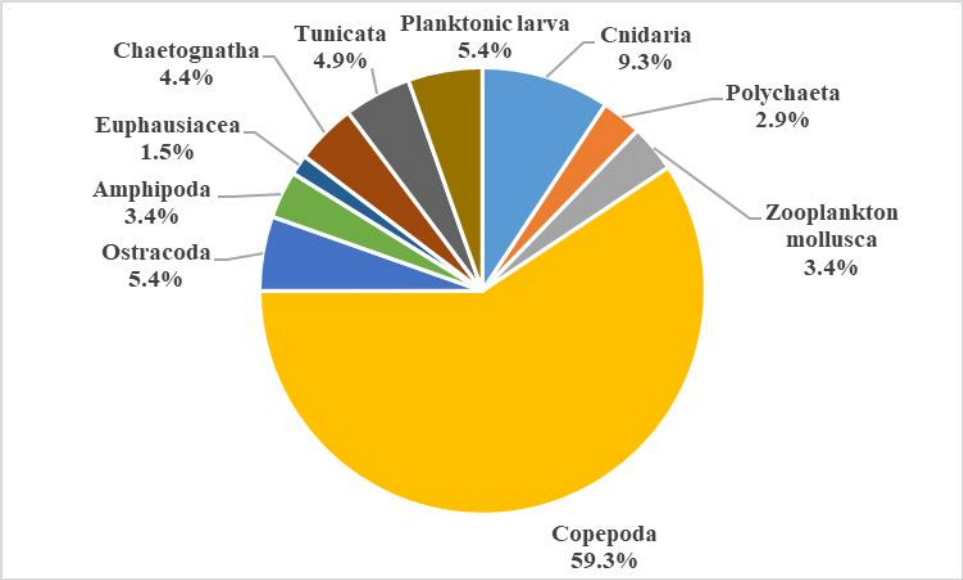

Figure 5.4-24 Structural composition of zooplankton community in the Block A-5

Table 5.4-2 Structural composition of zooplankton community in the Block A-5

Phylum	Genus	Number	%
Cnidaria phylum	Cnidaria	19	9.31
Annelida phylum	Polychaeta	6	2.94
Mollusca phylum	Zooplankton mollusk	7	3.43
Arthropoda	Copepoda	121	59.31
	Ostracoda	11	5.39
	Amphipoda	7	3.43
	Euphausiacea	3	1.47
Chaetognatha	Chaetognatha (Sagitta)	9	4.41
Urochordata	Tunicata	10	4.90
	Total	193	
	Planktonic larva	11	

(2) Vertical distribution of biomass and abundance

Analysis of samples collected with vertically towed net at 0-200 m depth layer around the Block A-5 shows that the biomass of zooplankton in 0-200 m depth layer only varies slightly, averaging about 39.13 mg/m^3.

On the whole, the biomass of zooplankton in the Block A-5 shows a decreasing

trend from the surface to the bottom, and the average biomass of the upper-layer ocean at 0-200 m depth is 76.23 mg/m^3. The highest nighttime values of all stations appears in the surface layer of 0-50 m depth, and the highest daytime values of most stations appear in the surface layer of 0-50 m depth. The abundance of zooplankton in the Block A-5 gradually decreases from the surface to the bottom, and the average abundance of the upper-layer ocean at 0-200 m is 58.27 ind./m^3.

(3) Vertical distribution of species diversity and abundance

With the increasing water depth, the species diversity decreases, and the structure of zooplankton communities varies obviously. In the 0-100 m depth layer, the main dominant species are *Farranula concinna*, *Acartia negligens*, *Oncaea venusta*, *Oithona plumifera*, *Clausocalanus arcuicornis*, and so on. In the 100-200 m depth layer, the main dominant species are *Rhincalanus cornutus*, *Oncaea venusta*, *Lucicutia flavicornis*, and so on.

5.4.1.6 Epipelagic fish diversity by eDNA analysis

During Minmetals' 2022 survey cruise, we have conducted surface-layer seawater sampling with ship-mounted equipment and CTD along the cruise route and in the euphotic zone of the Block A-5 and for eDNA test to estimate the diversity of epipelagic fish. The e-DNA OTU data are shown in Figure 5.4-25. Actinopterygii is dominant in the euphotic zone, while a few sharks (*Carcharhinus* sp.) were also detected. Of the Actinopterygii, Phosichthyidae is the dominant taxon represented by *Ichthyococcus elongatus* and *Cyclothone atraria*. The second dominant taxon is Myctophidae, represented by *Diogenichthys laternatus* and *Myctophum aurolaternatum*. Ranking in the third is *Leuroglossus* sp. of Argentiniformes. Besides, *Coryphaena* sp. and *Katsuwonus pelamis* were also detected to account for a certain proportion.

Figure 5.4-25 Epipelagic fish diversity based on eDNA data from seawater samples

Results of cluster analysis of the eDNA of surface seawater samples collected in the Block A-5 and along the route are shown in Figure 5.4-26. It can be seen that there is no obvious geographical differentiation between the stations in the Block A-5 and other stations along the route. This indicates that surface-layer nekton have no significant geographical isolation in the tropical Pacific; instead, they have good connectivity.

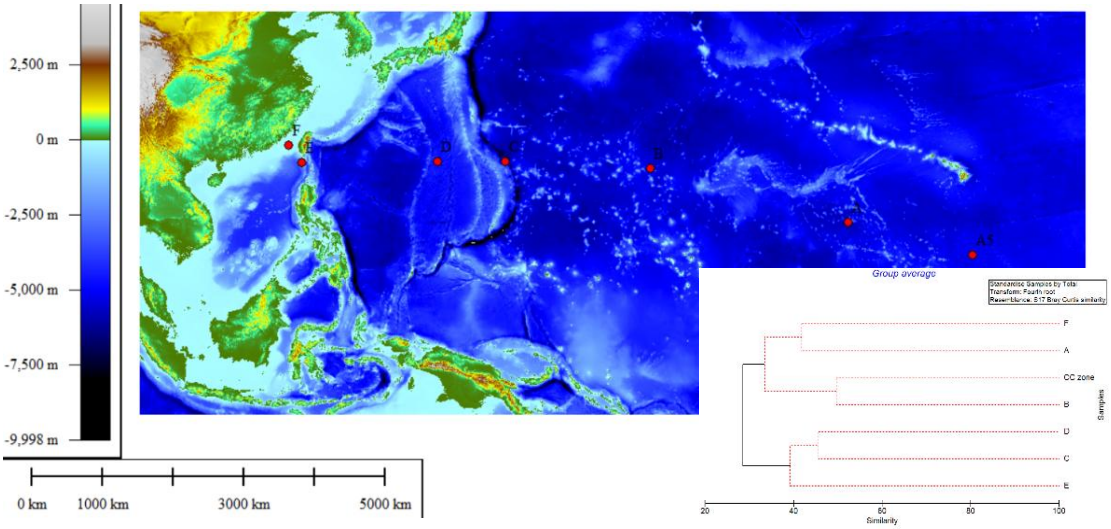

Figure 5.4-26 Seawater sampling stations for fish eDNA analysis

5.4.2 Middle layer

(1) Distribution of biomass

The biomass of zooplankton in the Block A-5 shows a decreasing trend from the surface to the deep sea, averaging 11.27 mg/m^3 in the upper part (200-450 m depth, OMZ layer) of the middle layer, and 6.08 mg/m^3 in the lower part (450-1,000 m depth) of middle layer (Figure 5.4-27).

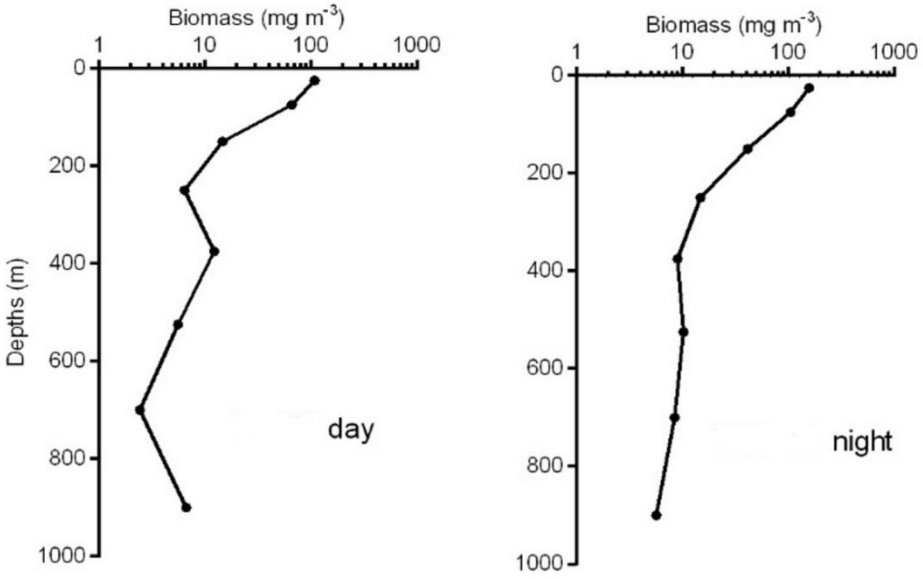

Figure 5.4-27 Vertical distribution of zooplankton biomass at the depth of 0-1,000 m in the Block A-5

(2) Distribution of abundance

The abundance of zooplankton in the Block A-5 shows a decreasing trend from the surface to the deep sea, averaging 5.26 ind./m^3 in the upper part (200-450 m depth) of mesopelagic zone (OMZ layer), and 1.19 ind./m^3 in the lower part (450-1,000 m depth) of mesopelagic zone (no-OMZ layer) (Figure 5.4-28).

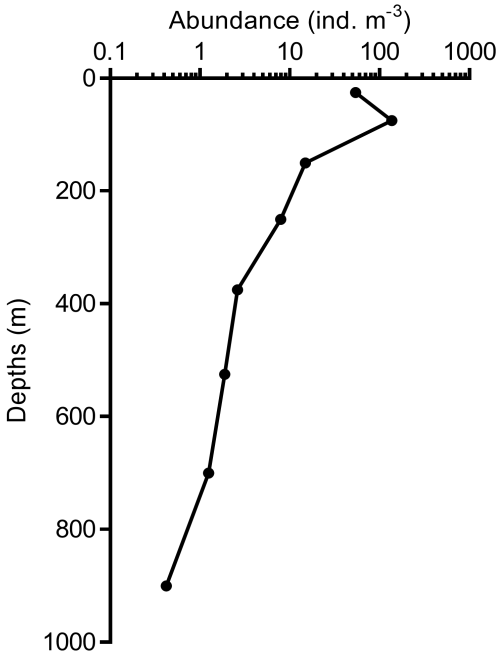

Figure 5.4-28 Vertical distribution of zooplankton abundance at the depth of 0-1,000 m in the Block A-5

(3) Vertical distribution of species diversity and abundance

With the increasing water depth, the species diversity tends to decrease (Figure 5.4-29), and the community structure of zooplankton varies obviously. In the 200-450 m depth layer, the main dominant species are *Rhincalanus cornutus*, *Pleuromamma robusta*, *P. gracilis*, etc. In the 450-600 m depth layer, the main dominant species is *P. robusta*. In the 600-1,000 m depth layer, the main dominant species are *Oncaea venusta*, *Oncaea venusta*, *Haloptilus paralongicirrus*, *Gaetanus minor*, etc.

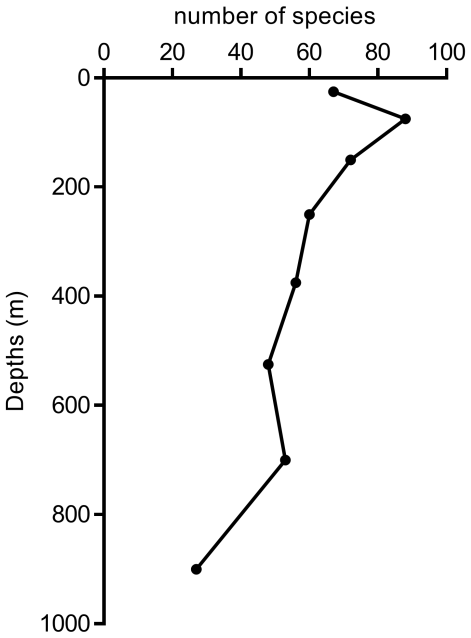

Figure 5.4-29 Variations of zooplankton species diversity with water depth at the depth of 0-1,000 m in the Block A-5

5.4.3 Bottom layer

5.4.3.1 Microorganisms

(1) Methods

Since the disturbance of the collection mechanism and the pressure of the traveling mechanism may affect a range of depths, we collected a high-quality stratified sediment sample up to a depth of 45 cm during the Minmetals' 2021 survey cruise (DY70 cruise) in order to obtain baseline data on the microbial community at larger depths. During this cruise (DY70), we conducted sediment sampling for microbial diversity analysis at two stations in the Block A-5, including one multicorer sampling at one station (DY70I-A5-MC01) and one box corer sampling at the other station (DY70I-A5-BC03). Surface-layer sediments were sampled with box corer. The multicorer samples were stratified by 29 layers, including 1 cm layers within the first 21 cm depth and then 3 cm layers over 21 cm depth. The aim of this study was to provide a data base for subsequent post-disturbance comparative studies, in particular to assess how deep the microbial communities within the sediments would be affected

by the disturbance of the collector vehicle.

During Minmetals' 2023 survey cruise (DY79), surface sediment samples were collected at two stations each in the IRZ, PRZ and ESRZ in the A5 region using a multicore sampler, and one station between the IRZ and PRZ (Figure 5.4-30). We carried out analyses of microbial diversity in these samples using molecular biology methods to reveal similarities in the biological communities of the IRZ, PRZ and ESRZ within the A-5 Block.

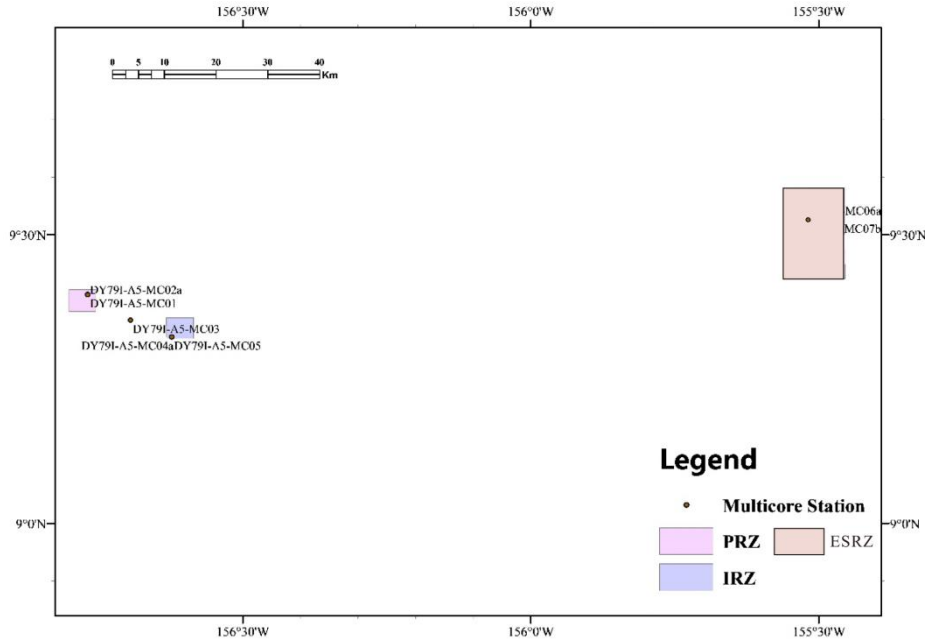

Figure 5.4-30 Location of surface sediment sampling sites (black circles) in the A-5 (Minmetals' 2023 survey cruise)

Genomic DNA was extracted using the Powersoil Max® kit according to the manufacturer's protocols. The DNA quantity and quality were determined using a NanoDrop Spectrophotometer (NanoDrop Technologies Inc., Wilmington, DE, USA). The primer 341F/806R was used for archaeal 16S rRNA gene amplification. Polymerase chain reaction (PCR) Polymerase chain reaction (PCR) was conducted in a 20-μL reaction system, and the parameters were 3 min at 95 °C, followed by 29 cycles at 95 °C for 30 s, 55 °C for 30 s, and 72°C for 45 s, ended with a final extension step at 72 °C for 10 min.

Sequencing was performed by Shanghai Majorbio Bio-pharm Technology

Company Ltd (Shanghai, China). DNA sequences were quality-filtered on the free online platform of Majorbio Cloud Platform (https://cloud.majorbio.com/) using QIIME v2 with the defined criteria. Amplicon Sequence Variants (ASVs) were clustered with 100% similarity and chimeric sequences were identified and removed. A representative sequence of each ASV was selected for taxonomic assignments. ASV taxonomy was assigned by RDP classifier against the SILVA database (http://www.arb-silva.de/).

The Good's coverage value of stratified sediment samples obtained with multicorer at DY70I-A5-MC01 station is between 0.959 and 0.999 (Figure 5.4-31), indicating that the current sequencing depth can cover most prokaryotic microbial groups. The OTU (97 %) of all samples is in the range of 379-1,855. The Shannon-Wiener Diversity Index of the samples is between 2.05 and 7.89, which shows that the prokaryotic microbial population in these deep-sea sediments has high diversity. Moreover, the OTU of shallow-surface-layer sediments is higher than that of deep-layer sediments, indicating that with the increasing sediment depth, there are certain differences in microbial community diversity, and shallow layer sediments contain higher species diversity and species abundance.

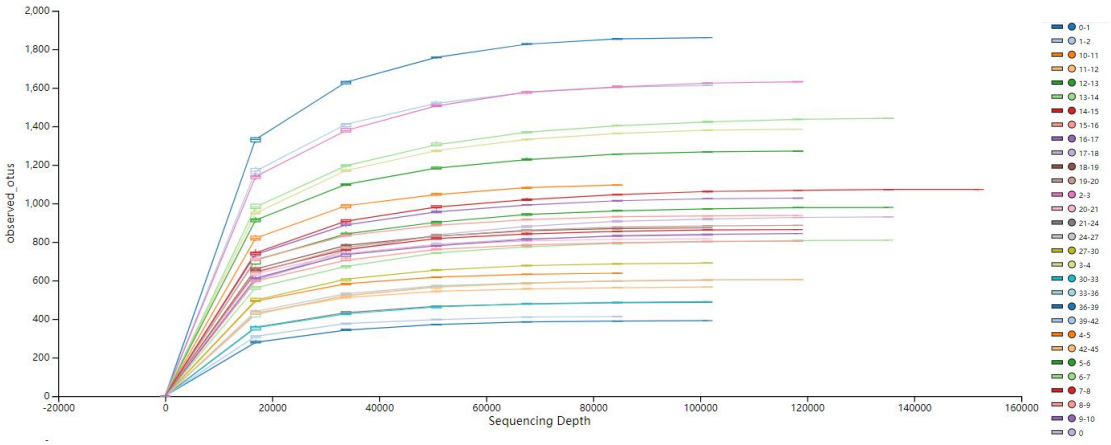

Figure 5.4-31 Dilution curve of prokaryotic microbial population sequencing of stratified sediment samples collected with multicorer at DY70I-A5-MC01 station

The ASV table for subsequent comparative analysis was rarefied to the same sequencing depth. The alpha diversity, including richness, shannon diversity,

shannoneven and phylogenetic diversity, was quantified using MOTHUR. The dissimilarity of beta diversity was estimated based on Bray-Curtis distances between each sample, and visualized by Principal Co-ordinates Analysis (PCoA). Permutational multivariate analysis of variance (PERMANOVA) was used to examine the significance of among groups.

(2) Variation of microbial diversity with sediment depth to 45 cm

By analyzing the amplicon results of stratified sediment samples collected with multicorer at DY70I-A5-MC01 station, we explored the species vertical distribution of composition and community structure of microorganisms. The sediment and overlying water samples collected at DY70I-A5-MC01 station are grouped according to depth, and the species accumulation map is drawn and visualized according to the order level, and compared with the surface-layer sediments collected with box corer at DY70I-A5-BC03. The results are shown in Figure 5.4-32.

Results show that Gammaproteobacteria is the dominant species in the surface-layer sediments collected at DY70I-A5-BC03 station and sediments of all layers collected at DY70I-A5-MC01 station. In Gammaproteobacteria, Burkholderiales and Pseudomonadales are the main groups, and the overall species richness of Gammaproteobacteria increases with the increasing depth at DY70I-A5-MC01 station. Alphaproteobacteria is less, accounting for only 5.004 % at the highest.

At all stations, Nitrosopumilales is the dominant taxon of archaea. Meanwhile, the species abundance of this community tends to decrease with the increasing depth, which may be due to the fact that this community is all aerobic archaea. With the increasing depth, the oxygen content gradually decreases, and the growth of this community is gradually limited. The community structure of microbes showed significant changes with depth, and was gradually steady over 10 cm depth.

The dominant taxa of bacteria and archaea in this area are consistent with those in the German Contract Area located in the eastern part of the CCZ, suggesting that the microbial ecological functioning of the deep-sea sediments in the Clarion-

Clipperton Zone is stable to some extent.

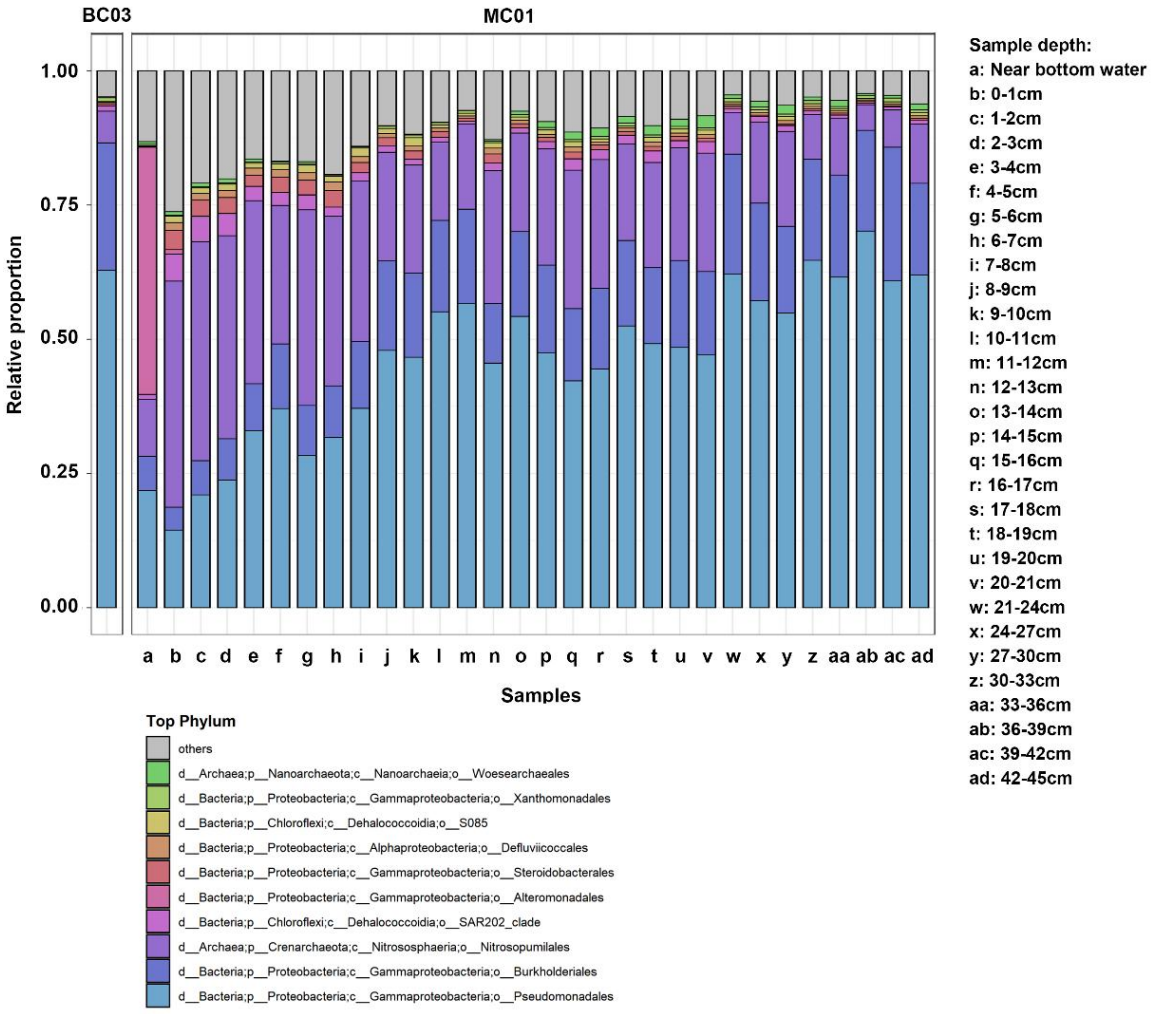

Figure 5.4-32 Composition analysis of prokaryotic microbial populations (on order level) in surface-layer sediments collected with box corer at DY70I-A5-BC03 station and stratified sediments collected with multicorer at DY70I-A5-MC01 station during Minmetals' 2021 survey cruise

(BC03 are surface-layer sediment samples collected with box corer, MC01 (from left to right) are the overlying water as well as sediment samples collected with multicorer at 0-1 cm, 1-2 cm, 2-3 cm, 3-4 cm, 4-5 cm, 5-6 cm, 6-7 cm, 7-8 cm, 8-9 cm, 9-10 cm, 10-11 cm, 11-12 cm, 12-13 cm, 13-14 cm, 14-15 cm, 15-16 cm, 16-17 cm, 17-18 cm 18-19 cm, 19-20 cm, 20-21 cm, 21-24 cm, 24-27 cm, 27-30 cm, 30-33 cm, 33-36 cm, 36-39 cm, 39-42 cm and 42-45 cm).

(3) Comparison of the IRZ and PRZ

A total of 34682 ASVs were identified in samples from this study area, spanning 46 phyla, 121 classes, 296 orders, 436 families, and 639 genera. The dominant bacterial phyla in this study area were Proteobacteria, Nitrospinota, NB1-j,

Myxococcota, Gemmatimonadota, Chloroflexi, Bacteroidota, Actinobacteriota and Acidobacteriota, with Proteobacteria being the most abundant (Figure 5.4-33). This study area had 32.8 % of unclassified species in the sediments, suggesting that its dark matter was yet to be explored.

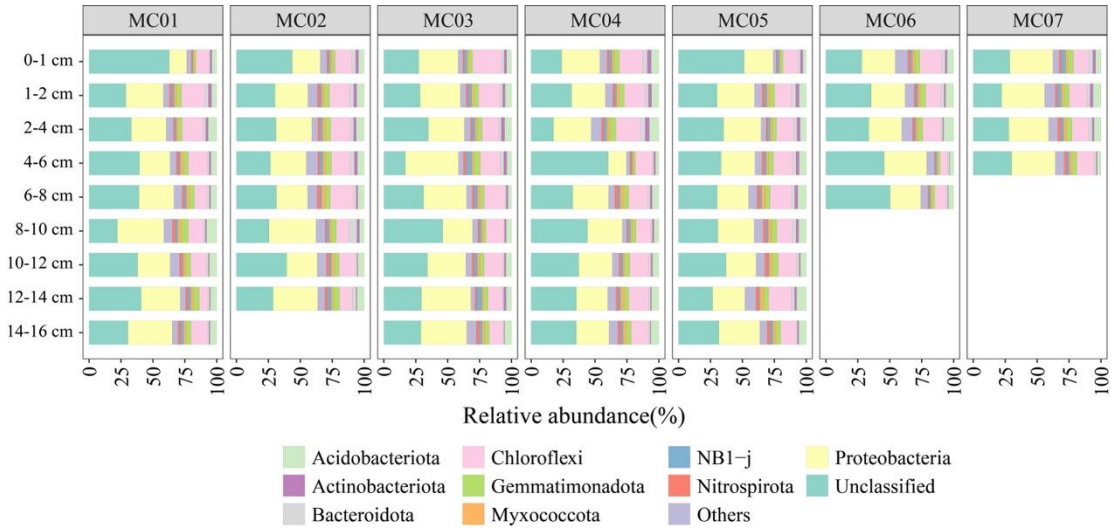

Figure 5.4-33 Composition of microbial communities at different depths at the phylum level

Four alpha diversity indexes, richness, Shannon-Wiener index and phylogenetic diversity, were calculated in this study to investigate the variation of alpha diversity indexes along depth. The Shannon-Wiener index of DY79I-A5-MC01 and DY79I-A5-MC02 had similar variation characteristics along the depth (Figure 5.4-34). Alpha diversity indexes of DY79I-A5-MC02 and MC03 had similar characteristics of variation along depth (Figure 5.4-34). Alpha diversity indexes of DY79I-A5-MC04 and DY79I-A5-MC05 had similar characteristics of variation along depth, except for 0-1 cm and 1-2 cm (Figure 5.4-34). Alpha diversity indexes of DY79I-A5-MC06 and DY79I-A5-MC07 had similar characteristics of variation along depth (Figure 5.4-34). Overall, alpha diversity showed a decreasing trend along depth, although there were some fluctuations.

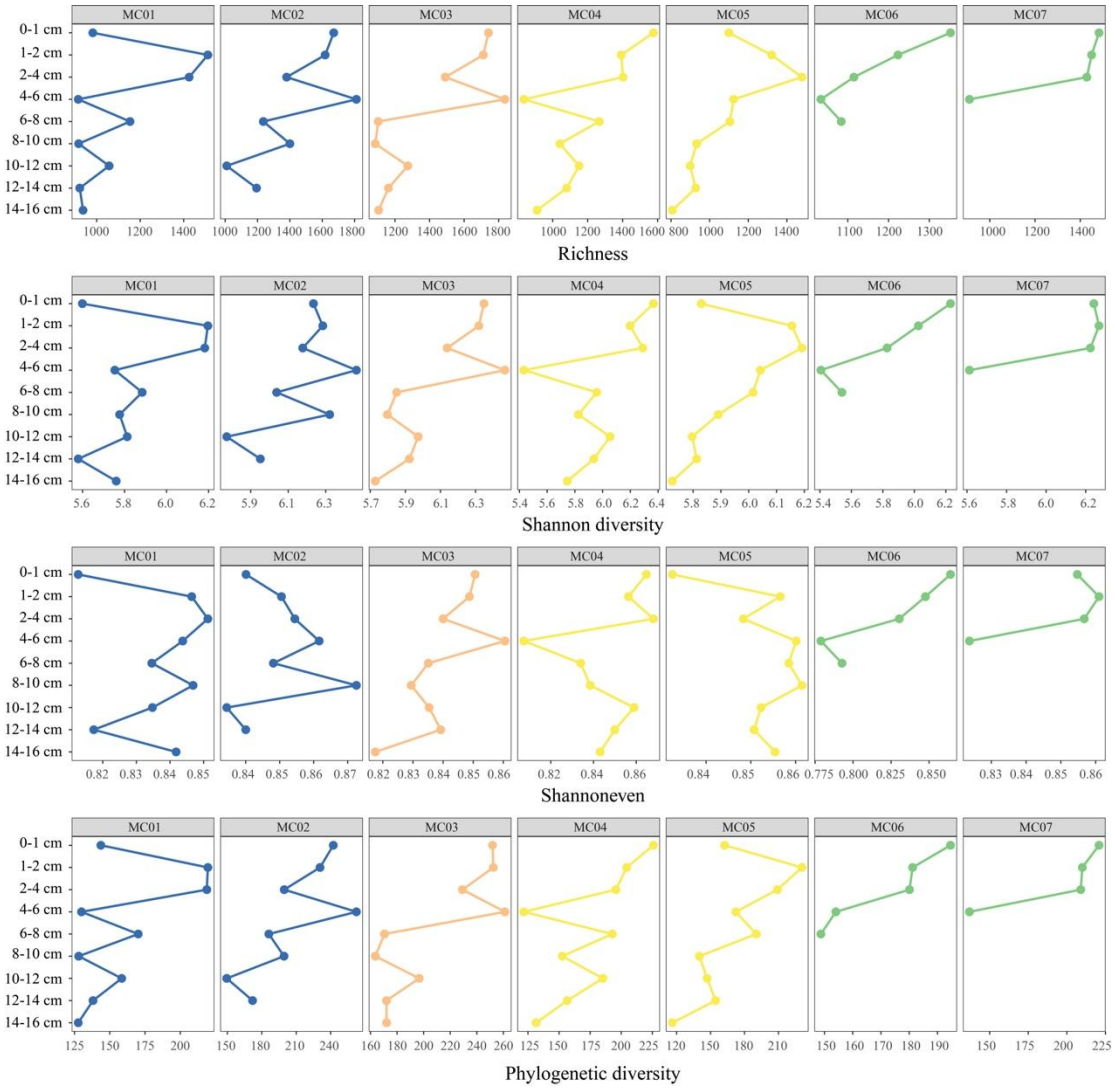

Figure 5.4-34 Characteristics of variation in alpha diversity along depth in each site

This study analyzed the beta diversity of microbial communities. PCoA analysis showed that microbial communities at different sites of sampling were relatively close to each other (Figure 5.4-35a).

The results of PERMANOVA analyses confirmed the significant effects of different sampling sites and different depths on microbial communities. Although the effect of different sampling sites on variation of community structure was significant (R^2 = 0.1962, p = 0.001), depth differences had a greater effect on the spatial variability of microbial community structure (R^2 = 0.2382, p = 0.001). This result suggests that the microbial communities in general were more affected by depth differences, although differences between sites could not be completely ignored

(Figure 5.4-35b).

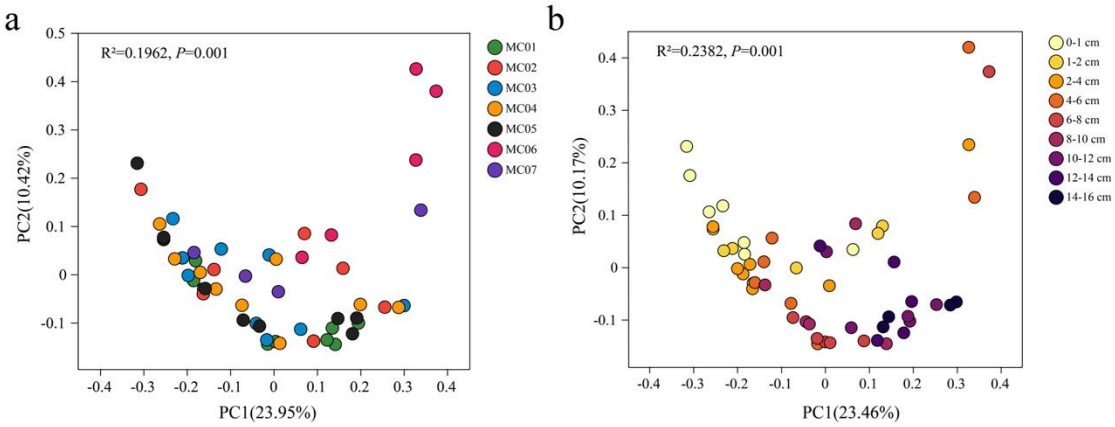

Figure 5.4-35 Beta diversity of microbial communities among different sites (a) and among different layers (b).

Further, PCoA analyses demonstrated differences in microbial communities among sites in each depth layer. In this study, the samples were divided into four groups, MC01-02, MC03, MC04-05, and MC06-07, based on the sampling area. The results showed that MC06-07 was different with MC01-02 in the PC1 axis, and MC01-02 was not significantly different from MC04-05 (Figure 5.4-36a-i). Combined with the previous results, microbial communities in the sediments of the A5 Block differed between MC06-07 and MC01-02 due to geographic distance, but the differences were weak relative to the differences caused by depth, and microbial communities were more similar in the same depth layer.

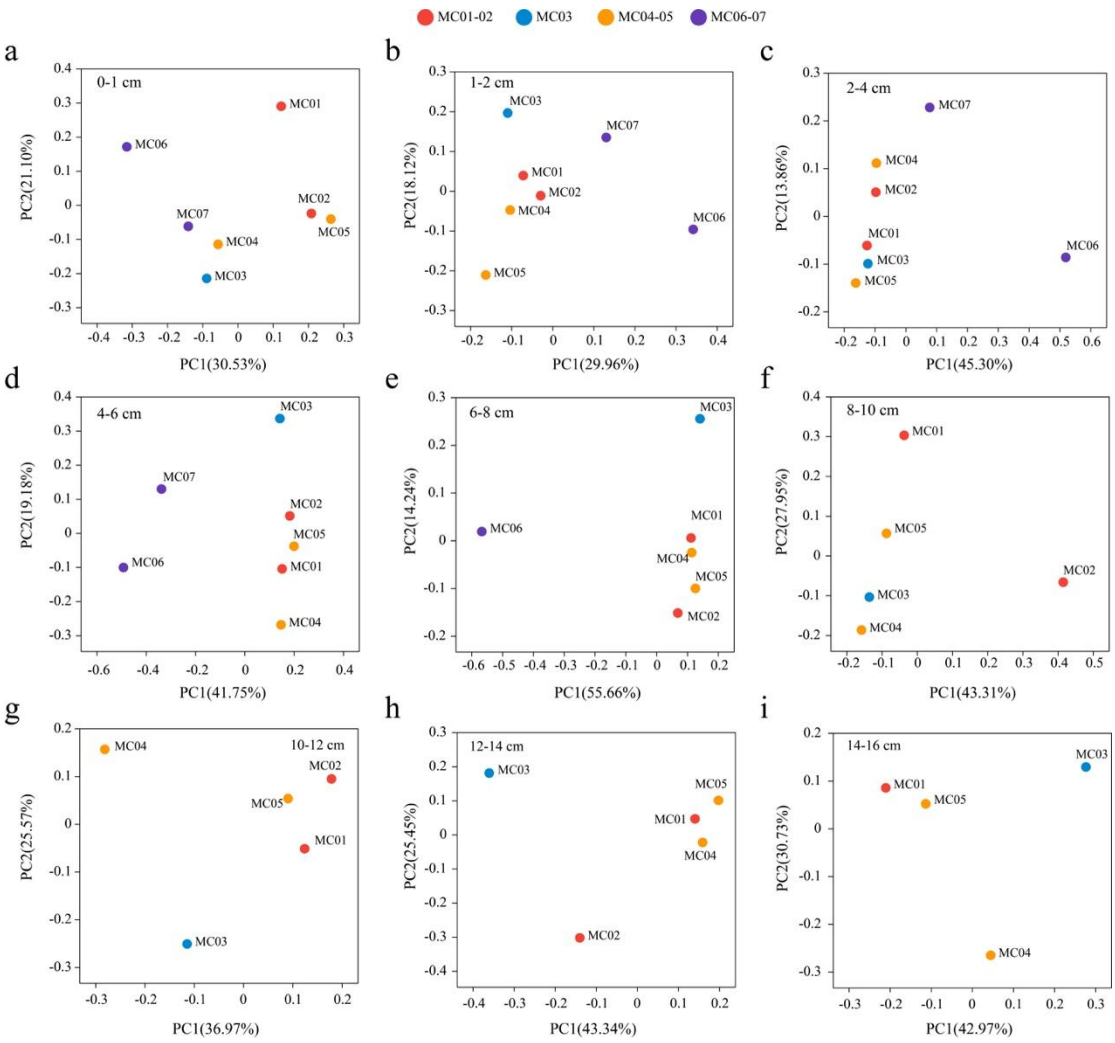

Figure 5.4-36 Beta diversity of microbial communities among different sites in each depth layer (a-i)

5.4.3.2 Meiofauna

So far, studies on meiofauna in the CCZ are mainly concentrated in the eastern part of the CCZ (EIS of BGR area, Uhlenkott, 2020). BGR report shows that meiofauna abundance in German Contract Area is 96-602 ind./10cm^2. Nematoda are the dominant taxon, accounting for 82-95 %, followed by Nauplius and Copepoda. The findings of TMC studies show that the average density of meiofauna in NORI-D Contract Area is 42.1167 ind./10cm^2, with Nematoda being the dominant taxon (67.4 %), an average density of 28.3931 ind./10cm^2, followed by Copepoda and Nauplius. On average, 68.8 % of meiofauna are distributed in the surface layer's 0-1 cm (51.0±33.9 ind./10cm^2), 23.3 % in the surface layer's 1-3 cm (17.3±12.4

ind./10cm^2) and 7.9 % in the surface layer's 3-5 cm (5.9±4.1 ind./10cm^2) (NORI 2022). The relative meiofauna abundance in the western part of the CCZ is relatively small. According to the studies in the COMRA Contract Area (Wang, 2013), the meiofauna abundance is 40-104 ind./10cm^2, and the dominant taxon is also Nematoda (91-93 %). This shows that the large-scale gradient variation of meiofauna abundance variation in the CCZ is in good agreement with the gradient of primary production in the upper layer of ocean.

5.4.3.2.1 IRZ

During Minmetals' 2021 survey cruise, we used multicorer to collect sediment samples for survey of meiofauna, as well as conducted four sampling operations (DY70I-A5-MC01, DY70I-A5-MC02, DY70I-A5-MC03 and DY70I-A5-MC04) at two stations in the IRZ of the Block A-5 of the Contract Area (parallel station sampling was conducted according to the requirements of the ISA).

(a) Community structure and abundance

Totally 11 groups of meiofauna have been found, including Nematoda Harpacticoida, Polychaeta, Oligochaeta, Ostracoda, Tardigrada, Acari, Nauplius, Isopoda, Gastrotricha, Kinorhyncha and other unidentified species (Figure 5.4-37), with an average abundance of 64.05 ind./10cm^2. Nematoda is the dominant group, accounting for 91.8 % of the total meiofauna, with an average abundance of 58.78 ind./10cm$^{2;}$ followed by Harpacticoida (an average abundance of 2.43 ind./10cm^2, 3.8 %) and Polychaeta (an average abundance of 0.76 ind./10cm^2, 1.2 %). Other groups each account for less than 1 %, with the sum only accounting for 3.2 % of total meiofauna abundance.

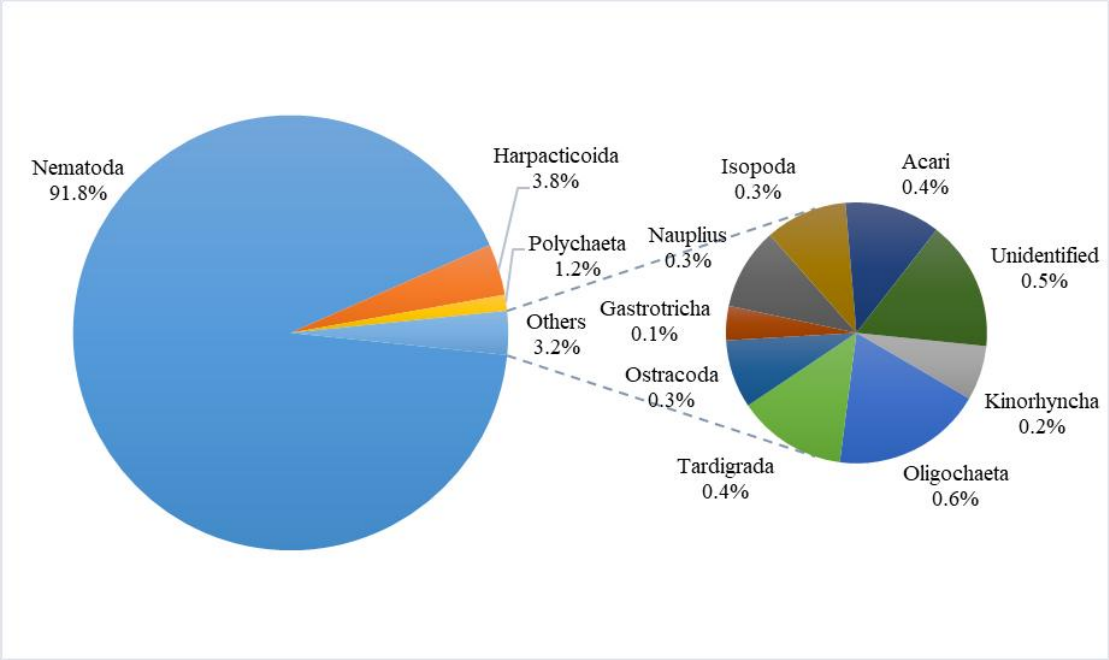

Figure 5.4-37 Meiofauna community structure in the IRZ

(b) Vertical distribution

The vertical distribution characteristics of meiofauna in sediments are shown in Figures 5.4-38 and 5.4-39. Approximately half of meiofauna are distributed in the uppermost layer (0-1 cm), and the sediment abundance below 4 cm depth only accounts for approximately 3 % of the total abundance.

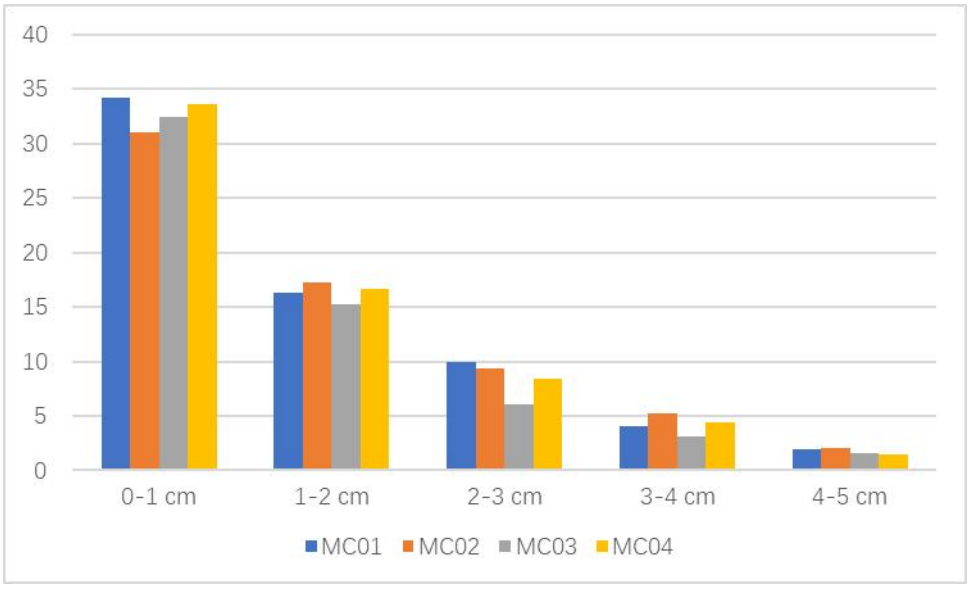

Figure 5.4-38 Vertical distribution characteristics of meiofauna abundance at different stations of the IRZ (Unit: 10 ind./cm^2)

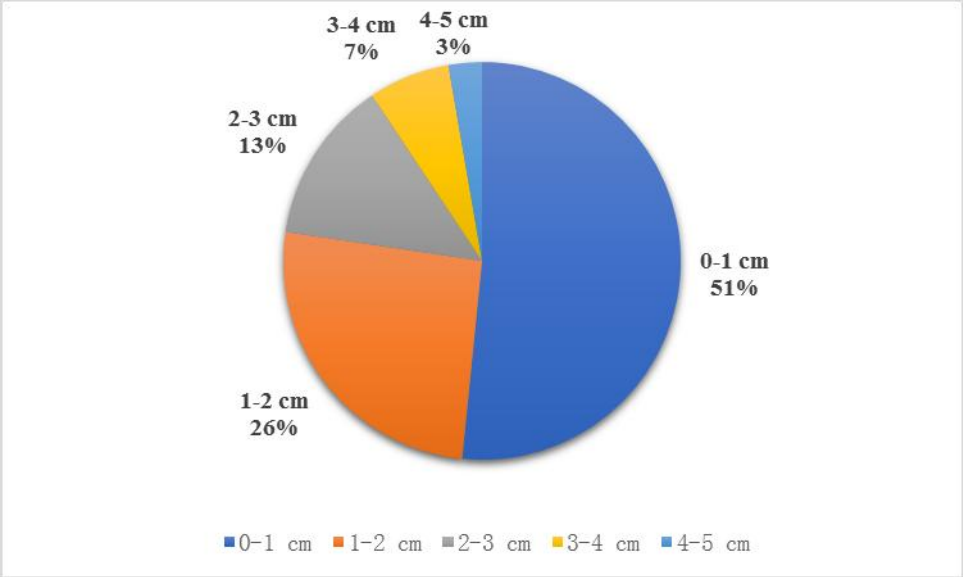

Figure 5.4-39 Vertical distribution of meiofauna abundance in the IRZ

5.4.3.2.2 PRZ

During Minmetals' 2019 survey cruise, we used multicorer to collect sediment samples for the survey of meiofauna, and conducted two sampling operations (DY54IV-A5-MC01 and DY54IV-A5-MC02) at one station in the PRZ of the Block A-5.

(a) Community structure and abundance

Eight groups of meiofauna have been found in the sediments of the survey area, including free-living marine Nematoda, Polychaeta, Oligochaeta, Harpacticoida, Isopoda, Cladocera, Tardigrada and Ostracoda (Figure 5.4-40), with an average abundance of 52.13 ind./10cm^2. Nematoda is the dominant group, accounting for more than 90 % meiofauna abundance, followed by Harpacticoida (an average abundance of 3.35 ind./10cm^2, 6.63 %) and Polychaeta (an average abundance of 0.60 ind./10cm^2, 1.19 %). Other groups only account for approximately 2 % of meiofauna abundance.

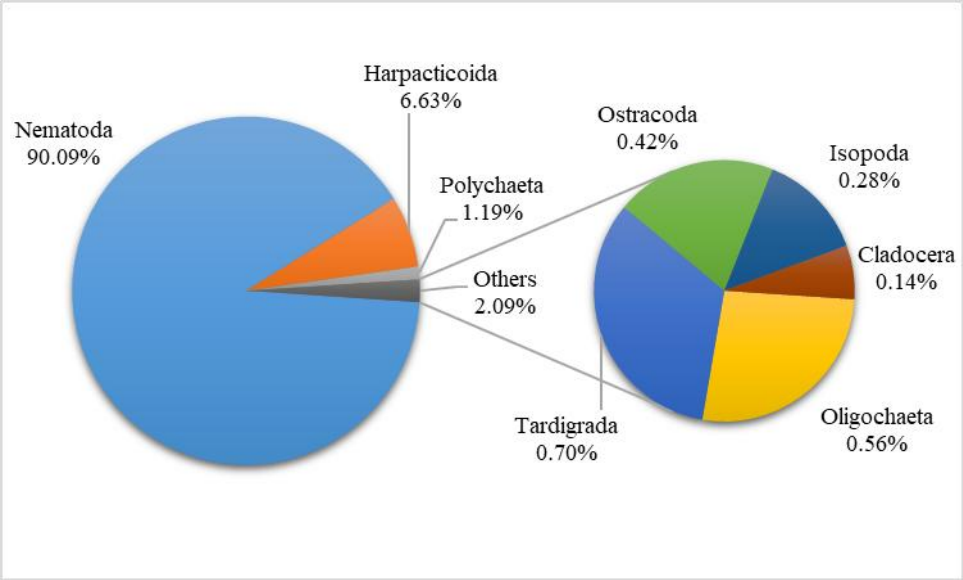

Figure 5.4-40 Community structures of meiofauna communities in the survey areas of PRZ

(b) Vertical distribution

The vertical distribution characteristics of meiofauna in sediments are shown in Figures 5.4-41 and 5.4-42. More than half of meiofauna in the Block A-5 are distributed in the 0-1 cm surface-layer sediments, and less than 5 % in sediments deeper than 4 cm.

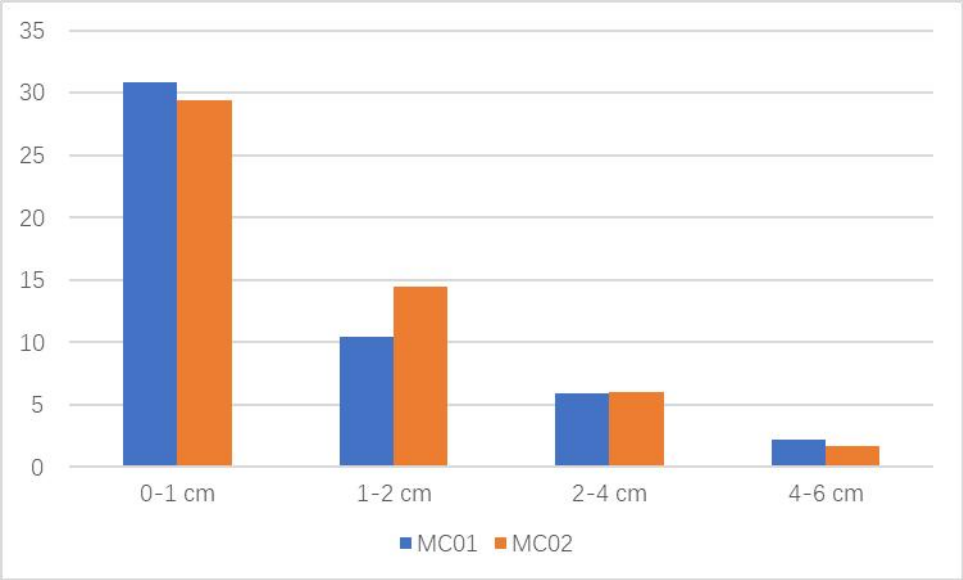

Figure 5.4-41 Vertical distribution characteristics of meiofauna abundance at different stations of PRZ (Unit: 10 ind./cm^2)

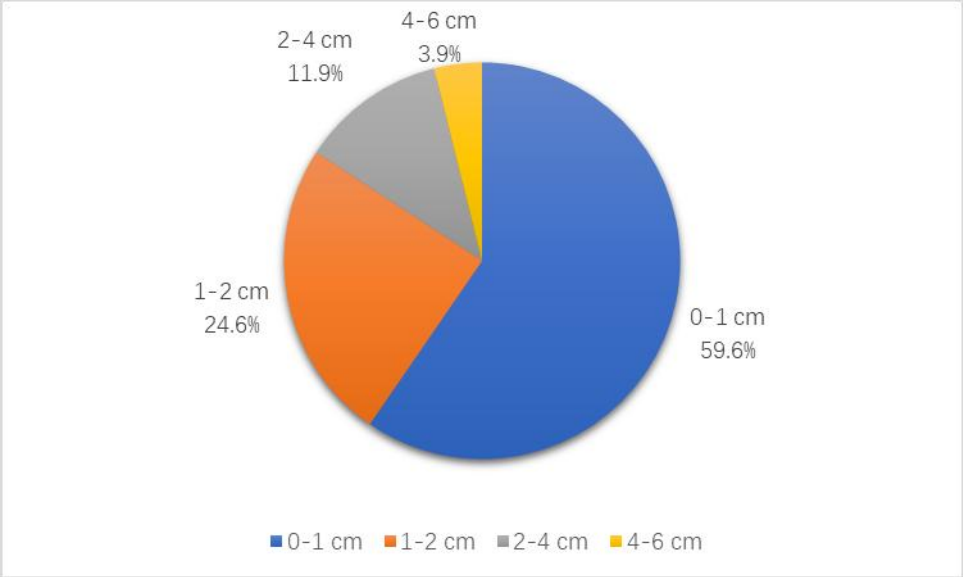

Figure 5.4-42 Vertical distribution of meiofauna abundance in the PRZ

5.4.3.2.3 Comparison of the IRZ and PRZ

(a) Community structure

During previous surveys, 12 groups of meiofauna were found in the PRZ and IRZ. Seven groups (i.e. Nematoda, Harpacticoida, Polychaeta, Oligochaeta, Tardigrada, Ostracoda and Isopoda) were found in both the IRZ and PRZ. There are four groups unique to the IRZ and one group unique to the PRZ. The diversity of biological groups in the PRZ and IRZ is similar. Nematoda is the dominant taxon (more than 90 %), followed by Harpacticoida and Polychaeta. The IRZ has many exclusive groups, possibly because there are no enough survey stations in the PRZ to cover all groups. The composition and dominant taxa of meiofauna in the PRZ and IRZ are the same as those in the COMRA Contract Area (Figure 5.4-43).

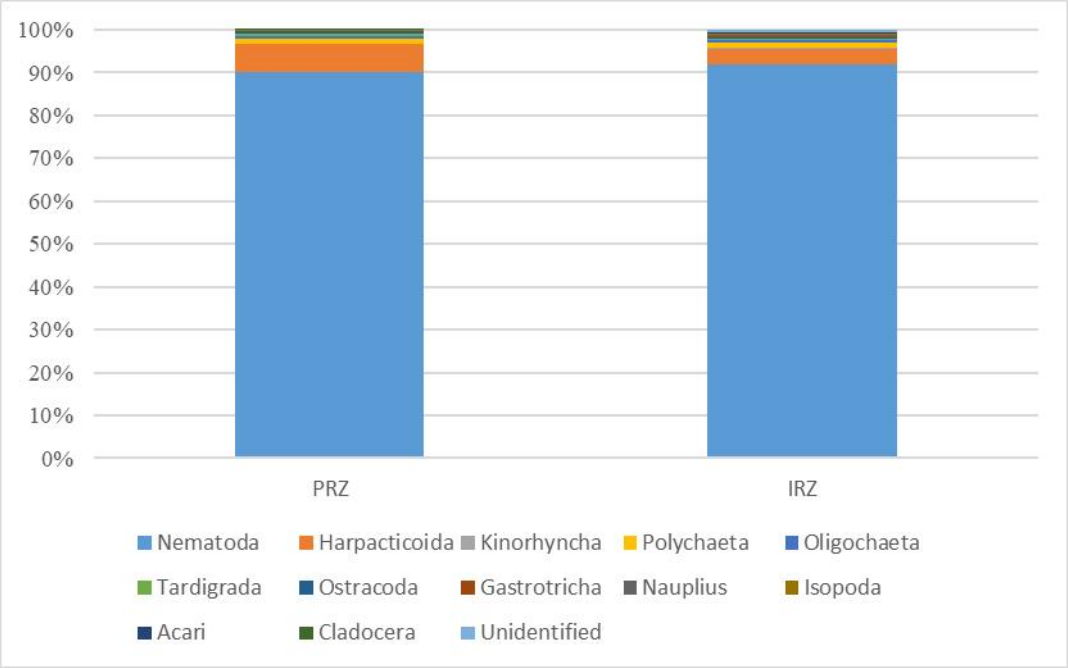

Figure 5.4-43 Comparison of meiofauna community structures between the IRZ and PRZ

(b) Distribution of abundance

Meiofauna abundance is similar in the PRZ and IRZ (Figure 5.4-44), averaging 64.05 ind./10cm^2 in the IRZ and 52.13 ind./10cm^2 (slightly lower) in the PRZ. The meiofauna abundance of the PRZ and IRZ is close to that of the COMRA Contract Area, which is also in the western part of the CCZ (40-104 ind./10cm^2).

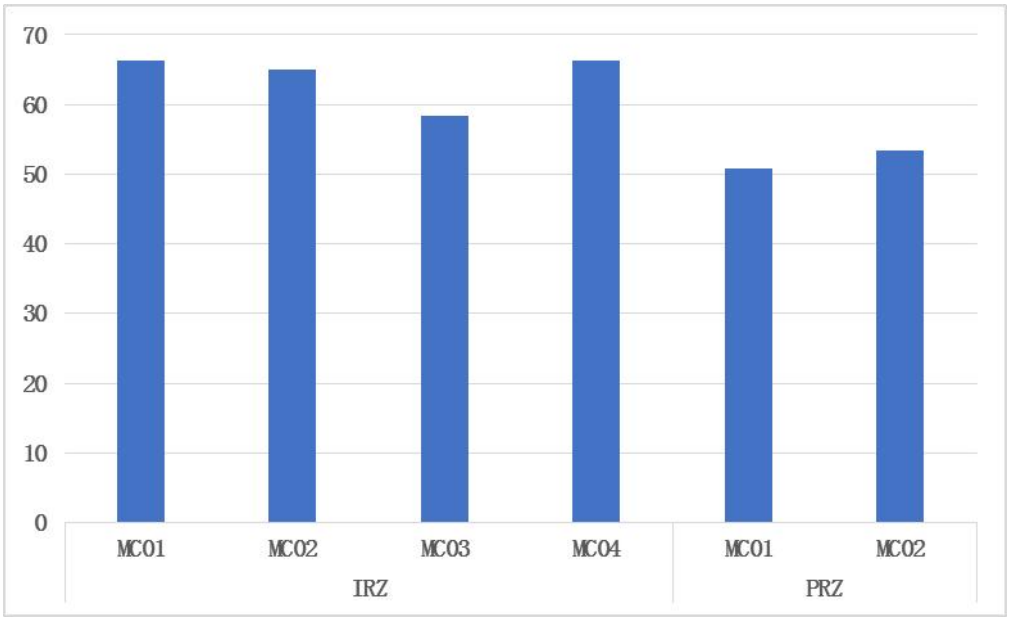

Figure 5.4-44 Comparison of meiofauna abundance between the IRZ and PRZ (Unit: ind./10cm^2)

(c) Vertical distribution

Comparison shows that the IRZ and PRZ are similar in the vertical distribution of meiofauna in sediments shallower than 4 cm. More than half of the abundance is concentrated in the surface-layer sediments of 0-1 cm, while sediments deeper than 2 cm account for 20 % of the total abundance (Figure 5.4-45).

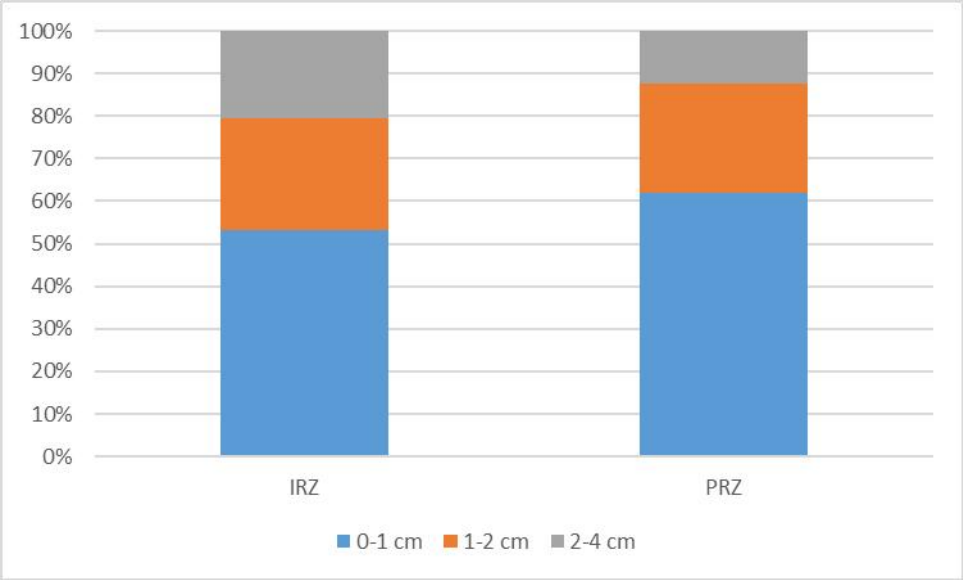

Figure 5.4-45 Comparison of vertical distribution of meiofauna between the IRZ and PRZ

(d) Interannual variability of meiofauna

Combined analysis of the meiofaunal survey data from five cruises in Block A-5 of contract area during the period 2017-2022 showed that the average abundance of PRZ meiofauna ranged from 50.5-62.8 ind./10cm^2 during the period of 2019-2023, with the lowest value occurring in 2019 and the highest value in 2022. The average abundance of IRZ meiofaunal ranged between 64.1-78.1 ind./10cm^2 during 2021-2022. The average abundance of meiofauna at stations outside of the reference areas ranged between 58.4-62.2 ind./10cm^2 during 2017-2022, with the lowest value occurring in 2022 and the highest in 2017 (Figure 5.4-46). There was little inter-annual variability in the abundance of meiofauna among stations outside of reference areas and in reference areas.

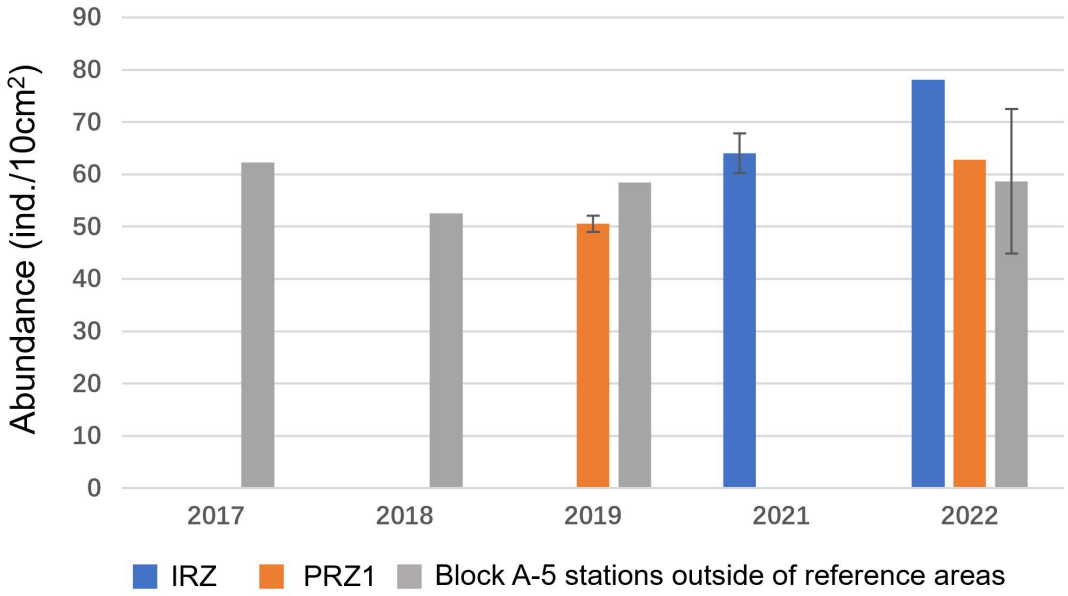

Figure 5.4-46 Comparison of of meiofauna between the IRZ and PRZ, showing the interannual variability

5.4.3.3 Macrofauna

So far, the studies on macrofauna in the CCZ are mainly concentrated in the eastern part of the CCZ (BGR 2018; De Smet, 2017). According to BGR report, the macrofauna abundance in the German Contract Area is 148-808 ind./m^2. Copepoda is the dominant taxon, followed by Polychaeta, and then by Tanaidacea and Isopoda. Other taxa are seldom seen. TMC report shows that the average macrofauna abundance in NORI Contract Area are 166±60.7 ind./m^2 and 278.8±34.3 ind./m^2 in Projects 5A and 5D, respectively. Among the identified species in Project 5A, the dominant taxa are Annelida, Echinodermata and Mollusca, while those in Project 5D include Arthropoda, Annelida and Mollusca (NORI 2022).

5.4.3.3.1 IRZ

During Minmetals' 2021 survey cruise, we used box corer to collect macrofauna samples at two stations (DY70I-A5-BC02 and DY70I-A5-BC04) in the IRZ of the Block A-5. According to the ISA's requirements, macrofauna samples were obtained at intervals of 0-3 cm, 3-5 cm and 5-10 cm.

(a) Community structure and abundance

Six types of macrofauna have been found in the survey area, including Polychaeta, Oligochaeta, Ostracoda, Isopoda, Amphipoda and Tanaidacea. The abundance varies in the range of 32-52 ind./m^2, averaging 44 ind./m^2. Polychaeta has the highest abundance (47 %), followed by Oligochaeta (24 %) and Ostracoda (14 %). The proportions of Isopoda, Amphipoda and Tanaidacea are all 5 % (Figure 5.4-47).

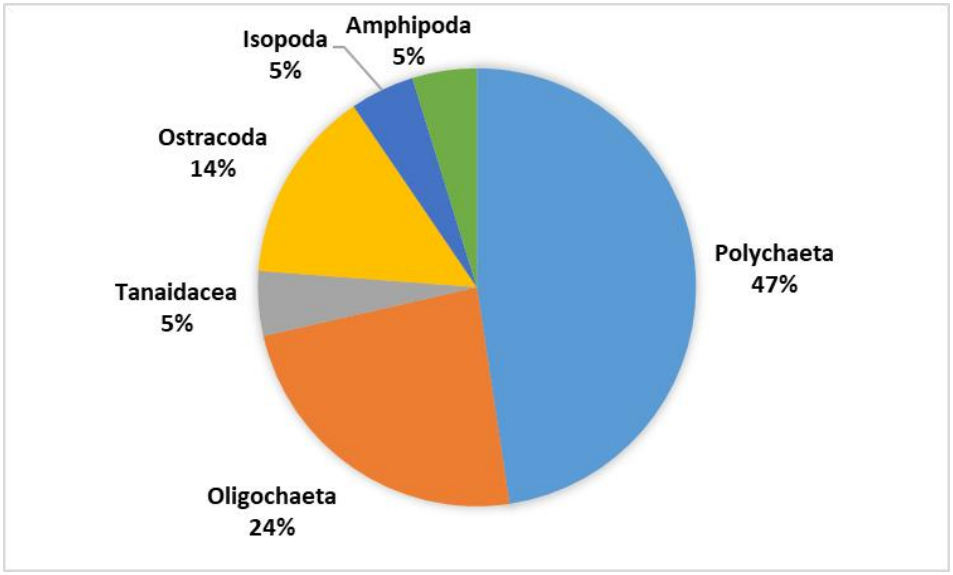

Figure 5.4-47 Macrofauna community structure in the IRZ

(b) Vertical distribution

We analyzed the vertical distribution characteristics of macrofauna in sediments. As shown in Figure 5.4-48, the abundance of macrofauna decreases obviously with the increase of sediment depth from the surface. More than 2/3 megafauna abundance are distributed in the uppermost layer (0-3 cm), and the proportion of sediments with depth of 5-10 cm is only 5 %.

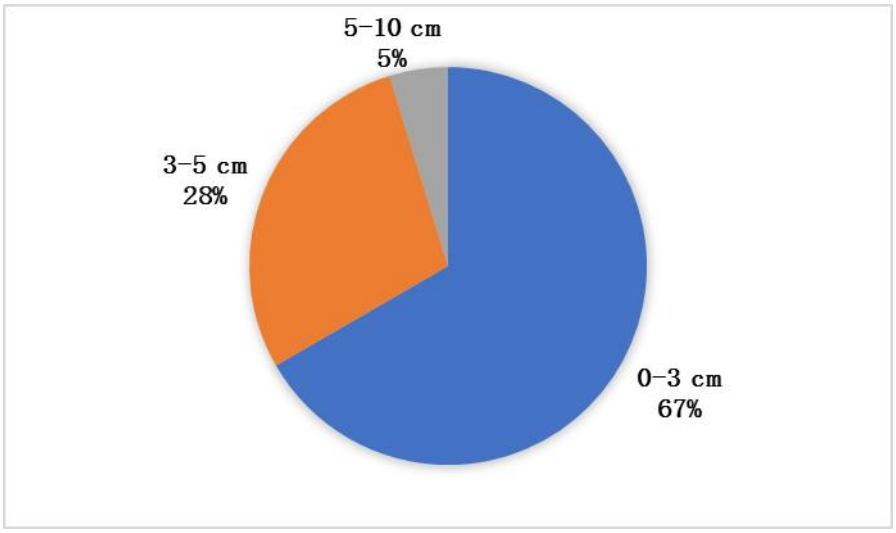

Figure 5.4-48 Vertical distribution of macrofauna in the IRZ

5.4.3.3.2 PRZ

During Minmetals' 2019 survey cruise, we used box corer to collect macrofauna samples at one station (DY54IV-A5-BC16) in the PRZ of the Block A-5, at intervals of 0-2 cm, 2-5 cm and 5-10 cm.

(a) Community structure and abundance

Five groups of macrofauna have been found in the survey area, including Polychaeta, Bivalve, Ostracoda, Isopoda, and Tanaidacea. The abundance is 56 ind./m^2. Polychaeta has the highest abundance (43%), while the proportions of Isopoda, Amphipoda and Tanaidacea are all in the range of 14-15 % (Figure 5.4-49).

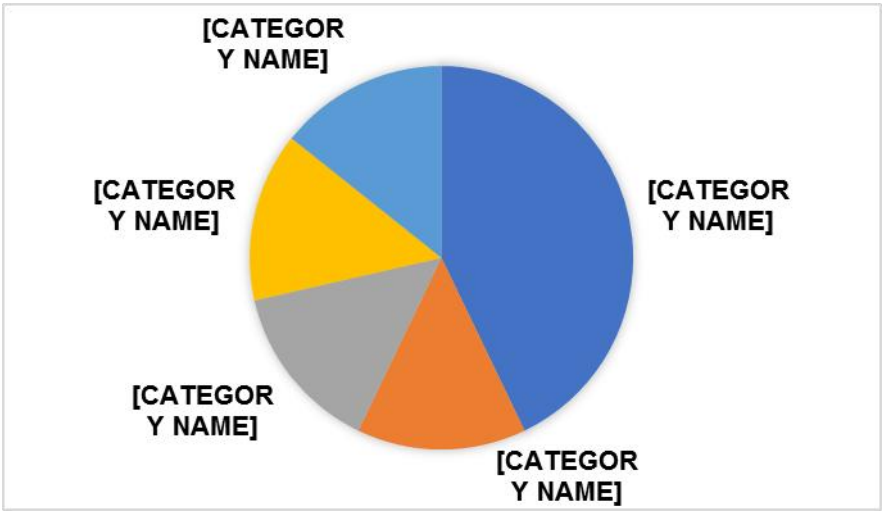

Figure 5.4-49 Macrofauna community structure in the PRZ

(b) Vertical distribution

The vertical distribution characteristics of macrofauna in sediments are shown in Figure 5.4-50. The abundance decreases obviously with the increase of horizon from the surface. Megafauna accounting for nearly half of the abundance is distributed in the uppermost-layer sediments (0-2 cm), while sediments deeper than 5 cm for only 28 % of abundance.

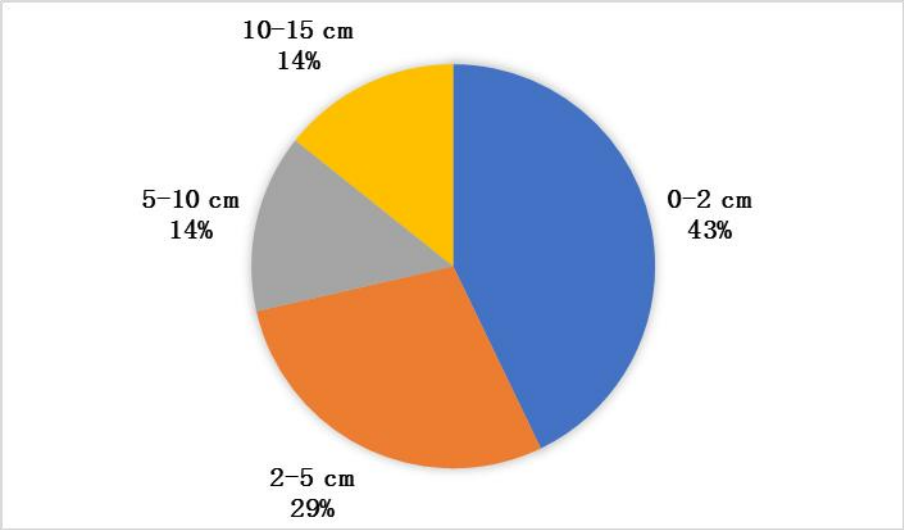

Figure 5.4-50 Vertical distribution of macrofauna in the PRZ

5.4.3.3.3 Comparison of the IRZ and PRZ

(a) Community structure and abundance

Seven groups of macrofauna were found in the PRZ and IRZ in the previous survey, including four groups (Polychaeta, Ostracoda, Isopoda and Tanaidacea) shared by the two regions. There are two groups unique to the IRZ and one group unique to the PRZ. Macrofauna abundance averages 32-52 ind./m^2 in the PRZ and IRZ. With abundance over 40 %, Polychaeta is the dominant taxon in the IRZ and PRZ. The composition and abundance of macrofauna in the IRZ and PRZ are similar, both less than that (148-808 ind./m^2) in the German Contract Area located in the eastern part of the CCZ and that (166-278 ind./m^2) in the NORI Contract Area. However, the dominant taxa and community structure of the communities were similar among the above regions (Figure 5.4-51) (NORI 2022).

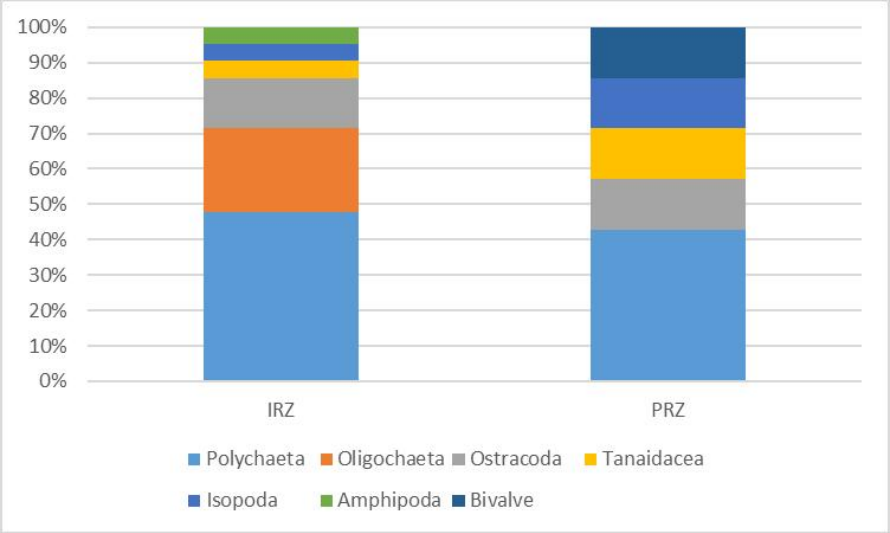

Figure 5.4-51 Comparison of meiofauna community structures between the IRZ and PRZ

(b) Species composition

Eight stations of macrobenthic samples (BC09, BC13, BC16, BC24, BC25 in 2022 cruise and BC10a, BC11, BC12 in 2023 cruise) were collected in Block A-5 using a box corer during the 2022 and 2023 cruises. We examined the species composition of the macrofauna and the results are presented below (Table 5.4-3).

Species richness of macrofauna in the IRZ, PRZ and other Block A-5 stations outside of reference areas was 32±5.7 species/m^2, 22.7±10.1 species/m^2 and 29.3±12.2 species/m^2, respectively. The difference in species richness between IRZ and PRZ was not significant, and the species composition of both areas was dominated by crustaceans and polychaetes.

Table 5.4-3 Comparison of macrobenthic diversity characteristics between PRZ and IRZ.

Area	Station No.	Specimens/station	Number of species/station	Dominant Taxa
IRZ	DY73I-A5-BC24	12	9	Polychaeta + Crustacea
	DY79I-A5-BC12	8	7	Polychaeta + Crustacea
	DY73I-A5-BC16	8	6	Polychaeta + Crustacea
PRZ	DY79I-A5-BC11	6	8	Polychaeta + Crustacea+ Mollusca
	DY79I-A5-BC10a	13	3	Polychaeta + Crustacea
Other A-5 stations outside of reference areas	DY73I-A5-BC09	7	4	Polychaeta + Crustacea
	DY73I-A5-BC13	11	8	Polychaeta + Crustacea+ Mollusca
	DY73I-A5-BC25	17	10	Polychaeta + Crustacea+ Mollusc+ Echinodermata

A total of 16 species have been recorded in the PRZ and 14 species in the IRZ. There are 5 species shared between the two areas (Table 5.4-4).

Table 5.4-4 Macrobenthic species list of IRZ and PRZ

Species	PRZ	IRZ
Allodaposia sp.	+	+
Conchostraca sp.3	+	
Conchostraca sp.4	+	
Conchostraca sp.5		+
Conchostraca sp.6		+
Harpacticoida sp.2	+	
Harpacticoida sp.3	+	
Isopoda sp.	+	
Isopoda sp.1	+	+
Isopoda sp.4	+	+
Isopoda sp.5		+
Isopoda sp.6		+
Isopoda sp.11		+
Tanaidacea sp.	+	
Tanaidacea sp.4	+	+
Tanaidacea sp.8		+
Ampharetidae sp.1		+
Cirratulidae sp.1		+
Glyceridae sp.	+	+
Opheliidae sp.	+	
Paralacydoniidae sp.		+
Praxillella sp.	+	
Spionidae sp.1	+	
Terebellida sp.5	+	
Veleropilina Starobogatov	+	

(c) Vertical distribution

The IRZ and PRZ have similar vertical distribution of meiofauna, which are concentrated in the surface layer of 0-5 cm depth, with the abundance accounting for over 80 %, and very small in the 5-10 cm depth layer (Figure 5.4-52).

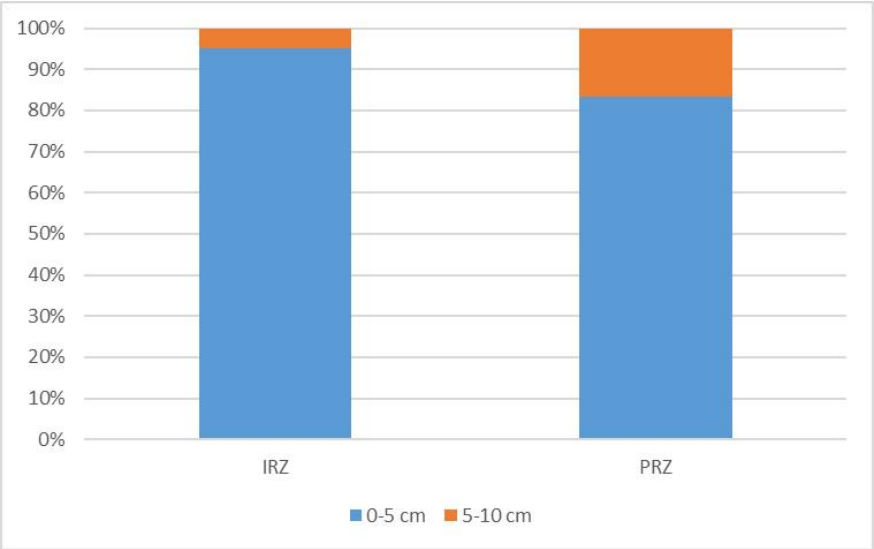

Figure 5.4-52 Comparison of vertical distribution of meiofauna between the IRZ and PRZ

(d) Interannual variability of macrofauna

Combined analysis of the macrofaunal survey data from six cruises in Block A-5 of contract area during the period 2017-2023 showed that the average abundance of PRZ macrobenthos ranged between 32-48 ind./m² during 2019-2023, with the lowest value occurring in 2022 and the highest in 2019. The average abundance of IRZ macrobenthos ranged between 32-48 ind./m^2 between 2022-2023, with the lowest value occurring in 2023 and the highest in 2022. The average abundance of macrobenthos at stations outside the reference zone ranged between 34.7-147 ind./m^2 during 2017-2022, with the lowest value occurring in 2022 and the highest in 2017, showing a large interannual variation (Figure 5.4-53). Interannual variability in macrobenthic abundance was lower in PRZ and IRZ, while interannual variability in abundance outside the reference area was higher.

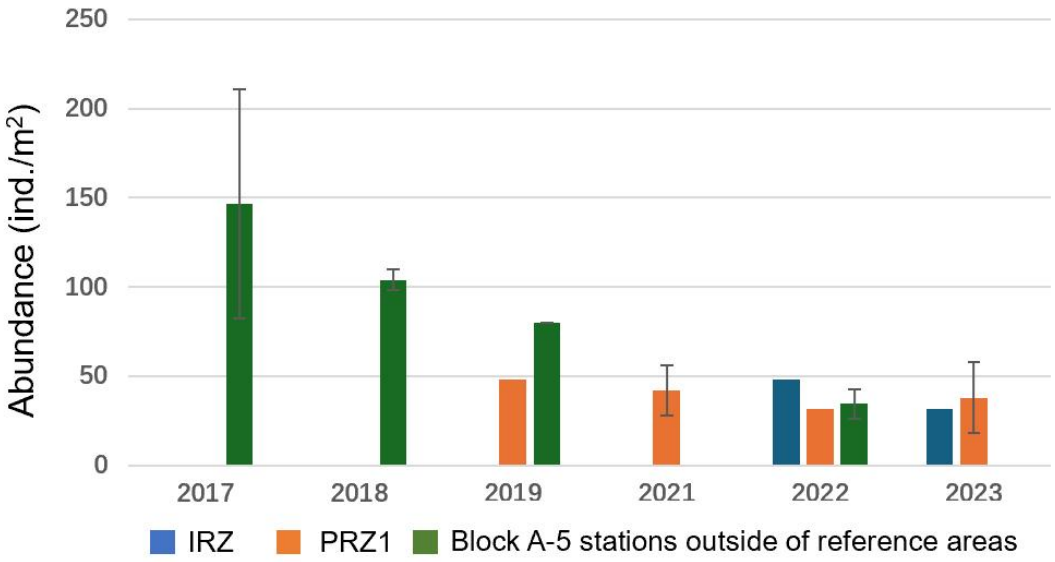

Figure 5.4-53 Comparison of of meiofauna between the IRZ and PRZ, showing the interannual variability

5.4.3.4 Megafauna

Based on the seabed videos obtained with towed camera, we analyzed the community composition and abundance of megafauna. The video data were obtained with towed camera photography survey lines in the Block A-5 of the Contract Areas during Minmetals' 2023 survey cruise. We conducted four towed camera photography survey lines (DY79I-A5-BVP01, DY79I-A5-BVP02, DY79I-A5-BVP03 and DY79I-A5-BVP04) in the Block A-5 of the Contract Area. The locations of survey lines (actual trajectory data from the Ultra-short baseline positioning system) are shown in Figure 5.4-54. Two lines are located in PRZ and its adjacent area, while the other two lines are located in the IRZ and its adjacent area; DY79I-A5-BVP01 survey line is about 24.5 km long, while others are about 20 km long. Every line has 5 km long in the IRZ (or PRZ), and the rest parts in adjacent areas. Towed camera survey lines are divided into six zones, which in PRZ and adjacent area are named as section 1-3, and in the IRZ and adjacent area are named as section 4-6.

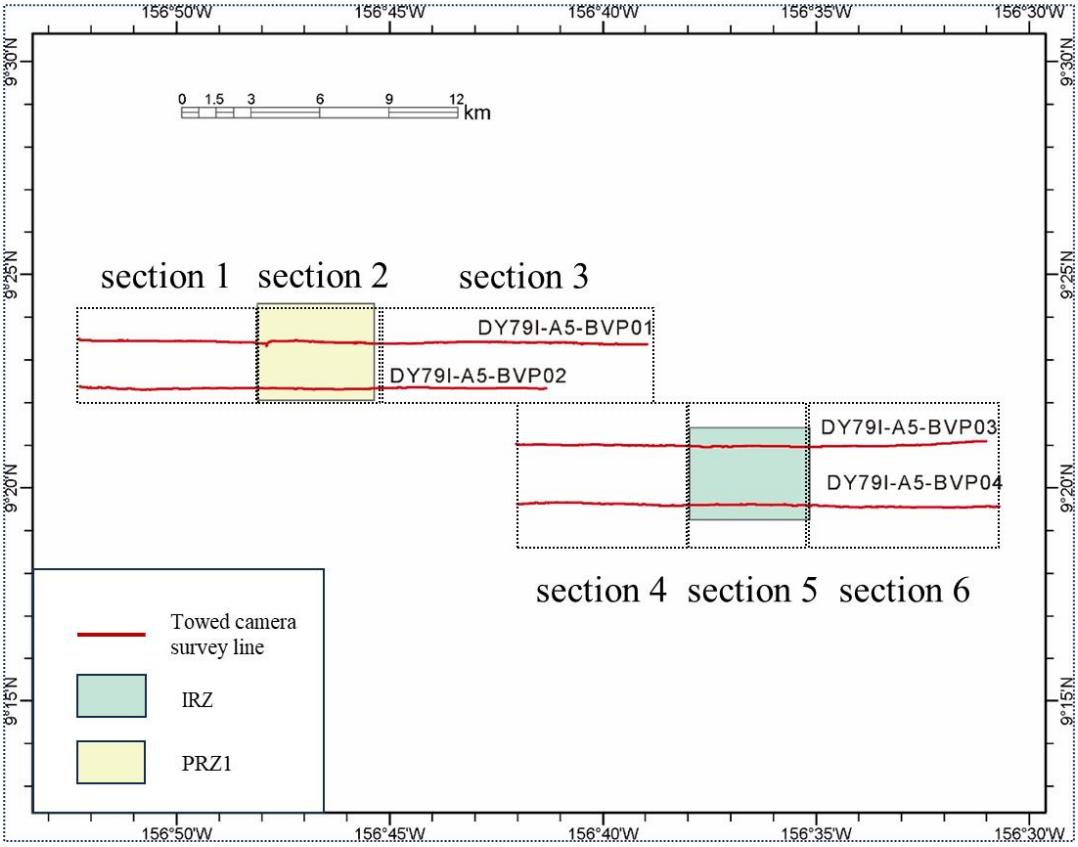

Figure 5.4-54 Towed camera survey lines and corresponding zones in the Block A-5 of the Contract Area

A total of 22,757 photographs have been recorded with towed camera, of which 13,858 were identified as megafauna. The average megafauna abundance is approximately 452.6 ind./ha. There are eight phyla: Protozoa, Porifera, Cnidaria, Echinodermata, Annelida, Mollusca, Arthropoda, Mollusca and Chordata. Among them, the average abundance of metazoan benthic invertebrates is 386.1 ind./ha, which is close to the abundance ar APEI 1, APEI 4 and APEI 7 in the western part of the CCZ (Durden et al. 2021) (Figure 5.4-57), and the community composition of megabenthic metazoa on phylum or class level is also consistent, with only the megafaunal foraminifera (Foraminifera) having lower abundance in the Block A-5. These results suggest that the abundance and community structure of megabenthic communities are largely similar at larger geographic scales in the western part of CCZ. Echinodermata, the dominated group megafauna in this region (44.3 %), consists of Holothuroidea (27.3 %), Opiuroidea (12.0 %), a small amount of Asteroidea (3.3 %)

and Echinoidea (1.3 %) and Crinoidea (0.4 %), followed by Porifera (18.0 %), megafaunal protozoa (14.1 %) (dominated by Xenophyophores), and Cnidaria (12.3 %) (dominated by corals and Actiniarian). Annelida (4.9 %) (dominated by Polychaeta), Mollusca (2.3 %), Arthropoda (42.1 %), and Chordata (2.1 %) are less common (Figures 5.4-55 and 5.4-56).

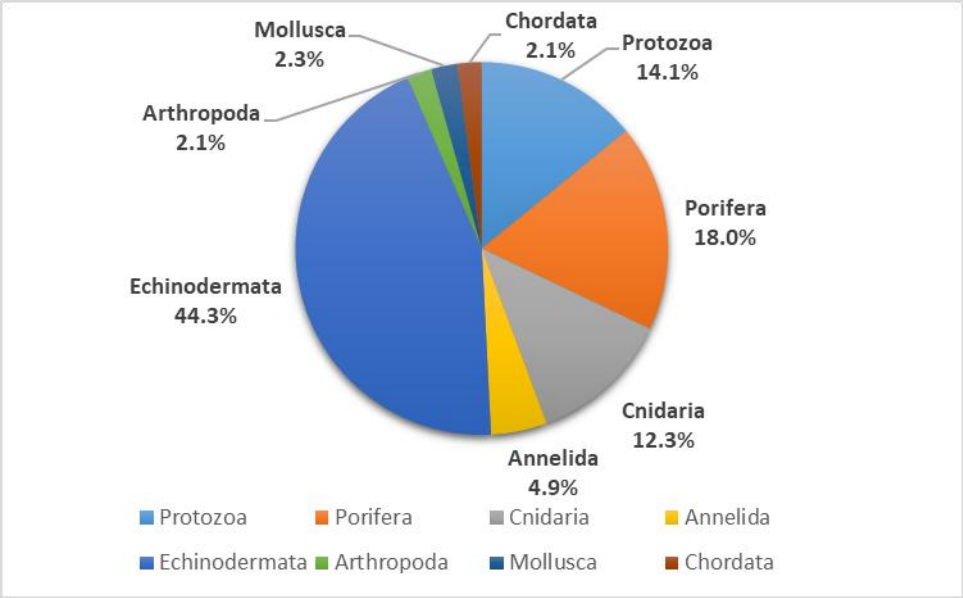

Figure 5.4-55 Distribution of megafauna abundance on phylum level

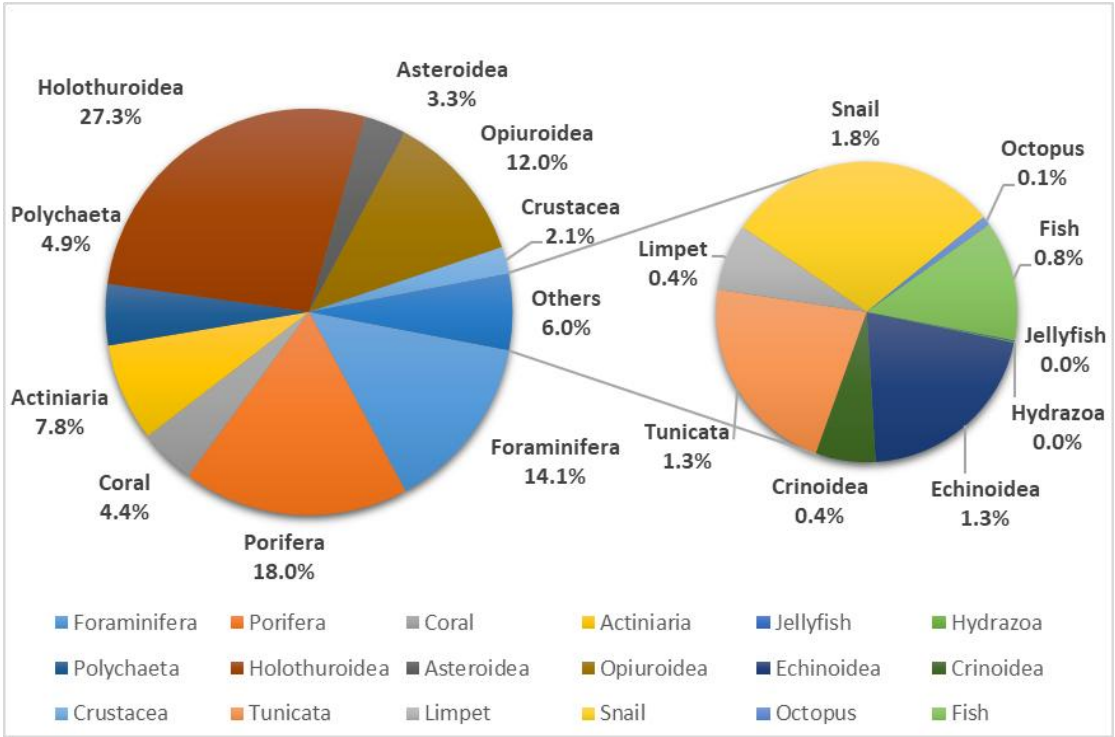

Figure 5.4-56 Distribution of megafauna abundance on class/order level

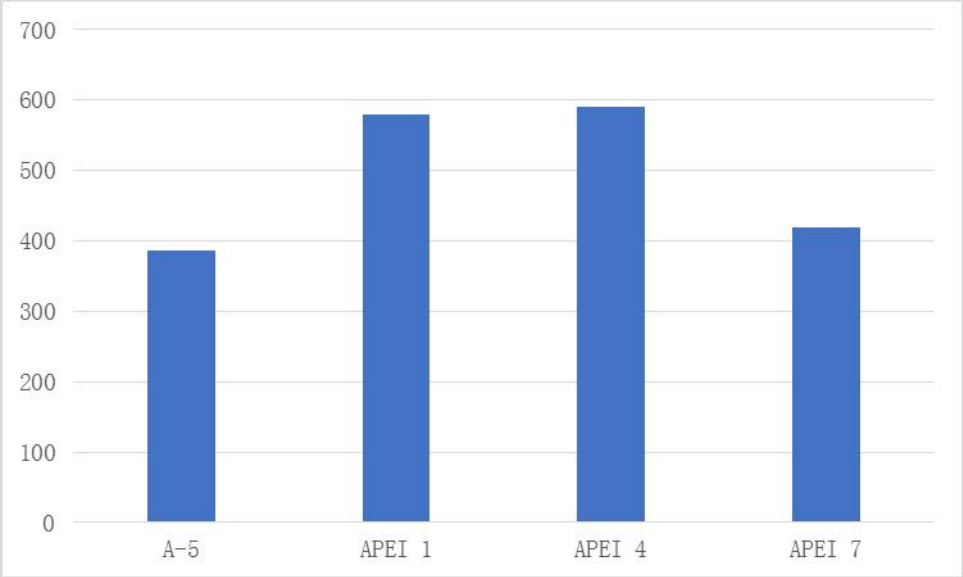

Figure 5.4-57 Comparison of the average abundance of macrobenthic invertebrates in the Block A-5 and the western part of the CCZ (Unit: ind./ha)

By their relationship with substrate, benthic fauna can be divided into three categories: fauna, nektobenthos (swimming fauna) and sessile fauna. Among them, vagile fauna and sessile fauna are dominant in this region, accounting for 47 % and 46 % of the total abundance. Most of vagile organisms belong to Echinodermata, among which most are Holothuroidea (27.3 %), followed by Opiuroidea (12.0 %) and few starfish, snails, capelin, and benthic arthropods represented by isopods. Protozoa (Foraminifera) (18 %) and sponges (14 %) dominated the sessile fauna, followed by actiniarians (7.8 %) and corals (4.4 %), while ascidians, sea lilies, and hydrozoans are rare, with abundances of less than 2 %. Nektobenthos are the least abundant, only accounting for about 7 % of total abundance, with polychaetes being more abundant (4.9 %) in this group, followed by swimming arthropods represented by shrimps, and fish, octopuses and jellyfish being rare (Figure 5.4-56 and Figure 5.4-58).

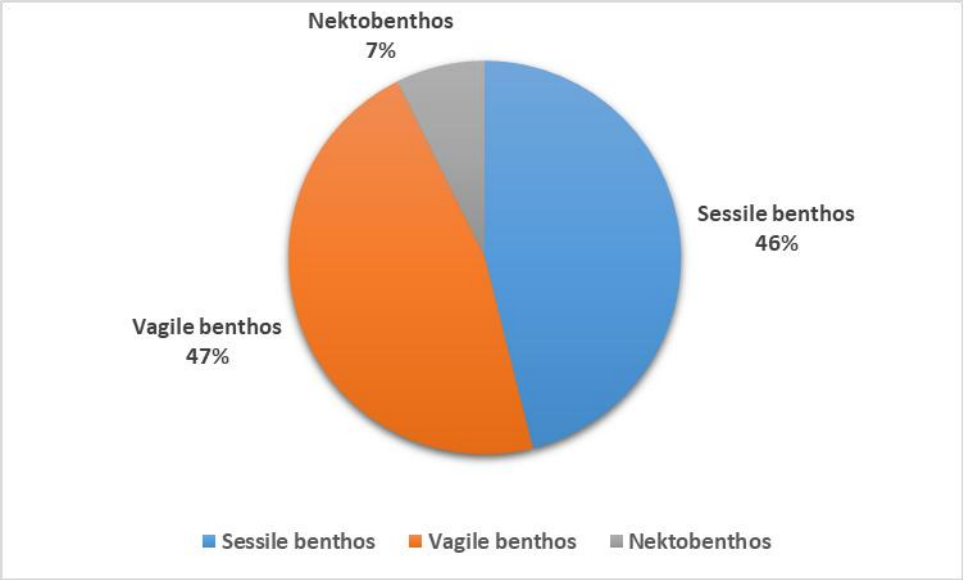

Figure 5.4-58 Megafauna community proportions by their relationship with substrate

Spatial analyses indicated differences in megabenthic abundance among six sections: the highest and lowest abundance values were found in section 4 and section 6, with 528.3 ind./ha and 325.8 ind./ha, respectively. Analysis also showed that there was no significant difference in the megafauna abundance of section 2 and section 5 located in the PRZ and IRZ respectively (431.0 ind./ha vs 510.6 ind./ha) (Figure 5.4-59). Except for a few rare taxa with abundances less than 0.1% (e.g., jellyfish, hydroids, and octopuses), the species composition and community structure of the megabenthos in PRZ and the IRZ are similar. (Figure 5.4-60).

In the study of NORI-D region, 605 metazoan megafauna specimens and 2657 Foraminifera were identified in the 597 m^2 seabed area surveyed in the NORI-D region, including 72 species of metazoan megafauna (with Cnidaria being the most abundant). In the whole NORI-D region, the distribution of megafauna is homogeneous, with abundances ranging from 0.93-1.08 ind./m^2 (NORI 2022). The megafauna abundance of the Block A-5 is lower than that of NORI-D.

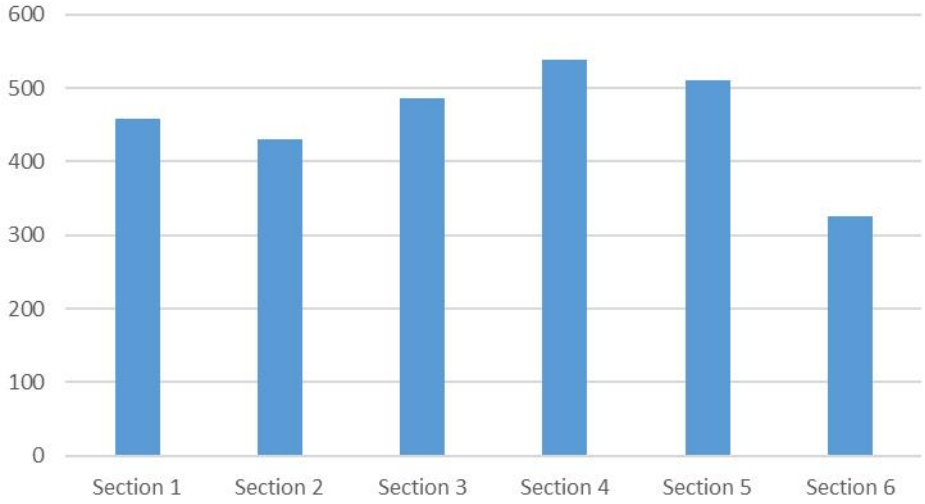

Figure 5.4-59 Comparison of megafauna abundance in the PRZ and IRZ (Unit: ind./ha)

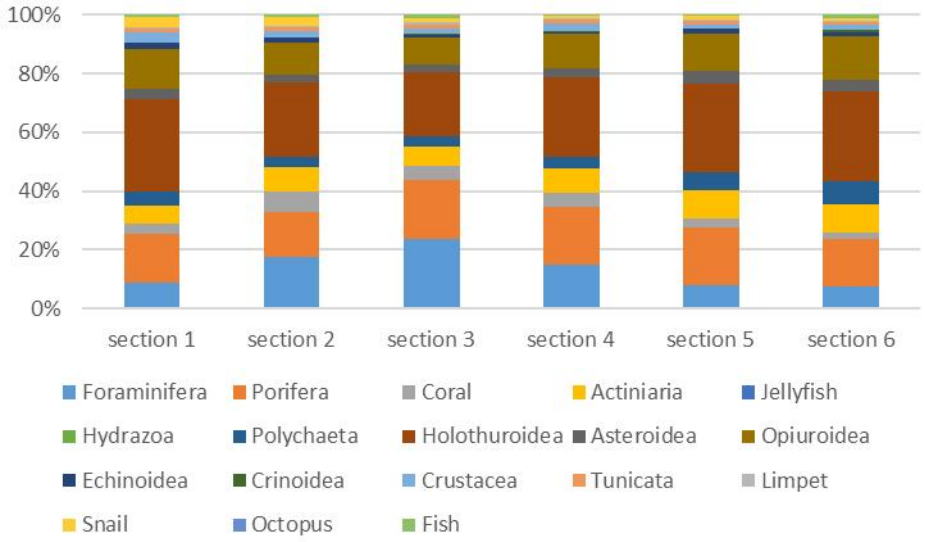

Figure 5.4-60 Comparison of megabenthic community structures in the PRZ and IRZ

The four long-distance camera trawl survey lines were divided into one sample block every 200 m, and the community structure of each sample block was analyzed by PCoA according to the grouping of the six zones mentioned above. The results showed that although there was a weak trend of spatial variability in the community in the east-west direction, the differences in community structure among the six blocks of Zone1-Zone6 were not significant (Figure 5.4-61). There was a high degree of similarity in the community structure of megabenthos between PRZ and IRZ as well as around the periphery of the two zones.

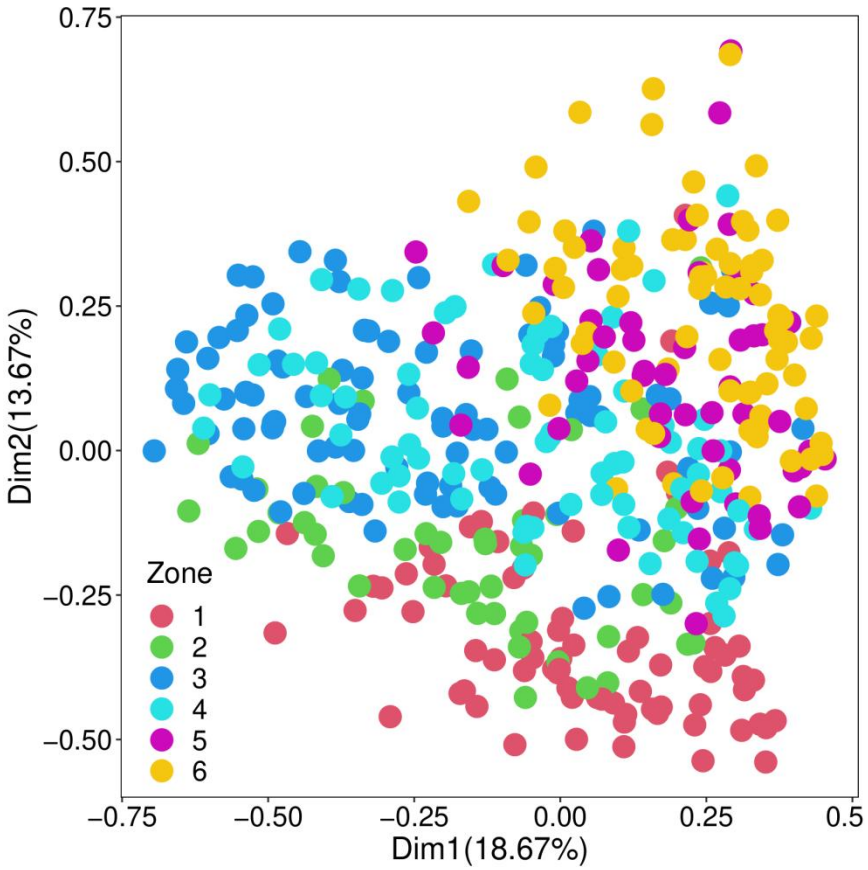

Figure 5.4-61 Result of PCoA to showing the spatial variation of megabenthic community structures between the PRZ and IRZ.

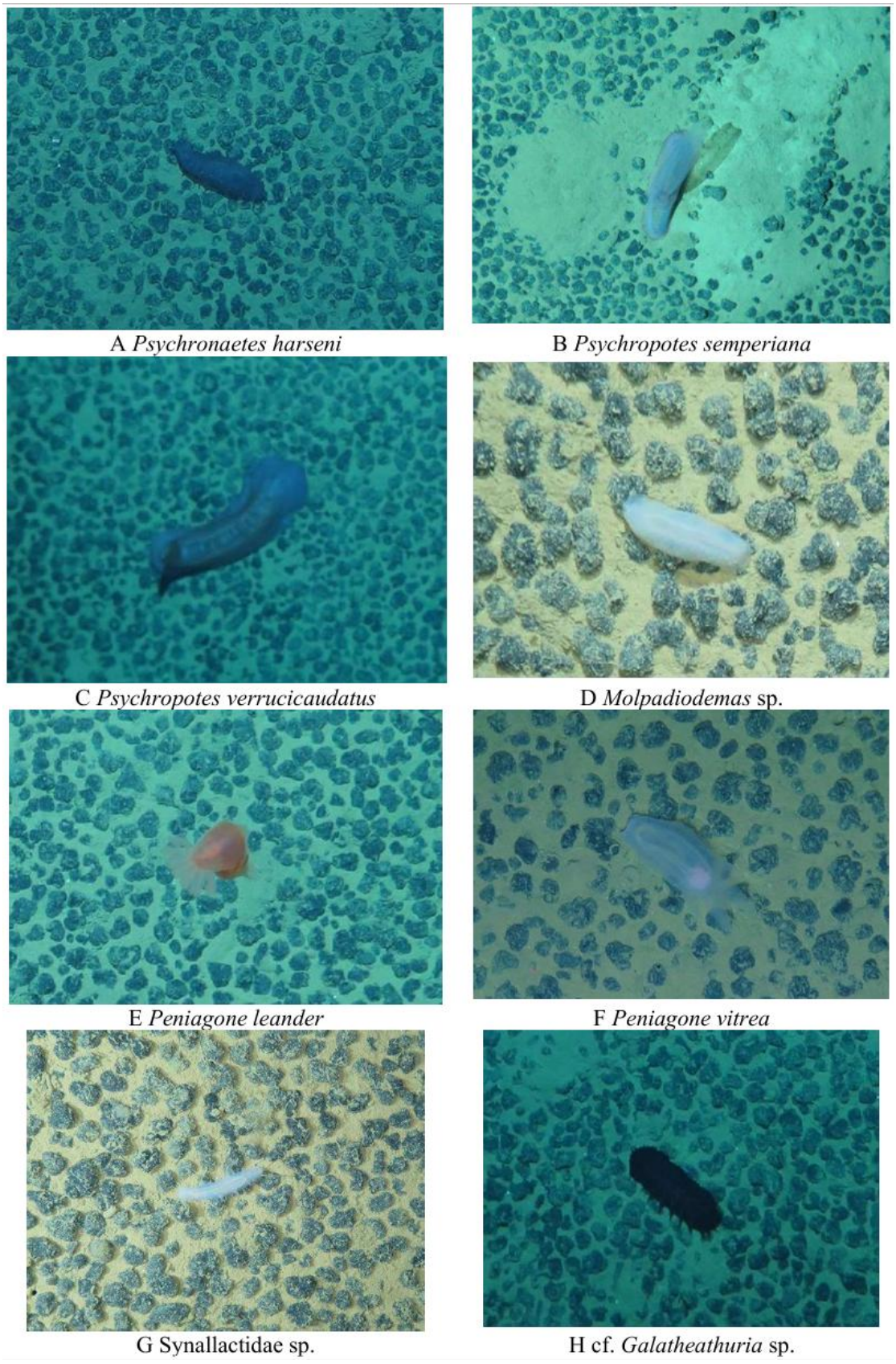

Figure 5.4-62 Representative megafauna in the Block A-5

(Photographs were taken during Minmetals' survey cruise DY73 and DY79, by AUV or deep-sea towed camera)

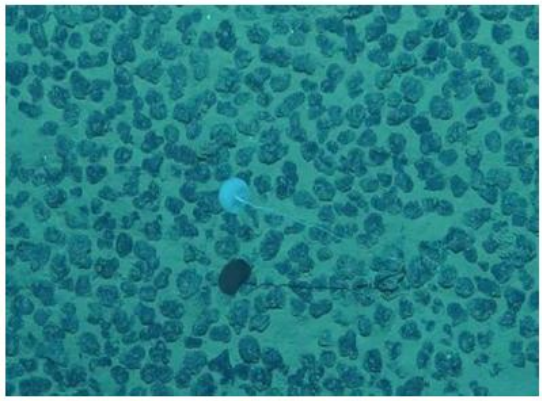

I *Caulophacus* sp

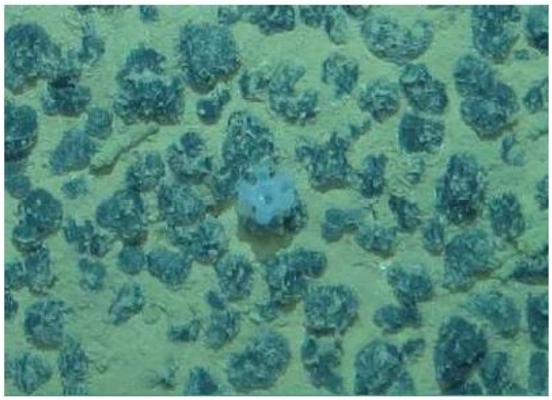

J *Cobitella* sp.

K *Hyalonema* sp.

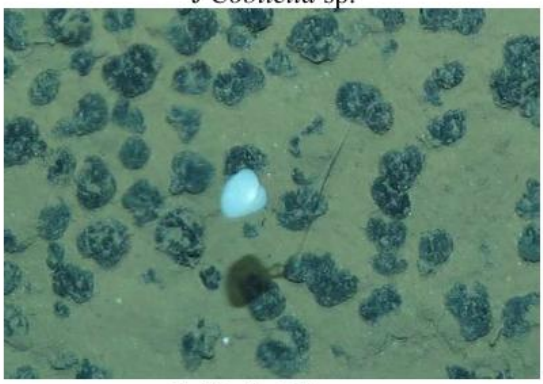

L *Hyalostylus* sp.

M Isididae sp.

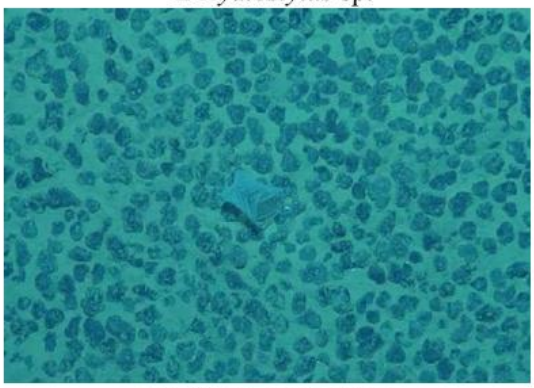

N *Abyssopathes lyra*

O Hormathiidae

P cf. *Cerianthus* sp

Figure 5.4-62 Representative megafauna in the Block A-5 (continued)

(Photographs were taken during Minmetals' survey cruise DY73 and DY79, by AUV or deep-sea towed camera)

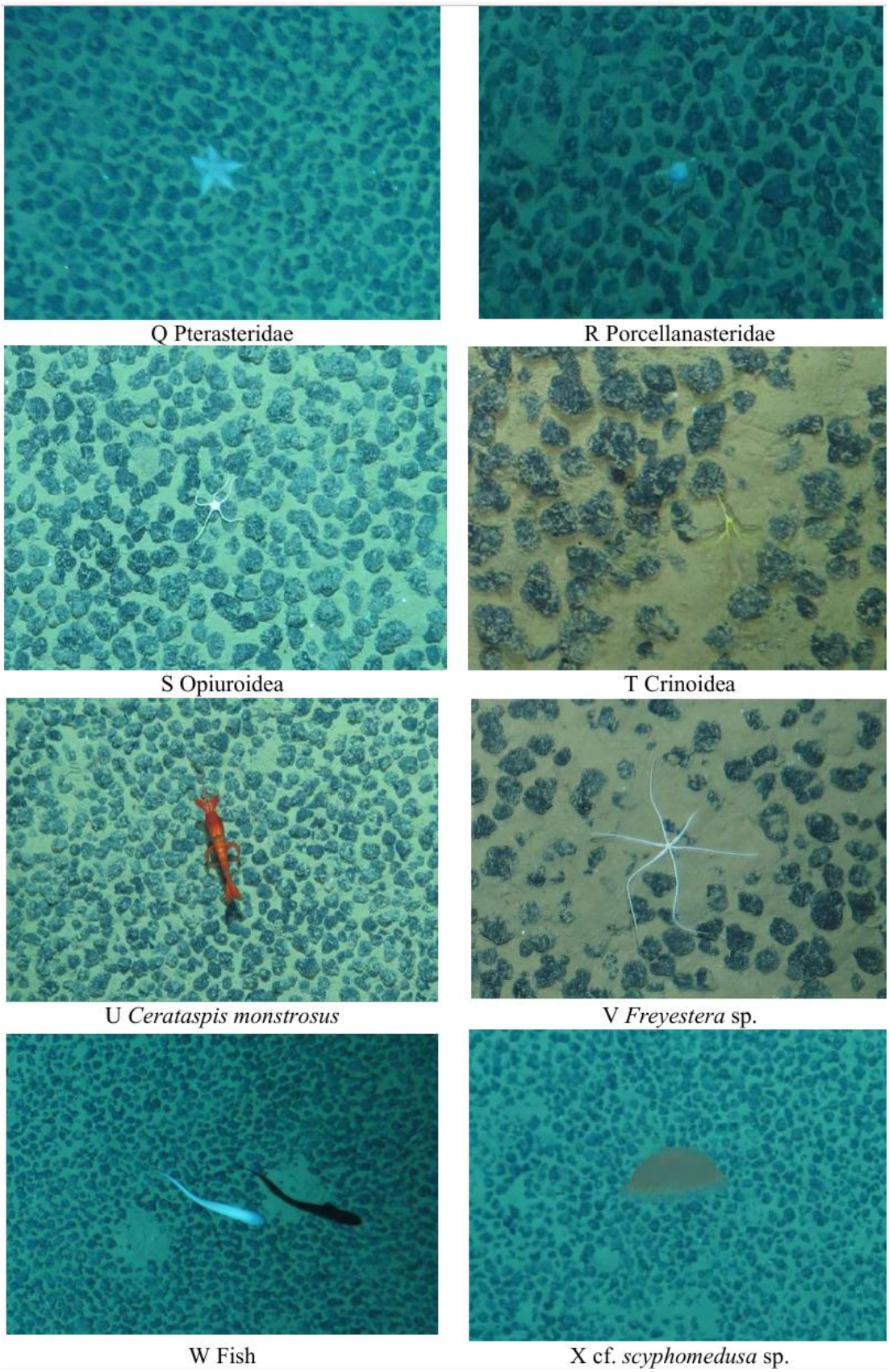

Figure 5.4-62 Representative megafauna in the Block A-5 (continued)

(Photographs were taken during Minmetals' survey cruise DY73 and DY79, by AUV or deep-sea towed camera)

The above megabenthos in situ photographs are taken from the AUV and deep-sea towed camera surveys conducted by Minmetals in Block A-5 in 2022 and 2023. Figures A, D, E, G, I, J, M-P, S-U are from DY73I-A5-AUV08; Figures B, C, H, K, Q, R, W, X are from DY73I-A5-AUV09; Figures L, V are from DY79II-A5-BVP01a; and Figures F are from DY79II-A5-BVP02. A large number of species have also been documented in other parts of the CCZ: figures A, N, U (Simon-Lledó, 2020), B, E, O, P (Tilot, 2006), L (Kersken, 2019) are also found in the eastern part of the CCZ; figures C, D, F, K, V (Bribiesca-Contreras, 2022), G-J, M (Durden, 2021) are also found in the western part of the CCZ.

5.4.3.5 Nodule fauna

During Minmetals' 2023 survey cruise, we have conducted investigation of samples collected by box corer at 40 stations in Block A-5, all of these samples remained low-disturbance. The site locations are shown in Figure 5.4-63. A total of 39 nodule fauna were collected during the field survey. The community structure of nodule fauna is shown in Figure 5.4-64. Preliminary results showed that the dominant groups of nodule fauna were protozoa (28.2 %) and bryozoa (17.9 %), while other groups included cnidarians, sponges, annelids, chordates, molluscs, echinoderms, and crustaceans, and 18 % were unidentified. Since each box corer covered an area of 0.25 m^2, we estimated that the abundance of nodule fauna in the Block A-5 was about 3.9 ind./m^2.

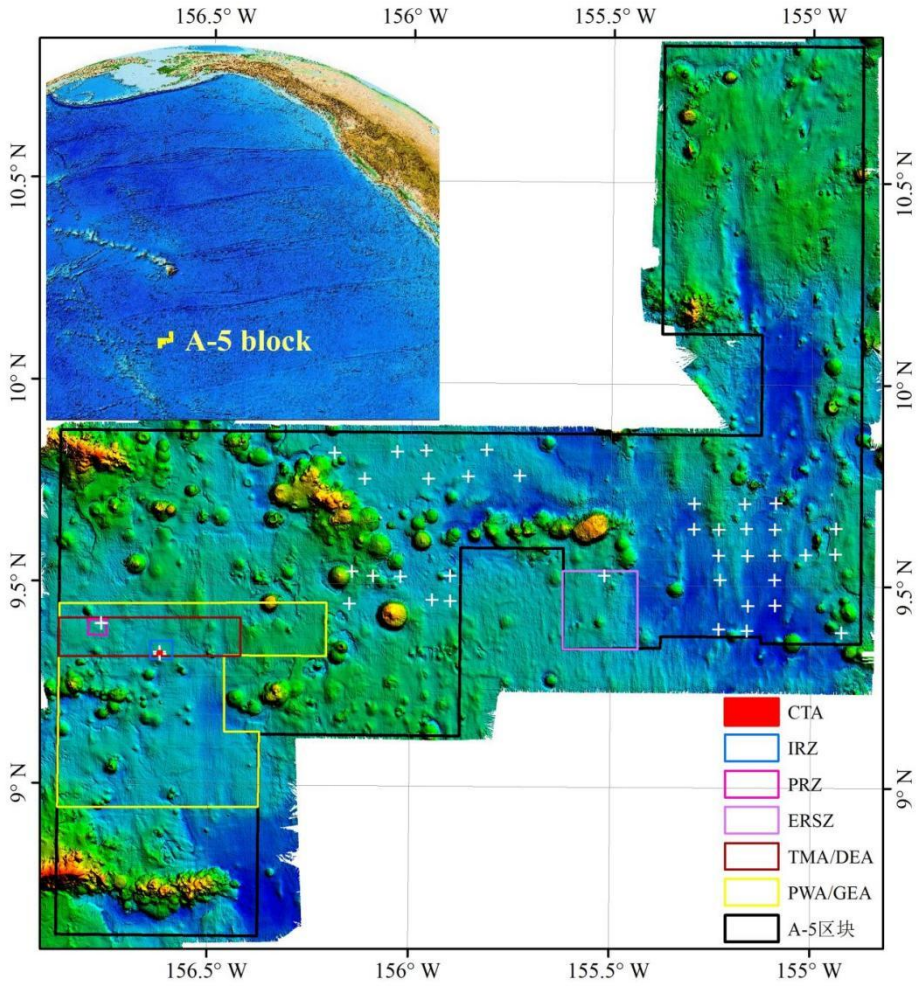

Figure 5.4-63 Box corer sampling stations with intact overlying water (PRZ to the west and ESRZ to the east of the Block A-5)

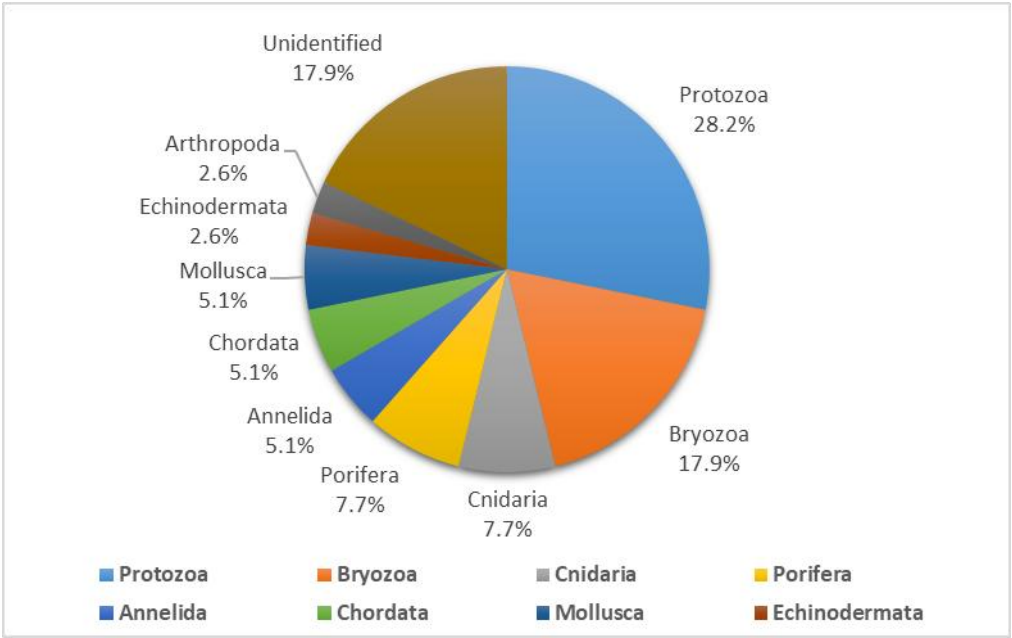

Figure 5.4-64 Nodule fauna community structure in the Block A-5

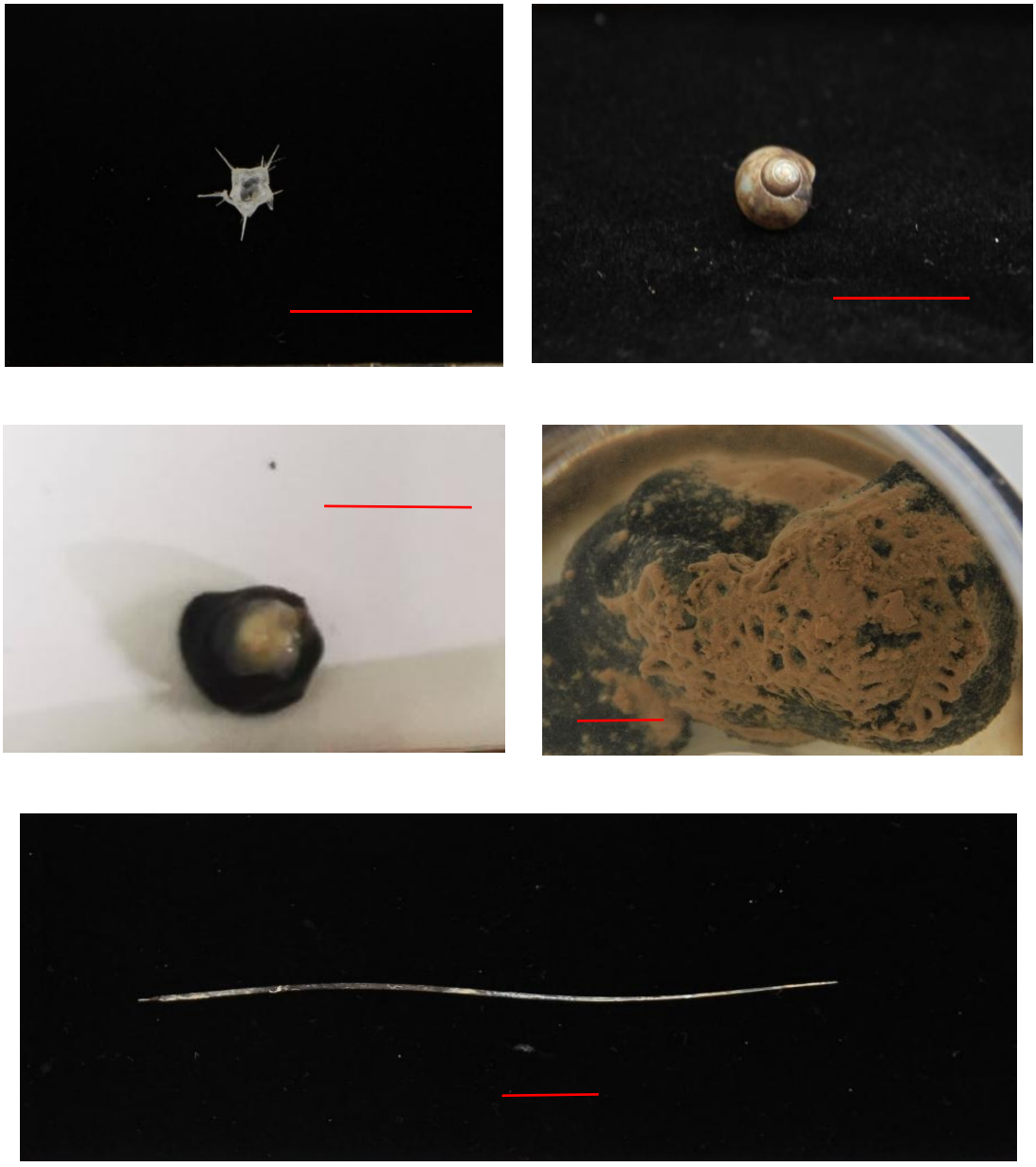

Figure 5.4-65 Photographs of some nodule fauna collected (scale: 1 cm)

According to the results of survey on the GSR German Contract Area in the eastern part of the CCZ, Foraminifera is the dominant Protozoa in nodule fauna, while Nematoda are the main nodule-related meiofauna (GSR 2018).

5.4.3.6 Scavengers

5.4.3.6.1 Scavenger biodiversity and DNA sequencing

During the Minmetals' 2021 and 2022 survey cruises, Minmetals conducted two

trap lander sampling operations in each of the IRZ and PRZ (including their peripheries). Scavengers such as fish and Gammarus were obtained (Figure 5.4-66). There are three species shared between the two areas, two species unique to PRZ and five species unique to IRZ (Table 5.4-5). The diversity of scavenger species was relatively similar. Considering that scavengers are mostly widely distributed species, the difference may be related to the relatively few sampling stations. The species of *Alicella* sp. were found the most in trapped species. So far, genus *Alicella* have been found mainly distributed at a water depth of 4,000-8,000 m in the Pacific Ocean (Ocean Biodiversity Information System, OBIS). In addition, the genus *Eurythenes*, a member of the family Eurythenidae, was trapped in high numbers, and two species of this genus were trapped in Block A-5, including *Eurythenes maldoror* and another unidentified species. The genus *Eurythenes* has a very wide distribution and has been recorded in the eastern, central and western parts of CCZ.

Table 5.4-5 List of scavengers in the Block A-5 Contract Area

Region	Species
PRZ	*Barathritis* sp.
	Alicella sp.
	Paralicella tenuipes
	Eurythenes sp.
	Eurythenes maldoror
IRZ	*Barathritis* sp.
	Coryphaenoides yaquinae
	Coryphaenoides lecointei
	Alicella sp.
	Eurythenes sp.
	Acanthonotozoma sp.
	Ichnopus sp.
	Hyperiidea

Figure 5.4-66 Scavengers trapped with lander in the Block A-5

We obtained the mitochondrial cytochrome c oxidase subunit I (COI) DNA barcode fragment from the sample of *Coryphaenoides yaquinae*, and searched the COI sequence data and geographical information of this species from NCBI and BOLD databases. The result of phylogenetic tree showed that the COI haplotypes of samples obtained in the IRZ of the Block A-5 are the same as most samples from the eastern part of the CCZ (Figures 5.4-67 and 5.4-68), which suggested the populations of *C. yaquinae* in the CCZ may not be obviously isolated and differentiated, and there is good connectivity.

A total of 10 lander operations have been conducted in the NORI-D region and a total of 15 scavengers were obtained. Among them, *Coryphaenoides* sp. is the most abundant species, followed by *Pachycara nazca* and *Barathritis iri* (NORI 2022). *Coryphaenoides* sp. and *Barathritis* sp. have been also found in the Block A-5.

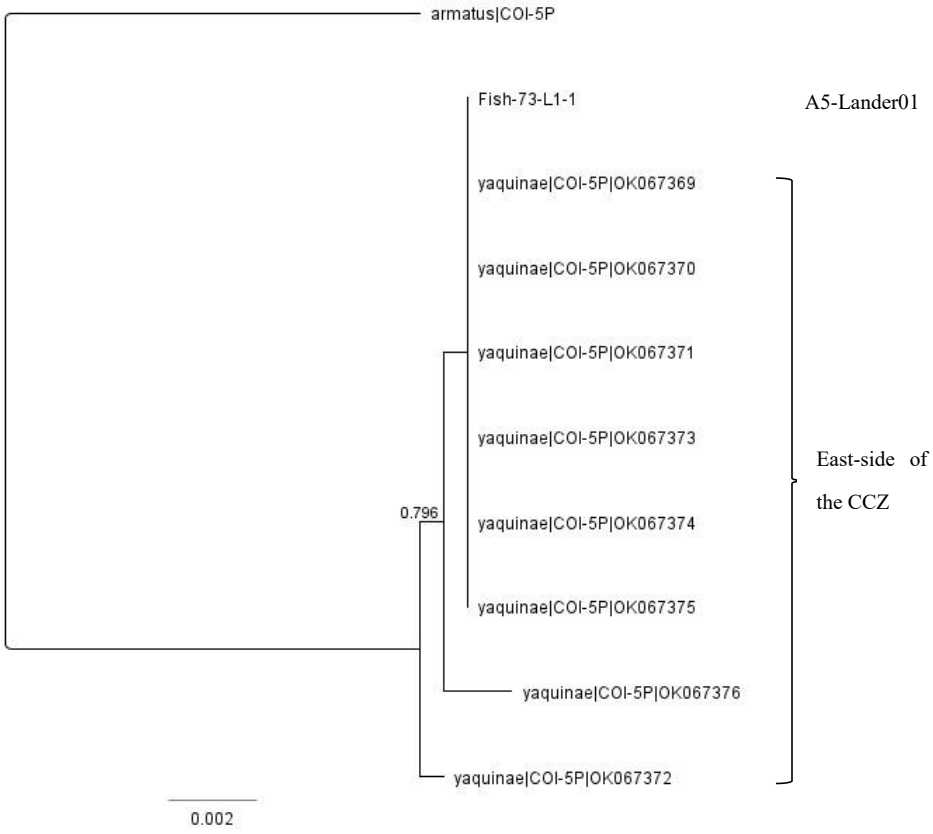

Figure 5.4-67 Phylogenetic tree for the COI of *C. yaquinae*

In this study, DY73Ⅰ-A5-Lander01 is the sampling station near the IRZ; the rest *C. yaquinae* sequence data are from NCBI and other databases; and the collection site is in the eastern part of the CCZ. See the following figure for the sampling stations.

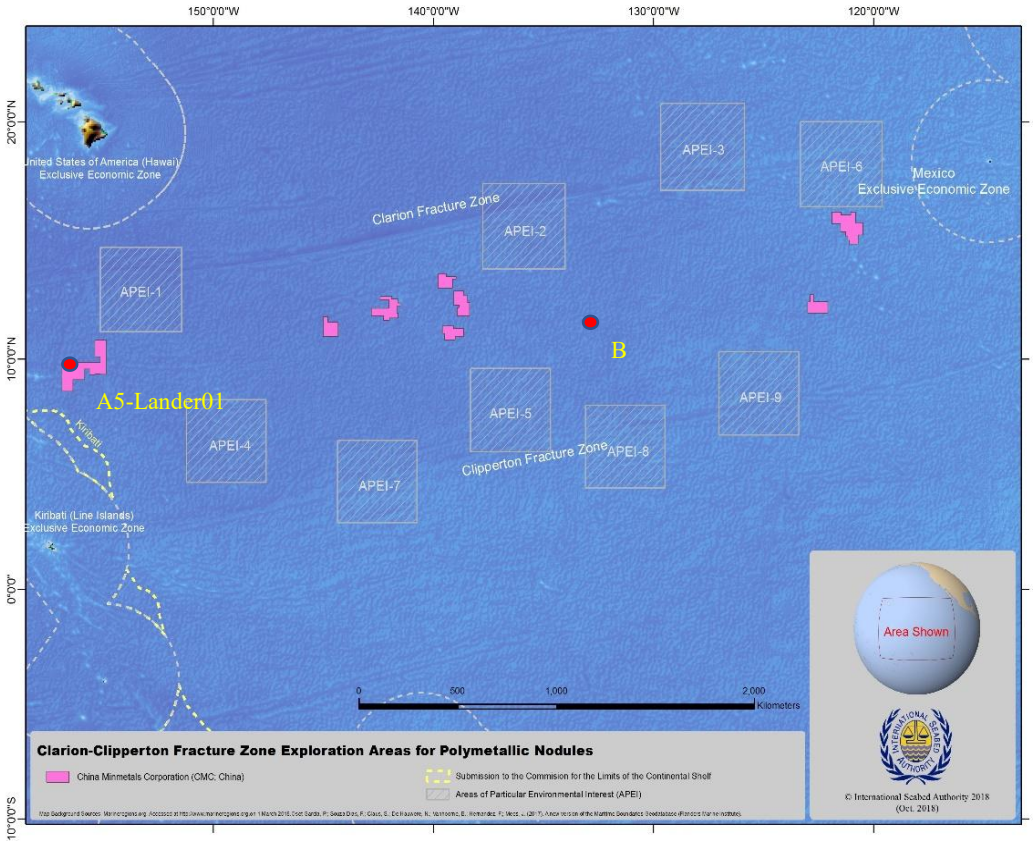

Figure 5.4-68 Map for *C. yaquinae* sampling stations

In this study, DY73Ⅰ-A5-Lander01 is the sampling station and B is the sampling station for sequence information obtained from NCBI, BOLD and other publicly available databases.

5.4.3.6.2 Biological trace elements

Several samples of demersal scavengers were obtained from Lander traps during the DY73 cruise. Two of these fish were selected and dissected to obtain dorsal muscle tissue, which was used to determine trace elements. Among them, 73-lander01-1 was a rat-tailed grenadier (*Coryphaenoides yaquinae*), and 73-lander02-4 was a weasel trevally (Ophidiidae sp.), and the photos of the fish specimens are shown in Figure 5.4-69.

73-lander01-1

73-lander02-04

Figure 5.4-69 Demersal scavengers for trace element measurements

Mercury was determined by cold atomic fluorescence spectrometry; the rest of the trace elements were determined by inductively coupled plasma mass spectrometry (ICP-MS) in μg /g dry weight. The results of biological trace elements were obtained by analyzing the specimens collected in DY73I-A5-Lander01-01 and DY73I-A5-Lander02-04 stations during Minmetals' 2022 survey cruise. See Table 5.4-6 for the determination results.

Table 5.4-6 Determination results of biological trace elements

Sample No.	As	Cd	Co	Cr	Ni	Cu	Pb	Hg	Mo	Mn
	μg/g	ng/g	μg/g	μg/g	μg/g	μg/g	μg/g	ng/g	μg/g	μg/g
73Ⅰ-A5-lander01-01	9.20	28.4	0.55	3.28	0.97	1.17	0.14	3186	0.03	2.80
73Ⅰ-A5-lander02-04	3.60	50.0	0.20	2.17	0.93	6.76	0.35	4336	0.07	7.86
Bottom seawater	0.0014	0.135	0.00061	0.00066	0.00072	0.0011	0.000036			
Sediment pore water	0.00165	0.215	0.00041	0.00084	0.00068	0.0017	0.000065			

Sample No.	Zn	Fe	Rb	Cs	Li	Mg	Na	P	Ca	K
	μg/g	μg/g	μg/g	μg/g	μg/g	%	%	%	%	%
73Ⅰ-A5-lander01-01	18.0	56.7	1.35	0.08	0.22	0.09	1.89	0.57	0.18	0.96
73Ⅰ-A5-lander02-04	42.8	117	1.71	0.08	1.18	0.20	8.32	0.78	0.36	1.01
Bottom seawater	0.005									
Sediment pore water	0.0155									

The result showed that various heavy metal elements were detected in two species of demersal fish in the Block A-5 in natural conditions, and there were obvious differences in the heavy metal concentrations of different fish species. Among them, the concentrations of arsenic, cobalt and chromium were higher in the muscle of *Coryphaenoides yaquinae*, while the concentrations of cadmium, copper, lead, zinc, iron, manganese and molybdenum were higher in Ophidiformes. The concentrations of mercury and nickel in the two species were similar. Except for iron and zinc, arsenic was the most abundant in *Coryphaenoides yaquinae*, manganese and copper were the most abundant in Ophidiformes and cadmium and molybdenum were the lowest in both species. Heavy elements in fish are 2-4 orders of magnitude higher than concentrations of the same elements in bottom seawater and sediment pore water, suggesting significant bioconcentration.

5.5 Summary of existing biological environments

Boobies are the dominant seabirds in this region. There is no direct sighting record of whales or dolphins in the Block A-5 of the Contract Area. Assessments based on publicly available data indicate that the Block A-5 is far from Marine Mammal Protected Areas and areas where scientific evidence suggests protection is needed. The nearest major global migratory corridor for cetaceans to the western portion of the CCZ is the migratory corridor between the area around the Hawaiian Islands and the high-latitude offshore areas of the northeastern Pacific Ocean. This corridor is far from the Block A-5.

Located in the western part of the CCZ, the Block A-5 of the Contract Area is an oligotrophic sea area affected by equatorial current. The Chl concentration and primary production in the Block A-5 are lower than those in the eastern part of the Clarion-Clipperton Zone (CCZ), and the interannual variations of surface-layer Chl concentration are small among the IRZ, PRZ and ESRZ.

In all seasons, the isolines of surface Chl concentration is roughly zonal, so the IRZ, PRZ and ESRZ in the Block A-5 are highly consistent and comparable in the spatio-temporal variations of primary production.

The maximum value of the primary production profile is in the subsurface layer (water depth of 50 m). The integral primary production of water column shows that the average total primary production of water column at this station is 51.44 mg C m^{-2} h^{-1}. The vertical variation of Chl *a* concentration was consistent in both PRZ and IRZ, with maximum values at about 50 m, 0.2 mg/m^3 and 0.28 mg/m^3, respectively.

The average phytoplankton abundance in the surveyed area is 338 cells/L. The community is dominated by Bacillariophyta, followed by Dinoflagellate. The dominant phyla are Bacillariophyta (e.g. *Bacteriastrum hyalinum* var. *hyalinum* and *Coscinodiscus jonesianus*), and Dinoflagellate (e.g. *Ceratium teres*).

A total of 193 zooplankton species belonging to six phyla have been identified. Copepoda is the dominant taxon, followed by Cnidaria, Ostracoda, Chaetognatha, Tunicata, etc. The biomass gradually decreases from the surface to deep sea.

Gammaproteobacteria is the dominant taxon of microbial community, with Burkholderiales and Pseudomonadales being the main orders. Nitrosopumilales is the dominant taxon of archaea. The community structure of microbes showed significant changes with depth, and was gradually steady over 10 cm depth. The dominant taxa of bacteria and archaea in this area are consistent with those in the German Contract Area located in the eastern part of the CCZ, suggesting that the microbial ecological functioning of the deep-sea sediments in the Clarion-Clipperton Zone is stable to some extent. The analysis of water and sediment microbial communities in the IRZ and PRZ suggests that the main drivers of spatial variation in microbial communities in the region are environmental changes along water and sediment depths, rather than changes in horizontal geographic gradients.

The results of meiofauna show that meiofauna communities in the IRZ and PRZ of the Block A-5 have similar compositions, with the dominant taxa being Nematoda (more than 90 %), followed by Harpacticoida and Polychaeta. The meiofauna abundance varies in the range of 50 - 66 ind./m^2, similar to the western CCZ but lower than the eastern CCZ. The taxa composition is closer to both the western and eastern

parts of the CCZ.

The results of macrofauna show that macrofauna communities in the IRZ and PRZ of the Block A-5 have similar compositions, including Polychaeta, Ostracoda, Isopoda, Tanaidacea, etc. The dominant taxon is Polychaeta, with abundance exceeding 40%. The abundance of macrofauna varies in the range of 32 - 52 ind./m^2, which is lower than that in the eastern CCZ, but with similarity in community composition.

The results of megafauna show that the dominant groups in this area include eight phyla: Protozoa, Porifera, Cnidaria, Echinodermata, Annelida, Mollusca, Arthropoda, Mollusca and Chordata. The average megafauna abundance is 452.6 ind./ha, and there is no significant difference in megafauna abundance (431.0 ind./ha vs 510.6 ind./ha) between PRZ and IRZ. The species composition and community structure of megafauna in PRZ and IRZ are similar.

The average abundance of nodule fauna in the Block A-5 is 3.9 ind./m^2, mainly including Protozoa, Bryozoa, Cnidaria, Porifera and Annelida.

The scavenger groups are mainly *Coryphaenoides yaquinae*, Anarhichadidae, *Alicella Gammarus* and *Eurythenes* sp. Among them, *Coryphaenoides yaquinae* has high connectivity on a large scale indicated by molecular biology analyses, while *Eurythenes* sp. is widely distributed in the Pacific Ocean (including the CCZ).

In summary, the biological environment characteristics in IRZ of the Block A-5 Contract Area are similar to those in PRZ, especially the characteristics of the benthic fauna. The Block A-5 has high similarity with other areas of CCZ, especially the western part.

5.6 References

Bailey H, Fossette S, Bograd SJ, Shillinger GL, Swithenbank AM, et al. (2012) Movement Patterns for a Critically Endangered Species, the Leatherback Turtle (Dermochelys coriacea), Linked to Foraging Success and Population Status. PLOS ONE 7(5): e36401.

BGR. 2018. Environmental Impact Assessment for the testing of a pre-protoype manganese nodule collector vehicle in the Eastern German license area (Clarion-Clipperton Zone) in the framework of the European JPI-O MiningImpact 2 research project.

Bribiesca-Contreras, G., Dahlgren, T. G., Amon, D. J., Cairns, S., Drennan, R., Durden, J. M., ...& Glover, A. G. (2022). Benthic megafauna of the western Clarion-Clipperton Zone, Pacific Ocean.ZooKeys, 1113, 1.

De Smet, B., Pape, E., Riehl, T., Bonifácio, P., Colson, L., & Vanreusel, A. (2017). The community structure of deep-sea macrofauna associated with polymetallic nodules in the eastern part of the Clarion-Clipperton Fracture Zone. Frontiers in Marine Science, 4, 103.

Durden, J. M., Putts, M., Bingo, S., Leitner, A. B., Drazen, J. C., Gooday, A. J., & Smith, C. R. (2021). Megafaunal ecology of the western Clarion Clipperton Zone.Frontiers in Marine Science, 8, 671062.

GSR. 2018. Environmental Impact Statement - Small-scale testing of nodule collector components on the seafloor of the Clarion-Clipperton Fracture Zone and its environmental impact. [place unknown].

Kersken, D., Janussen, D., & Arbizu, P. M. (2019). Deep-sea glass sponges (Hexactinellida) from polymetallic nodule fields in the Clarion-Clipperton Fracture Zone (CCFZ), northeastern Pacific: Part II—Hexasterophora. Marine Biodiversity, 49, 947-987.

McQuaid, K. A., Attrill, M. J., Clark, M. R., Cobley, A., Glover, A. G., Smith, C. R., & Howell, K. L. (2020). Using habitat classification to assess representativity of a protected area network in a large, data-poor area targeted for deep-sea mining. Frontiers in Marine Science, 7, 558860.

NORI. 2022. Collector Test Study – Environmental Impact Statement – Testing of polymetallic collector system components in the NORI-D contract area, Clarion Clipperton Zone, Pacific Ocean. Jamaica.

Rabone, M., Horton, T., Jones, D. O. B., Simon-Lledó, E., & Glover, A. G. (2023). A review of the International Seabed Authority database DeepData from a biological perspective: challenges and opportunities in the UN Ocean Decade. Database, 2023, baad013.

Simon-Lledó, E., Pomee, C., Ahokava, A., Drazen, J. C., Leitner, A. B., Flynn, A., ...& Jones, D. O. (2020). Multi-scale variations in invertebrate and fish megafauna in the mid-eastern Clarion Clipperton Zone.Progress in Oceanography, 187, 102405.

Tilot, V. (2006). Biodiversity and distribution of the megafauna.Unesco.

Spalding, M. D., Agostini, V. N., Rice, J., & Grant, S. M. (2012). Pelagic provinces of the world: a biogeographic classification of the world's surface pelagic waters. Ocean & Coastal Management, 60, 19-30.

Wang, Xiaogu, Zhou, Yadong, Zhang, Dongsheng, Hong, Lisha and Wang, Chunsheng. (2013). Study on Meiofauna in China's Polymetallic Nodules Area of the East Pacific Ocean in the Summer of 2005. Acta Ecologica Sinica, 33(2), 492-500.

Watling, L., Guinotte, J., Clark, M. R., & Smith, C. R. (2013). A proposed biogeography of the deep ocean floor. Progress in Oceanography, 111, 91-112.

Uhlenkott, K., Vink, A., Kuhn, T., & Martinez Arbizu, P. (2020). Predicting meiofauna abundance to define preservation and impact zones in a deep-sea mining context using random forest modelling. Journal of Applied Ecology, 57(7), 1210-1221.

6 Description of Existing Socioeconomic Environment

6.1 Key information

Through the collection and analysis of publicly available data, we have gained the following understandings of the existing socioeconomic environment in this Block A-5:

(1) The proposed TMA is not an important fishing ground in the East Pacific Ocean;

(2) This region is not the main marine traffic channel in the East Pacific Ocean;

(3) There is no tourism (e.g. fishing, whale watching and general sightseeing) in this region;

(4) Marine scientific research activities in this region mainly include resource exploration and environmental survey by various contractors in the Contract Area and APEIs under the ISA framework, such as the Tropical Pacific Observation System (TPOS) and the Array for Real-time Geostrophic Oceanography (Argo) Observation System;

(5) The CTA is more than 100 km away from the nearest seabed cable;

(6) There is no site of an archaeological or historical nature in this region

6.2 Existing utilizations

6.2.1 Fishery

Limited by the low level of primary production in this region, the western part of the CCZ is not an important fishing ground in the East Pacific Ocean. According to the data of Global Fishing Watch, the fishing intensity of high seas fishery in the region where Minmetals' Block A-5 is located is at the level of 500-1,000 h/500 km, which is significantly lower than those near the Hawaiian Islands to the west and the Equatorial Pacific region to the south of the region (Figure 6.2-1).

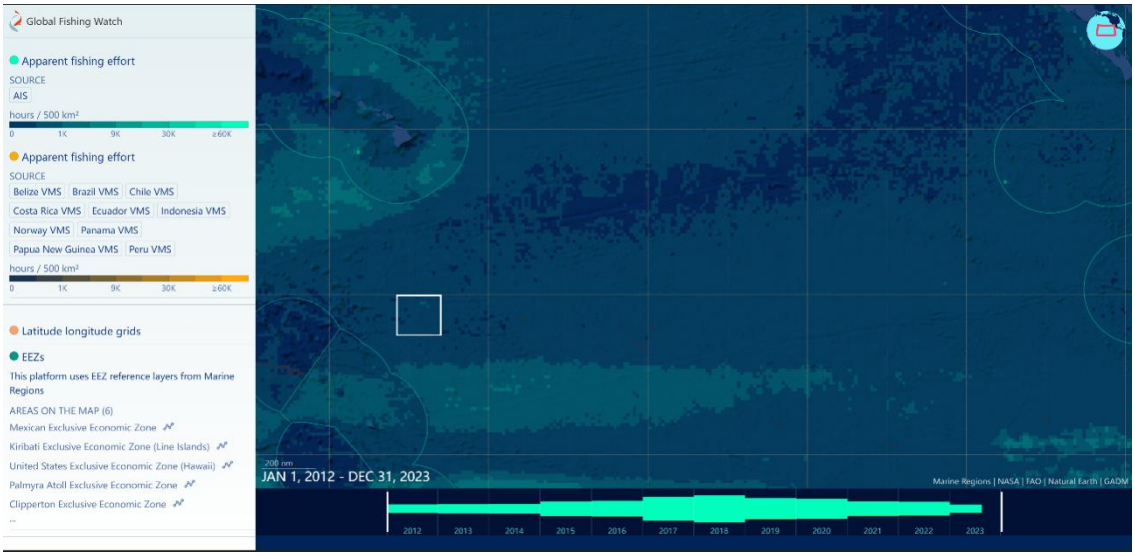

Figure 6.2-1 Fishing intensity in the Block A-5 of the Contract Area

(White box indicates this Project's site; source: Global Fishing Watch)

Despite the existence of tuna fishery, the western part of the CCZ, especially where Block A-5 is located, is not the main fishing area for any major fishing target of high seas fishery (Figure 6.2-2) (Sala et al., 2018). A recent study on the distribution of tuna fishery resources in the high seas integrated with the climate change model shows that under the future climate change conditions, the significance of the CCZ to the future tuna fishery in the high seas may increase significantly by the middle of this century (2044-2053). For example, the biomass of skipjack may increase by 30 %, thus becoming a more important high seas fishing ground in the future (Figure 6.2-3) (Amon et al., 2023). However, such increase is highly uneven. Only in the unlikely GHG emission scenario (RCP 8.5), the western part of the CCZ may become an important potential fishing ground, while in the GHG emission scenario closer to reality (RCP 4.5), the main tuna biomass increase occurs in the eastern and central parts of the CCZ.

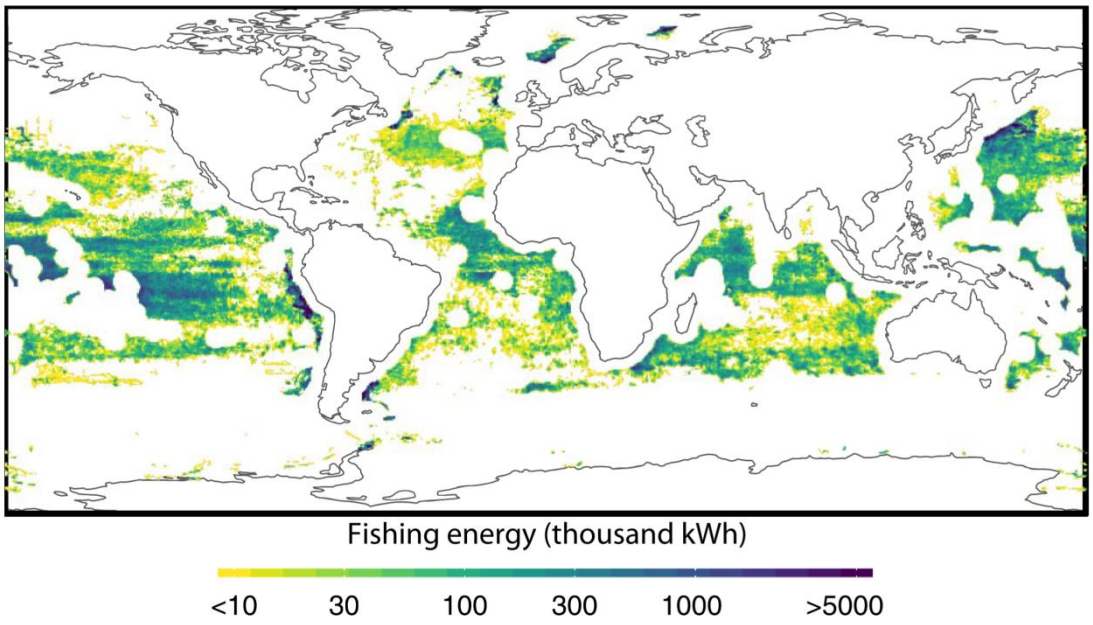

Figure 6.2-2 Distribution of high seas fishing grounds in the world (based on fishing efforts, Sala et al., 2018)

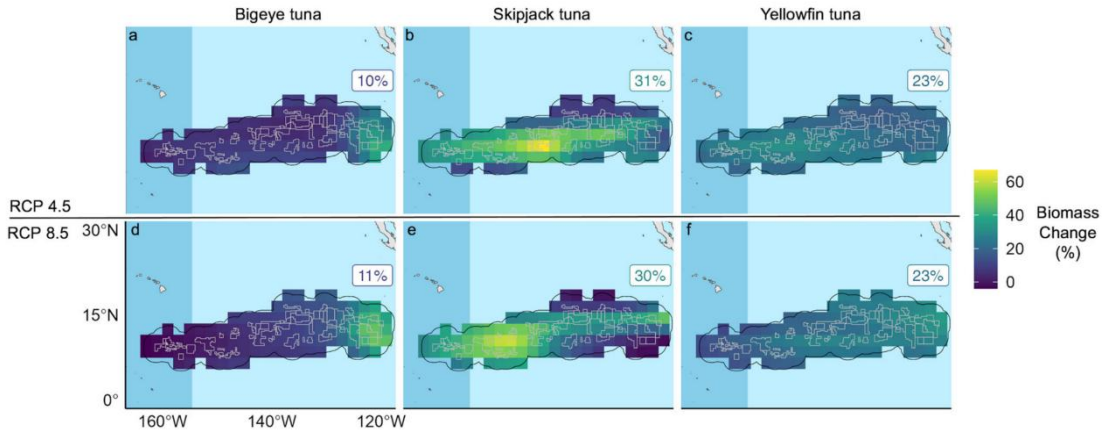

Figure 6.2-3 Tuna resource variations in the CCZ under future climate change scenarios (Amon et al., 2023)

6.2.2 Marine traffic

The main marine traffic channels involving the East Pacific Ocean are as follows: (1) East Asia-West Coast Route of North America, which is an important way to connect the two global economic centers of Northeast Asia and North America; (2) East Asia-Panama-Caribbean, East Coast route of North America, which passes through Honolulu Port in the Hawaiian Islands or bypasses the south of the Hawaiian Islands, crosses the Panama Canal and reaches the ports on the west coast of the Atlantic Ocean.

Among these two main routes, the East Asia-North America west coast route is far from the CCZ; the East Asia-Panama-Caribbean and the East Coast of North America passes through the northern part of the Block A-5 of the Contract Area but does not enter the Block A-5.

Figure 6.2-4 Marine traffic intensity in the Block A-5 of the Contract Area (White box indicates this Project's site)

(Source: IMF Working Paper, WP/20/57)

6.2.3 Tourism

At present, there are no tourism (e.g. fishing, whale watching and general sightseeing) in this region.

6.2.4 Marine scientific research

Marine scientific research activities conducted in this region mainly include resource exploration and environmental survey by various contractors in the Contract Area and APEIs under the ISA framework, TPOS and the Argo Observation System, etc.

(1) TPOS

TPOS is an important part of the Global Ocean Observing System (GOOS) under the responsibility of the Intergovernmental Oceanographic Commission of the United

Nations Educational, Scientific and Cultural Organization (IOC-UNESCO). It is a new generation of operational observation system after the Pacific TAO/TRITON buoy observation network, aiming at measuring the underwater, ocean surface and atmosphere in the tropical Pacific from approximately 10 °S to 10 °N. Ocean observation in the Western Tropical Pacific strengthens the targeted observation of air-sea heat flux, upper mixed layer of ocean and marine ecological elements, which is not only of great significance for supporting the study of weather and climate system variations affecting China and neighboring countries such as typhoons, monsoons and the ENSO, but also of great value for deeply understanding the response of marine ecological processes to weather or climate variations.

Although the Block A-5 of the Contract Area is located in the tropical Pacific (between 10 °N and 10 °S) concerned by TPOS, there is no TPOS buoy in the Block A-5, and there is no plan to deploy observation buoys in the future.

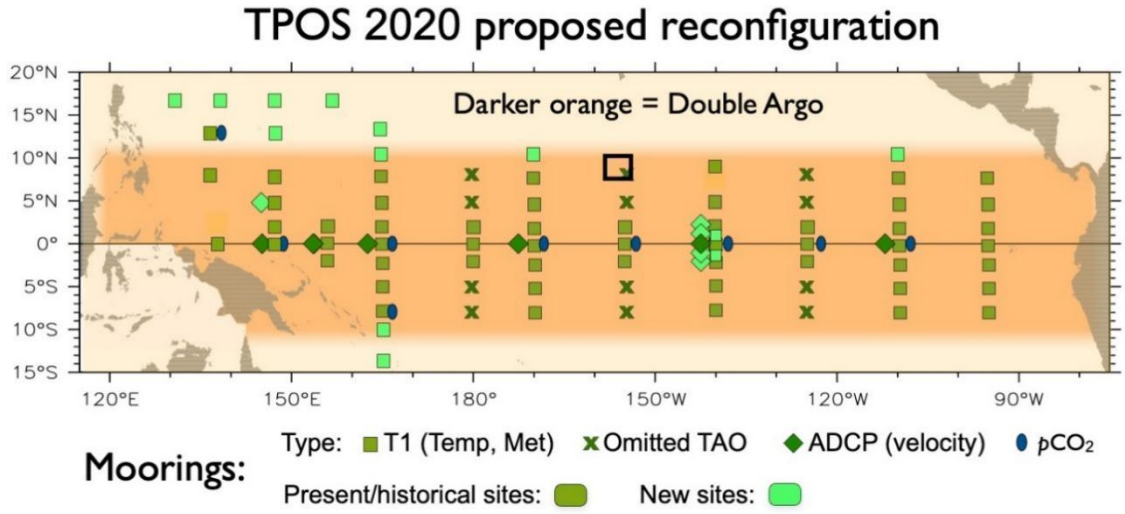

Figure 6.2-5 Location relationship between TPOS observation system and the Block A-5 of the Contract Area (black box indicates the Project's site)

(Source: https://tropicalpacific.org/)

(2) Argo observation system

The Argo program, which was put forward by marine and atmospheric scientists of the United States, France, Australia and other countries in 1998, is one of the most successful GOOS. So far, it has obtained a large number of observation data of

physical, biological and chemical elements in the global ocean. This Project was officially launched in 2000. With the joint efforts of more than 30 coastal countries, a real-time observation network consisting of nearly 4,000 active buoys has been built and maintained for a long time in the global ocean. At the outset, it only observed the temperature and salinity (core Argo) at the water depth within the range of 0-2,000 m in the global ice-free area. However, it has been extended to polar regions, deep seas (2,000-6,000 m) and the biogeochemistry (BGC) field. Long-time series and high-quality Argo data improve not only scientists' cognitive ability of the role of the ocean in global climate change, but also the studies level of global warming, ocean carbon cycle, hypoxia, acidification and other scientific issues.

The Block A-5 of the Contract Area is located in the impact area of the NEC, so a large number of Argo buoys will naturally drift through this region with ocean currents. Generally, oceanic activities (e.g. test-testing) do not adversely affect the work of Argo buoys.

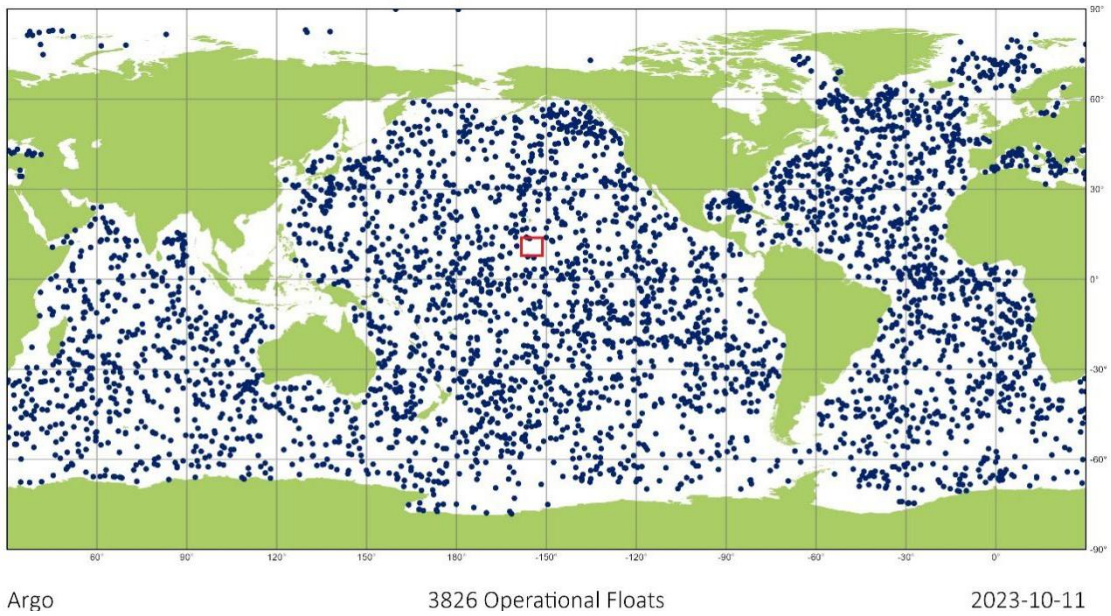

Figure 6.2-6 Location relationship between the Argo observation system and the Block A-5 of the Contract Area (red box indicates the Project's site)

(Source: https://www.ocean-ops.org)

6.2.5 Area-based management tools

There are already some area-based management tools in the CCZ and its adjacent areas, including the ISA's REMP for the CCZ and the marine protected areas in the US Pacific EEZ.

(1) REMP for the CCZ

In 2007, during the "Pew Workshop on Design of Marine Protected Areas for Seamounts and the Abyssal Nodule Province in Pacific High Sea", which was sponsored by the University of Hawaii, a group of scientists headed by Dr. Craig Smith proposed to the ISA that a marine protected area should be established in the high seas of the Pacific Ocean for deep-sea seamounts and nodule areas (biogeographic province) to protect the biodiversity and ecosystem functions of this region. The ISA's LTC subsequently assessed this proposal, and held a meeting to draft a REMP in 2011, aiming at designing a REMP for the CCZ of the East Pacific Ocean and establishing a network including nine APEIs. In 2012, the ISA Council adopted the "Decision on the Environmental Management Plan for the Clarion-Clipperton Zone" (hereinafter referred to as the "Decision") in accordance with Articles 145, 162 and 165 of the UNCLOS and the provisions herein requiring the ISA to fulfill its obligations of marine environmental protection. The REMP for the CCZ has been formally implemented. Since then, based on the new understanding of scientific research during the 10 years after the REMP for the CCZ was formulated, scientists have put forward new supplementary plans. In 2021, the ISA Council adopted a newly revised REMP to increase the number of APEIs to 14 (Figure 6.2-7).

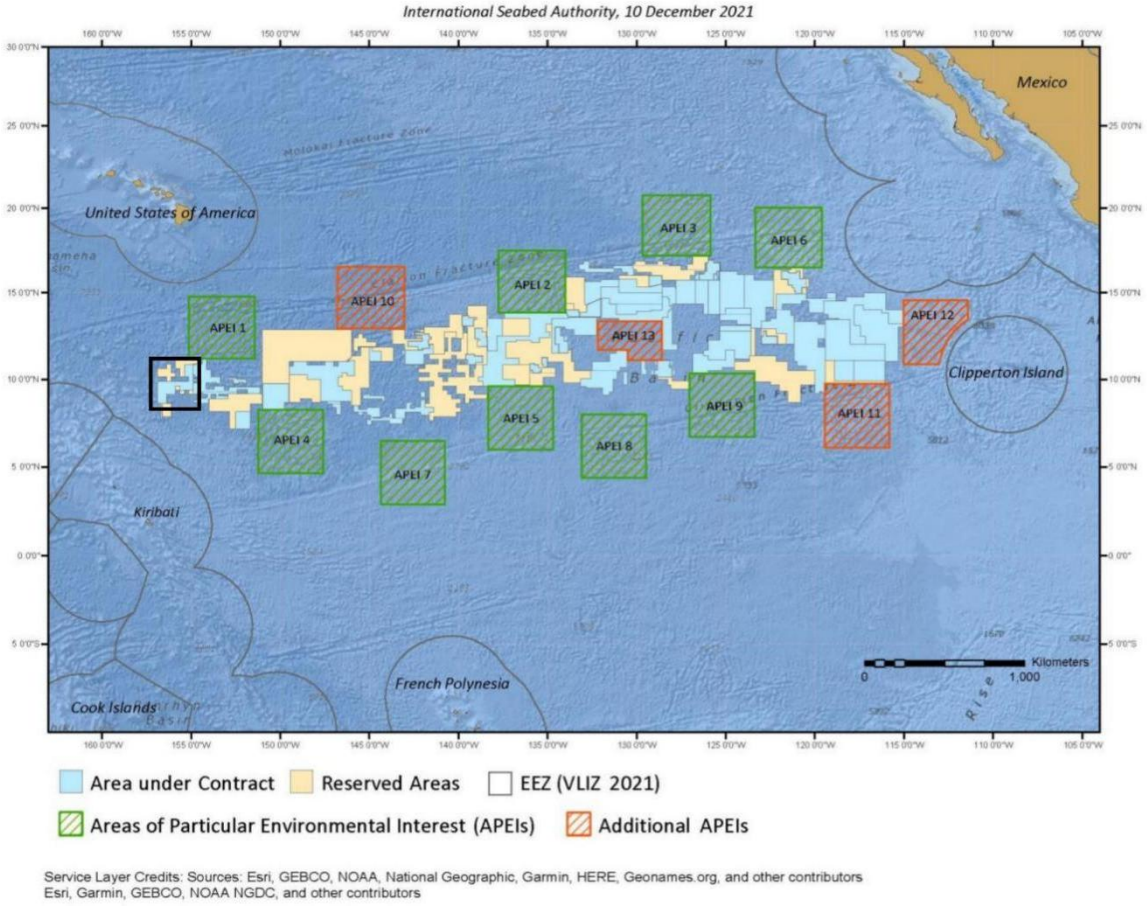

Figure 6.2-7 REMP for the CCZ

(Black box indicates this Project's site; source: ISBA/26/C/58)

The Block A-5 of the Contract Area is adjacent to the APEI-1 stipulated in the REMP. The benthic biodiversity and sedimentary environment in this region have been preliminarily studied recently (Durden et al., 2021), and this APEI will effectively preserve the benthic biodiversity in the western part of the CCZ. In Chapters 7 and 8 of this EIS, we assess the potential impact scope of this test, concluding that it will not cause potential environmental impact on APEI-1 or other APEIs.

(2) Marine protected areas in the US Pacific EEZ

The marine protected areas nearest to the Block A-5 of the Contract Area are the Papahānaumokuākea Marine National Monument of the United States, as well as the Johnston Atoll, Kingman Reef, Palmyra Atoll protected areas of the U.S. Pacific Remote Islands Marine National Monument. The Block A-5 is more than 500 nautical

miles away from the Papahānaumokuākea Marine National Monument and the Johnston Atoll National Wildlife Refuge, and more than 200 nautical miles away from Kingman Reef and Palmyra Atoll Reserves. Therefore, this test will not cause environmental impacts on these reserves

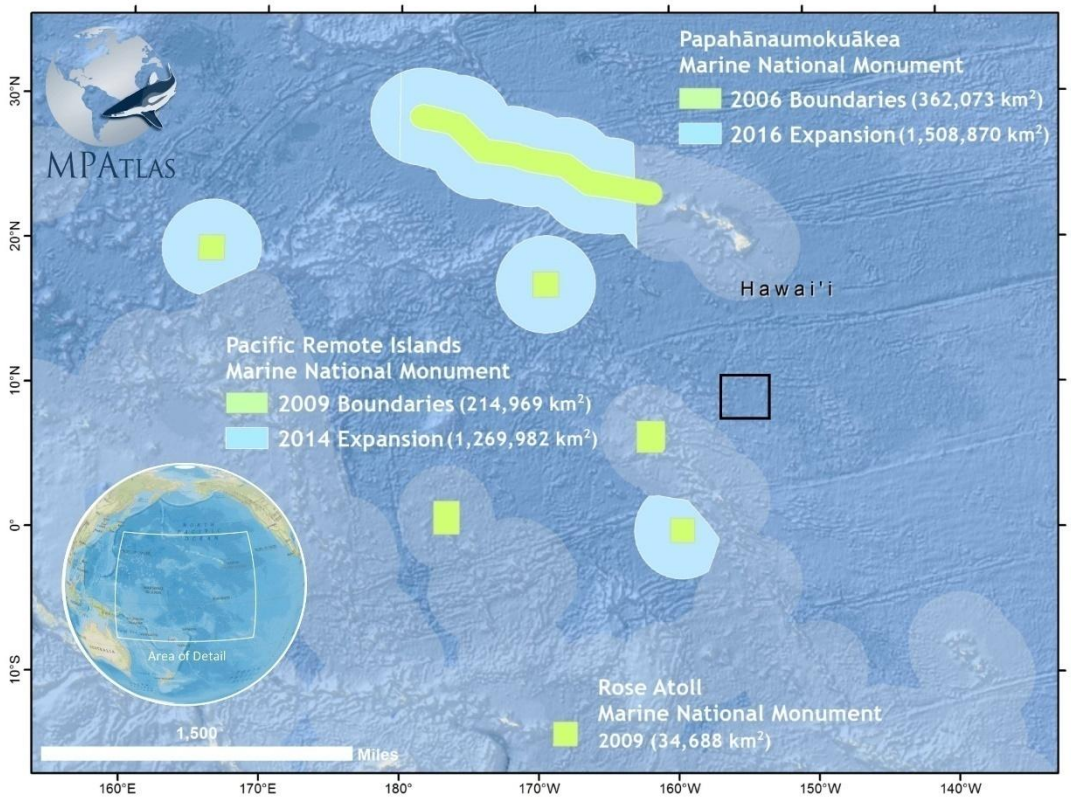

Figure 6.2-8 Marine protected areas in the US Pacific EEZ

(Black box indicates this Project's site; source: https://mpatlas.org/)

6.2.6 Others

An international seabed cable runs through the eastern part of the Block A-5 of the Contract Area, which belongs to Honutua cables owned by the Post and Telecommunications Office of French Polynesia (OPT French Polynesia). The cable is distributed in the Block A-5 of the Contract Area for approximately 20 km, and the specific location is shown in Figure 6.2-9 below.

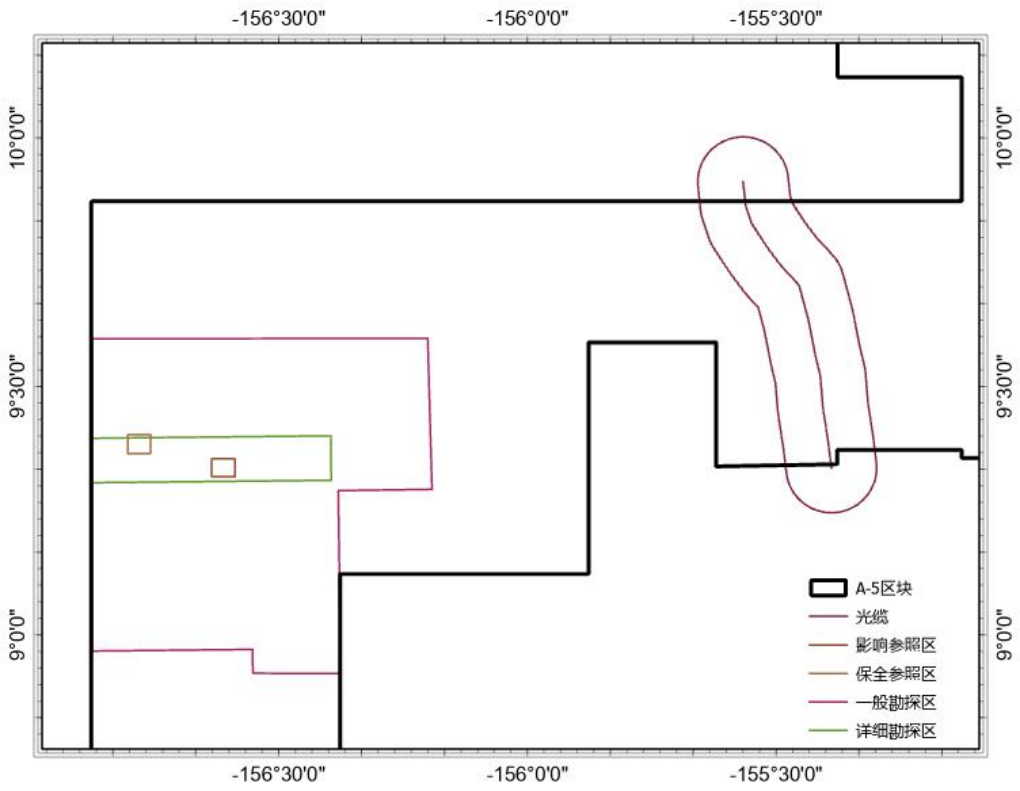

Figure 6.2-9 Schematic diagram for optical cable locations in the Block A-5

The cable of OPT French Polynesia was laid in 2008. According to the ICPC recommendation standard, the seabed cable has a safe distance of 10 km (20 km) left and right. The distance between the location involved in this collector vehicle test and the Honutua cable is more than 100 km, which meets the safety requirements of the cable, thus the cable will not be affected by this collector vehicle test.

6.3 Sites of an archaeological or historical nature

Survey results show that the project area does not involve any site of an archaeological or historical nature.

6.4 Summary

According to the above analysis results, the CTA of this Project is far away from areas with frequent human social activities. In view of the small scale and short duration of this Project, we estimate that it is extremely unlikely that the test-mining activities in this Project will have a significant impact on the socioeconomic

environment.

6.5 References

Amon, D.J., Palacios-Abrantes, J., Drazen, J.C. et al. Climate change to drive increasing overlap between Pacific tuna fisheries and emerging deep-sea mining industry. npj Ocean Sustain 2, 9 (2023). https://doi.org/10.1038/s44183-023-00016-8

Sala E, Mayorga J, Costello C, Kroodsma D, Palomares MLD, Pauly D, Sumaila UR, Zeller D. 2018. The economics of fishing the high seas. Sci Adv. 4(6): eaat2504. https://doi.org/10.1126/sciadv.aat2504

7 Assessment of Impacts on the Physicochemical Environment and Proposed Mitigation Measures

7.1 Key information

This Chapter analyzes the potential impacts of the collector vehicle testing on the physico-chemical environment, and introduces multiple measures for mitigating environmental impact.

This collector vehicle testing aims to verify its technical feasibility and reliability, and to collect the environmental disturbance data under different operation conditions. These key data are indispensable for developing a collector vehicle that is technically reliable, economically feasible and with only moderate environmental disturbance. The physico-chemical environment baselines in and around the Block A-5 have been described in Chapter 4 of this EIS. The assessment in this Chapter is based on the above-mentioned contents, relevant literature and/or reports, established sediment plume dispersal and redeposition model, etc.

On the one hand, we have identified the potential impact of the collector vehicle at four different depths/habitats in the water column: (1) atmosphere, (2) sea surface and euphotic zone (0-200 m depth), (3) meso-pelagic zone (200-1,000 m depth), (4) deep layer (1,000 m water depth to 200 m above the bottom) and (5) bottom layer (water columns and seabed within 200 m above the bottom). In Table 7.2-1 below, we explain the specific contents of these potential impact categories at different water depths. The purpose is to identify the most important environmental impact of this test on the basis of a comprehensive description. On the other hand, we describe these potential impacts in the order of air quality, geological setting, physical oceanography environment, chemical oceanography environment, seabed sedimentary environment, natural disasters, noise and light, GHG emissions and climate change, maritime safety, waste management, cumulative impact and residual impact.

Since this test does not involve large-scale ore/sediment lifting and tail water

discharge, and the total test duration is controlled to the shortest, the potential environmental impact of this test is mainly in the bottom layer and slight on biological communities living in other depths/habitats.

7.2 Description of potential impact categories

All potential sources of environmental impact in this test include the following two types of activities, which are not overlapped and located outside and inside the Block A-5 respectively.

(1) Outside the Block A-5, there will be the noise and internal combustion engine exhaust generated by the SSV and EMV during their trip between the Zhoushan home port in China and the Block A-5 of the Contract Area in the CCZ.

(2) Inside the Block A-5, there will be the following potential environmental disturbance:

a variations in the original habitat, including nodule removal, sediment removal and sediment disturbance, caused by the testing of the collector vehicle;

b The testing of the collector vehicle will cause sediment plumes, which may further lead to variations in the physicochemical environment of the bottom-layer water column and variations in the geological setting and chemical environment of the habitat caused by sediment redeposition;

c Light from the collector vehicle, SSV/EMV and ROV;

d Noise from the collector vehicle, SSV/EMV and;

e Exhaust emissions from the internal combustion engines of SSV/EMV;

f Potential leakage of toxic substances (e.g. fuel oil, lubricating oil and hydraulic oil) from the collector vehicle, SSV/EMV and ROV;

g Potential risks caused by natural disasters.

Table 7.2-1 Categories and spatial scopes of potential impacts from this collector vehicle test

Atmosphere	Sea surface and euphotic zone	Mesopelagic zone	Deep layer	Bottom layer
●	●	●	●	●
-	-	-	-	●
-	-	-	●	●
●	●	●	-	●
●	●	●	●	●
●	-	-	-	-
-	●	-	-	●
●	-	-	-	-

Note: See the above section for the definitions and detailed descriptions of "potential impact categories".

7.3 Air quality

7.3.1 Potential impacts and problems to be solved

While sailing to and from between the home port in China to the Block A-5 and operating in the Block A-5, the main engines, auxiliary engines and redundant generator systems of the SSV and EMV will consume diesel fuel and emit carbon dioxide, nitrogen oxides, sulfur oxides and particles. The discharge of these pollutants may impact the air quality level along the route and in the Block A-5. To reduce such potential environmental impacts, we choose to use vessels that meet the IMO's requirements and Chinese laws, as well as clean fuel.

See section 7.10 below for the potential impact of GHG emissions.

7.3.2 Environmental management measures to mitigate impacts

(1) The SSV and EMV in this test do not use ozone-depleting substances as the

working medium of equipment during their day-to-day work. Ozone-depleting substances are those mentioned in Article 2, Paragraph 16, Chapter 1 of Annex VI of MARPOL 73/78.

(2) During this test, all plastic wastes from the working and living activities will be classified and stored in-situ; they will not be burned on board.

(3) The emissions of nitrogen oxides, sulfur oxides and particles of the SSV and EMV will strictly meet the requirements of the second-stage emission limit of nitrogen oxides stipulated in MARPOL 73/78.

(4) During the survey cruise, the scheduled route does not pass through the sulfur oxide emission control areas stipulated in the MARPOL. While on the high seas, the SSV and EMV will use fuel, strictly meeting the requirement (sulfur content >0.50 %m/m) of MARPOL 73/78.

7.3.3 Residual impact

According to the general practice of the marine traffic industry, the correct use of shipboard exhaust pollution control devices and the use of compliant fuels within the specified areas are not considered as having a clearly harmful residual impact on the environment through.

7.4 Geological setting

7.4.1 Potential impacts and problems to be solved

In this test, the operation zone of the collector vehicle on the seabed is 0.6 km^2 (1,000 m long, 600 m wide). The plan for the collector vehicle test involves two separate underwater tests. The disturbed area during the first underwater operation is 24,200 m^2 and that during the second underwater operation is 75,800 m^2, totaling 0.1 km^2. The total weight of nodules collected is estimated to be approximately 1,300 t, and the wet nodules lifted with the collector vehicle to the surface platform to be no more than 10 t.

There are obvious environmental gradients in the whole CCZ, in terms of water

depth, sediment deposition flux, topography and geomorphology, nodule abundance. However, such gradients have not caused a small part of the CCZ to become a unique habitat in a specific geological setting (McQuaid et al. 2020). The CTA for this test is in the western part of the Block A-5, which is located in the western part of the CCZ. The topography of the CTA is flat, without any seamount or sea knoll, and the slope is less than 2 %. The sedimentary parameters, nodule coverage and topographic and geomorphological features are not unique in the Block A-5 or in a wider spatial scope (see Chapter 4).

The depth of sediment disturbance by the collector vehicle's collector head is approximately 4-6 cm (it depends on the buried depth of nodules and can be adjusted to realize the shallowest sediment disturbance while effectively collecting nodules). The direct depth of disturbance by the collector vehicle's crawler belts is approximately 10 cm; there will inevitably be a certain degree of subsidence impact on deeper sediments. This test only has a direct collection area of approximately 0.1 km^2, and the direct disturbance area accounts for only 0.000438 % of the total area of the Block A-5 (22,821 km^2). Therefore, we infer that direct removal of nodules and sediments will not cause great disturbance to the seabed.

According to the sediment plume dispersal and sediment redeposition models, the sediment redeposition range in this test is measured by the threshold of 0.1 mm redeposition thickness. The maximum redeposition area is no more than 1 km^2 (see Section 7.5 of this Chapter), accounting for only 0.0044 % of the total area of the Block A-5. So, we infer that sediment redeposition will not cause great disturbance to the seabed.

7.4.2 Environmental management measures to mitigate impacts

The main mitigation measures adopted in the collector vehicle test include an optimized design for the system and equipment of the collector vehicle and an optimized test scheme in the test operation stage. These mitigation measures aim to minimize impacts on the environment.

(1) An optimized design for the system and equipment of the collector vehicle:

- A topography-adaptive collection mechanism to avoid unnecessary or too-deep disturbance in the sediment
- Wide crawler belts and weight reduction designs to avoid unnecessary or too-deep disturbance in the sediment
- Disturbance shielding and slowing devices on the crawler belts to reduce the intensity of disturbance in the sediment

(2) An optimized test scheme:

- A centralized and compact test route design to minimize the total area of the CTA
- On the premise of ensuring the minimum requirements of the test, the duration of 100 % power collection test will be shortened

7.4.3 Residual impact

The disturbance and recolonization experiment (DISCOL) found that the variations of micro-topography and micro-geomorphology caused by the disturbance of plows and harrows were still clearly visible 26 years after the test (Stratmann et al. 2018). This gives a few examples for the natural recovery rate of geological setting in the oligotrophic deep-sea environment. Since the sedimentation rate in the central and western parts of the CCZ is only 3-5 mm/kyr (Pälike et al. 2014), it may take 20,000-30,000 years for the micro-geomorphological variation of approximately 10 cm caused by this disturbance to be landfilled when only gravity settlement is considered. However, due to the existence of periodic high-current-speed events such as "undersea storm" in the near-bottom layer of the East Pacific Ocean (Kontar and Sokov 1994), the natural restoration (redeposition) process may be accelerated. Due to lack of sufficiently long-term observation data, this is the best estimation for the time being.

7.5 Physical oceanography environment

7.5.1 Potential impacts and problems to be solved

Since the collector vehicle's collector head will disturb the sediment to 4-6 cm of depth, the main components of the sediment plume caused by the collector vehicle are from the surface-layer sediment (clay-grade and silt-grade particles). Most of the sand- and silt-grade particles are of biological origin, mainly radiolarians and Bacillariophyta. In this test, the main sediment plumes are in the bottom layer, which are mainly caused by the collector vehicle's traveling and nodule-collecting activities. There will be near- and far-field environmental impacts.

In the near field, the sediments produced in the seabed mining process quickly redeposit near the Contract Area. This may cover benthic fauna and block their food filters, causing more oxygen consumption by unstable organic matters or reduced metals, and releasing toxic substances. These processes will affect the structure and function of deep-sea ecosystem, but the quantitative impact remains to be seen. This Project plans to strengthen the near- and far-field monitoring and assess the degree and scope of impact on the environment. The collector vehicle will be equipped with an environmental inspection and monitoring ROV (with cable length of approximately 20 m) to dynamically monitor the plume generation and dispersal around the collector vehicle. A monitoring network at far, middle and near fields will be arranged near the CTA to monitor the plume dispersal process.

In the far field, the numerical model will be used to simulate the dispersal process of sediment plume, the raising height of mining plume and the impact scope. So far, there are only a handful of similar studies. The numerical simulation adopted in this EIS will integrate the physicochemical properties of sediments, hydrodynamic characteristics, bottom topography, mining equipment types, mining rate and emission rate to simulate the plume dispersal process under different conditions.

7.5.1.2 Modelling

A numerical model of plume dispersal resulting from seabed mining in the CTA of the Block A-5 has been established. It is an FVCOM (an Unstructured Grid, Fine-volume Coastal Ocean Model) based on a triangular grid and adopting the finite volume method and the ocean model of three-dimensional primitive equations. The integral method of volume flux is used to solve the original governing equations of fluid dynamics, thus ensuring the conservation of momentum, energy and mass in a single grid and the whole calculation area, and solving key problems in ocean numerical calculation. The S coordinate system is adopted in the vertical direction to deal with complex topography variations and simulate the dynamic process in the bottom layer in a better way. An unstructured triangular mesh in the horizontal direction is used to locally encrypt the key areas of concern (e.g. the CTA) and improve the calculation efficiency.

The FVCOM's governing equations are as follows:

$$\frac{\partial \zeta}{\partial t}+\frac{\partial Du}{\partial x}+\frac{\partial Dv}{\partial y}+\frac{\partial w}{\partial z}=0$$

$$\frac{\partial uD}{\partial t}+\frac{\partial u^2D}{\partial x}+\frac{\partial uvD}{\partial y}+\frac{\partial uw}{\partial \sigma}-fvD$$
$$=-gD\frac{\partial \zeta}{\partial x}-\frac{gD}{\rho_0}[\frac{\partial}{\partial x}(D\int_{\sigma}^{0}\rho d\sigma')+\sigma\rho\frac{\partial D}{\partial x}]+\frac{1}{D}\frac{\partial}{\partial \sigma}(K_m\frac{\partial u}{\partial \sigma})+DF_u$$

$$\frac{\partial vD}{\partial t}+\frac{\partial uvD}{\partial x}+\frac{\partial v^2D}{\partial y}+\frac{\partial vw}{\partial \sigma}+fuD$$
$$=-gD\frac{\partial \zeta}{\partial y}-\frac{gD}{\rho_0}[\frac{\partial}{\partial u}(D\int_{\sigma}^{0}\rho d\sigma')+\sigma\rho\frac{\partial D}{\partial y}]+\frac{1}{D}\frac{\partial}{\partial \sigma}(K_m\frac{\partial v}{\partial \sigma})+DF_v$$

$$\frac{\partial \theta D}{\partial t}+\frac{\partial \theta uD}{\partial x}+\frac{\partial \theta vD}{\partial y}+\frac{\partial \theta w}{\partial \sigma}=\frac{1}{D}\frac{\partial}{\partial \sigma}(K_h\frac{\partial \theta}{\partial \sigma})+DH+DF_\theta$$

$$\frac{\partial SD}{\partial t}+\frac{\partial SuD}{\partial x}+\frac{\partial SvD}{\partial y}+\frac{\partial Sw}{\partial \sigma}=\frac{1}{D}\frac{\partial}{\partial \sigma}(K_h\frac{\partial S}{\partial \sigma})+DH+DF_S$$

$$\frac{\partial q^2D}{\partial t}+\frac{\partial q^2uD}{\partial x}+\frac{\partial q^2vD}{\partial y}+\frac{\partial q^2w}{\partial \sigma}=2D(P_s+P_b-\varepsilon)+\frac{1}{D}\frac{\partial}{\partial \sigma}(K_q\frac{\partial q^2}{\partial \sigma})+DE_q$$

$$\frac{\partial q^2 lD}{\partial t} + \frac{\partial q^2 luD}{\partial x} + \frac{\partial q^2 lvD}{\partial y} + \frac{w}{D}\frac{\partial q^2 lw}{\partial \sigma}$$
$$= lE_l D(P_s + P_b - \frac{\widetilde{W}}{E_l}\varepsilon) + \frac{1}{D}\frac{\partial}{\partial \sigma}(K_q \frac{\partial q^2 l}{\partial \sigma}) + DF_l$$

$$\rho = \rho(\theta, S)$$

Where x, y, σ are the coordinates in the middle, north and vertical directions in the Cartesian coordinate system; u, v, w are velocity components in x, y, σ directions; T is temperature; S is salinity; ρ is density; P is pressure; f is the Coriolis force parameter; g is the acceleration of gravity; is the vertical eddy viscosity coefficient; is thermal vertical vortex friction coefficient; F_u , F_v , and represent horizontal momentum, temperature and salinity dispersal.

For this collector vehicle test, a scope of 40 km × 40 km is set in the simulation model, with a mesh resolution of 2,000 m at the model boundary and 100 m in the test-mining center (5 km × 5 km). In the vertical direction, the generalized coordinate system is adopted; the grid is encrypted near the bottom and divided into 61 layers. At the depth of 10 m above the bottom, the resolution is 1 m (Figure 7.5-1).

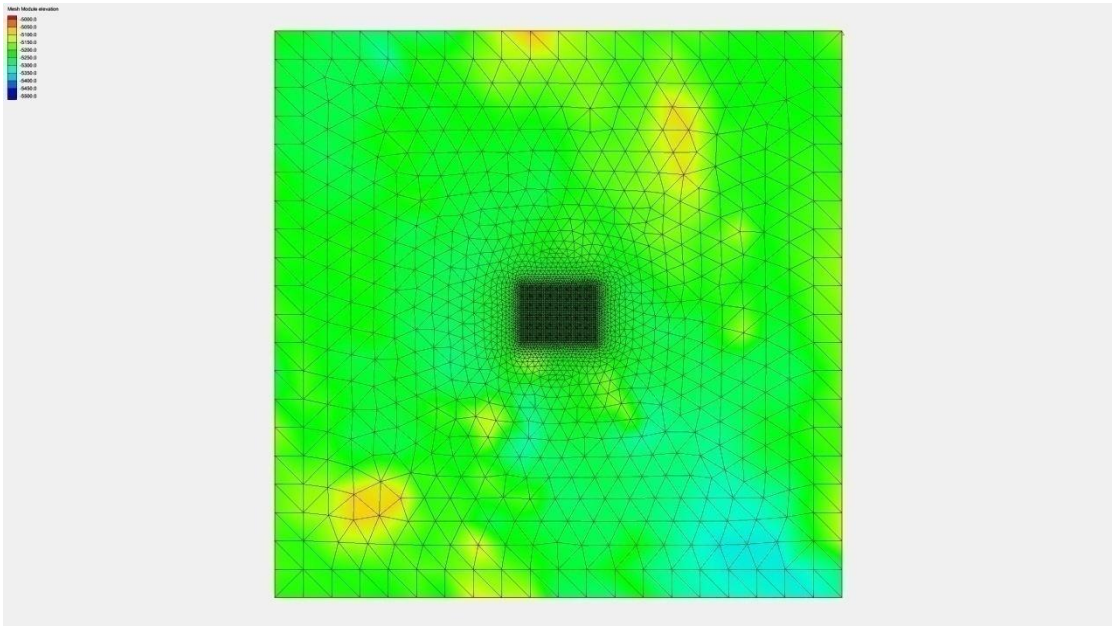

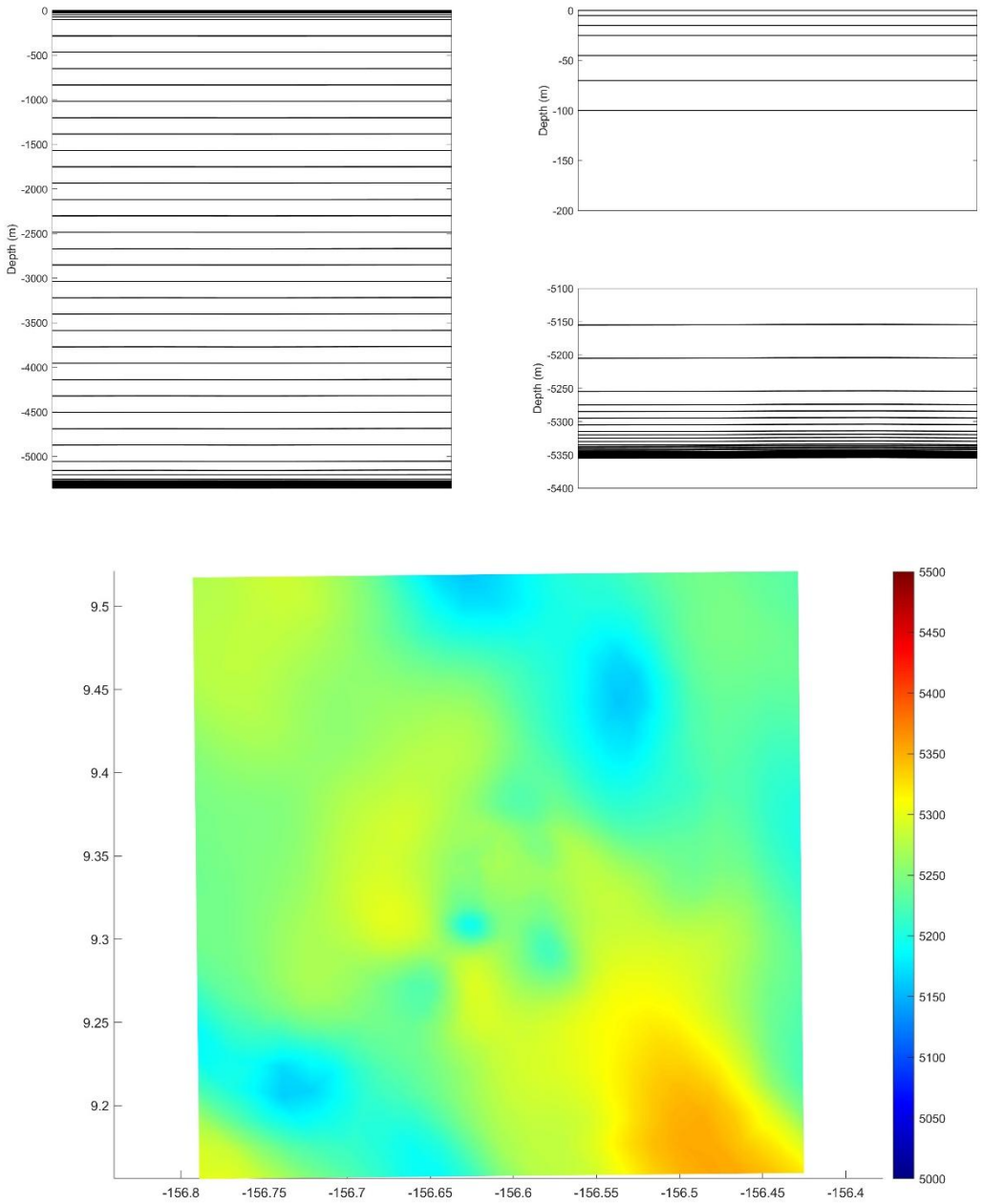

Figure 7.5.1 Model's horizontal grid (upper), vertical grid (middle) and water depth map (lower)

Mode setting and open-boundary conditions:

There is no obvious variation in temperature and salinity in the bottom layer, as shown in the structure of temperature and salinity profiles. The CTA is located in the bottom layer, and there is no emission in the surface and middle layers, so the plume model will be calculated as a barotropic model.

The open boundary tidal level is obtained by using the TPXO global tidal model.

Assuming that the background flow field in the bottom layer of the simulation area is always the same, the residual current field obtained by filtering out high-frequency variations (e.g. tidal currents) according to the measured flow field is taken as the open boundary condition of the flow field of the model.

Sediment Module:

The sediment module considers the coupling of water and sediment density and the process of flocculation settling. The suspended sand diffusion equation is as follows:

$$\frac{\partial C}{\partial t}+\frac{\partial (uC)}{\partial x}+\frac{\partial (vC)}{\partial y}+\frac{\partial \left[(w-w_s)C\right]}{\partial z}=\frac{\partial}{\partial x}\left(A_H\frac{\partial C}{\partial x}\right)+\frac{\partial}{\partial y}\left(A_H\frac{\partial C}{\partial y}\right)+\frac{\partial}{\partial z}\left(K_h\frac{\partial C}{\partial z}\right)$$

where C, w_s represent the suspended sediment concentration and settling velocity, A_H represents the horizontal eddy viscosity coefficient, K_h represents the vertical eddy viscosity coefficient.

The sediment flux boundary conditions are as follows:

$$K_h\frac{\partial C}{\partial z}=0,\quad z=\zeta$$

$$K_h\frac{\partial C}{\partial z}=E-De,\quad z=-H$$

where E represents the sediment resuspension flux, $De = C_b w_b$ represents the sediment deposition flux at the lowest layer, Cb, wb represent the suspended sediment concentration and settling velocity at the lowest layer.

Setting of suspended sediment parameters for plume:

According to the study reports of relevant survey cruises, the particle sizes of the bottom-layer sediments exhibit a bimodal distribution pattern. So, the particle sizes of suspended sediments are set as 0.0028 mm and 0.0625 mm. The settling speed of 0.0028 mm and 0.0625 mm particles are set at 0.36 mm/s and 8.33 mm/s, with reference to the article by Zhan et al. (2023).

The simulated plume discharge port is 1 m above the bottom, the density of

plume sediment is 1700 kg/m^3, critical shear stress for deposition is 0.1 N/m^2.

Refer to Section 3.3 for the traveling path of the collector vehicle. Since the collector vehicle only creates small disturbance during traveling, the model only simulates the plume during the collecting operation. The specific schematic diagram of the simulated collecting path is shown in Figure 7.5-2. The disturbance intensity is calculated according to the relevant technical parameters of the collector vehicle. It is 7.2 kg/s at 0.2 m/s, 14.4 kg/s at 0.4 m/s, 18.0 kg/s at 0.6 m/s, 19.2 kg/s at 0.8 m/s and 24.0 kg/s at 1.0 m/s.

Considering that the lower limit of the effective detection concentration of the turbidity sensor is 0.1mg/l (Munoz Royo et al. 2022), and referring to the boundary values for plume diffusion evaluation in NORI-D EIS, therefore, in the subsequent analysis of the horizontal and vertical distribution characteristics of suspended sediment concentration, 0 1 mg/l is used as the boundary value for the effect of plume diffusion.

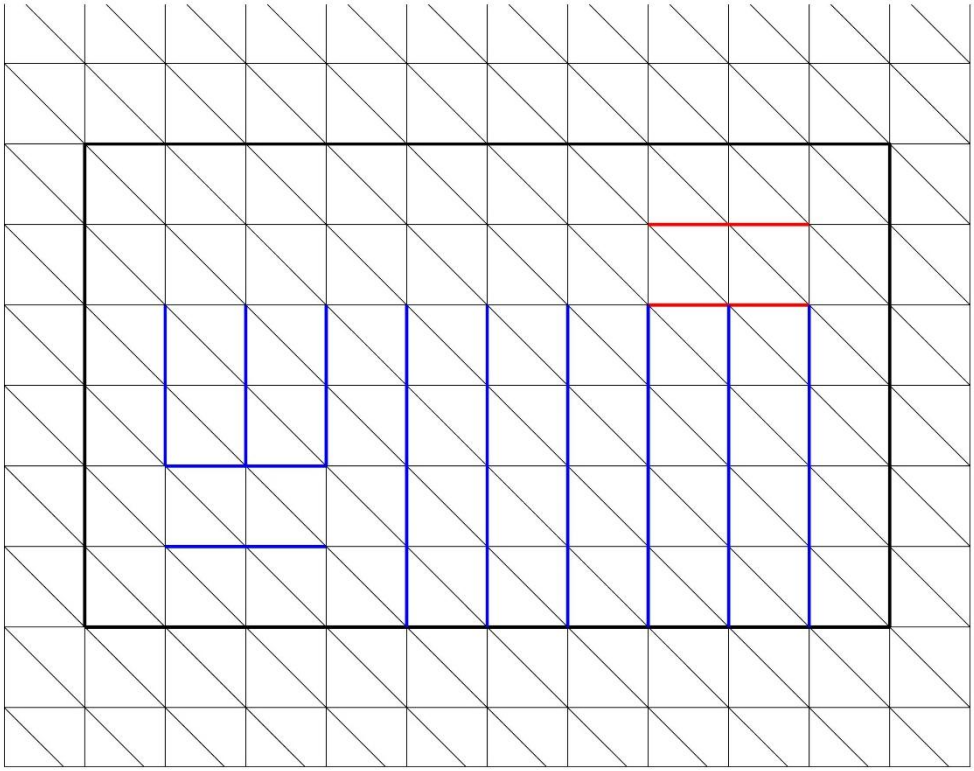

Figure 7.5-2 Schematic diagram for the simulated collecting path of the collector vehicle

(The thin black line is the pattern grid line; the thick black line is the CTA; the red line is the path of first test-mining; and the blue line is the path of second test-mining)

7.5.1.3 Model validation

Comparison of the model flow field results from July to August in 2020 with the measured flow field (20m above the seafloor at station DY70II-A5-MX01), as in Figure 7.5-2, shows that the simulated flow current speed is in good agreement with the measured flow current speed.

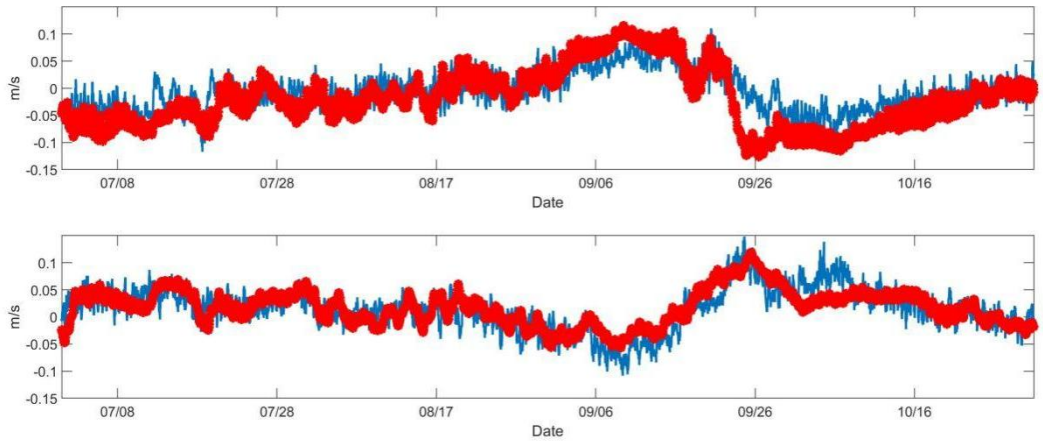

Figure 7.5-3 Comparison of model results (red) and measured current speeds (blue)

(Upper picture shows the east-west component of current speed; lower picture shows the north-south component of current speed.)

Warner and other methods are adopted to quantify the calculation accuracy of the numerical value model. The calculation formula is as follows:

$$Skill = 1 - \frac{\sum_{i=1}^{N} \left| X_{mod} - X_{obs} \right|^2}{\sum_{i=1}^{N} \left(\left| X_{mod} - \bar{X}_{obs} \right| + \left| X_{obs} - \bar{X}_{obs} \right| \right)^2}$$

Where: X represents the parameter to be compared,

$\bar{X}$ represents the average,

mod represents the calculation result of the model,

obs indicates the measured results.

The calculated results are in the range of 0-1.0; where 1.0 means that the

calculated results of the model are consistent with the measured results, while 0 means that they are inconsistent. The closer the value is to 1, the higher the simulation accuracy of the model is.

The Skill values of the simulated current speeds and the measured current speeds are calculated. On the U component, the magnitude and variation trend of the two are basically the same, and the Skill value is 0.85. In the V component, the magnitude and variation trend of the two are basically the same, and the average Skill value is 0.86. The average Skill of current speed reaches 0.855, indicating that the simulation accuracy of the model is high and the results of the hydrodynamic numerical model are credible.

7.5.1.4 Plume model results

Since the operation time is undetermined, we only simulated plumes under the flow field conditions in July, August, September and October. We assume that the first underwater operation starts at 00:00 on the 10th of each month, and the test-mining lasts for about 5 hours in total; the second underwater operation starts at 00:00 on the 11th of each month, and the test-mining lasts for about 36 hours in total. The distribution of plume dispersal is simulated with two particle sizes. See Table 7.5-1 for specific cases.

Table 7.5-1 Parameters of plume model cases

Case	Sediment particle size	Start time
Case,1	0.0625	07/10
Case,2	0.0028	07/10
Case,3	0.0625	08/10
Case,4	0.0028	08/10
Case,5	0.0625	09/10
Case,6	0.0028	09/10
Case,7	0.0625	10/10
Case,8	0.0028	10/10

7.5.1.4.1 Horizontal distribution of suspended sediment concentrations

The disturbance duration is relatively short during the first test-mining, so all the water columns with suspended sediment concentration higher than 10 mg/L at 1 m above the bottom are located in the CTA. During the second test-mining, because the collector vehicle's path is close to the edge of the CTA, the number of water columns with suspended sediment concentration higher than 10 mg/L is slightly higher in the south of the CTA than in the whole CTA. The bottom-layer suspended sediment concentration is the highest during the test-mining, and the concentration gradually decreases after the test-mining. The dispersal range of plume is controlled by the bottom-layer current speed. The impact scope of mining plume is small in August due to slow current speed in the month. The plume disappeared four days after the start of the test-mining (2.5 days after the end of the test-mining) in Case 3; and disappeared 5 days after the start of the test-mining (3.5 days after the end of the test-mining) in other cases. The dispersal direction of plume is controlled by the bottom-layer flow field, so the dispersal direction is northwest in July and east in September. The maximum impact distance of plume varies from month to month, being the smallest in August and the largest in September. The dispersal distribution range of fine-grained sediments is larger than that of coarse-grained sediments, and the maximum impact distance in the cases is 2.1 km (Case 2).

Analysis of the comprehensive sea surface conditions shows that August is the most suitable for the collector vehicle test. See Figures 7.5-4 and 7.5-5 for the ranges of bottom-layer plume dispersal under different case conditions in August.

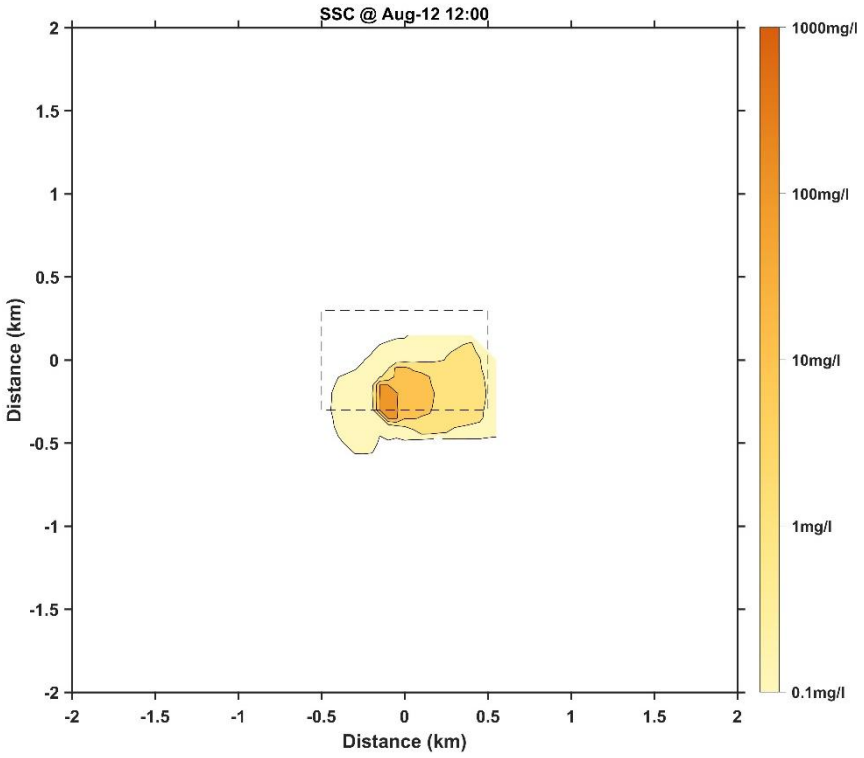

Figure 7.5-4 Distribution of suspended sediment concentrations at the end of second test-mining in Case 3

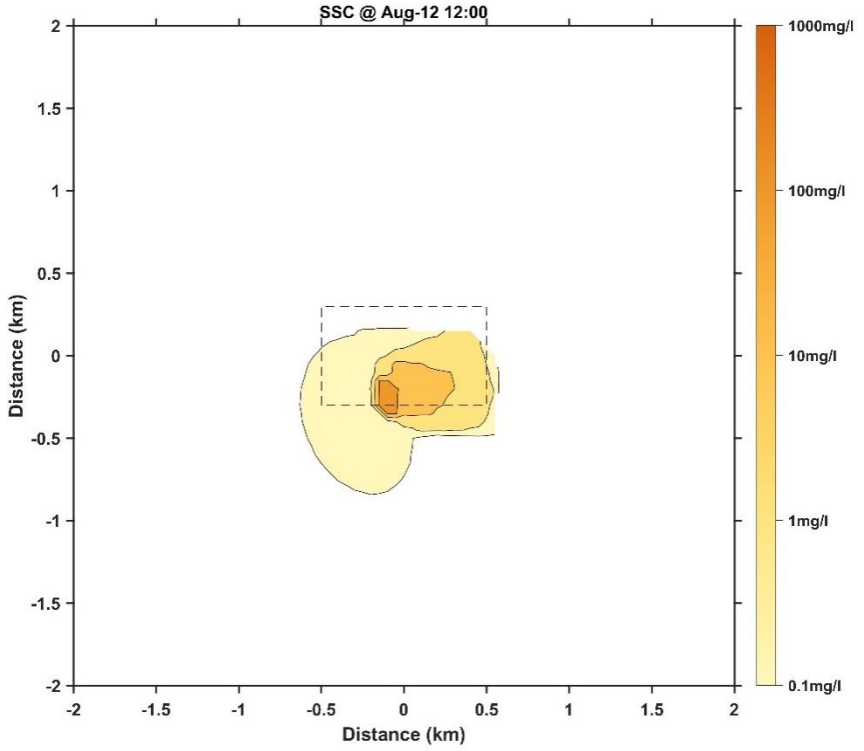

Figure 7.5-5 Distribution of suspended sediment concentrations at the end of second test-mining in Case 4

7.5.1.4.2 Vertical distribution of suspended sediment concentrations

Referring to the vertical distribution characteristics of suspended sediment concentration at the midpoint of the CTA, if the 0.1 mg/L isoline is taken as the vertical impact scope of plume, then the vertical impact height of plume is 124 m at most. If the isoline of 1 mg/L (higher than the detection limit of background turbidity) is taken as the influence range, the maximum height of the vertical plume dispersal is about 80 m. The plume disappears within 1-1.5 days after the test-mining. Fine-grained sediments bring higher impact than coarse-grained sediments. Figures 7.5-6 and 7.5-7 are the numerical simulation results of vertical distribution of suspended sediment under different case conditions in August.

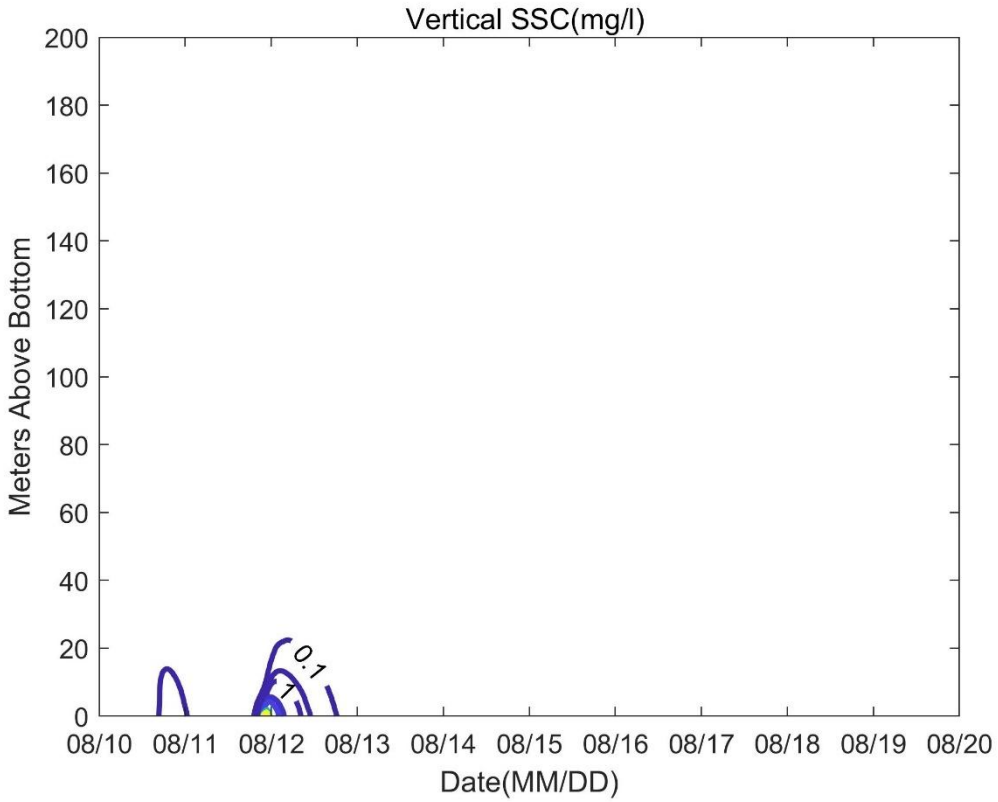

Figure 7.5-6 Vertical distribution of suspended sediment concentrations in Case 3

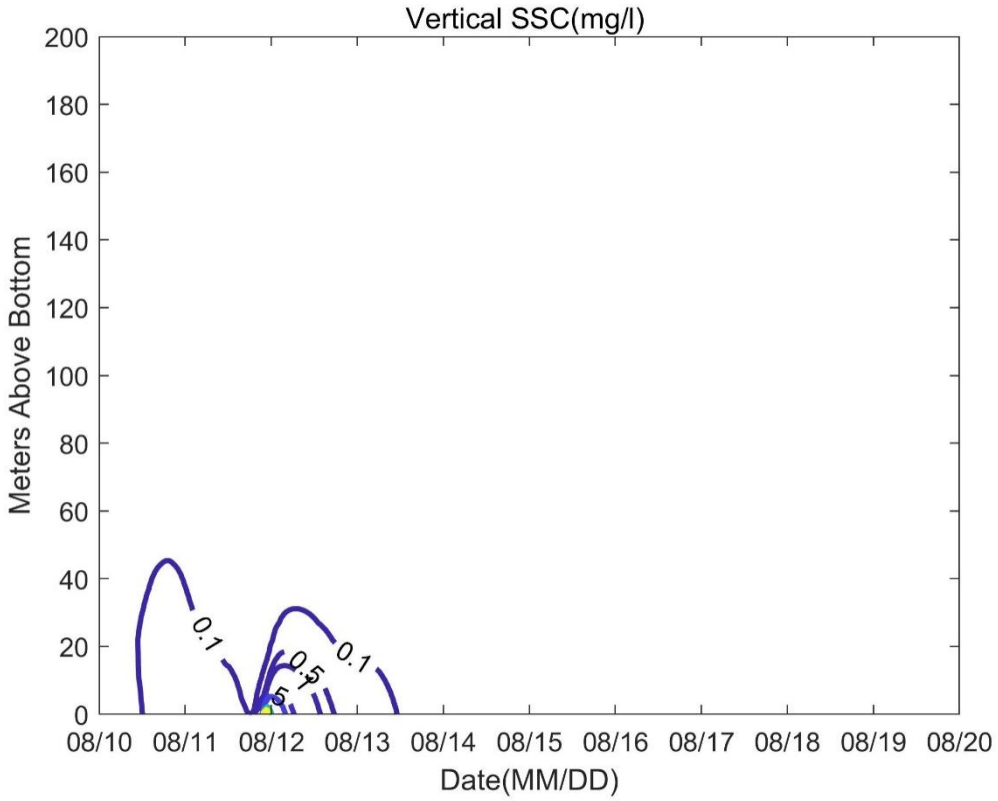

Figure 7.5-7 Vertical distribution of suspended sediment concentrations in Case 4

7.5.1.4.3 Distribution of redeposition thickness

Most of the sediment plumes produced by the nodule-collecting activity will settle around the nodule-collecting area, gradually thinning from near to far field, with the maximum deposition thickness being 0.33 cm (Case 3). Figures 7.5-8 and 7.5-9 show the numerical simulation results of redeposition thickness under different case conditions in August.

See Tables 7.5-2 and 7.5-3 for the maximum dispersal range, maximum redeposition thickness and redeposition area of plume. The areas with redeposition thickness greater than 0.1 mm are located within 100 m outside the CTA; the areas with redeposition thickness greater than 1 mm are mainly located in the CTA with a distance of 0 m between the first and second areas for continuous nodule collection.

The area with redeposition thickness greater than 1 mm is 0.06-0.12 km^2, and the area with redeposition thickness greater than 0.1 mm is 0.59-0.64 km^2.

The maximum redeposition thickness is the largest in August and the smallest in

September. By redeposition thickness greater than 1 mm, the largest area appears in September and the smallest area in August. These are the characteristics of flow field variations in corresponding months.

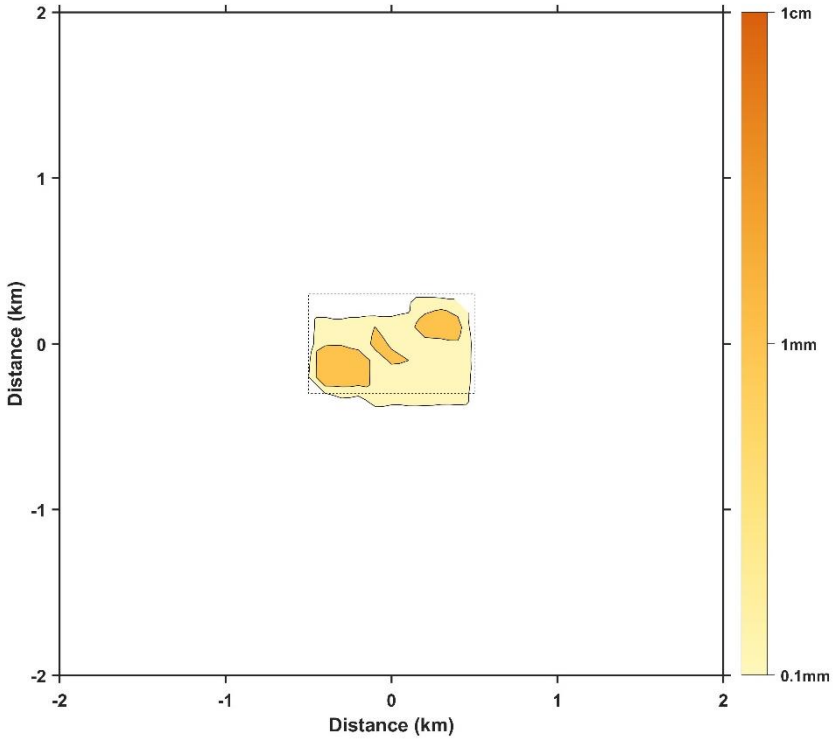

Figure 7.5-8 Distribution of redeposition thicknesses in Case 3

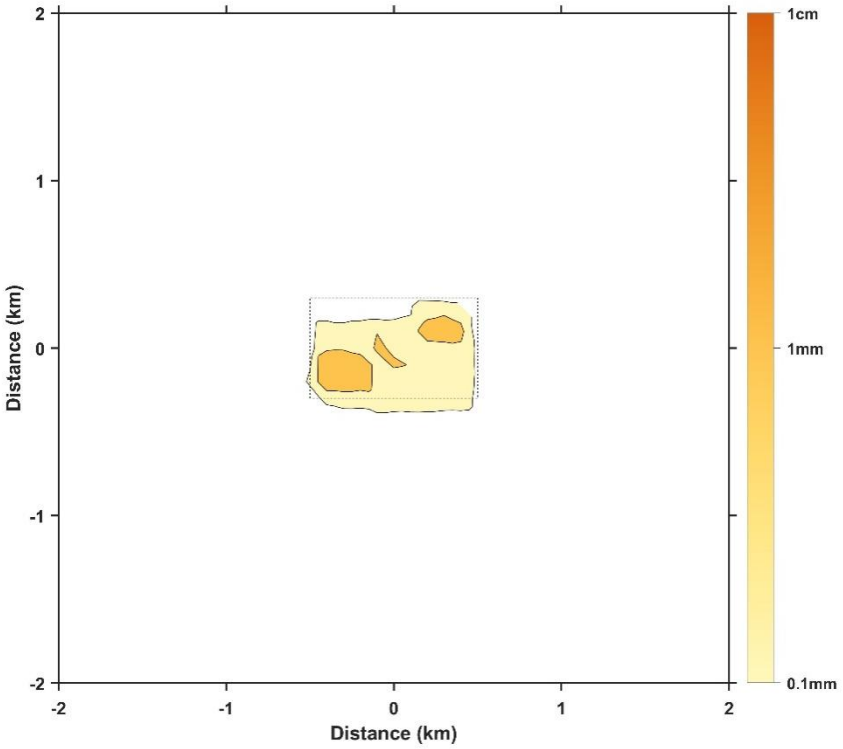

Figure 7.5-9 Distribution of redeposition thicknesses in Case 4

Table 7.5-2 Maximum plume dispersal scopes and maximum redeposition thicknesses

Case	Maximum dispersal range of plume (km)	Maximum redeposition thickness (cm)	Maximum height of impact (m)
Case,1	1.5	0.28	70
Case,2	2.1	0.24	79
Case,3	0.6	0.33	22
Case,4	0.9	0.30	45
Case,5	1.7	0.23	121
Case,6	2.1	0.19	124
Case,7	1.1	0.30	67
Case,8	1.7	0.26	75

Table 7.5-3 Areas of plume redeposition

Case	Area with redeposition thickness greater than 1 cm (km^2)	Area with redeposition thickness greater than 1 mm (km^2)	Area with redeposition thickness greater than 0.1 mm (km^2)
Case,1	0	0.10	0.62
Case,2	0	0.09	0.64
Case,3	0	0.12	0.59
Case,4	0	0.11	0.60
Case,5	0	0.09	0.60
Case,6	0	0.06	0.60
Case,7	0	0.11	0.61
Case,8	0	0.09	0.63

7.5.1.5 Summary

For seabed mining of nodules, we have established a plume model for seabed mining, and simulated the plume dispersal and redeposition process with different sediment particle sizes under different flow field conditions in July, August, September and October. Simulation results show that water columns with high

concentrations and redeposition of suspended sediments are mainly located in the CTA. The maximum impact of plume is horizontally 2.1 km and vertically 124 m. The plume dispersal varies obviously under the flow field conditions in different months. Fine-grained sediments can bring larger impact horizontally and vertically than coarse-grained sediments.

7.5.2 Environmental management measures to mitigate impacts

The most effective measure to reduce the environmental impact is optimizing the collector vehicle design, which can reduce the disturbance during traveling and nodule-collecting activities. Meanwhile, we select reasonable traveling mode and speed of the collector vehicle through numerical simulation, so as to reduce the environmental impact, and choose suitable time for the collector vehicle test to reduce plume dispersal. See Section 7.14 for the environmental impact mitigation measures included in the design of the collector vehicle.

7.5.3 Residual impact

Simulation results show that the plume with suspended particulate matter (SPM) concentration of 0.1 mg/L will disappear within four days after the end of the test. Therefore, this test has little residual impact on the physical oceanography environment.

7.6 Chemical oceanography environment

7.6.1 Potential impacts and problems to be solved

Since this test does not involve tail water discharge, the impact on seawater environment mainly occurs in the bottom layer, and there is little impact on the chemical environment of seawater column. Although the toxicity of heavy metals to organisms is widely regarded as an important part of the potential environmental impact of seabed mining (Hauton et al. 2017), it is unlikely that simple mechanical disturbance will change the properties of oxidized minerals and lead to large-scale heavy metal release in the extensive oxidation environment in the bottom layer of the

CCZ (BGR 2018). There are a lot of nutrients and heavy metals in the pore water of surface-layer sediments in the nodule area. The simulated disturbance experiment shows that the release of heavy metals has significant element specificity (Figure 7.6-1, Shi et al. 2023), and only four kinds of heavy metals (i.e. vanadium, rubidium, molybdenum and cadmium) with significant and stable precipitation behavior. Similar results have also been found in other people's studies (Koschinsky et al. 2001). Some in-situ toxicity tests of heavy metals in deep sea show that the toxicity of heavy metals can have a significant impact on the hypobenthos (Kwan et al. 2019). However, these tests were obviously incredible, because they adopted heavy metal precipitation concentrations much higher than the reality and some unlikely types of heavy metals (e.g. Cu). Due to undetermined threshold of heavy metal concentration, it remains very difficult to assess the impact on the bottom-layer chemical environment.

In order to provide a quantitative assessment, surface sediment samples from block A-5 were flushed and analyszd the main heavy metal species in the precipitates. The results show that Cd, Cu and Cr are the three main biotoxic heavy metals, while the other heavy metals are not significantly toxic. Further, we evaluated the binary joint toxicity of these biotoxic heavy metals with other non-biotoxic heavy metals, by the luminescent Vibrio fischeri method. The results show that the EC50 is much higher than the heavy metal concentrations in sediment pore water or bottom water, both for single metal toxicity and binary combined toxicity (Annex 3). Therefore, considering the relatively short time and limited scale of this test, the toxic effects due to heavy metal releases are limited.

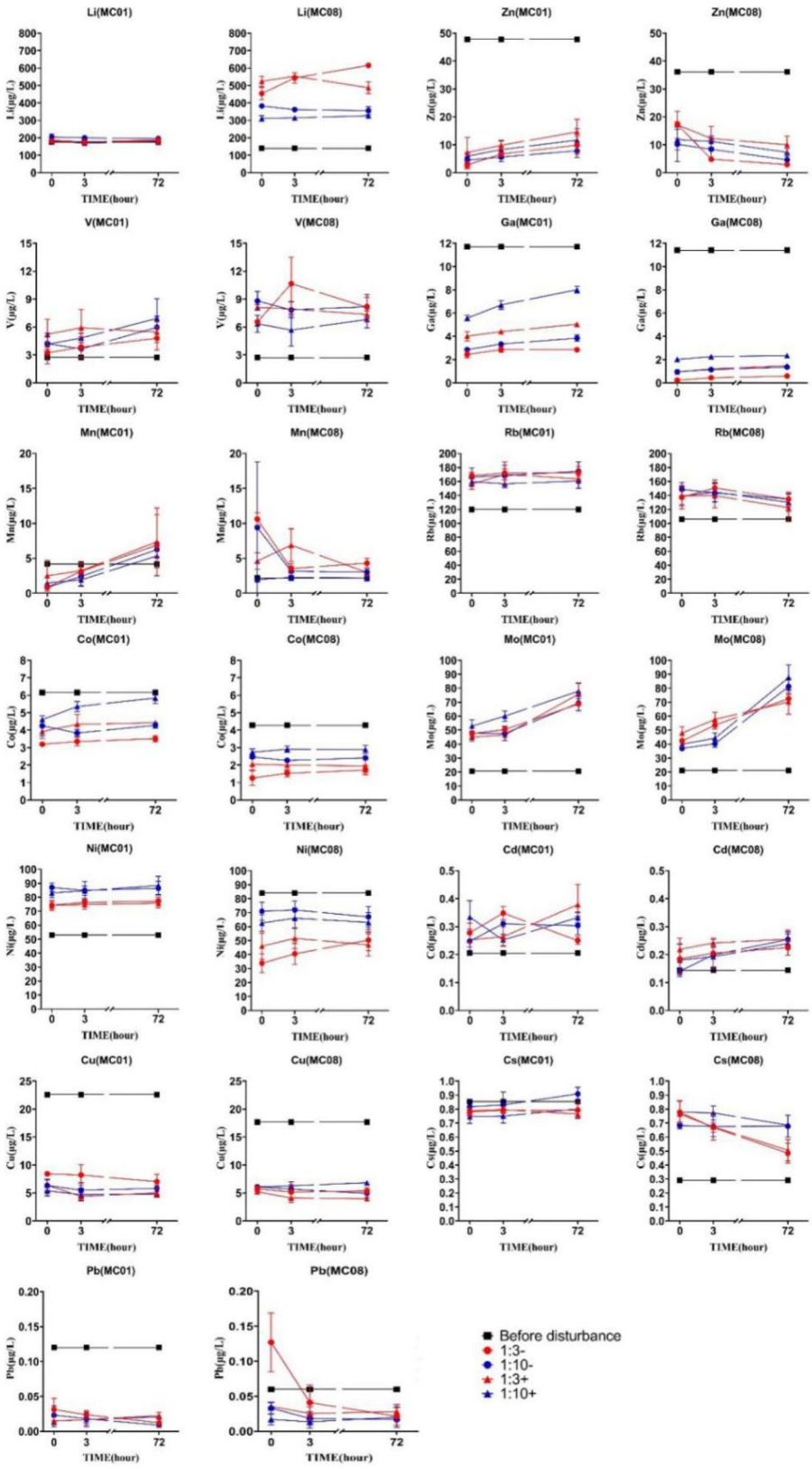

Figure 7.6-1 Simulation results of heavy metal release after sediment disturbance in nodule area (Shi et al. 2023)

(Results show that only four kinds of heavy metals, namely vanadium, rubidium, molybdenum and cadmium, have significantly stable precipitation behavior)

In addition to the potential release of heavy metals, the consumption of active organic carbon (AOC) in plume by biological activities and the further oxidation of metal ions may also cause the consumption of DO in the near-bottom-layer water column (GSR 2018). The organic carbon content of surface-layer sediments in the CTA is less than 0.5 % (Figure 4.5-15), and a large amount of TOC in deep-sea sediments is inert organic carbon (Arndt et al. 2013). Since the small total disturbance scale and the fluidity of bottom-layer seawater in this test, the variation of DO in the bottom-layer seawater tends to be slight.

7.6.2 Environmental management measures to mitigate impacts

Since there is no ore lifting and tail water discharge in this test, the main environmental disturbance mitigation measures are the same as those to reduce the plume. See section 7.5.2.

7.6.3 Residual impact

Since this test only brings small disturbance to sediments and seawater (see Sections 7.4, 7.5 and 7.7), we expect there is not any significant residual impact.

7.7 Seabed sediment environment

Since this test does not involve surface-layer/middle-layer/deep-layer tail water discharge, the disturbance to marine planktonic ecosystem and BGC environment of water column will be extremely slight. Under the current scientific framework (Honjo et al. 2014), there is no evidence that this kind of disturbance will directly lead to the variation of sedimentary flux from the upper-layer ocean to the seabed.

However, this test-mining will bring direct and obvious disturbance to the sediment environment. This process can occur in at least two different ways: 1. When traveling on the soft seabed sediment surface, the collector vehicle's crawler belts will cause the sediment to be pressed in a certain depth range; 2. The collector vehicle's disturbance to the sediment will cause plume dispersal, resulting in redeposition of sediment in this area. Under the technical conditions adopted in this test, it is difficult

to completely avoid these two kinds of disturbances. The range of redeposition caused by plume is analyzed in Section 7.5 of this EIS, so we only briefly discussed the compaction of sediment resulting from the collector vehicle here.

Analysis in Section 4.8 of this EIS shows that the strengths of in-situ penetration into surface-layer sediments are in the range of 25.1-30.3 kPa in and around the CTA. The design based on this value will ensure that the collector vehicle's crawler belts will sink no more than 10 cm into the subsoil. Recent evidence shows that the content of heavy metals in the pore water of sediments in the shallow-surface layer (0-20 cm depth) of the deep-ocean basin in the Pacific Ocean has a wide vertical uniformity (Yang et al. 2023), so the impact of such extrusion and disturbance on the content of heavy metals in the pore water may be slight. Up to now, there has been no sufficient direct evidence in this regard. In this test, we plan to collect columnar sediment samples at the depth of 0-40 cm in the trajectory after the collector vehicle travels without mining in the trajectory, and compare them with those collected before the test. Subsequent analysis data will help us make a more objective assessment of the disturbance of seabed sediment environment caused by the compaction effect of the collector vehicle.

7.8 Natural disasters

Known scientific evidence shows that the geological structure of this region is stable and the topography is flat. So, there is no risk of inducing geological disasters such as landslides, collapses, deep-sea turbidity currents, volcanic eruptions and earthquakes in this test.

There are typhoons and other severe weather phenomena in the CCZ, especially from July to September every year. Available historical records show that a very small number of cyclones (with the central wind force up to 30 m/s) will cross the Block A-5, which will significantly affect the collector vehicle testing and cause potential risks (see Section 10.1 for details). Since the fast movement speed and strong predictability of tropical cyclones, we can decide to recover the test equipment or even move the

vessel to the area beyond the impact of typhoons on the spot according to the forecast data provided 48 h and 96 h in advance. Therefore, the impact of typhoon natural disasters on this test can be avoided.

7.9 Noise and light

7.9.1 Noise

On the high seas, vessels are the main sources of artificial noise. In this test, the EMV, SSV and collector vehicle are the main sources of noise. Strong artificial noise may cause a series of adverse effects on marine organisms, at least on whales, fish and the larvae of benthic fauna. However, data in this regard are highly insufficient. So, there is a large variation range about the impact threshold of noise on marine animals. For example, some studies concluded that the noise intensity above 120 dB re 1μPa will affect whales (Williams et al. 2022b), but other studies reckoned that noise sources below 150 dB re 1μPa were safe at 500 m away from whales (Arranz et al. 2021). Recent studies have also found that soundscapes formed by marine background noise may be of great significance to the colonization of lower invertebrate larvae (Williams et al. 2022a), so the variation of soundscape caused by mining activities may also cause risks in this respect.

China's R/V *DAYANG HAO* will be used as the EMV, which has the classification certificate issued by the CCS (No. GZ17NB00014; valid until: June 27, 2024). The classification certificate clearly indicates: Underwater Noise (3, 10-1,000Hz); Underwater Noise (1, 1,000-100,000Hz). Level 1 indicates the highest noise reduction level and the lowest noise.

China's *R/V ZHANG JIAN* will be used as the SSV, and has the classification certificate issued by the CCS (No. BJ18SS05145; valid until: July 12, 2024). R/V *ZHANG JIAN* has passed the inspection of the whole vessel noise by Shanghai Sinoking Marine S&T Co., Ltd. Test results show that the loudest noise position of the whole vessel is the propeller room in the stern, and the peak noise at the standard

speed is 107 dB, which meets the requirements of the CCS and IMO for vessels of this class and purpose.

According to NORI's estimation, the impact scope of surface vessels is 0.62 km^2, measured by the threshold of 140 dB re 1μPa rms (beyond which the destructive behavior of baleen whales may be affected). If stricter standards are adopted, the impact scope of noise can reach 19.5 km^2 and 62.7 km^2 respectively under the thresholds of 130 dB re 1μPa rms and 120 dB re 1μPa rms. In this test, the EMV is of the similar tonnage as the vessel in the NORI test. However, the SSV is 4,800 t, much smaller than the Hidden Gem (60,000 t) used in the NORI test. Therefore, the impact of water surface noise will be less in this test than in the NORI test.

See 3.3.2 for the detailed engineering description of the collector vehicle. The noise level of the equipment has not yet been tested in the deep-sea environment. Our collector vehicle's collecting capacity and power are similar to those in the NORI test. So, we refer to the NORI test result (NORI 2022) for the estimation. According to the threshold of 120 dB re 1μPa rms, the horizontal range of impact can reach 562 m radius, or approximately 0.99 km^2.

During the test, we will deploy a hydrophone array to measure the collector vehicle's noise source strength and distance attenuation.

7.9.2 Light

Artificial light sources in the environment will have adverse effects on biological communities and ecosystems. This has become a widespread environmental problem (Davies et al. 2016). Although studies in this regard remain scarce, there is a view that the environmental impact of artificial light sources is extensive, even from the cell level of an individual organism to the macro-ecosystem level (Gaston et al. 2013). So far, the known and potential disturbance from artificial light sources on marine ecosystems include: (a) inhibiting or changing the vertical migration of zooplankton; (b) attracting seabirds to hit brightly lit vessels or at-sea platforms; (c) extending the visual foraging behavior of coastal wading birds from normal daytime to nighttime; (d)

obstructing and changing the colonization of some invertebrate larvae; (e) triggering fish schools to and aggregate for intensified predation; (f) disturbing the reproductive behavior controlled by the moon phase (e.g. Anthozoa); (g) interfering with the navigation of adult turtles, thus affecting their reproduction and the navigation of turtle hatchling, and even their survival rate (Davies et al. 2014). The studies on the impact of two kinds of artificial light sources (i.e. LED lamps and halogen lamps) on the behavior of Amphipoda in shallow water shows that both kinds of light sources can attract the gathering of Amphipoda, while LED lamps have more intense impact (Navarro-Barranco and Hughes 2015). However, in the deep-sea environment (thousands of meters below surface), there is no scientific evidence to prove that artificial lighting will directly lead to adverse effects on biological communities or ecosystems. Another evidence in this regard is that when the baited trap lander system was used to survey the scavengers on the seabed, the flashing light did not cause any identifiable interference to the behavior of scavengers and crustaceans (no data from the survey conducted in the CCZ has been published).

From the technical and engineering point of view, the SSV and collector vehicle must have appropriate lighting to ensure the safety of equipment and personnel.

In the surface layer, both the SSV and EMV have to use necessary lighting at night to ensure the safety of normal operation. Especially during the underwater testing of the collector vehicle, the SSV will turn on the lighting facilities on the whole deck at night. When lighting is not absolutely necessary or allowed to be reduced, both the SSV and EMV will only use minimum lighting on board. Since the Block A-5 is not located in an area of high marine traffic and is not a concentrated distant-water fishing area, the cumulative impact of lighting disturbance in this test is small.

At the bottom of the sea, the collector vehicle needs to keep lighting in the front, the rear and on itself. Lighting in the front will help the operator judge the nodule coverage and micro-topography, so as to adaptively adopt the collecting mode with

the lowest environmental disturbance. Lighting in the rear will assist the operator judge the collector vehicle's nodule-collecting efficiency and the disturbance to the sediment environment under different working conditions. Lighting on the vehicle is for helping the operator monitor the control capsule, hydraulic pipes, electrical sockets, cables and connectors of the vehicle, thus ensuring the safety of test equipment and monitoring whether there is accidental leakage of toxic substances (e.g. hydraulic oil). Apart from these necessary lighting, other lighting equipment on the collector vehicle will only be turned on when absolutely necessary.

To minimize environmental impact, halogen lamps will be used as the main lighting source on the water surface and underwater in this test as appropriate as possible.

7.10 GHG emissions and climate change

The GHG emissions in this test mainly include those from the SSV and EMV and the potential GHG emissions from seabed sediments due to disturbance by the collector vehicle.

7.10.1 GHG emissions from vessels

Before the test, the SSV and EMV set out from Zhoushan Port in China and went to the Block A-5 by the shortest route (8,900 km), with the round-trip distance being 17,800 km (9,611 nautical miles). The standard speed of the SSV (R/V *ZHANG JIAN*) is 10 knots, while that of the EMV (R/V *DAYANG HAO*) is 12 knots. Calculated with the standard speed, the SSV and EMV will sail for 40 days and 33.4 days respectively during the round-trip. The diesel consumption rates under standard speed are 8 t/d for the SSV (R/V *ZHANG JIAN*) and 13 t/d for the EMV (R/V *DAYANG HAO*), respectively.

The total test duration in the CTA is estimated to be 15 days. Due to necessary maneuvering and dynamic positioning operations, both vessels will be calculated according to 50 % of converted speed. The diesel fuel consumption rates in this state

are for the SSV (R/V *ZHANG JIAN*) and 13 t/d for the EMV (R/V *DAYANG HAO*), respectively.

During the underwater testing of the collector vehicle, the SSV will operate an additional generator system with a power of 3,000 kW to provide power supply for the collector vehicle and other support equipment on board. The diesel consumption per hour is 0.78 t, and the total duration is one day.

We use these indexes and the EPA GHG equivalent calculator to estimate the emissions from the collector vehicle testing (Table 7.10-1).

Table 7.10-1 Estimation of GHG emissions

Round-trip of R/V *ZHANG JIAN*	320.0	1,024.5	2,414.6
Round-trip ferry of R/V *DAYANG HAO*	434.2	1,390.1	
Operation of R/V *ZHANG JIAN* in the Block A-5	72.0	230.5	
Auxiliary generator (providing full power for the collector vehicle and surface support system)	187.2	599.3	1,214.0
Operation of R/V *DAYANG HAO* in the Block A-5	120.0	384.2	
			3,628.6

7.10.2 Potential GHG emissions from seabed sediments due to disturbance by the collector vehicle

Due to the lack of studies on the stability of inert organic carbon in sediments after disturbance, there is no scientific and effective estimation method in this respect. Therefore, this study does not estimate this part of GHG emissions. In this test, relevant data (especially DO and DIC in the bottom layer) will be collected to provide reference data assessment.

7.11 Maritime safety, and interactions between this test and existing shipping routes

The main marine traffic routes passing through the CCZ of the East Pacific Ocean are in the south edge of the Panama Canal-Hawaii exclusive economic zone (200 nautical miles) and in the north edge of the CCZ (approximately 15 °N) (March et al. 2021). The Block A-5 of the Contract Area is at approximately 9 °N, which is far from the main marine traffic routes (Figure 7.11-1). Therefore, this test is not expected to cause obvious interference to existing shipping.

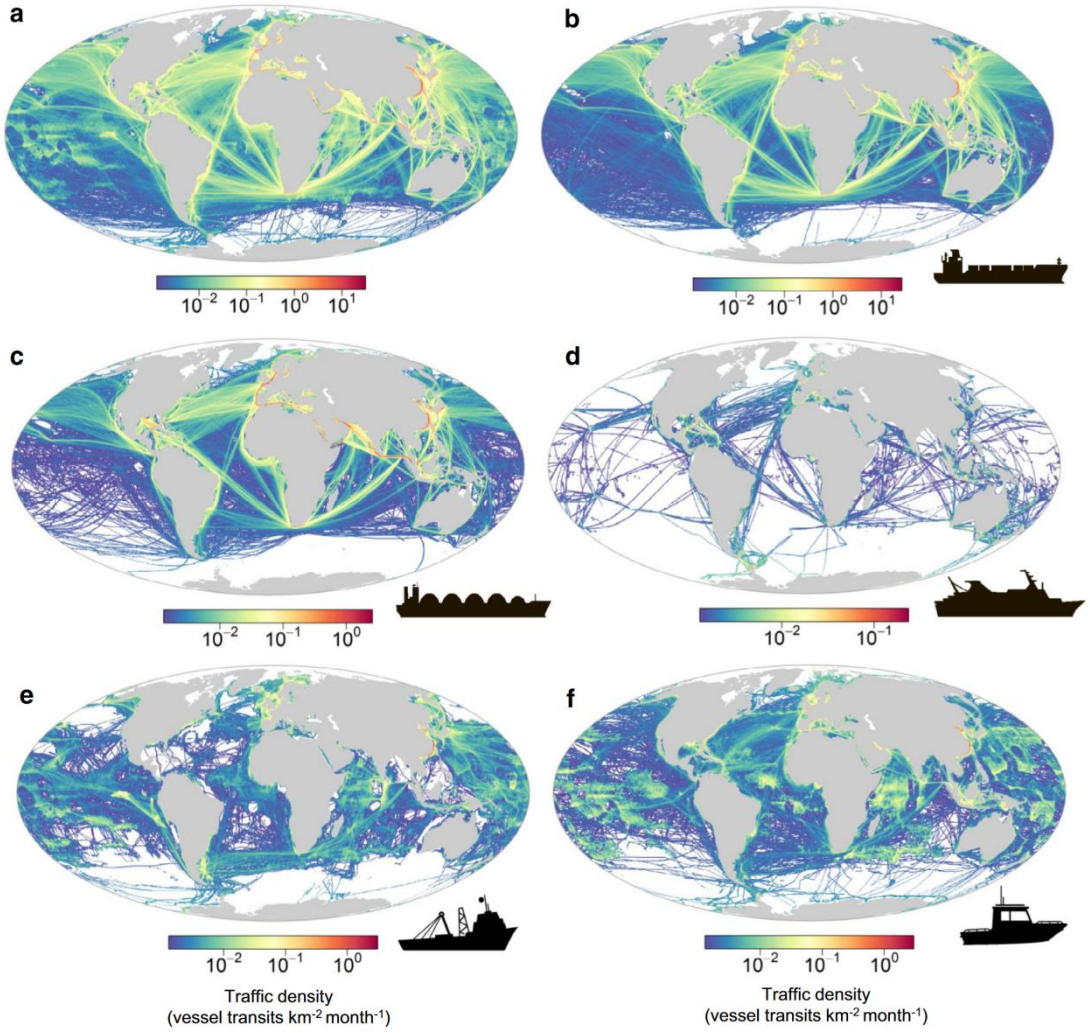

Figure 7.11-1 Thermodynamic chart of main shipping routes in the world (March et al. 2021)

7.12 Waste management

The SSV and EMV used in this test meet the requirements of "International

Management Code for the Safe Operation of Ships and for Pollution Prevention" (ISM Code-1993) and the Annex 1 of "International Convention for the Prevention of Pollution from Ships". They will not discharge or discard substances that may cause pollution or harm to the marine environment, and will strictly abide by the above provisions during the test.

7.13 Cumulative impact

Mining site impacts may be multifaceted. Multiple sources of stressors or repeated strengthening of the same stressor at different times can have cumulative impacts on a habitat or region. Multiple stressors can also result in a cumulative impact greater than the impact of individual stressor (Levin et al. 2016). Understanding the cumulative impact will help to identify serious hazards across multiple departments, and it is very important to formulate strategic environmental assessment and management plans.

Spatially, cumulative impacts can occur at many levels. Examples are as follows. Multiple tests or mining activities by one or more contractors in a specific area; overlapping of different types of deep-sea resources exploitation activities in a region; other human activities unrelated to seabed mining, but overlapping in the spatial sense (e.g. fishing) and the multiple impacts of seabed mining on specific species or ecosystems. The assessment of cumulative impacts of seabed mining activities should include past, present and reasonably foreseeable future impacts. However, due to the lack of understanding of deep-sea ecosystem and biodiversity, especially the source-sink relationship of larval migration and dispersal, larval migration ability and colonization survival rate, key ecotoxicological thresholds, complete food web structure and energy flow path, and ecosystem resilience, it is still very challenging to assess the cumulative impact of seabed mining activities (Clark et al. 2020).

(1) Nodule removal, sediment disturbance and the physicochemical environment of bottom-layer water column

So far, the bottom environment of the CCZ is not disturbed by other human

activities, so there is no pressure source other than test-mining activities. The removal of nodules in the test-mining process will change the benthic habitat on the geological timescale for a long time, and the removal and redeposition of sediments will also change the benthic habitat on the scale of at least several decades. In terms of scale, the removal of nodules and surface-layer sediments directly caused by this test only involves about 0.1 km^2 of collection area, while the total area of the Block A-5 is 22,821 km^2. This means that the direct disturbance area is only 0.000438 % of the total area of the Block A-5. So, we infer that the cumulative impact of removal of nodules and surface-layer sediments is limited. The sediment range in this test is measured by the threshold of 0.1 mm redeposition thickness, and the maximum redeposition area is less than 1 km^2, accounting for only 0.0044 % of the total area of the Block A-5. So, we infer that sediment redeposition will not cause great disturbance to the seabed.

Plume dispersal caused by the testing of the collector vehicle will impact the physicochemical environment at the bottom layer. However, due to the existence of the bottom-layer ocean currents and the good dispersal ability of seawater, the recovery of physicochemical environment at the bottom layer is much faster. Since the small scope and duration of this test, the cumulative impact in this respect is limited.

(2) Noise and light

At present, the main human activities in the CCZ, such as shipping and offshore fishing, may produce noise and light impacts. However, as mentioned above (6.2.1 and 6.2.2), the area where Block A-5 is located is not an important fishing ground and ocean route, and most of the CCZ belongs to the "Marine Wilderness Outside EEZ" (Jones et al. 2018) with little human activity. Therefore, the noise and light generated by this test-mining will not have cumulative impacts with other pressure sources other than the test-mining activities.

(3) GHG emissions

At present, the GHG emissions in the CCZ are mainly generated by a small

amount of shipping and offshore fishing activities. Because of the low frequency of these activities, the GHG emissions are very small. The sources of GHG emissions in this test include direct emissions from the SSV and EMV and indirect emissions from seabed sediments due to disturbance by the collector vehicle. In Chapter 7.10.1 of this EIS, the emissions from the former source are estimated (the total emission of carbon dioxide in the Block A-5 is 1,214 t); the emissions from the latter source are not considered, because there is no effective technical method to estimate them for the time being. Take the main vessels (20,000 TEU container ships) passing through the "East Asia-Panama-Caribbean, East Coast of North America" near the CCZ for example. The daily fuel consumption of this type of vessels at normal speed is about 200 t, and the carbon dioxide emissions are about 640 t. Comparison shows that the total GHG emissions (only from the SSV and EMV) in this test are about two days' emissions from large container ships passing through the CCZ. Since this area has good air dispersal conditions, the cumulative effect of GHG emissions will not be significant.

Timescale wise, in the Block A-5 where this test is to be conducted, the main types of human activities include a very small number of merchant vessels sailing through and a very small number of fishing activities. Other human activities include Minmetals' 2-3 months of resource exploration and environment baseline survey cruises every year. Within the current scientific understanding, these activities have a slight disturbance to the marine environment, so there will be no obvious cumulative impact between this test and other activities in the region.

7.14 Environmental impact mitigation measures in the design of the collector vehicle

To strike a balance between obtaining sufficient and effective test data and reducing the environmental impact of this test as appropriate as possible, we have taken a series of measures in the design of the collector vehicle to try our best to

reduce the potential impact of test collection activities on the physicochemical environment. The main measures are as follows

1) The PCV is generally half scale of the the proposed commercial size (with a collecting capacity of approximately 1/4 scale of a full-size commercial collector vehicle), which is considered to be sufficient to minimize the environmental interference footprint while achieving test objectives.

2) The collection mechanism of the collector vehicle is designed to use a combination of mechanical disturbance and hydraulic transportation to minimize disturbance to sediment in the process of nodule collection.

3) The working height of the collector vehicle can be adjusted according to the variation of micro-topography. Changing the depth of mechanical disturbance teeth inserted into the sediments can reduce the disturbance to the thin soft bottom material, thus minimizing the sediment disturbance.

4) In the rear-drive crawler-belt traveling mechanism, a group of high-pressure jet nozzles are arranged at a proper distance to the crawler belt at the traveling wheel end, and the waterjet from the nozzle will remove the attached deposits between the bottom treads when they leave the ground and start to roll upwards, thus reducing the amount of seabed sediments to the surface of crawler belt.

5) The crawler belts are equipped with surrounding box covers, which will gather the sediment plume formed by traveling disturbance during the traveling of the crawler belt and reduce its dispersal range.

6) The nodule desliming treatment system separates the nodules collected by the collector vehicle from the sediments. A spiral channel structure powered by water pump is adopted to completely separate sediments from nodules on the seabed as far as possible, and the height and speed of discharge after separation are lowered to reduce the dispersal range of sediments on the seabed.

7.15 References

Arndt S, Jørgensen BB, LaRowe DE, Middelburg JJ, Pancost RD, Regnier P. 2013.

Quantifying the degradation of organic matter in marine sediments: A review and synthesis. Earth-Sci Rev. 123:53–86. https://doi.org/10.1016/j.earscirev.2013.02.008

Arranz P, de Soto NA, Madsen PT, Sprogis KR. 2021. Whale-watch vessel noise levels with applications to whale-watching guidelines and conservation. Marine Policy. 134:104776. https://doi.org/10.1016/j.marpol.2021.104776

BGR. 2018. Environmental Impact Assessment for the testing of a pre-protoype manganese nodule collector vehicle in the Eastern German license area (Clarion-Clipperton Zone) in the framework of the European JPI-O MiningImpact 2 research project. [place unknown].

Clark MR, Durden JM, Christiansen S. 2020. Environmental Impact Assessments for deep-sea mining: Can we improve their future effectiveness? Marine Policy. 114:103363. https://doi.org/10.1016/j.marpol.2018.11.026

Davies TW, Duffy JP, Bennie J, Gaston KJ. 2014. The nature, extent, and ecological implications of marine light pollution. Front Ecol Environ. 12(6):347–355. https://doi.org/10.1890/130281

Davies TW, Duffy JP, Bennie J, Gaston KJ. 2016. Stemming the Tide of Light Pollution Encroaching into Marine Protected Areas: Light pollution in marine protected areas. Conserv Lett. 9(3):164–171. https://doi.org/10.1111/conl.12191

Gaston KJ, Bennie J, Davies TW, Hopkins J. 2013. The ecological impacts of nighttime light pollution: a mechanistic appraisal: Nighttime light pollution. Biol Rev. 88(4):912–927. https://doi.org/10.1111/brv.12036

GSR. 2018. Environmental Impact Statement - Small-scale testing of nodule collector components on the seafloor of the Clarion-Clipperton Fracture Zone and its environmental impact. [place unknown].

Hauton C, Brown A, Thatje S, Mestre NC, Bebianno MJ, Martins I, Bettencourt R, Canals M, Sanchez-Vidal A, Shillito B, et al. 2017. Identifying Toxic Impacts of Metals Potentially Released during Deep-Sea Mining—A Synthesis of the Challenges to Quantifying Risk. Front Mar Sci [Internet]. [accessed 2023 Jul 18] 4. https://www.frontiersin.org/articles/10.3389/fmars.2017.00368

Honjo S, Eglinton T, Taylor C, Ulmer K, Sievert S, Bracher A, German C, Edgcomb V, Francois R, Iglesias-Rodriguez MD, et al. 2014. Understanding the Role of the Biological Pump in the Global Carbon Cycle: An Imperative for Ocean Science. oceanog. 27(3):10–16. https://doi.org/10.5670/oceanog.2014.78

Jones KR, Klein CJ, Halpern BS, Venter O, Grantham H, Kuempel CD, Shumway N, Friedlander AM, Possingham HP, Watson JEM. 2018. The Location and Protection Status of Earth's Diminishing Marine Wilderness. Curr Biol. 28(15):2506-2512.e3. https://doi.org/10.1016/j.cub.2018.06.010

Kontar EA, Sokov AV. 1994. A benthic storm in the northeastern tropical Pacific over the fields of manganese nodules. Deep Sea Res Part I. 41(7):1069–1089. https://doi.org/10.1016/0967-0637(94)90019-1

Koschinsky A, Gaye-Haake B, Arndt C, Maue G, Spitzy A, Winkler A, Halbach P. 2001. Experiments on the influence of sediment disturbances on the biogeochemistry of the deep-sea environment. Deep Sea Research Part II: Topical Studies in Oceanography. 48(17):3629–3651. https://doi.org/10.1016/S0967-0645(01)00060-1

Kwan YH, Zhang D, Mestre NC, Wong WC, Wang X, Lu B, Wang C, Qian P-Y, Sun J. 2019. Comparative Proteomics on Deep-Sea Amphipods after in Situ Copper Exposure. Environ Sci Technol. 53:13981–13991.

Levin LA, Mengerink K, Gjerde KM, Rowden AA, Van Dover CL, Clark MR, Ramirez-Llodra E, Currie B, Smith CR, Sato KN, et al. 2016. Defining "serious harm" to the marine environment in the context of deep-seabed mining. Marine Policy. 74:245–259. https://doi.org/10.1016/j.marpol.2016.09.032

March D, Metcalfe K, Tintoré J, Godley BJ. 2021. Tracking the global reduction of marine traffic during the COVID-19 pandemic. Nat Commun. 12(1):2415. https://doi.org/10.1038/s41467-021-22423-6

McQuaid KA, Attrill MJ, Clark MR, Cobley A, Glover AG, Smith CR, Howell KL. 2020. Using Habitat Classification to Assess Representativity of a Protected Area Network in a Large, Data-Poor Area Targeted for Deep-Sea Mining. Front Mar Sci. 7:558860. https://doi.org/10.3389/fmars.2020.558860

Navarro-Barranco C, Hughes LE. 2015. Effects of light pollution on the emergent fauna of shallow marine ecosystems: Amphipods as a case study. Mar Pollut Bull. 94(1–2):235–240. https://doi.org/10.1016/j.marpolbul.2015.02.023

NORI. 2022. Collector Test Study – Environmental Impact Statement – Testing of polymetallic collector system components in the NORI-D contract area, Clarion Clipperton Zone, Pacific Ocean. Jamaica.

Pälike H, Lyle MW, Nishi H, Raffi I. 2014. The Pacific Equatorial Age Transect. In: Developments in Marine Geology [Internet]. Vol. 7. [place unknown]: Elsevier; [accessed 2023 Jul 22]; p. 329–357. https://doi.org/10.1016/B978-0-444-62617-2.00013-X

Shi P, Yang J, Sun D, Wang C. 2023. A simulation from offsite disturbance experiments on the metal resuspension process in the seafloor of the Western Pacific. Chemosphere. 311:137042. https://doi.org/10.1016/j.chemosphere.2022.137042

Stratmann T, Mevenkamp L, Sweetman AK, Vanreusel A, Van Oevelen D. 2018. Has Phytodetritus Processing by an Abyssal Soft-Sediment Community Recovered 26 Years after an Experimental Disturbance? Front Mar Sci. 5:59. https://doi.org/10.3389/fmars.2018.00059

Williams B, McAfee D, Connell S. 2022a. Oyster larvae swim along gradients of sound. J Appl Ecol. 59(7):1815–1824. https://doi.org/10.1111/1365-2664.14188

Williams R, Erbe C, Duncan A, Nielsen K, Washburn T, Smith C. 2022b. Noise from deep-sea mining may span vast ocean areas. Science. 377(6602):157–158. https://doi.org/10.1126/science.abo2804

Yang J, Nie H, Sun D, Wang C. 2023. Environmental controls on the distribution of metals in porewater and their diffusion fluxes at the sediment-water interface of the western Pacific. Appl Geochem. 148:105520. https://doi.org/10.1016/j.apgeochem.2022.105520

8 Assessment of Impacts on the Biological Environment and Proposed Mitigation Measures

8.1 Key information

This Chapter analyzes the potential impacts of this collector vehicle test on the biological environment, and introduces multiple measures for mitigating environmental impact.

This collector vehicle test aims to verify its technical feasibility and reliability, and to collect the environmental disturbance data under different operation conditions. These key data are indispensable for developing a collector vehicle that is technically reliable, economically feasible and with only moderate environmental disturbance. The biological environment baselines in and around the Block A-5 have been described in Chapter 5 of this EIS. The assessment in this Chapter is based on the above-mentioned contents, relevant literature and/or reports, established sediment plume dispersal and redeposition model, etc.

On the one hand, we have identified the potential impact of the collector vehicle at four different depths/habitats in the water column: (1) atmosphere, (2) sea surface and euphotic zone (0-200 m depth), (3) mesopelagic zone (200-1,000 m depth), (4) deep layer (1,000 m water depth to 200 m above the bottom) and (5) bottom layer (water columns and seabed within 200 m above the bottom). In Table 8.2-1 below, we explain the specific contents of these potential impact categories at different water depths. The purpose of identification is to focus on the most important environmental impact on the biological communities and ecosystems in this region on the basis of a comprehensive description of the impacts of this test on the environment. On the other hand, we have described these potential impacts in the order of surface layer, middle layer, bottom layer, community/ecosystem and cumulative impact.

Since this test does not involve large-scale ore/sediment lifting and tail water discharge, and the total test duration is controlled to the shortest, the potential

environmental impact of this test is mainly in the bottom layer and slight on biological communities living in other depths/habitats.

8.2 Description of potential impact categories

All potential sources of environmental impact in this test include the following two types of activities, which are not overlapped and located outside and inside the Block A-5 respectively.

(1) Outside the Block A-5, there will be mainly noise and direct collision of the SSV/EMV with whales, turtles and other large marine organisms during their trip between the Zhoushan home port in China and the Block A-5 of the Contract Area in the CCZ. Since ocean-going vessels will not turn on high-illuminance lighting facilities during normal navigation, there is no impact of artificial lighting on marine organisms at this stage.

(2) Inside the Block A-5, there will be mainly the following potential environmental disturbance categories:

a The collector vehicle test, including nodule removal, sediment removal and sediment disturbance, will change the original habitat. This will have an impact on benthic microorganisms, meiofauna, macrofauna, megafauna and nodule fauna.

b The collector vehicle test will cause the plume dispersal of sediments, which may further lead to the burial effect on benthic fauna caused by sediment redeposition;

c Lighting from the collector vehicle, SSV/EMV and ROV, especially disturbance to phototactic plankton and nekton;

d Noise from the collector vehicle, SSV/EMV, especially disturbance to large marine mammals (e.g. whales);

e The potential leakage of toxic substances (e.g. fuel oil, lubricating oil and hydraulic oil) from the collector vehicle, SSV/EMV and ROV may lead to acute toxic effects on plankton.

Table 8.2-1 Biological community components to be impacted in this test

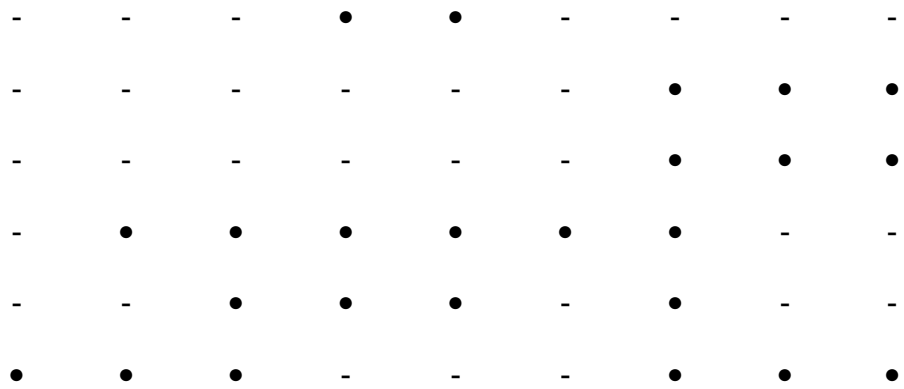

Note 1: See above section for the definition and detailed description of "potential impact categories".

Note 2: The categories of biological community components are as follows:

A. Phytoplankton and other primary producers
B. Zooplankton
C. Nekton (e.g. fish and cephalopods) in the surface and middle depth (excluding bottom-layer nekton)
D. Whales
E. Turtles
F. Seabirds
G. Bottom-layer nekton and scavengers
H. Benthic fauna
I. Nodule fauna

8.3 Surface layer

8.3.1 Potential impacts and problems to be solved

In this test, the SSV and EMV will sail from Zhoushan Port in China and to the Block A-5 of the Contract Area in the CCZ. During the survey cruise, both vessels will strictly abide by IMO regulations, especially the requirements on exhaust emission and garbage disposal. During their survey cruise and operation in the CTA of the Block A-5 of the Contract Area, no KBA (Figure 8.3-1) or IMMA (Figure 8.3-2)

will be involved. Based on the location beacon tracking data of 23 kinds of top-tier/large marine organisms (e.g. turtles, whales, sharks and seabirds) in the North Pacific Ocean, we judge that the CTA is not an important habitat for most of these top-tier predators (Figure 8.3-3) (Block et al. 2011). Only leatherback turtles are commonly seen in this region. However, this species is distributed globally, and their main spawning areas are the Caribbean Sea and the coast of West Africa (https://www.fisheries.noaa.gov/species/leatherback-turtle). The CCZ is not an area for leatherback turtles in their key life stages (spawning area and nursery). Therefore, the overall potential risk to large, rare and endangered marine animals such as marine mammals, seabirds and turtles is very low.

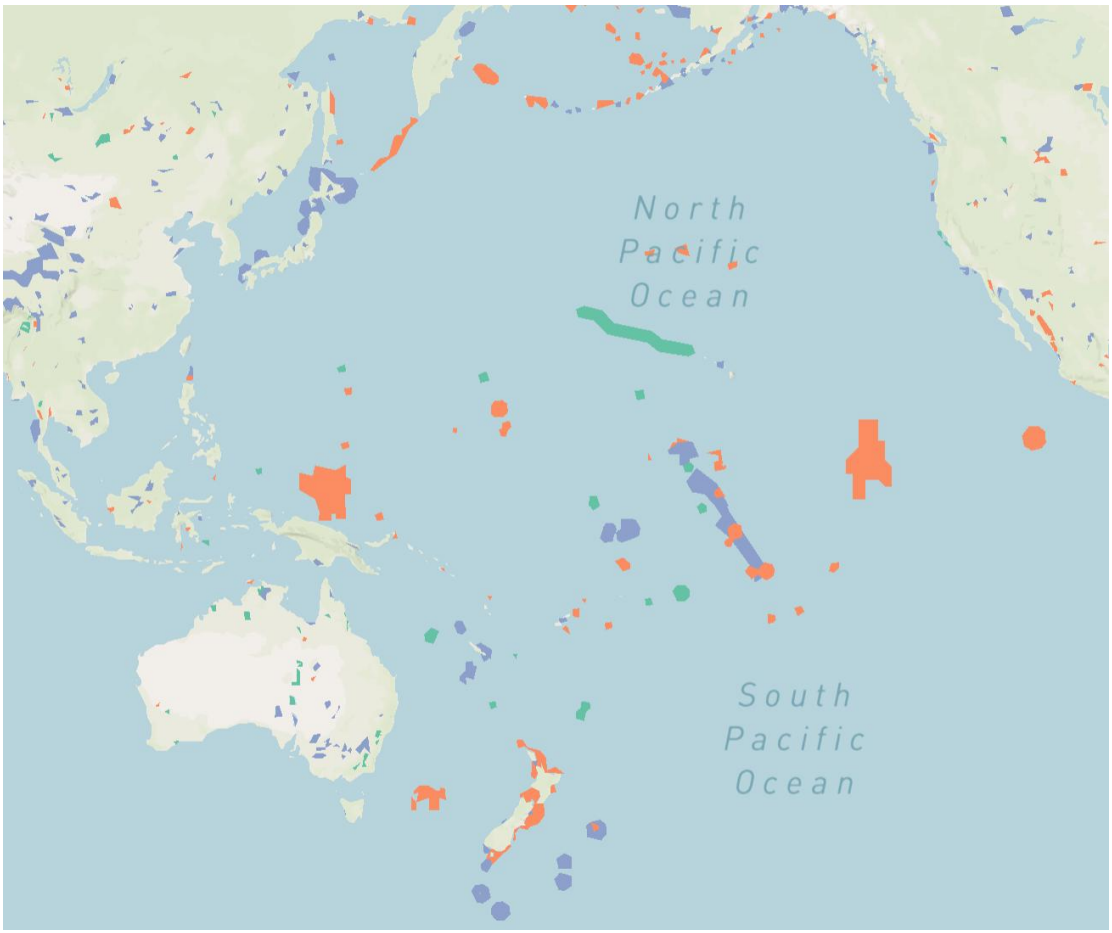

Figure 8.3-1 KBAs in the Pacific Ocean

(Map from: Protected Planet Report 2020)

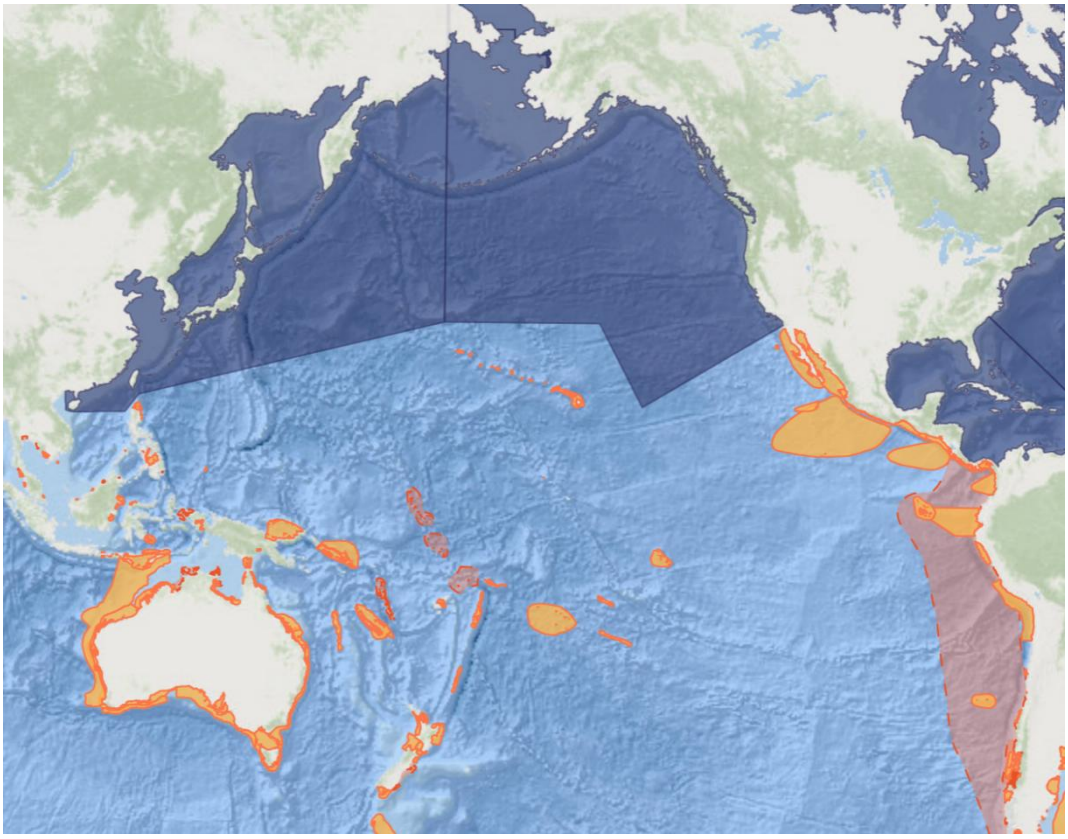

Figure 8.3-2 IMMAs in the Pacific Ocean

(Map from: https://www.marinemammalhabitat.org/)

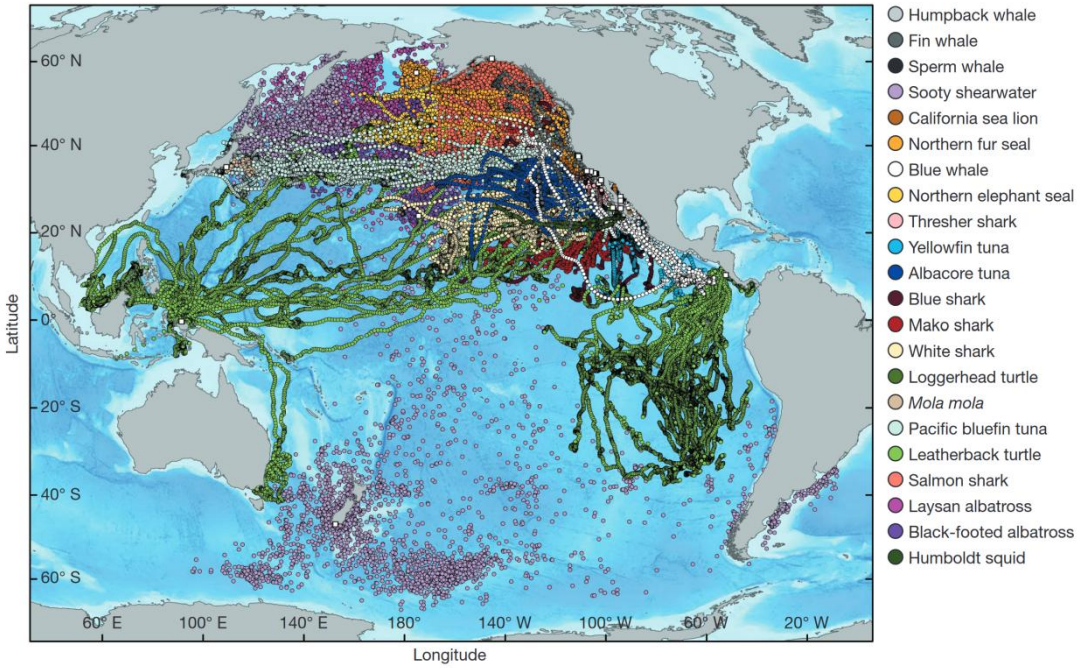

Figure 8.3-3 Distribution of 23 top-tier marine predators in the Pacific Ocean(Block et al. 2011)

8.3.1.1 Noise

Although the noise generated by vessels may have adverse effects on seabirds, turtles, marine mammals, etc., including behavioral effects on their feeding, reproduction, migration and even direct death (Hawkins et al. 2020; Duarte et al. 2021), it is generally believed that whales can be protected from the serious adverse effects of noise when they are 500 m away from vessels with underwater noise of 150 dB re 1 μPa (Arranz et al. 2021). However, it should be noted that the quantitative assessment of this impact degree is largely limited by the tolerance threshold of whales to underwater noise. For example, if this threshold is set at 130 dB re 1 μPa, it is obvious that marine organisms in a farther range will be threatened by noise (Williams et al. 2014). Recent studies on the stricter threshold (120 dB re 1 μPa) show that the direct impact of mining activities on marine mammals will extend to a radius of 4-5 km (Williams et al. 2022b). In this assessment, one of the main difficulties at present is the lack of direct observation data of the main cetaceans affected by noise from human activities in deep ocean areas with low frequency and intensity of human activities, such as the CCZ in the East Pacific Ocean. A large number of similar studies have been conducted in coastal areas or areas with frequent human activities and serious underwater noise from various human sources (Rolland et al. 2012), and the target species and populations of these studies will be subjected to cumulative impacts from multiple sources. Some studies also show that strong noise may also affect invertebrate larvae (Williams et al. 2022a), but such studies also lack reference data in deep-sea environment and for deep-sea species. Considering that the tonnage of the vessel used in this test is significantly smaller than that of the vessel used in NORI's test in 2022, and referring to the results of its EIS (NORI 2022), we reckon that the impact of water surface noise generated in this test on marine organisms is low and the scope is small.

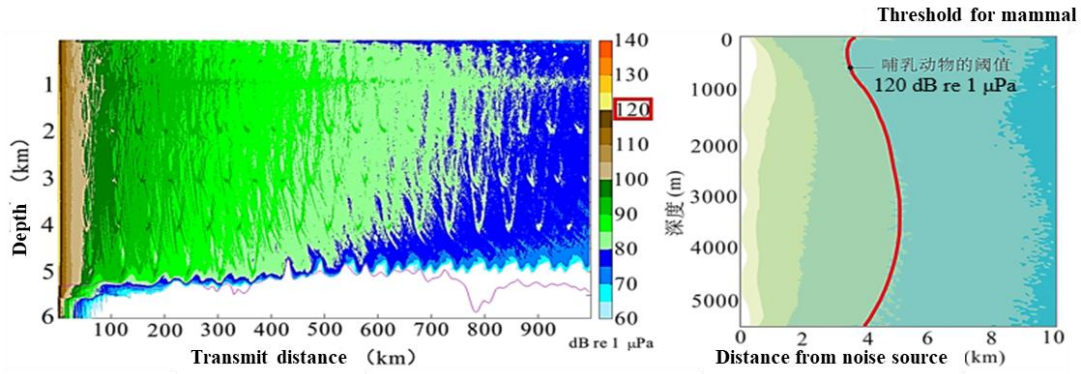

Figure 8.3-4 Simulated propagation distances of seabed mining noise (Williams et al. 2022b)

8.3.1.2 Light

Although light trapping has been widely used in marine fisheries for a long time (Nguyen and Winger 2019), lighting disturbance caused by human activities has been universally regarded as an environmental problem with significant adverse effects on marine organisms in recent twenty years (Longcore and Rich 2004). For example, a lobster fishing boat will emit bright light at night, which may cause seabirds (e.g. sea swallows) to lose their way and even crash into the boat and die (Ryan et al. 2021). Intense artificial lighting near the sea is also considered to significantly affect the navigation ability of turtle hatchlings to correctly orient towards ocean and enter the seawater as soon as possible after breaking out of their shells, which will have a significant impact on the continuation and maintenance of turtle population (Kamrowski et al. 2015). The more significant impact of artificial lighting may be on species that migrate vertically between the upper and middle layers, such as small squid and some zooplankton (Song et al. 2022). Since these organisms usually sink to the mesopelagic zone during the day and float to the euphotic zone at dusk and night, they can meet their feeding needs while avoiding visual predators to the maximum extent, and long-term artificial light at night will induce predators of these organisms to gather and prey, thus causing certain interference to the normal interspecific relationship (Gaston et al. 2013; Davies et al. 2014). The duration of this test is limited (no more than several weeks) and the intensity of light source is significantly weaker than that of squid fishing boats commonly seen in the East Pacific Ocean.

Therefore, we reckon that the water surface illuminance generated in this test has a low impact on marine organisms.

8.3.1.3 Potential impacts on the planktonic ecosystem

This test only involves the collector vehicle. Under normal circumstances, it will not produce surface discharge (e.g. tail water), so there is no impact on the planktonic ecosystem in the surface layer of the ocean.

8.3.2 Environmental management measures to mitigate impacts

8.3.2.1 Noise

We will equip professionals to observe and monitor the activities of large marine organisms (e.g. turtles and whales) around the vessels during the cruise and test in the Block A-5. adopting proactive collision avoidance measures to avoid damage to these organisms.

The underwater noise levels of the SSV and EMV meet the requirements of IMO and China for vessels of the same class, so as to minimize the noise impact on marine organisms.

8.3.2.2 Light

We will refrain from unnecessary lighting during the cruise and test in the Block A-5. During the test, both the SSV and EMV only use necessary lighting to ensure the safety of normal operation, especially when the collector vehicle is conducting tests underwater, the SSV will turn on the lighting facilities on the whole deck at night.

8.3.2.3 Others

The SSV and EMV used in this test meet the requirements of "International Management Code for the Safe Operation of Ships and for Pollution Prevention" (ISM Code-1993) and the Annex 1 of "International Convention for the Prevention of Pollution from Ships". They will not discharge or discard substances that may cause pollution or harm to the marine environment, and will strictly abide by the above provisions during the test.

During the deck preparation, the collector vehicle to be tested will not cause uncontrollable discharge of toxic and harmful substances. Necessary chemicals (e.g. hydraulic oil) required for equipment test will be properly controlled. Wastes generated will be stored properly instead of being dumped into the sea.

8.3.3 Residual impact

Different from other impact sources, artificial noise and light can be regarded as non-persistent point source impact. That is, once the source is removed, its impact will drop rapidly (Parsons et al. 2020). Therefore, there is no residual impact on the surface layer.

8.4 Middle layer

There are zooplankton, small nekton and other marine biological groups in the middle ocean layer of the CTA. Most of them are sensitive to light. While being lowered the deck to the seabed, the collector vehicle does not need to turn on lighting facilities, so there is no lighting disturbance on the midwater biological communities. To maintain the posture of the collector vehicle and ensure the safety of the collector vehicle and the load-bearing steel cable during the lowering process, the small propeller of the collector vehicle will be started when necessary. Similar to that on the ROV, this small propeller features low noise, which is expected to only have a slight noise impact on the midwater biological communities.

Different from the whole system test, there will be only the collector vehicle test this time, so it does not bring discharge or impact to the middle layer. There is no facility to produce light and noise in the middle layer except necessary steel cables and power cables. Therefore, we believe that the impact of this test on the midwater biological communities is slight.

8.5 Bottom layer

8.5.1 Potential impacts and problems to be solved

8.5.1.1 Immediate impact

In the Block A-5 of the Contract Area, meiofauna are mainly distributed in the surface layer of sediments (0-4 cm, this depth accommodates more than 95 % of the total biomass). About half of the meiofauna are distributed in the uppermost layer of sediments (0-1 cm). In other blocks of the CCZ, the vertical distribution of meiofauna also presents similar characteristics (Tong et al. 2022). Our studies also found that the spatial distribution of meiofauna in the Block A-5 was relatively uniform (Figure 5.4-30). This spatial distribution uniformity in the middle and small scale is similar to that in the NORI-D region (NORI 2022). Similar results have also been found in the Central Indian Ocean Basin (Singh et al. 2019). There is no contradiction between the uniformity of the above-mentioned meiofauna community density on the middle and small scale and its strong gradient on the large scale (for example, the spatial scale of the whole CCZ) (Tong et al. 2022). On the large scale, the trend that the meiofauna community density gradually increases from west to east is consistent with the strong gradient of primary production in this region (McQuaid et al. 2020).

The depth of sediment disturbance by the collector vehicle's collector head is approximately 4-6 cm (it depends on the buried depth of nodules and can be adjusted to realize the shallowest sediment disturbance while effectively collecting nodules). The direct depth of disturbance by the collector vehicle's crawler belts is approximately 10 cm; there will inevitably be a certain degree of subsidence impact on deeper sediments. After the sediment around the nodule is sucked away by the collector head, the organisms in the sediment are inevitably caught in the collector head, and then dispersed or re-settled with the ocean current. This process may lead to the direct death of some organisms living in the sediments or being eaten by larger organisms, thus reducing the biological density. The DISCOL and the BIE in the

1980s and 1990s revealed the long-term impact of simulated disturbance on benthic fauna after sediments were removed. During the 1988-1998 DISCOL in Germany, the environmental variations were surveyed before and after the simulated disturbance (six months, three years and seven years). Results showed that the abundance of all fauna except bacteria decreased significantly after the disturbance, and did not reach the value of undisturbed sediments after half a year. After seven years, although the density of macrofauna recovered to the original level, the species composition of Polychaeta was significantly lower than that before disturbance (Schriever et al. 1997). Further studies show that the Nematoda community had not recovered to its original state after 26 years. The total density and biomass of Nematoda communities in the disturbed track were significantly lower than those outside the track, and the biodiversity index showed that the diversity of *Nematoda* in the track was significantly lower, and the structure of Nematoda communities in the track was significantly lower than that in two undisturbed sites outside the track (Miljutin et al. 2011). Therefore, the collector vehicle passes will have a serious direct impact on the meiofauna community in the area it travels.

This test only has a direct collection area of approximately 0.1 km^2 while Block A-5 has an area of 22,821 km^2. Since the area with direct disturbance this time is only 0.000438 % of the total area of the Block A-5, we infer that the overall scale of direct impact is small, and the overall impact on the vast deep-sea ecosystem of the CCZ is even smaller.

8.5.1.2 Nodule removal

From a global perspective, the deep-sea plain is generally a soft substrate environment, and the proportion of hard basement required by sessile fauna is very low (Riehl et al. 2020). In the CCZ, nodules provide a hard basement for Anthozoa, Porifera, Vestimentifera, Crinoidea and so on, and constitute a unique and important micro-habitat (Simon-Lledó et al. 2019). The results of ROV survey in the CCZ show that the density of epifauna in the area with high nodule coverage is more than twice

as high as that in the area without nodules, and almost no key sessile fauna such as soft Anthozoa and black Anthozoa are found in the area without nodules (Vanreusel et al. 2016). These fauna will be directly affected by the operation of the collector vehicle. The collector vehicle test this time will remove most of nodules on the nodule-collecting track, which obviously will destroy almost all the surface life-forms such as Porifera, Anthozoa, and Crinoidea attached to these nodules. A track disturbed by the test-mining 37 years ago was also re-investigated in the study, and it was found that there was almost no redistribution of the above-mentioned megafauna on the nodule mining track, which indicated that mining would permanently destroy the nodule habitat and lead to the extremely slow recovery of such nodule fauna (Vanreusel et al. 2016).

When the collector vehicle travels, organisms with weak mobility (e.g. Asteroidea, sea urchins and sea cucumbers) will be crushed to death or sucked into the collector vehicle and then minced because they have no time to escape. Besides, due to the removal of nodules, the larvae of sessile benthic communities moved in from outside the Contract Area will die soon because they cannot find the needed hard basement to attach.

In addition to the megafauna such as Porifera and Anthozoa, there are many kinds of microorganisms, Protozoa and Metazoa (e.g. Nematoda) attached to nodules, which constitute the nodule biological communities (Thiel et al. 1993). There is a significant difference in the community structure between the organisms in the cracks of nodules and the meiofauna in the surrounding sediments. The former is small in size and low in density, and the genera *Camacolaimus*, *Leptolaimus* and *Acantholaimus* are abundant. Among them, *Camacolaimus* may be the dominant genus of Nematoda in nodule cracks. Studies have found that there are significant differences in the species composition of Nematoda between the areas with and without nodules in the French Contract Area of the CCZ, and the density of Nematoda in the areas without nodules is twice as high as that in the areas with nodules

(Miljutina et al. 2010). However, the results of study in the nodule areas of the Central Indian Ocean Basin show that the diversity of Nematoda distributed in the crevices of nodules is low, but the existence of nodules may help to increase the density of *Leptolaimus* and *Camacolaimus*. These suggests that these two genera may be endemic genera in the nodule micro-habitat (Singh et al. 2019). It can be inferred from these evidences that the disappearance or disturbance of this micro-habitat will inevitably lead to a decrease in the biodiversity of local meiofauna living in the crevices of nodules. However, there still lacks quantitative studies for the time being.

This test only has a direct collection area of approximately 0.1 km^2 while Block A-5 has an area of 22,821 km^2. Since the area with direct disturbance this time is only 0.000438 % of the total area of the Block A-5, we infer that the overall scale of direct impact is small, and the overall impact on the vast deep-sea ecosystem of the CCZ is even smaller.

8.5.1.3 Sediment plume and sediment cover

The organic carbon content in deep-sea sediments is approximately two levels of magnitude lower than that in the particles deposited in the upper layer (Kim et al. 2015). Therefore, although there are a lot of particles in the sediment plume caused by resuspension, these particles are not a good food resource, which means it is unlikely to provide an additional food source for benthic fauna.

The sediment of larger particles in the plume will soon fall to the seabed, which is expected to have a direct impact on hypobenthos, such as physical burial/suffocation effect, blocking breathing and filter feeding organs, or releasing potential toxic or oxygen-depleting substances. The finer particles in the plume have a slow settling speed, and will stay in the water for a long time. They will spread under the action of the bottom-layer ocean current and redeposit in a large area of the seabed. If the organisms in these plume dispersal areas are disturbed by low-level deposition for a long time, there will also likely be chronic impacts. The said impacts are in the following aspects:

（1） **Physical burial/suffocation effect:** Physical burial/suffocation effect is one of the focuses of biological impacts related to plume and redeposition.

When faced with the plume caused by a limited-scale collector vehicle, organisms with strong swimming ability can escape quickly and proactively to avoid such impact. However, there may be a negative impact on epifauna close to the disturbance source, with poor mobility or no mobility at all, such as Opiuroidea, Porifera and Anthozoa. For example, existing deep-sea studies have tested and observed the different reactions of Anthozoa and Porifera exposed to various types of particles: When exposed to fine SPM, a cold-water stone Anthozoa (*Lophelia pertusa*) significantly reduced its bone growth rate, and its respiration and fatty acid ratio in tissues were not significantly negatively affected, but at the same time, this study also found that Anthozoa larvae may be particularly vulnerable to high-concentration particles (Larsson et al. 2013). With short-term (4 h) high-concentration particle stress, the metabolic oxygen consumption rate of some *Geodia baretti* will be significantly reduced by 50 %, but once the SPM load returns to the background level, the oxygen consumption will quickly return to the level before contact. However, after 29 days of continuous exposure to high-concentration SPM (50 mg/L), the metabolic oxygen consumption rate of sponge will be permanently reduced by 60 %, which indicates that the tolerance of sponge to persistent physical stress is low (Kutti et al. 2015).

（2） **Obstructing breathing and filtering:** For zooplankton near the bottom or other fauna that breathe through gills, high-concentration SPM may block gills or other filtering organs, thus impairing their respiration and feeding capacities, and even causing the death of zooplankton such as Copepoda and krill (Anderson and Mackas 1986). There is a view that DO in the water column may be consumed by the oxygen-consuming decomposition of microorganisms after the bottom-layer sediments are released into the water column, which may lead to the deoxygenation of the near-bottom-layer seawater. Nevertheless, this problem can be ignored in the deep-sea area where the bottom-layer water column is well exchanged (Christiansen et al. 2020).

（3） **Lowering the quality of food:** After being covered by sediment plume, the passive intake of particles with low nutritional value will lead to an

increase in energy consumption, which in turn will lead to a decrease in energy intake and eventually lead to de facto hunger. At the level of food web, this will further affect organisms with high trophic level through trophic cascade effect (Christiansen et al. 2020). Studies on Copepoda with different feeding habits show that herbivorous and omnivorous Copepoda (*Undinula vulgaris*, *Euchaeta rimana*, *Labidocera acutifrons* and others) will ingest SPM in mining tail water, but for *Oncaea venusta*, which mainly eats debris (sea snow), it is not easy to ingest SPM in these mining tailings (Hu 1981). However, so far, the data of this kind of studies are obtained in the at-sea and upper-layer ocean, and the studies data for hypobenthos are still very scarce.

（4） **Olfactory interference:** Olfactory sensation may be the main mechanism to attract and guide benthic scavengers to prey on food (Sainte-Marie 1992). The sediment plume produced by mining activities will interfere with the odor plume released by food, reduce the probability of finding food, and may lead to a general decrease in the food supply of scavengers, which will further affect other high-trophic organisms in the food web through the trophic cascade.

（5） **Visual interference:** Although sunlight cannot penetrate the thick seawater to reach the depth of 1,000 m, vision is not generally degraded in hypobenthos. Instead, it plays a key role in intraspecific and interspecific communication, such as predation, escaping from enemies and finding mates (Warrant and Adam Locket 2004). Many hypobenthos can emit light by themselves. Such bioluminescence is also of great significance to their life activities (Haddock et al. 2010). The increase of turbidity/SPM concentration in sediment plume caused by mining activities will weaken the light transmittance, so it may have adverse effects on visual organisms and luminous organisms.

According to the sediment plume dispersal model and sediment redeposition model we constructed, the sediment redeposition range in this test is measured by the threshold of 0.1 mm redeposition thickness, and the maximum area is no more than 1 km^2 (see Section 7.5 of this Chapter). These two areas account for 0.0044 % of the

Block A-5, so we infer that sediment redeposition will not cause great disturbance to the benthic communities. It should also be pointed out that the studies on the direct effect of sediment burial on benthic fauna are not sufficient at present. In the similar sediment burial experiments conducted with shallow-sea species, it was found that macrofauna can tolerate in-situ sediment burial of less than 3 mm (Schaanning et al. 2008). If the benthic communities in the deep sea have similar tolerance, this assessment may also overestimate the potential environmental impact caused by the coverage of plume redeposition.

8.5.1.4 Release of heavy metals

The release of toxic substances caused by seabed mining activities is considered as one of the important environmental impacts (Levin et al. 2016). In the extensive oxidation environment in the bottom layer of the CCZ, it is unlikely that the properties of oxidized minerals will be changed due to simple mechanical disturbance and result in large-scale release of heavy metals (BGR 2018). There are a lot of nutrients and heavy metals in the pore water of surface-layer sediments in the nodule area. The simulated disturbance experiment shows that the release of heavy metals has significant element specificity (Shi et al. 2023), and only four kinds of heavy metals (i.e. vanadium, rubidium, molybdenum and cadmium) with significant and stable precipitation behavior. Similar results have also been found in other people's studies (Koschinsky et al. 2001). See Section 7.6 for the results.

The EIA for the above-mentioned heavy metal release behaviors is based on the data of toxicological studies. In fact, most toxicological studies aiming at the EIA for seabed mining are limited by various conditions and have to use shallow water and at-sea biological species as test organisms (Yamagishi et al. 2019). Before MIDAS started, there was no toxicological assessment record of hypobenthos as test subjects in the database of EPA in the United States in 2013, (Hauton et al. 2017). Since today's mining processes and technologies do not involve discharge in the surface and middle layers of the ocean, the data of toxicological assessment using shallow water and at-sea species cannot be directly used as the basis for EIA for seabed mining activities. Some studies have compared the effects of low-temperature and high-pressure environment in deep sea on the results from the toxicity assessment of many heavy metals. Using high-pressure and low-temperature culture equipment, these

studies found that the toxicity of copper increased significantly under high hydrostatic pressure, while the toxicity of cadmium did not increase significantly (Brown et al. 2017a). Some studies have put forward the method of "temperature correction factor", trying to convert a large number of toxicological test data under normal temperature and pressure to assess the actual toxicity under different temperature backgrounds (Wang et al. 2014). This method may not be helpful in solving the toxicological assessment problems in seabed mining environment, because under high hydrostatic pressure, a "temperature correction factor" for any metal is inconsistent and must be determined according to experience and actual species (Hauton et al. 2017). Therefore, it is still difficult to accurately assess the toxicity of seabed mining to the bottom-layer ecosystem on the basis of available data.

In addition to the above-mentioned toxicological assessment with the semi-lethal concentration (LC_{50}) as the key parameter, a large number of studies have found that organisms can proactively escape when facing the threat of heavy metals so as to avoid or alleviate the behavioral response to heavy metal stress (Hauton et al. 2017). Brown et al. compared the behavioral responses of shallow-water and deep-sea species to the toxicity of heavy metals. In the toxicological experiment at 4 °C in the laboratory, the sea cucumber was observed to climbed to the side of the experimental pool to avoid being polluted by copper with a concentration of 5 mg/L. In the exposure experiment of copper-polluted sediments in the Peruvian basin at the depth of 4,167 m, deep-sea sea cucumbers were also observed to have similar avoidance behavior (Brown et al. 2017b). The results of this study suggest that it is very likely for hypobenthos to escape from heavy metal stress. When faced with heavy metal stress in sediment plume, benthic fauna in nodule areas can make similar escape reactions.

8.5.1.5 Noise

The main noise sources of seabed mining activities include the SSV, the riser/lifting system, the collector vehicle, etc. In this test, the riser/lifting system is not involved, so the impact on the bottom layer is mainly caused by the collector vehicle. Besides, the noise of the SSV can also vertically spread to the deep seabed (NORI 2022).

A great deal of noise will be inevitably produced during the operation of the

collector vehicle. This also has potential impact on the deep-sea bottom layer and aquatic organisms. However, studies in this aspect are scarce at present. Monitoring data about background noise in the deep-sea bottom layer of the western part of the CCZ are limited. There are only long-time series data collected from the water depth of 300 m (see 4.10). Studies have found that the background noise of the Mediterranean deep-sea environment does not exceed 50 dB in the frequency range of 10-45 kHz and 60 dB in the lower frequency range of 2-10 kHz. It can be inferred that most hypobenthos may live in a low-noise environment (Riccobene 2009). There is a significant difference between sound frequencies of toothed whales and baleen whales. The former often reaches 3-5 kHz, while the latter can be as low as 30 kHz. Bottom-layer fish usually communicate with low-frequency (<1.2 kHz) sounds (Rountree et al. 2012). Generally speaking, the main frequency of sound produced by percussion mechanism in mechanical noise is below 1,000 Hz, while the main frequency of sound produced by friction pronunciation mechanism is in the range of 3,000-5,000 Hz. The durations, pulse intervals and other characteristics of these sounds vary greatly, which may affect the exchange of information and induce species-specific reactions. There is evidence that fish will respond to the calls of the same species during mating, the calls of potential predators, the calls of prey and the sounds that bounce off objects during echolocation.

See 3.3.2 for the detailed engineering description of the collector vehicle. The noise level of the equipment has not yet been tested in the deep-sea environment. Considering that the collector vehicle's collecting capacity and power are similar, we refer to the NORI test result (NORI 2022) for estimation in this regard. According to the threshold of 120 dB re 1μPa rms, the horizontal impact can extend to a radius of 562 m (i.e. approximately 0.99 km^2). According to the latest estimation, the horizontal disturbance of the collector vehicle's noise in the bottom layer can extend to a radius of approximately 4 km (Figure 8.3-4) (Williams et al. 2022b).

8.5.1.6 Light

The collector vehicle needs a light source to illuminate the seabed along the mining path, so that the operator can accurately control the operation and avoid risks. The ROV, AUV and lander used for survey, monitoring and maintenance will also emit strong light when necessary. Sunlight cannot penetrate into the deep sea with depth of 1,000 m, and many hypobenthos have no eyes or photosensitive organs at all. However, many fish and invertebrates have not completely lost their photosensitive ability. There are few examples of artificial light sources causing direct biological stress in the deep sea. It has been found that some deep-sea shrimps living in hydrothermal vents will suffer permanent damage to their retinas when they are illuminated by floodlights on manned submersibles (Herring et al. 1999). Considering the small scale and short duration of this test, we believe that the risk of such impact is low.

8.5.2 Environmental management measures to mitigate impacts

During the test, multiple measures will be taken to minimize or mitigate the environmental impact.

（1） Disturbance of the collector vehicle to bottom-layer sediments

During the test, we will adopt multiple measures to reduce the disturbance of bottom-layer sediments, including: (1) Reasonable arrangement of test plan, trying to reduce the traveling distance and disturbed area of the collector vehicle on the premise of completing necessary test contents; (2) Optimizing the design of the collector vehicle's collector head and crawler belts according to laboratory test results, and installing crawler belt covers to reduce the depth of sediment disturbance; and (3) Developing a nodule density identification device, so as to shut down the collector vehicle's collector head in the areas with low nodule density. See sections 3.3 and 7.14 for details.

（2） Impact of noise from the collector vehicle

During the test, we will adopt multiple measures to reduce the impact of noise from the collector vehicle, including: (1) Reasonably arranging the plan for collector vehicle test, and reducing the duration of full-power operation on the premise of completing necessary test contents; (2) Adding simple noise shielding devices on main noise sources (e.g. crushing devices, hydraulic pumps, etc.) to slow down the spread of noise; and (3) Reasonably arranging the plan for collector vehicle test to shorten the working duration of underwater positioning device, thus reducing the noise generated by underwater positioning.

（3） Lighting disturbance from the collector vehicle and support equipment such as the ROV and AUV

During the test, we will refrain from using unnecessary lighting as appropriate as possible. When the collector vehicle, ROV, AUV and other equipment are being lowered through the mesopelagic zone (water depth of 200-1,000 m) with relatively dense organisms, the underwater lighting and other facilities will not be turned on. While working underwater, the AUV will not turn on lateral and forward lighting devices. Only illumination on the seabed below will be turned on during the near-bottom optical survey, so as to avoid the interference of artificial light source to a wider area. During the operation of the collector vehicle, the illuminance of the lighting facilities will be controlled to the minimum level for safe operation. Disorderly and excessive illumination will be avoided.

8.5.3 Residual impact

The residual impact on the benthic communities is mainly reflected in two aspects. First, after the nodules are collected and removed, the nodule fauna cannot colonize because they lose the hard basement on which they depend, which will lead to the lack of necessary conditions for the subsequent growth of these organisms in the range (0.1 km^2) where the collector vehicle travels and collects directly in this test, thus leading to the loss of nodule fauna in the benthic communities in this small area. Second, within the impact scope of sediment plume cover (measured by the threshold

of 0.01 mm redeposition thickness, the maximum area does not exceed 1 km^2), organisms will be impacted by the burial of habitats by sediments. According to the data of DISCOL, this effect will last for several years to decades depending on the different responses of different biological taxon.

8.6 Cumulative impact

The cumulative impact of human activities on the marine ecosystem is very complex. The cumulative impact of different stressors on specific components in the ecosystem can show additive effect, synergistic effect or antagonistic effect, while the interaction types of different stressors in the cumulative impact will also change with the organizational level and trophic level in the ecosystem (Crain et al. 2008). The disturbance of this test-mining is mainly in the bottom layer. As mentioned above, direct factors such as the removal of nodules, sediment disturbance (removal, compaction, redeposition, etc.), plume containing high concentration of SPM, release of heavy metals, noise and light, as well as potential factors such as the variation of DO concentration and conductivity incurred therefrom are the stressors to the groups of microorganisms, meiofauna, macrofauna, megafauna, nodule fauna and benthic nekton in benthic communities. So far, there lacks quantitative study on the cumulative impact of disturbed deep-sea ecosystems on a regional scale. For example, the cumulative impact of the Mediterranean deep-sea ecosystem under the pressure of climate change and human activities was studied by using the quantitative analysis method of food web (Ecosim with Ecopath). It was found that the impact caused by trawl fishing grounds may be more serious than the reduction of sea snow caused by climate change (Tecchio et al. 2015). In the Peruvian basin in the Southeast Pacific Ocean, based on the disturbance of the DISCOL experiment conducted in 1989 to the seabed, the study team revisited the test area in 2015, and built a relatively comprehensive food web model based on multi-source data to assess the recovery of the deep-sea ecosystem function after 26 years (De Jonge et al. 2020). Regrettably, there is no similar food web model in the CCZ, and there is no observation data on the

impact of different disturbance pressure sources on different key components in the food web. Therefore, similar quantitative methods cannot be used in this project area.

NORI's EIS classifies the stressors of cumulative impact as follows. Type I is the sum of different stressors that have, are, or may have an impact on the ecosystem. Type II refers to the repeated effects of the same type of stressors on the ecosystem over time. Type III is the impact on migratory species, which may encounter the same or different types of stressors in other parts of the migration path. Because the disturbance of this Project is mainly concentrated in the bottom layer and lasts for a short time, the potential cumulative impact on deep-sea biodiversity, ecosystem functions and biological system services is mainly caused by Type I stressors.

Since our collector vehicle test only has a limited duration and scope, we can reasonably assume that the cumulative impact on deep-sea biodiversity, ecosystem functions and biological system services is low.

8.7 References

Anderson EP, Mackas DL. 1986. Lethal and sublethal effects of a molybdenum mine tailing o n marine zooplankton: Mortality, respiration, feeding and swimming behavior in Calanus marshallae, Metridia pacifica and Euphausia pacifica. Mar Environ Res. 19(2):131–155. https://doi.org/10.1016/0141-1136(86)90043-7

Arranz P, de Soto NA, Madsen PT, Sprogis KR. 2021. Whale-watch vessel noise levels with a pplications to whale-watching guidelines and conservation. Marine Policy. 134:104776. https://doi.org/10.1016/j.marpol.2021.104776

BGR. 2018. Environmental Impact Assessment for the testing of a pre-protoype manganese n odule collector vehicle in the Eastern German license area (Clarion-Clipperton Zone) in t he framework of the European JPI-O MiningImpact 2 research project. [place unknown].

Block BA, Jonsen ID, Jorgensen SJ, Winship AJ, Shaffer SA, Bograd SJ, Hazen EL, Foley D G, Breed GA, Harrison A-L, et al. 2011. Tracking apex marine predator movements in a dynamic ocean.Nature. 475(7354):86–90. https://doi.org/10.1038/nature10082

Brown A, Thatje S, Hauton C. 2017a. The Effects of Temperature and Hydrostatic Pressure on Metal Toxicity: Insights into Toxicity in the Deep Sea. Environ Sci Technol. 51(17):102 22–10231. https://doi.org/10.1021/acs.est.7b02988

Brown A, Wright R, Mevenkamp L, Hauton C. 2017b. A comparative experimental approach t o ecotoxicology in shallow-water and deep-sea holothurians suggests similar behavioural responses. Aquatic Toxicology. 191:10–16. https://doi.org/10.1016/j.aquatox.2017.06.02

8

Christiansen B, Denda A, Christiansen S. 2020. Potential effects of deep seabed mining on pelagic and benthopelagic biota.Mar Policy. 114:103442. https://doi.org/10.1016/j.marpol.2019.02.014

Crain CM, Kroeker K, Halpern BS. 2008. Interactive and cumulative effects of multiple human stressors in marine systems. Ecol Lett. 11(12):1304–1315. https://doi.org/10.1111/j.1461-0248.2008.01253.x

Davies TW, Duffy JP, Bennie J, Gaston KJ. 2014. The nature, extent, and ecological implications of marine light pollution. Front Ecol Environ. 12(6):347–355. https://doi.org/10.1890/130281

De Jonge DSW, Stratmann T, Lins L, Vanreusel A, Purser A, Marcon Y, Rodrigues CF, Ravara A, Esquete P, Cunha MR, et al. 2020. Abyssal food-web model indicates faunal carbon flow recovery and impaired microbial loop 26 years after a sediment disturbance experiment. Prog Oceanogr. 189:102446. https://doi.org/10.1016/j.pocean.2020.102446

Duarte CM, Chapuis L, Collin SP, Costa DP, Devassy RP, Eguiluz VM, Erbe C, Gordon TAC, Halpern BS, Harding HR, et al. 2021. The soundscape of the Anthropocene ocean. Science. 371(6529):eaba4658. https://doi.org/10.1126/science.aba4658

Gaston KJ, Bennie J, Davies TW, Hopkins J. 2013. The ecological impacts of nighttime light pollution: a mechanistic appraisal: Nighttime light pollution. Biol Rev. 88(4):912–927. https://doi.org/10.1111/brv.12036

Haddock SHD, Moline MA, Case JF. 2010. Bioluminescence in the Sea. Annu Rev Mar Sci. 2(1):443–493. https://doi.org/10.1146/annurev-marine-120308-081028

Hauton C, Brown A, Thatje S, Mestre NC, Bebianno MJ, Martins I, Bettencourt R, Canals M, Sanchez-Vidal A, Shillito B, et al. 2017. Identifying Toxic Impacts of Metals Potentially Released during Deep-Sea Mining—A Synthesis of the Challenges to Quantifying Risk. Front Mar Sci. 4:368. https://doi.org/10.3389/fmars.2017.00368

Hawkins AD, Johnson C, Popper AN. 2020. How to set sound exposure criteria for fishes. J Acoust Soc Am. 147(3):1762–1777. https://doi.org/10.1121/10.0000907

Herring PJ, Gaten E, Shelton PMJ. 1999. Are vent shrimps blinded by science? Nature. 398(6723):116–116. https://doi.org/10.1038/18142

Hu VJH. 1981. Ingestion of deep-sea mining discharge by five species of tropical copepods. Water Air Soil Pollut. 15(4):433–440. https://doi.org/10.1007/BF00279425

Jones KR, Klein CJ, Halpern BS, Venter O, Grantham H, Kuempel CD, Shumway N, Friedlander AM, Possingham HP, Watson JEM. 2018. The Location and Protection Status of Earth's Diminishing Marine Wilderness. Curr Biol. 28(15):2506-2512.e3. https://doi.org/10.1016/j.cub.2018.06.010

Kamrowski RL, Limpus C, Pendoley K, Hamann M, Kamrowski RL, Limpus C, Pendoley K, Hamann M. 2015. Influence of industrial light pollution on the sea-finding behaviour of flatback turtle hatchlings. Wildl Res. 41(5):421–434. https://doi.org/10.1071/WR14155

Kim HJ, Kim D, Hyeong K, Hwang J, Yoo CM, Ham DJ, Seo I. 2015. Evaluation of Resuspended Sediments to Sinking Particles by Benthic Disturbance in the Clarion-Clipperton Nodule Fields. Mar Georesour Geotec. 33(2):160–166. https://doi.org/10.1080/1064119X.2013.815675

Koschinsky A, Gaye-Haake B, Arndt C, Maue G, Spitzy A, Winkler A, Halbach P. 2001. Experiments on the influence of sediment disturbances on the biogeochemistry of the deep-sea environment. Deep Sea Research Part II: Topical Studies in Oceanography. 48(17):3629–3651. https://doi.org/10.1016/S0967-0645(01)00060-1

Kutti T, Bannister RJ, Fosså JH, Krogness CM, Tjensvoll I, Søvik G. 2015. Metabolic responses of the deep-water sponge Geodia barretti to suspended bottom sediment, simulated mine tailings and drill cuttings. J Exp Mar Biol Ecol. 473:64–72. https://doi.org/10.1016/j.jembe.2015.07.017

Larsson AI, van Oevelen D, Purser A, Thomsen L. 2013. Tolerance to long-term exposure of suspended benthic sediments and drill cuttings in the cold-water coral Lophelia pertusa. Mar Pollut Bull. 70(1):176–188. https://doi.org/10.1016/j.marpolbul.2013.02.033

Levin LA, Mengerink K, Gjerde KM, Rowden AA, Van Dover CL, Clark MR, Ramirez-Llodra E, Currie B, Smith CR, Sato KN, et al. 2016. Defining "serious harm" to the marine environment in the context of deep-seabed mining.Marine Policy. 74:245–259. https://doi.org/10.1016/j.marpol.2016.09.032

Longcore T, Rich C. 2004. Ecological light pollution. Front Ecol Environ. 2(4):191–198. https://doi.org/10.1890/1540-9295(2004)002[0191:ELP]2.0.CO;2

McQuaid KA, Attrill MJ, Clark MR, Cobley A, Glover AG, Smith CR, Howell KL. 2020. Using Habitat Classification to Assess Representativity of a Protected Area Network in a Large, Data-Poor Area Targeted for Deep-Sea Mining. Front Mar Sci. 7:558860. https://doi.org/10.3389/fmars.2020.558860

Miljutin DM, Miljutina MA, Arbizu PM, Galéron J. 2011. Deep-sea nematode assemblage has not recovered 26 years after experimental mining of polymetallic nodules (Clarion-Clipperton Fracture Zone, Tropical Eastern Pacific). Deep Sea Research Part I: Oceanographic Research Papers. 58(8):885–897. https://doi.org/10.1016/j.dsr.2011.06.003

Miljutina MA, Miljutin DM, Mahatma R, Galéron J. 2010. Deep-sea nematode assemblages of the Clarion-Clipperton Nodule Province (tropical north-eastern Pacific). Mar Biol. 40:1–15.

Nguyen KQ, Winger PD. 2019. Artificial Light in Commercial Industrialized Fishing Applications: A Review. Rev Fish Sci Aquac. 27(1):106–126. https://doi.org/10.1080/23308249.2018.1496065

NORI. 2022. Collector Test Study – Environmental Impact Statement – Testing of polymetallic collector system components in the NORI-D contract area, Clarion Clipperton Zone, Pacific Ocean. Jamaica.

Parsons MJ, Duncan AJ, Parsons SK, Erbe C. 2020. Reducing vessel noise: An example of a solar-electric passenger ferry.The Journal of the Acoustical Society of America. 147(5):35

75–3583.

Riccobene G. 2009. Long-term measurements of acoustic background noise in very deep sea. Nuclear Instruments and Methods in Physics Research Section A: Accelerators, Spectro meters, Detectors and Associated Equipment. 604(1, Supplement):S149–S157. https://do i.org/10.1016/j.nima.2009.03.195

Riehl T, Wölfl A-C, Augustin N, Devey CW, Brandt A. 2020. Discovery of widely available a byssal rock patches reveals overlooked habitat type and prompts rethinking deep-sea bio diversity. Proc Natl Acad Sci USA. 117(27):15450–15459. https://doi.org/10.1073/pnas.1 920706117

Rolland RM, Parks SE, Hunt KE, Castellote M, Corkeron PJ, Nowacek DP, Wasser SK, Kraus SD. 2012. Evidence that ship noise increases stress in right whales. P Roy Soc B-Biol Sc i. 279(1737):2363–2368. https://doi.org/10.1098/rspb.2011.2429

Rountree RA, Juanes F, Goudey CA, Ekstrom KE. 2012. Is Biological Sound Production Imp ortant in the Deep Sea? In: Popper AN, Hawkins A, editors. The Effects of Noise on Aqu atic Life. New York, NY: Springer; p. 181–183. https://doi.org/10.1007/978-1-4419-7311 -5_41

Ryan PG, Ryan EM, Glass JP. 2021. Dazzled by the light: the impact of light pollution from s hips on seabirds at Tristan da Cunha. Ostrich. 92(3):218–224. https://doi.org/10.2989/00 306525.2021.1984998

Sainte-Marie B. 1992. Foraging of Scavenging Deep-Sea Lysianassoid Amphipods. In: Rowe GT, Pariente V, editors. Deep-Sea Food Chains and the Global Carbon Cycle [Internet]. Dordrecht: Springer Netherlands; [accessed 2023 Oct 7]; p. 105–124. https://doi.org/10.1 007/978-94-011-2452-2_7

Schaanning MT, Trannum HC, Øxnevad S, Carroll J, Bakke T. 2008. Effects of drill cuttings on biogeochemical fluxes and macrobenthos of marine sediments. J Exp Mar Biol Ecol. 361(1):49–57. https://doi.org/10.1016/j.jembe.2008.04.014

Schriever C, Ahnert A, Bluhm H, Borowski C, Thiel H. 1997. Results of the large scale deep-sea environmental impact study DISCOL during eight years of investigation. In: ISOPE I nternational Ocean and Polar Engineering Conference [Internet]. Hawaii: ISOPE; [access ed 2023 Oct 6]; p. ISOPE-I. https://onepetro.org/ISOPEIOPEC/proceedings-abstract/ISO PE97/All-ISOPE97/23760

Shi P, Yang J, Sun D, Wang C. 2023. A simulation from offsite disturbance experiments on the metal resuspension process in the seafloor of the Western Pacific. Chemosphere. 311:13 7042. https://doi.org/10.1016/j.chemosphere.2022.137042

Simon-Lledó E, Bett BJ, Huvenne VAI, Schoening T, Benoist NMA, Jones DOB. 2019. Ecolo gy of a polymetallic nodule occurrence gradient: Implications for deep-sea mining. Limn ol Oceanogr. 64(5):1883–1894. https://doi.org/10.1002/lno.11157

Singh R, Sautya S, Ingole BS. 2019. The community structure of the deep-sea nematode com munity associated with polymetallic nodules in the Central Indian Ocean Basin. Deep Se a Research Part II: Topical Studies in Oceanography. 161:16–28. https://doi.org/10.1016/

j.dsr2.2018.07.009

Song Y, Wang C, Sun D. 2022. Both Dissolved Oxygen and Chlorophyll Explain the Large-Scale Longitudinal Variation of Deep Scattering Layers in the Tropical Pacific Ocean. Front Mar Sci. 9:782032. https://doi.org/10.3389/fmars.2022.782032

Tecchio S, Coll M, Sardà F. 2015. Structure, functioning, and cumulative stressors of Mediterranean deep-sea ecosystems. Prog Oceanogr. 135:156–167. https://doi.org/10.1016/j.pocean.2015.05.018

Thiel H, Schriever G, Bussau C, Borowski C. 1993. Manganese nodule crevice fauna. Deep Sea Research Part I: Oceanographic Research Papers. 40(2):419–423. https://doi.org/10.1016/0967-0637(93)90012-R

Tong SJW, Gan BQ, Tan KS. 2022. Community structure of deep-sea benthic metazoan meiofauna in the polymetallic nodule fields in the eastern Clarion-Clipperton Fracture Zone, Pacific Ocean. Deep Sea Res Part I. 188:103847. https://doi.org/10.1016/j.dsr.2022.103847

Vanreusel A, Hilario A, Ribeiro PA, Menot L, Arbizu PM. 2016. Threatened by mining, polymetallic nodules are required to preserve abyssal epifauna. Sci Rep. 6(1):26808.

Wang Z, Kwok KWH, Lui GCS, Zhou G-J, Lee J-S, Lam MHW, Leung KMY. 2014. The difference between temperate and tropical saltwater species' acute sensitivity to chemicals is relatively small. Chemosphere. 105:31–43. https://doi.org/10.1016/j.chemosphere.2013.10.066

Warrant EJ, Adam Locket N. 2004. Vision in the deep sea. Biol Rev. 79(3):671–712. https://doi.org/10.1017/S1464793103006420

Williams B, McAfee D, Connell S. 2022a. Oyster larvae swim along gradients of sound. J Appl Ecol. 59(7):1815–1824. https://doi.org/10.1111/1365-2664.14188

Williams R, Erbe C, Ashe E, Beerman A, Smith J. 2014. Severity of killer whale behavioral responses to ship noise: A dose–response study. Mar Pollut Bull. 79(1):254–260. https://doi.org/10.1016/j.marpolbul.2013.12.004

Williams R, Erbe C, Duncan A, Nielsen K, Washburn T, Smith C. 2022b. Noise from deep-sea mining may span vast ocean areas. Science. 377(6602):157–158. https://doi.org/10.1126/science.abo2804

Yamagishi T, Ota S, Yamaguchi H, Koshikawa H, Tatarazako N, Yamamoto H, Kawachi M. 2019. Ecotoxicological Bioassay Using Marine Algae for Deep-Sea Mining. In: Environmental Issues of Deep-Sea Mining: Impacts, Consequences and Policy Perspectives. [place unknown]: Springer; p. 255–271.

9 Natural Hazards and Accidental Events

9.1 Extreme weather

9.1.1 Tropical cyclones

The East Pacific Ocean, where the Contract Area is located, is one of the regions with the most frequent occurrence and development of tropical cyclones in the world. Second only to the Northwest Pacific Ocean by tropical cyclone activity, it has approximately 17 tropical cyclones every year on average, accounting for about 20 % of the total tropical cyclones in the world (Scareck et al., 2014).

With regard to the changing tropical cyclone generation positions in the East Pacific Ocean and possible causes, Zhao et al. (2021) pointed out that Hadley circulation and ITCZ position change are the key circulation systems for the meridional movement of tropical cyclone generation position in the East Pacific Ocean. In the timescale of a decade or longer, tropical cyclones in the East Pacific Ocean showed a significant trend of northward movement in 1979-2018, mainly due to the northward expansion of the ITCZ and Hadley circulation caused by hemispheric temperature difference. Different from the interdecadal or longer timescale, the interannual variation of the north-south movement of the tropical cyclone generation position in the East Pacific Ocean is mainly caused by the meridional variation of Hadley and the ITCZ positions caused by ENSO and hemispheric temperature difference.

Figures 9.1-1 to 9.1-8 show the optimal paths and central maximum wind force distribution of tropical cyclones in the North Pacific Ocean for 42 years in 1980-2022, on the basis of the global historical data set of International Best Track Archive for Climate Stewardship (IBTrACS) 4th edition (Knapp et al., 2010). The yellow area indicates where the CTA is in the Block A-5 of the Contract Area, and the colored lines represent the maximum wind force in the center, as given by the World Meteorological Organization (WMO). The West Pacific Ocean is the sea area where

the warm pool is located. From April to May, a strong typhoon occurrs in the Northwest Pacific Ocean. In June, the typhoon moves westward, and with an obviously higher probability of landing in South China. Under the influence of subtropical high, the probability of tropical cyclones occurring and landing in the Northwest Pacific Ocean increases from July to September, and the damage to eastern Asian countries grows accordingly. The probability of typhoon landing lowers significantly in October, except for South China.

It may be because the sea surface temperature in the East Pacific Ocean is lower than that in the West Pacific Ocean, and the tropical cyclones in the northeast Pacific occur later than those in the West Pacific Ocean. They mainly occur from June to October, with the largest number in July-September, a small number in May and November, and only occur sporadic in April, December and January. There is no tropical cyclone in the East Pacific Ocean in February and March. Tropical cyclones that affect the IRZ are most likely to occur from July to September every year. When individual cyclones cross the Block A-5, the central wind force can reach 30 m/s, which will significantly affect the test-mining activities and cause potential risks.

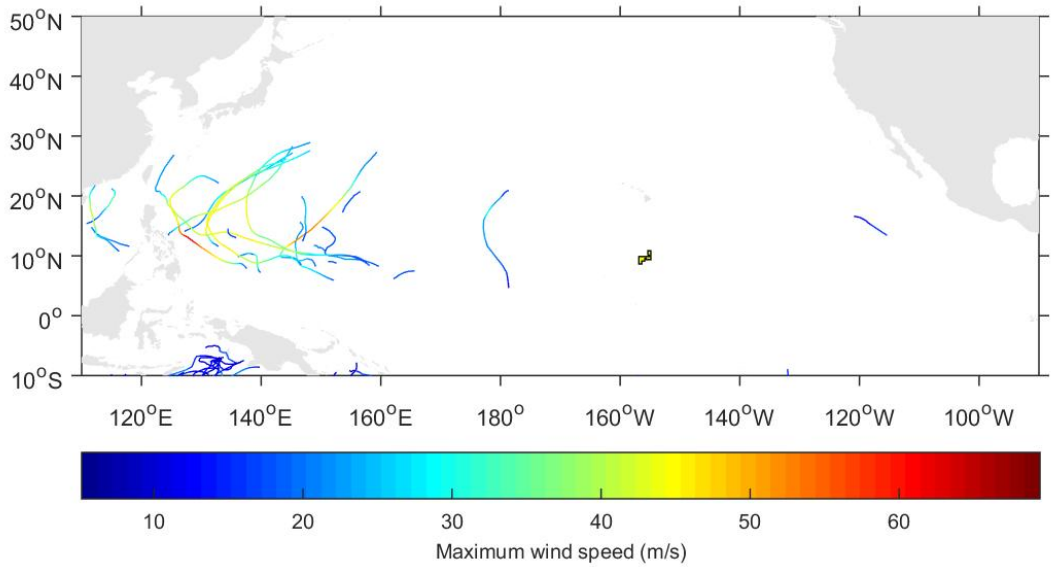

Figure 9.1-1 Tropical cyclone paths in April over the past 42 years (1980-2022) in the survey area

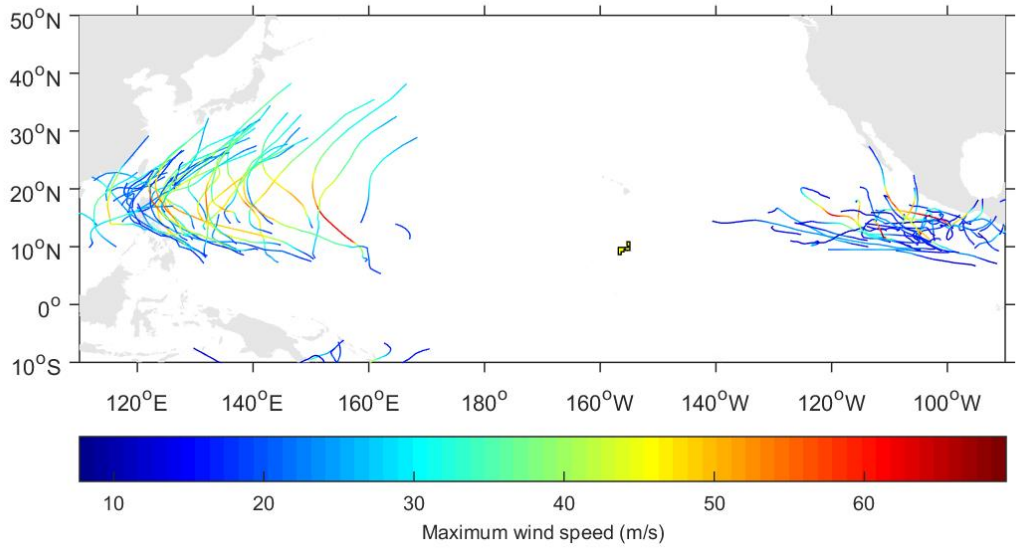

Figure 9.1-2 Tropical cyclone paths in May over the past 42 years (1980-2022) in the survey area

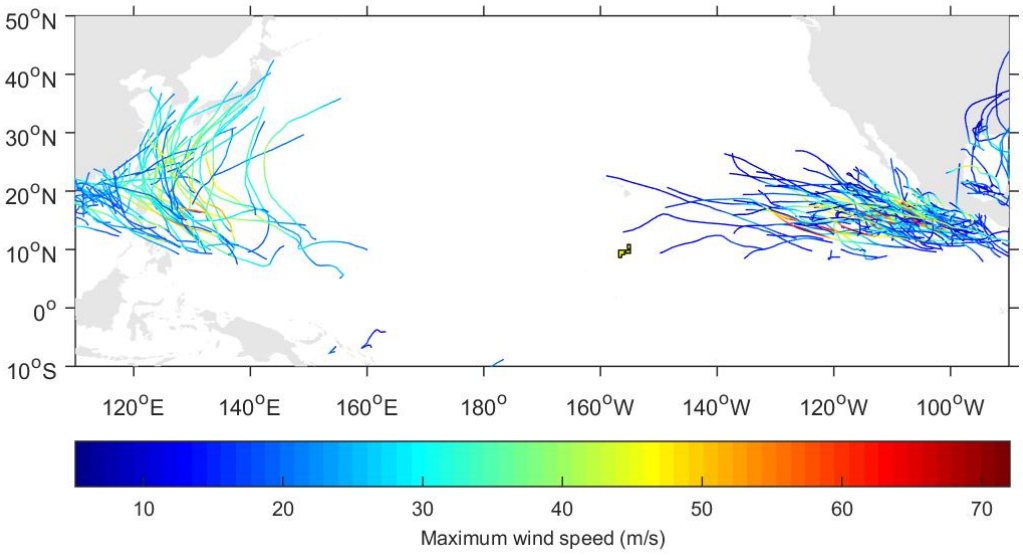

Figure 9.1-3 Tropical cyclone paths in June over the past 42 years (1980-2022) in the survey area

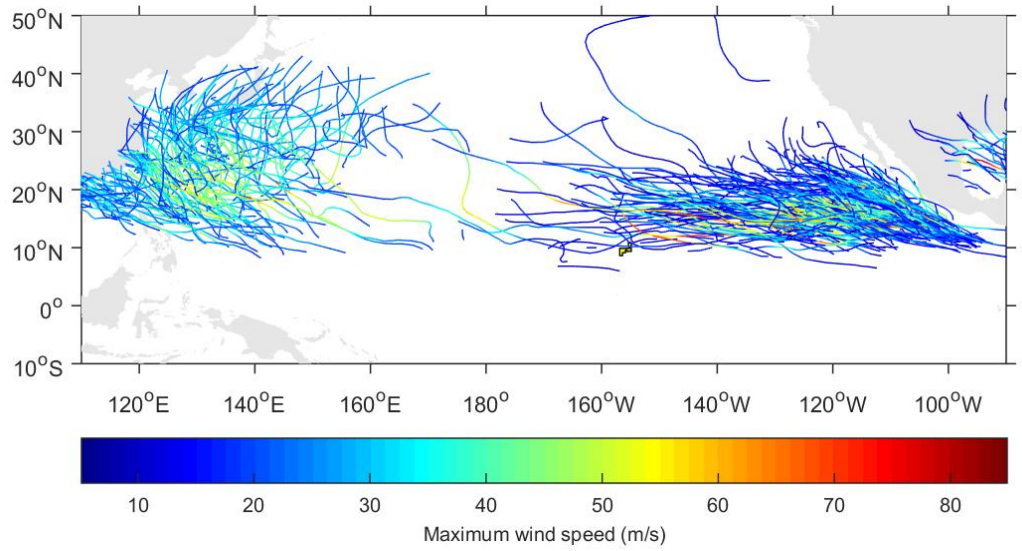

Figure 9.1-4 Tropical cyclone paths in July over the past 42 years (1980-2022) in the survey area

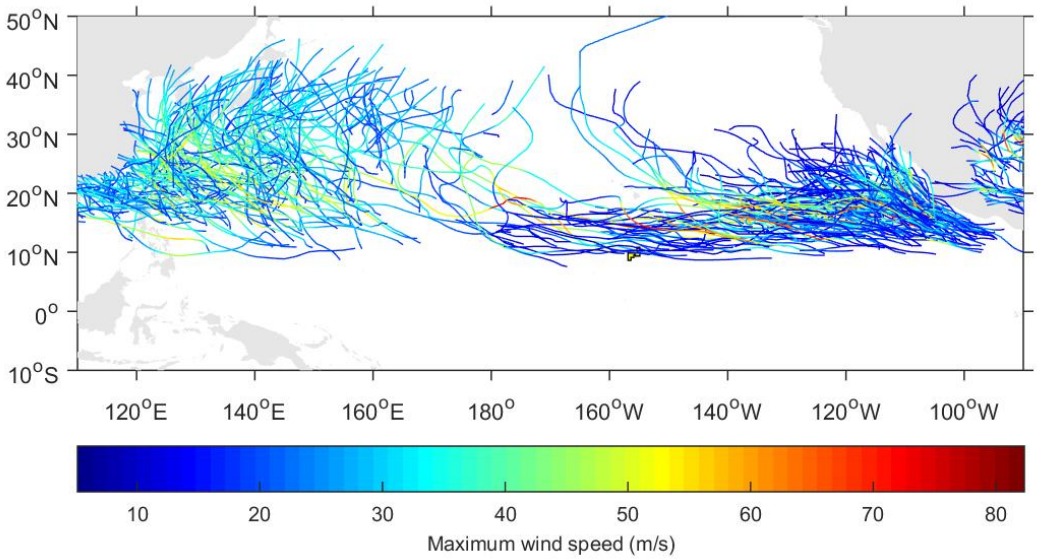

Figure 9.1-5 Tropical cyclone paths in August over the past 42 years (1980-2022) in the survey area

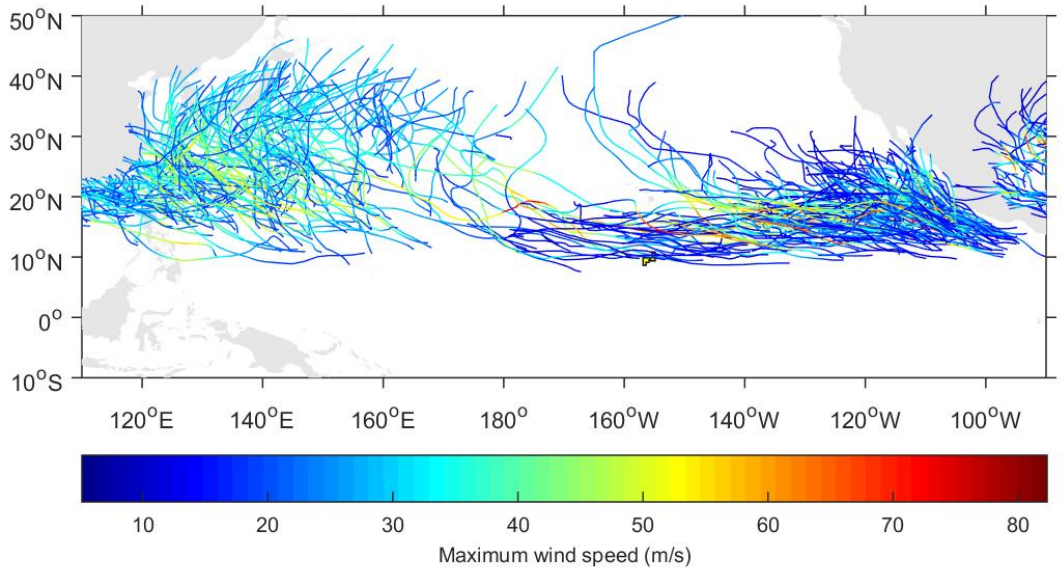

Figure 9.1-6 Tropical cyclone paths in September over the past 42 years (1980-2022) in the survey area

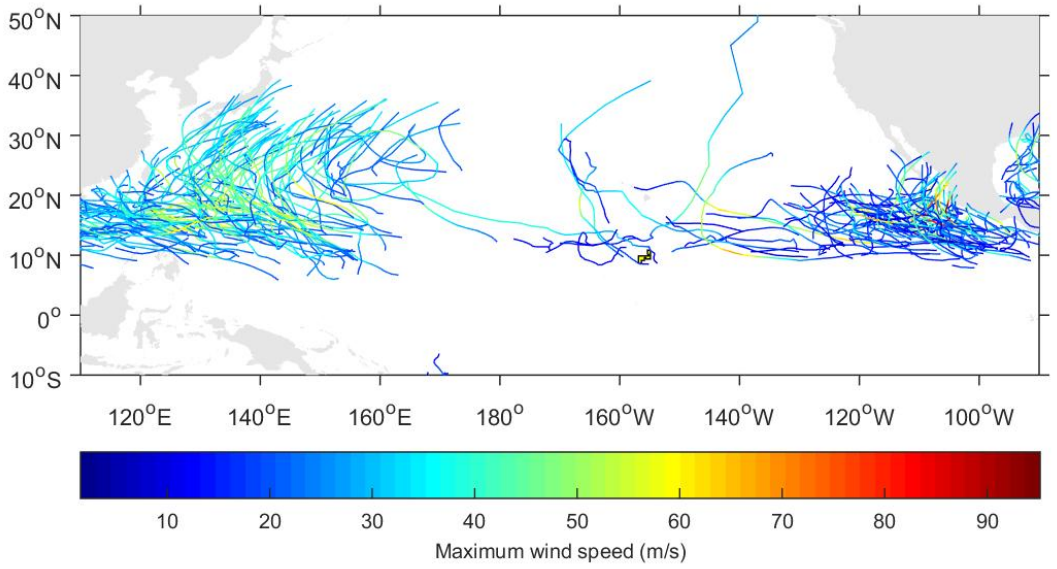

Figure 9.1-7 Tropical cyclone paths in October over the past 42 years (1980-2022) in the survey area

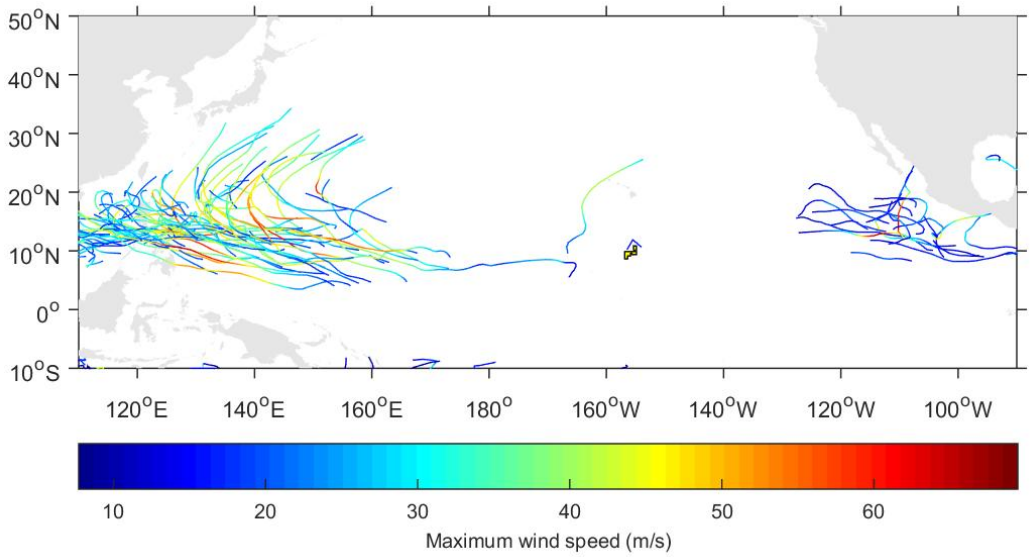

Figure 9.1-8 Tropical cyclone paths in November over the past 42 years (1980-2022) in the survey area

9.1.2 Adverse weather conditions other than hurricanes

Considering the safety of vessels and equipment during the test, we set the daily average wind speed smaller than magnitude 6 as the safe operation window, and analyzed the daily average wind speeds on the sea surface in 2019-2022 (Figure 9.1-9). Gales exceeding magnitude 6 mainly occur in spring (January-April), and the extreme wind speed can reach 20 m/s. The probability of extreme wind speed in summer and autumn is very low. It is especially so in July-October, with daily average extreme wind speed no more than 12 m/s (magnitude 5).

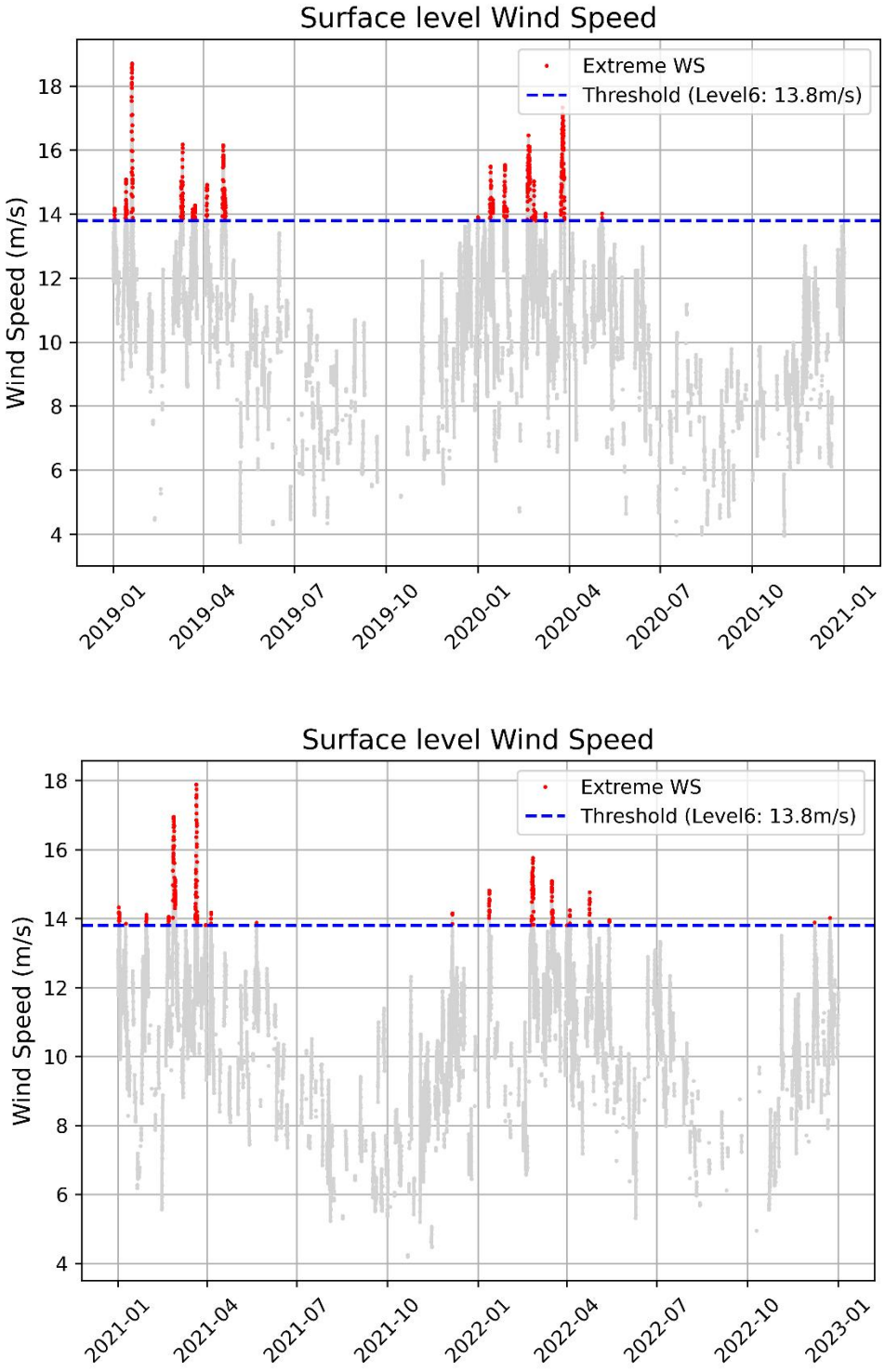

Figure 9.1-9 Daily average sea surface wind speeds in the Block A-5 in 2019-2022 (wind speeds above magnitude 6 are marked in red)

9.2 Natural disasters

There is no significant seismic activity or clear record of underwater volcanic activity in this region.

9.3 Accidental events

The emissions of environmental hazards caused by accidental events and extreme natural events are essentially different from those under normal operation. These are basically unplanned events but might happen, so preventive measures and/or passive response measures are needed. Hazards associated with the collector vehicle test and vessel operation have been identified and will be discussed below. In offshore waters, such incidents are usually related to accidents that lead to fuel or chemical leakage, fire, explosion and/or dangerous discharge.

The probability of accidental events is low, given that the design of Project components and the selection of contractors are subject to the requirements of relevant technical codes, operating procedures, and control measures designed to minimize the likelihood of accidents. Similarly, natural events of sufficient magnitude to cause severe consequences have a low probability of occurrence and specific operational procedures will be developed and implemented under such circumstances.

While rare, accidents and extreme events can occur and there is potential for loss of life, environmental harm, asset loss and reputational damage. The focus of this assessment is to evaluate the potential consequences associated with major hazards, in terms of the criteria provided in Section 4.

Should accidents occur, Minmetals will mobilize resources according to established emergency response plan. Hazard and risk assessment of such events is integral to the Project and will be undertaken from Project design through to execution. This process includes:

9.3.1 Vessel accidental events and emergency measures

(1) Chemical leakage or spillage

Chemical or fuel leakage may occur due to leakage, equipment failure or extreme events (e.g. vessel collision or out of control). A spill may have detrimental impacts on water quality and adversely affect the marine ecosystem.

A spill risk assessment will be undertaken following the completion of the final project design. This will identify specific activities where there is potential for spills and describe mitigation measures to minimize the risk.

Mitigation measures and operating procedures will be reviewed and revised as needed considering the outcomes of the spill risk assessment. Proactive and reactive measures will be used to minimize the risk of fuel and other hazardous materials and their potential impacts. Proactive measures may include:

—Appropriate material selection and corrosion control in hoses, equipment and storage tanks.

—Maintenance and monitoring programs to ensure the integrity of equipment and detect loss of containment.

—Emergency shutdown and containment systems.

—Provision and maintenance of spill response and containment equipment appropriate to the level and type of risk and located at all areas of possible spills.

—Ensure sufficient containment or bunding of chemical storage areas to prevent rain/drainage water being contaminated.

—Personnel training and field drills on leakage prevention, containment and response.

—Reporting all spills and near misses followed by a root cause analysis and corrective actions plan to prevent recurrence.

—Implementation of waste (solid and liquid) management plans.

—Implementation of a vessel water management plan that separates clean runoff from potentially contaminated water to minimize the potential for the release of contaminated water.

In case of an accident, emergency measures will be taken in strict accordance with the emergency instructions for vessel spill to avoid or reduce pollution to the marine environment. Reactive measures in the event of an incident will be dependent on the level of the spill, consistent with international government and industry

approaches to spill response management. All activities associated with the implementation of the project will be subject to the requirements of the "International Convention for the Prevention of Pollution from Ships" (MARPOL) which includes regulations aimed at preventing both accidental pollution and pollution from routine vessel operations. MARPOL includes six technical annexes the requirements of which will be adhered to throughout the Project. In case of a spill, emergency measures will be taken to avoid or reduce pollution to the marine environment.

(2) Fire and explosion

The Project will involve the storage and handling of flammable and combustible substances that can lead to the generation of potentially explosive and/or flammable gas emissions resulting in a fire or explosion. While the Project does not require the use of explosives, potential environmental impacts associated with the use of other flammable and combustible substances, such as fuel, may result in fire, release of significant quantities of hazardous smoke to the air.

Preliminary mitigation measures include:

—Induction to include all areas of risks of fire and types of fire, reporting fire events, response actions, locations/usage of fire-fighting equipment;

—Restricted access to high fire-risk areas;

—Storage and handling of all flammable and combustible substances, including waste, under conditions which minimize the risk of fire or toxic emissions. For example, provide adequate separation distances between potential ignition sources and flammable materials and classify hazard areas.

—Specific design criteria for fire prevention, detection, control and personnel safety requirements.

—Ensuring that "hot works" do not take place near flammable materials.

—Implementation of passive and active fire prevention and fire-fighting techniques for each hazard area.

—Identification and regular maintenance and testing of fire equipment adequate

for the level of risk to ensure good working order.

The emergency measures taken in case of vessel fire/explosion will depend on the severity of the accident, and the crew and special personnel at all levels will conduct emergency operations in strict accordance with the emergency instructions for fire and explosion to minimize losses.

(3) Vessel collision

Transit routes will intersect with many international routes, some of which are highly utilized. International maritime practices will be observed and the vessel equipped with communication and navigation aids.

Vessel collisions may occur during extreme weather conditions or due to human error, for example, due to poor coordination and communication with third-party vessels, mechanical faults, poor visibility and rough sea conditions. Resulting impacts includes injuries to people, the release of ballast water and spills of fuels and other hazardous materials that have the potential to impact water and sediment quality and ecological receptors.

A number of mitigation measures will be implemented to minimize the potential for impacts associated with vessel collisions:

—Notifying relevant maritime authorities of the planned collector vehicle test as required.

—Notifying third parties potentially operating in the vicinity of the test site of the timing of the test and any safety exclusion zones.

—Use of vessel positioning equipment, including marine radar and a global navigation satellite system (i.e. the United States Government NAVSTAR Global Positioning System).

In case of vessel collision, emergency measures will be taken in strict accordance with the emergency instructions for vessel collision to minimize casualties, environmental pollution and property losses.

9.3.2 Collector vehicle accidental events and emergency measures

(1) Separation of the collector vehicle from umbilical cable

When the collector vehicle is working on the seabed, if the umbilical cable is broken or cut off due to special circumstances, the collector vehicle, quite different from most ROVs, is unable to float to the surface by beacon control due to its insufficient buoyancy. If the collector vehicle cannot work or move, it will remain stationary on the seabed, and there will be no risk of pollution to the seabed environment in the short term.

The collector vehicle is equipped with an acoustic beacon, which can provide the accurate position information of the collector vehicle. To cope with this special situation, the collector vehicle is designed with a mechanism for connection with lifting cables. For the at-sea test, the SSV is equipped with a working-class ROV capable of working at the water depth of 6,000 m. The ROV can carry the lifting cable to the top of the collector vehicle, and connect the lifting cable with the docking mechanism of the collector vehicle. In this way, the collector vehicle can be recovered.

(2) Oil spill from the collector vehicle

Thanks to its high efficiency, reliability and remote operability, hydraulic system is vital in the traveling and control mechanisms of the collector vehicle. The hydraulic system's normal operation of is directly related to the performance and safety of all underwater operation equipment. The leakage of hydraulic oil is a problem that cannot be ignored. Leakage of hydraulic oil may lead to serious consequences, such as equipment performance degradation and equipment out of control. Causes of hydraulic oil leakage from the collector vehicle may include:

1) Aging or wear of seals;
2) Too high pressure of hydraulic oil;
3) Poor or loose connection of hydraulic oil pipeline;
4) Crack in or damage of Hydraulic oil tank or oil pipeline.

The total amount of hydraulic oil for the collector vehicle is approximately 600-

700 L of hydraulic oil (Shell Tellus S2 V series or another brand with similar performance). Shell Tellus S2 V series hydraulic oil is a kind of high-performance mineral hydraulic oil. It has many advantages, such as excellent protection ability, good wear resistance, excellent low-temperature performance and prolonging the service life of hydraulic oil. According to the Globally Harmonized System of Classification and Labelling of Chemicals (GHS), this series of hydraulic oils are not classified as physical hazards, health hazards or environmental hazards.

To prevent the leakage of hydraulic oil, the following measures will be taken:

1) Making that the hydraulic system of the collector vehicle strictly follow the relevant standards during design and manufacture, so as to ensure that the hydraulic system is well sealed;

2) Ensuring that the temperature and pressure of hydraulic oil are within the tolerable range during normal operation;

3) Regularly checking and maintaining the hydraulic system to identify and eliminate hidden dangers in a timely manner;

4) Monitoring the liquid level variation of the pressure compensator of the hydraulic system through a displacement sensor, and observing the key part of the collector vehicle through a vehicle-mounted camera;

5) Formulating an emergency response plan for hydraulic oil leakage, conducting trainings and drills on emergency response ability, and improving the comprehensive quality of personnel to deal with emergencies; and

We will take effective measures to ensure personal and environmental safety during emergency disposal of leakage, and follow the requirements of relevant laws and regulations.

9.4 References

Knapp, K. R., Kruk, M. C., Levinson, D. H., Diamond, H. J. & Neumann, C. J. (2010). The International Best Track Archive for Climate Stewardship (IBTrACS) Unifying Tropical Cyclone Data. Bull. Am. Meteor. Soc. 91, 363–376.

Schreck, C. J., Knapp, K. R., & Kossin, J. P. (2014).The impact of best track discrepancies on

global tropical cyclone climatologies using IBTrACS. Monthly Weather Review, 142(10), 3881–3899.

Zhao, H., Zhao, K., Cao, J., Klotzbach, P. J., Raga, G. B., & Ma, Z. (2021). Meridional migration of eastern north pacific tropical cyclogenesis: Joint contribution of interhemispheric temperature differential and ENSO. Journal of Geophysical Research: Atmospheres, 126, e2020JD034504.

10 Environmental Management, Monitoring and Reporting

10.1 Organizational structure and responsibilities

10.1.1 Organization and management and personnel responsibilities of the project team

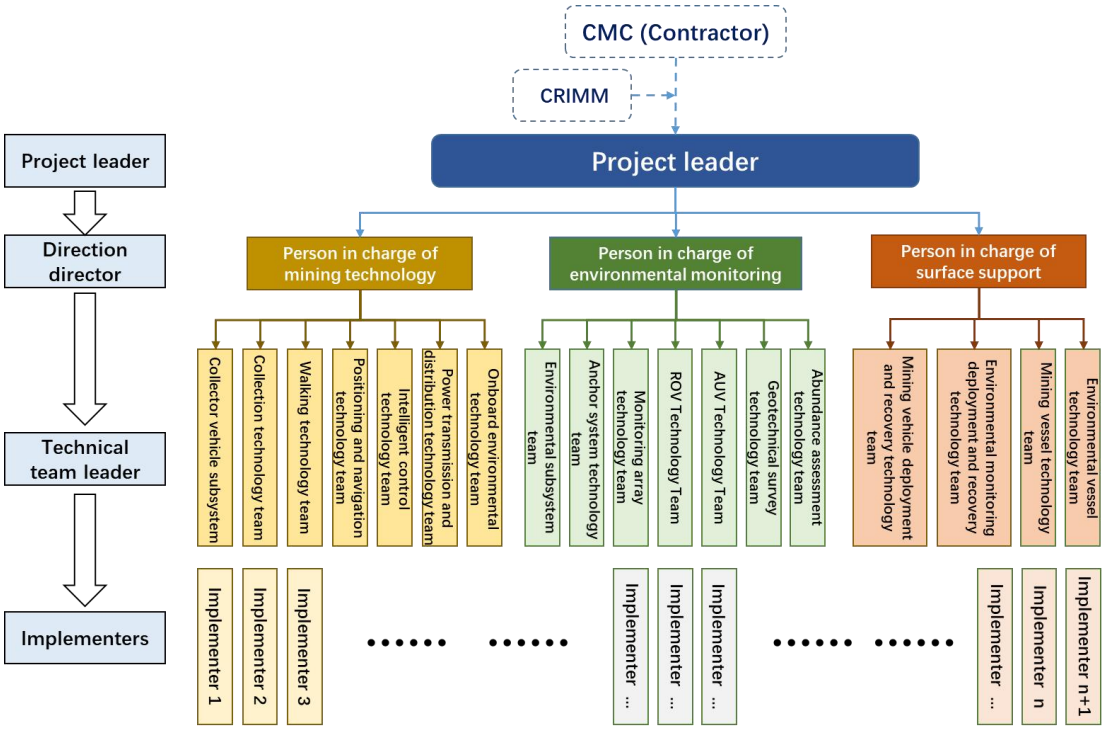

Figure 10.1-1 Organization and management architecture of the project team

A project leader takes full responsibility for the whole team, and the whole organizational management structure is divided into four levels: project leader, direction director, technical team leader and implementer.

（1） **Project leader**

The project leader is appointed by the Contractor to be responsible for the whole project's organization, implementation, technical check and schedule management. Mao Guiting is the project leader.

（2） **Direction director**

During the implementation of this Project, the person in charge of mining technologies, environmental monitoring and surface support are set up separately. The person in charge of mining technologies is responsible for the research, design,

manufacture and at-sea testing ofcollector vehicle. The person in charge of environmental monitoring is responsible for the preparation of environmental scheme, R&D of environmental equipment and marine environmental monitoring of the whole project. The person in charge of surface support is responsible for the R&D of the launch and recovery technologies for the collector vehicle and monitoring equipment, the launch and recovery operation of at-sea equipment, and the support of surface vessels.

The person in charge of mining technologies is Cheng Yangrui; the persons in charge of environmental monitoring are Sun Dong and Liu Yuwei; and the person in charge of surface support is Li Manhong.

（3） Technical team leaders

Technical team leaders are responsible for the relevant work of their respective special technologies, equipment and operations. They follow the overall arrangements of the direction director.

（4） Implementers

Implementers are responsible for the implementation of specific tasks such as technology R&D, equipment development and at-sea operation.

10.1.2 Organization, management and personnel responsibilities related to at-sea survey

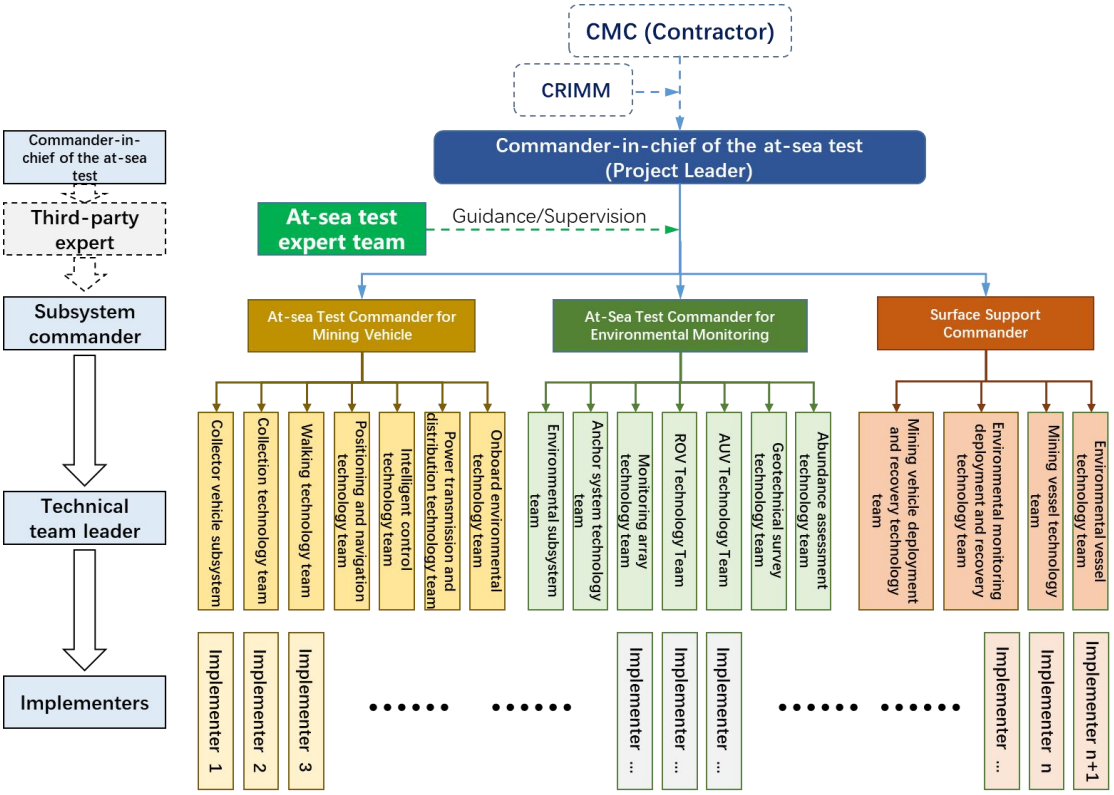

Figure 10.1-2 Organization and management architecture of at-sea survey

During the at-sea testing of this Project, there will be a commander-in-chief responsible for the overall at-sea test. The entire at-sea test organization and management structure will be divided into four levels: at-sea test commander-in-chief, subsystem commander, technical team leader and implementer. There will also be third-party experts.

（1） At-sea test commander-in-chief

Appointed by the Contractor, the commander-in-chief of the at-sea test is responsible for the organization, implementation, technical check and schedule management of the at-sea testing of the whole project. Mao Guiting, the project leader, serves concurrently as the commander-in-chief of the at-sea test.

（2） Third-party experts

The third-party experts include technical experts and environmental experts designated by the relevant management agencies of sponsoring States. They are

responsible for technical guidance, consultation and environmental monitoring operation supervision during the at-sea test.

（3） **Subsystem commanders**

During the at-sea test, there will be commanders for the at-sea testing of the collector vehicle, environmental monitoring and surface support respectively. The commander for the at-sea testing of the collector vehicle is responsible for the planning and testing of seabed collecting equipment. The commander for environmental monitoring during at-sea test is responsible for the preparation of EMP, data collection and preliminary analysis of marine environmental monitoring data of the whole project. The commander for surface support is responsible for the launch and recovery of the collector vehicle and monitoring equipment, and managing the SSV and EMV.

Cheng Yangrui is the commander for the at-sea testing of the collector vehicle. Sun Dong and Liu Yuwei are commanders for environmental monitoring of the at-sea test. Li Manhong is the commander for surface support.

（4） **Technical team leaders**

Technical team leaders are respectively responsible for the at-sea test operation, data collection, maintenance and guarantee of their corresponding technologies and equipment. They follow the overall arrangements of corresponding subsystem commanders.

（5） **Implementers**

Implementers are responsible for the implementation of specific tasks such as at-sea operation, maintenance and data collection of specific technologies and equipment.

10.2 Environmental management system

Testing of collecting equipment is an integral part of the baseline studies required by the ISA, as well as the primary inputs to the EIA for commercial mining (ISBA/25/LTC/6/Rev.1(s.VI(B)(33)). This test can facilitate the improvement of scientific cognition and the progress of engineering technologies. In this way, we can better understand the operation mechanism of the collector vehicle, the impact on the

bottom marine ecosystem and the natural recovery of the ecosystem after nodule collection. All the obtained data and information will be used for optimizing the design of the collector system and preparation of the EMMP.

10.2.1 Division of test stages

This equipment test and environmental monitoring will be conducted in the following stages:

(1) Survey of baseline characteristics before the collector vehicle test

a. Survey of and studies on baseline characteristics in 2017-2024;

b. Survey of and studies on baseline characteristics 1-2 weeks before the test in 2025.

(2) Testing and monitoring of the collector vehicle's performance

a. Monitoring of the collector vehicle's status;

b. Near- and far-field environmental monitoring during the collector vehicle test (including fixed-point monitoring and mobile monitoring).

(3) Post-test monitoring

a. Environmental monitoring in areas directly disturbed by the collector vehicle;

b. Environmental monitoring in plume-impacted areas;

c. Environmental monitoring in the PRZ.

In 2017-2023, Minmetals signed contracts with the scientists of nearly 10 scientific research institutions to conduct on-going environment baseline studies in the Block A-5. Minmetals will continue environment baseline studies in 2024-2025. After seven years' continuous survey of and studies on environment baselines, Minmetals now can comprehensively describe and compare the environment baselines of the IRZ and PRZ. Before the test is carried out in the third quarter of 2025, Minmetals will keep surveying the environment baselines. The baseline data of the IRZ and PRZ collected before the testing will be used as the benchmark for studying the environmental impact of this collector vehicle test, as well as for comparing the variations and long-term recovery of the near-bottom environmental ecosystem after

the test.

The testing and monitoring of the functions and performance of the collector vehicle, as well as the environmental impact of the test-mining are planned in the third quarter of 2025.

The monitoring will be conducted prior to, during and following the collector vehicle test. The short-term monitoring (within hours, days and weeks) will mainly focus on the technical functions, performance verification and direct impact of the collector vehicle. The collector vehicle test this time will provide good references for collector system design and plume model validation.

Post-test monitoring will be conducted within hours, days, weeks or months after the end of this collector vehicle test. The EMP aims to quantify the direct impact of mining on the bottom-layer marine environment, and the results will be used in the EIA for Commercial Mining.

(4) Long-term studies on environmental restoration

Long-term studies on environmental restoration will be conducted within several years to decades after the test. Relevant details will be incorporated into the EMMP for Commercial Mining. Such long-term studies aim to monitor the recovery of benthic communities after disturbance. The monitoring results will be based on the IRZ's environment baselines before the test and the ongoing survey results of the PRZ's environment baselines.

10.2.2 Data management

All monitoring data of this Project will be input into the "Integrated Analysis & Management System for the Contract Area", which was designed and developed by Minmetals for the EIA and relevant studies.

Objectives of data management system:

- Realizing the classified storage, query and display of metadata related to various monitoring activities;
- Registering the sample collection platform and process;

- Registering sampling events;
- Registering data and objects generated by sampling events, such as images, physical samples, data files, sensor readings, observation data and drawing files (e.g. rasters and spatial data);
- Tracking the integrity of input data objects and the integrity of backtracking information.

To achieve the above-mentioned objectives, the "Integrated Analysis & Management System for the Contract Area" will be equipped with professional operators for at-sea data management system, necessary hardware & software and internet link. According to the obligation of reporting to the ISA and providing data to the ISA's DeepData database, Minmetals adopts a standardized data format in its data management system that meets the ISA's structure requirements for uploading data.

10.2.3 Sample management

For the samples obtained in this Project, including but not limited to nodules, biological samples, etc., Minmetals will earnestly fulfill the relevant obligations stipulated in the "Law of the People's Republic of China on the Exploration and Development of Resources in Deep Seabed Areas" and submit the samples to the China Ocean Sample Repository. With comprehensive sample preservation conditions and management system, the China Ocean Sample Repository can ensure the professional and standardized management of the samples obtained in this Project.

10.3 EMMP

10.3.1 Mitigation and management

This Project will follow the best scientific knowledge and a feasible technical scheme to mitigate the potential environmental impact caused by the test, and adopt the impact mitigation measures throughout the test to minimize environmental impact.

Minmetals hereby promises that it will conduct comprehensive environmental monitoring for the bottom layer prior to, during and following the test. After test-

related data and environmental monitoring data are studied and analyzed by a professional team, a scientific report will be prepared and then submitted to the ISA as the common scientific heritage of all mankind. The biological and environmental samples obtained during the studies will be kept in the national sample management institutions in China according to relevant Chinese laws. Any scientist with the purpose of scientific research may apply to the State Oceanic Administration of China for access according to the "Law of the People's Republic of China on the Exploration and Development of Resources in Deep Seabed Areas" (2016) and the "Regulations of the People's Republic of China on the Administration of Ocean Samples" (2009).

10.3.2 EMP

10.3.2.1 Summary

Only the collector vehicle test will be conducted this time. Environmental impact analysis results (in the previous chapters of this EIS) show that the possible environmental impact of this Project is mainly on the seabed and the near-bottom-layer seawater. Therefore, this EMP focuses on the monitoring of the bottom environment, benthic ecosystem and near-bottom-layer ecosystem.

According to the ISA's "Recommendations for the guidance of contractors for the assessment of the possible environmental impacts arising from exploration for marine minerals in the Area", the monitoring should focus on: (1) key environmental parameters such as temperature, salinity, DO, pH, turbidity and redox potential in the bottom layer; (2) parameters such as the particle concentration, turbidity, emission volume of seabed sediment plume, as well as the redeposition range and thickness of plume dispersal trajectory; (3) parameters of chemical elements such as nutrients (nitrate, carbonate, silicate), key heavy metal elements (copper, zinc, lead, nickel, cadmium, etc.), organic pollutants, oil in bottom-layer seawater; (4) the diversity, community structure and quantitative variations of benthic communities.

To effectively obtain all kinds of environmental monitoring data in this test, we will adopt four environmental monitoring measures: (1) Installing on the collector

vehicle an environmental monitoring and in-situ sampling system, including a small ROV for simultaneous environmental monitoring and assessing operational safety risk during the test; (2) Deploying environmental monitoring arrays in and around the CTA; (3) Monitoring and sampling with shipboard equipment, the ROV and the AUV, etc.; (4) Deploying a set of near-bottom long-term environmental observation equipment in the CTA, and conducting annual return visit and sampling during subsequent survey cruises to obtain the natural recovery data of the disturbed CTA.

According to the test schedule, the EMP will be implemented in the following order:

a) Before the collector vehicle test: The submerged buoys of mooring for deep-sea environmental observation, the distributed environmental monitoring array with high precision, and the redeposition thickness monitoring device will be deployed in the CTA and PRZ. Ship-mounted sampling equipment will be used to collect environment baseline samples and data, and the AUV will be used to collect near-bottom environmental data and survey benthic fauna;

b) During the collector vehicle test: (1) The pre-installed environmental monitoring system, vehicle-mounted monitoring system and simultaneous monitoring system will be used to conduct point-line-plane environmental monitoring, as well as to collect time-series environmental samples and data in the vicinity of the collector vehicle and the affected area under multiple working conditions. Ship-mounted sampling equipment will be used to collect near-bottom-layer seawater samples along the plume dispersal gradients. (2) The performance parameters (e.g. temperature, pressure, flow rate, etc.) of the collector vehicle's operation will be monitored in a real-time manner to ensure that the collector vehicle is in normal operation state. In case of any abnormality, timely intervention and operation will be conducted to ensure that there will be no abnormality of the collector vehicle that will affect the at-sea test;

c) After the collector vehicle test: Re-sampling and observation will be conducted

by using ship-mounted sampling equipment to obtain the post-mining sediment environment and residual nodules. The AUV will be used to collect near-sediment environmental data and survey benthic fauna re-entry along the track before the collector vehicle test. A long-time-series observation device of the sediment environment will be set up in the CTA to obtain the monitoring data of the natural recovery of the sediment environment and biological communities for many years to come.

10.3.2.2 Environmental monitoring and in-situ sampling system installed on the collector vehicle

In view of the requirements for monitoring the working mode and conditions of the collector vehicle during the test, the variations of seabed hydrology and chemical environmental parameters during the test-mining, an environmental monitoring and sample collecting system will be installed on the collector vehicle to obtain key environmental impact parameters such as sediment concentration, discharge flow and pressure, temperature, salinity, turbidity, pH and DO discharged during the collector vehicle test in a real-time manner, as well as to collect seawater, sediment and scavenger samples. The collected data and samples will be used as references in the subsequent EIA.

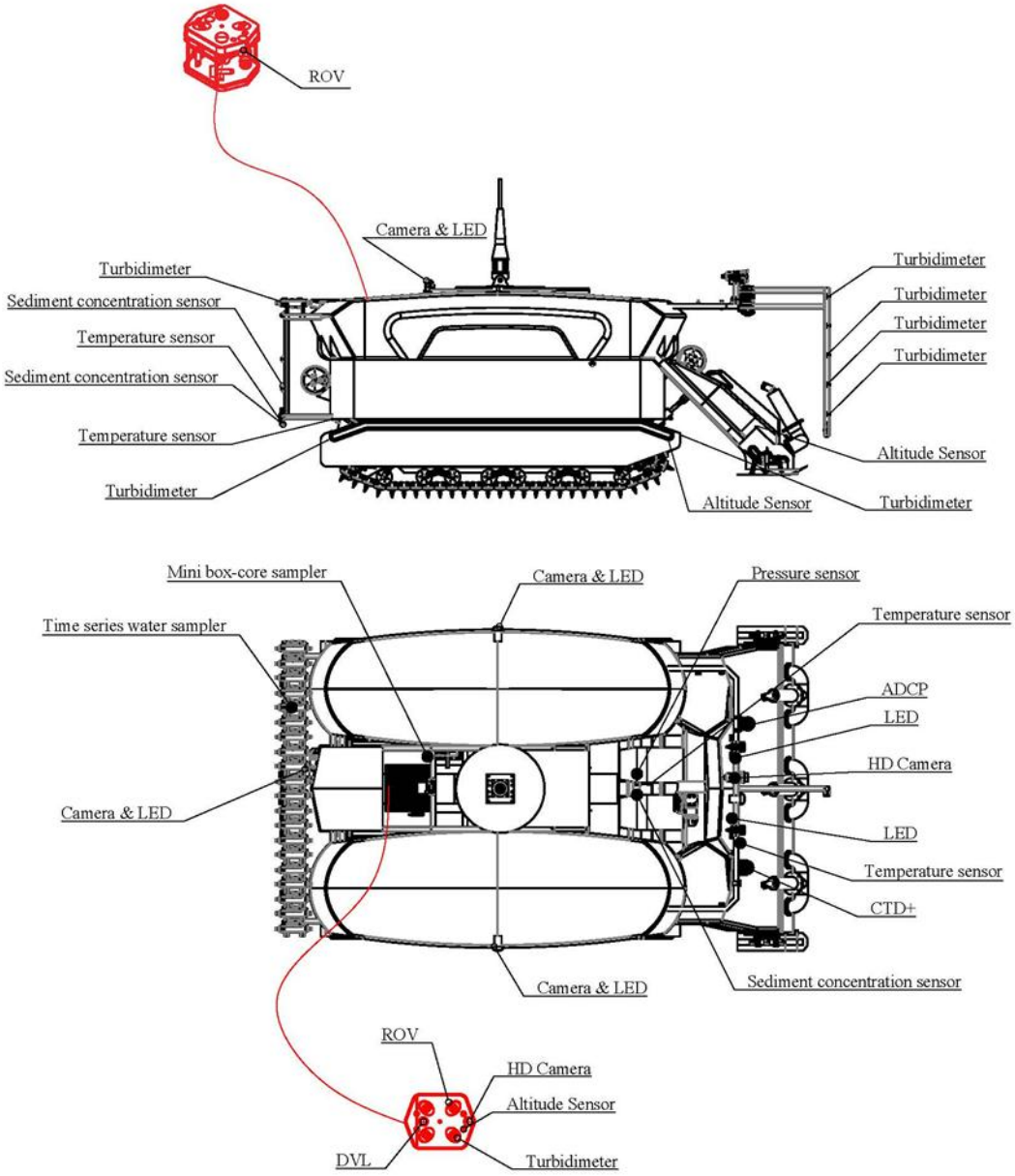

Figure 10.3-1 Design for the multi-parameter online environmental monitoring system of the collector vehicle

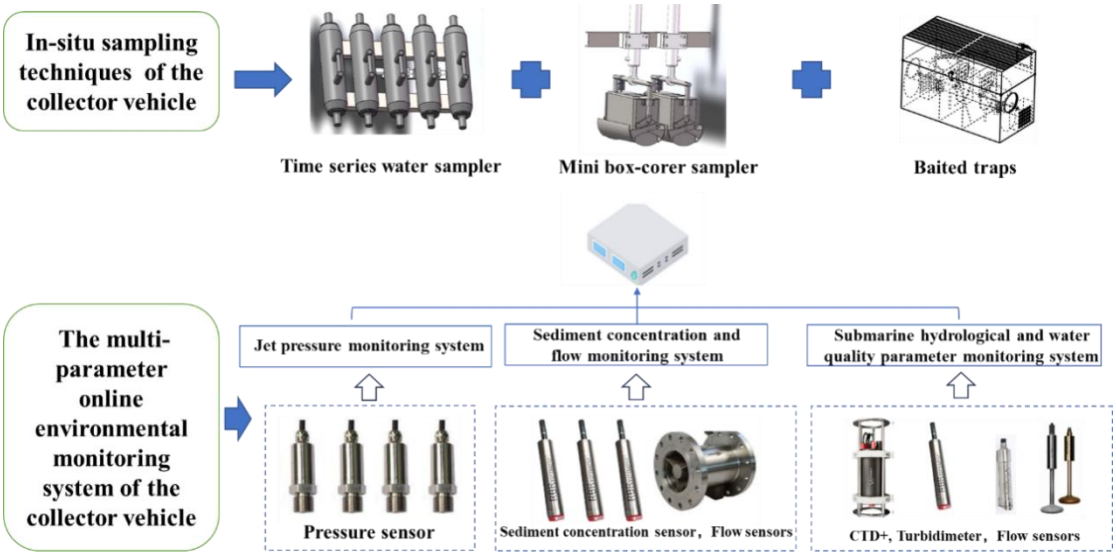

Figure 10.3-2 Schematic diagram for the main subsystems of the multi-parameter online environmental monitoring system of the collector vehicle

Table 10.3-1 Main subsystems of the multi-parameter online environmental monitoring system of the collector vehicle

S.N.	Name of monitoring instrument	Quantity	Monitoring purpose
1	ADCP	1 set	For monitoring the ocean current profile and water column sediment concentration in the vicinity of the collector vehicle
2	CTD	1 set	For monitoring the variations of parameters (e.g. CTD) in the vicinity of the collector vehicle
3	Underwater HD camera	1	For observing the seafloor environment during the traveling of the collector vehicle
4	Underwater lamp	5	For observing the seafloor environment during the traveling of the collector vehicle
5	Sediment concentration sensor	4	For monitoring the variations of sediment concentration at the tail of the collector vehicle and the sediment concentration at the cargo hatch
6	Temperature sensor	4	For monitoring the impact of discharged sludge on water temperature
7	Water sampling bottle	10 sets	For collecting seawater samples in the vicinity of the collector vehicle
8	Box corer on the collector vehicle	2 sets	For collecting mud samples in the vicinity of the collector vehicle
9	Turbidimeter	8	For monitoring that turbidity around the collector vehicle at different positions and heights
10	Pressure sensor	1	For monitoring the water pressure of the cargo hatch

10.3.2.3 Environmental monitoring array

The main environmental disturbance during the test is in the bottom layer.

Disturbed by mining activities, the water column may have strong material and energy exchange with sediments. Impacted by near-bottom-layer ocean currents, sediments will be eroded, resuspended and transported to cause transport of seabed chemicals. Especially during the test-mining, the sediment plume discharged by the collector vehicle on the seabed will spread to the surrounding water columns within a large radius. Therefore, it is necessary to deploy benthic boundary layer observation devices to monitor the variations of key chemical and biological parameters in the bottom-layer seawater.

To this end, we will deploy an environmental monitoring array during the test, which mainly includes the following three types of monitoring devices:

(1) Distributed environmental monitoring array (node)

a) Bottom-layer ocean current + turbidity monitoring platform;

b) ADCP monitoring platform;

c) Bottom-layer temperature and salinity + turbidity monitoring platform;

d) Bottom-layer ocean current + sediment concentration monitoring platform;

e) Turbidity monitoring platform

f) Near-bottom platform for monitoring the characteristics of ocean current plume;

(2) Redeposition thickness measuring system

(3) Submerged buoy of mooring

Table 10.3-2 Number and composition of the monitoring nodes in the environmental monitoring array

S.N.	Name	Quantity	Composition of monitoring instruments for each set of equipment	Monitoring purpose
1	Bottom-layer ocean current + turbidity monitoring platform	2	Current meter × 1, turbidity sensor × 1	For monitoring the variations of ocean current and turbidity in the CTA
2	ADCP monitoring platform	2	300K ADCP×1	Vertical profiles of ocean current and sediment in the near-bottom water layer of the CTA
3	Bottom-layer temperature and salinity + turbidity monitoring platform	3	CTD × 1, turbidity sensor × 1	For monitoring the CTD and turbidity variations outside the CTA
4	Bottom-layer ocean current + sediment concentration monitoring platform	2	Current meter × 1, sediment concentration sensor × 1	Vertical profiles of ocean current and sediment in the near-bottom water layer of the CTA
5	Turbidity monitoring platform	5	Turbidity sensor × 1	For monitoring the variations of turbidity along the control line of the CTA

6	Near-bottom platform for monitoring the characteristics of ocean current plume	1	Laser holographic imaging equipment, redeposition thickness measuring equipment, multi-parameter CTD binocular imaging equipment (with Chl, turbidity and dissolved oxygen sensors), electrochemical monitoring sensor and current meter.	Imaging of plume particles, collection and measurement of redeposited plume, image monitoring of deposition process, and variations of near-bottom-layer environmental parameters (ocean current, temperature, salinity, turbidity, Chl, DO, conductivity, pH and redox potential)
7	Redeposition thickness measuring device	14	Redeposition thickness measuring device (SLIC box with optimized design) × 1	For monitoring redeposition thickness along the control line of the CTA
8	Submerged buoys of mooring—Type I	3	CTD × 1, current meter × 1, turbidity sensor × 2, DO sensor × 1, hydrophone × 1, acoustic release device × 1 (including acoustic positioning function)	For monitoring temperature, salinity, current, turbidity and noise in the bottom-layer water column
9	Submerged buoy of mooring — Type II	4	CTD × 1, turbidity sensor × 2, acoustic release device × 1 set (acoustic with positioning function)	For monitoring the variations of temperature and salinity in the bottom-layer water column and the turbidity of water column under the impact of mining
10	Submerged buoys of mooring—Type III	2	CTD × 1 set, current meter × 1, turbidity sensor × 4, acoustic release device × 1 (including acoustic positioning function), sediment trap × 1, hydrophone × 1	For long-term monitoring of ocean current, turbidity, plume dispersal height, SPM re-settlement, noise and so on in the IRZ

11	Submerged buoys of mooring—Type IV	1	CTD × 4, current meter × 5, turbidity sensor × 2, 75K or 150K ADCP × 2, acoustic release device × 1, sediment trap × 2, DO sensor × 2, hydrophone × 1	For long-term monitoring of the vertical profiles of ocean current, the variations of background turbidity, the re-settlement of SPM, noise, etc. in the PRZ
12	Submerged buoys of mooring—Type V	3	Sediment trap × 1, electrochemical monitoring nodes × 30, acoustic release transponder, acoustic communication system	Used for sediment capture, monitoring of impact on conventional electrochemical parameters (conductivity, pH and redox potential), and inversion of plume vertical distribution by establishing turbidity-electrical parameter inversion model
13	Submerged buoys of mooring—Type VI	4	Electrochemical monitoring, biological trap and acoustic release transponder	Used for conventional electrochemical parameters (conductivity, pH and redox potential), monitoring and biological trap

10.3.2.3.1 Distributed environmental monitoring array (node)

The purpose of distributed environmental monitoring array (node) is to monitor near-bottom-layer ocean current, temperature and salinity, sediment concentration and turbidity. The heights of the nodes of the distributed environmental monitoring array are generally less than 2 m, they can be deployed closer to the CTA (the outer edge of the CTA) than the submerged buoys of mooring to form an inner ring of monitoring nodes.

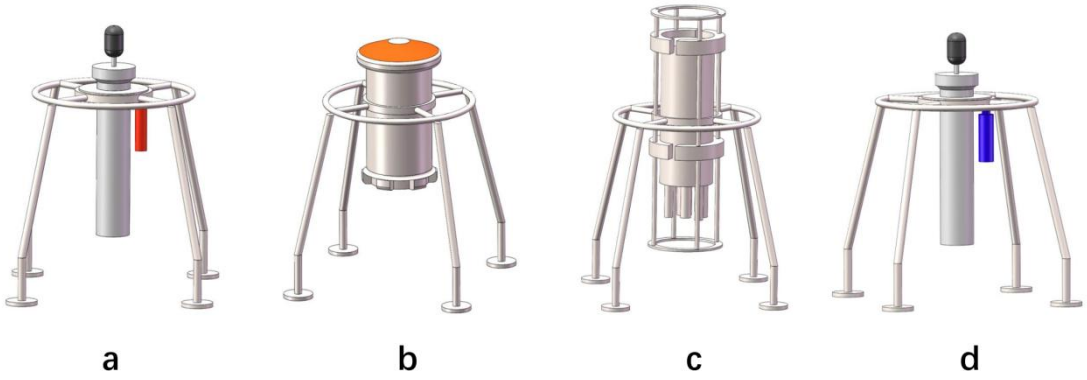

Figure 10.3-3 Distributed environmental monitoring array

(a. Bottom-layer ocean current + turbidity monitoring platform; b. ADCP monitoring platform; c. Bottom-layer temperature and salinity + turbidity monitoring platform; d. Bottom-layer ocean current + sediment concentration monitoring platform)

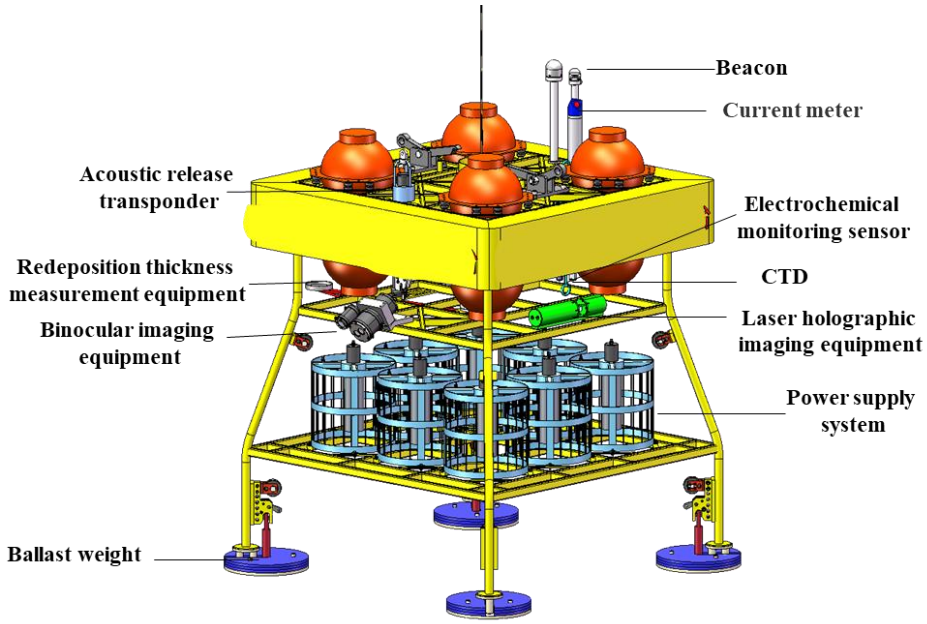

Figure 10.3-4 Near-bottom platform for monitoring the characteristics of ocean current plume

10.3.2.3.2 Redeposition thickness measuring system

Germany's GEOMAR Helmholtz Centre for Ocean Research Kiel has developed a simple redeposited sediment monitoring device—SLIC box in the environmental impact monitoring of seabed test mining in the CCZ of the East Pacific Ocean. More accurate monitoring data of redeposition thickness can be obtained with existing technologies (i.e. acoustic and optical measurement based on AUV/ROV). These data

are vital in assessing the simulation results of plume model and further improving the precision of model simulation. In this test, we will also use similar equipment, but with some improvements: (i) Using sawtooth waveform instead of sine waveform as the bottom plate of the monitoring box; increasing the slope, reducing the peak area and simplifying the width-thickness conversion process. (ii) Changing the other half waveform to a black-and-white checkerboard, so as to monitor the thickness of sediment below 1 mm through color variations, and also calibrate the camera through the checkerboard.

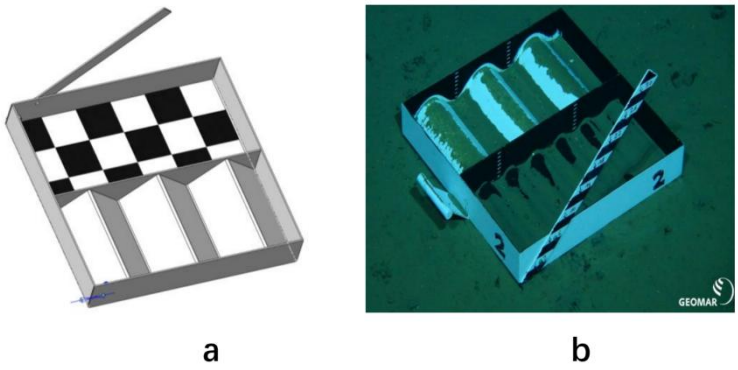

Figure 10.3-5 Redeposition thickness measuring system

(a. The redeposition thickness measuring system to be used in this test; b. Similar systems used by GEOMAR)

10.3.2.3.3 Submerged buoy of mooring

According to different monitoring purposes, all the submerged buoys of mooring system to be deployed near the CTA will be divided into short mooring and long mooring. The short mooring will be used to monitor the vertical profiles of ocean current, sediment concentration and turbidity data in the water column, noise, and so on. The long mooring will be used for long-term monitoring of the vertical profiles of ocean current, turbidity and plume dispersal, re-settlement of SPM, noise and so on in the CTA and PRZ as well as the areas between them.

The submerged buoys of mooring will be mainly used for monitoring the source intensity and dispersal of sediment plume. The monitoring of source intensity is mainly based on the whole-process monitoring of vehicle monitoring system and

environmental impact inspection and monitoring, so as to obtain more accurate and reliable data of plume source intensity. The monitoring data obtained with the submerged buoys of mooring system, distributed environmental monitoring array and redeposition thickness measuring system will provide the basis for quantitative analysis of plume dispersal path, range and law.

The turbidity monitoring positions of the monitoring station in the CTA are 2 m and 6 m above the bottom. According to the results of the near-field numerical simulation of GSR test and the far-field numerical model of this plan, the turbidity of the bottom-layer nepheloid formed by test-mining rapidly decays at the depth of 2 m above the bottom, so turbidimeters near the bottom are set at the depth of 2 m and 6 m above the bottom to observe SPM concentration in the near-bottom layer during this test (GSR, 2018). The SPM concentration monitoring device will be set at 20 m above the bottom, and the concentration is within 1.0 mg/L of the simulated vertical distribution concentration value of SPM in this plan, which is convenient for comparison with the background turbidity value, and then for confirming the mining impact.

Among them, Types I-III submerged buoys of mooring will be used for environmental monitoring in the CTA, and Type IV submerged buoy of mooring will be used for environmental monitoring in the PRZ.

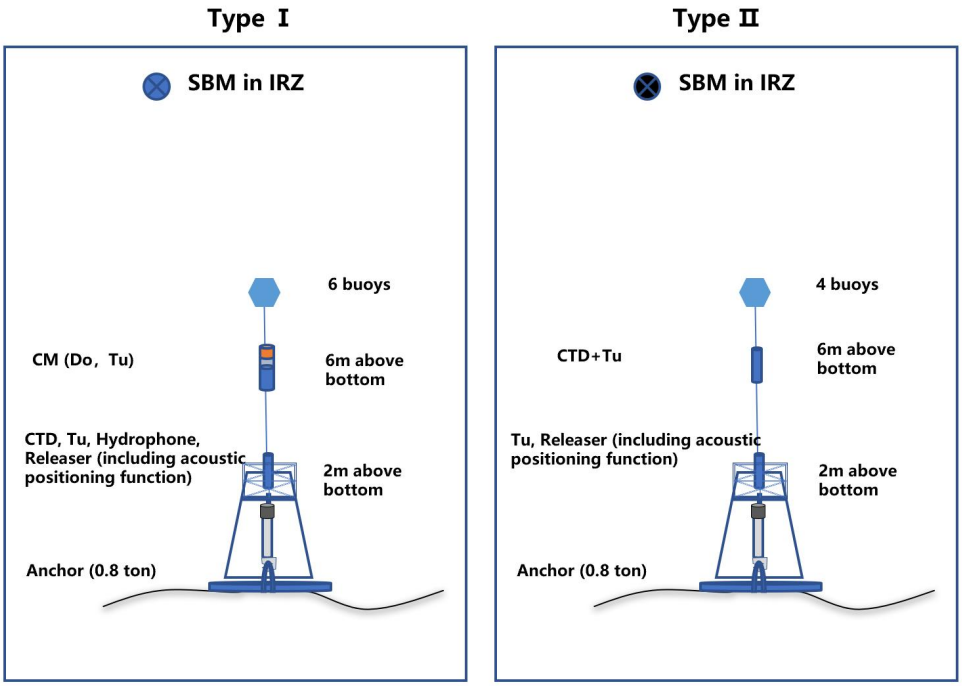

Figure 10.3-6 Design drawing of submerged buoy of mooring (Types I and II)

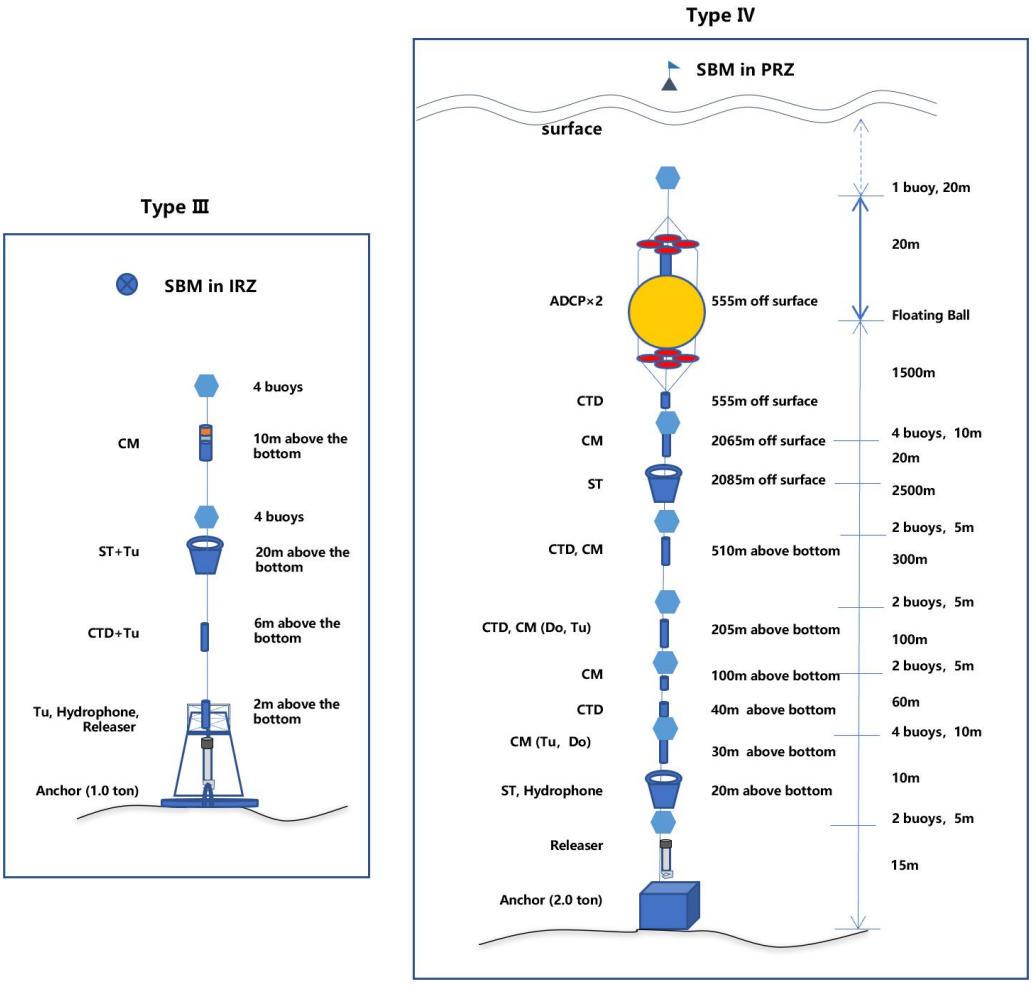

Figure 10.3-7 Design drawing of submerged buoy of mooring (Types III and IV)

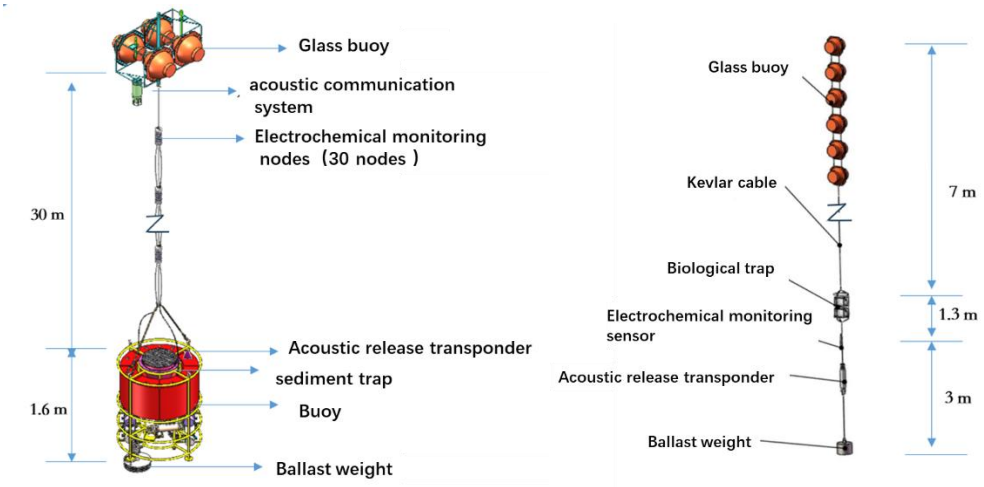

Figure 10.3-8 Design drawing of submerged buoy of mooring (Types V and IV)

10.3.2.3.4 Design of monitoring arrays

A three-layer surrounding monitoring array will be deployed according to the basic law of sediment plume dispersal and the results of numerical simulation. The direction and size of the bottom-layer ocean current play a vital role in plume dispersal, determining the dispersal direction and scope of the plume. Therefore, it is necessary to grasp the direction of the underflow through field observation before putting it into the monitoring station and reasonably increase the distribution of the downstream monitoring stations.

Based on the above-mentioned principles, we initially designed the monitoring array as follows:

a) First monitoring ring: At the outer boundary of the CTA, the near-bottom distributed environmental monitoring array is used to monitor the variations of ocean current and sediment concentration/turbidity in the CTA. The direct measurement data of redeposition thickness are obtained by using the redeposition thickness measuring system;

b) Second and third monitoring rings: The submerged buoys of mooring will be deployed along the second and third monitoring rings. The second monitoring ring is as close as possible to the CTA, within the range of 1 mg/L plume turbidity (initial radius of approximately 600 m). The third

monitoring ring is located in the range of 0.1-1 mg/L plume turbidity (initial radius of approximately 2,000 m). The radii of the second and third monitoring rings will be determined according to the numerical simulation results of near-bottom-layer sediment plume, with reference to historical documents and the data of other collector vehicle tests in the CCZ.

c) Monitoring of peripheral areas and the PRZ: Depending on the variations of topography, a set of long submerged buoys (Type IV) will be deployed at the same water depth, at a station approximately 6-8 km upstream to the CTA or the PRZ, so as to obtain the monitoring data beyond the plume impact range;

d) The initial design is based on the historical monitoring data (July-October) and the numerical simulation results of plume dispersal based thereon (Annex 1). Before the above-mentioned equipment is launched, LADCP and short-term lander system will be used to re-observe the near-bottom-layer flow field, and the design of monitoring array will be adjusted as appropriate.

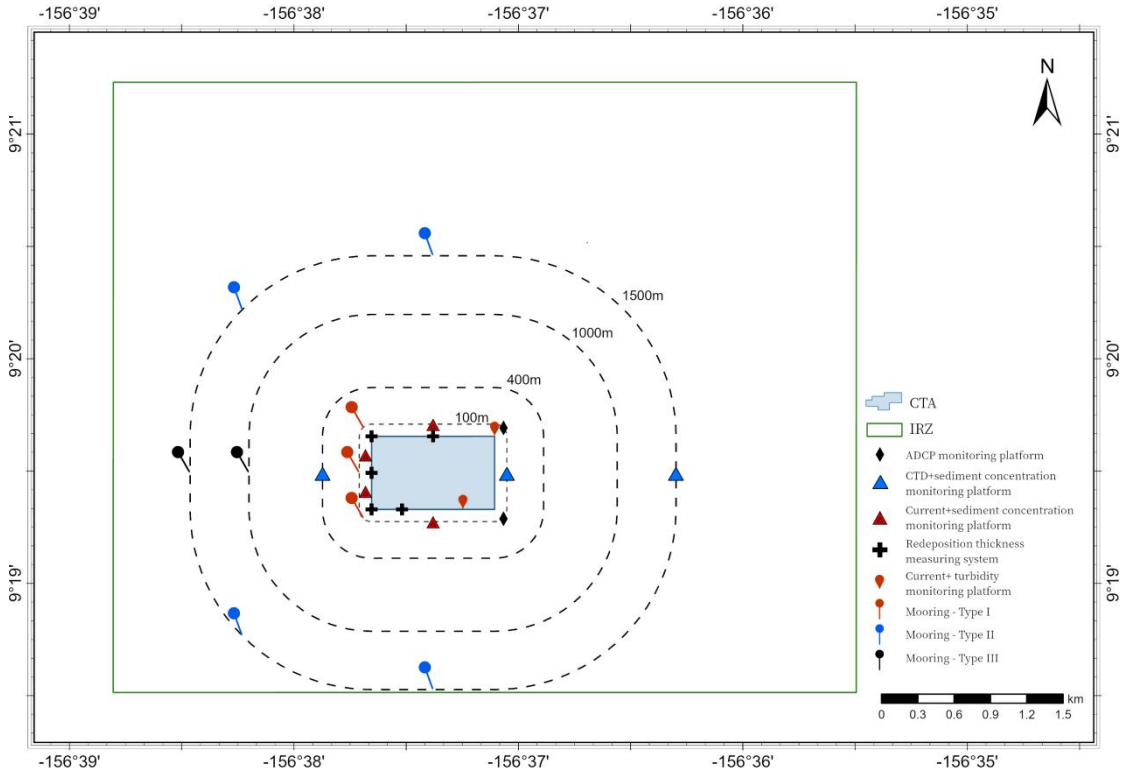

Figure 10.3-9 Design of monitoring arrays

The near-bottom distributed environmental monitoring array, DEMA; The submerged buoys of mooring (SBM); Source intensity monitoring system (SIMS); Plume diffusion monitoring system

(PDMS)

10.3.2.4 Other environmental monitoring measures during the test

10.3.2.4.1 Monitoring of near-bottom layer with AUV

Before and after the test-mining, the AUV *QIANLONG-IV* will be used to conduct near-bottom-layer photography survey of the CTA, the PRZ and the main direction of plume dispersal. We will perform near-bottom survey at 3-5 m above the bottom with the AUV, and determine the coverage area of photographs with laser ruler, thus obtaining quantitative data. The AUV will travel at a speed of 0.8-1.0 knots, and synchronously record environmental parameters such as temperature, salinity and turbidity in water. We will interpret the obtained photographs, identify megafauna in the photographs, and obtain information such as the number, distribution and diversity of morphospecies. For the benthic community data obtained from photography survey, we will conduct multivariate analysis to identify the spatial variations of benthic community indexes (species number, abundance, biomass, Margalef richness index, Shannon-Wiener diversity index and Pielou's evenness index) before and after the collector vehicle test, as well as the main influencing factors, so as to judge the impact of mining activities on benthic communities.

Figure 10.3-10 AUV *QIANLONG-IV* to be used for near-bottom monitoring

10.3.2.4.2 Collection of sediment samples and monitoring of benthic communities

a. EMP design

Sampling of shallow-surface-layer sediments:

We will sample the shallow-surface-layer sediments with the shipboard box corer/multicorer in and around the CTA before and after test, as well as analyze meiofauna and macrofauna therein.

Prior to the test-mining, we will set up two stations in the CTA and PRZ to survey environment baselines and obtain sediment samples (combined with the environment baseline survey tasks and exploration tasks in the Contract Area). Six stations (100 m, 250 m, 500 m, 1,000 m, 3,000 m and 5,000 m away from the CTA) will be set along the main direction of plume dispersal to obtain sediment samples.

After the test-mining, we will revisit the site and take samples at the above-mentioned stations.

b. Specific analysis methods

Meiofauna (Nematoda, etc.) will be sampled by multicorer, stratified and stored in 4 % formaldehyde solution and -80 °C refrigerator. Macrofauna (Polychaeta, small crustaceans, etc.) will be sampled with box corer, screened by 250 μm screen in-situ and stored in anhydrous ethanol for subsequent morphological identification and DNA barcode extraction.

For the benthic community data obtained from sediment survey, we will perform multivariate analysis to identify the spatial variations of benthic community indexes (species number, abundance, biomass, Margalef richness index, Shannon-Wiener diversity index and Pielou's evenness index) before and after the collector vehicle test as well as the main influencing factors, so as to judge the impact of mining activities on benthic communities.

10.3.2.4.3 Collection of seawater samples and monitoring of water environment

The purpose of hydrochemical monitoring is to compare and study the variations

of SPM, nutrient, dissolved organic carbon (DOC), DIC, POC and DO concentrations in seawater prior to, during and following the collector vehicle test, and to assess the impact and intensity of environmental variations caused by mining activities.

a. EMP design

In this study, SPM, nutrients, DOC, DIC, POC and DO concentrations will be collected from a site with 12 layers (5 m, 10 m, 15 m, 20 m, 25 m, 30 m, 40 m, 50 m, 75 m, 100 m, 150 m and 200 m above the bottom) in the CTA and PRZ respectively.

During the testing of the collector vehicle, six stations (100 m, 250 m, 500 m, 1,000 m, 3,000 m and 5,000 m away from the mining site) will be set up along the main direction of plume dispersal. Seawater samples will be extracted at 12 layers (5 m, 10 m, 15 m, 20 m, 25 m, 30 m, 40 m, 50 m, 75 m, 100 m, 150 m and 200 m) for determination of SPM, nutrient, DOC, DIC, POC and DO concentrations, which will be used as the environmental sample values during the disturbance.

After the testing of the collector vehicle, six stations (100 m, 250 m, 500 m, 1,000 m, 3,000 m and 5,000 m away from the mining site) will be set up along the main direction of plume dispersal. Seawater samples will be extracted at 12 layers (5 m, 10 m, 15 m, 20 m, 25 m, 30 m, 40 m, 50 m, 75 m, 100 m, 150 m and 200 m) for determination of SPM, nutrient, DOC, DIC, POC and DO concentrations, which will be used as the environmental sample values after the disturbance. We will also conduct comprehensive analysis of environmental pollution variations prior to, during and following disturbance to assess the environmental impact and intensity of disturbance.

b. Specific analysis methods

(a) DOC

Immediately after being collected, the seawater samples will be filtered by Whatman GF/F glass fiber filter membrane that has been burned at 450 °C for 4 h in advance, and 50 mL of filtrate will be collected in a brown glass bottle that has been

burned at 550 °C for 2 h. Then, the seawater samples will be acidified to pH of 2 by dropping in excellent pure concentrated phosphoric acid. After shaking for several minutes, the glass bottle will be plugged, sealed and stored in a freezer. Back in the laboratory, the seawater samples will be determined (at data precision of 0.01 mg/L) with Multi C/N 3100 produced by Analytik Jena AG of Germany.

(b) POC

The collected seawater samples will be filtered by Whatman GF/F glass fiber filter membrane (burned at 450 °C for 2 h in advance), and then the filter membrane will be stored at -20 °C and brought back to the laboratory for analysis. Before analysis, inorganic carbon will be removed through fumigation with concentrated HCl for more than 12 h. After distillation, washing and drying, the samples will be put into the TOC analyzer—SSM (TOC-5000A, manufactured by Shimadzu of Japan) to determine the POC content, with a data precision of 0.01 mg/L.

(c) DIC

In-situ seawater samples will be collected with a clean silicone tube. The small amount of bubbles in the silicone tube should be discharged, and then a 150 mL sampling bottle should be moistened for three times. Insert the silicone tube to the end, and take it out after the seawater sample exceeds the 100 mL mark. Add 1.5 mL of saturated mercuric chloride solution, mix well and fix it, and then store it at 4 °C.

The working curve will be drawn according to Article 8.2 of "Determination of dissolved inorganic carbon in seawater using non-dispersive infrared absorption" (HY/T 196-2015), and the sample will be determined by total inorganic carbon analyzer.

Connect the seawater sample to the sample injection end of the digital pump, set the sample injection volume so that the apparatus response value of the sample measurement falls in the middle of the working curve, run the analysis program, pump the sample and phosphoric acid solution into the reaction tank, blow the generated carbon dioxide into the drying system with high-purity nitrogen as the carrier, and

then put the sample into the detector for determination, record the corresponding instrument response value, and calculate the total DIC content of the sample according to the working curve.

$$DIC_v = \frac{A - a}{(b \times V) \times 1{,}000}$$

DIC_v indicates the total DIC content of the sample, with the unit being μmol/L; A indicates the response value of the apparatus; a represents the intercept of the working curve; $b$indicates the slope of the working curve; V indicates the injection volume of seawater sample during determination, with the unit being mL.

$$\mathrm{DIC} = \frac{\mathrm{DIC_v}}{\frac{(1-\mathrm{x})}{\rho}}$$

DIC represents the total DIC content in seawater samples, with the unit being μmol/kg); ρ indicates the density of seawater at the sample temperature, with the unit being kg/dm^3; x represents the ratio of the added volume of saturated mercuric chloride solution to the volume of the sample bottle.

(d) DO

According to "Specifications for oceanographic survey - Part 3: Marine meteorological observations" (GB/T 12763-2007), the iodometric titration method will be used. The seawater sample will be gradually filled into a 125 mL brown glass bottle until overflow; and then the bottle will be covered with a bottle cap.

Add 1 mL of manganese chloride solution and 1 mL of alkaline potassium iodide solution, shake well and fix the bottle.

Dissolve the precipitate completely with 1 mL sulfuric acid solution and then titrate with sodium thiosulfate.

Calculate DO concentration in the seawater sample:

$$\rho_{O_2} = \frac{c \times V \times 8}{V_0} \times 1{,}000$$

ρ_{O_2} represents DO concentration in seawater sample, with the unit being mg/L; c

represents the concentration of sodium thiosulfate, with the unit being mol/L; V represents the volume of sodium thiosulfate consumed in the titration process, with the unit being mL; V_0 represents the actual seawater sample volume for titration (= the volume of water sampling bottle - the volume of fixative for fixing water samples), with the unit being mL.

All DO samples will be measured in-situ.

(e) Inorganic nutrients

Nutrients will be determined according to GB/T 12763-2007. Seawater samples will be filtered by Whatman GF/F glass fiber filter membrane and determined by 7230 spectrophotometer. The nutrients are mainly nitrite, nitrate, phosphate and silicate.

Nitrite: Take 500 mL seawater sample, filter it with Whatman GF/F glass fiber filter membrane, measure 50 mL and add it into a colorimetric tube with plug. Referring to the method of drawing standard curve in 37.5.1 of GB/T 12763-2007, use 7230 spectrophotometer to determine the absorbance A_w of seawater sample. Measure 50 mL of secondary deionized water and add it into the colorimetric tube with plug. According to the method of drawing standard curve in 37.5.1 of GB/T 12763-2007, use 7230 spectrophotometer to measure the absorbance A_h of analytical blank.

Calculate A_n

$$A_n = A_w - A_{\mathrm{h}}$$

Calculate the concentration of nitrite nitrogen in seawater sample:

$$\rho(\mathrm{NO_2\text{-}N}) = \frac{A_n - a}{b}$$

$\rho(\mathrm{NO_2\text{-}N})$ represents the concentration of nitrite nitrogen, with the unit being mg/L; A_n represents the absorbance of nitrite nitrogen in seawater sample; a represents the intercept of standard curve; b indicates the slope of standard curve.

Nitrate (cadmium column reduction method): Take 500 mL seawater sample, filter it with Whatman GF/F glass fiber filter membrane, measure 50 mL and add it into a 125 mL conical flask with stopper, add 50 mL ammonium chloride buffer

solution and mix well. Referring to the method of drawing standard curve in 38.1.5.2 of GB/T 12763-2007, determine the absorbance A_w of seawater sample with 7230 spectrophotometer. Measure 50 mL of secondary deionized water, add it into a 125 mL conical flask with stopper, add 50 mL of ammonium chloride buffer solution, and mix well. Referring to the method of drawing standard curve in 38.1.5.2 of GB/T 12763-2007, determine the absorbance A_h of analytical blank with 7230 spectrophotometer. The concentration of nitrate nitrogen and nitrite nitrogen (mg/L) c_{Total} will be calculated by the standard working curve A_w-A_h or linear regression equation.

Calculate the concentration of nitrate nitrogen in seawater samples:

$$c(NO_3 - N) = c_{Total} - c(NO_2 - N)$$

Phosphate (ascorbic acid-based phosphorus molybdenum blue method): Take 500 mL seawater sample, filter it with Whatman GF/F glass fiber filter membrane, and seal it for later use.

Measure 25 mL seawater sample (2 parallel samples for each seawater sample) to 50 mL reaction flask and mix well. Referring to 9.6.1.2-9.6.1.3 of GB/T 12763-2007, determine the absorbance of seawater samples. Meanwhile, determine the absorbance of blank group (25 mL water).

Calculate the concentration of phosphate phosphorus

$$c(PO_4 - Si) = \frac{(\overline{A_w} - A_b) - a}{b}$$

$c(PO_4 - Si)$ represents the concentration of reactive phosphate in seawater sample, with the unit being μmol/mL; $\overline{A_w}$ represents the average absorbance measured from the seawater samples; A_b is the blank absorbance; a is the intercept of standard curve; b is the slope of standard curve.

Silicate (silicon molybdenum yellow method): Take 500 mL seawater sample, filter it with Whatman GF/F glass fiber filter membrane, and seal it for later use.

Measure 3 mL of ammonium molybdate solution and put it into a 50 mL

colorimetric tube with plug, add 25 mL seawater sample (two parallel samples for each seawater sample) and mix well. Referring to 8.6.1.2-8.6.1.3 of GB/T 12763-2007, determine the absorbance A_w of seawater sample. Meanwhile, determine the absorbance A_b of blank group (25 mL water).

Calculate the concentration of silicate silicon

$$c(SiO_3 - Si) = \frac{(\overline{A_w} - A_b) - a}{b}$$

$c(SiO_3 - Si)$ represents the concentration of reactive silicate in seawater sample, with the unit being μmol/mL; $\overline{A_w}$ represents the average absorbance measured from the seawater samples; A_b is the blank absorbance; a is the intercept of standard curve; b is the slope of standard curve.

(f) SPM

For the determination of SPM, refer to China's national standard (GB/T 17378.4-2007).

Use an aspirator filter pump (pressure of 5×10^4-6×10^4 Pa) to suck 8 L seawater sample through a Whatman GF/F glass fiber filter membrane with a pre-weighed weight W_2 of 0.45 μm (SPM with high concentration can be caused by mining disturbance, and the seawater sample volume after disturbance is 1 L). See 27.4.3.2-27.4.3.5 of national standard GB 17378.4-2007 for details.

Put the filter membrane into an electric heating constant temperature drying oven (40-50 °C) to dehydrate at a constant temperature for 6-8 h, take it out and put it into a silica gel dryer. 6-8 h later, weigh it with a scale of 1:100,000 to obtain W_1.

Calculate the weight of SPM:

$$\rho = \frac{W_1 - W_2}{V}$$

ρ represents the concentration of SPM, with the unit being mg/L; W_1 represents the dry weight of the filter membrane after filtering the SPM, with the unit being mg; W_2 represents the dry weight of the filter membrane, with the unit being mg; V represents the volume of seawater sample, with the unit being L.

10.3.2.4.4 Monitoring of microbial communities and ecosystem service functions

The purpose of monitoring microbial community and ecosystem service functions is to compare the variations of microbial community structure, diversity and functional genes in seawater and shallow-surface-layer sediments prior to, during and following mining activities, as well as to assess the impact of mining activities on the service functions of deep-sea microbial communities and deep-sea ecosystems.

a. EMP design

The design of stations for ship-mounted CTD measurement is consistent with that of stations for hydrochemical monitoring. There will also be analysis of microorganisms and functional genes in time series seawater samples obtained with in-situ environmental sampler carried by the collector vehicle. For each seawater sample, use a 0.2 μm PC filter membrane to filter 4 L of seawater sample in-situ, and store it at -80 °C in refrigerator or liquid nitrogen for use in subsequent analysis.

We will sample the shallow-surface-layer sediments with the ship-mounted box corer/multicorer in and around the CTA before and after mining, as well as analyze microorganisms therein.

Prior to the test-mining, we will set up two stations in the CTA and PRZ to survey environment baselines and obtain sediment samples (combined with the environment baseline survey tasks and exploration tasks in the Contract Area). Six stations (100 m, 250 m, 500 m, 1,000 m, 3,000 m and 5,000 m away from the mining site) will be set along the main direction of plume dispersal to obtain sediment samples.

After the test-mining, we will revisit the site and take samples at the above-mentioned stations.

Samples will be divided into three layers by depth (0-2 cm, 2-5 cm and 5-10 cm) and stored at -80 °C in refrigerator or liquid nitrogen for use in subsequent analysis. Corresponding samples will also be stored for use in the analysis of sedimentary environment parameters.

b. Specific analysis methods

(a) Analysis of microbial communities

Both DNA extraction and PCR amplification will be conducted according to standard methods. For the V4-V5 variable region amplification of bacterial 16S rRNA gene adopted archaea-bacteria universal primers 515F-Y (5'-GTGYCAGCMGCCGCGGTAA-3') and 926R (5'-CCGYCAATTYMTTTRAGTTT-3') recommended by the Earth Microbiome Project, which have high coverage for both archaea and bacteria. Finally, the amplification products of each sample will be mixed to purify the PCR product; then a library will be constructed to conduct paired-ended sequencing (2 × 300 bps) on the Illumina NovaSeq high-throughput sequencing platform. FLASH will be used to merge paired-ended sequences. Qiime will be used to filter the sequence quality, denoise, splice and remove chimera, so as to obtain high-quality sequences. UCLUST method will be used to cluster high-quality sequences according to 100 % sequence similarity, and generate characteristic sequences (ASVs) and abundance data tables. Then the Blast method will be used to compare the sequence annotation database, and the species annotation of each ASV will be obtained to form a table of total data for subsequent analysis.

Furthermore, nonparametric multivariate analysis of variance, similarity analysis, SIMPER analysis and LEfSe analysis will be used to analyze the difference degree and species of bacterial communities before and after mining. The co-occurrence network will be used to analyze the co-occurrence mode of bacterial species during the mining process, and the molecular ecological network will be used to analyze the biological interaction inside a bacterial community, including network construction and network analysis. Based on modular feature factor analysis, we will find the core species to maintain the stability of bacterial community. The environmental driving factors of bacterial community change before and after mining will be identified by environmental association analyses (EAA). The ecological mechanism analysis methods such as zero model will be used to analyze the variations of bacterial

community ecological process before and after mining. With the above-mentioned studies, we will systematically and comprehensively assess the disturbance caused by the testing of collector vehicle to the deep-sea microbial community and the response mechanism of the microbial community to this disturbance.

(b) Analysis of microbial ecosystem service functions

DNA extraction and PCR amplification will be conducted according to standard methods. A metagenomic library will be constructed and 2 × 150 bps paired-ended sequencing will be performed on the Illumina HiSeq platform. For the metatranscriptome library, it is necessary to remove ribosomal RNA, synthesize cDNA and construct it, and use the Illumina HiSeq platform for 2 × 150 bps paired-ended sequencing. Bioinformatics processing will be performed for RawReads obtained by metagenome and metatranscriptome sequencing by using complete MetaWRAP processing flow and recommended database. The Read_qc module in MetaWRAP will be used to control the original reads of a single sample, and then FASTQC and MultiQC will be called to generate the quality reports of raw reads and clean reads to assess the quality control results. The clean reads of each sample are assembled by MetaWRAP Assembly module, boxed by MetaWRAP Binning module, and divided into two halves as differential coverage information. Then the Bin_refinement module of MetaWRAP will be used to optimize the generated bins into the final BIN-based genome set. CheckM software will be used to assess the integrity and pollution rate of each MAG. METABOLIC will be used to predict the metabolic characteristics of deep-sea microbial genome and the pathways involved in the main biogeochemical cycles. The role of deep-sea microorganisms in other biogeochemical cycles such as carbon cycle and nitrogen cycle will be obtained, and the total abundance information of each cycle path will be calculated according to the abundance information of genome. The environmental mRNA sequence will be read and mapped to the metabolic pathway genes in the reconstructed genome box to assess the in-situ activity. The expression of functional genes in the reconstructed

genome will be analyzed by combining with the metatranscriptome. Furthermore, the variations of functional gene abundance, functional gene expression abundance and cycle path abundance of carbon and nitrogen cycle before and after mining will be explored by statistical methods such as difference test between groups. The variations of microbial community diversity involved in carbon and nitrogen cycle before and after mining will be analyzed by nonparametric test and ranking analysis. The microbial communities, functional genes and cycle paths related to carbon and nitrogen cycle will be correlated with carbon and nitrogen fixation rates, and the effects of microbial function variations on carbon and nitrogen fixation rates will be analyzed. Through the above-mentioned studies, we can systematically and comprehensively assess the disturbance caused by the testing of collector vehicle to the carbon and nitrogen cycle function of microorganisms, as well as analyze the response mechanism of carbon and nitrogen fixation rate to this disturbance at the microbial level.

10.3.2.5 Long-term EMP after the test-mining

To obtain the long-term observation data of natural variations in the environment after the test-mining, we will set up a long-term observation system in this region after the collector vehicle test, which has the long-term monitoring ability for environmental parameters such as turbidity, ocean current, pH, noise and near-bottom video.

In the next few years, seawater and sediment samples in the CTA and PRZ will be collected with CTD, box corer and multicorer for the EIA of this test.

10.3.3 EIA scheme

Using the environment baselines of the IRZ and PRZ constructed by the exploration task in the Contract Area, and the environmental survey and monitoring data prior to, during and following the test-mining, we will improve the sediment plume model and the EIA model. Using the pre-built EIA index (threshold) and comparative assessment method, we will compare and study the biological

communities and bottom environment characteristics of the IRZ and PRZ before and after the test, assess the impact of this collector vehicle test on benthic communities, benthic ecosystem functions and bottom-layer physicochemical environment, and report the results to the ISA.

10.3.3.1 Assessment of plume impact scope and intensity

SPM generated by the collector vehicle traveling and collecting nodules on the seabed will form near-bottom-layer sediment plume under the action of bottom-layer ocean current, which will have a direct impact on near-bottom-layer seawater environment, shallow-surface-layer sedimentary environment, benthic communities and benthic ecosystem functions. Based on the monitoring data of submerged buoys of mooring, distributed monitoring arrays and follow-up monitoring system, we will revise and improve the pre-built plume model, so as to calculate the impact scope, intensity, duration and redeposition intensity of plume, as well as assess the environmental impact of plume.

10.3.3.2 Assessment of mining disturbance to benthic communities

The collector vehicle's traveling and nodule-collecting activities will generate plume. The redeposition of the plume and the direct removal of nodules will have an impact on the benthic communities. Based on the analysis data of samples collected with multicorer and box corer, and the photography survey data of AUV, we will comparatively analyze the abundance, species diversity and community structure of meiofauna, macrofauna and megafauna before and after the testing of the collector vehicle. Based on the baseline data of the CTA before the test-mining and the PRZ, we will assess the impact of the disturbance of the collector vehicle on the benthic communities.

10.3.3.3 Assessment of mining disturbance to benthic ecosystem functions:

The collector vehicle's traveling and nodule-collecting activities will generate plume. The redeposition of the plume and the direct removal of nodules will have an

impact on the functions of benthic communities. Based on the samples collected with multicorer, near-bottom-layer CTD water sampler and vehicle-mounted time series water sampler, we will conduct the metagenome analysis of the microbial communities, as well as compare the variations of carbon and nitrogen cycle functional gene abundance, functional gene expression abundance and cycle path abundance before and after mining, so as to assess the disturbance caused by the testing of collector vehicle to the carbon and nitrogen cycle function of deep-sea microorganisms, and thus assess the impact of mining disturbance on the benthic ecosystem functions.

10.3.3.4 Assessment of mining disturbance to bottom-layer hydrochemical environment

The plume generated by the collector vehicle will dramatically change the characteristics of the bottom-layer hydrochemical environment. Based on the analysis of data collected with CTD water sampler and vehicle-mounted time series water sampler in the near-bottom layer, we will compare the short-term variations of chemical parameters before and after the testing of the collector vehicle, as well as assess the impact of mining disturbance on the bottom-layer hydrochemical environment in combination with the variations of biological communities and ecosystem functions.

10.3.3.5 Assessment of mining disturbance to sedimentary environment

The collector vehicle's traveling and nodule-collecting activities will generate plume. The redeposition of the plume and the direct removal of nodules will have an impact on the area's sedimentary environment. Based on the samples of multicorer, the AUV photography survey and monitoring data obtained with the distributed redeposition thickness monitoring array, the variations of redeposition thickness and physical and chemical properties of shallow-surface-layer sediments before and after the testing of the collector vehicle are compared, and the impact of mining disturbance on sedimentary environment is assessed in combination with the

variations of biological communities and ecosystem functions.

10.3.3.6 Assessment of mining-related noise and light disturbance

The noise of the collector vehicle operating on the seabed will disturb the bottom environment. The nighttime lighting of the SSV and EMV will also have a certain impact on seabirds. We will assess mining-related noise and light disturbance, based on the monitoring data of vehicle-mounted hydrophone and photometer and follow-up monitoring system, and of ship-mounted photometer, as well as after consulting on the spatio-temporal distribution scale of the main rare and endangered marine organisms in the CCZ of the East Pacific Ocean and their tolerance to noise and nighttime lighting.

Table 10.3-3 Main indicators of environmental monitoring and impact assessment

S.N.	Specific impact assessment contents	Field data and sample collection indicator	In-situ data and sample collection means	Final evaluation indicator
1	Plume impact scope and intensity	Data: Bottom-layer and near-bottom-layer temperature, salinity, turbidity, DO concentration, sediment concentration, current speed and direction Sample: None	Submerged buoys of mooring (including three depth types: Bottom layer, near-bottom layer and full depth profile), distributed monitoring array and vehicle-mounted follow-up monitoring system; the above-mentioned system includes CTD, single-point current meter, Doppler current meter (ADCP), DO sensor, turbidity sensor, sediment sensor, etc.	Impact scope, intensity and duration of sediment plume Thickness and scope of redeposition
2	Impact of mining disturbance on benthic communities	Data: Seabed videos and photographs Sample: Shallow-surface-layer sediment	AUV system, multicorer and box corer	Microbial community structure: Densities and community structures of meiofauna and macrofauna; Density and community structure of megafauna
3	Impact of mining disturbance on benthic ecosystem functions:	Data: None Sample: Shallow-surface-layer sediments, bottom-layer and near-bottom-layer seawater	Multicorer, box corer, CTD water sampler and in-situ water sampling system carried by the collector vehicle	Abundance of carbon and nitrogen cycle functional genes Functional gene expression abundance and circulating pathway abundance
4	Impact of mining disturbance on bottom-layer hydrochemical environment	Data: DO concentration, turbidity, water fluorescence Sample: Bottom-layer and near-bottom-layer seawater	CTD water sampler and in-situ water sampling system carried by the collector vehicle	DO concentration in bottom-layer seawater Bottom-layer seawater pH Concentration of POC, DOC and DIC in bottom-layer seawater

5	Impact of mining disturbance on sedimentary environment	Data: Seabed videos and photographs; high-precision shallow stratum profile data detected near the bottom; photographs of in-situ redeposition thickness Sample: Shallow-surface-layer sediments and pore water	AUV system, multicorer, box corer and distributed monitoring array (redeposition thickness monitoring system)	Concentration of dissolved inorganic salts in bottom-layer seawater Concentration of SPM in bottom-layer seawater Distribution of particle sizes in shallow-surface-layer sediment profile AOC and TOC in shallow-surface-layer sediments Heavy metal ion concentration, redox potential, pH in pore water Redeposition thickness
6	Impact of mining-related noise and light disturbance	Data: Noise; illumination intensity Sample: None	Deep-sea hydrophone and photometer	Noise intensity and frequency Illumination intensity

10.4 Report

10.4.1 Reporting the monitoring results to the ISA

The results of monitoring activities will be recorded in a monitoring report, which contains data for assessing the following contents: The collector vehicle's performance and the effectiveness of design and management measures. The survey results will be used to verify the plume model and impact forecast in this EIS, as well as provide a basis for the EIS and the EMMP for Commercial Mining. The general structure of the monitoring report will include:

—Introduction

—Legislative framework and standards

—Monitoring standards

—Monitoring methods

—Monitoring results

—Audit

—Recommendations and corrective actions

Minmetals will submit a monitoring report to the ISA every year. According to Regulation 32 of ISBA/19/C/17,

the Contractor shall report annually in writing to the Secretary-General on the implementation and results of the EMP, and submit data and information, taking into account all recommendations issued by the LTC.

These reports will explain the compliance with the EMMP and make recommendations for any corrective actions.

Minmetals will also disclose the results of other assessment and monitoring activities to the ISA every year.

Minmetals plans to hold a public stakeholder event to announce the results of the collector vehicle test.

10.4.2 Reporting unexpected accidents and disposal results to the ISA

Any spill, accident or uncontrolled release into the marine environment will be reported to the ISA as an emergency within the specified reporting time. Regulation 33 of ISBA/19/C/17 states:

A contractor shall promptly report to the Secretary-General in writing, using the most effective means, any incident arising from activities which have caused, are causing or pose a threat of serious harm to the marine environment.

The notification to the ISA will include the following:

—The event and all the important facts and circumstances known about the event at that time;

—Any and all actions taken to avoid or mitigate any adverse environmental impact;

—Any and all corrective measures that have been taken or may be taken to prevent similar incidents from happening again.

Minmetals will also notify any relevant third-party institutions as required by the MARPOL OPRC-HNS Protocol 2000.

11 Product Stewardship

It is estimated that no more than 10 t of wet nodules will be collected and lifted onto the deck in this test. These nodules will be used for scientific research, especially for the study of smelting process. Minmetals has advanced mineral processing and metallurgical processing technologies. All smelting experiments conducted in China are strictly regulated by domestic laws and regulations, so it is unlikely to cause adverse environmental impact.

12 Consultation

12.1 General introduction

This report is released for public comment on 2nd April and 11th April, 2024 on the official website of Minmetals and ISA, respectively. Deadline for comments was by the end of May, 2024 (The website is http://www.minmetals.com.cn/xxgk/qygg/202404/t20240 402_303328.html).

A total of 8 stakeholders' comments on this EIS have been received as of the end of the stakeholder consultation period.

(1) Deep Sea Conservation Coalition

(2) Deep-Ocean Stewardship Initiative

(3) Ocean North

(4) The Ocean Foundation

(5) The Pew Charitable Trusts

(6) U.S. Observer Delegation to the International Seabed Authority

(7) UK Foreign Ocean Policy Unit

(8) World Wide Fund for Nature

Minmetals subsequently organized and summarized these opinions. Beside opinions that clearly oppose deep-sea mining, there are also 57 general comments and suggestions, and 301 specific comments and suggestions, mainly related to EIA procedures, environmental baselines, reference area selection, plume modelling, monitoring plan, impact assessments, and some text and charts errors.

The current version of the EIS has been updated in response to public comments provided as part of the stakeholder consultation process. The modifications mainly include biological baselines (microbial diversity, more detailed biological classification and identification results, annual variation characteristics of benthic

communities, comparison results of IRZ and PRZ, statistical analysis of spatial differences in megafauna communities, heavy metal concentrations in organisms, etc), description of plume modeling method, and results of heavy metal toxicology tests.

We appreciate all stakeholders' feedback, which greatly improved this report.

Article 140 of the Convention provides that activities in the Area shall be carried out for the benefit of mankind as a whole. China Minmetals Corporation does not agree with a one-sided emphasis on exploitation at the expense of environmental protection, nor does it agree with a one-sided emphasis on environmental protection at the expense of exploitation, as a one-sided emphasis on one aspect is contrary to the purpose of the Convention. The protection of the deep-sea environment is an inherent requirement of the international seabed development regime itself, and the work of China Minmetals Corporation is aimed at striking a balance between deep-sea environmental protection and deep-sea development, so as to promote the process of deep-sea development and fundamentally enhance the well-being of humankind as a whole.

12.2 Response to stakeholder comments

12.2.1 EIS process

Regarding the issue of EIS process, it mainly focuses on the following four aspects.

(1) Some stakeholders as PEW believed that from a procedural perspective, a formal EIA Scoping is required.

In accordance with regulation 18 (c) of “Regulations on Prospecting and Exploration for Polymetallic Nodules in the Area” (ISBA/19/C/17), the applicant for a plan of work for exploration is required to submit with its application a "preliminary assessment of the possible impact of the proposed exploration activities on the marine environment". The Recommendations for Guidance have listed the activities during the exploration phase that do not require environmental impact assessment, as well as

the activities that require environmental impact assessment during the exploration phase. It has specified the information and measurements to be provided, the baseline data requirements, and provided guidance on the currently best available techniques and methods for the main areas or issues, in order to "support the contractors in implementing these exploration recommendations and effectively protect the marine environment from potential harmful effects of activities in the 'Area'". The "Regulations on Exploration" and the "Recommendations for Guidance" do not require a separate scoping procedure in the process of conducting environmental impact assessment for mining tests.

Based on this, China Minmetals Corporation believes that scoping is one of the component steps in the environmental impact assessment procedures during the exploration phase, and the specific content related to scoping has been integrated and reflected in the environmental impact report. Therefore, the environmental impact report for the mining test does not need to have a separate scoping stage.

(2) Some stakeholders (U.S. Delegation, DSCC, The Ocean Foundation) recommend additional description of the stakeholder consultation efforts, including consultation with adjacent coastal States.

In accordance with the recommendations of the ISA secretariat and LTC (ISBA/25/LTC/6/Rev.3), China Minmetals Corporation conducted consultations with stakeholders after the EIS report was made public and fully ensured that the consultations were open, transparent and involved all parties fairly. The location of the test was remote from the coastal State and did not involve crossing the seabed under the jurisdiction of the coastal State, and the estimation of the environmental impacts indicated that the extent of the impacts did not involve the coastal State, and therefore no specific consultation with the coastal State was required by ISA.

(3) Some stakeholders (PEW) believe that environmental risk assessment, impact mitigation and alternative options are needed.

We have already listed the environmental risk assessment, development of impact mitigation and alternative measures in the EIS report, which will be further revised and improved in accordance with the relevant comments and based on current best practices and scientific understanding.

(4) Some stakeholders recommend extending the consultation period

"Recommendations for the guidance of contractors for the assessment of the possible environmental impacts arising from exploration for marine minerals in the Area" (ISBA/25/LTC/6/Rev.3) do not provide guidance on the time period for stakeholder consultations on environmental impact statements, and the time period for stakeholder consultations on environmental impact statements has varied among several previous contractors. China Minmetals Corporation has determined the time period for stakeholder consultation in accordance with the relevant regulations of the China Ocean Affairs Administration and relevant domestic practices. The time period was ranged from 2nd April to 31st May, 2024.

12.2.2 Environmental baseline issues

The main issues with environmental baselines include the insufficient surveys to characterize temporal and spatial variation, and the lack of some environmental baseline parameters. The specific classifications and modifications are as follows.

12.2.2.1 Spatio-temporal characteristics of environmental baseline

In this report, we describe the spatio-temporal variation characteristics of some baseline elements. For example, chlorophyll a data based on satellite remote sensing**.** The annual average Chl a concentration in the surface layer of the IRZ is 0.08±0.03 μg/L, reaching maximally 0.09±0.05 μ g/L in April-June and minimally 0.06±0.02 μg/L in October.

In section 4.6.4 of the report, we analyzed the changes in seawater temperature, salinity, turbidity, and ocean currents in the survey area based on the annual observation results of the submersible mooring system. Section 4.7.7 also presents time-series sediment flux data collected by sediment capture devices. Section 5.4.3 also compared the interannual variation characteristics of abundance of meiofauna and macrofauna from 2017 to 2022.

The environmental recommendations suggest the need for survey data covering different seasons, and we approve of this concept based on scientific integrity. After several cruises since 2017, we have obtained a lot of scientific data and understanding of the environmental baseline in the area, with a time period covering three seasons, including summer, autumn and winter from August to December (Appendix 5), and the relevant data have been submitted to the ISA.In addition, with the help of satellite remote sensing and observations from the moorings+sediment traps, we have also gained a more complete knowledge of the seasonal variations. Our understanding of seasonal variations in the region will be further deepened and enriched with the continuation of the survey cruises.

About the spatial variation, we have added information on the environmental baseline and biodiversity survey stations for each of the previous cruises conducted by China Minmetals Corporation. Initially (e.g., 2017-2019), we carried out a broad range of surveys in the China Minmetals Corporation contract area, including Blocks A-1, A-2, A-3, A-5, A-6, A-7, A-8, etc., which enriched our baseline information for the CC zone. Subsequently, in accordance with the exploration contract provisions and China Minmetals' plan, we focused our environmental surveys on Block A-5 and organized survey cruises for 2021-2023. The survey contents and station information of these cruises have been added in this revision of the EIS report (Appendix 4 and Appendix 5).

In addition, according to the monitoring plan, Minmetals will continue to conduct environmental baseline investigations in the TMA and PRZ during the 2024

cruise and 2025 before the test to further obtain a statistically reliable environmental baseline data.

12.2.2.2 Relevant baseline data has not been collected

As pointed out by many stakeholders, previous EIS had missing or insufficient environmental baseline parameters. We divided into four categories for processing.

(1) Added some baseline parameters in this report

Microbe: as point out by DOSI **"inadequate for any meaningful microbial assessment or baseline"**. We conducted analysis based on existing microbe samples and supplemented relevant results in the report in sections 5.4.1.3 and 5.4.3.1 of the revised EIS.

Macrofauna: "**lacks taxonomic resolution**". we identified samples collected by box samplers and added more detailed taxonomic identifications. Results was shown in section 5.4.3.3.3.

Megafauna: For megafauna, we analyzed the photographic data obtained from deep-sea cameras for manual identification and added more detailed taxonomic identifications (to morphospecies). For these species, we have also provided photographic data from our photographs. In the initial version of EIS report, readers misinterpreted our accompanying photographs as references to images of megafauna from other literature, when in fact this was due to misleading descriptions. These photographs have not appeared in any published literature and are copyrighted by us. We have made changes to the representations. All of these were obtained from surveys during the cruise DY79.

Marine mammals, birds, turtles, sharks: "no systematic/detailed survey for seabirds and marine mammals". Since no direct observations of cetaceans have been recorded during the field observations of the China Minmetals cruises to date, we consulted and referenced data on globally important marine mammal sanctuaries

provided by the IUCN SSC-WCPA Marine Mammal Protected Areas Inter-Commission. This database is maintained on an ongoing basis by a number of global organizations, including the International Commission on Marine Mammal Protected Areas (ICMMPA), the World Commission on Protected Areas (WCPA) of the World Conservation Union (IUCN), and the IUCN Species Survival Commission (SSC). The assessments associated with this database indicate that the Block A-5 is far from being an "Important Marine Mammal Area".

The "Whale Superhighway" report, published by WWF in collaboration with dozens of research organizations around the world, also clearly describes the major migratory corridors for cetaceans globally, with the closest corridor to the western portion of the CC region being between the area around the Hawaiian Islands and the high-latitude offshore areas of the northeastern Pacific Ocean. The closest corridor to the western portion of the CCZ is the migratory corridor between the area around the Hawaiian Islands and the high latitude offshore areas of the Northeast Pacific. This corridor is far from the Block A-5, which is located south of the Hawaiian Islands. In addition, because no direct observations of sea turtles have been documented during field observations on the various cruises to date, we retrieved data on the primary sea turtle in the eastern Pacific, the leatherback turtle (*Dermochelys coriacea*). The Pacific leatherback turtle is one of the flagship species for marine conservation. As such, this species receives significant attention for monitoring and conservation (public data enrichment). Leatherback turtles in the eastern Pacific tend to move within migratory corridors to foraging grounds in the southeastern Pacific, with areas of concentration overlapping with areas of high chlorophyll concentration, with their central distribution areas located in the CC zone and in the eastern Pacific east of 120° W.

(2) samples have not yet analyzed

eDNA: Samples were also collected during the cruise DY79 (2023), and a descriptive and comparative study of the species diversity of multiple taxa in Block A-

5 is being conducted using eDNA methods. This study is ongoing and it is anticipated that this information is expected to be submitted to ISA in the 2024 annual report.

Noise: We deployed hydrophones on mooring system in the Block A-5 on 2022 cruises. These hydrophones recorded not only ocean background noise but also some cetacean voicing data. These data will be analyzed by professional marine acoustic experts and the results will be submitted to ISA, which may be useful for understanding the diversity and distribution patterns of cetaceans in the western part of the CCZ.

(3) Sample or data not yet collected but planned for 2024 and 2025 cruises

AUV optical data: It is planned to conduct video surveys using AUVs during the 2024 and 2025 cruises.

Food web: We expect to use ROV during 2025 cruise, which will enable us to obtain qualified samples for isotope analysis which would be used for food web analysis.

(4) Other unresolved baseline parameters

Sediment oxygen consumption: We plan to survey benthic communities using ROVs during 2025, which will provide a unique opportunity to deploy in situ DO measurement equipment onto the seafloor, which will provide us with the feasibility of measuring oxygen consumption in benthic communities in the A-5 region.

12.2.3 Comparison of IRZ and PRZ

PEW, DOSI, and the UK Foreign Ocean Policy Unit have raised the issue that existing data cannot fully prove the similarity between IRZ and PRZ.

For the comparison of the PRZ and IRZ, we added more data to the EIS report. The environmental and sediment characteristics of the PRZ and IRZ within Block A-5 exhibit a high degree of similarity, including seafloor current velocity, temperature, salinity, water depth, nodule coverage, sediment properties, sedimentation flux, primary productivity, and other features.

We report the results in terms of microbial community structure at full water depth, microbial community structure in surface sediments, community structure of meiofauna, macrofauna and megafauna. We believe that these results are sufficient to demonstrate the environmental and biological community similarities between two regions (PRZ and IRZ) that are so close in horizontal distance.

These characteristics may imply that the habitats in these two areas are highly comparable.

12.2.4 Plume modeling

PEW, DSCC, DOSI and UK Foreign Ocean Policy Unit pointed out that the plume model was poorly described and appears not to use any of the recent increases in knowledge of mining plume behaviour.

Our response is as follows.

(1) FVCOM is a three-dimensional unstructured grid primitive equation numerical model with a triangular mesh in the horizontal direction and a generalized random-bottom coordinate system in the vertical direction. It contains a sediment transport module for sediment dynamics processes and has been shown to be effective for the simulation of sediment dynamics processes (Chen et al. 2003, 2006, Ge et al. 2015, 2020, Li et al. 2023). In the ESI report, we have added a description of the sediment transport module and parameter settings (see Section 7.5.1 Model-Sediment Module and Annex 1 for details).

(2) Turbidity generated by the mining plume occurs mainly in the near field of the Collector Vehicle, i.e., within 100 m of the truck and within 2 m of the bottom ("The observations suggest that 92 to 98% of the sediment mobilized by the collector were below 2 m at the time and location of the observations." (Muñoz-Royo et al. 2022). "It was found that the generated sediment plume extended no >2 m above the seabed close to the source (<100 m) but increased in height at greater distance. Furthermore, turbidity values decreased rapidly with increasing distance to the source." (Haalboom et al. 2023).). Our plume model focuses primarily on the effect of

the mining plume on the far field (>100 m from the Collector Vehicle) and therefore does not include the effect of turbidity in the near field (<10 times the distance of the truck length) in the model. This would result in our model predicting a larger plume impact than is actually the case, as more than 90% of the disturbed sediment is located near the Collector Vehicle, within 2 m of the bottom, and does not spread out with the bottom flow field. Meanwhile, the turbidity currents generated by deep-sea mining were also found in the test of GSR's Collector Vehicle, and many parameters of the modeling of mining turbidity currents are still unclear. Therefore, we need to collect relevant data (both near-field and far-field) in this sea test to establish and validate the near-field turbidity model, which will also provide a good foundation for future work on deep-sea mining plume modeling.

12.2.5 Ecotoxicology

Pew, DOSI and other organizations comment that this report lack of ecotoxicology information.

This report supplements some ecotoxicology study including two aspects:

(1) we used the luminescent bacteria method to evaluate the toxicity of sediment eluates from A-5 on *Vibrio fischeri*. An important innovative finding is that some metal elements in this area, which are not typically considered to have significant heavy metal toxicity, can significantly alter the toxicity of copper, cadmium, and chromium, which are known to have significant heavy metal toxicity. For detailed results of this part, please see Annex 3 (Toxicity assessment to Vibrio fischeri of heavy metals released from disturbed surface sediments in the Block A-5).

(2) Polymetallic nodule minerals are oxides, which are naturally stable, and heavy metals are very difficult to dissolve in the ionic state. This was also confirmed by data from an in-laboratory high-pressure crushing simulation experiment carried out by China Minmetals Corporation (Zeng et al. 2019). In this experiment, “The results show that under the optimal dissolution conditions, including manganese nodule pulp at the concentration of 15% by volume (liquid - solid mass ratio of 1.65:1),

dissolution time of 30 min, dissolution temperature at 25 °C, stirring speed at 200 r/min, and dissolution pressure of 10 MPa, the concentration of heavy metals of Pb, Zn, Ni and Mn reach the highest level. Under all conditions, the heavy metal concentration will not be higher than 200 μg/L.

12.2.6 Environmental Monitoring Programmes

Deep Ocean Stewardship Initiative, Ocean North, UK Foreign Ocean Policy Unit and other organizations comment that the Environmental Monitoring Programme are not clearly defined.

In this report, we built a plume model (verifies the model using measured mooring observation data), and conduct a preliminary numerical simulation to predict the spatio-temporal changes of plume. Our environmental monitoring programme was based on this result. This EMMP has been supplemented and improved in section 10.3.2 of this report.

12.2.7 Impact assessment

UK Foreign Ocean Policy Unit, World Wide Fund for Nature and other organizations believed that the existing assessment cannot support the conclusion that this activity will not have a significant impact on the marine environment.

This test is small-scale within the framework of the "Exploration Regulations", and not a large-scale test for commercial or quasi-commercial purposes. As mentioned by several stakeholders, any disturbance in the deep sea may lead to relatively persistent impact. However, in evaluating the impact of deep-sea activities, it is more important to take the scale and duration of the impact into consideration. The direct disturbance area of the seabed in this test is only within the range of 600m*1000m, and the range of sediment plumes and re-sedimentation is also only within a few kilometers. Compared to the total area of the China Minmetals contract area, this disturbance only occupies a negligible proportion. Based on the assessment data in this report, the maximum impact distance of the plume caused by this activity is 2.1

km, and the maximum vertical impact height is 124 m. The plume will disappear 1-1.5 days after the mining test is completed. The area where the sediment plume re-sedimentation thickness exceeds 0.1 mm does not exceed 1 km^2 in this test. Additionally, the entire test will be completed within two or three weeks, and the underwater working time of the mining vehicle is only about 100 hours. Based on these reasons, we believe the environmental disturbance of this test is at a relatively low level.

13 Terminology and Abbreviation

Terminology

Terminology	Interpretation
Contract Area	An exploration area according to the contract signed between the Contractor and the ISA.
Polymetallic nodules	One of the resources in the Area, including any deposit or accretion of nodules, on or just below the surface of the deep seabed, which contain manganese, nickel, cobalt and copper
General exploration zone (GEA)	An area in the prospecting zone with further exploration value. The exploration work is mainly conducted by systematic sampling. After the exploration work is completed, the indicated resources should be estimated. It is part of the prospecting zone.
Primary working area (PWA)	In this Project, the PWA is located in the western basin of the Block A-5, with an area of approximately 4,590 km^2, and grid cells of 7 km × 7 km for resource exploration. It is also referred to as the GEA.
Detailed exploration area (DEA)	The first planned mining area in the GEA. The exploration work is mainly conducted by intensive sampling. After the exploration work is completed, the measured resources should be estimated. It is a part of the GEA.
Target mining area (TMA)	In this Project, the TMA is the DEA.
Impact reference zone (IRZ)	It is located in a portion of the Area scheduled to be mined and to be directly affected, will be used for assessing the effect of test-mining in the Area on the marine environment.
Collector test area (CTA)	Located in the TMA, it is where the collector vehicle test will be conducted in this Project.
Preservation reference zone (PRZ)	It is mostly located in the Contractor's Contract Area, with species composition and environmental characteristics similar to the IRZ, far away from the IRZ and not affected by the test-mining.
Areas of particular environmental interest (APEI)	Areas established by the ISA for the purpose of implementing the REMP.
Cumulative impact	Impact resulting from the incremental impact of the action when added to the other past, present or reasonably foreseeable future actions.
Plume	It contains a large number of suspended sediment particles, minerals and benthic debris, and it is a diffused water flow.
Megafauna	The epifauna that inhabit the water-sediment interface and can be clearly distinguished on the seabed photographs. They are usually larger than 1 cm in size.

Macrofauna	The epifauna that inhabit the surface and bottom of sediments and will be blocked by 250μm mesh screen during sorting of sediment samples.
Meiofauna	Metazoa and their larvae, which inhabit the surface and bottom of sediments and will be blocked by 32μm mesh screen during sorting of sediment samples.

Abbreviation

AABW	Antarctic Bottom Water
ADCP	Acoustic Doppler Current Profiler
AFS	International Convention for the Control of Harmful Anti-fouling Systems on Ships
APEI	Areas of Particular Environmental Interest
Argo	Array for Real-time Geostrophic Oceanography
As	Arsenic
ASVs	Amplicon Sequence Variants
AUV	Autonomous Underwater Vehicle
BC	Box Corer
BIE	Benthic Impact Experiment
BPI	Bathymetric Position Index
BWMC	Ballast Water Management Convention
CBD	Convention on Biological Diversity
CCD	Carbonate Compensation Depth
CCZ	Clarion-Clipperton Zone
Cd	Cadmium
cDNA	complementary Deoxyribonucleic acid
Chl *a*	Chlorophyll *a*
Co	Cobalt
COI	Cytochrome c oxidase subunit I
COMRA	China Ocean Mineral Resources Research and Development Association
Cr	Chromium
CTA	Collector Test Area
CTD	Conductivity Temperature Depth
Cu	Copper
Minmetals	China Minmetals Group Co., Ltd.
MLC	Maritime Labor Convention
DIC	Dissolved Inorganic Carbon
DISCOL	Disturbance and recolonization experiment in a manganese nodule area of the deep South Pacific
DNA	Deoxyribonucleic acid
DO	Dissolved Oxygen
DOC	Dissolved Organic Carbon
ECWMF	European Centre for Medium-Range Weather Forecasts
EDGAR	Emissions Database for Global Atmospheric Research
eDNA	Environmental Deoxyribonucleic Acid
EEZ	Exclusive Economic Zone
EIS	Environmental Impact Statement

EMMP	Environmental Management and Monitoring Plan
EMP	Environmental Monitoring Programme
ENSO	El Niño-Southern Oscillation
EPA	U.S. Environmental Protection Agency
EUC	Equatorial Undercurrent
Fe	Iron
FTU	Formazan Turbidity Units
FVCOM	An Unstructured Grid, Finite-Volume Coastal Ocean Model
GC	Gravity Core
GEOMAR	GEOMAR Helmholtz Centre for Ocean Research Kiel
GOOS	Global Ocean Observing System
GSR	Global Sea Mineral Resources
IBTrACS	International Best Track Archive for Climate Stewardship
IMMAs	Important Marine Mammal Areas
IMO	International Maritime Organization
IMO-BIE	International Maritime Organization- Benthic Impact Experiment
Ind.	Individual
IOM-BIE	Interoceanmetal Joint Organization- Benthic Impact Experiment
IRZ	Impact Reference Zone
ISA	International Seabed Authority
ISM	The International Safety Management
ITCZ	Intertropical Convergence Zone
JET	Japan Deep-Sea Impact Experiment
KBAs	Key Biodiversity Areas
LADCP	Lowered Acoustic Doppler Current Profiler
LC50	Lethal Concentration 50
L-PMOC	The lower deep branch of the Pacific Meridional Overturning Circulation
MARPOL	The International Convention for the Prevention of Pollution from Ships
MC	Multicore
MEOW	Marine Ecoregions Of the World
MIDAS	Managing impacts of deep-sea resources exploitation
Mn	Manganese
MX	Mooring
NEC	North Equatorial Current
NECC	North Equatorial Countercurrent
NEG	Nickel equivalent grade
NEP	Northeast Pacific
NESC	North Equatorial Subsurface Current
NEUC	North Equatorial Undercurrent
NGCC	New Guinea Coastal Current
Ni	Nickel
NOAA-BIE	National Oceanic and Atmospheric Administration- Benthic Impact Experiment
NUC	Equatorial Undercurrent
OBIS	Ocean Biodiversity Information System
OMZ	Oxygen minimum zone
OTU	Operational Taxonomic Unit
Pb	Lead
PCR	Polymerase Chain Reaction

POC	Particulate Organic Carbon
PPOW	Pelagic Provinces Of the World
PRZ	Preservation Reference Zone
PSD	Power Spectral Density
Ra	Radium
RCP	Representative Concentration Pathway
REMP	Regional Environmental Management Plan
ROV	Remote Operated Vehicle
rRNA	Ribosomal ribonucleic acid
SEC	South Equatorial Current
SNP	Single Nucleotide Polymorphisms
SOLAS	International Convention for the Safety of Life at Sea
SPL	Sound Pressure Level
SPM	Suspended Particulate Matter
TAO	Tropical Atmosphere Ocean
TMC	The Metals Company
TN	Total Nitrogen
TOC	Total Organic Carbon
TPOS	Tropical Pacific Observation System
TRITON	Triangle Trans-Ocean Buoy Network
TSM	Total Suspended Matter
UNCLOS	United Nations Convention on the Law of the Sea
U-PMOC	The upper deep branch of the Pacific Meridional Overturning Circulation
V	Vanadium
VMEs	Vulnerable Marine Ecosystems
WMO	World Meteorological Organization
Zn	Zinc

14 Study Teams

Table 14.1-1 List of study team members

Name	Professional title	Employer	Study contents
Sun Dong	Research fellow	SIOMNR	Marine ecosystem
Liu Yuwei	Senior engineer	CRIMM of Minmetals	Plume impact
Mao Guiting	Professor-level senior engineer	CRIMM of Minmetals	Mining technology
Cheng Yangrui	Senior engineer	CRIMM of Minmetals	Mining technology
Lu Bo	Associate research fellow	SIOMNR	Marine biology
Wang Jun	Associate research fellow	SIOMNR	Plume impact
Lin Shiquan	Associate research fellow	SIOMNR	Marine biology
Chen Shiping	Engineer	CRIMM of Minmetals	Plume impact
Hao Xiangli	Engineer	CRIMM of Minmetals	Marine geology
Zhang Wenqian	Engineer	CRIMM of Minmetals	Marine biology
Li Zhenggang	Associate research fellow	SIOMNR	Marine geology
Li Weiwen	Associate research fellow	TIOMNR	Chemical oceanography
Jiang Yuhuan	Assistant research fellow	TIOMNR	Environmental management
Li Xiaohu	Research fellow	SIOMNR	Marine geology
Zhang Weiyan	Research fellow	SIOMNR	Marine geology
Yang Chenghao	Research fellow	SIOMNR	Physical oceanography

Ding Han	Research fellow	Carnegie Mellon University	Meteorology
Jia Yonggang	Professor	Ocean University of China	Plume impact
Shi Bing	Professor	Ocean University of China	Plume impact
Ding Haibing	Professor	Ocean University of China	Plume impact
Zou Li	Professor	Ocean University of China	Plume impact
Zhang Xueqing	Professor	Ocean University of China	Plume impact
Quan Yongzheng	Senior engineer	Ocean University of China	Plume impact
Fan Zhihan	Post-doctoral research fellow	Ocean University of China	Plume impact
Lei Yanli	Professor	IOCAS	Marine ecosystem
Zhao Feng	Research fellow	IOCAS	Marine biology
Zhan Zifeng	Associate research fellow	IOCAS	Marine biology
Li Haotian	Post-doctoral research fellow	IOCAS	Marine biology
Sun Chengjun	Research fellow	IOCAS	Plume impact
Chi Wanqing	Research fellow	FIOMNR	Plume impact
Zhou Yubin	Associate research fellow	National Deep Sea Center	Environmental assessment
Li Jun	Senior engineer	The CRIMM of Minmetals	Mining technology
Shuang Zhi	Senior engineer	The CRIMM of Minmetals	Mining technology
Li Manhong	Professor-level senior	The CRIMM of	Mining technology

	engineer	Minmetals	
Chen Bingzheng	Senior engineer	The CIMR of Minmetals	Mining technology
Chu Fengyou	Research fellow	SIOMNR	Marine geology
Lin Zhilan	Associate research fellow	TIOMNR	Marine ecosystem
Lin Ruijuan	Assistant research fellow	TIOMNR	Laws and regulations
Chen Siting	Assistant research fellow	TIOMNR	Chemical oceanography
Yuan Zheng	Assistant research fellow	TIOMNR	Environmental engineering
He Weiyi	Assistant research fellow	TIOMNR	Marine biology
Xu Xuewei	Research fellow	SIOMNR	Marine biology
Shao Qianwen	Assistant research fellow	SIOMNR	Marine ecosystem
Feng Yunzhi	Assistant research fellow	SIOMNR	Marine ecosystem
Tang Qinqin	Assistant research fellow	SIOMNR	Marine ecosystem
Li Qing	Assistant engineer	The WSGRI of Minmetals	Physical oceanography
Liu Nuan	Assistant research fellow	SIOMNR	Physical oceanography
Jiang Nan	Engineer	SIOMNR	Technical support for submersibles
Liu Wei	Engineer	SIOMNR	Technical support for submersibles
Chen Li	Engineer	SIOMNR	Technical support for submersibles
Lou Tiaohua	Engineer	SIOMNR	Technical support for submersibles

List of Abbreviations:

CIMR: Changsha Institute of Mining Research Co., Ltd.

CRIMM: Changsha Research Institute of Mining & Metallurgy Co., Ltd.

DOSI: Deep-Ocean Stewardship Initiative

DSCC: Deep Sea Conservation Coalition

FIOMNR: First Institute of Oceanography, Ministry of Natural Resources

IOCAS: Institute of Oceanology, Chinese Academy of Sciences

PEW: The Pew Charitable Trusts

SIOMNR: Second Institute of Oceanography, Ministry of Natural Resources

TIOMNR: Third Institute of Oceanography, Ministry of Natural Resources

WSGRI: WSGRI Engineering and Technology Co., Ltd.

WWF: World Wide Fund for Nature

15 References

See related sections.

16 Annexes

Annex 1 Study Report on Modeling Sediment Plume Caused by Bottom-layer Disturbance.

Annex 2 Survey Methods and Quality Assessment for Environment Baseline Studies

Annex 3 Toxicity Assessment to *Vibrio fischeri* of Heavy Metals Released from Disturbed Surface Sediments in the Block A-5

Annex 4 Environmental Survey Station in the IRZ and PRZ

Annex 5 Minmetals' Environmental Survey Stations in History and Plans for the Future Environmental Survey

Annex 1 Study Report on Modeling Sediment Plume Caused by Bottom-Layer Disturbance

中国五矿

长沙矿冶院

Study Report on Modeling Sediment Plume Generated from Bottom-Layer Disturbance by Collector vehicle test (1/4 Commercial Size) in the Block A-5 of the Contract Area

Compiled by: Wang Jun, Yang Chenghao, Sun Dong

SIOMNR

March 2024

Table of Contents

Figures

Tables

1 Modelling

A numerical model of plume dispersal resulting from seabed mining in the CTA of the Block A-5 has been established. It is an FVCOM (an Unstructured Grid, Fine-volume Coastal Ocean Model) based on a triangular grid and adopting the finite volume method and the ocean model of three-dimensional primitive equations. The integral method of volume flux is used to solve the original governing equations of fluid dynamics, thus ensuring the conservation of momentum, energy and mass in a single grid and the whole calculation area, and solving key problems in ocean numerical calculation. The S coordinate system is adopted in the vertical direction to deal with complex topography variations and simulate the dynamic process in the bottom layer in a better way. An unstructured triangular mesh in the horizontal direction is used to locally encrypt the key areas of concern (e.g. the CTA) and improve the calculation efficiency.

The FVCOM's governing equations are as follows:

$$\frac{\partial \zeta}{\partial t}+\frac{\partial Du}{\partial x}+\frac{\partial Dv}{\partial y}+\frac{\partial w}{\partial z}=0$$

$$\frac{\partial uD}{\partial t}+\frac{\partial u^2D}{\partial x}+\frac{\partial uvD}{\partial y}+\frac{\partial uw}{\partial \sigma}-fvD$$
$$=-gD\frac{\partial \zeta}{\partial x}-\frac{gD}{\rho_0}[\frac{\partial}{\partial x}(D\int_{\sigma}^{0}\rho d\sigma')+\sigma\rho\frac{\partial D}{\partial x}]+\frac{1}{D}\frac{\partial}{\partial \sigma}(K_m\frac{\partial u}{\partial \sigma})+DF_u$$

$$\frac{\partial vD}{\partial t}+\frac{\partial uvD}{\partial x}+\frac{\partial v^2D}{\partial y}+\frac{\partial vw}{\partial \sigma}+fuD$$
$$=-gD\frac{\partial \zeta}{\partial y}-\frac{gD}{\rho_0}[\frac{\partial}{\partial u}(D\int_{\sigma}^{0}\rho d\sigma')+\sigma\rho\frac{\partial D}{\partial y}]+\frac{1}{D}\frac{\partial}{\partial \sigma}(K_m\frac{\partial v}{\partial \sigma})+DF_v$$

$$\frac{\partial \theta D}{\partial t}+\frac{\partial \theta uD}{\partial x}+\frac{\partial \theta vD}{\partial y}+\frac{\partial \theta w}{\partial \sigma}=\frac{1}{D}\frac{\partial}{\partial \sigma}(K_h\frac{\partial \theta}{\partial \sigma})+DH+DF_\theta$$

$$\frac{\partial SD}{\partial t}+\frac{\partial SuD}{\partial x}+\frac{\partial SvD}{\partial y}+\frac{\partial Sw}{\partial \sigma}=\frac{1}{D}\frac{\partial}{\partial \sigma}(K_h\frac{\partial S}{\partial \sigma})+DH+DF_S$$

$$\frac{\partial q^2D}{\partial t}+\frac{\partial q^2uD}{\partial x}+\frac{\partial q^2vD}{\partial y}+\frac{\partial q^2w}{\partial \sigma}=2D(P_s+P_b-\varepsilon)+\frac{1}{D}\frac{\partial}{\partial \sigma}(K_q\frac{\partial q^2}{\partial \sigma})+DE_q$$

$$\frac{\partial q^2 lD}{\partial t} + \frac{\partial q^2 luD}{\partial x} + \frac{\partial q^2 lvD}{\partial y} + \frac{w}{D}\frac{\partial q^2 lw}{\partial \sigma}$$
$$= lE_l D(P_s + P_b - \frac{\widetilde{W}}{E_l}\varepsilon) + \frac{1}{D}\frac{\partial}{\partial \sigma}(K_q \frac{\partial q^2 l}{\partial \sigma}) + DF_l$$

$$\rho = \rho(\theta, S)$$

Where x, y, σ are the coordinates in the middle, north and vertical directions in the Cartesian coordinate system; u, v, w are velocity components in x, y, σ directions; T is temperature; S is salinity; ρ is density; P is pressure; f is the Coriolis force parameter; g is the acceleration of gravity; K_m is the vertical eddy viscosity coefficient; K_h is thermal vertical vortex friction coefficient; F_u, F_v, F_θ and F_S represent horizontal momentum, temperature and salinity dispersal.

For this test-mining, a scope of 40 km × 40 km is set in the simulation model, the multibeam bathymetric survey data (Figure 1) are adopted for topography inside the model, with a mesh resolution of 2,000 m at the model boundary and 100 m in the test-mining center (5 km × 5 km). In the vertical direction, the generalized coordinate system is adopted; the grid is encrypted near the bottom and divided into 61 layers. At the depth of 10 m above the bottom, the resolution is 1 m (Figure 7.5-1).

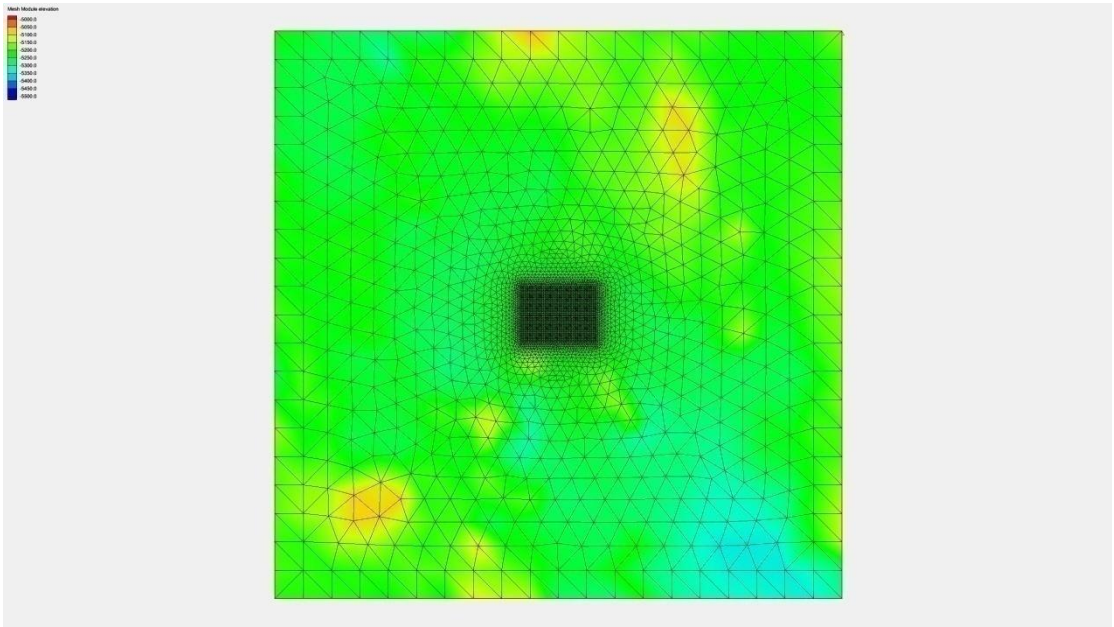

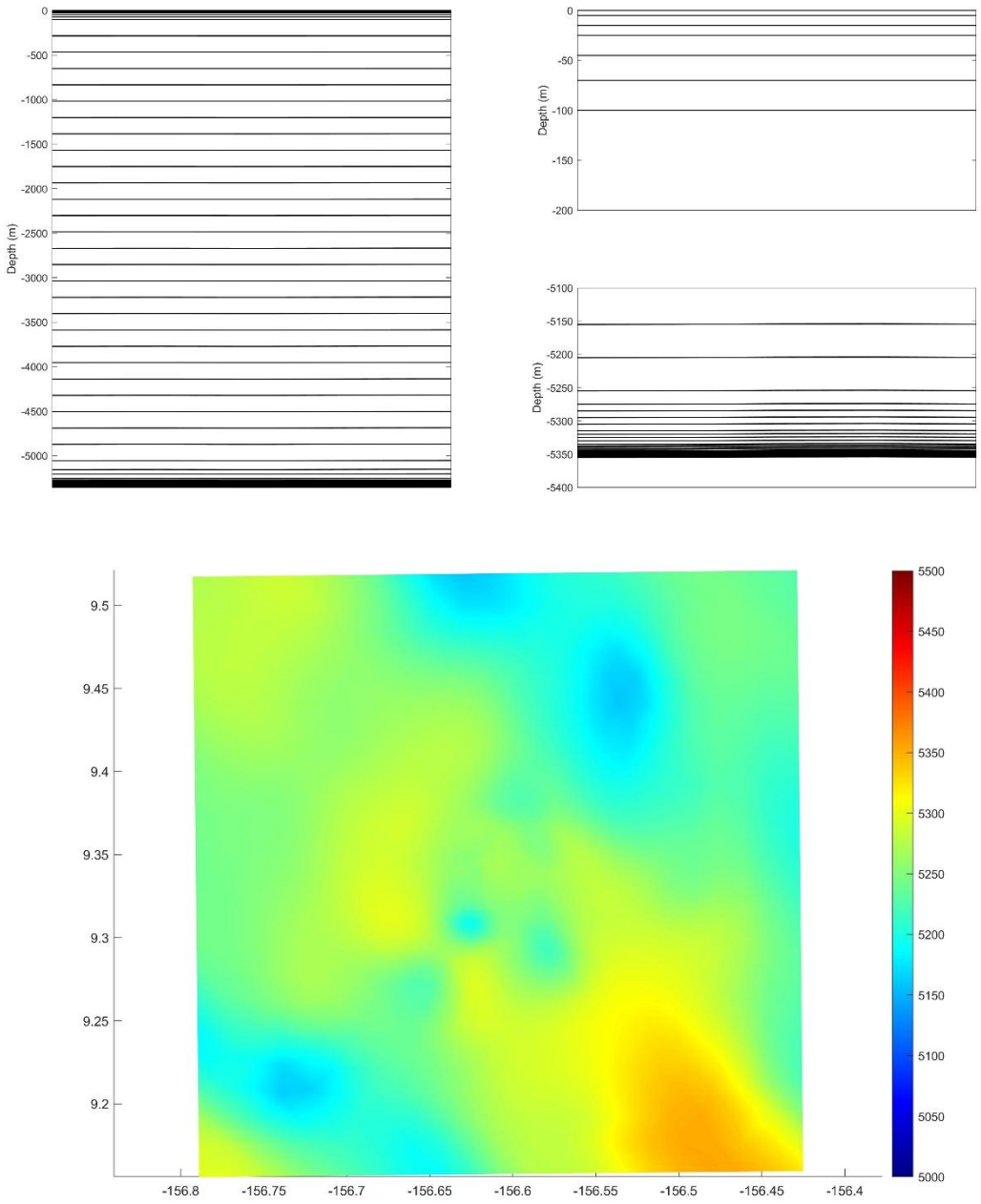

Figure 1 Model's horizontal grid (upper), vertical grid (middle) and water depth map (lower)

Mode setting and open-boundary conditions:

There is no obvious variation in temperature and salinity in the bottom layer, as shown in the structure of temperature and salinity profiles. The CTA is located in the bottom layer, and there is no emission in the surface and middle layers, so the plume model will be calculated as a barotropic model.

The open boundary tidal level is obtained by using the TPXO global tidal model. Assuming that the background flow field in the bottom layer of the simulation area is

always the same, the residual current field obtained by filtering out high-frequency variations (e.g. tidal currents) according to the measured flow field is taken as the open boundary condition of the flow field of the model.

Sediment Module:

The sediment module considers the coupling of water and sediment density and the process of flocculation settling. The suspended sand diffusion equation is as follows:

$$\frac{\partial C}{\partial t}+\frac{\partial (uC)}{\partial x}+\frac{\partial (vC)}{\partial y}+\frac{\partial \left[(w-w_s)C\right]}{\partial z}=\frac{\partial}{\partial x}\left(A_H\frac{\partial C}{\partial x}\right)+\frac{\partial}{\partial y}\left(A_H\frac{\partial C}{\partial y}\right)+\frac{\partial}{\partial z}\left(K_h\frac{\partial C}{\partial z}\right)$$

where C, w_s represent the suspended sediment concentration and settling velocity, A_H represents the horizontal eddy viscosity coefficient, K_h represents the vertical eddy viscosity coefficient.

The sediment flux boundary conditions are as follows:

$$K_h\frac{\partial C}{\partial z}=0,\quad z=\zeta$$

$$K_h\frac{\partial C}{\partial z}=E-De,\quad z=-H$$

where E represents the sediment resuspension flux, $De = C_b w_b$ represents the sediment deposition flux at the lowest layer, Cb, wb represent the suspended sediment concentration and settling velocity at the lowest layer.

Setting of suspended sediment parameters for plume:

According to the study reports of relevant survey cruises, the particle sizes of the bottom-layer sediments exhibit a bimodal distribution pattern. So, the particle sizes of suspended sediments are set as 0.0028 mm and 0.0625 mm. The settling speed of 0.0028 mm and 0.0625 mm particles are set at 0.36 mm/s and 8.33 mm/s, with reference to the article by Zhan Lin et al. (2023).

The simulated plume discharge port is 1 m above the bottom, the density of plume sediment is 1700 kg/m^3, critical shear stress for deposition is 0.1 N/m^2.

Refer to Section 3.3 for the traveling path of the collector vehicle. Since the

collector vehicle only causes small disturbance during traveling, the model only simulates the plume during the collecting operation. The specific schematic diagram of the simulated collecting path is shown in Figure 2. The disturbance intensity is calculated according to the relevant technical parameters of the collector vehicle. It is 7.2 kg/s at 0.2 m/s, 14.4 kg/s at 0.4 m/s, 18.0 kg/s at 0.6 m/s, 19.2 kg/s at 0.8 m/s and 24.0 kg/s at 1.0 m/s.

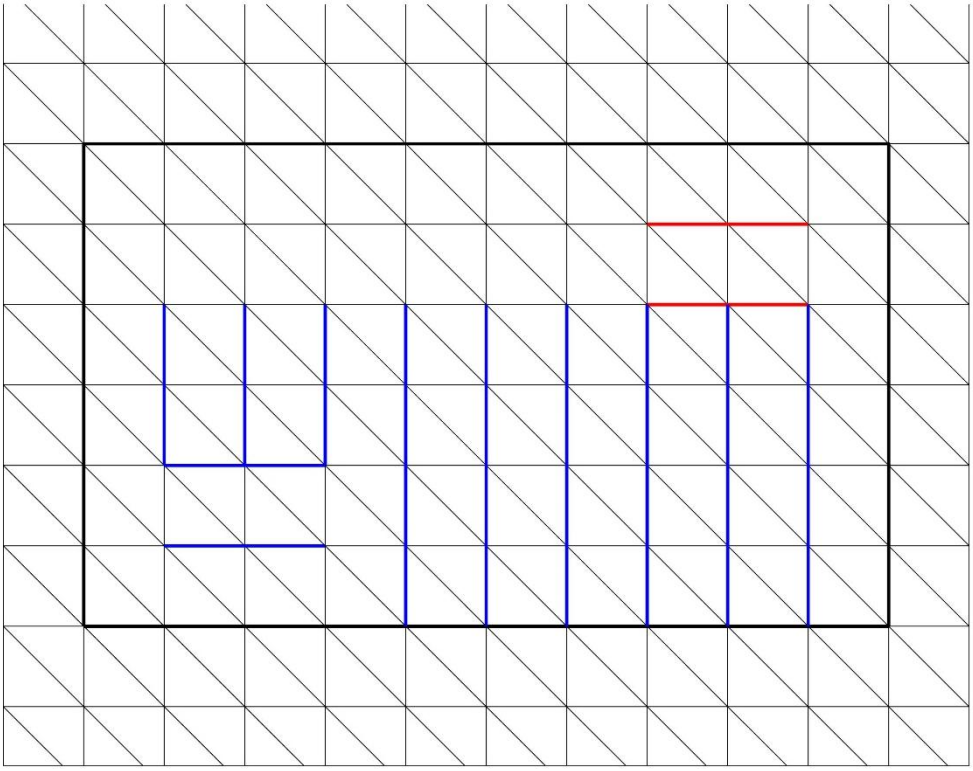

Figure 2 Schematic diagram for the simulated collecting path of the collector vehicle

(The thin black line is the pattern grid line; the thick black line is for the CTA; the red line is the path of first test-mining; and the blue line is the path of second test-mining)

Table 1. Parameters of the first underwater testing

The first underwater testing	
start time	10th 00:00
collector speed	0.6m/s
collector disturbance	18.0kg/s
collecting distance per line	200m
collecting time per line	600s
inspection time per line	1200s

collecting test lines	10
total testing time	300min

Table 2 Parameters of the second underwater testing

The second underwater testing					
start time	11th 00:00				
Path spacing: 0m					
collector speed	0.2m/s	0.4m/s	0.6m/s	0.8m/s	1.0m/s
collector disturbance	7.2kg/s	14.4kg/s	18.0kg/s	19.2kg/s	24.0kg/s
collecting distance per line	200m				
collecting time per line	1270s	720s	597s	534s	300s
inspection time per line	3600s				
collecting test lines	2				
testing time	842min				
Path spacing: 15m					
collector speed	0.2m/s	0.4m/s	0.6m/s	0.8m/s	1.0m/s
collector disturbance	7.2kg/s	14.4kg/s	18.0kg/s	19.2kg/s	24.0kg/s
collecting distance per line	200m				
collecting time per line	910s	482s	357s	294s	257s
inspection time per line	3600s				
collecting test lines	5	4	3	3	3
testing time	454min				
Path spacing: 25m					
collector speed	0.2m/s	0.4m/s	0.6m/s	0.8m/s	1.0m/s
collector disturbance	7.2kg/s	14.4kg/s	18.0kg/s	19.2kg/s	24.0kg/s
collecting distance per line	200m				
collecting time per line	990s	535s	410s	348s	310s
inspection time per time	3600s				
collecting test lines	4				
testing time	473min				
Path spacing: 50m					
collector speed	0.2m/s	0.4m/s	0.6m/s	0.8m/s	1.0m/s
collector disturbance	7.2kg/s	14.4kg/s	18.0kg/s	19.2kg/s	24.0kg/s
collecting distance per line	200m				
collecting time per line	1185s	665s	540s	498s	440s

inspection time per time	3600s				
collecting test lines	4	2	2	2	2
testing time	434min				
total testing time	2203min				

2 Model validation

Comparison of the model flow field results in July-October of 2020 with the measured bottom flow field (as in Figure 3), shows that the simulated flow current speed is in good agreement with the measured flow current speed.

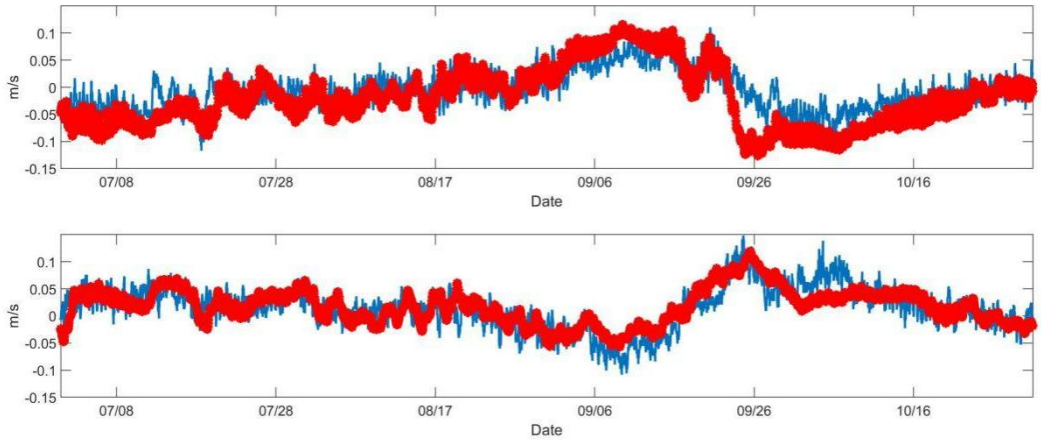

Figure 3 Comparison of model results (red) and measured current speeds (blue)

(Upper picture shows the east-west component of current speed; lower picture shows the north-south component of current speed.)

Warner and other methods are adopted to quantify the calculation accuracy of the numerical value model. The calculation formula is as follows:

$$Skill = 1 - \frac{\sum_{i=1}^{N} \left| X_{mod} - X_{obs} \right|^2}{\sum_{i=1}^{N} \left(\left| X_{mod} - \bar{X}_{obs} \right| + \left| X_{obs} - \bar{X}_{obs} \right| \right)^2}$$

Where: X represents the parameter to be compared,

$\bar{X}$ represents the average,

mod represents the calculation result of the model,

obs indicates the measured results.

The calculated results are in the range of 0-1.0; where 1.0 means that the calculated results of the model are consistent with the measured results, while 0 means that they are inconsistent. The closer the value is to 1, the higher the simulation accuracy of the model is.

The Skill values of the simulated current speeds and the measured current speeds are calculated. On the U component, the magnitude and variation trend of the two are basically the same, and the Skill value is 0.85. In the V component, the magnitude and variation trend of the two are basically the same, and the average Skill value is 0.86. The average Skill of current speed reaches 0.855, indicating that the simulation accuracy of the model is high and the results of the hydrodynamic numerical model are credible.

3 Plume model results

Since the operation time is undetermined, we only simulated plumes under the flow field conditions in July, August, September and October. We assume that the first underwater operation starts at 00:00 on the 10th of each month, and the test-mining lasts for about 5 hours in total; the second underwater operation starts at 00:00 on the 11th of each month, and the test-mining lasts for about 36 hours in total. The distribution of plume dispersal is simulated with two particle sizes. See Table 3 for specific cases.

Table 3. Parameters of plume model cases

Case	Sediment particle size	Start time
Case,1	0.0625	07/10
Case,2	0.0028	07/10
Case,3	0.0625	08/10
Case,4	0.0028	08/10
Case,5	0.0625	09/10
Case,6	0.0028	09/10
Case,7	0.0625	10/10
Case,8	0.0028	10/10

3.1 Horizontal distribution of suspended sediment concentrations

Figures 4 ~ 66 show variations in the horizontal distribution of suspended sediment concentrations at the depth of 1 m above the bottom in all cases, from the start of first test-mining to the disappearance of plume (the limit is 0.1 mg/L, considering that the lower limit of the effective detection concentration of the turbidity sensor is 0.1mg/l (Munoz Royo et al. 2022), and referring to the boundary values for plume diffusion evaluation in NORI-D EIS, therefore, in the subsequent analysis of the horizontal and vertical distribution characteristics of suspended sediment concentration, 0 1 mg/l is used as the boundary value for the effect of plume diffusion). It can been seen from the Figure that the disturbance duration is relatively

short during the first test-mining, so all the water columns with suspended sediment concentration higher than 10 mg/L are located in the CTA. During the second test-mining, because the collector vehicle's path is close to the edge of the CTA, the number of water columns with suspended sediment concentration higher than 10 mg/L is slightly higher in the south of the CTA than in the whole CTA. The bottom-layer suspended sediment concentration is the highest during the test-mining, and the concentration gradually decreases after the test-mining. The dispersal range of plume is controlled by the bottom-layer current speed. The impact scope of mining plume is small in August due to slow current speed in the month. The plume disappeared four days after the start of the test-mining (2.5 days after the end of the test-mining) in Case 3; and disappeared 5 days after the start of the test-mining (3.5 days after the end of the test-mining) in other cases. The dispersal direction of plume is controlled by the bottom-layer flow field, so the dispersal direction is northwest in July and east in September. The maximum impact distance of plume varies from month to month, being the smallest in August and the largest in September. The dispersal distribution range of fine-grained sediments is larger than that of coarse-grained sediments, and the maximum impact distance in the cases is 2.1 km (Case 2).

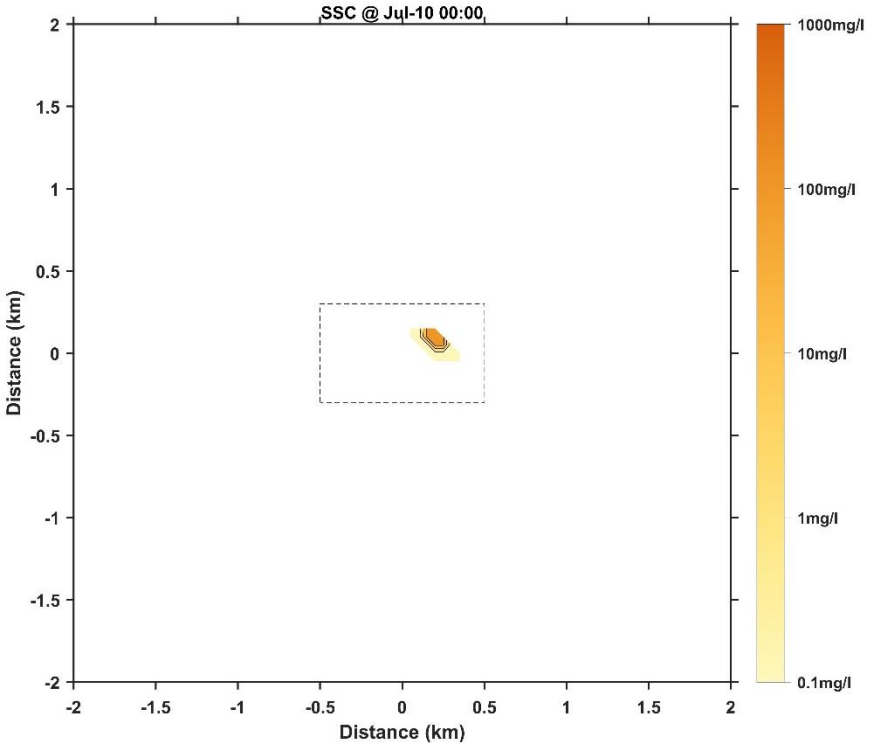

Figure 4 Distribution of bottom-layer suspended sediment concentrations at the start of first test-mining in Case 1

(Black dotted line indicates the CTA, the same below)

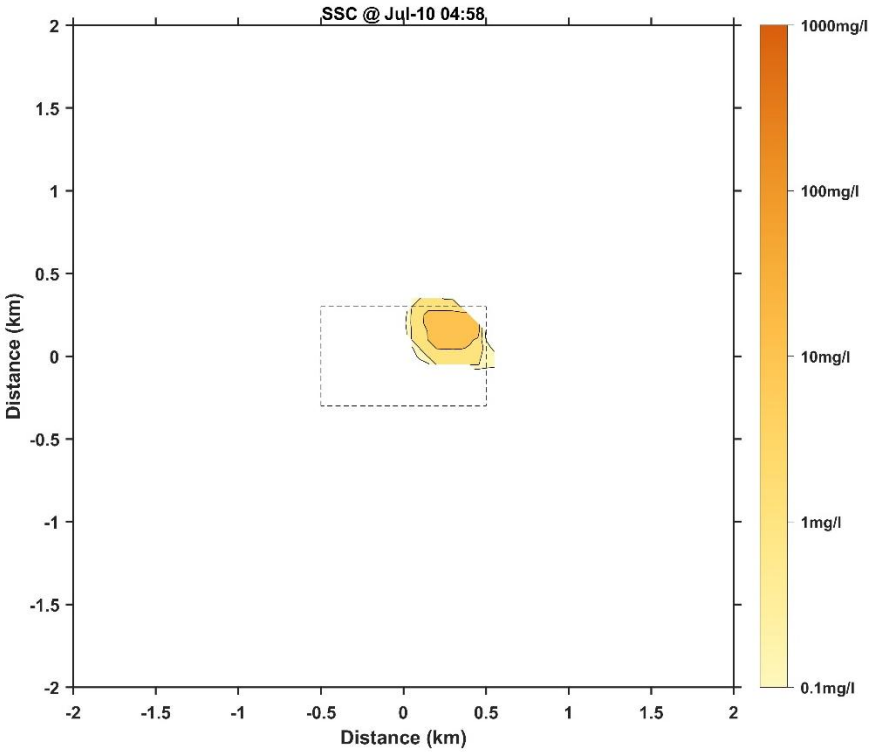

Figure 5 Distribution of bottom-layer suspended sediment concentrations at the end of first

test-mining in Case 1

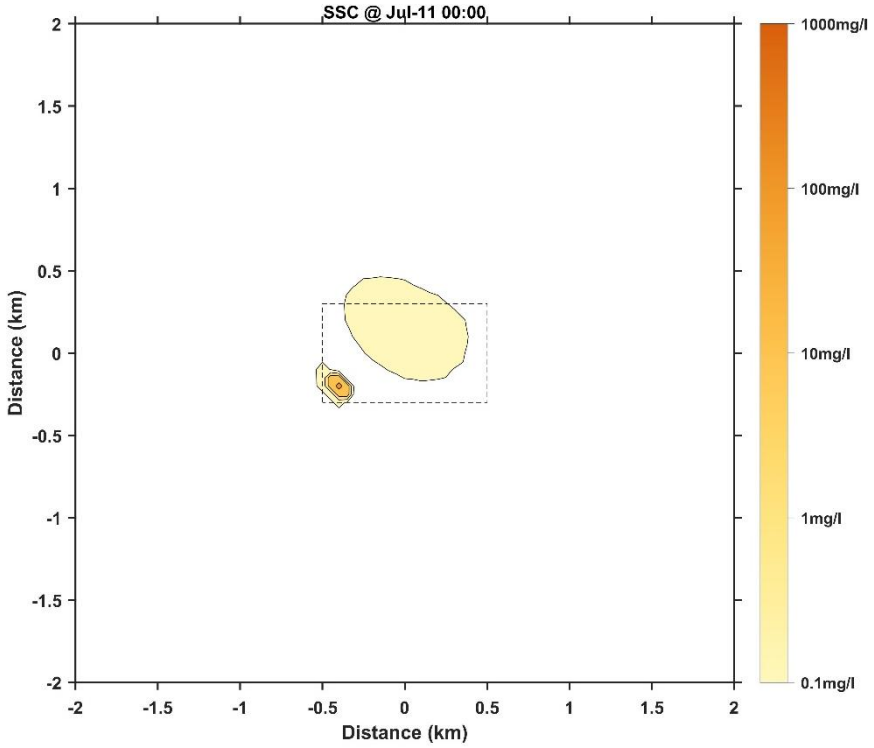

Figure 6 Distribution of bottom-layer suspended sediment concentrations at the start of second test-mining in Case 1

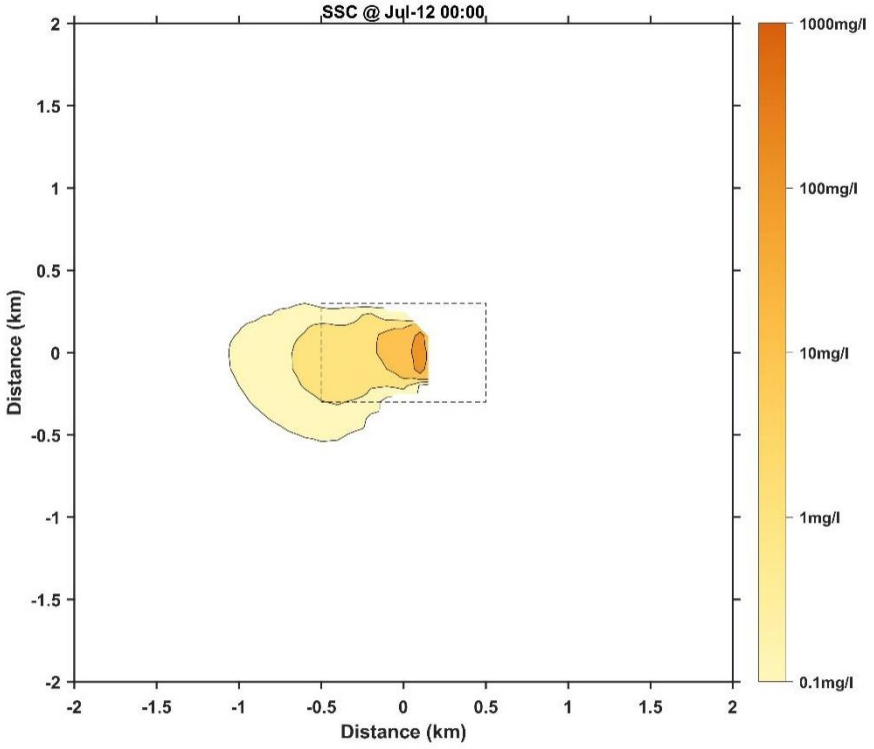

Figure 7 Distribution of bottom-layer suspended sediment concentrations on day 2 of test-mining in Case 1

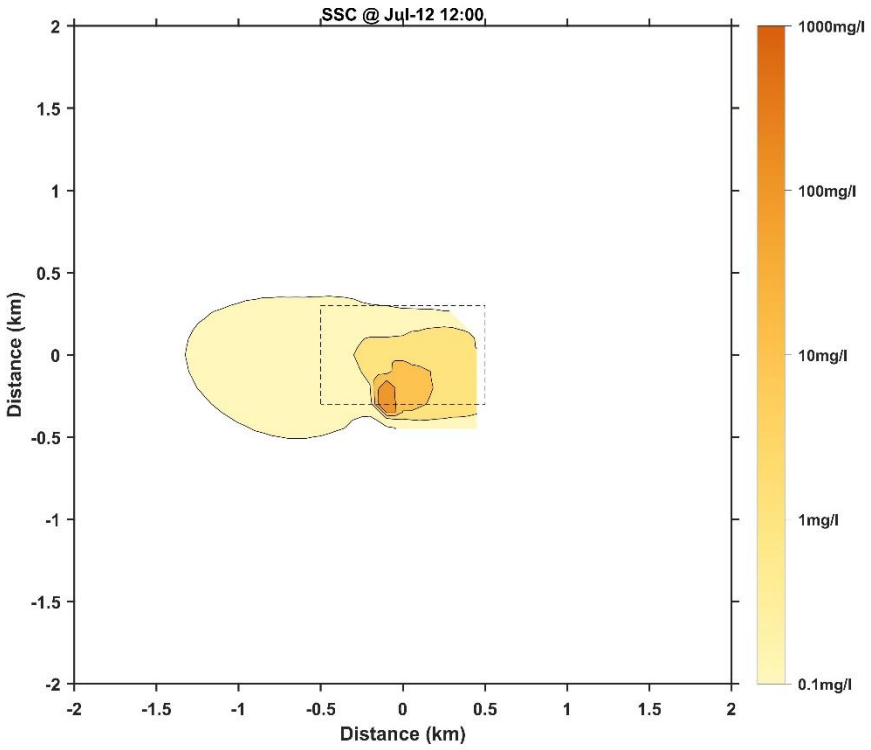

Figure 8 Distribution of bottom-layer suspended sediment concentrations at the end of second test-mining in Case 1

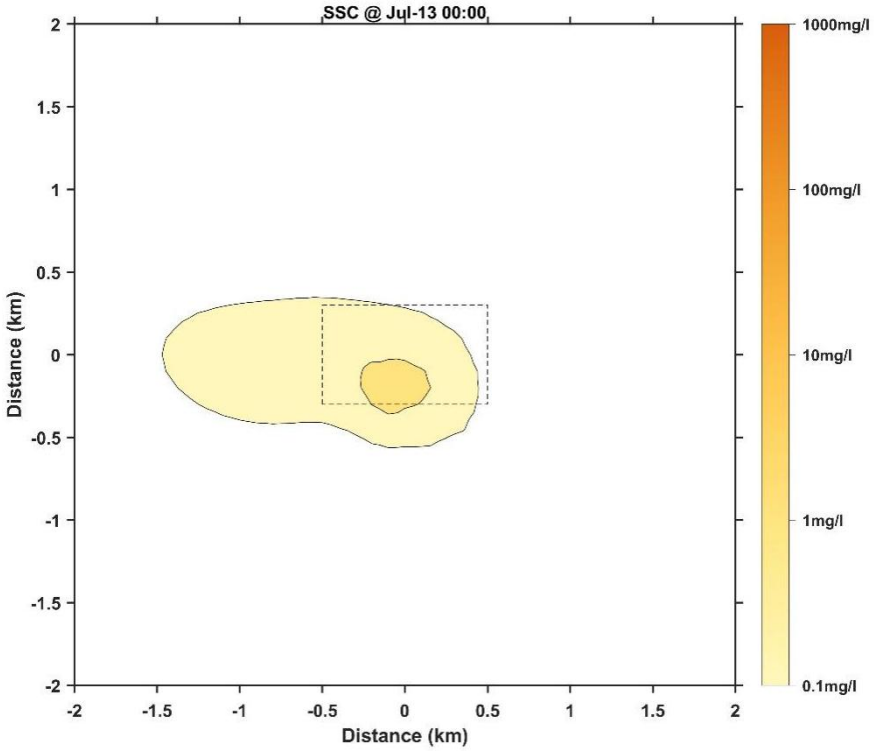

Figure 9 Distribution of bottom-layer suspended sediment concentrations on day 3 of test-mining in Case 1

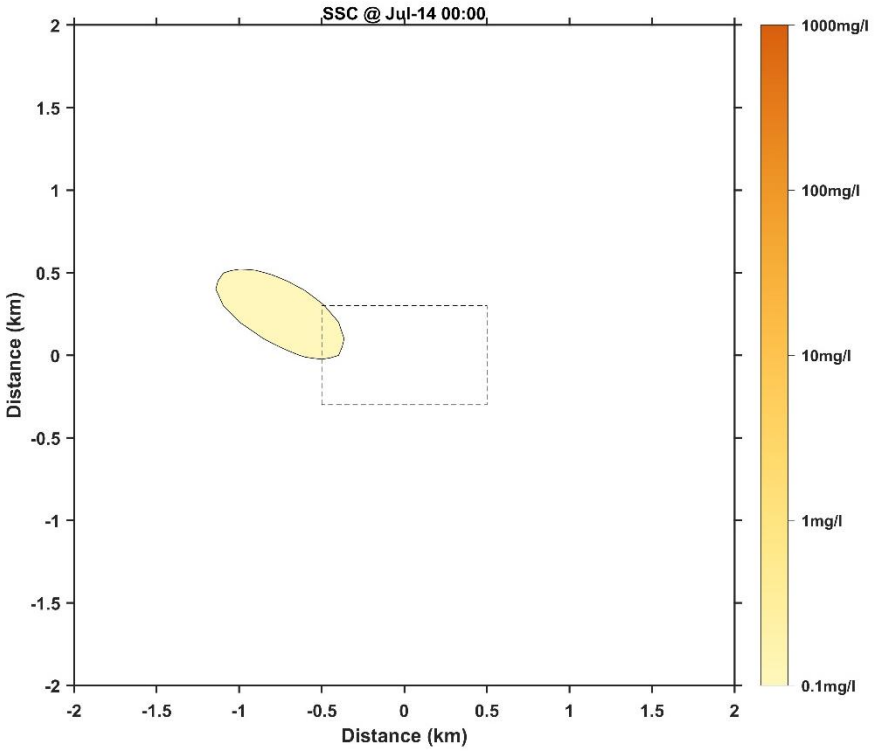

Figure 10 Distribution of bottom-layer suspended sediment concentrations on day 4 of test-mining in Case 1

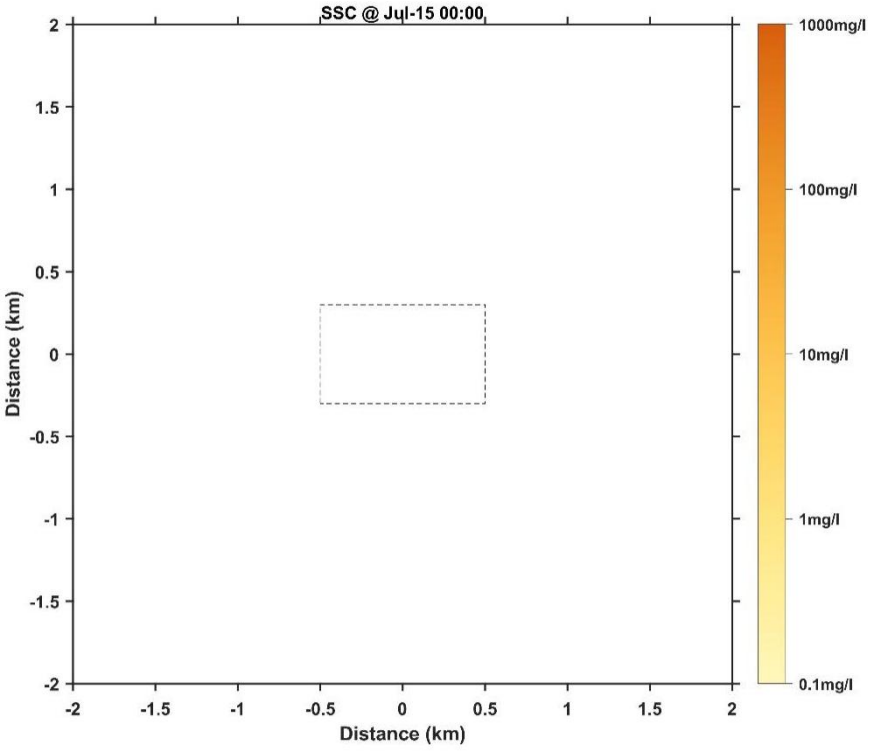

Figure 11 Distribution of bottom-layer suspended sediment concentrations on day 5 of test-mining in Case 1

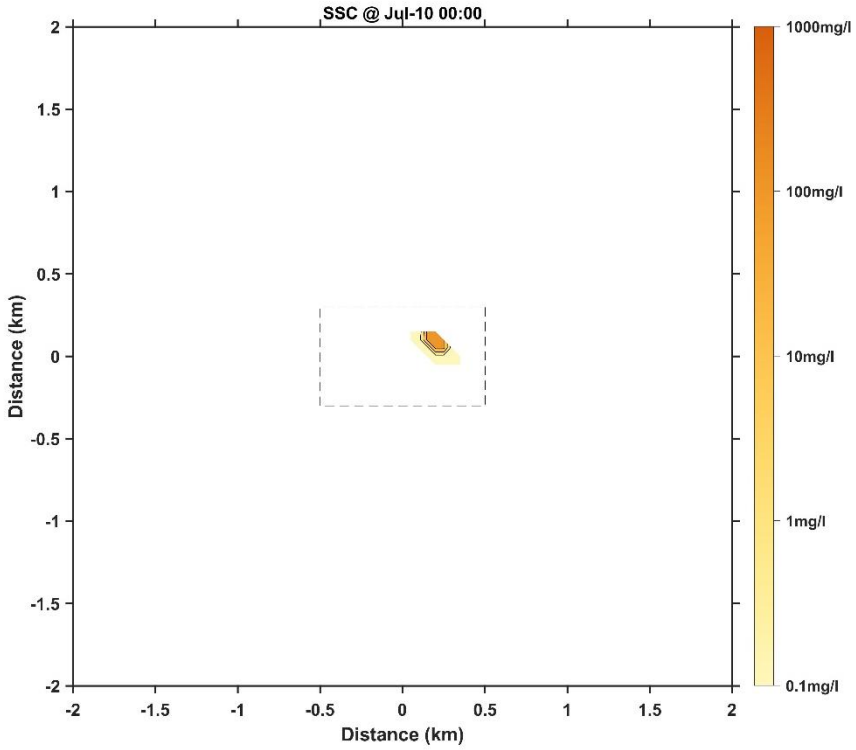

Figure 12 Distribution of bottom-layer suspended sediment concentrations at the start of first test-mining in Case 2

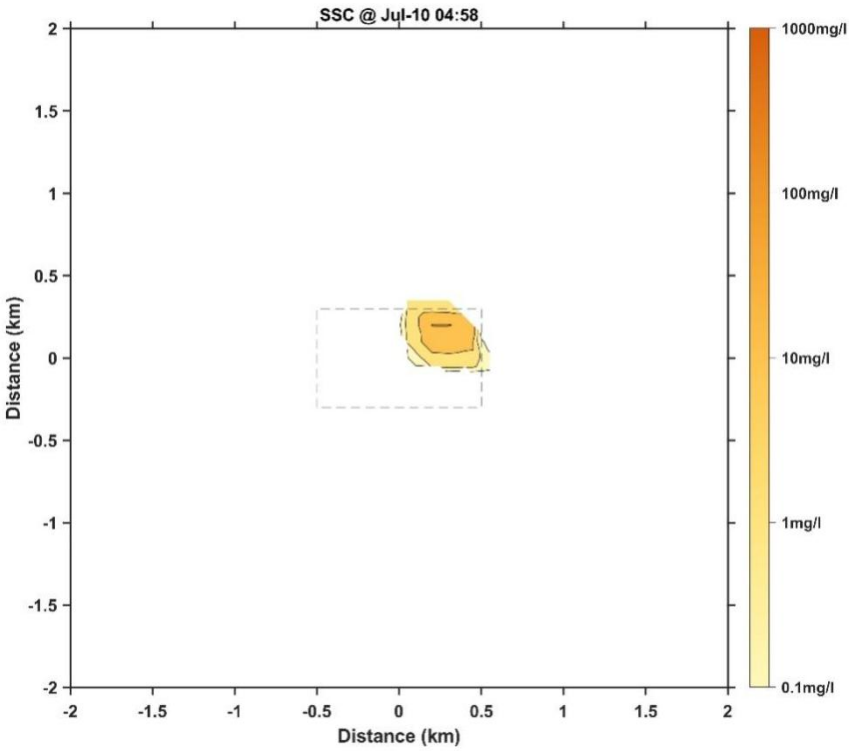

Figure 13 Distribution of bottom-layer suspended sediment concentrations at the end of first test-mining in Case 2

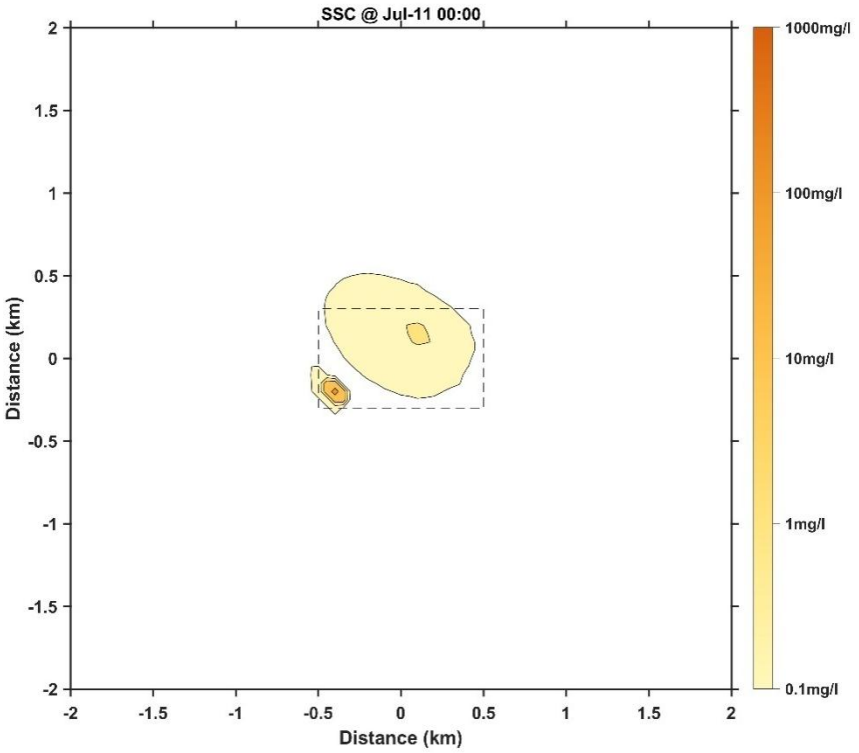

Figure 14 Distribution of bottom-layer suspended sediment concentrations at the start of second test-mining in Case 2

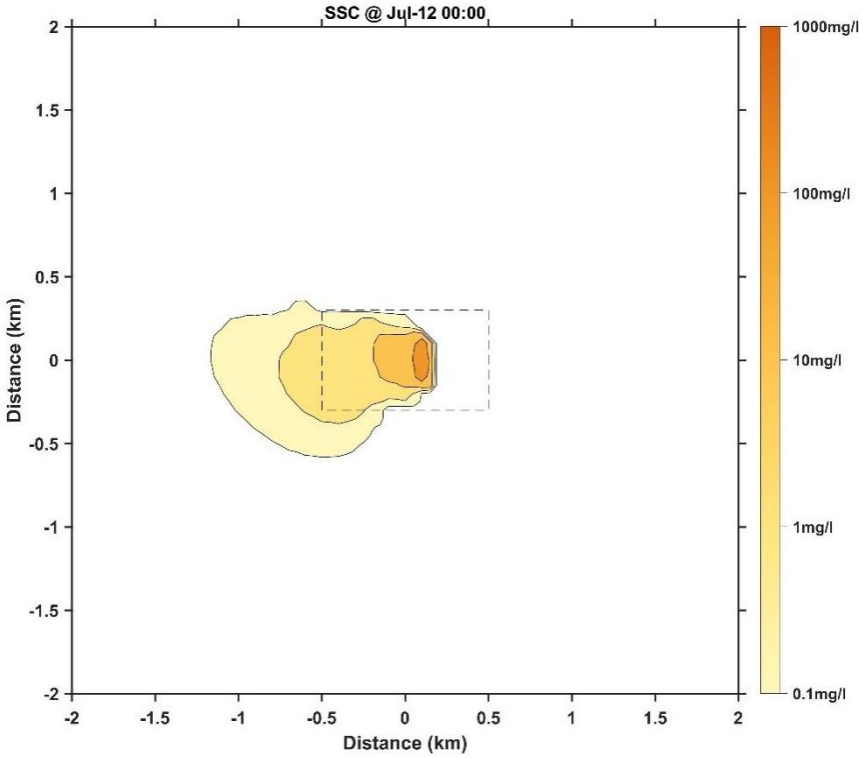

Figure 15 Distribution of bottom-layer suspended sediment concentrations on day 2 of test-mining in Case 2

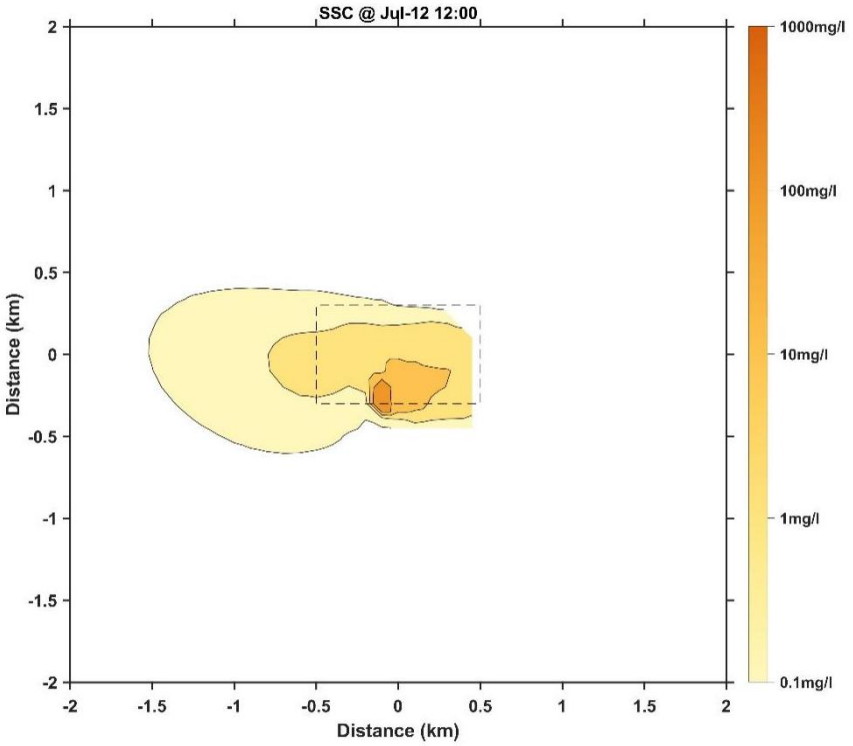

Figure 16 Distribution of bottom-layer suspended sediment concentrations at the end of second test-mining in Case 2

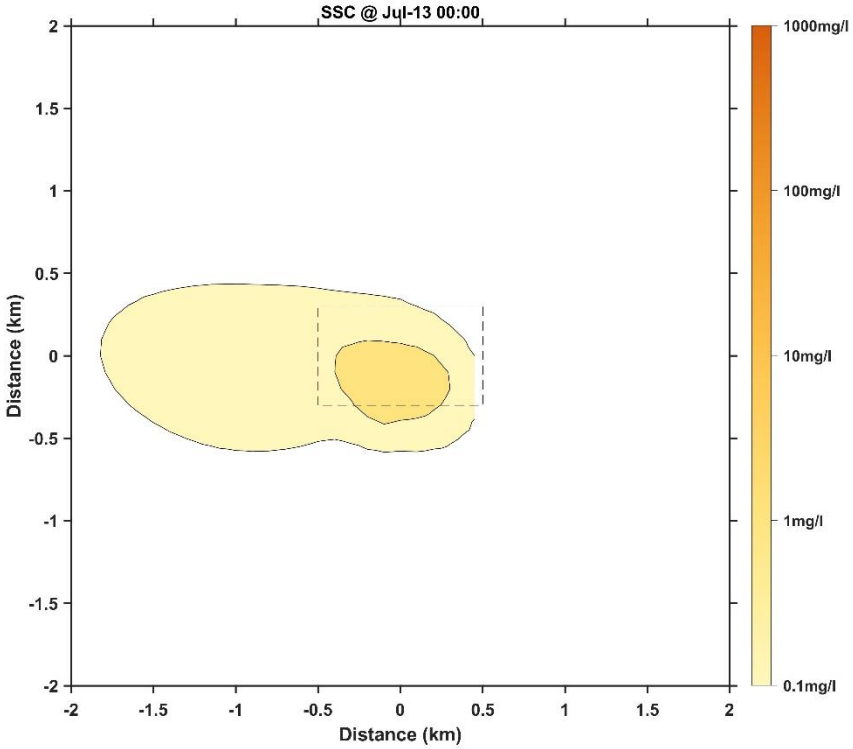

Figure 17 Distribution of bottom-layer suspended sediment concentrations on day 3 of test-mining in Case 2

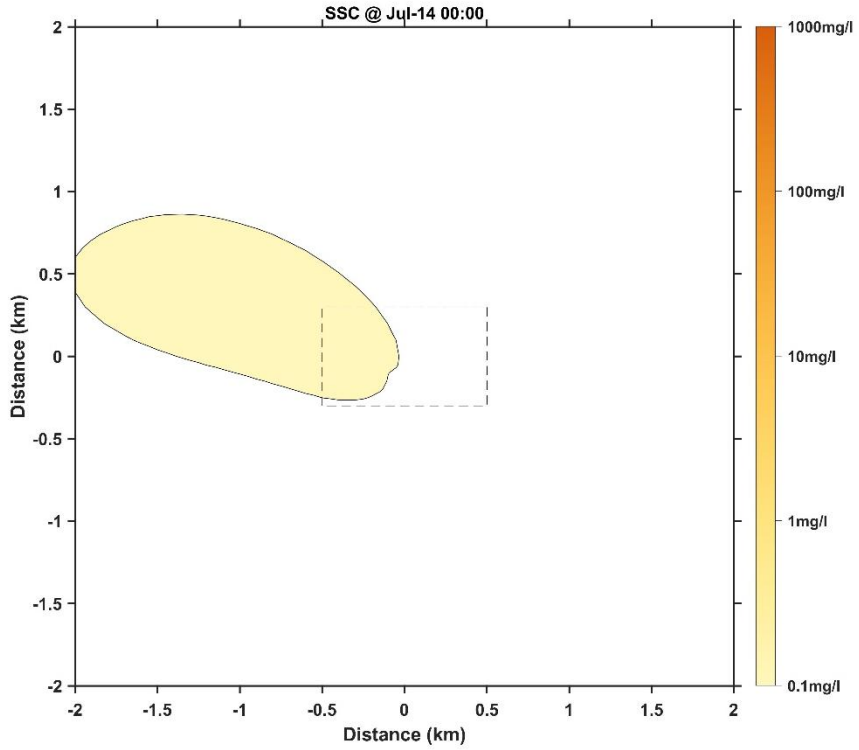

Figure 18 Distribution of bottom-layer suspended sediment concentrations on day 4 of test-mining in Case 2

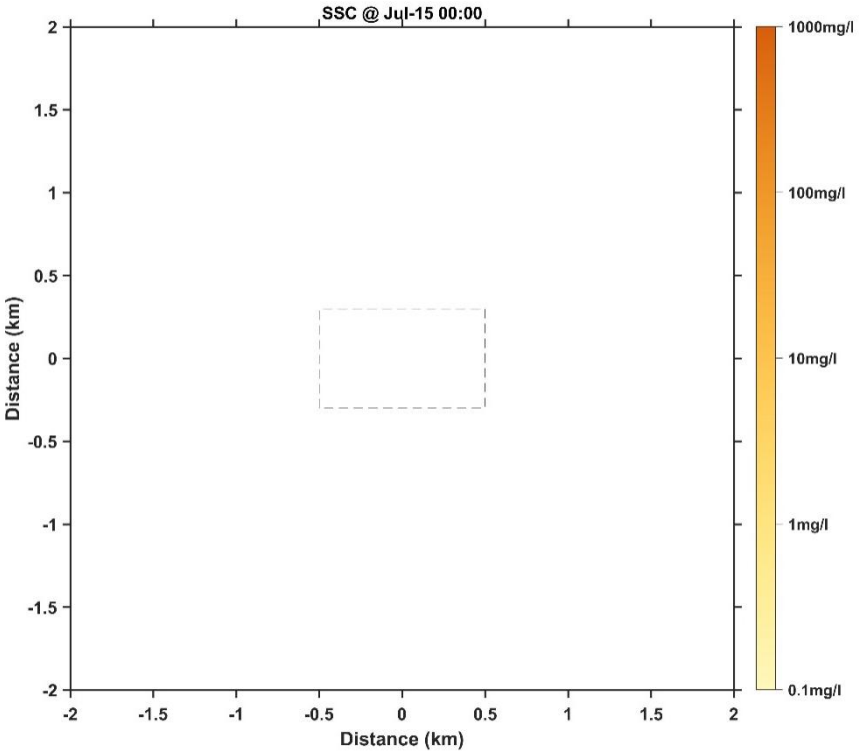

Figure 19 Distribution of bottom-layer suspended sediment concentrations on day 5 of test-mining in Case 2

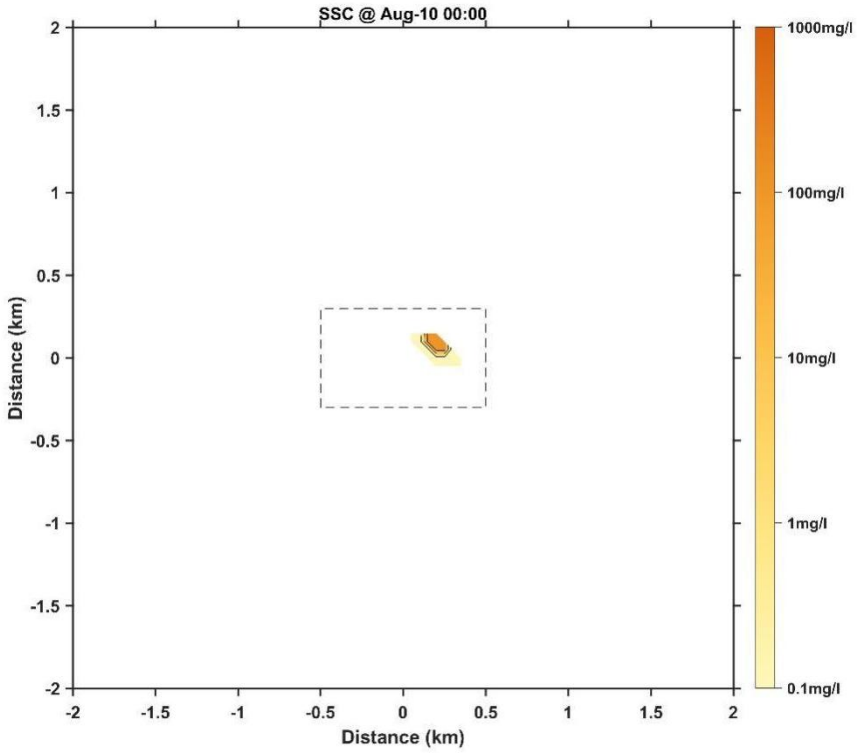

Figure 20 Distribution of bottom-layer suspended sediment concentrations at the start of first test-mining in Case 3

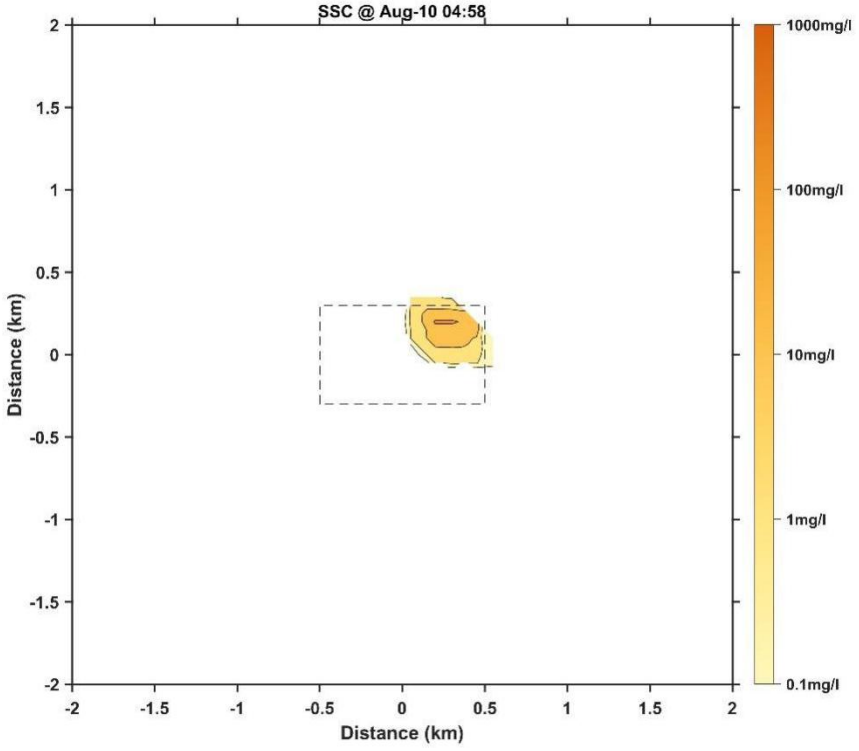

Figure 21 Distribution of bottom-layer suspended sediment concentrations at the end of first test-mining in Case 3

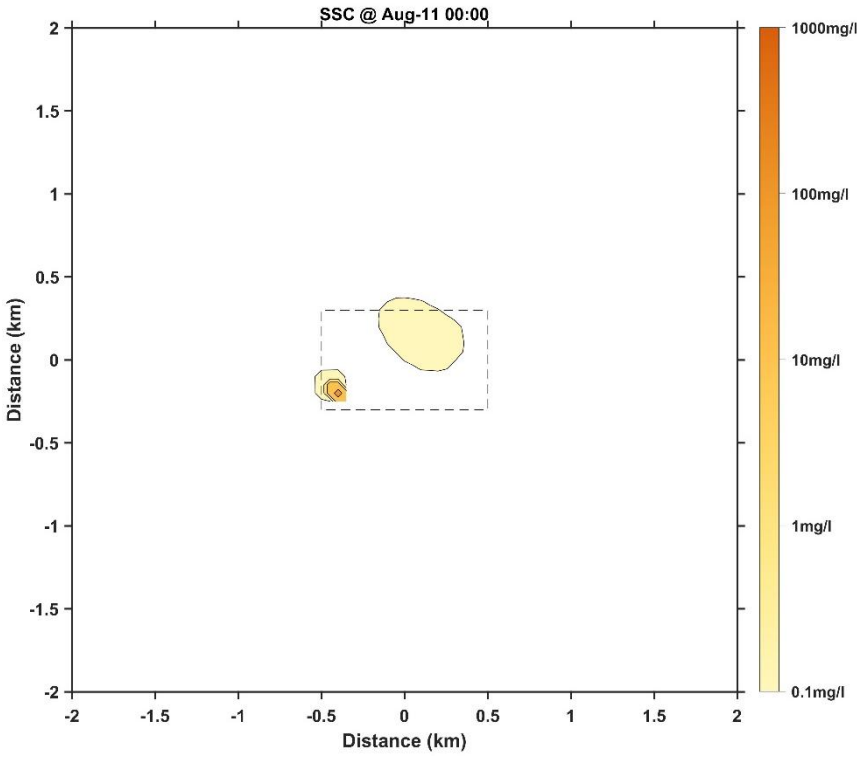

Figure 22 Distribution of bottom-layer suspended sediment concentrations at the start of second test-mining in Case 3

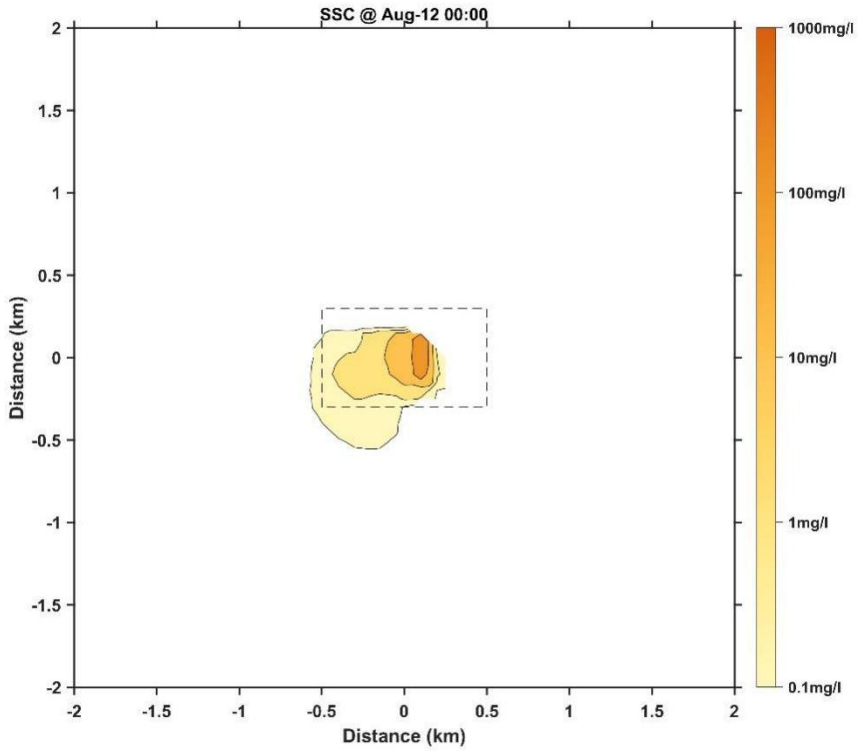

Figure 23 Distribution of bottom-layer suspended sediment concentrations on day 2 of test-mining in Case 3

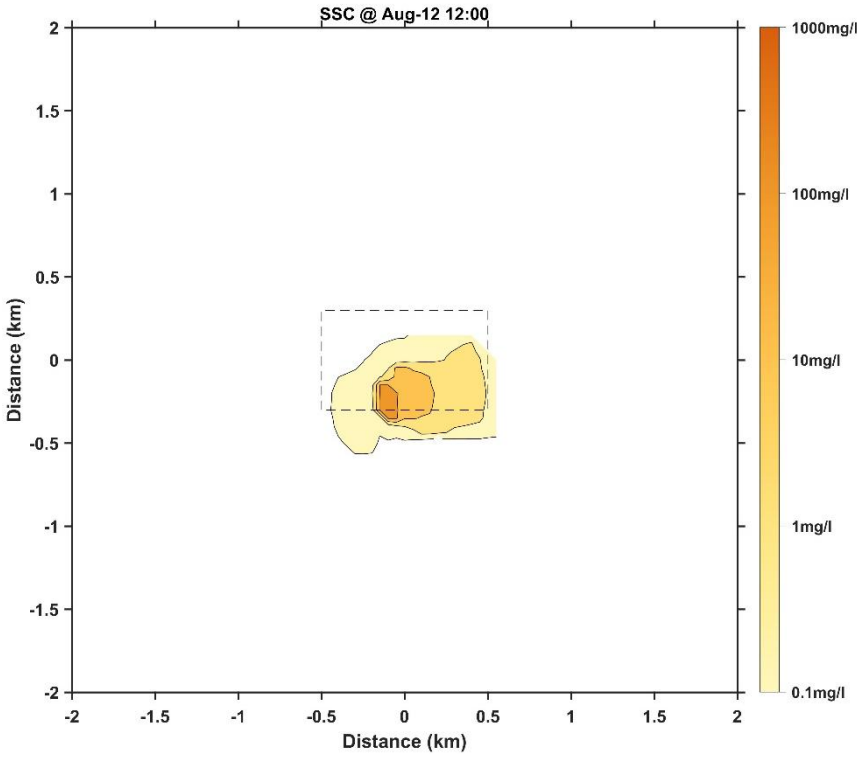

Figure 7.5-4 Distribution of bottom-layer suspended sediment concentrations at the end of second test-mining in Case 3

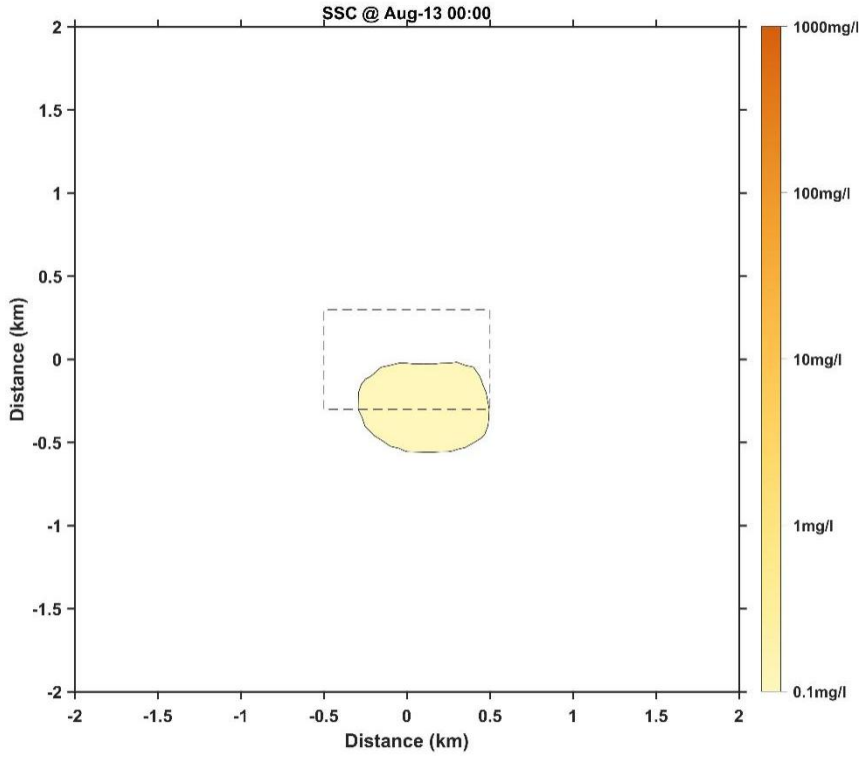

Figure 25 Distribution of bottom-layer suspended sediment concentrations on day 3 of test-mining in Case 3

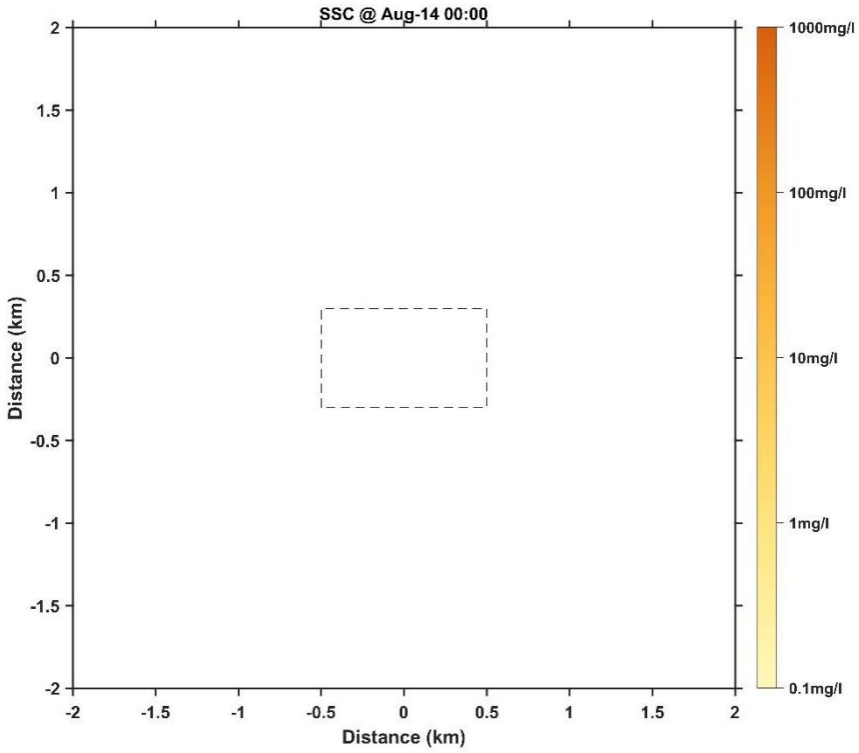

Figure 26 Distribution of bottom-layer suspended sediment concentrations on day 4 of test-mining in Case 3

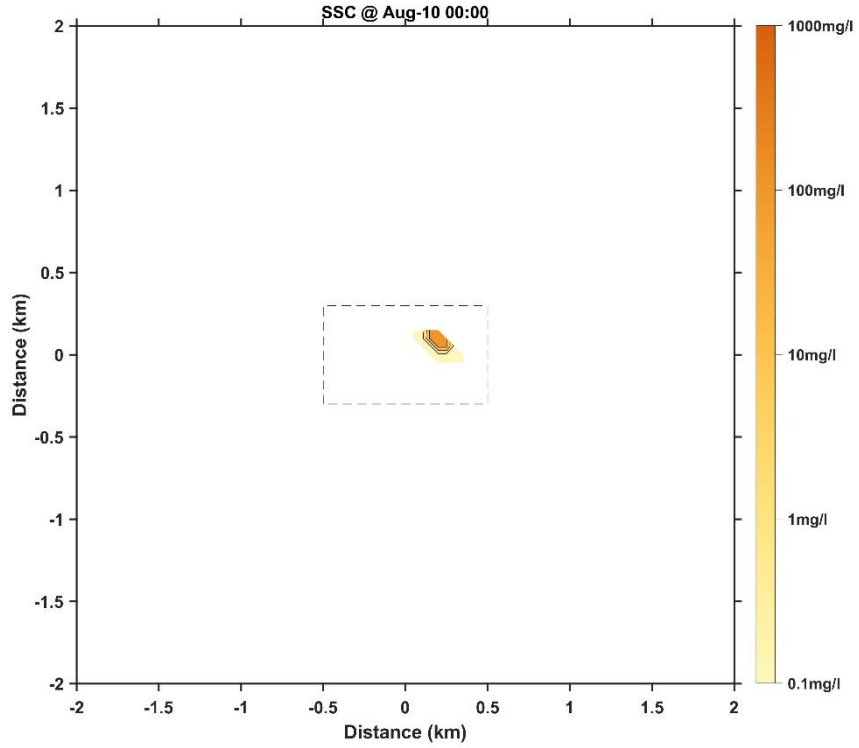

Figure 27 Distribution of bottom-layer suspended sediment concentrations at the start of first test-mining in Case 4

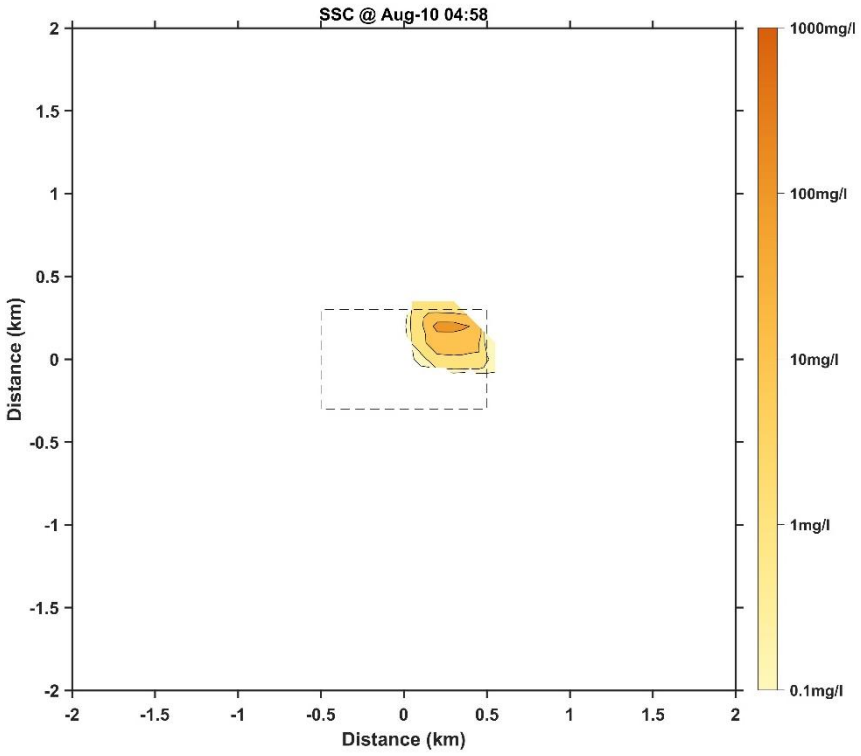

Figure 28 Distribution of bottom-layer suspended sediment concentrations at the end of first test-mining in Case 4

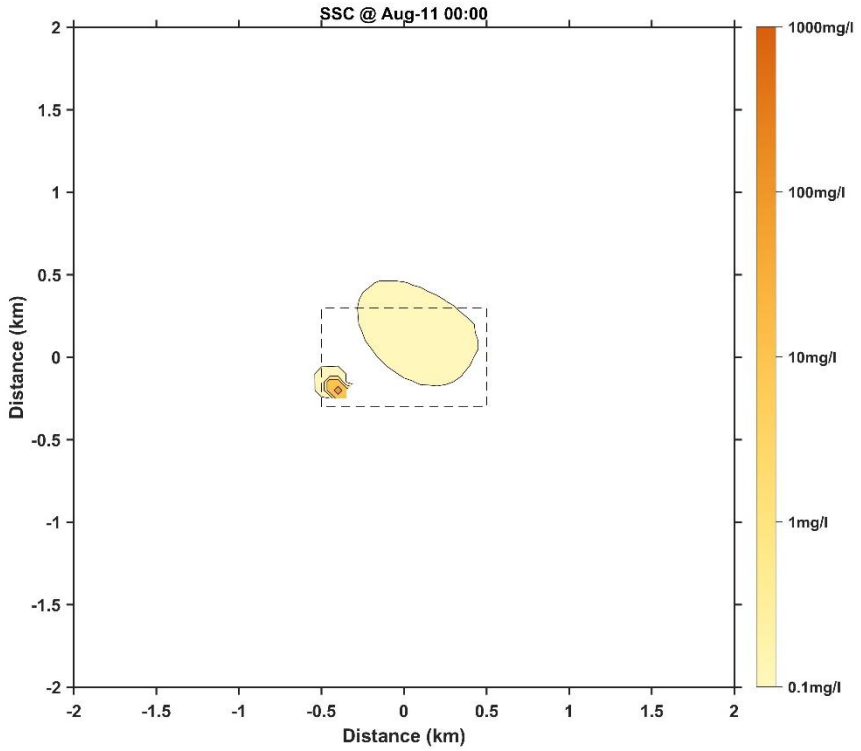

Figure 29 Distribution of bottom-layer suspended sediment concentrations at the start of second test-mining in Case 4

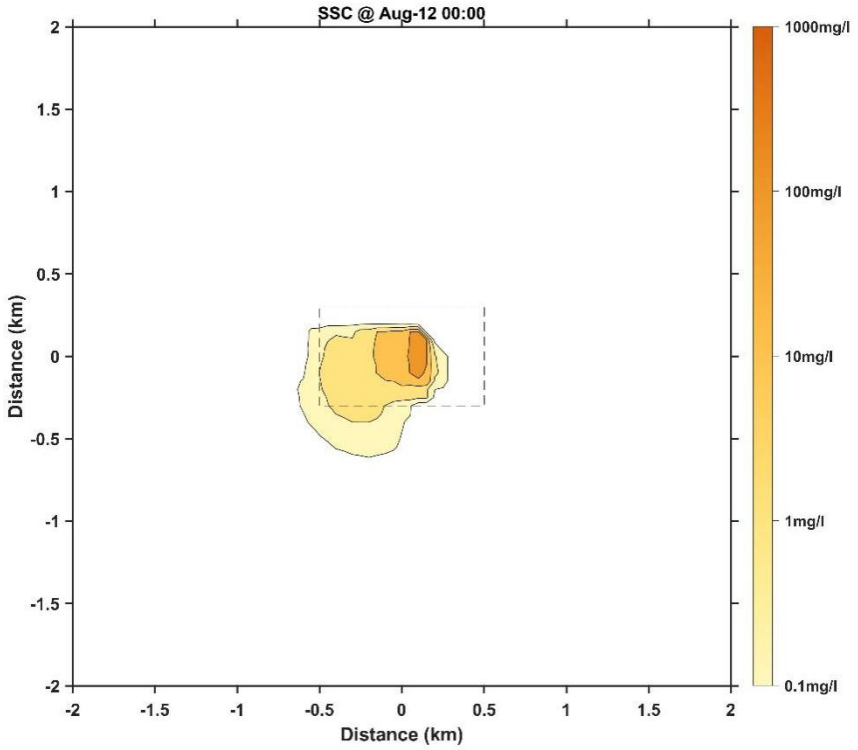

Figure 30 Distribution of bottom-layer suspended sediment concentrations on day 2 of test-mining in Case 4

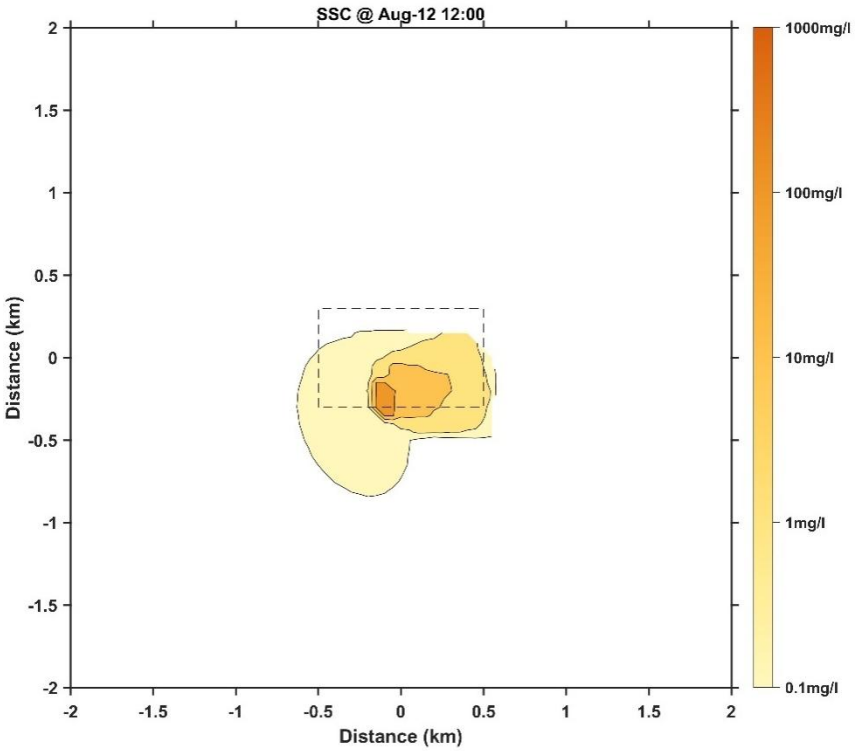

Figure 31 Distribution of bottom-layer suspended sediment concentrations at the end of second test-mining in Case 4

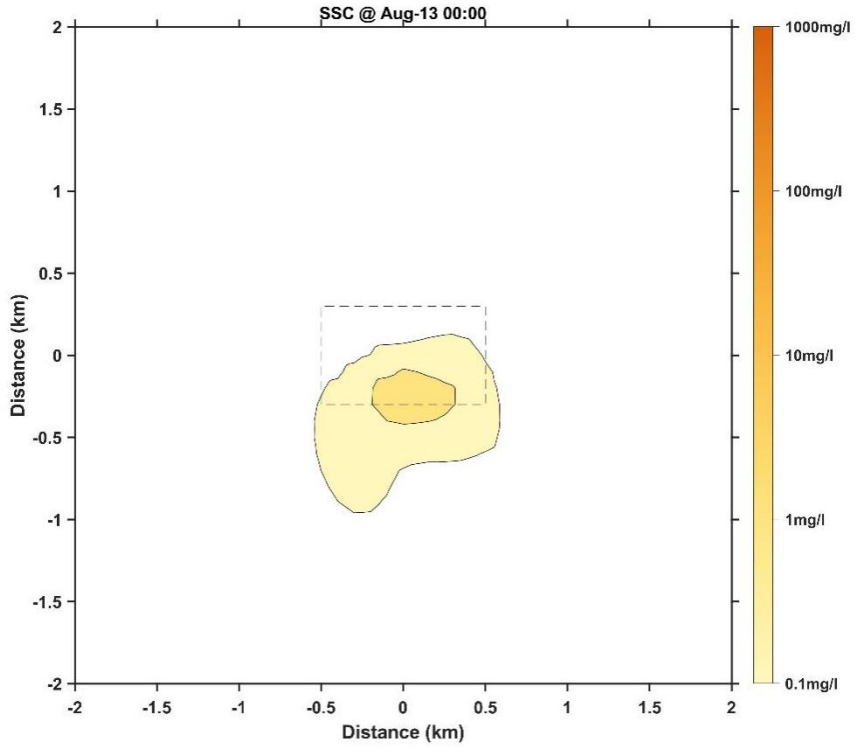

Figure 32 Distribution of bottom-layer suspended sediment concentrations on day 3 of test-mining in Case 4

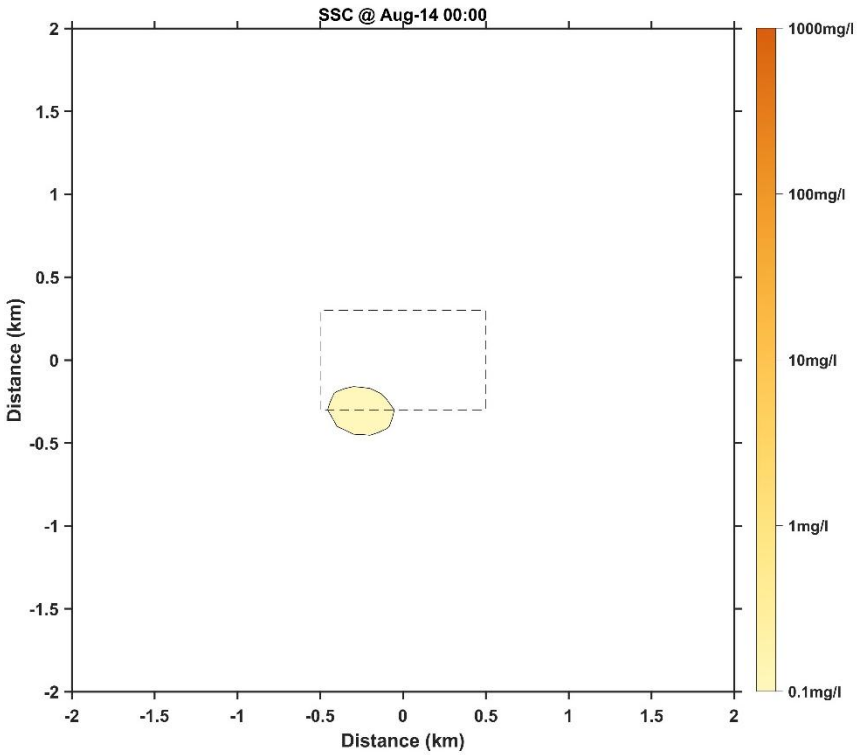

Figure 33 Distribution of bottom-layer suspended sediment concentrations on day 4 of test-mining in Case 4

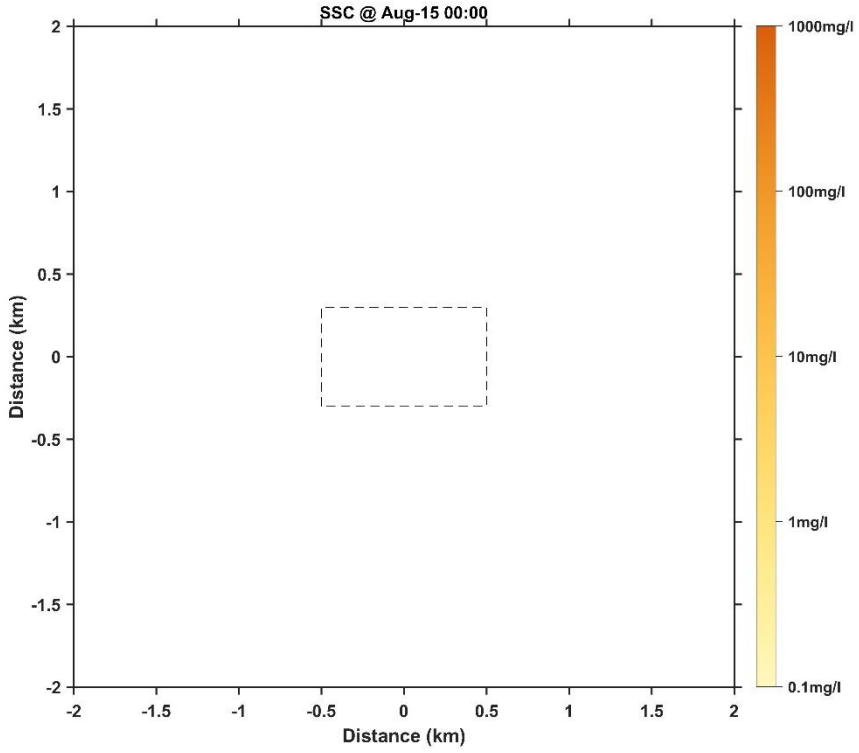

Figure 34 Distribution of bottom-layer suspended sediment concentrations on day 5 of test-mining in Case 4

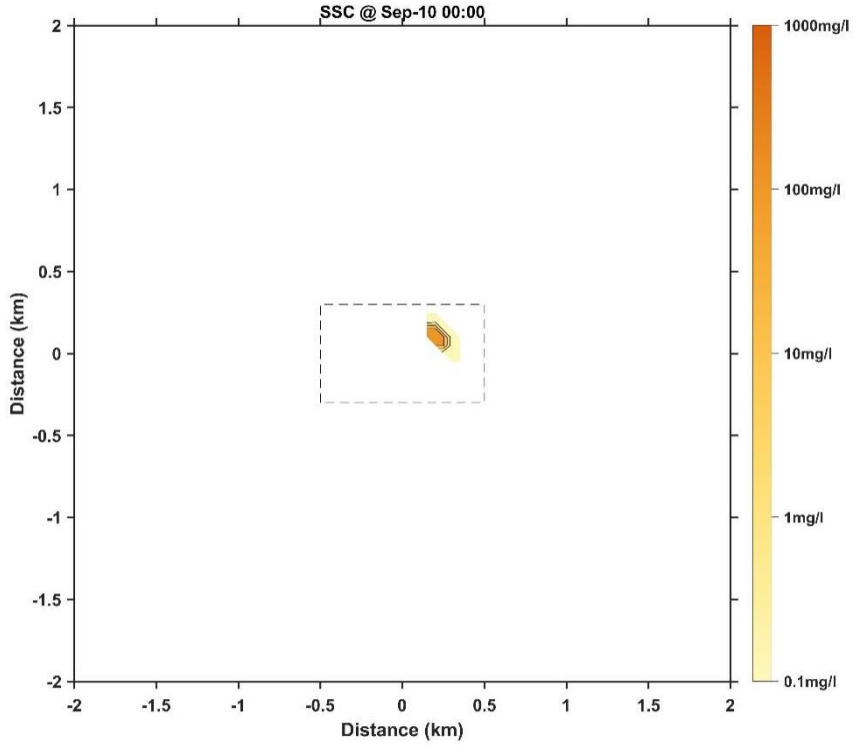

Figure 35 Distribution of bottom-layer suspended sediment concentrations at the start of first test-mining in Case 5

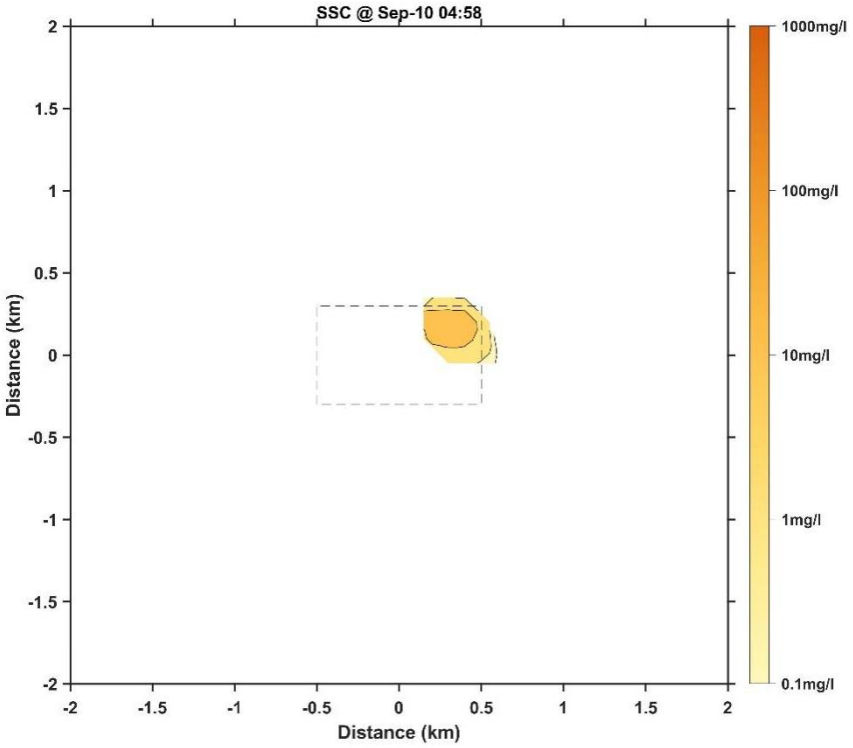

Figure 36 Distribution of bottom-layer suspended sediment concentrations at the end of first test-mining in Case 5

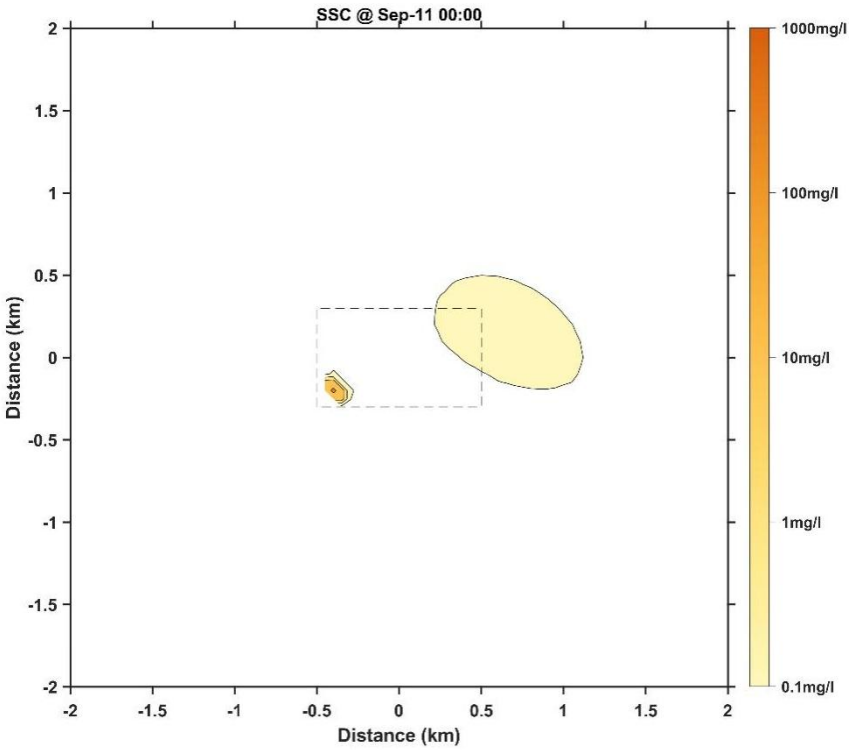

Figure 37 Distribution of bottom-layer suspended sediment concentrations at the start of second test-mining in Case 5

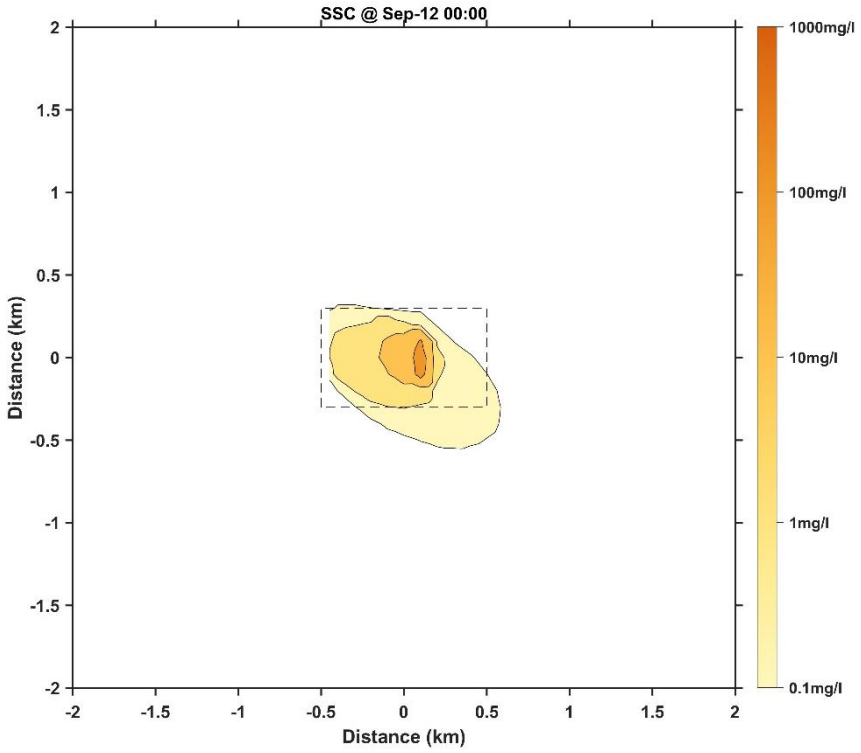

Figure 38 Distribution of bottom-layer suspended sediment concentrations on day 2 of test-mining in Case 5

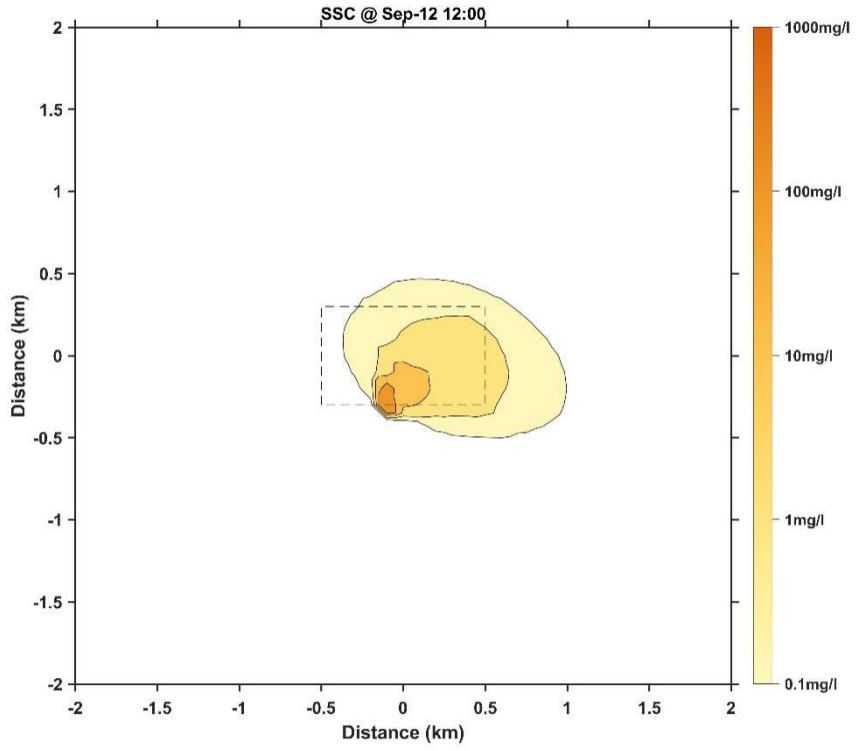

Figure 39 Distribution of bottom-layer suspended sediment concentrations at the end of second test-mining in Case 5

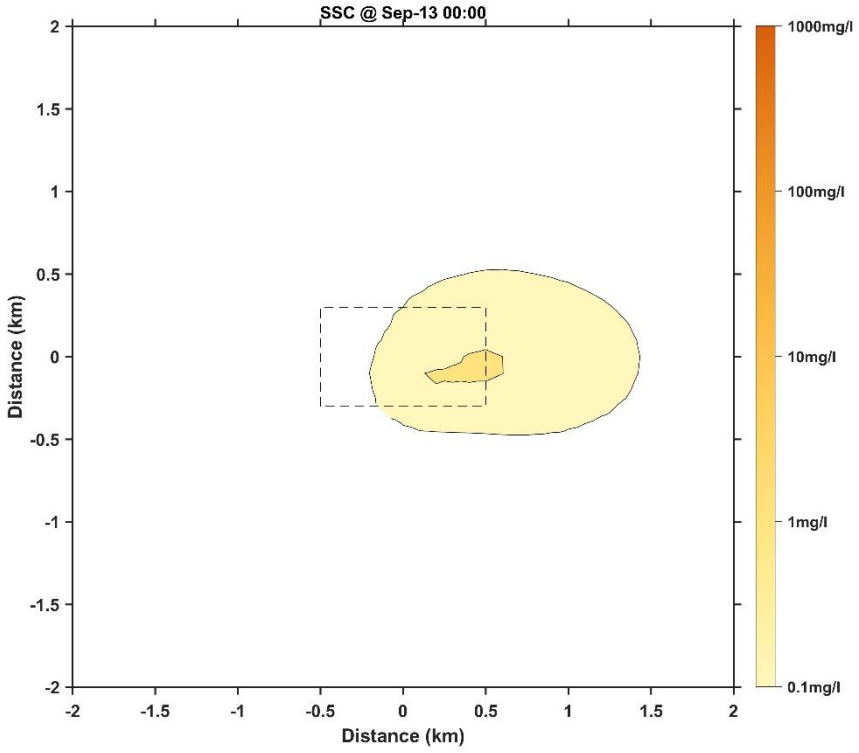

Figure 40 Distribution of bottom-layer suspended sediment concentrations on day 3 of test-mining in Case 5

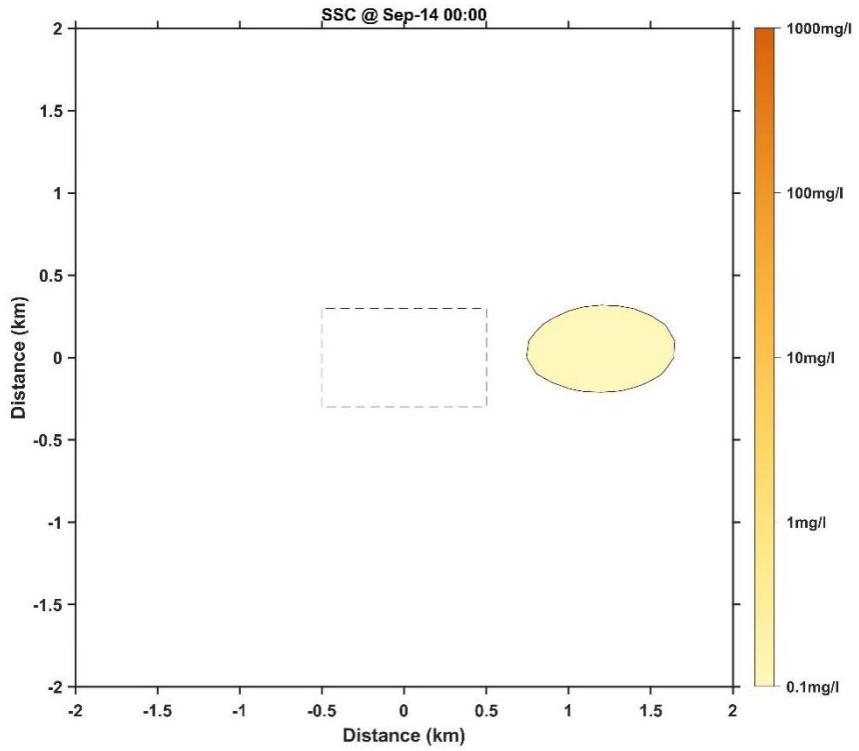

Figure 41 Distribution of bottom-layer suspended sediment concentrations on day 4 of test-mining in Case 5

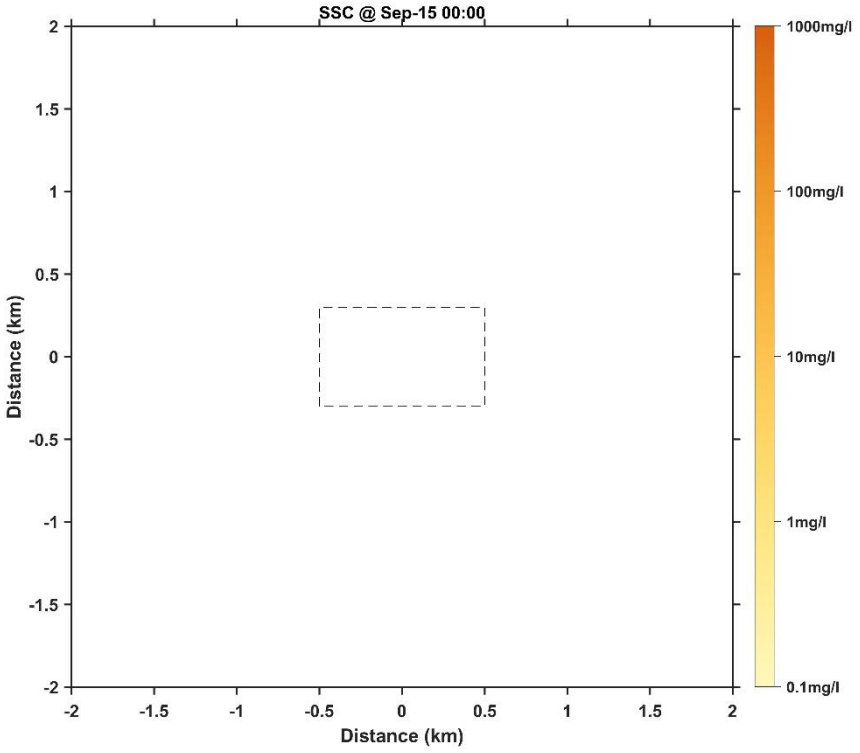

Figure 42 Distribution of bottom-layer suspended sediment concentrations on day 5 of test-mining in Case 5

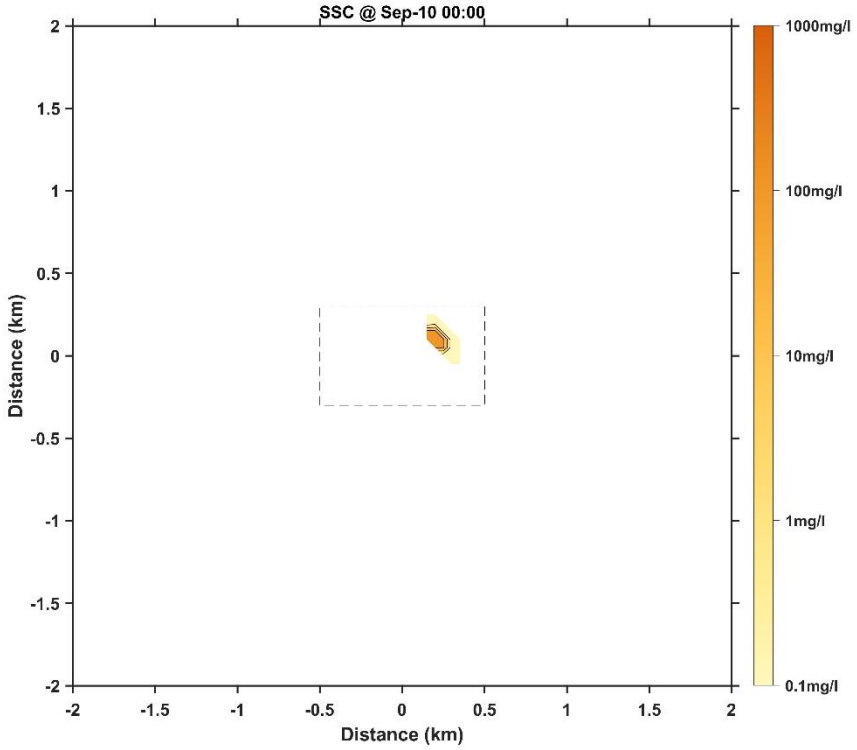

Figure 43 Distribution of bottom-layer suspended sediment concentrations at the start of first test-mining in Case 6

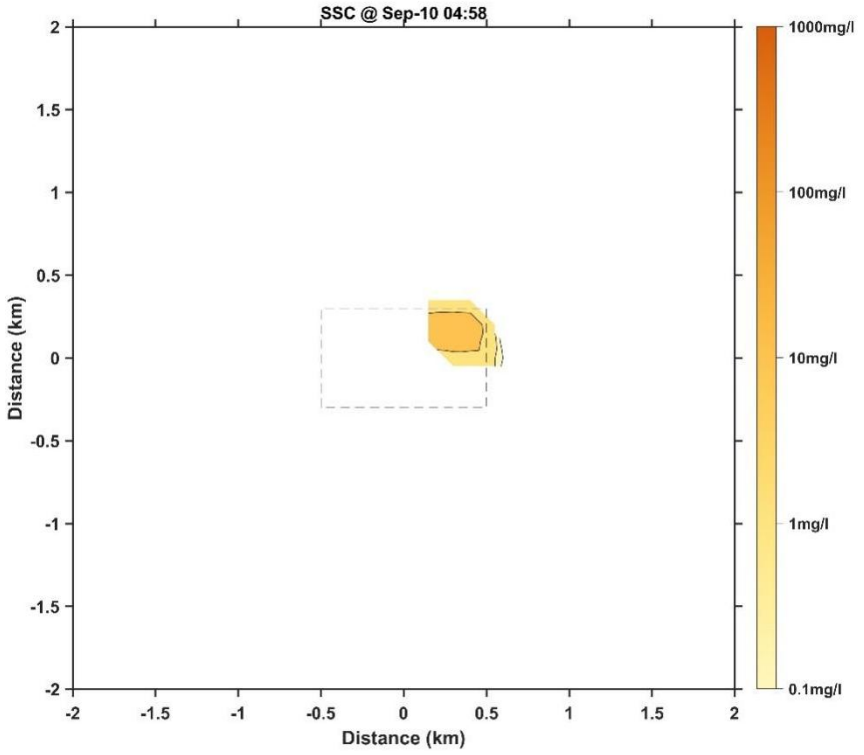

Figure 44 Distribution of bottom-layer suspended sediment concentrations at the end of first test-mining in Case 6

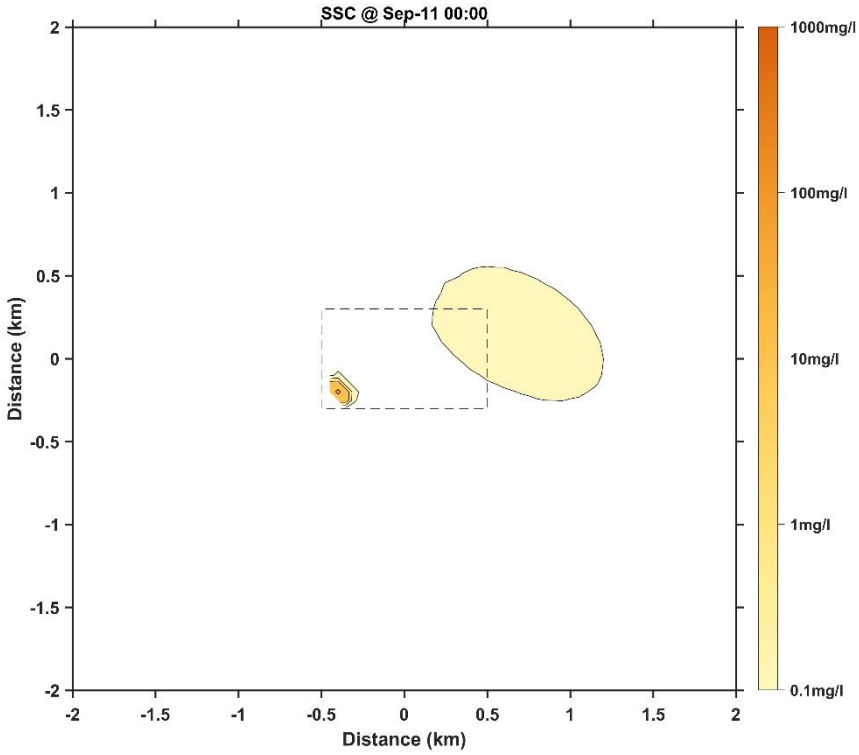

Figure 45 Distribution of bottom-layer suspended sediment concentrations at the start of second test-mining in Case 6

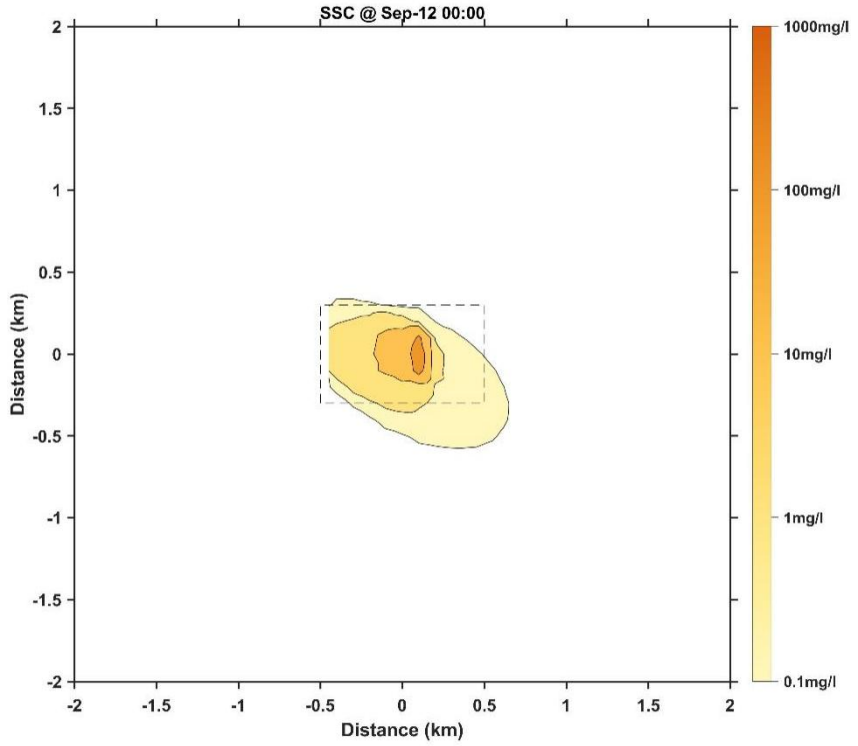

Figure 46 Distribution of bottom-layer suspended sediment concentrations on day 2 of test-mining in Case 6

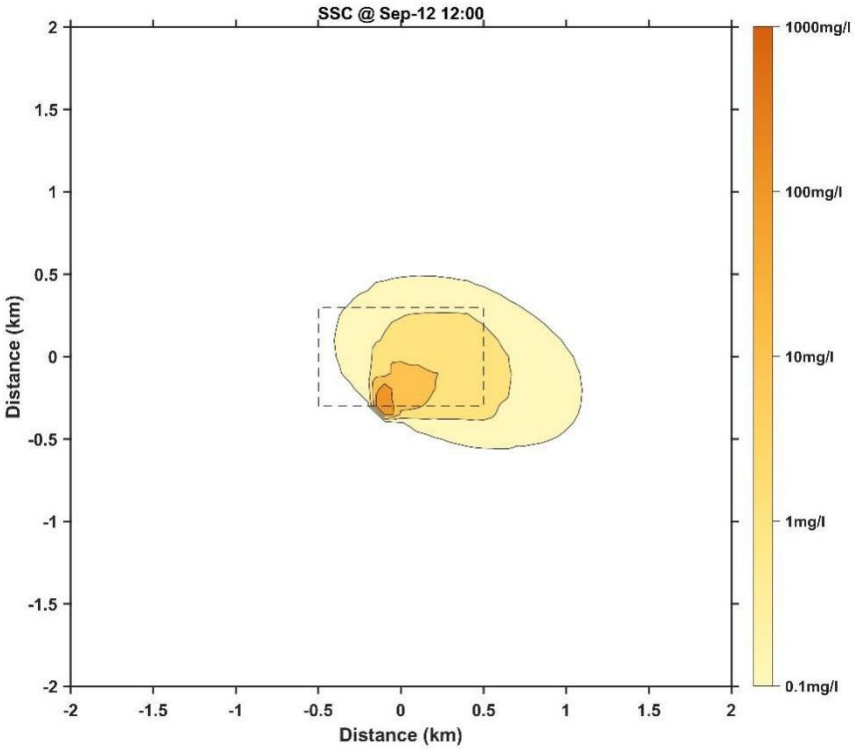

Figure 47 Distribution of bottom-layer suspended sediment concentrations at the end of second test-mining in Case 6

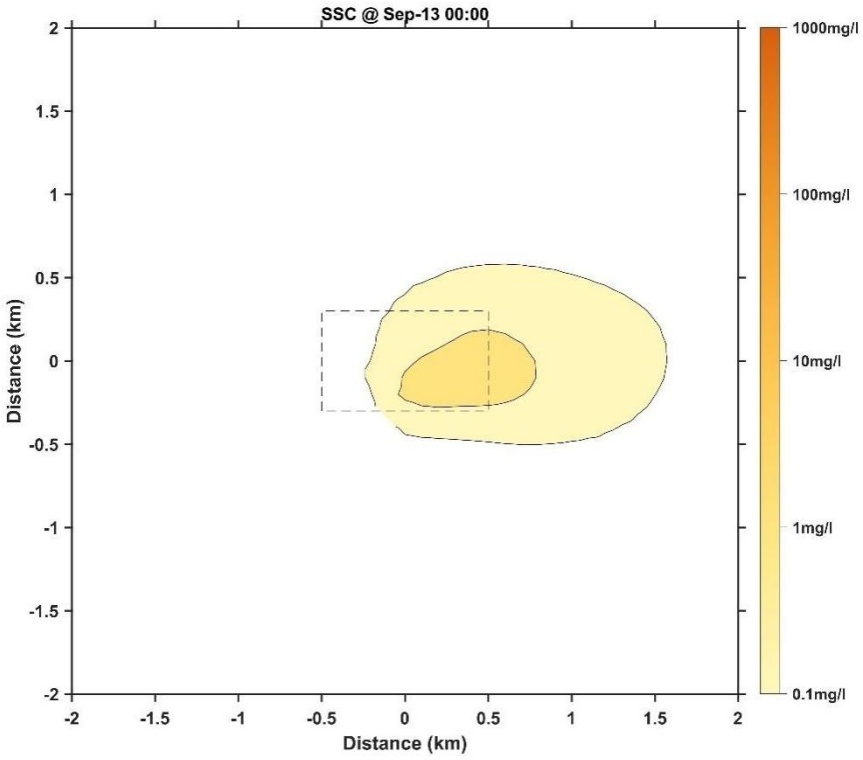

Figure 48 Distribution of bottom-layer suspended sediment concentrations on day 3 of test-mining in Case 6

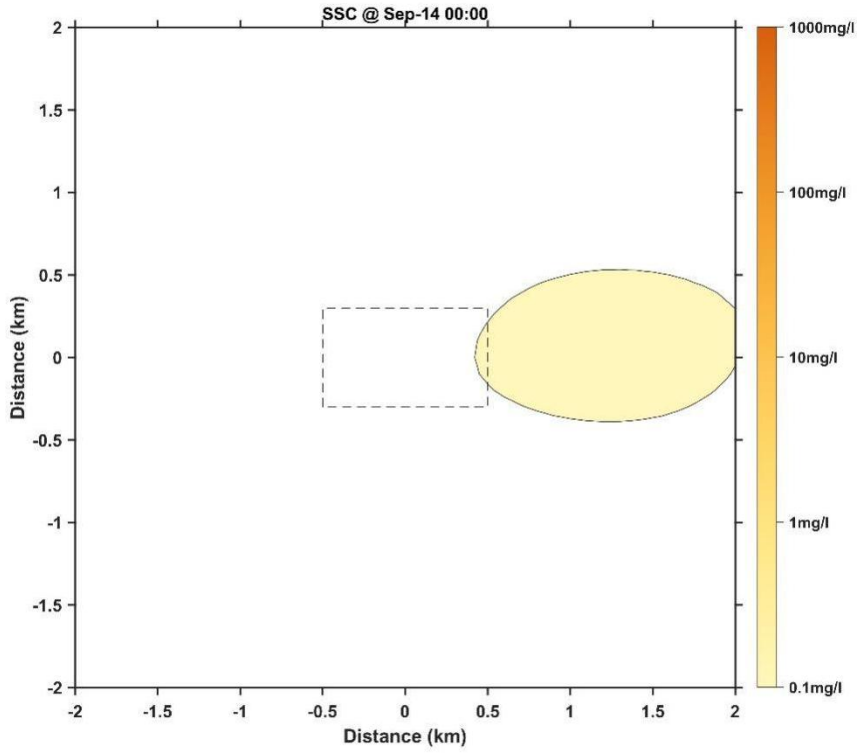

Figure 49 Distribution of bottom-layer suspended sediment concentrations on day 4 of test-mining in Case 6

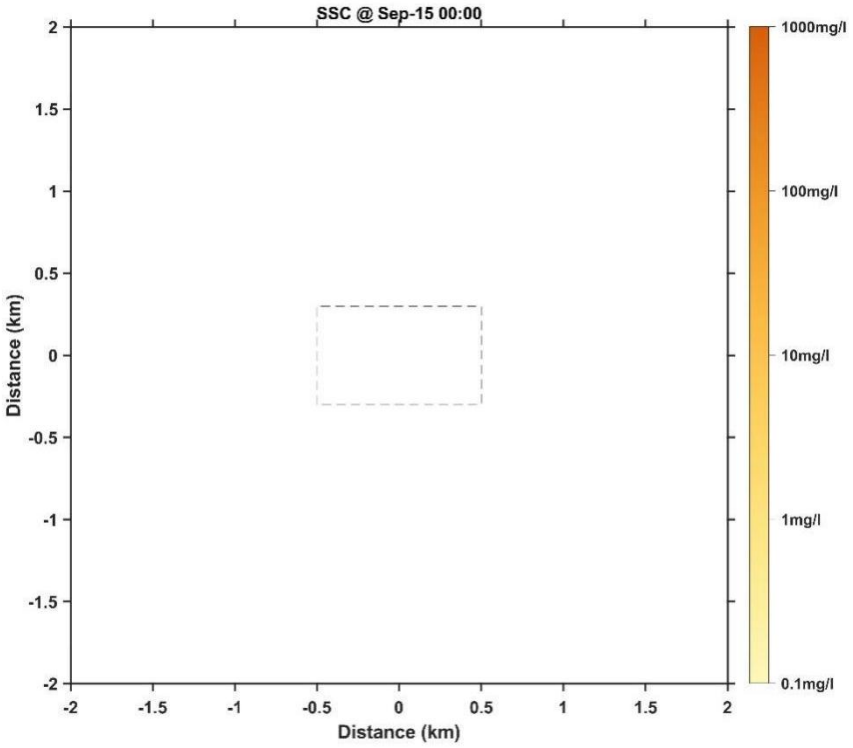

Figure 50 Distribution of bottom-layer suspended sediment concentrations on day 5 of test-mining in Case 6

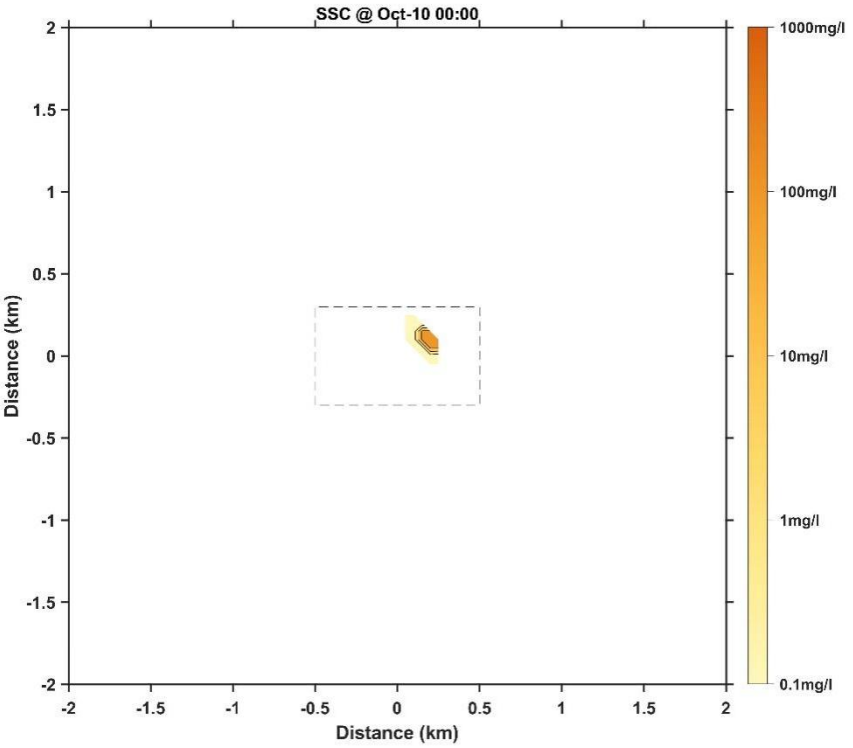

Figure 51 Distribution of bottom-layer suspended sediment concentrations at the start of first test-mining in Case 7

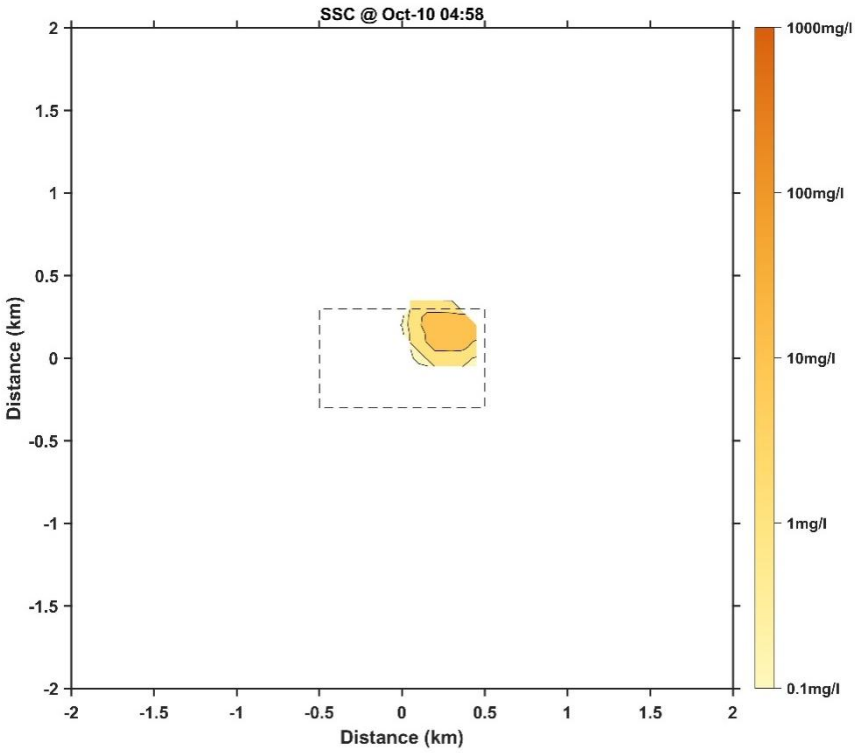

Figure 52 Distribution of bottom-layer suspended sediment concentrations at the end of first test-mining in Case 7

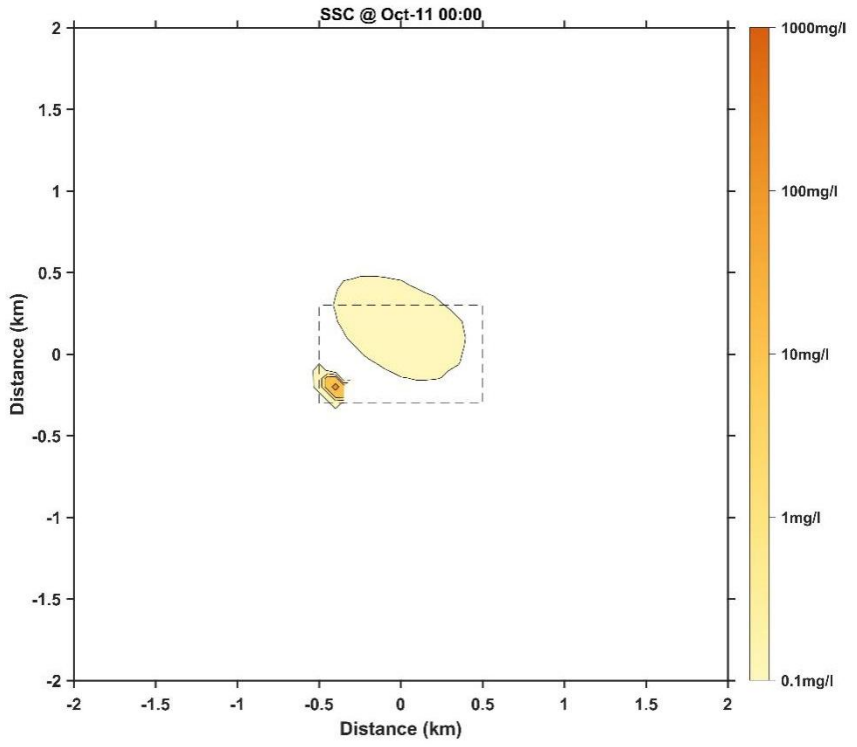

Figure 53 Distribution of bottom-layer suspended sediment concentrations at the start of second test-mining in Case 7

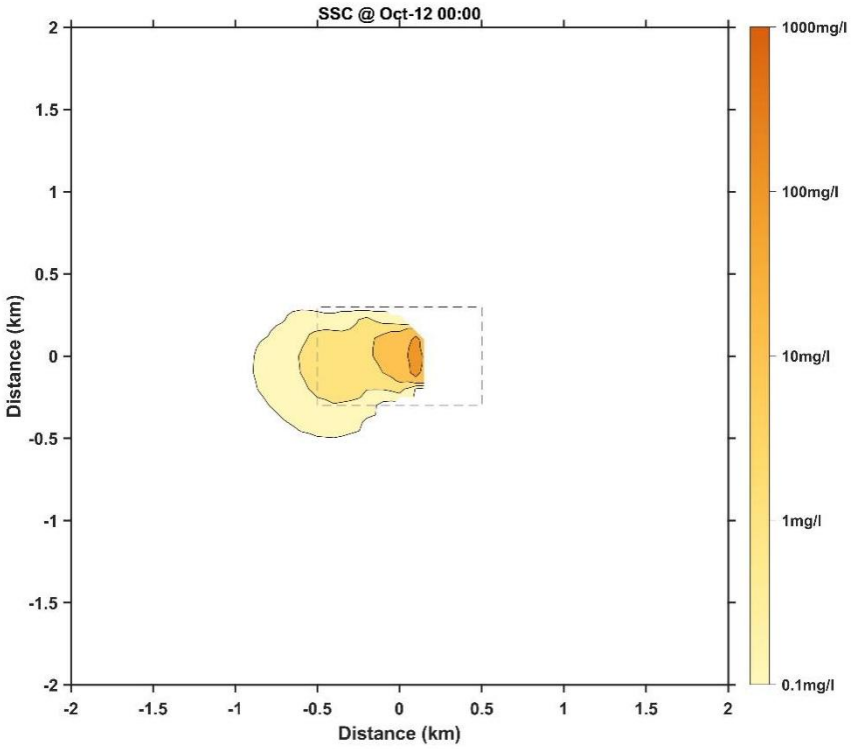

Figure 54 Distribution of bottom-layer suspended sediment concentrations on day 2 of test-mining in Case 7

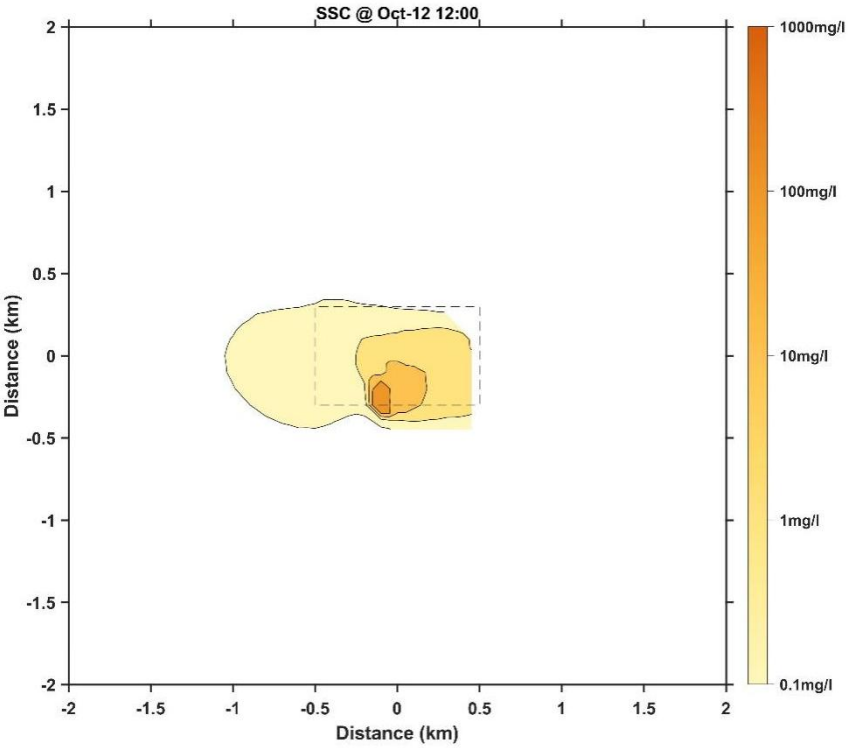

Figure 55 Distribution of bottom-layer suspended sediment concentrations at the end of second test-mining in Case 7

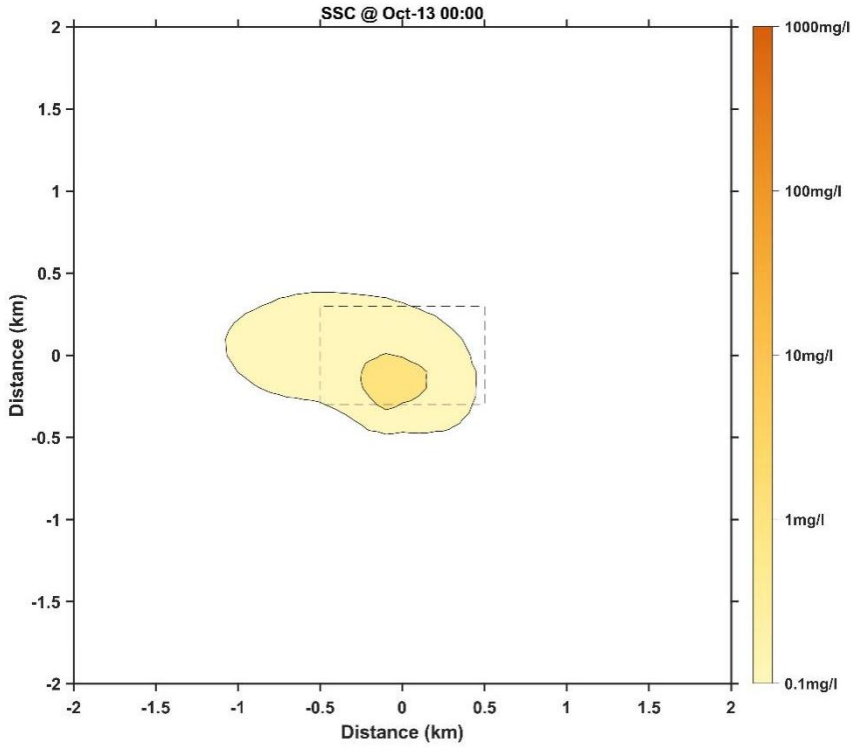

Figure 56 Distribution of bottom-layer suspended sediment concentrations on day 3 of test-mining in Case 7

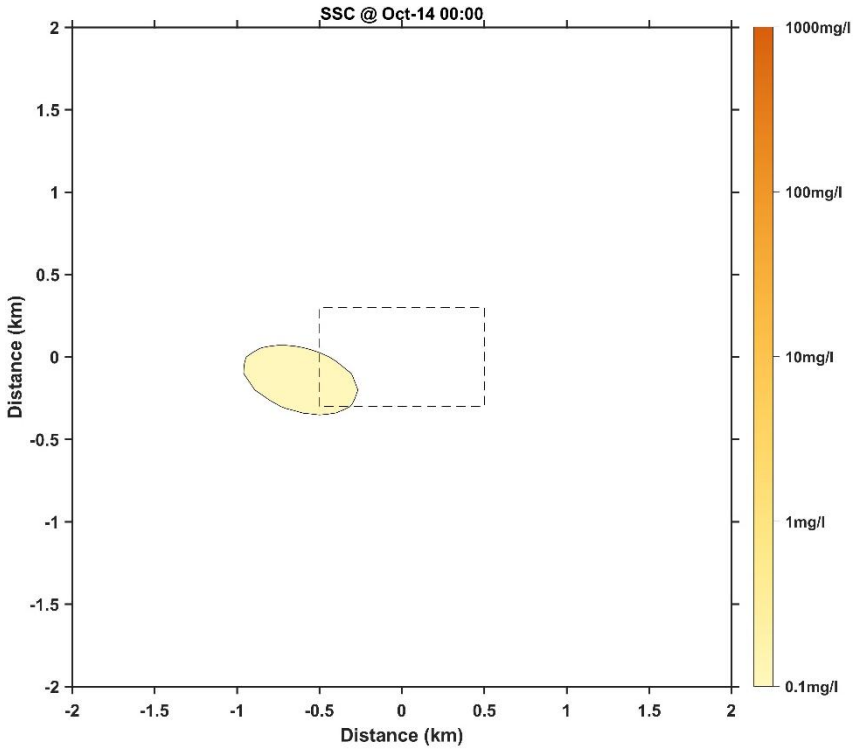

Figure 57 Distribution of bottom-layer suspended sediment concentrations on day 4 of test-mining in Case 7

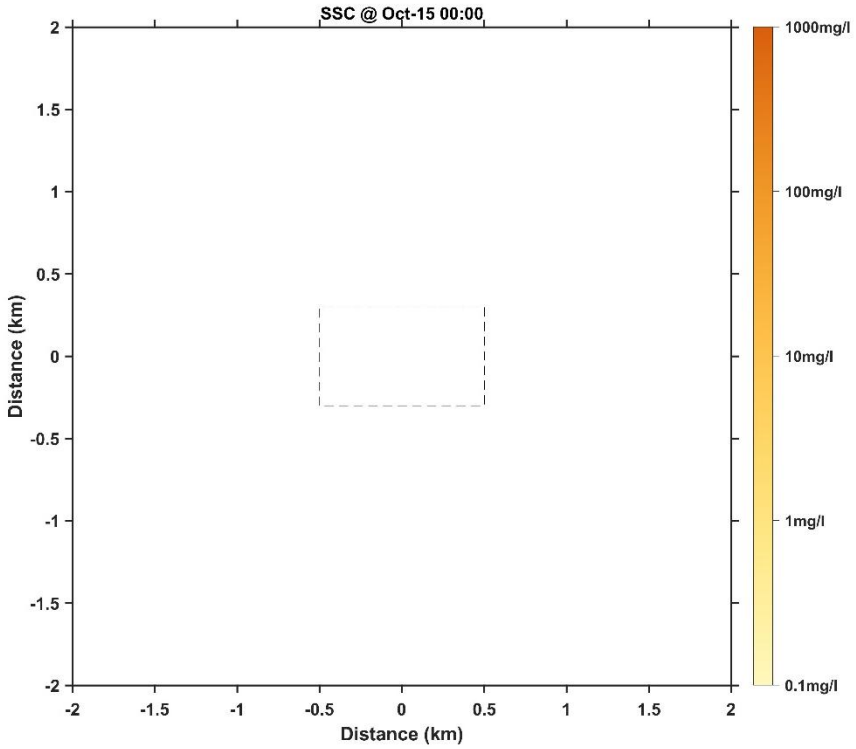

Figure 58 Distribution of bottom-layer suspended sediment concentrations on day 5 of test-mining in Case 7

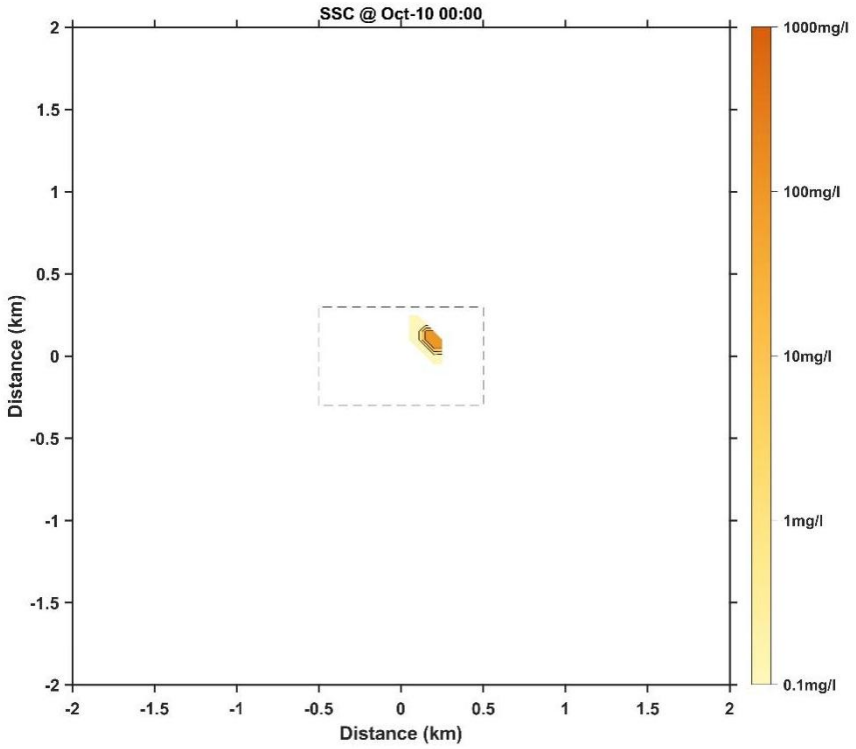

Figure 59 Distribution of bottom-layer suspended sediment concentrations at the start of first test-mining in Case 8

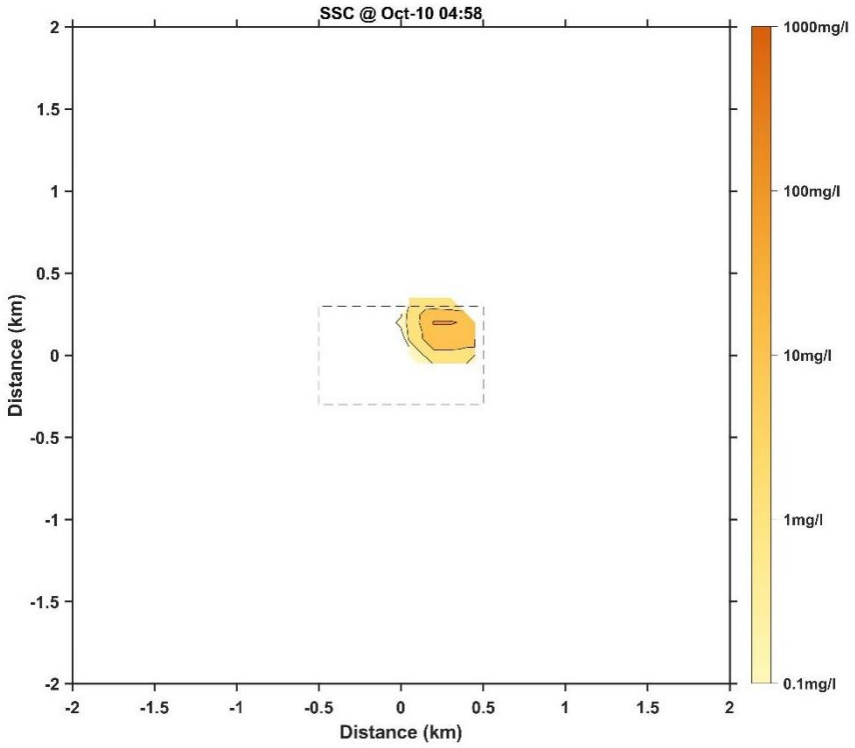

Figure 60 Distribution of bottom-layer suspended sediment concentrations at the end of first test-mining in Case 8

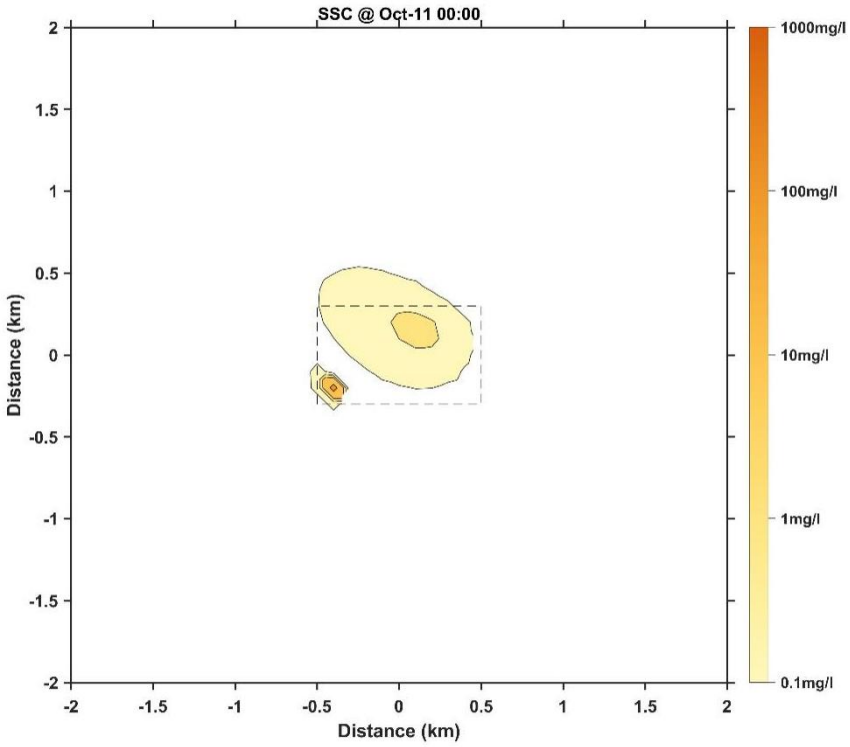

Figure 61 Distribution of bottom-layer suspended sediment concentrations at the start of second test-mining in Case 8

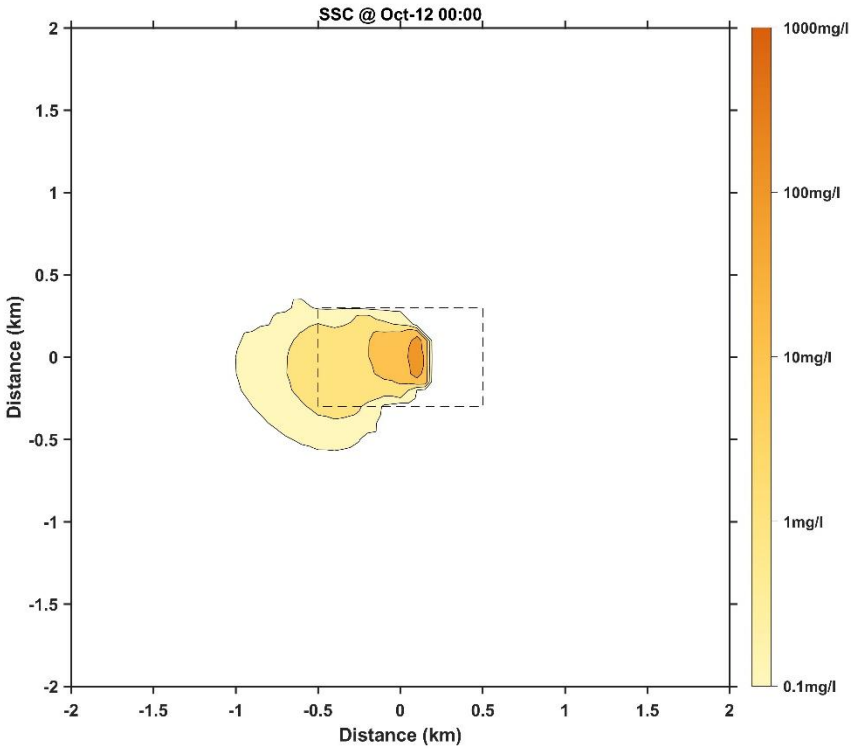

Figure 62 Distribution of bottom-layer suspended sediment concentrations on day 2 of test-mining in Case 8

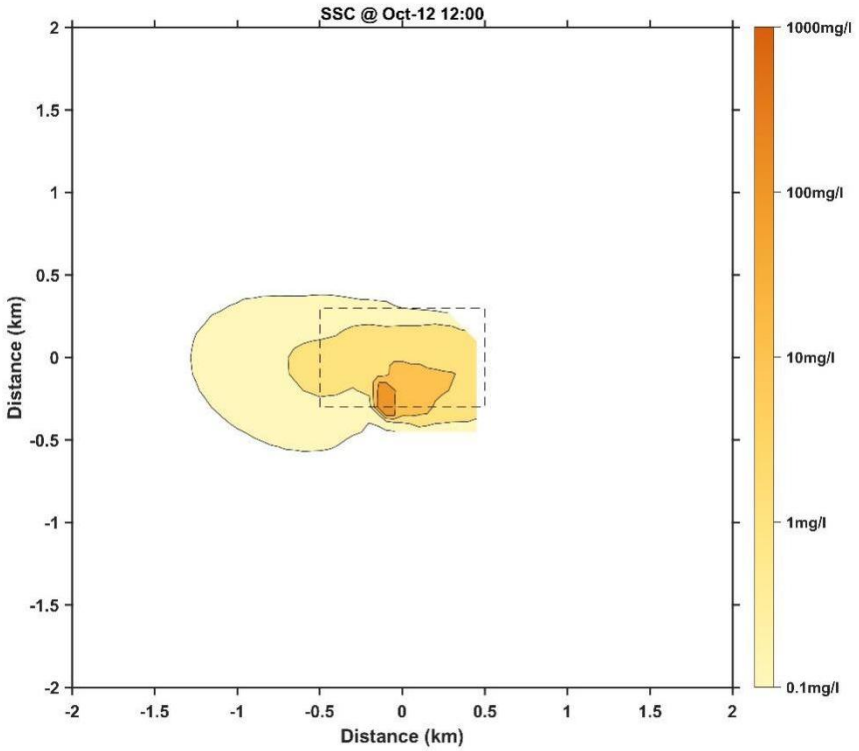

Figure 63 Distribution of bottom-layer suspended sediment concentrations at the end of second test-mining in Case 8

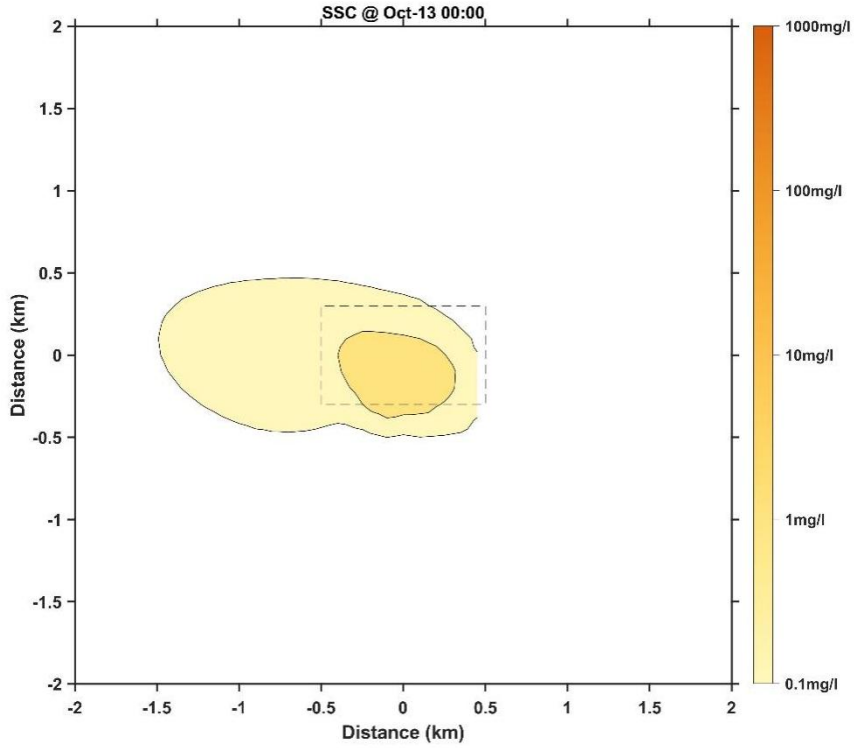

Figure 64 Distribution of bottom-layer suspended sediment concentrations on day 3 of test-mining in Case 8

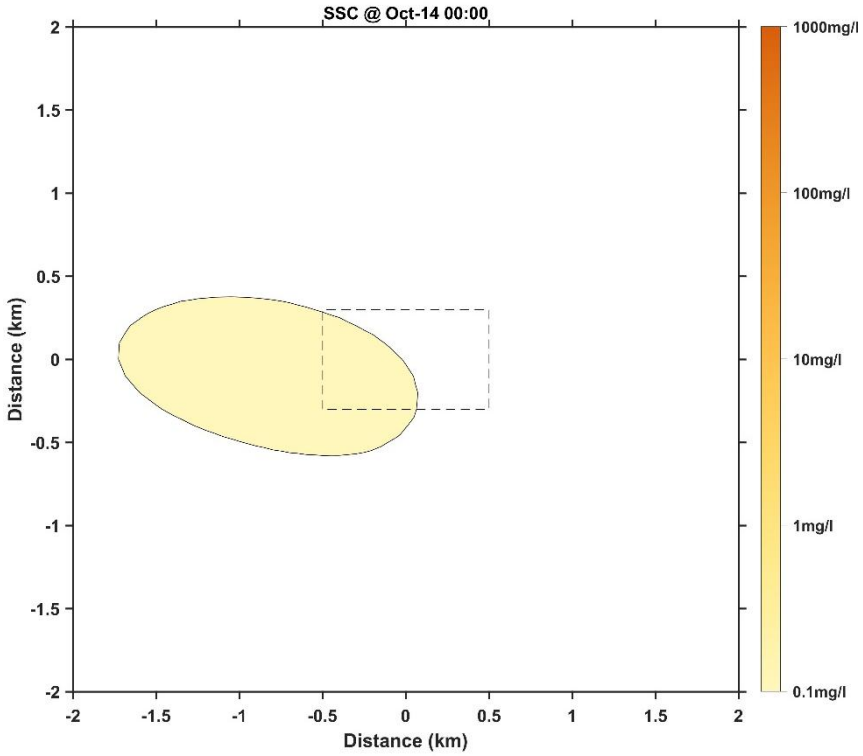

Figure 65 Distribution of bottom-layer suspended sediment concentrations on day 4 of test-mining in Case 8

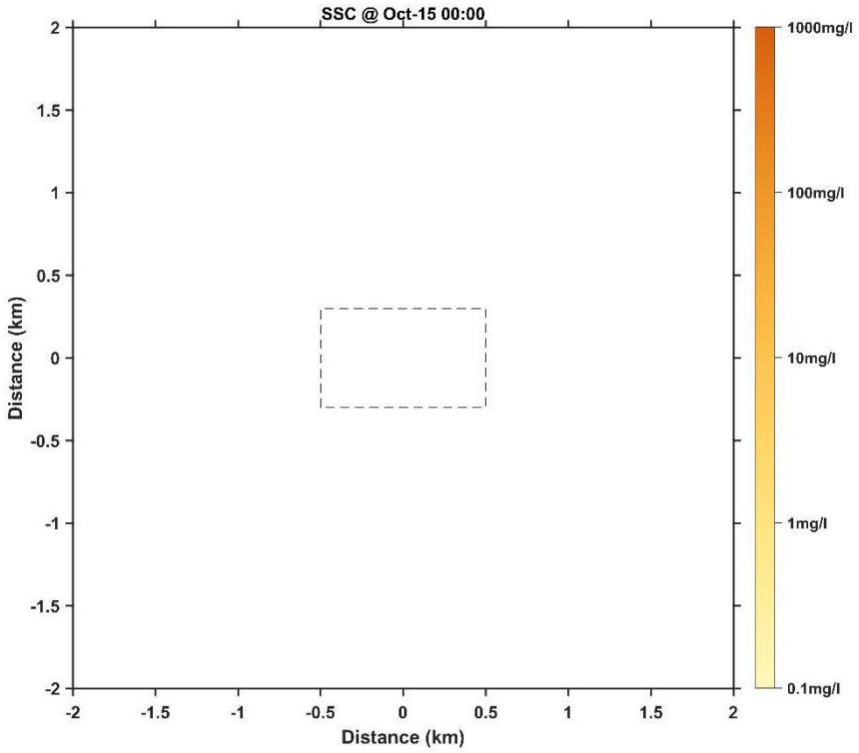

Figure 66 Distribution of bottom-layer suspended sediment concentrations on day 5 of test-mining in Case 8

3.2 Vertical distribution of suspended sediment concentrations

Figures 67-74 show the vertical distribution characteristics of suspended sediment concentration at the midpoint of the CTA. It can be seen from the Figures that the vertical impact of the plume is 124 m at most, and the plume at this point disappears within 1-1.5 days after the collector vehicle test is ended. Fine-grained sediments bring higher impact than coarse-grained sediments. The height of caused plume increases with the speed of the collector vehicle.

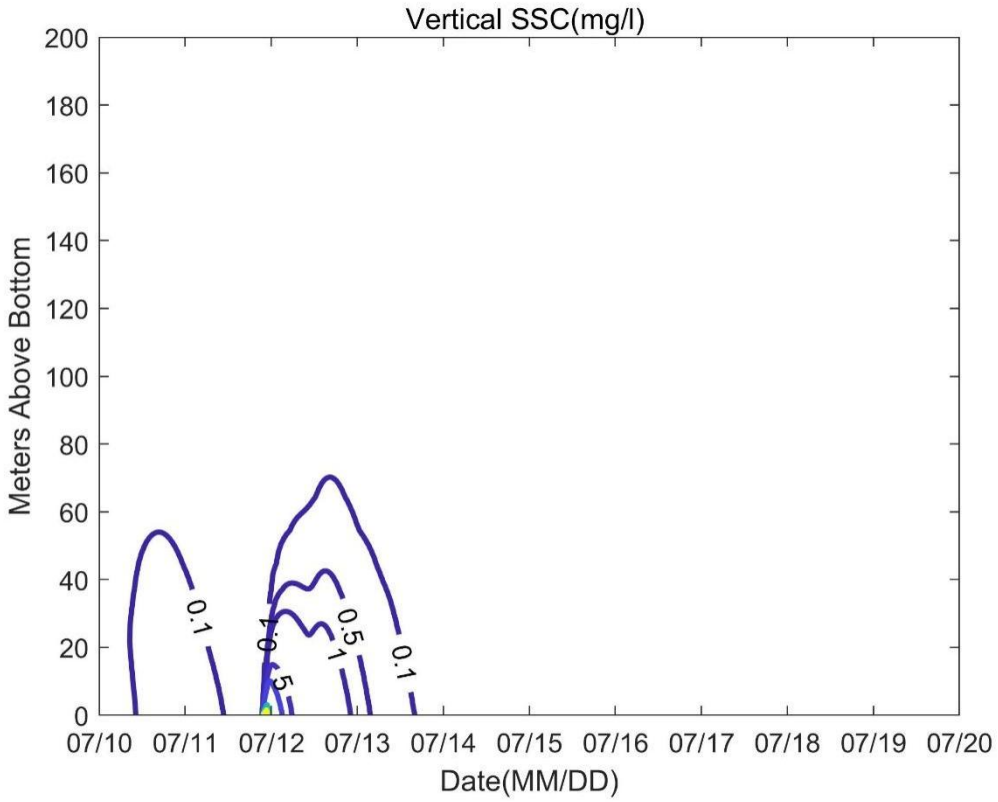

Figure 67 Vertical distribution of suspended sediment concentrations in Case 2

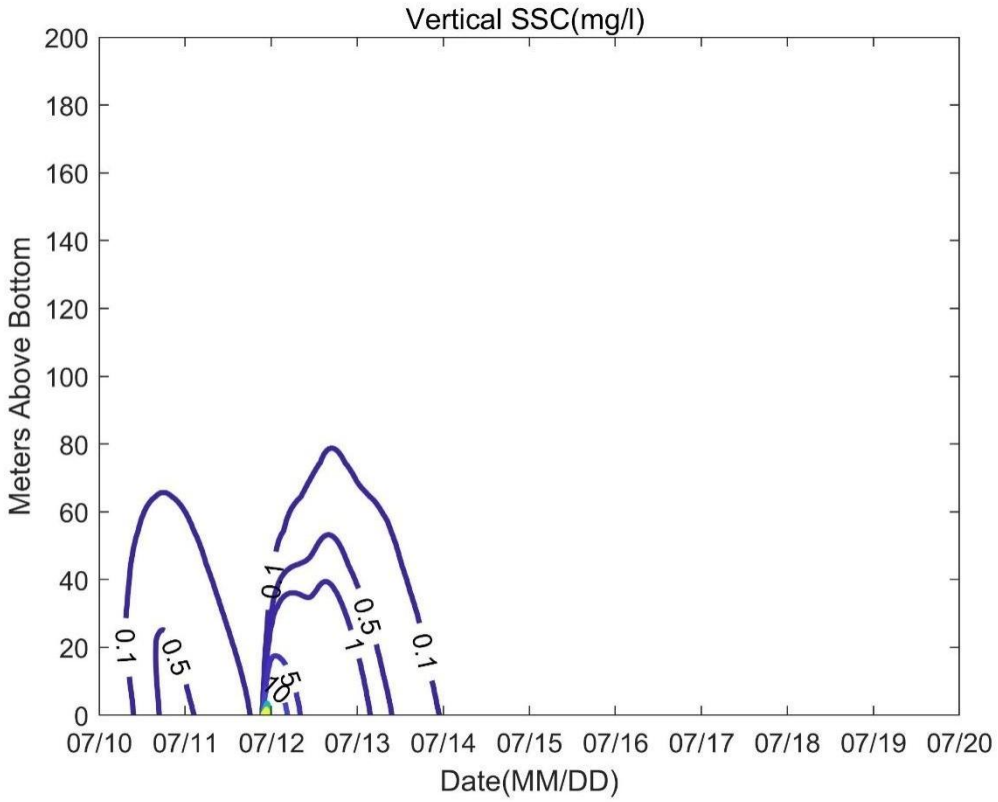

Figure 68 Vertical distribution of suspended sediment concentrations in Case 2

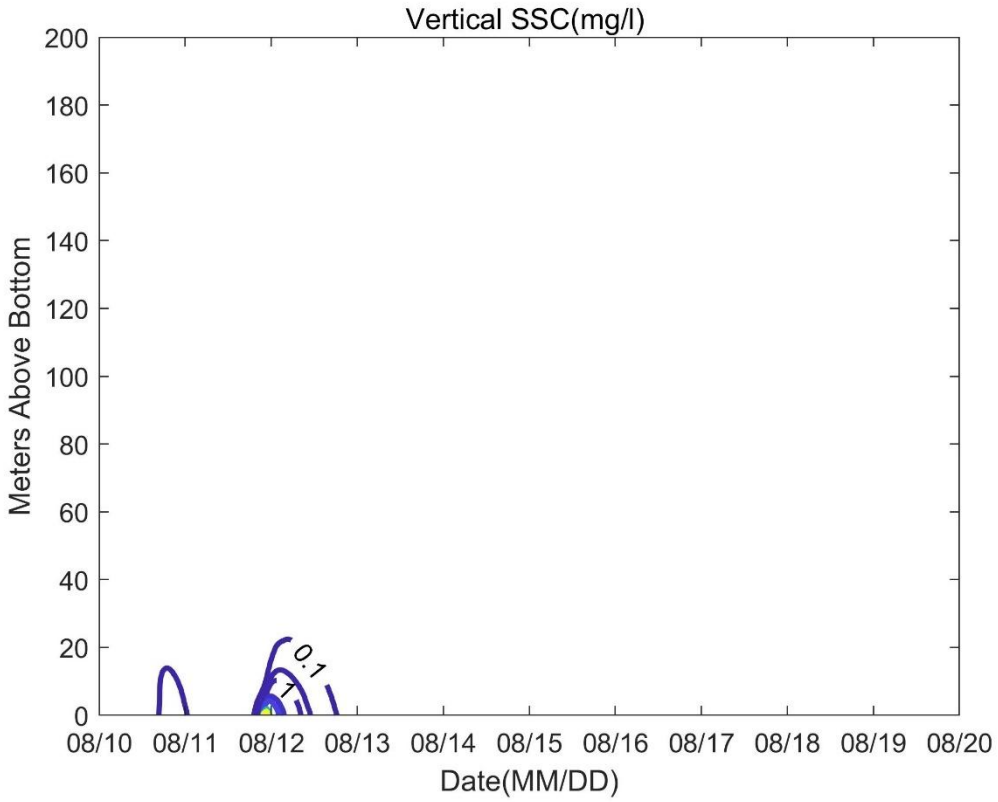

Figure 69 Vertical distribution of suspended sediment concentrations in Case 3

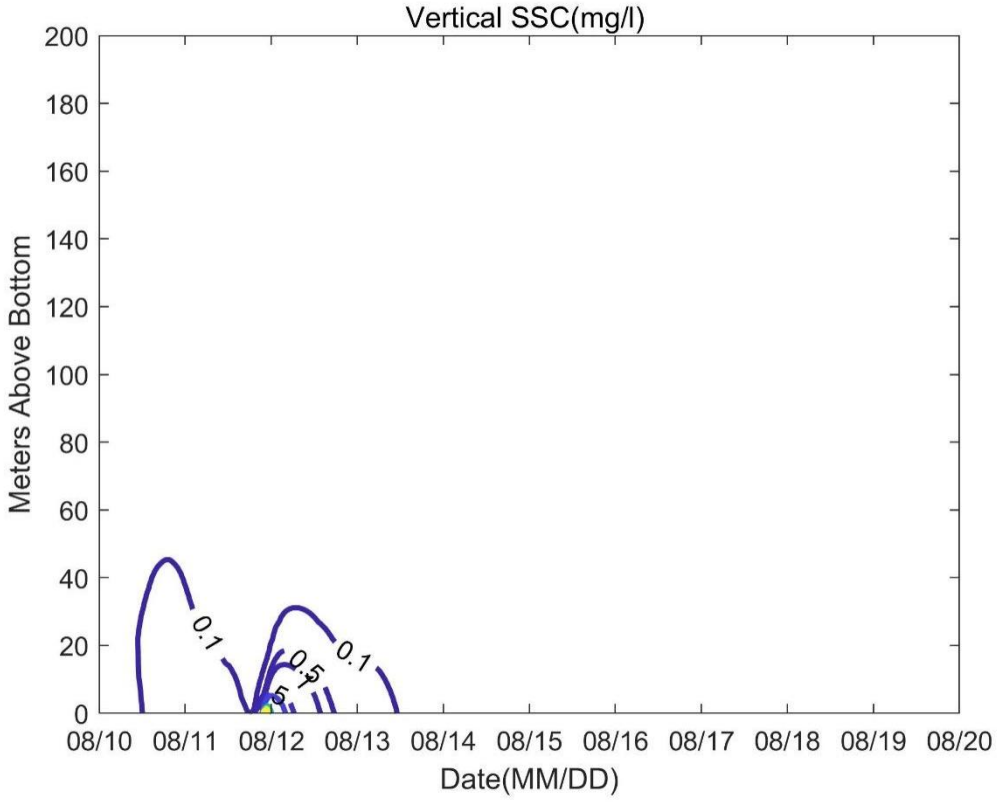

Figure 70 Vertical distribution of suspended sediment concentrations in Case 4

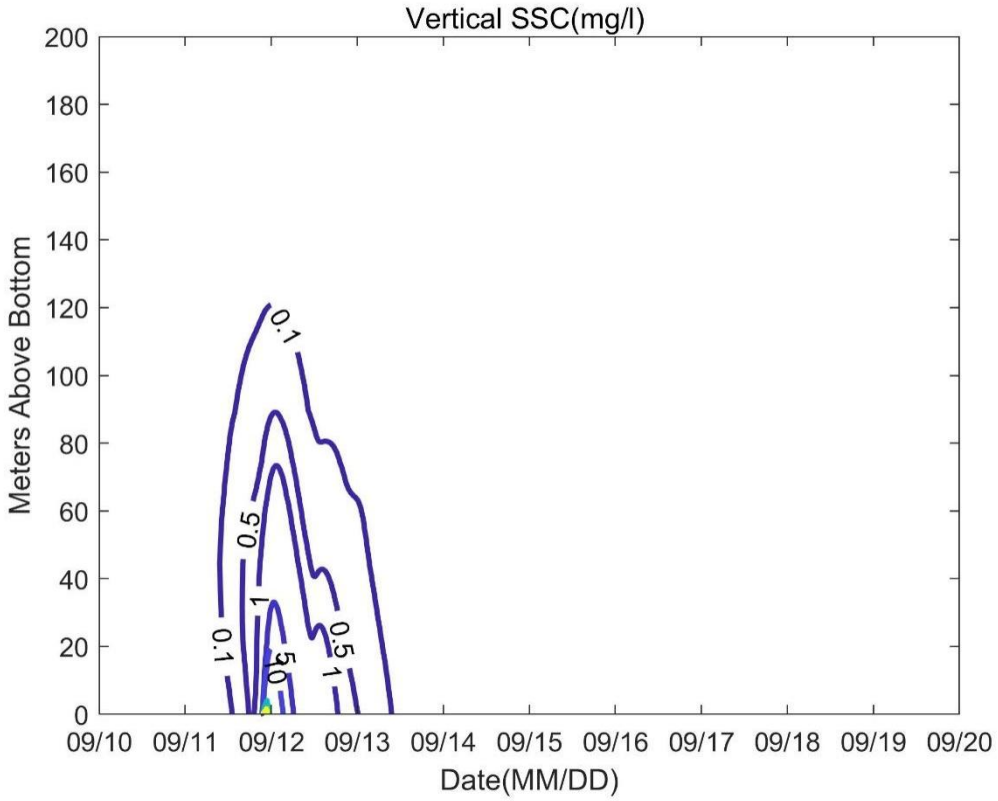

Figure 71 Vertical distribution of suspended sediment concentrations in Case 5

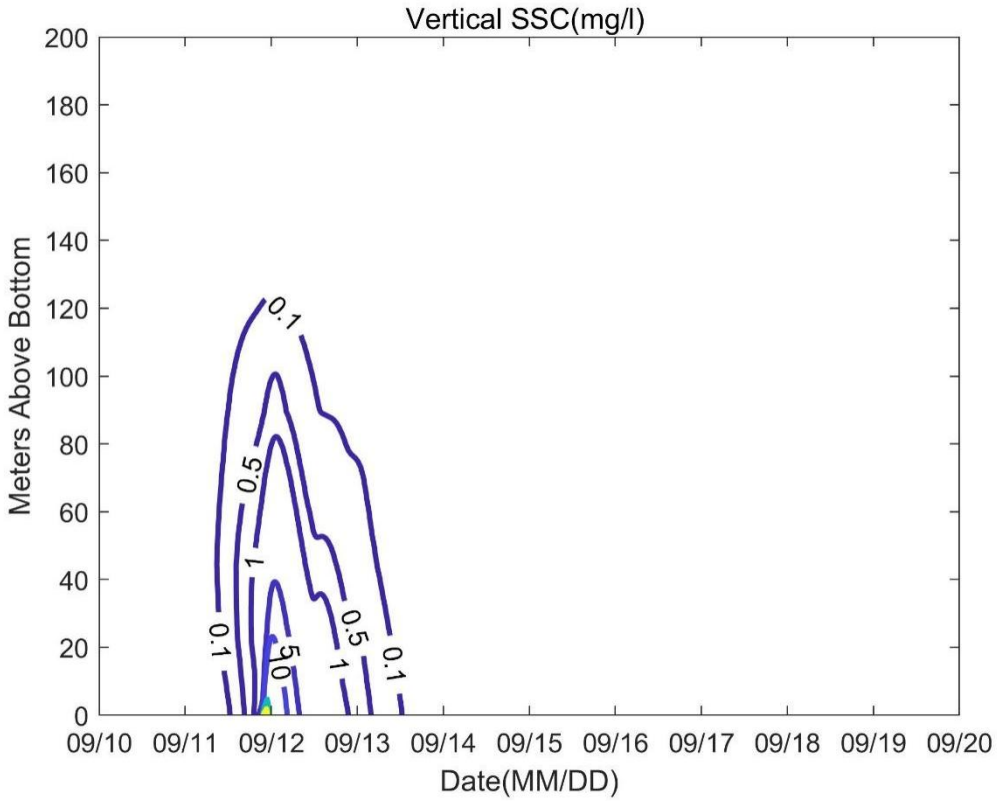

Figure 72 Vertical distribution of suspended sediment concentrations in Case 6

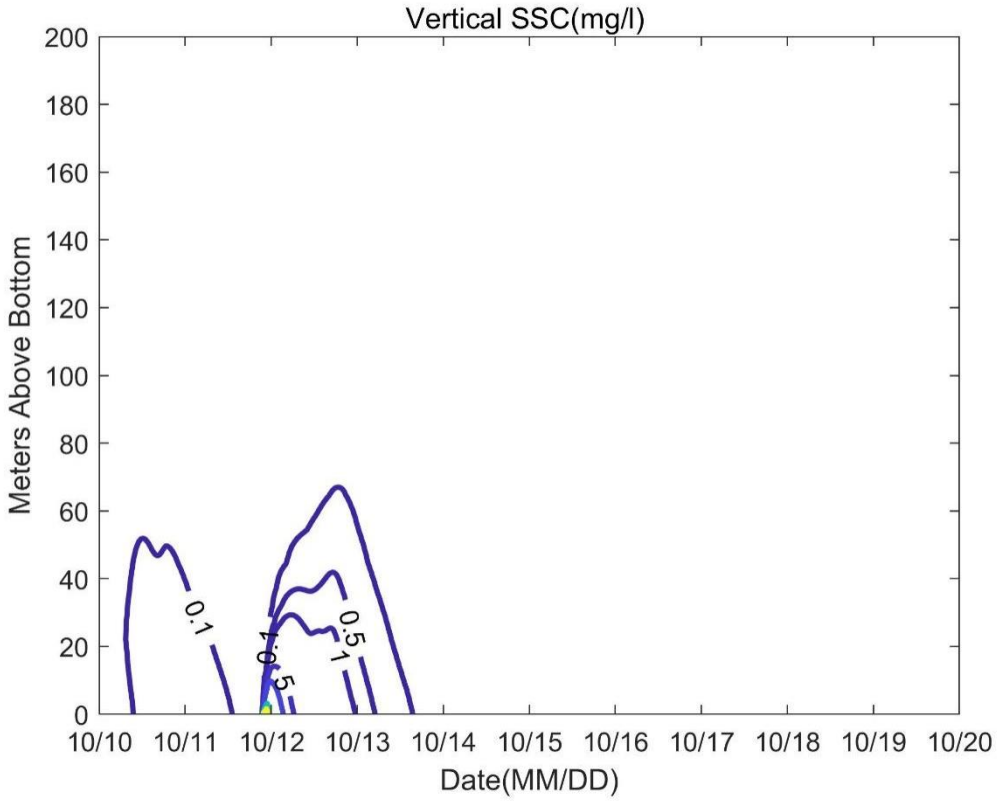

Figure 73 Vertical distribution of suspended sediment concentrations in Case 7

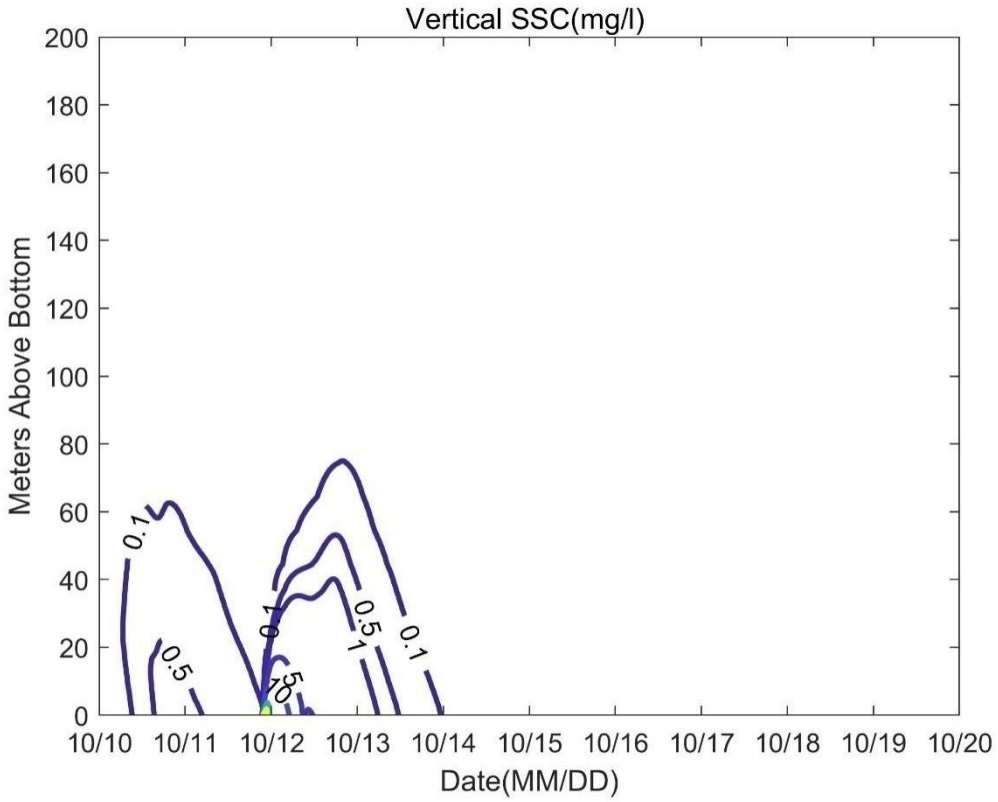

Figure 74 Vertical distribution of suspended sediment concentrations in Case 8

3.3 Distribution of redeposition thickness

Figures 75-82 show the distribution of sediment redeposition thicknesses in all cases. As can be seen from the figures, redeposition thicknesses are smaller than 1 cm, with the maximum value being 0.33 cm (Case 3). The areas with redeposition thickness greater than 0.1 mm are located within 100 m outside the CTA; the areas with redeposition thickness greater than 1 mm are mainly located in the CTA with a distance of 0 m between the first and second areas for continuous nodule collection (see red operation zone in Figure 3.3-6).

The area with redeposition thickness greater than 1 mm is 0.06-0.12 km^2, and the area with redeposition thickness greater than 0.1 mm is 0.59-0.64 km^2.

The maximum redeposition thickness is the largest in August and the smallest in September. With redeposition thickness greater than 1 mm, the largest area appears in September and the smallest area in August. These are the characteristics of flow field variations in corresponding months.

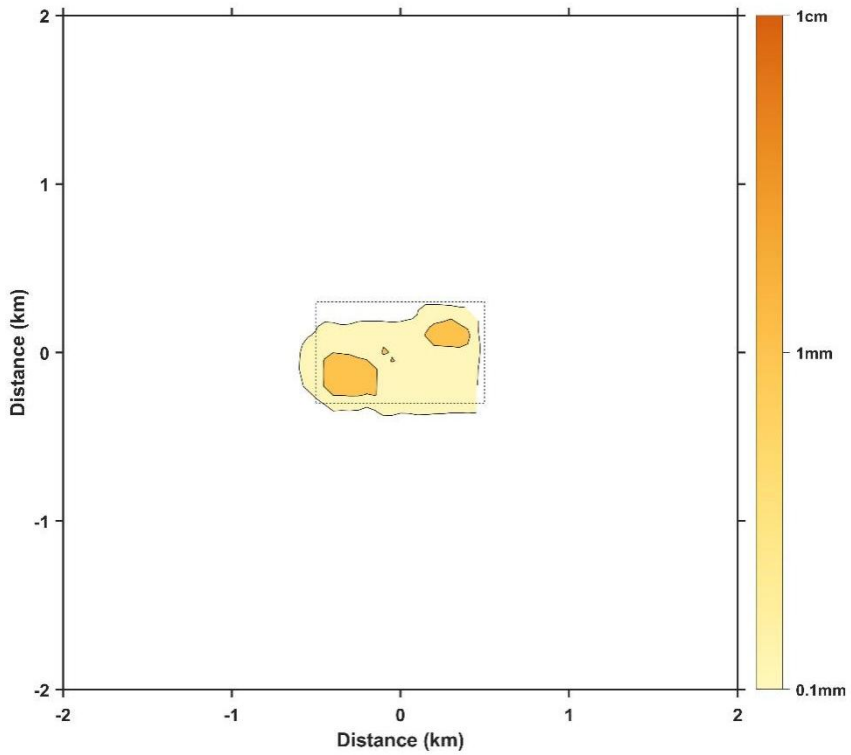

Figure 75 Distribution of redeposition thicknesses in Case 1

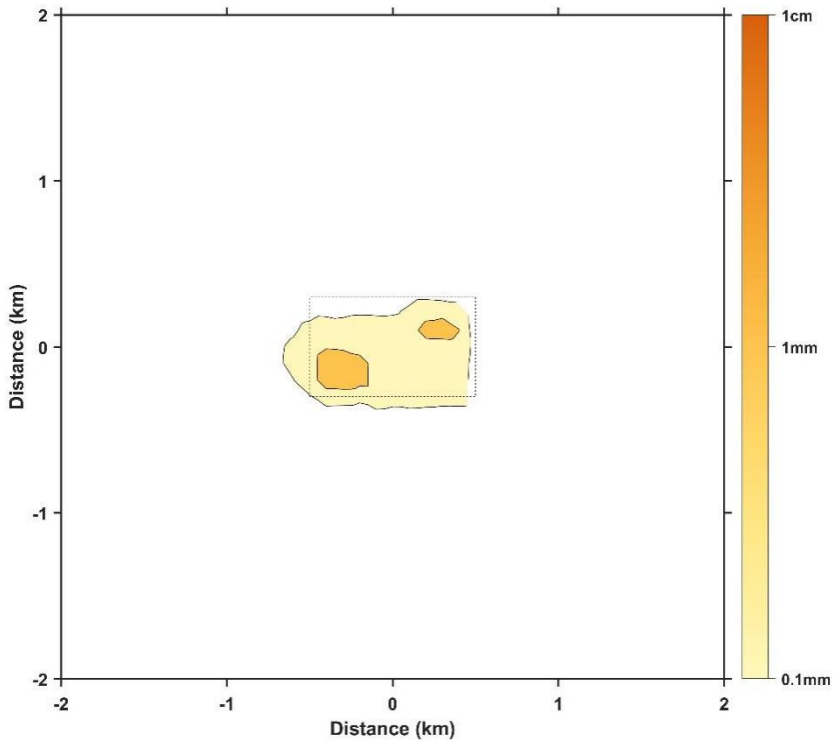

Figure 76 Distribution of redeposition thicknesses in Case 2

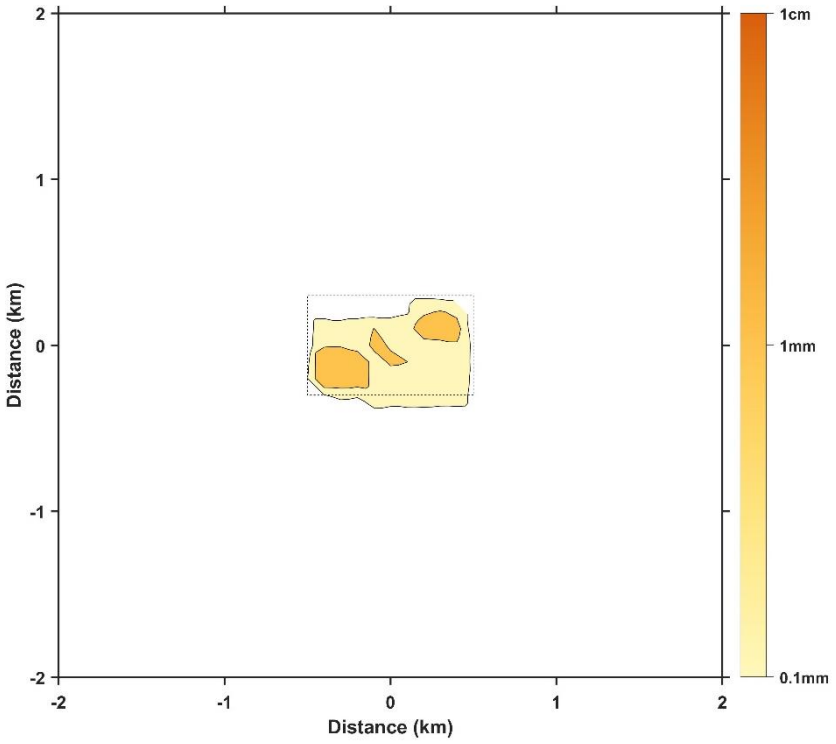

Figure 77 Distribution of redeposition thicknesses in Case 3

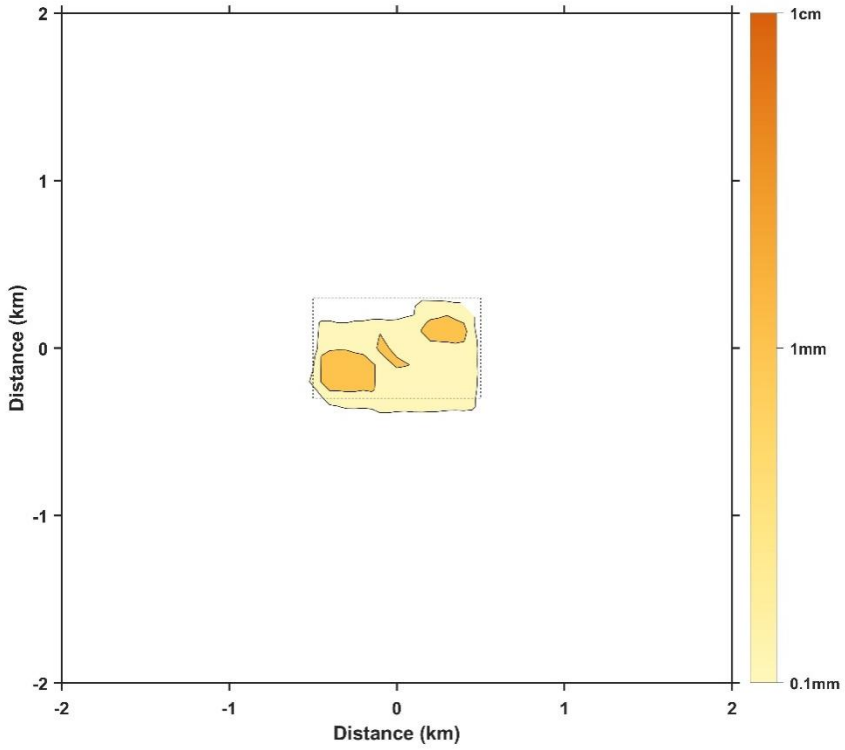

Figure 78 Distribution of redeposition thicknesses in Case 4

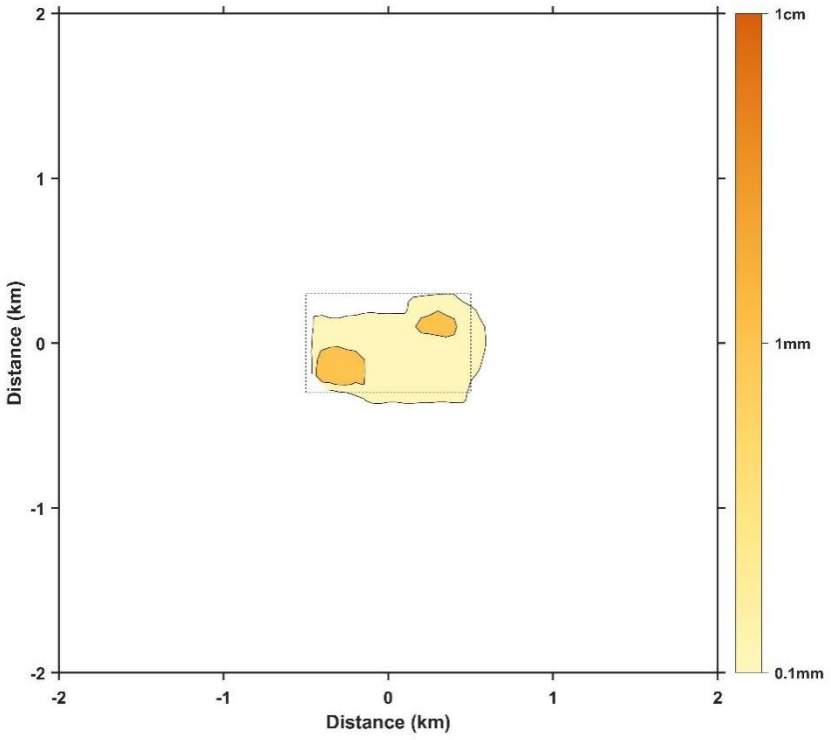

Figure 79 Distribution of redeposition thicknesses in Case 5

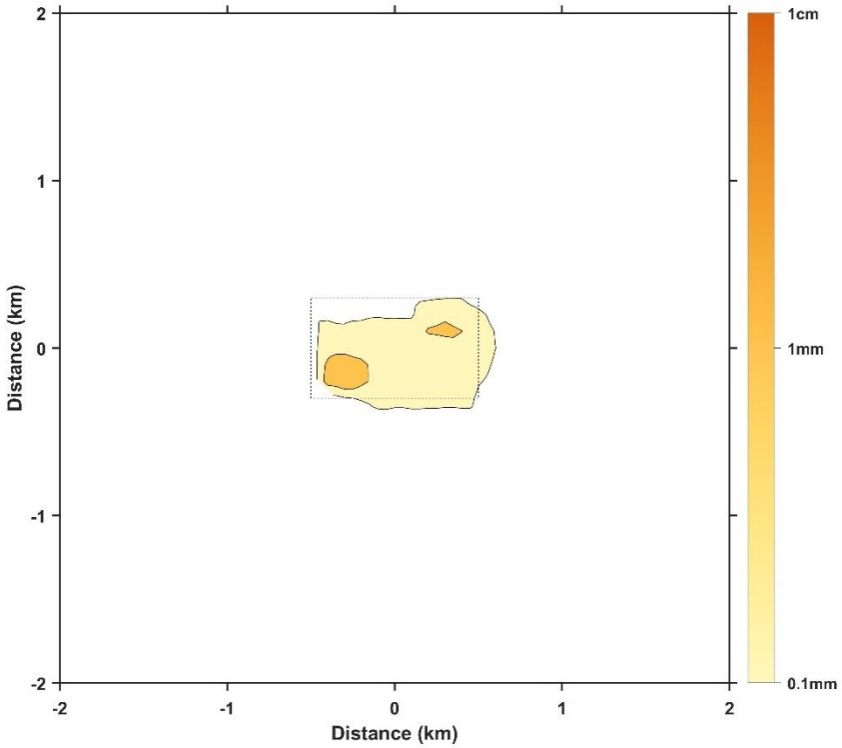

Figure 80 Distribution of redeposition thicknesses in Case 6

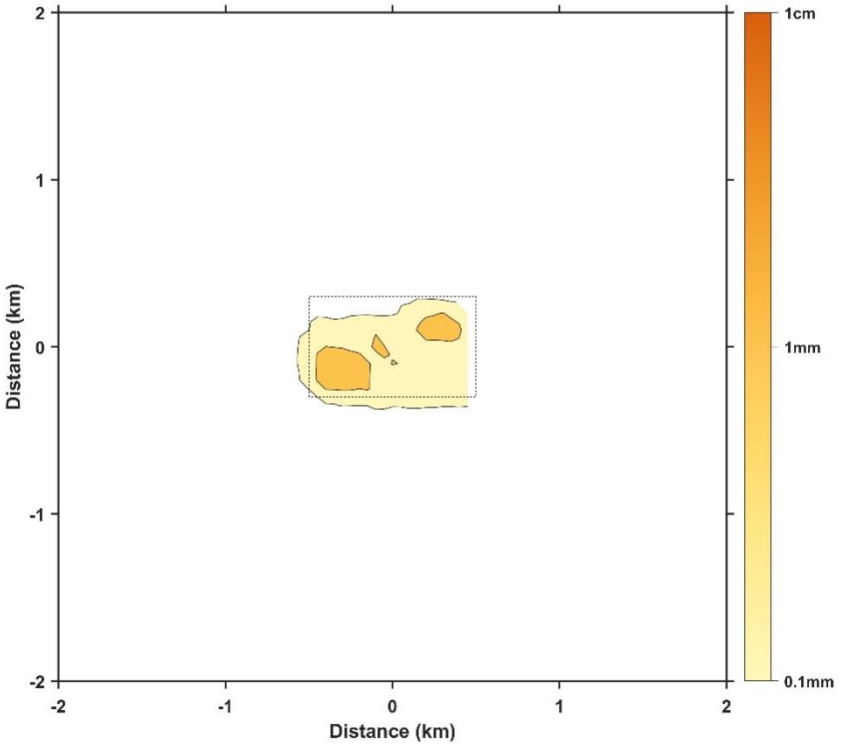

Figure 81 Distribution of redeposition thicknesses in Case 7

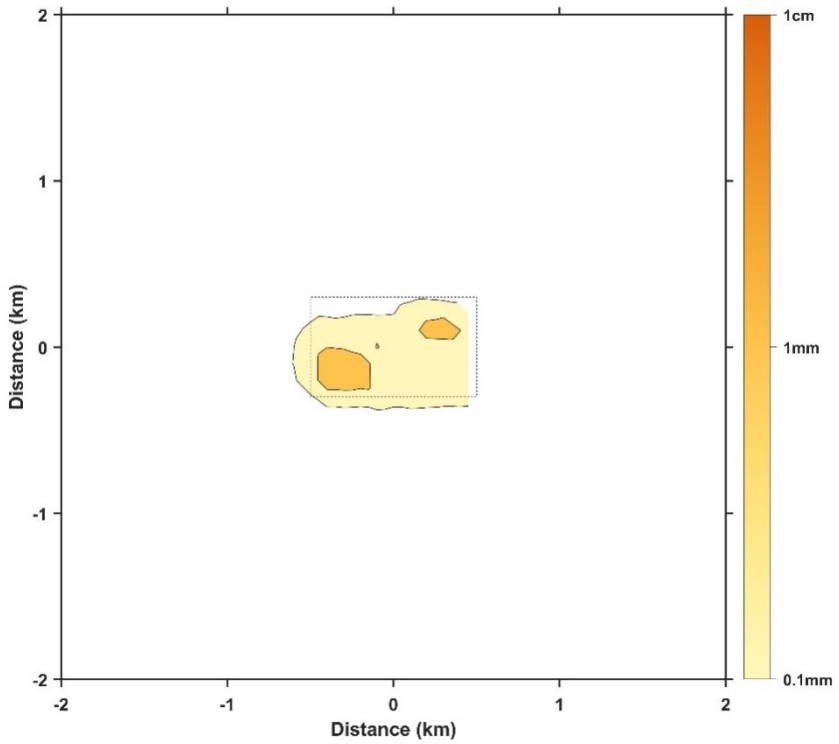

Figure 82 Distribution of redeposition thicknesses in Case 8

Table 4. Maximum plume dispersal scopes and maximum redeposition thicknesses

Case	Maximum dispersal range of plume (km)	Maximum redeposition thickness (cm)	Maximum height of impact (m)
Case,1	1.5	0.28	70
Case,2	2.1	0.24	79
Case,3	0.6	0.33	22
Case,4	0.9	0.30	45
Case,5	1.7	0.23	121
Case,6	2.1	0.19	124
Case,7	1.1	0.30	67
Case,8	1.7	0.26	75

Table 5. Areas of plume redeposition

Case	Area with redeposition thickness greater than 1 cm	Area with redeposition thickness greater than 1 mm (km^2)	Area with redeposition thickness greater than 0.1 mm (km^2)
Case,1	0	0.10	0.62
Case,2	0	0.09	0.64
Case,3	0	0.12	0.59
Case,4	0	0.11	0.60
Case,5	0	0.09	0.60
Case,6	0	0.06	0.60
Case,7	0	0.11	0.61
Case,8	0	0.09	0.63

4 Summary

We have established a plume model for seabed mining, and simulated the plume dispersal and redeposition process with different sediment particle sizes under different flow field conditions in July, August, September and October. Simulation results show that water columns with high concentrations and redeposition of suspended sediments are mainly located in the CTA. The maximum impact of plume is horizontally 2.1 km and vertically 124 m. The plume dispersal varies obviously under the flow field conditions in different months. Fine-grained sediments can bring larger impact horizontally and vertically than coarse-grained sediments.

Annex 2 Survey Methods and Quality Assessment for Environment Baseline Studies

1 Geological baselines

1.1 Topography and geomorphology

1.1.1 Multibeam bathymetric survey data

Topographic data and backscatter strength data of the operation zone mainly came from the measured data of multibeam bathymetry survey by China's R/V *XIANGYANGHONG LIUHAO* and R/V *XIANGYANGHONG SHIHAO* in the East Pacific Ocean in 2017 and 2018. The multibeam bathymetric survey systems used in the at-sea survey were EM122 and SeaBeam3012 multibeam systems.

Multibeam bathymetric survey data collected by EM122 and SeaBeam3012 multibeam systems were processed by the mature processing software CARIS Hips/Sips (version 11.0) developed in Canada. The data processing method and process all followed China's national standard "Technical regulations for application of marine multibeam bathymetric survey" (DZ/T 0292-2016).

Assessment of the precision of multibeam bathymetric survey data: The precision of post-processing data of water depth was assessed in accordance with "Technical regulations for application of marine multibeam bathymetric survey" (DZ/T 0292-2016).

In field measurement, the number of effective beams received by each transmitted pulse was mostly greater than 75 % of the total beam number. The full-coverage multibeam sounding survey had a more than 10 % overlapping rate for adjacent survey lines. Topographic survey of water depth requires synchronous positioning and bathymetric survey under dynamic conditions. To avoid accidental or systematic errors, no less than 5 % inspection lines have been laid in the vertical main survey line according to the specifications, so as to comprehensively check the quality

of water depth results. The specification stipulates that: (1) The accuracy of depth measurement results is assessed according to the statistical characteristics of depth discrepancy at the intersection of the main survey line and the inspection line; (2) There should be systematic error and gross error test on the inconsistent value of the intersection depth, and after eliminating systematic error and gross error, the tolerance of the inconsistent value should be 0.6 m for a water depth less than 30 m; with the water depth greater than 30 m, the tolerance of discrepancy value should be 2 % of the water depth; (3) The over-limit points shall not exceed 10 % of the total points in the comparison. According to the requirements of the specification, comparison calculation of the inspection line and the main survey line at the same position was conducted in the first and second legs of cruise respectively. The cumulative statistical points of the first leg of cruise were 34,508 (with a coincidence rate of 98.3 %), meeting the requirements of the specification. The error in water depth was 40.7 m, meeting the requirements of the specification. The cumulative statistical points of the second leg of cruise were 68,116 (with a coincidence rate of 99.9 %), meeting the requirements of the specification. The error in water depth was 12.1 m, meeting the requirements of the specification.

1.1.2 Multibeam backscatter strength data

For the backscatter strength data collected with EM122 and SeaBeam3012 multibeam systems, the self-developed multibeam backscatter strength post-processing software MbPPP were used to refine the backscatter data.

(1) Data outliers and the elimination of noise points

Since the multibeam topographic survey data have not been subjected to in-situ refined processing, there are still some abnormal values and noise points in the strength data. Therefore, filtering the backscatter strength data can effectively remove the abnormal values and noise points of the strength data. In this way, the quality of the strength data can be further improved.

(2) Correction of acoustic propagation loss

In the original data (xse format) recorded by SeaBeam3012 multibeam system, the obtained backscatter strength has been rid of all sonar system enhancements, so the acoustic propagation loss of regional backscatter strength was corrected first. The acoustic propagation loss was the acoustic energy loss caused by the interaction between the acoustic signal transmitted by sonar and the water column. It mainly includes two parts: the acoustic expansion loss and the acoustic absorption loss. In deep-water environments, the longest round-trip propagation distance of acoustic signals can reach more than 10 km, and the loss of acoustic energy is often much greater than that in shallow-water environments (Figure 1-1). Therefore, it is necessary to accurately calculate and correct the acoustic propagation loss of backscatter strength to ensure the accuracy of backscatter strength level.

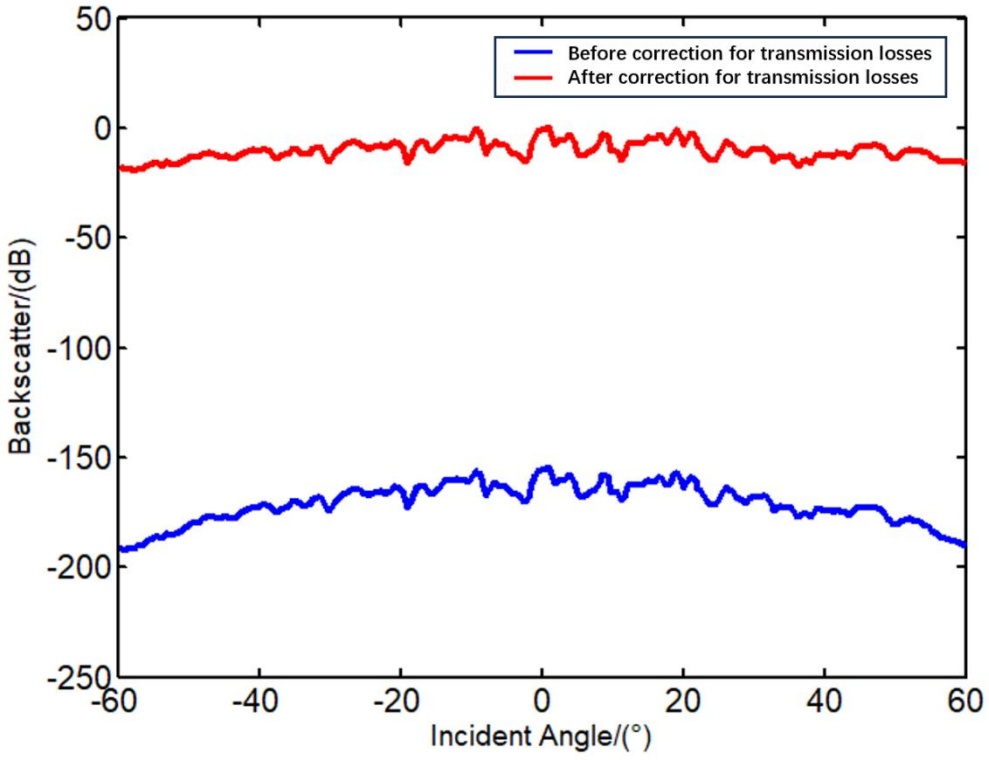

Figure 1-1 Comparison of the intensity levels of backscatter strength propagation losses before and after correction

In the process of beam propagation, with the spherical expansion and the absorption of seawater, the reduction of energy TL (propagation loss) is:

$$TL = 20lgR + \alpha R(dBre\ 1m), \left(R(m), \alpha(dB/m)\right)$$

Where α is the absorption parameter, which is a function of parameters such as sound wave frequency and water turbidity. After the correction of the acoustic propagation loss, the acoustic energy loss of the regional sonar image is accurately compensated and the image texture becomes clearer (Figure 1-2).

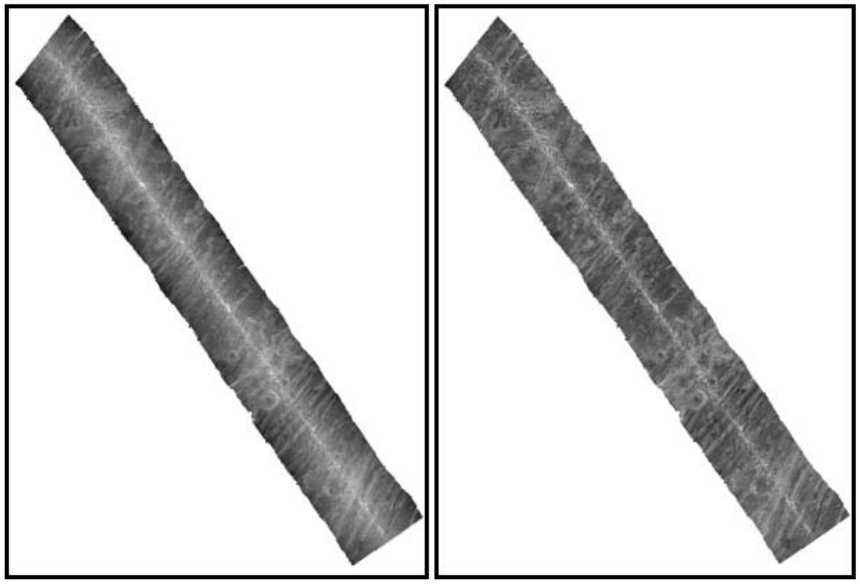

Figure 1-2 Comparison of sonar strip image propagation losses before and after correction (Left: Before correction; Right:After correction)

(3) Angle response correction

The backscatter strength of multibeam is affected by the scattering model mechanism. Different backscatter strengths can be obtained at different angles. The impact of angle response on backscatter data can reduce the quality of sonar images and affect the accurate interpretation of images. To obtain the natural backscatter strength of the seabed that only reflects the characteristics of the seabed sediment, it is necessary to correct the angular response. A quadratic differential model was used as the angular response model in the previous in-situ processing. After the correction, there are still "stripes" on the sonar image (Figure 1-3). This means that the correction effect still needs to be improved.

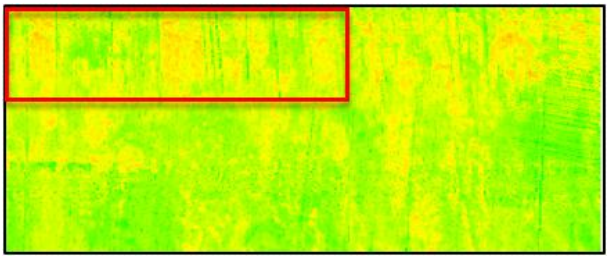

Figure 1-3 Remaining "stripes" after the correction with quadratic differential model

Therefore, the Brownian Passage Time (BPT) model was used to correct the angle response in the post-processing of strength. Many areas with similar and uniform bottom materials in the Block were selected by using a BPT model. Then, based on the angular response curve (Figure 1-4) extracted according to these areas, the area was corrected as a whole.

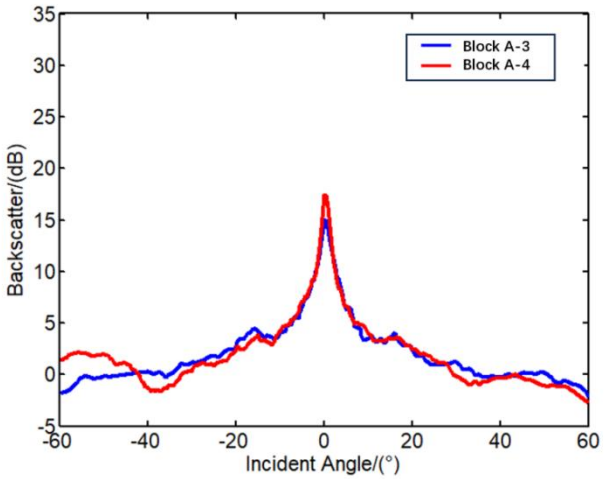

Figure 1-4 Angle response curve of BPT model

It can be seen from the comparison that the "stripe" trace is improved and the texture becomes clearer after the correction with BPT model (Figure 1-5). The correction effect for the complex area of sediment variation in the Block is also improved.

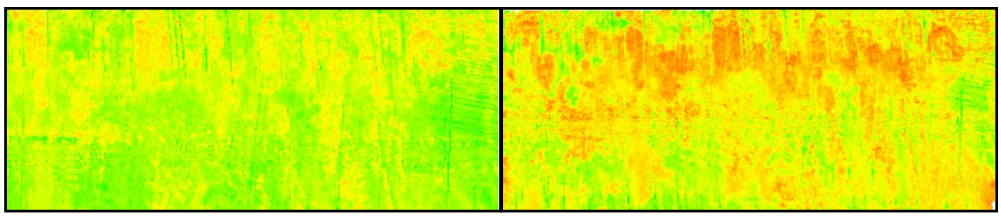

Figure 1-5 Comparison of the correction effects of two angle response models (Left: Quadratic differential model; Right: BPT model)

(4) Correction of central mirror reflection abnormalities

Due to the strong reflection from the mirror directly below the bottom of the vessel, the backscatter strength in the central beam area of multibeam sonar image is relatively strong. Even after the correction of incident angle effect, the multibeam acoustic scattering model is not satisfactory, due to the complexity of the interaction between sound waves and the seabed. After the correction, there is still a large system residual, presenting a narrow strip illusion along the track direction. To mitigate the influence of central beam specular reflection, we adopted the correction method of equal mean variance fitting model. Firstly, the trend line was fitted by using the backscatter strength of ping the normal area with continuous numbers, and then the mean and variance of the backscatter strength in the area directly below the bottom of the vessel and in a certain range on both sides were calculated. By comparing the variance between the normal area and the abnormal area, the correction coefficient was obtained, and compressing and moving the backscatter data in the area directly below the bottom of the vessel, the mean and variance of the abnormal area and the normal area on both sides tended to be consistent. Finally, the course equalization was conducted to correct the backscatter residual existing at the fixed incident angle position, so as to correct the abnormal data directly below the bottom of the vessel (Figure 1-6).

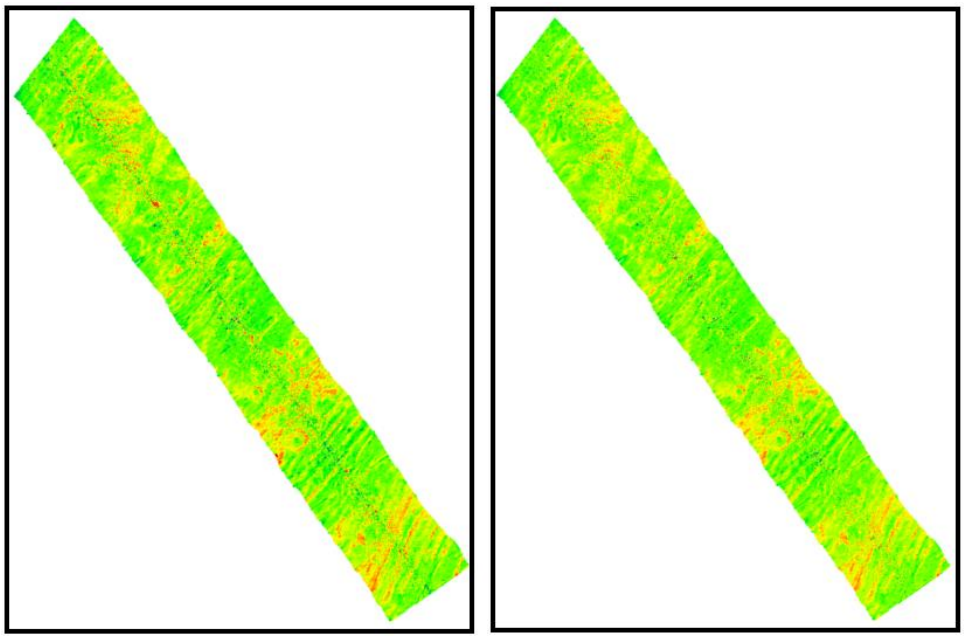

Figure 1-6 Comparison of central mirror reflection abnormalities before and after correction (Left: Before correction; Right:After correction)

1.2 Sediment parameters

1.2.1 Main trace elements in sediments

The chemical composition analysis of sediment samples was completed in the seabed science laboratory of the SIOMNR. Among them, the major elements were analyzed by melting sheet method, using X-ray fluorescence spectrum analyzer (model: AxiosMAX), and referring to the national standard "Methods for chemical analysis of silicate rocks—Part 28: Determination of 16 major and minor elements content" (GB/T 14506.28-2010). Trace elements were analyzed by acid dissolution in wet chemical analysis, using inductively coupled plasma mass spectrometry (Model No.: PE Elan DRC-e), and referring to the national standard "Methods for chemical analysis of silicate rocks—Part 30: Determination of 44 elements" (GB/T 14506.30-2010).

Two national first-class reference materials (GBW07103 and GBW07316) and six rock standard samples (AGV-2 (andesite), GSP-2 (granodiorite), W-2a (diabase), BHVO-2 (basalt), DTS-2b (peridotite) and BCR-2 (basalt) were used as internally controlled samples in the analysis of chemical composition of sediments.

The relative errors of major and trace elements in each standard sample are shown in Figures 1-7 and 1-8 respectively. The analysis errors of major elements in sediments are mostly within 3 %, and the errors of trace elements are mostly controlled within 10 %.

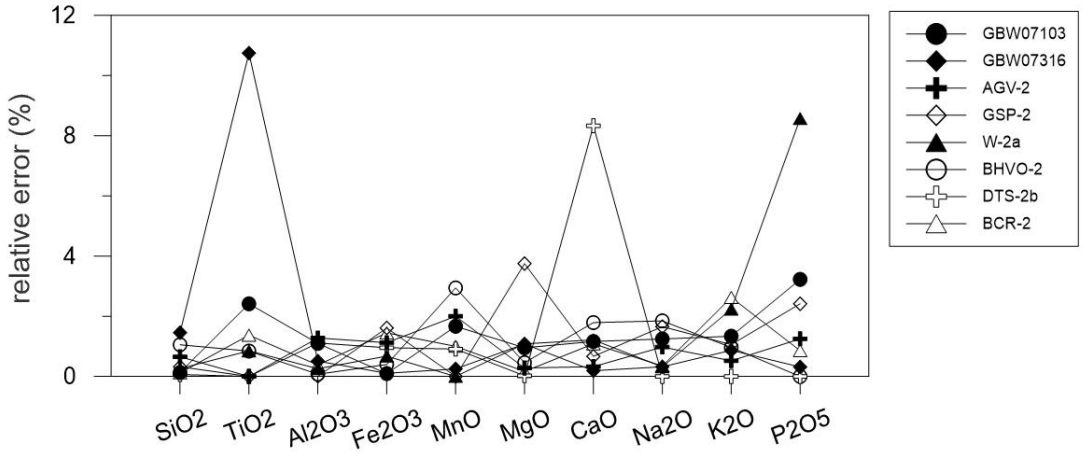

Figure 1-7 Relative errors of major elements in sediment standard samples

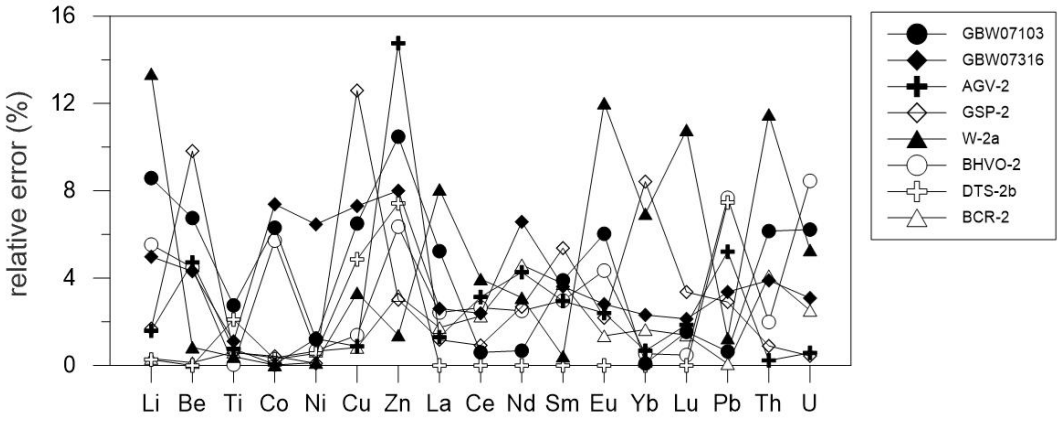

Figure 1-8 Relative errors of trace elements in sediment standard samples

From the reproducibility results, except for a few samples, the relative deviation of major elements is mostly better than 1 % (Figure 1-9a), and the large deviation of MnO content may be related to its low content (average content of MnO = 0.69 wt%). The relative deviations of trace elements (except Be) are mostly better than ±2 % (Figure 1-9b), which shows that the test results have good reproducibility. The relative deviation of Be in trace elements is large, which may be related to the low Be content in sediments (~2 ppm).

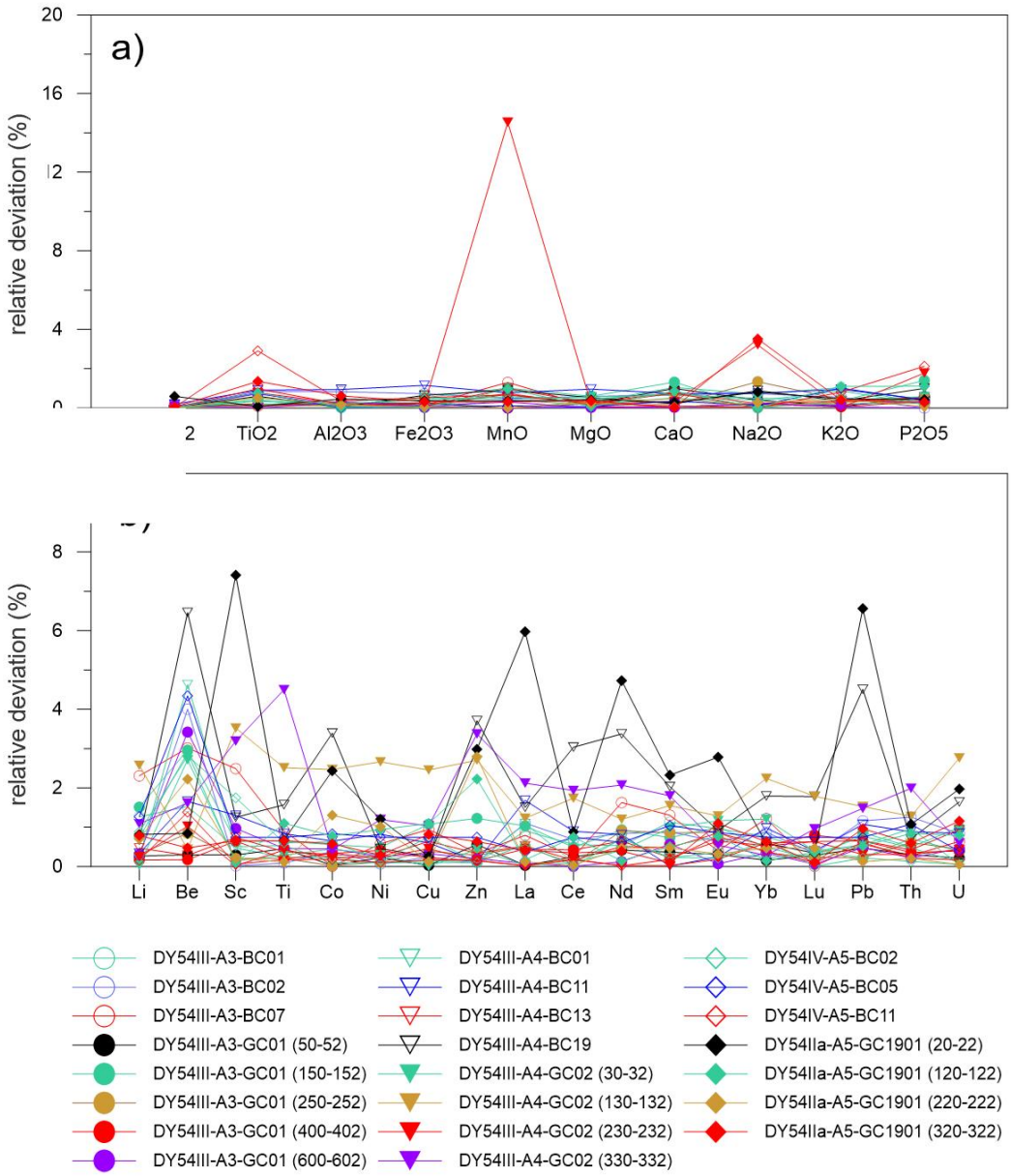

Figure 1-9 Relative deviations of major and trace elements in the parallel samples of sediments

1.2.2 Grain size analysis

Grain size analysis is completed in the Submarine Science Laboratory of the SIOMNR with a laser diffraction particle size analyzer (Mastersizer 2000, UK).

Before sampling, the samples to be tested are mixed evenly. Then the sampling quantity is determined according to the particle size of the sample. Generally, 0.1-0.2 g of fine-grained sediments, such as clayey silt or silty clay, 0.3-0.4 g sediment and fine sand, as well as 0.5-0.6 g medium-coarse sand were sampled. The sample with

excessive hydrogen peroxide (H_2O_2) solution is dissolved, and a little 30 % H_2O_2 is added into the beaker containing the sample. A large number of bubbles are generated later. When bubbles no longer occur, a small amount of hydrogen peroxide is added. If no bubbles are generated, it means that the organic matter has been completely oxidized. If no bubble is generated, it is necessary to repeat the above steps until no bubble is generated. After an addition of distilled water, the beaker containing samples is stirred with a glass rod, and then stood for 24 h, and the supernatant in the cup is sucked. Repeat the previous step. Finally, a few drops of 0.5 N sodium hexametaphosphate are added into the beaker, which is stirred with a glass rod or vibrated with ultrasonic wave to fully disperse the sample. The processed samples are tested on the computer. During the test, all the processed samples are poured into a sample pool, and the samples remaining on the beaker wall are also washed into the sample pool by using washing bottles.

The calculation method of granularity analysis parameters is based on "Specifications for oceanographic survey—Part 8: Marine geology and geophysics survey" (GB/T 12763.8-2007), the grain size parameters, mainly including average particle size (Mz), sorting coefficient (σi), skewness (Ski) and peak state (Kg), were calculated with Fokker and Ward formulas.

It can be seen from the table that among the 18 duplicate samples, the average particle size error of all samples is less than 0.15φ, and the sorting coefficient error of 17 samples is less than 0.1φ, which basically meets the error detection requirements of GB/T 12763.8-2007. Therefore, the data quality is acceptable.

Table 1.1 Analysis errors of repeated samples by particle size test

Sample name	Primitive sample		Duplicate sample		Error	
	Average particle size (φ)	Sorting coefficient (φ)	Average particle size (φ)	Sorting coefficient (φ)	Average particle size (φ)	Sorting coefficient (φ)
54III-A3-BC01-5-6	6.60	2.42	6.65	2.45	0.05	0.03
54III-A3-BC02-0-2	6.44	2.44	6.38	2.46	0.06	0.02
54III-A3-GC01-50-52	7.58	1.96	7.64	1.91	0.06	-0.05
54III-A3-GC01-250-252	7.39	1.85	7.32	1.82	0.07	-0.03
54III-A3-GC01-400-402	7.35	1.78	7.43	1.88	0.08	0.1
54III-A3-GC01-600-602	7.57	1.45	7.57	1.48	0.00	0.03
54III-A4-BC01-35-36	8.02	1.47	8.05	1.49	0.03	0.02
54III-A4-BC19-35-36	8.11	1.39	8.06	1.37	-0.05	-0.02
54III-A4-BC14-0-2	7.99	1.86	7.91	1.86	-0.08	0
54III-A4-GC02-30-32	8.36	1.35	8.36	1.35	0.00	0
54III-A4-GC02-230-232	8.31	1.42	8.29	1.48	-0.02	0.06
54III-A4-GC02-330-332	8.10	1.54	8.08	1.55	-0.02	0.01
54IV-A5-BC02-0-2	6.00	2.49	5.94	2.47	-0.06	-0.02
54IV-A5-BC05-0-2	6.42	1.84	6.29	1.89	-0.13	0.05
54IV-A5-BC11-25-26	6.34	1.40	6.27	1.35	-0.07	-0.05
54IIa-A5-GC1901-220-222	6.91	1.88	7.00	1.82	0.09	-0.06
54IIa-A5-GC1901-320-322	7.38	1.73	7.50	1.73	0.12	0
54IIa-A5-GC1901-398-400	6.25	1.27	6.14	1.25	-0.11	-0.02

1.2.3 Geotechnical properties

The in-situ testing of geotechnical properties at sea mainly includes the testing and analysis of penetration resistance and shear strength of vane. The penetration resistance test is conducted with a pocket penetrometer, and the shear strength test is conducted with a miniature vane shear apparatus.

(1) Test basis and specifications

The test and analysis of geotechnical properties of surface-layer sediments are mainly based on the following specifications and standards:

- "The expertise for oceanic polymetallic nodules survey" (GB/T 17229-1998)
- "Standard for soil test method" (GB/T 50123-1999)
- "Test Methods of Soils for Highway Engineering" (JTG E40-2007)
- "Rules of Pocket Penetrometer Test" (CECS 54:93)

(2) Penetration strength

The penetration resistance test is completed by TT-MP1 pocket penetrometer, which consists of penetration probe, connecting rod, dynamometer and other components. 20 N, 40 N or 60 N dynamometer with different specifications, and cone, small cylinder or large cylinder penetration probe are applicable.

(3) Shear strength

The shear strength test is completed with the TT-MVS1 miniature vane shear apparatus, which is composed of vane head, torsion spring, force cylinder and sliding pointer.

1.2.3.1 Laboratory geotechnical properties test

The analysis of physical properties, including natural moisture content, specific gravity, natural wet density, natural void ratio, plastic limit, liquid limit, plastic index, liquid index, and mechanical properties, such as compressibility, compressive modulus, cohesion and internal friction coefficient are completed in laboratory test.

Natural moisture content: The soil sample left after geotechnical properties test with cutting-ring method is dried to a constant weight at 100-105 °C, the ratio of the lost water mass to the constant weight soil mass obtained is the natural moisture content, expressed as a percentage. The test equipment is an electrothermal constant temperature drying box. The test equipment includes an electric thermostatic drying oven and an electronic balance.

Natural wet density: The cutting-ring method is adopted in the test, and the columnar samples are divided at intervals of 5 cm to be 2 cm high and a cross-sectional area of 30 cm^2. After weighing the soil samples, the natural wet density of the sediments is calculated in g/cm^3. The test equipment includes a cutting ring and an electronic balance.

Specific gravity: The soil samples are dried and ground, and then tested with a 50 mL pycnometer. The test equipment includes a 50 mL pycnometer, an electronic balance, and a vacuum pump, etc.

1.2.4 Data processing methods and quality status

The samples obtained in the operation zone meet the requirements of "Specifications for oceanographic survey—Part 8: Marine geology and geophysics survey" (GB/T 12763.8-2007) regarding the technical indexes for testing the physical and mechanical properties of sediments.

Main technical requirements for testing the physical and mechanical properties of sediments are as follows.

- The soil sample must be an undisturbed soil sample without water loss;
- A group of test samples, approximately 25-30 cm in length and 6-8 cm in diameter;
- Water content, relative density of sedimentary soil, shear strength of vane and natural adhesion shall be determined in-situ as possible.

During the geotechnical properties test, the equipment are in good condition, the

apparatuses are used correctly, and the test operation meets the requirements of Part 4 "Testing the physical and mechanical properties of sediments" of the "Technical Specification for Environmental Survey in International Seabed Areas", the "Standard for soil test method" (GB/T 50123-1999) and the "Rules of Pocket Penetrometer Test" (CECS 54:93). The shift report records are clear, accurate and neat, the test data are accurate and reliable, and the self-inspection meets requirements. The measurements meet the requirements of "Recommendations for the guidance of contractors for the assessment of the possible environmental impacts arising from exploration for marine minerals in the Area" (ISBA/19/LTC/8) and the "Standardization of Environmental Data and Information: Development of guidelines" (ISA/02/02), especially the requirements in Chapter 23. The test records of geotechnical properties of sediments are complete and integrate, showing a 100 % qualified rate after self-inspection by professional groups and on-site quality administrator.

2 Physical oceanography baselines

2.1 Submerged buoy of mooring

2.1.1 Survey equipment and parameters

The launched and recovered mooring observation equipment mainly includes CTD, ADCP, single-point current meter, sediment trap, acoustic release transponder and buoys. The main technical indexes of all kinds of equipment are as follows:

SBE16plus and SBE37 (made by Sea-bird Scientific of the United States) for CTD is used to observe pressure, temperature, conductivity, which can be obtained synchronously. The technical requirements are shown in Table 2-1.

Table 2-1 Observation requirements for temperature, conductivity and pressure indexes

Parameters	Resolution	Accuracy	Stability
Temperature	0.0001 ℃	±0.002 ℃	0.0002 ℃/month
Conductivity (salinity)	0.00001 s/m	±0.0003 s/m	0.0003 s/m/month

Pressure	0.002 % × full range	0.1 % × full range	0.1 % of full range/year

Seaguard RCM (RCM for short) made by Aanderaa is adopted as the single-point current meter. It measures the current speed distribution around the equipment using Doppler effect, and has built-in tilt and compass sensors. It can also be used as a platform extension to add other measurement parameters, such as temperature, conductivity, depth, DO and so on. The technical requirements are shown in Table 2-2.

The sediment trap is mainly used to collect microparticles of sediment at a fixed depth in the ocean. The sampling time can be set as required, and samples can be taken underwater for several days to several weeks or as long as one and a half years. The sampling bottles automatically collect sediment samples at least once a month, and at least 12 bottles in the first year after sampling.

Oceano 2500s made by IXSEA of France is adopted as the releaser, which uses an integrated transducer to receive the instructions from the deck unit and execute them. The safe working load is 2,500 kg and the pressure resistance is 6,000 m.

See Figures 2-1 and 2-2 for the structure diagram of the mooring.

Table 2-2 Technical indexes for monitoring current elements

Current meter	Resolution of current speed	Accuracy of current speed	Resolution of current direction	Accuracy of current direction
RCM	0.1 mm/s	±0.15 cm/s	0.01°	±2°

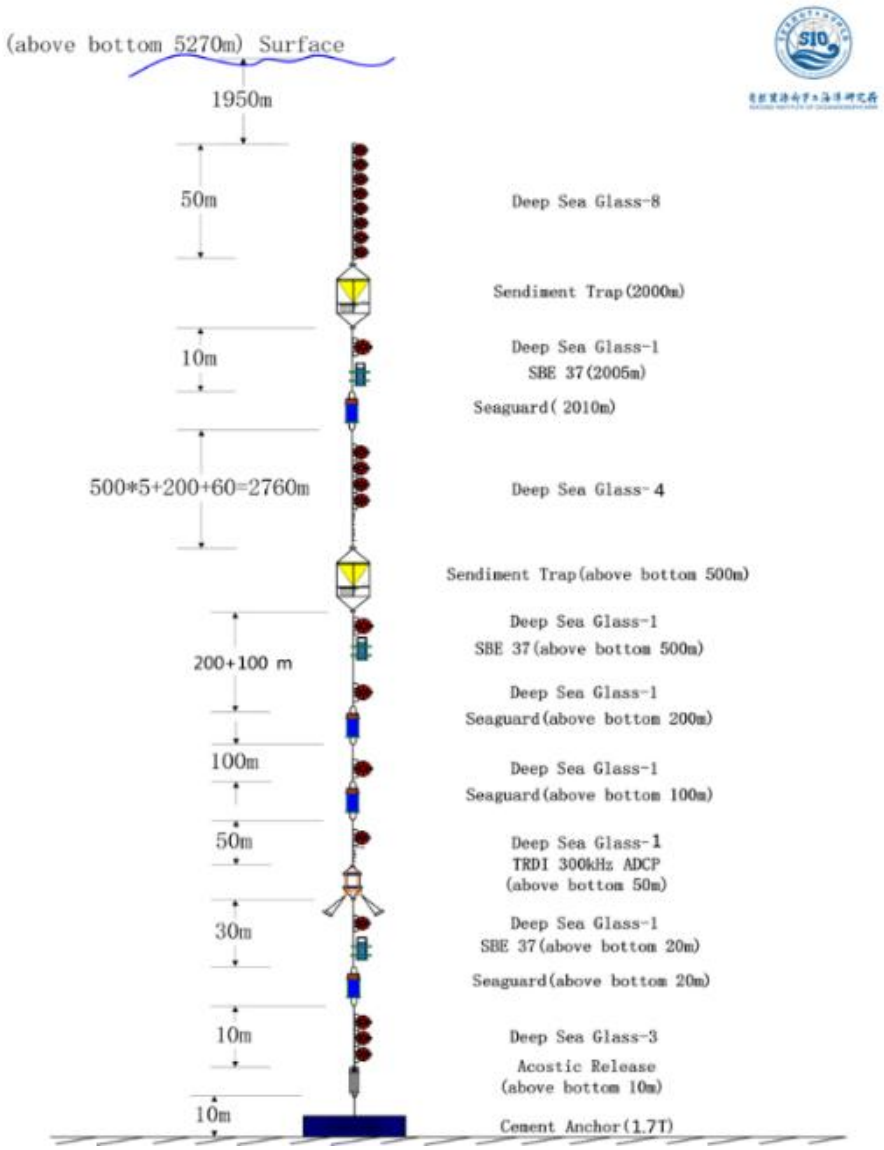

Figure 2-1 Structural diagram for mooring recovered at DY70II-A5-MX01 during the 2021 survey cruise

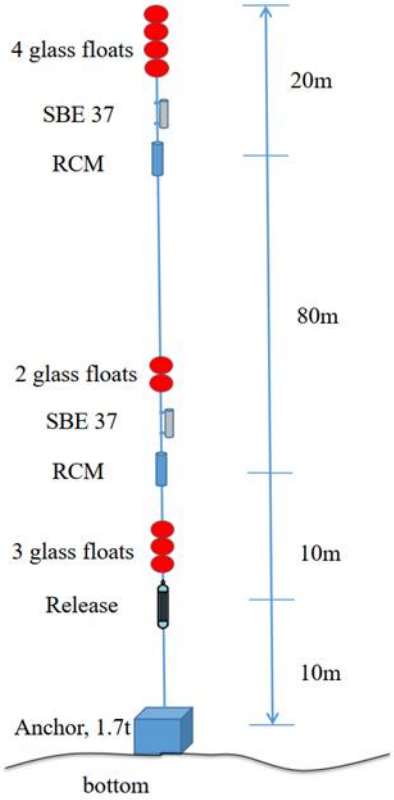

Figure 2-2 Structural diagram for DY73I-A5-MX02 mooring recovered during the 2022 survey cruise

2.1.2 Analysis methods and quality control

2.1.2.1 Temperature and salinity data

Data preprocessing: The CTD data of submerged buoy is processed by SBEDataProcessing-Win32 software of Sea-bird Scientific, and the original observation data (hexadecimal) of temperature-depth sensor and temperature and salinity sensor are converted into data in ASCII format.

Data quality control:

- Delete the data in the air, and eliminate the data collected during launch and recovery.
- Scope check: Check the data according to the extreme values of historical data of temperature and salinity elements in the sea area with the submerged buoy system. Exclude the data outside the extreme value interval, and use the adjacent normal data to fill in by linear interpolation.

- Trend check: The observed data should not exceed the corresponding variation range within a certain period of time. Perform subsection test, with each section being 15 days; data with more than 2.5 times the standard deviation are regarded as abnormal data. Exclude the abnormal data, and use the adjacent normal data to fill in by linear interpolation.
- Time series diagram test: Human judgment and audit will be conducted by drawing the time series diagram of seawater temperature and salinity.

2.1.2.2 Ocean current data

1) Data preprocessing:

The current data obtained with the ADCP through submerged buoys were converted from hexadecimal original data of ADCP to ASCII data by WINADCP software. Elements such as current speed, current direction and intact rate were extracted from the data at 1 h intervals. Single-layer ocean current data obtained with Aanderaa current meter are exported with Seaguard Studio software, while elements such as current speed and direction are extracted at 0.5 h intervals.

2) Data quality control

- Data processing begins with data inspection to understand the basic information of observation data. The basic information includes instrument model, installation depth, instrument blind area, layer thickness setting, layer number setting, sampling interval, etc., as well as sea conditions during observation, a preparation for further data processing.
- Preliminary control is conducted according to the relevant parameters of the observation apparatus. Missing data, signal interruption data and data not meeting the requirements of important parameters are excluded. Basic submerged buoy observation data in time series are formed.
- The rationality test and instrument error correction are conducted on the data after the above preliminary quality control. Rationality check covers garbled and unreasonable characters in the data file, observed data such as current

speed and current direction beyond the normal range, and too-large data mutation of two adjacent layers. Instrument error correction covers compass value correction, instrument inclination correction, instrument position change correction, etc. These data are checked for their rationality and correction of errors.

- Range test, discreteness check and statistical analysis are used to filter out the more significant anomalies in the data. The time series diagrams of submerged buoy data and other related maps are drawn. Combined the historical experience of understanding the sea area, the rationality of seabed data are judged artificially. Then necessary corrections are made to the data with problems.

The CTD carried by the mooring are calibrated before sailing, and other equipment (e.g. current meter) are self-checked. The observed data of temperature, salinity, pressure and current are of good quality and high precision to fully and truthfully reflect the hydrological conditions of the surveyed waters and meet the technical requirements set forth in the "Specifications for oceanographic survey—Part 2: Marine hydrographic observation" (GB/T 12763.2-2007).

2.2 Temperature and salinity structure

2.2.1 Sampling equipment

SBE911plus CTD made by Sea-bird Scientific of the United States is adopted as the direct-reading CTD measuring system. The system consists of SBE9plus underwater CTD equipment, SBE11plus deck equipment, armored cable and data acquisition computer. Through the armored cable, the SBE 911plus CTD system can achieve collection and storing of data in a real-time manner. When the 911plus CTD system is launched, the power supply for the underwater unit is provided by the deck unit through the armored cable. The armored cable is also used to transmit data to the SBE11plus deck unit. The deck unit decodes the data collected with 911plus CTD, and then transmitted them to the data acquisition computer, which displays the data in

a real-time manner and records the data on the disk. This system can observe hydrological factors such as pressure, temperature, conductivity, etc. It is also equipped with 24 10 L water sampling bottles with automatic excitation function (controlled by the underwater unit), which can provide seawater samples for chemical and biological analysis. See Table 2-3 for the main technical parameters of SBE911plus CTD system

Table 2-3 Main technical parameters of SBE911plus CTD system

Technical parameters	Measuring range	Precision	Stability (monthly)	Response time (s)
Conductivity (s/m)	0-7	0.0003	0.0003	0.065
Temperature (°C)	-5~+35	0.001	.0002	0.065
Pressure (psia)	10,000	0.015%FS	0.0015%FS	0.015

2.2.2 Data processing

The SBE Data Processing software developed by Sea-bird Scientific of the United States is used to process CTD data. The data processing steps are as follows:

1) Data conversion

Convert the original observation data (hexadecimal) into ASCII data. The specific data elements include pressure, water temperature, conductivity, pump state, etc.

2) Pressure correction and deletion of records in the air

Average the pressure data of CTD before and after entering the water, and then subtract the average value from the observed pressure value. Artificially exclude the data before and after entering the water and the temperature sensing stage of CTD, according to the pressure, conductivity and pump state.

3) Smoothing (filter)

The low pass filter made by Sea-bird Scientific of the United States is used to filter one or several items of data, so as to smooth the noise of high-frequency (fast-

varying) data. The pressure smoothing time constant is 0.15 s, and the others are 0.0 s.

4) Hysteresis calibration (Align CTD)

To ensure that all the elements based on pressure are consistent in time, and other factors (e.g. conductivity) are calculated for the same seawater sample in data processing. Align CTD is used for hysteresis calibration. The Align CTD module is used to perform hysteresis calibration of conductivity, with the conductivity parameter being +0.073.

5) Heat flux correction (Cell Thermal Mass)

To eliminate the measurement error of conductivity caused by large temperature gradient, the Cell Thermal Mass program is run to correct the heat flux. The heat flux correction parameters Amplitude Alpha and Lag time Tau are 0.03 and 7, respectively.

6) Backpressure elimination (Loop Edit)

To eliminate the reverse jitter of water depth caused by vessel swing, the Loop Edit program is used to eliminate the backpressure of the data, and the minimum lowering speed of CTD is 0.25 m/s.

7) Water depth calculation (Derive)

Water depth is calculated with the Derive program.

8) Data averaging (bin average)

Average the data according to the depth of 1 m, and select 0.5 m for the surface layer, with the value being 0.

9) Salinity calculation (Derive)

Use the Derive program to calculate salinity.

10) Inspection and correction of data quality

Draw the vertical distribution map of each element, and make necessary manual corrections according to the vertical distribution map and in combination with empirical analysis. The observation data of the entire water column and 1,500 m CTD in this survey cruise are of good quality and need no correction.

11) Splitting uplink and downlink data (Split)

Split the uplink and downlink data of CTD.

12) Data output (ASCII Out)

Remove header information and only retain data.

2.3 Surface-layer ocean currents

2.3.1 Survey equipment

Ship-mounted OS38K ADCP produced by RD Instruments of the United States is adopted. The ADCP consists of in-hull transducer, deck unit, external compass, GPS and operation computer. The main technical indexes are shown in Table 2-4.

Table 2-4 Main technical indexes of OS38K ADCP

Model name	OS38K
Center frequency	38 kHz
Number of beams	Four beams generated by the beamformer
Beam angle	30° from perpendicular line
Long-term precision	1 %V±0.5 cm/s (V is the current speed value)
Maximum profile depth	Broadband mode: 730-780 m Narrowband mode: 800-1,000 m
Blind zone	16 m
Number of depth units	1-128
Length of depth unit	16 m, 24 m or optional
Maximum pulse emissivity	0.4 Hz
Precision	<2 cm/s
Speed range	10 m/s

According to its technical parameters, the OS38K ADCP is applicable for observation at the water depth of 38-800 m. The parameter settings used in the ship-mounted ADCP are shown in Table 2-5.

Table 2-5 Operating parameter settings of ship-mounted ADCP

Parameters	OS38K
BINSIZE	8 m
NUMBER OF BINS	128
BLANK	16 m

TRANDUCER DEPTH	5 m
Transducer drift angle	45°
Short-term average duration	60 s
Long-term average duration	300 s

2.3.2 Analysis method

At a water depth not exceeding the bottom tracking depth of ADCP, WINADCP, a software developed by RDI, is used to convert the hexadecimal original data of ship-mounted ADCP into ASCII data, and extract the horizontal current speed, horizontal current direction, vertical current speed, current speed error, data integrity rate, GPS, water depth, vessel speed, vessel direction and water temperature data at the transducer from the average data of 5 min. At a water depth exceeding the bottom tracking depth of ADCP, various data corrected by GPS vessel speed are extracted and processed.

The ship-mounted ADCP works according to the principle of acoustic Doppler, and various environmental conditions in the ocean will affect its measurement and cause observation errors. According to the data processing requirements of water survey, it is necessary to control the quality of ocean current data in data processing.

1) Data processing. It begins with data inspection to understand the basic information of data, such as instrument model, installation depth, instrument blind area, layer thickness setting, layer number setting, sampling interval, etc., so as to prepare for further data processing.

2) Determining the stability of the ship-mounted ADCP current direction by whether the current direction at the corner of the route changes with the course variation of the EMV in the plan. It can be seen from the figure that the current direction does not change with the course change, which proves that the ship-mounted ADCP instrument works stably and there is no abnormal phenomenon.

3) Conducting preliminary control and deleting the data with poor quality, based on the data integrity rate (greater than 50 %) and the correlation coefficient (greater than 0.8).

4) Deleting the data obtained when the GPS signal is interrupted.

5) Deleting the data without vessel speed or direction.

6) Deleting data with surface-layer abnormalities. Due to the disturbance of the hull, the surface-layer data obtained with the apparatus are often of poor quality. Therefore, it is necessary to judge and analyze the surface-layer data and delete the abnormal values.

7) Deleting the bottom-layer data with abnormalities. Data with a survey depth greater than the water depth are deleted. The reflection of sound beam above the bottom affects the data quality of several BINs in the bottom layer, so it is necessary to analyze and judge the abnormal values and delete them. Usually, the sudden change (greater than 50 cm/s) of current speeds of two adjacent layers is considered as abnormal.

8) Due to weather, sea conditions, vessel swaying and other unknown reasons, the data obtained with ADCP in individual observation periods are obviously too large (greater than 250 cm/s) and the variation of current direction obviously does not conform to the actual tidal current change law in the sea area. Such data will be deleted as appropriate according to the actual situation.

After the above-mentioned data processing and quality control, the ship-mounted ADCP observation data are of reliable quality.

3 Chemical oceanography baselines

3.1 Sampling and analysis methods

The chemical oceanography survey is conducted in accordance with "Code of practice for international seabed area and high seas environmental survey—Part 2: Marine chemical survey" (GB/T 42629.2-2023) and the requirements of relevant technical specifications and documents.

The seawater samples required for chemical oceanography survey are collected through SBE 911plus CTD system by layer. The seawater samples obtained through

CTD are analyzed for such items as pH, DO, nitrate, silicate, phosphate, nitrite, DIC and SPM in seawater. See Table 3-1 for the methods for analysis of all elements.

Table 3-1 Methods for analysis of chemical oceanography elements

Monitored elements	Name of monitoring method	Instrument name	Detection limit	Accuracy	Precision
pH	pH meter method	Orion Star pH meter	/	0.01 level	±0.01
DO	Iodometric titration	Dropping funnel	5.3μmol/L	/	/
Nitrate	Zinc-cadmium reduction method	723C spectrophotometer	0.05μmol/L	When the concentration is 10.0 μmol/L, the relative error is ±4.0 %	When the concentration is 10.0 μmol/L, the relative deviation is ±3.0 %
Nitrite	Diazo-azo method	723C spectrophotometer	0.02μmol/L	When the concentration is 1.0 μmol/L, the relative error is ±3.0 %	When the concentration is 1.0 μmol/L, the relative deviation is ±2.0 %
Phosphate	Phosphorus molybdenum blue method	7230 spectrophotometer	0.02μmol/L	When the concentration is 2.0 μmol/L, the relative error is ±3.5 %	When the concentration is 2.0 μmol/L, the relative deviation is ±3.0 %
Silicate	Silicon molybdenum	7230 spectrophotometer	0.10μmol/L	/	/

Monitored elements	Name of monitoring method	Instrument name	Detection limit	Accuracy	Precision
	blue method				
Ammonium	Sodium hypobromite oxidation method	723C spectrophotometer	0.03μmol/L	When the concentration is 7.0 μmol/L, the relative error is ±4.0 %	When the concentration is 7.0 μmol/L, the relative deviation is ±3.0 %
SPM	Gravimetric method	Balance AL204	0.1 mg	/	/
DIC	Non-dispersive infrared spectrophotometry	DIC analyzer	/	<±0.2%	<±0.2%

3.2 Data processing methods and quality control

Those could not be verified or calibrated have passed self-inspection. The reference materials used are provided by qualified suppliers and used within the validity period. The quality control requirements for analysis of chemical oceanography characteristics are shown in Table 3-1.

(1) Seawater pH

The seawater pH is determined in-situ during survey cruises. Orion Star A series pH meter produced by Thermo, an America firm, is used for the determination. The equipment consists of a host and a pH electrode. Parameters of pH/temperature modules are as follows: pH resolution: 0.01; measuring range: -2.00-20.00 mV/RmV; working environment: ambient temperature: 5-35 °C; relative humidity: ≤85 %. In the process of pH analysis and determination, pH standard solution was used for calibration in advance to ensure controllable quality in the analysis process.

(2) DO in seawater

The DO in seawater is determined in-situ during survey cruises by iodometric titration. For DO parameters, parallel samples are used to control the analysis quality. The proportion of parallel samples determined in-situ is 100 %. The relative deviations of DO in-situ parallel samples are in the range of 0.0-3.88 %, averaging 0.81 %, all meeting the requirements of allowable deviation range stipulated in relevant specifications.

(3) Seawater nutrients

The methods for analyzing five seawater nutrients are shown in Table 3-1. In the analysis process, the standard samples are determined to control the data quality. Nitrite, nitrate, ammonium, silicate and phosphate are determined twice, with the relative errors in the ranges of 0.4-6.4 %, 2.6-3.6 %, 0.1-3.4 %, 1.0-4.3 % and 0.3-3.2 % respectively. All are in line with the allowable deviation range specified in the "The specification for marine monitoring — Part 7: Ecological survey for offshore pollution and biological monitoring" (GB 17378.7-2007). See Figure 3-1 for the standard working curves of nutrients.

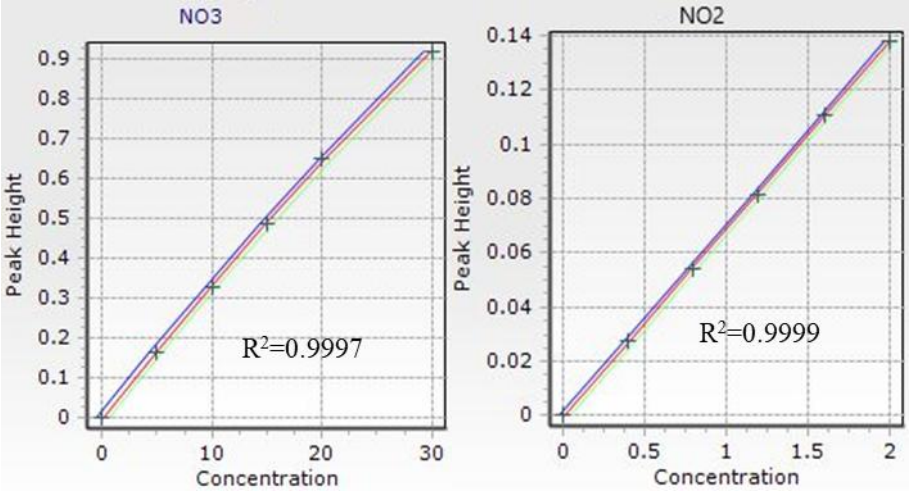

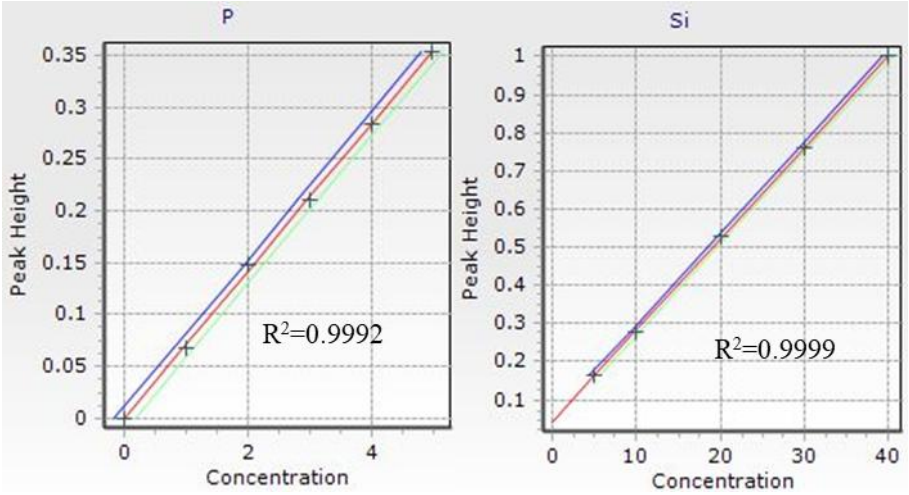

Figure 3-1 Standard working curves of nutrients

Standard working curves of nitrate (NO_3-), nitrite (NO_2-), phosphate (P) and silicate (Si) (x-axis shows the concentration, with the unit being μmol/L, and y-axis shows the corrected peak height).

In the determination process, the relative error and relative standard deviation of a single batch of samples are calculated with multiple measurements of standard solution (a standard solution called Drift was inserted every 20 samples. Generally, they are similar to most samples in the batch in content and slightly higher than them in concentration. Their role in Skalar analysis is to calibrate the drift of substance peaks), so as to assess and control the accuracy and precision of analytical test results. The specific formulas (1) and (2) for calculating relative error and relative standard deviation are as follows.

$$\textbf{Relative error}\boldsymbol{d_r}(\%) = \frac{|\textbf{Single measurement value}x_i - \textbf{Average value of multiple measurements}\bar{x}|}{\textbf{Average value of multiple measurements}\bar{x}} \times \mathbf{100\%} \textbf{(1)}$$

$$\textbf{Relative standard deviation}\boldsymbol{S_r}(\%) = \frac{\sqrt{\frac{\sum_{i=1}^{n} |\textbf{Single measurement value}x_i - \textbf{Average value of multiple measurements}\bar{x}|^2}{n-1}}}{\textbf{Average value of multiple tests}\bar{x}} \times \mathbf{100\%} \textbf{(2)}$$

The relative errors and relative standard deviations of the analysis results for different batches of nitrate, nitrite, phosphate and silicate are listed in Tables 3-2 and 3-3, and also shown in Figures 3-2 and 3-3.

Table 3-2 Relative errors of the analysis and determination results of various nutrient

parameters (%, accuracy)

Batch	Parameters			
	NO_2^-	Si	P	NO_3^-
1	0.87	1.76	0.45	0.56
2	1.77	1.30	0.70	0.56
3	1.12	0.94	0.96	0.43
4	1.10	0.10	0.40	0.70
5	0.00	0.90	0.70	0.50
6	—	—	—	0.40

Note: — indicates that the parameter is analyzed for the batch

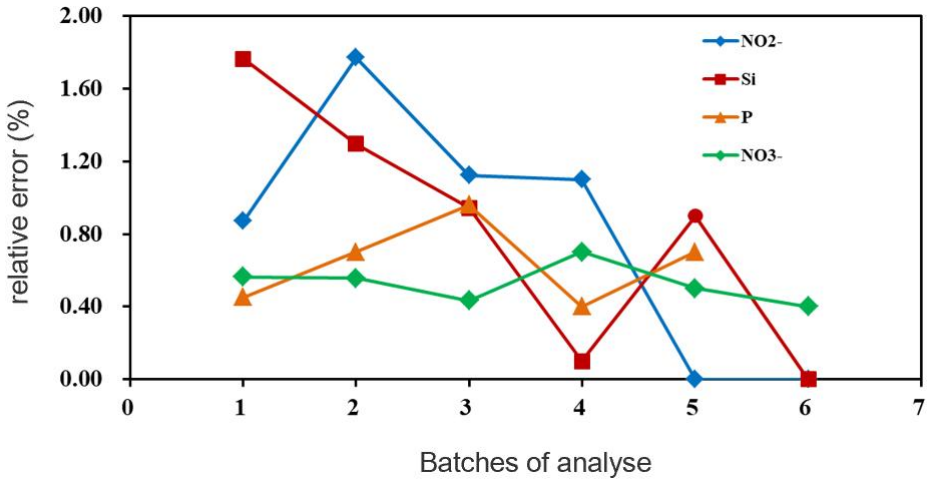

Figure 3-2 Relative errors of the analysis and determination results of various nutrient parameters (%, accuracy)

As can be seen from Table 3-3 and Figure 3-3, the relative errors of the analysis and determination results for different batches of nitrate, nitrite, phosphate and silicate are controlled within 0.7 %, 1.8 %, 1.0 % and 1.8 %, respectively. This shows that the results have high accuracy.

Table 3-3 Relative standard deviations of the analysis and determination results of various nutrient parameters (%, precision)

Batch	Parameters			
	NO_2^-	Si	P	NO_3^-
1	0.56	2.04	0.37	0.63
2	1.04	1.40	0.54	0.50

3	0.93	0.86	0.98	0.36
4	0.90	0.20	0.40	0.70
5	0.00	0.80	0.60	0.40
6	—	—	—	0.50

Note: — indicates that the parameter is analyzed for the batch

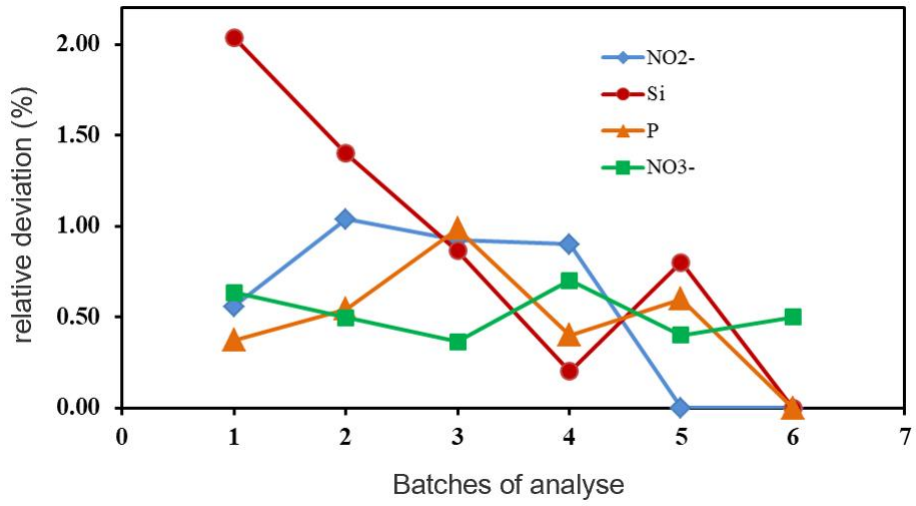

Figure 3-3 Relative standard deviations of the analysis and determination results of various nutrient parameters (%, precision)

(4) SPM

In the process of SPM analysis, quality control is conducted by using blank membrane for correction, controlling temperature and humidity, and putting the dried filter membrane into a silica gel dryer for constant-temperature drying. Approximately 1 % of the dried and standby filter membranes are randomly taken and filtered respectively with 1 L distilled water (50 pieces are taken). After drying, they are put into a silica gel dryer for 6-8 h at a constant temperature, with the temperature and humidity before and after weighing basically the same. Then, the weight loss value of the blank filter membrane is calculated, and the average value is taken as the correction value of the blank filter membrane in this Project, being at 0.3 mg/L as shown in the results. In the process of indoor analysis, laboratory parallel sample analysis and standard sample determination are conducted to control the quality of the

analysis process.

(5) DIC in seawater

The DIC analyzer (AS-C3) is adopted for measuring DIC in seawater. Main technical indexes included: reproducibility: ±0.1 % (DIC concentration: ~2,000 μmol/L); sample volume: 0.2-1.5 mL for each measurement. In the process of DIC analysis, calibration curve determination is conducted for approximately every 5-10 samples, resulting in a total of 12 calibration curves. The relative deviation between adjacent calibration curve determinations is 0.10±0.09 %.

4 Biological environment baselines

The methods adopted for the survey of biological communities are mainly according to the requirements of "Code of practice for international seabed area and high seas environmental survey—Part 3: Marine biological survey" (GB/T 42629.3-2023), "The technology specification for the pre-treatment of deep-sea microorganism samples" (GB/T 30744-2014) and related technical specifications and documents. The biological community elements analyzed in this EIS mainly include the species diversity and abundance of Chl *a*, photosynthetic pigments, microorganisms, phytoplankton, zooplankton, meiofauna, macrofauna, scavengers, seabirds and mammals.

4.1 Chl *a* and photosynthetic pigments

4.1.1 Survey method

The SBE911plus CTD water sampler is used to collect seawater samples for Chl *a* analysis. The collected water samples (0.6 L) from each layer are filtered through a six-way filter equipped with Whatman GF/F filter membrane with a diameter of 25 mm, and then through Jinteng diaphragm vacuum pump at a negative pressure of 0.02 MPa. The collected samples are wrapped with aluminum foil paper tape, kept in the ultra-low temperature refrigerator and taken to the laboratory for analysis. The extraction of Chl *a* should be at 4 °C. The samples are first stored in the dark at room

temperature for 0.5 h before determination, and then determined by TURNER-10-AU-005-CE fluorometer after acidization for 30 s.

The seawater samples for photosynthetic pigment analysis are filtered and collected on the filter membrane by the multi-way inverted filter device, with the negative pressure of filtration controlled within the pressure range of less than 100 mmHg, and the filter membrane able to be isolated from the outside world. They are then filtered by Millipore Swinnex® membrane exchange filter equipped with Merck GF/D filter membrane with a diameter of 25 mm, and by SHB-III circulating water vacuum pump at a negative pressure of 0.02 MPa, with an air extraction rate of 10 L/min and a frequency of 50 Hz. The collected samples are stored in a 2 mL freezing tube in an ultra-low temperature refrigerator (-80 °C) and taken to the laboratory for analysis. The operation steps of extracting photosynthetic pigment samples are as follows. Firstly, suck the residual seawater outside the filter membrane, and then cut the filter membrane into pieces; add 3 mL of N,N-dimethylformamide (DMF) and perform extraction at -20 °C in the dark for one hour (Furuya et al., 1998). Secondly, shake the extracting solution for tens of seconds under the condition of darkroom and take the supernatant. Then, filter the supernatant through Whatman® GF/F Swinnex Filter Holder with a diameter of 13 mm. Finally, mix 0.6 mL of filtered supernatant with 0.6 mL of ammonium acetate with a concentration of 1 mol L^{-1} in a brown chromatographic bottle with a volume of 1.5 mL, and store it at -20 °C in a refrigerator in the dark for high performance liquid chromatography (HPLC) analysis. In this study, dimethyl formamide (DMF) is used as the organic extraction solvent for extracting photosynthetic pigments.

Agilent 1100 Series liquid chromatography workstation is the photosynthetic pigment analysis system. The elution peak is detected by diode array detector (DAD), with the scanning band at 300-700 nm and the peak spectrum characteristics recorded at fixed wavelengths of 440 nm and 663 nm. The Eclipse XDB C8 separation column with a particle size of 3.5 μm (100 × 4.6 mm; Agilent Technologies, Germany) is

adopted. The mobile phase A is methanol with a volume ratio of 4:1: 1 mol L^{-1} ammonium acetate buffer solution, while the mobile phase B is methanol. The gradient elution procedure is shown in Table 4-1, with the mobile phase flow rate at 1 mL min^{-1}. The time interval between every two sample injections and the start of the procedure is 10 min, making the polar state of the chromatographic column fully balanced (Mendes et al., 2007).

Table 4-1 Gradient elution procedure for HPLC separation and analysis of photosynthetic pigments

Duration (min)	Mobile phase A (%)	Mobile phase B (%)	Gradient system
0	100	0	Sample injection
2	100	0	Linear gradient
16	55	45	Linear gradient
27	0	100	Linear gradient
32	0	100	Linear gradient
36	100	0	Balance

4.1.2 Data processing methods and quality control

The collection, preprocessing, storage and transportation of Chl *a* and photosynthetic pigment samples are conducted in accordance with the requirements of the "Specifications for oceanographic survey — Part 6: Marine biological survey" (GB/T 12763.6-2007). The Chl *a* quality control is mainly the determination of parallel samples in the laboratory to test the relative error of sample repeatability in the determination of *Chl* a. The specific quality control measure is to select a certain proportion of stations that can cover the whole sea area to a certain extent, and conduct double-sample determination. The number of parallel samples is 26, accounting for 33.3 % of the total samples. The quality control results from determining repeated Chl *a* samples show that the repeatability error of the samples is 0.20-8.00 %, less than ±10 %. The determination precision meets the requirements of "Code of practice for international seabed area and high seas environmental survey — Part 3: Marine biological survey" (GB/T 42629.3-2023).

The quality control and assessment scheme for photosynthetic pigment

concentration is conducted according to the suggestions of Roy et al. (2011). The steps are as follows. (1) Injecting standard samples every day to determine the resolution and retention time of chromatographic peaks; (2) Determining the changes in chromatographic peak absorbance and retention time every day according to the standard peak spectrogram; (3) Correcting Chl *a* concentration every day; (4) Checking and analyzing the efficiency of sample extraction every day; analyzing the HPLC spectrum of standard samples every day to confirm the variation of absorption wavelength; (5) confirming that the working curve of Chl *a* will not change greatly when the chromatographic column is replaced; and (6) Analyzing and controlling the noise value of detector.

4.2 Microorganisms

4.2.1 Survey technique

Microbial diversity analysis and culturable microorganism survey in seawater and sediments, according to the "Specifications for oceanographic survey—Part 6: Marine biological survey" (GB/T 12763.6-2007).

The microbial samples collected are pre-treated according to "The technology specification for the pre-treatment of deep-sea microorganism samples" (GB/T 30744-2014). In-situ sediment samples are all preserved in three ways: refrigerated at 4 °C, frozen at -20 °C and frozen at -80 °C.

By extracting DNA from seawater and sediment samples, and specifically amplifying one or two continuous hypervariable regions, we sequence the hypervariable regions by high-throughput sequencing platform. Then, the sequencing data are processed and analyzed by bioinformatics analysis method to obtain the composition of microbial community and species annotation information in the samples.

FastDNA® SPIN Kit is used for DNA extraction from deep-sea sediments, and PowerWater DNA Isolation Kit is used for DNA extraction from water filter membrane. 16S rRNA gene amplification primers:

27F:5'-AGAGTTTGATCCTGGCTCAG-3'

1492R: 5'-ACGGCTACCTTGTTACGACT-3'

Genomic DNA is used as templates in PCR amplification and product electrophoresis detection. Primer with barcode and PremixTaq (TaKaRa) are used for PCR amplification. After comparing the concentration of PCR products by Gene Tools Analysis Software (Version 4.03.05.0, SynGene), we calculate the required volume of each sample according to the principle of equal mass, and mix the PCR products. During the analysis, E.Z.N.A. E.Z.N.A® Gel Extraction Kit is used to recover PCR mixed products, while TE buffer solution is used to elute and recover target DNA fragments. Subsequently, a library is built for the recovered DNA samples according to the standard process of NEBNext® Ultra™ DNA Library Prep Kit for Illumina®, so as to ensure the accuracy and reliability of sequencing. After the establishment of the library, the samples are sequenced by high-throughput sequencing platform Hiseq or Miseq.

The original image data files obtained by sequencing are analyzed by BaseCalling, and transformed into RawReads. The sequencing results are stored in FASTQ (a file format abbreviated as fq), which contains the sequence information of Reads and corresponding sequencing quality information. For information about the genome composition and genetic variation characteristics of the samples, bioinformatics analysis (e.g. sequence alignment, species annotation and SNP detection) can be conducted based on these data.

4.2.2 Data processing methods and quality control

Microbial diversity analytical process is shown in the Figure 4-1.

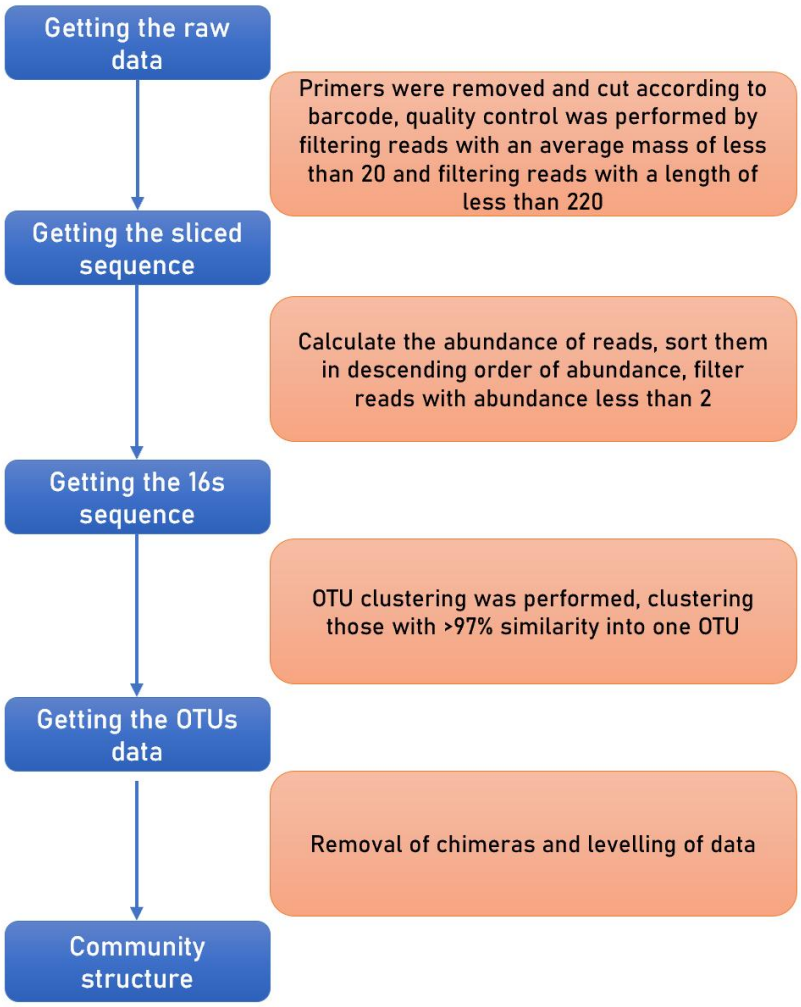

Figure 4-1 Microbial diversity analytical process

(1) Quality control: Data quality control is a crucial step in bioinformatics studies. This step usually involves checking the sequencing quality of the original data and removing low-quality reads and pollution to ensure the accuracy and reliability of the analysis results in the next step.

(2) Chimera removal and clustering: Qiime is a kind of software for processing high-throughput sequencing data, which can help to remove Chimeras from sequencing data and cluster reads. In the process of clustering, the reads are sorted by abundance in a descending order, and clustered according to the standard of 97 % similarity to derive OTU. Each OTU is considered to represent a species.

(3) Random levelling: The tags of each sample are randomly levelled and the corresponding OTU sequence is extracted. This step aims to reduce the differences

between samples and make the comparison between samples more accurate and reliable.

(4) Dilution curve of diversity index: Qiime is a widely used software for microbial community analysis. In this step, the Qiime software is used to draw the dilution curves of α and β diversity indexes to help select the appropriate levelling parameters.

(5) OTU classification: In this step, the representative sequence is compared with the 16S database to classify OTU by species.

(6) Drawing OTU abundance table: The OTU abundance table is drawn based on the number of sequences in each OTU. The table will be used in subsequent analysis, such as species diversity analysis, community structure analysis and function analysis.

Since there is a big gap in the numbers of reads corresponding to different samples, the data about each sample are randomly leveled to ensure the rationality of the later analysis results. This approach could eliminate the impact of the difference in the numbers of reads in different samples on the analysis results, making the analysis results more reliable and comparable. The selection of levelling parameters is very important. We determine levelling parameters based on the dilution curve of alpha diversity index.

In analyzing the microbial community structure of concentrated flora and environmental samples, we mainly use SMRT Link Analysis 6.0 to process the original reads of PacBio, so as to obtain circular consistent sequence (CCS) reads. The steps are as follows: the minimum pass times and prediction accuracy are set to be 3 and 0.99, respectively; The original reads are processed through SMRT Portal to screen the length (1,300-1,500 bps) and quality of the sequence. Further filtering is conducted by removing barcode, primer sequence, chimera and sequence containing 10 consecutive identical bases. OTU is clustered by UPARSE (version 7.1, http://drive5.com/uparse/) based on the similarity threshold of 98.65 %, and the chimeric sequences are identified and removed by UCHIME. Based on the Silva

(SSU132) 16S rRNA database, RDP Classifier (http://rdp.cme.msu.edu/) is adopted to use a 70 % confidence threshold to analyze the phylogenetic relationship of each 16S rRNA gene sequence.

4.3 Picoplankton

4.3.1 Survey technique

Flow cytometry (Olson et al., 1993) is adopted to identify the species and abundance of picophytoplankton. Water samples are collected using SBE 911plus CTD water sampler, fixed with 500 μL of 20 % paraformaldehyde and stored in liquid nitrogen. After moved to the laboratory, they are thawed in a water bath; and the species and abundance of picophytoplankton are then identified by flow cytometer (BD FACSCalibur). When used for cytometry detection, the flow cytometer should be checked for sensitivity and accuracy (expressed in CV value, which should be less than 2.0) according to the method provided by the apparatus manufacturer to ensure that the apparatus is in good condition.

4.3.2 Data processing methods and quality control

Picophytoplankton quality control is mainly about the determination of parallel samples in the laboratory to test the relative error of sample repeatability in the determination of picophytoplankton. The number of parallel samples is 26, accounting for 33.3 % of the total number of samples. Quality control results show that the repeatability error of the samples is 0.20-9.50 %, less than ±10 %. The determination precision meets the requirements of "Code of practice for international seabed area and high seas environmental survey — Part 3: Marine biological survey" (GB/T 42629.3-2023).

4.4 Phytoplankton

4.4.1 Survey technique

Plankton vertically towed net and CTD are adopted for phytoplankton collection and survey. The phytoplankton samples are vertically dragged to the surface from a

depth of 200 m with net of 20 μm in mesh size, washed and collected in sample bottles through a continuous seawater supply system, fixed with 5 % formaldehyde solution and stored at room temperature. The volume of water filtered is measured by the Hydro-Bios No.438115 mesh flowmeter fixed at the mesh mouth.

In the laboratory analysis, the phytoplankton samples are first placed for more than 48 h, then concentrated by extracting the supernatant by siphon, and then put under the microscope for the identification and counting of species, by category or the lowest taxonomic category as appropriate as possible.

4.4.2 Data processing methods and quality control

The plankton sampling nets, plankton sampling procedures, the processing and preservation of samples obtained and laboratory analysis methods are all conducted in accordance with the "Specifications for oceanographic survey" and internationally recognized methods to ensure the quality of samples.

The logarithm calculation formula with the base of 2 is adopted for diversity index:

$$H'=-\sum(p_i \ln p_i)$$

Uniformity calculation formula:

$$J'=H'/\ln S$$

The data obtained from identification and analysis are counted and processed by SPSS software, and maps are drawn.

4.5 Zooplankton

4.5.1 Survey technique

In the survey of large and medium-sized plankton, the samples are vertically dragged to the surface from a depth of 200 m with WP2 net of 200 μm in mesh size, washed and collected in sample bottles through a continuous seawater supply system, fixed with 5 % formaldehyde solution and stored at room temperature. The volume of water filtered is measured by the Hydro-Bios mesh flowmeter fixed at the mesh

mouth.

In the survey of the stratification and distribution characteristics of plankton, samples are vertically dragged from depths of 0-50 m, 50-100 m, 100-200 m, 200-500 m and 500-1,000 m by HydroBios Multinet System Maxi (with a mesh mouth area of 0.5 m^2 and a mesh screen pore size of 200 μm), and then washed and collected in sample bottles through a continuous seawater supply system, fixed with 5 % formaldehyde solution and stored at room temperature. The volume of water filtered and other environmental parameters are collected with sensors equipped in the apparatus.

4.5.2 Data processing methods and quality control

The diversity analysis and quality control methods for zooplankton are shown in 4.4.2.

4.6 Meiofauna

Meiofauna samples are collected with multicorer, and then undisturbed core samples are collected from the multicorer and divided into five layers of 0-1 cm, 1-2 cm, 2-3 cm, 3-4 cm and 4-5 cm. The organisms in overlying water in each tube are intercepted by a 32 μm mesh screen and packed with the sediment samples at 0-1 cm depth layer, while the sediment samples at other layers are bottled separately. The sediment samples are fixed with 5 % formaldehyde and taken to the laboratory. The samples of meiofauna are separated by Ludox centrifugation, and then treated and analyzed according to the requirements of "Code of practice for international seabed area and high seas environmental survey — Part 3: Marine biological survey" (GB/T 42629.3-2023).

4.7 Macrofauna

Macrofauna are sampled with a box corer with a side length of 50 cm, and the samples are pretreated in accordance with "Code of practice for international seabed area and high seas environmental survey — Part 3: Marine biological survey" (GB/T

42629.3-2023) and the ISA recommended specification of "Standardization of Environmental Data and Information" (2001). The sediments of all layers are collected at intervals of 0-3 cm, 3-5 cm and 5-10 cm, and washed by a 250 μm mesh screen in-situ to obtain macrofauna samples, which are then fixed and preserved by adding 5 % formaldehyde. After the samples of macrofauna are taken to the laboratory and sorted by groups, they are handed over to taxonomists of corresponding groups for corresponding morphological identification and counting. The samples are weighed by an analytical balance with a sensitivity of 0.0001 g, with the water on their surface sucked dry.

Macrofauna are sampled quantitatively by layers at stations with good sampling effect, while surface-layer sediments are sampled qualitatively at stations with ordinary sampling effect. Both sampling and sample pretreatment are conducted in accordance with "Code of practice for international seabed area and high seas environmental survey — Part 3: Marine biological survey" (GB/T 42629.3-2023). Sample analysis and identification are completed by personnel with professional qualification certificates related to marine survey, and checked by a second person to ensure the reliability of the obtained data.

4.8 Scavengers

Sampling and photography survey of deep-sea scavengers are conducted by using lander, a deep-sea hypobenthic fauna trapping and observation system. The survey process is as follows: Set the image recording system to start on time after the lander arrives at the seabed, with the camera taking one photo per minute and the video camera sleeping for 30 min after continuous recording for 30 min. Take the equipment back after it lands on the seabed for observation for approximately 48 h. Immediately collect the biological samples in the trap cage and keep in seawater at 4 °C after the equipment returns to the deck. Store some samples at -80 °C and the rest in 100 % alcohol after photographs are taken on the spot.

By biological morphology, swimming trajectory and other characteristics, it is

judged whether the similar individuals that appear continuously in a short period of time are the same individuals. The types and individual numbers of all benthic fauna at the station are observed and recorded, and then the data are summarized and analyzed.

4.9 Seabirds, turtles and mammals

The diversity of sea turtles, marine mammals and seabirds, especially the species composition of marine mammals such as pinnipeds and whales and seabirds, is surveyed through ship-based observation, alongside available data.

The survey of seabirds is mainly based on the "Technical guidelines for biodiversity monitoring — birds" (HJ710.42014) and the "Draft regulations on the exploitation of mineral resources in the Area" (ISBA/27/C/11) issued by the ISA. Shipboard observation is usually conducted in weather conditions with high visibility (≥500 m) and small wind and waves (sea conditions ≤4). In addition to naked eyes, a telescope is used on the observation platform for observation. The observation ranges are 100° on both left and right sides. That is, the waters from 90° on each side to 10° across the midline, with the course direction as 0°. The information is recorded after the discovery of animals, including the exact time and location for the discovery.

4.10 Primary production

4.10.1 Survey technique

The ^{14}C light-and-dark bottle technique was adopted to determine primary production. The whole process is as follows. Firstly, measure the transparency of seawater with a transparency scale to determine the optical depth of sampling; use SBE 911plus CTD to collect seawater at different water-depth layers and pack it in 175 mL narrow-necked square bottles; set two white bottles and one black bottle at each depth, and add ^{14}C markers to them. Then pack the sample bottles for different water-depth layers respectively into the corresponding light attenuation films, with six gradients of 100 %, 50 %, 30 %, 10 %, 5 % and 1 % of the surface light intensity.

Place the film box in the deck culture tank, whose temperature is controlled by surface running water, for 4-6 h. Collect the seawater sample back to the isotope container laboratory after the culture is completed, and filter it by the isotope six-way negative-pressure filtration device, under the filter funnel equipped with a polycarbonate filter membrane with a diameter of 25 mm and a pore diameter of 0.22 μm, and by a diaphragm vacuum pump at a negative pressure of 0.02MPa. Then, put the filter membrane into a scintillation vial, fumigate it with concentrated hydrochloric acid and store it in a refrigerator at -20 °C. Add scintillation liquid to the scintillation bottle with filter membrane after taking the sample to the land-based laboratory, place the scintillation bottle in the liquid scintillation counter Tricarb-3110TR after it is shaken, and determine the sample after the dark adaptation completely reaches the determination standard.

In addition, we have downloaded data about the monthly spatial distribution of global ocean primary production since 2003 with 9 km resolution from the "Digital Journal of Global Change Data Repository". Based on six kinds of monthly data, including phytoplankton absorption coefficient, Chl concentration, euphotic zone depth, diffuse attenuation coefficient of 490 nm, photosynthetic effective radiation and sea surface temperature provided by Moderate Resolution Imaging Spectroradiometer (MODIS), the remote-sensing monitoring data of global ocean primary production are calculated by using SABPM model. The data set is time series data (monthly) and stored in the hierarchical data format (HDF) (Tao Zui et al., 2019).

4.10.2 Data processing methods and quality control

For primary production, quality control is mainly about the determination of parallel samples in white and dark bottles in the laboratory to test the relative error of sample repeatability in the determination of primary production. The specific quality control measure is to determinate parallel samples for all black and white bottle samples. The number of parallel samples is 108, accounting for 100 % of the total number of samples. The quality control results from determining the repeated primary

production samples show that the repeatability error of the samples is 0.12-7.50 %, less than ±10 %. The determination precision meets the requirements of "Code of practice for international seabed area and high seas environmental survey — Part 3: Marine biological survey " (GB/T 42629.3-2023).

Annex 3 Toxicity Assessment to *Vibrio fischeri* of Heavy Metals Released from Disturbed Surface Sediments in the Block A-5

1 Materials and methods

1.1 Sediment elution experiment

To simulate the release of heavy metals caused by disturbance of surface sediments due to mining activities, an elution experiment was conducted on 0-14 cm sediment samples from Cruise DY 79: 10 g of sediment samples were weighed, deionized water (salinity: 34, pH: 6.7±0.2) as a solvent, with a soil-to-water ratio of 1:3, add it to a 100 mL Erlenmeyer flask; shake it in a constant temperature shaking box at 100 r/min for 24 hours at room temperature; finally, the suspension was filtered through a Buchner funnel and a 0.45μm filter membrane, and repeat it until the filtrate is clear and transparent to obtain the sediment leachate, and test the heavy metal concentration through inductively coupled plasma mass spectrometry (ICP-MS) technology.

According to the results of elution experiment, it was determined that the heavy metals Li^{+} Rb^{+} Mn^{2+} Mo^{6+} V^{5+} Cs^{+} with high concentrations released in the sediment and the three heavy metals Cu^{2+} Cr^{6+} Cd^{2+} with obvious toxic effects were selected as the objects for subsequent toxicity assessment. The single toxicity of Cu^{2+} Cr^{6+} Cd^{2+} and its binary combined toxicity changes with heavy metals released in higher concentrations in sediments were studied at 4°C and 20°C.

1.2 Test reagents

The freeze-dried luminescent bacteria, *Vibrio fischeri* (NRRL B-11177), and the reconstitution solution.

1.3 Apparatus and chemicals

Microtox® FX; 4℃ incubator; $CdCl_2·2.5H_2O$, $CuSO_4·5H_2O$, $K_2Cr_2O_7$, Na_3VO_4, $Na_2MoO_4·2H_2O$, RbCl, LiCl, CsCl, $MnSO_4$ H_2O, NaCl, all analytical grade.

1.4 Resuscitate the luminous bacteria

Resuscitate the luminous bacteria. Take out the lyophilized powder of *Vibrio fischeri* and warm it at room temperature; quickly pour 1mL of recovery solution into the reagent bottle, mix thoroughly with a pipette to make a hydration reagent (aspirate 500 μL each time and put it back again, repeat the operation for at least 10 times), wait for 15 minutes for resuscitation; dilute the luminous bacteria hydration solution with diluent (2% NaCl) at a ratio of 1:10 to prepare a luminous bacteria recovery solution.

1.5 Biological toxicity test

Before toxicity measurement, the heavy metal to be tested was diluted into a series of concentration gradients with 3.4% NaCl. Add 0.1 mL of bacterial solution to the sample tube and measure the initial luminescence intensity; add 0.9 mL of the substance to be measured into the corresponding sample tube, activate it at a specific temperature for 15 minutes, and then use the Microtox® FX toxicity analyzer to measure the luminescence inhibition rate. For each batch of experiments, a group of 3.4% NaCl was added as a blank control group, with 2 parallels for each concentration.

1.6 Single toxicity

A series of Cd^{2+} Cu^{2+} Cr^{6+} solutions with different mass concentrations were prepared. After the luminous bacteria were in contact with the prepared test sample for 15 minutes, a toxicity detector was used to measure the change rate of luminescence intensity. According to the ISO11348 standard, the luminescence inhibition rate of *Vibrio fischeri* was within 20 When 20%-80%, there is a linear

relationship between the logarithm of the inhibitor concentration and the inhibition rate. Finally, the EC_{50} value is calculated by regression analysis of the linear relationship between the logarithm of the heavy metal concentration and the inhibition rate.

1.7 Binary joint toxicity

Binary joint toxicity uses equal concentration ratios to obtain a binary mixture of Cd^{2+} Cu^{2+} Cr^{6+} and Li^{+} Rb^{+} Mn^{2+} Mo^{6+} V^{5+} Cs^{+}. The EC_{50} determination method of each mixed system is the same as that of a single system.

2 Result

2.1 Biological toxicity of Cd^{2+} to *Vibrio fischeri*

(1) Toxicity changes of Cd^{2+} at 20°C

Compare to Cd^{2+} EC_{50}=16.85 mg/L, Cd^{2+}+Mo^{6+} toxicity decreased, Cd^{2+}+V^{5+} toxicity decreased, Cd^{2+}+Rb^{+} toxicity decreased, Cd^{2+}+Li^{+} toxicity decreased, Cd^{2+}+Mn^{2+} toxicity increased, Cd^{2+}+Cs^{+} toxicity increased.

(2) Toxicity changes of Cd^{2+} at 4°C

Compare to Cd^{2+} EC_{50}=33.97 mg/L, Cd^{2+}+Mo^{6+} toxicity decreased, Cd^{2+}+V^{5+} toxicity decreased, Cd^{2+}+Rb^{+} toxicity decreased, Cd^{2+}+Li^{+} toxicity increased, Cd^{2+}+Mn^{2+} toxicity increased, Cd^{2+}+Cs^{+} toxicity decreased.

(3) Toxic effects of temperature on Cd^{2+}

For all treatment groups, the single and binary toxicity of Cd^{2+} decreased at 4℃ compared with 20℃.

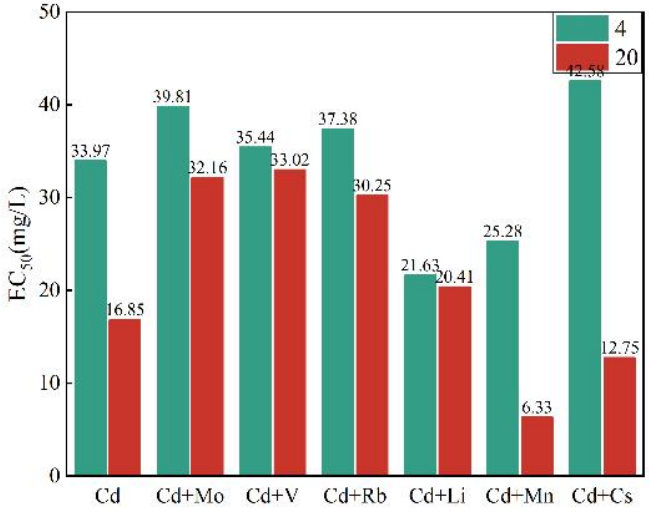

Figure 1 Biological toxicity of Cd^{2+} to *Vibrio fischeri*

2.2 Biological toxicity of Cu^{2+} to *Vibrio fischeri*

(1) Toxicity changes of Cu^{2+} at 20℃

Compare to Cu^{2+} EC_{50}=2.1 mg/L, Cu^{2+}+Mo^{6+} toxicity slightly decreased, Cu^{2+}+V^{5+} toxicity decreased, Cu^{2+}+Rb^{+} toxicity slightly increased, Cu^{2+}+Li^{+} toxicity decreased, Cu^{2+}+Mn^{2+} no change in toxicity, Cu^{2+}+Cs^{+} toxicity increased.

(2) Toxicity changes of Cu^{2+} at 4℃

Compare to Cu^{2+} EC_{50}=1.53 mg/L, Cu^{2+}+Mo^{6+} toxicity slightly increased, Cu^{2+}+V^{5+} toxicity decreased, Cu^{2+}+Rb^{+} no change in toxicity, Cu^{2+}+Li^{+} toxicity decreased, Cu^{2+}+Mn^{2+} toxicity slightly increased, Cu^{2+}+Cs^{+} toxicity increased.

(3) Toxic effects of temperature on Cu^{2+}

Compared with 20℃, the toxicity of Cu^{2+}+Rb^{+} and Cu^{2+}+Cs^{+} was basically unchanged at 4℃, and the toxicity of other treatment groups was enhanced.

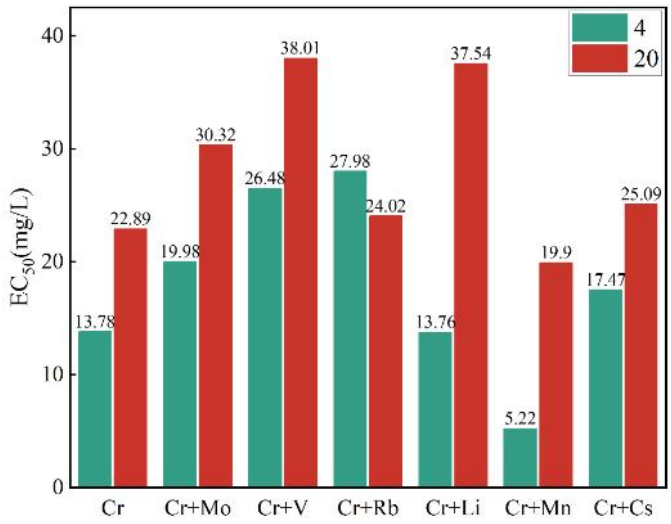

Figure 2 Biological toxicity of Cu^{2+} to *Vibrio fischeri*

2.3 Biological toxicity of Cr^{6+} to *Vibrio fischeri*

(1) Toxicity changes of Cr^{6+} at 20°C

Compare to Cr^{6+} EC_{50}=22.89 mg/L, Cr^{6+}+Mo^{6+} toxicity decreased, Cr^{6+}+V^{5+} toxicity decreased, Cr^{6+}+Rb^{+} toxicity decreased, Cr^{6+}+Li^{+} toxicity decreased, Cr^{6+}+Mn^{2+} toxicity increased, Cr^{6+}+Cs^{+} toxicity decreased.

(2) Toxicity changes of Cr^{6+} at 4°C

Compare to Cr^{6+} EC_{50}=13.78 mg/L, Cr^{6+}+Mo^{6+} toxicity decreased, Cr^{6+}+V^{5+} toxicity decreased, Cr^{6+}+Rb^{+} toxicity decreased, Cr^{6+}+Li^{+} no change in toxicity, Cr^{6+}+Mn^{2+} toxicity increased, Cr^{6+}+Cs^{+} toxicity decreased.

(3) Toxic effects of temperature on Cr^{6+}

Compared with 20°C, except for the reduced toxicity of Cr^{6+}+Rb^{+}, the toxicity of other treatment groups was enhanced at 4°C.

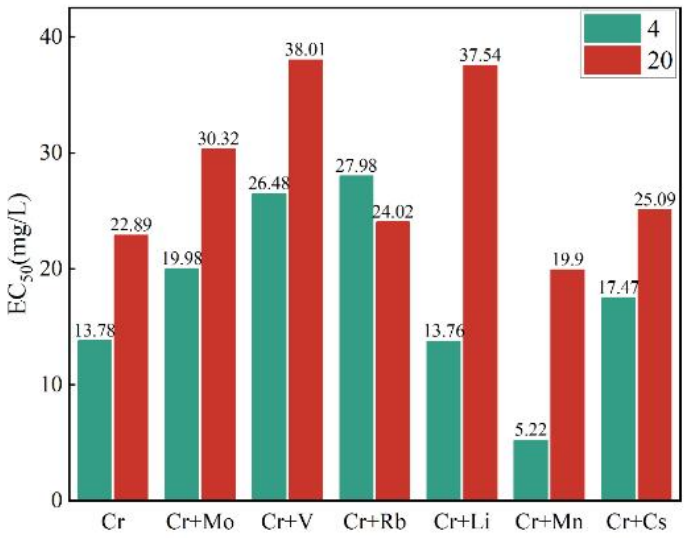

Figure 3 Biological toxicity of Cr^{6+} to *Vibrio fischeri*

3 Brief conclusion

(1) The concentration of Cu^{2+} Cr^{6+} Cd^{2+} released by surface sediment disturbance in the polymetallic nodule area is much lower than its EC_{50} effect value on *Vibrio fischeri*, so it has less toxic effect on the microbial population of the marine ecosystem.

(2) The presence of the heavy metals Li^{+} Rb^{+} Mn^{2+} Mo^{6+} V^{5+} Cs^{+} affects the toxicity of Cu^{2+} Cr^{6+} Cd^{2+} to *Vibrio fischeri*. The combined toxic effects of heavy metals released by sediment disturbance on microorganisms should be considered.

(3) The toxic effect of Cu^{2+} Cr^{6+} Cd^{2+} on *Vibrio fischeri* will be affected by temperature, and the toxic effect of the temperature of mining tailwater discharge on microorganisms should be considered.

Annex 4 Environmental Survey Station in the IRZ and PRZ

1 Environmental survey station in 2017

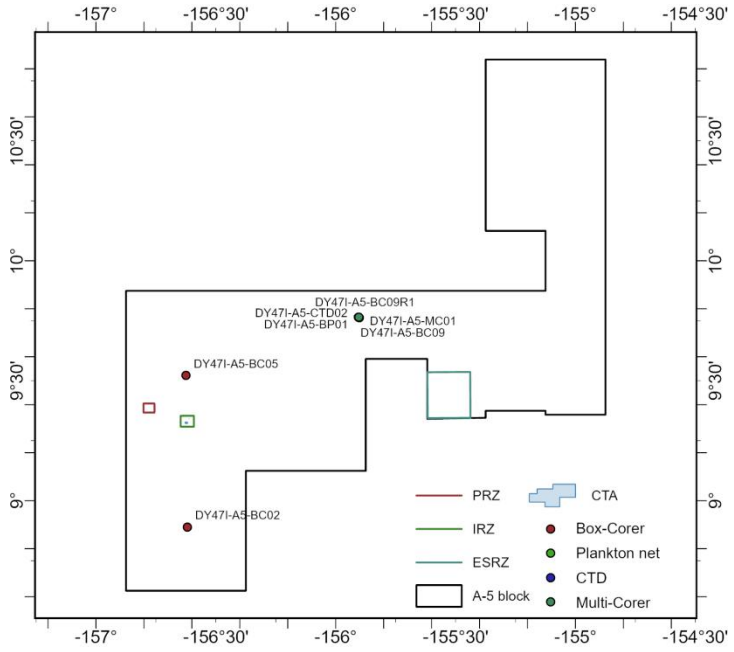

Figure 1 Information about environmental survey stations in 2017

2 Environmental survey station in 2018

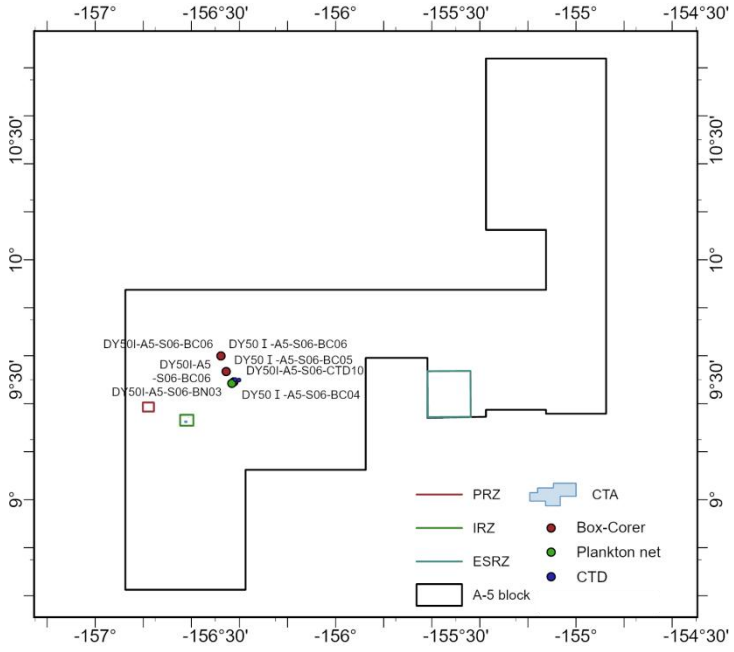

Figure 2 Information about environmental survey stations in 2018

3 Environmental survey station in 2019

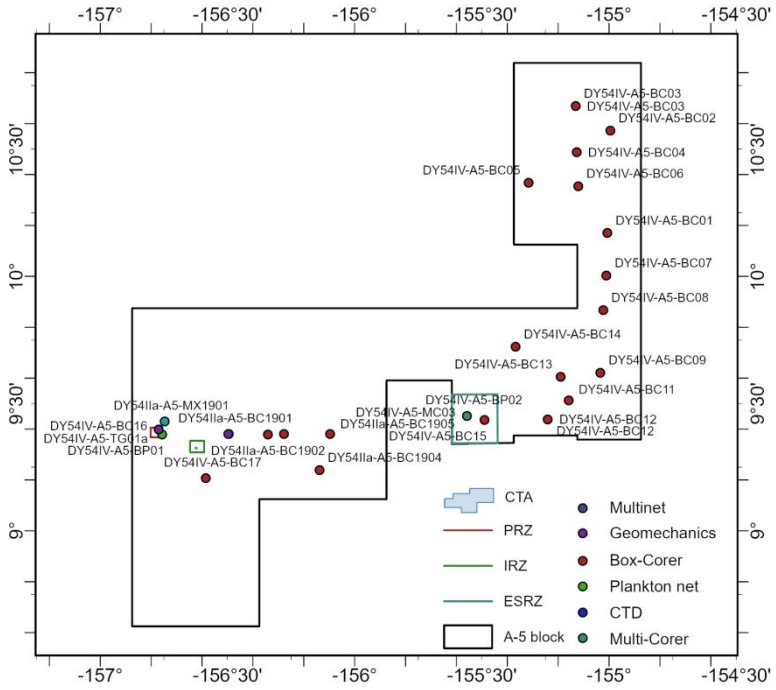

Figure 3 Information about environmental survey stations in 2019

4 Environmental survey station in 2021

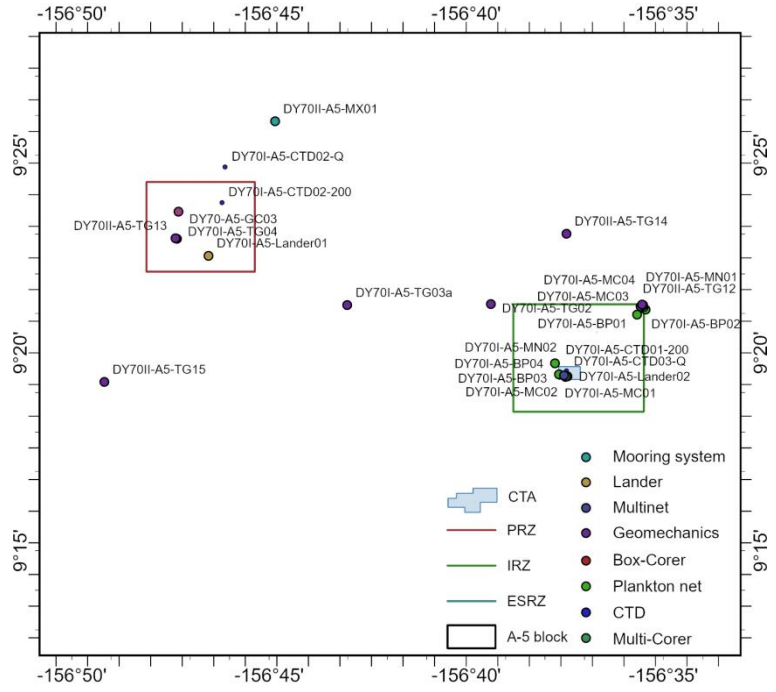

Figure 4 Information about environmental survey stations in 2021

5 Environmental survey station in 2022

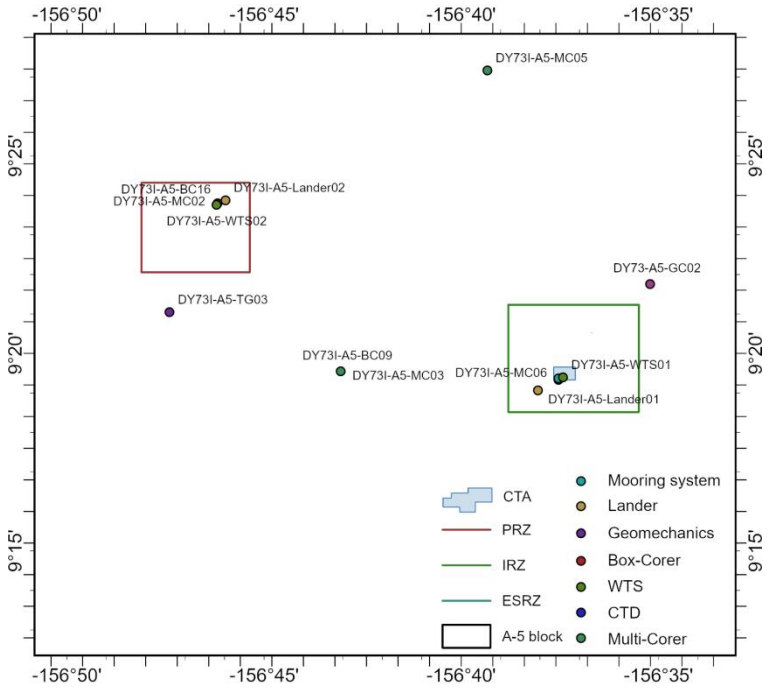

Figure 5 Information about environmental survey stations in 2022

6 Environmental survey station in 2023

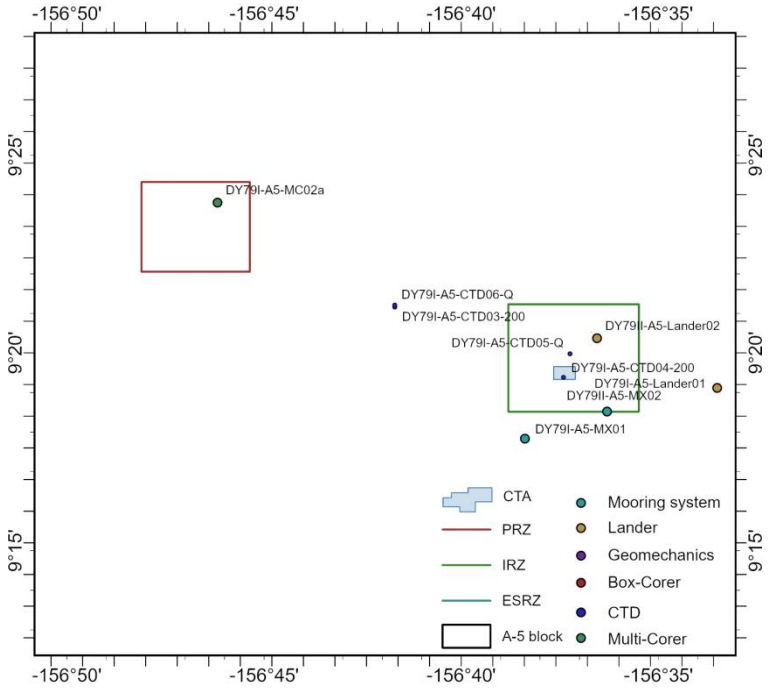

Figure 6 Information about environmental survey stations in 2023

Annex 5 Minmetals' Environmental Survey Stations in History and Plans for the Future Environmental Survey

Table 1 The information of Minmetals' environmental survey Stations in history

Station	Data	Longitude	Latitude	Analysis	Data Submission
DY47I-A5-BC02	20170921	-156.618097	8.890673	Macrofauna	Submitted
DY47I-A5-BC05	20170925	-156.624777	9.521445	Macrofauna	Submitted
DY47I-A5-BC09	20170927	-155.901898	9.76358	Macrofauna	Submitted
DY47I-A5-BC09R1	20170927	-155.904666	9.76459	Macrofauna	Submitted
DY47I-A5-BP01	20170927	-155.90484	9.764479	Phytoplankton	Submitted
DY47I-A5-CTD01(500m)	20170928	-155.902751	9.761195	Reactive phosphate, Nitrite, Nitrate, Silicate, DO, pH, Hydrology, Hydrogen and oxygen isotopes, Chlorophyll	Submitted
DY47I-A5-CTD02	20170928	-155.915	9.769	Reactive phosphate, Nitrite, Nitrate, Silicate, DO, pH, Hydrology, Hydrogen and oxygen isotopes	Submitted
DY47I-A5-MC01	20170928	-155.90351	9.764847	Meiofauna, Chlorophyll in Sediment , Nutrient contents in the pore water(Nitrate, Reactive phosphate, Silicate)	Submitted
DY47I-A5-MC01R1	20170930	-155.902732	9.764001	Meiofauna, Chlorophyll in Sediment	Submitted
DY47I-APEI-CTD03	20171007	-154.230234	14.839641	Reactive phosphate, Nitrite, Nitrate, Silicate, DO, pH, Hydrology, Hydrogen and oxygen isotopes	Submitted
DY47I-APEI-CTD04(250m)	20171008	-154.221962	14.820848	Reactive phosphate, Nitrite, Nitrate, Silicate, DO, pH, Hydrology, Chlorophyll	Submitted
DY47II-A1-BP02	20171027	-141.888287	12.220674	Phytoplankton	Submitted
DY47II-A1-CTD01	20171027	-141.881288	12.189036	Reactive phosphate, Nitrite, Nitrate, Silicate, DO, pH, Hydrology, Microorganisms	Submitted
DY47II-A1-	20171027	-141.881	12.189	Reactive phosphate, Nitrite, Nitrate, Silicate, DO, pH, Hydrology,	Submitted

CTD02(200m)				Chlorophyll	
DY47II-A2-BP04	20171103	-138.570589	12.04152	Phytoplankton	Submitted
DY47II-A2-CTD01	20171103	-138.569449	12.04098	Hydrology, Hydrogen and oxygen isotopes, Chlorophyll	Submitted
DY47II-A6-BP01	20171025	-144.48749	11.338284	Phytoplankton	Submitted
DY47II-A6-CTD01	20171024	-144.504	11.326	Reactive phosphate, Nitrite, Nitrate, Silicate, DO, pH, Hydrology, Microorganisms	Submitted
DY47II-A6-CTD02(250m)	20171025	-144.493148	11.332977	Reactive phosphate, Nitrite, Nitrate, Silicate, DO, pH, Hydrology, Chlorophyll, Hydrogen and oxygen isotopes	Submitted
DY47II-A6-MX01	20171024	-144.515409	11.309659	Sedimentary flux, Current meters, CTD	Submitted
DY47II-A7-BP05	20171106	-139.463813	11.370867	Phytoplankton	Submitted
DY47II-A7-CTD01(200m)	20171106	-139.470276	11.371137	Reactive phosphate, Nitrite, Nitrate, Silicate, DO, pH, Hydrology, Microorganisms, Chlorophyll	Submitted
DY47II-A7-CTD02	20171106	-139.453985	11.363813	Reactive phosphate, Nitrite, Nitrate, Silicate, DO, pH, Hydrology, Microorganisms	Submitted
DY47II-A8-BP03	20171030	-139.654659	13.415384	Phytoplankton	Submitted
DY47II-A8-CTD01	20171030	-139.636128	13.407558	Reactive phosphate, Nitrite, Nitrate, Silicate, DO, pH, Hydrology, Microorganisms	Submitted
DY47II-A8-CTD02(200m)	20171030	-139.679143	13.421479	Reactive phosphate, Nitrite, Nitrate, Silicate, DO, pH, Hydrology, Chlorophyll	Submitted
DY50I-A5-S06-BC04	20180809	-156.4227167	9.490075	Macrofauna	Submitted
DY50I-A5-S06-BC05	20180810	-156.45427	9.533353333	Macrofauna	Submitted
DY50I-A5-S06-BC06	20180810	-156.4764633	9.598985	Macrofauna	Submitted
DY50II-A1-S03-BC23	20180917	-142.1643617	12.09953333	Macrofauna	Submitted
DY50II-A1-S03-BC24	20180917	-142.1662167	12.099575	Macrofauna	Submitted
DY50II-A6-S02-BC35	20180921	-144.63686	11.27299	Macrofauna	Submitted
DY50II-A6-S02-BC36	20180922	-144.6369567	11.27263833	Macrofauna	Submitted
DY50II-A8-S03- BC03	20180906	-139.296435	13.305	Macrofauna	Submitted
DY50II-A8-S03-BN01	20180906	-139.29432	13.32741	Zooplankton, Phytoplankton	Submitted

DY50II-A8-S03-CTD01	20180906	-139.2942	13.32	Chlorophylla, Photosynthetic pigments, Primary production	Submitted
DY50II-A8-S03-Lander01	20180905-0909	-139.366	13.316	Lander	Submitted
DY50II-A8-S03-Multinet01	20180907	-139.29359	13.33641	Multinet	Submitted
DY50I-A5-S06-BC06	20180810	-156.4764633	9.598985	Meiofauna	Submitted
DY50I-A5-S06-BC06	20180810	-156.4764633	9.598985	DO, pH, Temperature, Eh, Heavy metal in the pore water	Submitted
DY50I-A5-S06-BN03	20180809	-156.4309683	9.485283333	Zooplankton, Phytoplankton	Submitted
DY50I-A5-S06-CTD10	20180809	-156.401	9.499	Hydrology, Reactive phosphate, Nitrite, Nitrate, Silicate, DO, pH, Ammonium	Submitted
DY50I-A5-S06-CTD11	20180809	-156.417	9.5	Hydrology, Reactive phosphate, Nitrite, Nitrate, Silicate, DO, pH, Ammonium	Submitted
DY50I-A5-S06-CTD11	20180809	-156.417	9.5	Chlorophylla, Photosynthetic pigments, Primary production	Submitted
DY50II-A1-S01-BC26	20180918	-142.5870933	12.09651167	Meiofauna	Submitted
DY50II-A1-S02-BC25	20180917	-142.40209	12.102215	Meiofauna	Submitted
DY50II-A6-S05-BC29	20180919	-144.9127383	11.27713167	Meiofauna	Submitted
DY50II-A6-S07-BC28	20180918	-144.7730717	11.40659667	Meiofauna	Submitted
DY50II-A8-S03-BC04	20180906	-139.2960317	13.30506	DO, ph, Temperature, Eh, Heavy metal in the pore water, BSi, Moisture content, Total carbon, Total organic carbon, Total organic nitrogen, Total Phosphorus, Total calcium, Heavy metal	Submitted
DY50II-A8-S03-CTD01	20180906	-139.2942	13.32	Hydrology, Reactive phosphate, Nitrite, Nitrate, Silicate, DO, pH, Ammonium, Total alkalinity, DIC, Total nitrogen, Total Phosphorus, TSM, Total calcium, TOC	Submitted
DY50II-A8-S03-CTD02	20180906	-139.294	13.327	Hydrology, Reactive phosphate, Nitrite, Nitrate, Silicate, DO, pH, Ammonium, Total alkalinity, DIC, Total nitrogen, Total Phosphorus, TSM, Total calcium, TOC	Submitted
DY50II-A8-S03-MC01	20180906	-139.2965633	13.30513	Reactive phosphate, Nitrite, Nitrate, Silicate, DO, pH, Ammonium, Total nitrogen, Total Phosphorus	Submitted
DY50II-A8-S03-MC01	20180906	-139.2965633	13.30513	Meiofauna	Submitted
DY54IIa-A5-BC1901	20190815	-156.4953333	9.380316667	pH, Eh in Sediment	Submitted

DY54IIa-A5-BC1902	20190815	-156.3407833	9.379133333	pH, Eh in Sediment	Submitted
DY54IIa-A5-BC1903	20190815	-156.2784333	9.379716667	pH, Eh in Sediment	Submitted
DY54IIa-A5-BC1904	20190815	-156.1382833	9.2392	pH, Eh in Sediment	Submitted
DY54IIa-A5-BC1905	20190816	-156.0959833	9.380266667	pH, Eh in Sediment	Submitted
DY54IIa-A5-BC1906	20190826	-120.6264	15.5245	pH, Eh in Sediment	Submitted
DY54IIa-A5-MX1901	20190812	-156.7469667	9.429266667	CTD, ADCP, Current meters, Temperature,Salinity, Ocean current, Sedimentary flux	Submitted
DY54IIa-A5-TG1901	20190814	-156.4956667	9.38005	In-situ geotechnical properties	Submitted
DY54III-A3-BC01	20190916	-122.8944667	12.12426667	overlying water pH, DO, Eh; pH, DO, Eh in Sediment	Submitted
DY54III-A3-BC02	20190916	-122.8314833	12.06921667	overlying water pH, DO, Eh; pH, DO, Eh in Sediment	Submitted
DY54III-A3-BC03	20190916	-122.8074333	12.31225	Nodule fauna	Submitted
DY54III-A3-BC03	20190916	-122.8074333	12.31225	overlying water pH, DO, Eh; pH, DO, Eh in Sediment	Submitted
DY54III-A3-BC04	20190917	-122.1843833	12.26793333	pH, DO, Eh in Sediment	Submitted
DY54III-A3-BC05	20190918	-122.2175667	12.26756667	pH, DO, Eh in Sediment	Submitted
DY54III-A3-BC06	20190919	-122.1598833	12.34123333	Macrofauna	Submitted
DY54III-A3-BC06	20190919	-122.1598833	12.34123333	Nodule fauna	Submitted
DY54III-A3-BC06	20190919	-122.1598833	12.34123333	overlying water pH, DO, Eh; pH, DO, Eh in Sediment	Submitted
DY54III-A3-BC07	20190921	-122.2241833	12.26671667	Macrofauna	Submitted
DY54III-A3-BC07	20190921	-122.2241833	12.26671667	overlying water pH, DO, Eh; pH, DO, Eh in Sediment	Submitted
DY54III-A3-BC08	20190922	-122.8386	12.69218333	pH, DO, Eh in Sediment	Submitted
DY54III-A3-BC08	20190922	-122.8386	12.69218333	Macrofauna	Submitted
DY54III-A3-BC08	20190922	-122.8386	12.69218333	Nodule fauna	Submitted
DY54III-A3-BC09	20190923	-122.8055	12.6004	Macrofauna	Submitted
DY54III-A3-BC09	20190923	-122.8055	12.6004	overlying water pH, DO, Eh; pH, DO, Eh in Sediment	Submitted
DY54III-A3-BP01	20190920	-122.1835667	12.28758333	Phytoplankton	Submitted

DY54III-A3-CTD01(200m)	20190917	-122.184	12.268	Hydrology, Chlorophyll	Submitted
DY54III-A3-CTD01	20190917	-122.186	12.268	Hydrology, DO, pH, Ammonium, Reactive phosphate, Nitrite, Nitrate, Silicate	Submitted
DY54III-A3-Lander01	20190920	-122.1833167	12.28706667	Scavengers, Mitochondrial	Submitted
DY54III-A3-MC01	20190917	-122.1844167	12.26795	Meiofauna	Submitted
DY54III-A3-MC02	20190918	-122.1843833	12.26796667	Meiofauna	Submitted
DY54III-A3-MP-01	20190921	-122.1859833	12.28333333	Microplastic	Submitted
DY54III-A3-TG01	20190921	-122.2229667	12.26726667	In-situ geotechnical properties	Submitted
DY54III-A4-BC01	20190925	-121.0811833	15.30335	overlying water pH, DO, Eh; pH, DO, Eh in Sediment	Submitted
DY54III-A4-BC02	20190927	-120.89385	15.39288333	Macrofauna	Submitted
DY54III-A4-BC02	20190927	-120.89385	15.39288333	overlying water pH, DO, Eh; pH, DO, Eh in Sediment	Submitted
DY54III-A4-BC03	20190929	-121.05055	15.18066667	overlying water pH, DO, Eh; pH, DO, Eh in Sediment	Submitted
DY54III-A4-BC04	20190929	-120.9806833	14.99176667	Macrofauna	Submitted
DY54III-A4-BC04	20190929	-120.9806833	14.99176667	Nodule fauna	Submitted
DY54III-A4-BC04	20190929	-120.9806833	14.99176667	overlying water pH, DO, Eh; pH, DO, Eh in Sediment	Submitted
DY54III-A4-BC05	20190930	-120.78365	15.44781667	overlying water pH, DO, Eh; pH, DO, Eh in Sediment	Submitted
DY54III-A4-BC06	20191002	-121.5133833	16.2006	overlying water pH, DO, Eh; pH, DO, Eh in Sediment	Submitted
DY54III-A4-BC07	20191003	-121.4854	16.09193333	Macrofauna	Submitted
DY54III-A4-BC07	20191003	-121.4854	16.09193333	Nodule fauna	Submitted
DY54III-A4-BC07	20191003	-121.4854	16.09193333	overlying water pH, DO, Eh; pH, DO, Eh in Sediment	Submitted
DY54III-A4-BC08	20191003	-121.5818167	16.02908333	overlying water pH, DO, Eh; pH, DO, Eh in Sediment	Submitted
DY54III-A4-BC09	20191003	-121.6585333	15.98125	overlying water pH, DO, Eh; pH, DO, Eh in Sediment	Submitted
DY54III-A4-BC10	20191003	-121.7525667	15.9193	overlying water pH, DO, Eh; pH, DO, Eh in Sediment	Submitted
DY54III-A4-BC11	20191004	-121.4070833	15.84941667	overlying water pH, DO, Eh; pH, DO, Eh in Sediment	Submitted
DY54III-A4-BC12	20191004	-121.2877667	15.6598	Macrofauna	Submitted

DY54III-A4-BC12	20191004	-121.2877667	15.6598	overlying water pH, DO, Eh; pH, DO, Eh in Sediment	Submitted
DY54III-A4-BC13	20191006	-121.0843	15.85481667	overlying water pH, DO, Eh; pH, DO, Eh in Sediment	Submitted
DY54III-A4-BC14	20191007	-121.2851333	15.93181667	overlying water pH, DO, Eh; pH, DO, Eh in Sediment	Submitted
DY54III-A4-BC15	20191008	-121.0916833	16.01643333	overlying water pH, DO, Eh; pH, DO, Eh in Sediment	Submitted
DY54III-A4-BC16	20191008	-120.92635	16.0988	overlying water pH, DO, Eh; pH, DO, Eh in Sediment	Submitted
DY54III-A4-BC17	20191009	-121.1206667	15.55071667	overlying water pH, DO, Eh; pH, DO, Eh in Sediment	Submitted
DY54III-A4-BC18	20191009	-120.8842667	15.65335	overlying water pH, DO, Eh; pH, DO, Eh in Sediment	Submitted
DY54III-A4-BC19	20191010	-120.6840167	15.7292	overlying water pH, DO, Eh; pH, DO, Eh in Sediment	Submitted
DY54III-A4-BC20	20191011	-120.5632167	15.58613333	overlying water pH, DO, Eh; pH, DO, Eh in Sediment	Submitted
DY54III-A4-CTD01(200m)	20190928	-120.897	15.336	Hydrology, Chlorophyll	Submitted
DY54III-A4-CTD01	20190928	-120.897	15.336	Hydrology, DO, pH, Ammonium, Reactive phosphate, Nitrite, Nitrate, Silicate	Submitted
DY54III-A4-CTD02(200m)	20191007	-121.029	15.854	Hydrology, Chlorophyll	Submitted
DY54III-A4-CTD02	20191007	-121.029	15.855	Hydrology, DO, pH, Ammonium, Reactive phosphate, Nitrite, Nitrate, Silicate	Submitted
DY54III-A4-MC01	20190927	-120.89725	15.33686667	Meiofauna	Submitted
DY54III-A4-MC02	20190928	-120.8971667	15.7292	Meiofauna	Submitted
DY54III-A4-TG01	20190926	-121.0812	15.30338333	In-situ geotechnical properties	Submitted
DY54IV- A5-CTD01	20191129	-156.77	9.399	Hydrology, DO, pH, Ammonium, Reactive phosphate, Nitrite, Nitrate, Silicate	Submitted
DY54IV- A5-CTD02	20191205	-155.558	9.456	Hydrology, DO, pH, Ammonium, Reactive phosphate, Nitrite, Nitrate, Silicate	Submitted
DY54IV-A5-BC01	20191121	-155.0068333	10.17013333	overlying water pH, DO, Eh; pH, DO, Eh in Sediment	Submitted
DY54IV-A5-BC02	20191122	-154.9955833	10.5726	overlying water pH, DO, Eh; pH, DO, Eh in Sediment	Submitted
DY54IV-A5-BC03	20191123	-155.1317167	10.66906667	Macrofauna	Submitted
DY54IV-A5-BC03	20191123	-155.1317167	10.66906667	overlying water pH, DO, Eh; pH, DO, Eh in Sediment	Submitted

DY54IV-A5-BC04	20191123	-155.1276167	10.48811667	overlying water pH, DO, Eh; pH, DO, Eh in Sediment	Submitted
DY54IV-A5-BC05	20191123	-155.3163833	10.36831667	pH, DO, Eh in Sediment	Submitted
DY54IV-A5-BC06	20191123	-155.1218833	10.35463333	overlying water pH, DO, Eh; pH, DO, Eh in Sediment	Submitted
DY54IV-A5-BC07	20191124	-155.0098833	10.00333333	overlying water pH, DO, Eh; pH, DO, Eh in Sediment	Submitted
DY54IV-A5-BC08	20191124	-155.0235	9.867433333	overlying water pH, DO, Eh; pH, DO, Eh in Sediment	Submitted
DY54IV-A5-BC09	20191124	-155.0343833	9.621816667	overlying water pH, DO, Eh; pH, DO, Eh in Sediment	Submitted
DY54IV-A5-BC11	20191125	-155.1576	9.5128	overlying water pH, DO, Eh; pH, DO, Eh in Sediment	Submitted
DY54IV-A5-BC12	20191125	-155.2409833	9.43835	Macrofauna	Submitted
DY54IV-A5-BC12	20191125	-155.2409833	9.43835	overlying water pH, DO, Eh; pH, DO, Eh in Sediment	Submitted
DY54IV-A5-BC13	20191127	-155.1908	9.60485	overlying water pH, DO, Eh; pH, DO, Eh in Sediment	Submitted
DY54IV-A5-BC14	20191128	-155.3676	9.723433333	overlying water pH, DO, Eh; pH, DO, Eh in Sediment	Submitted
DY54IV-A5-BC15	20191128	-155.4897333	9.435683333	overlying water pH, DO, Eh; pH, DO, Eh in Sediment	Submitted
DY54IV-A5-BC16	20191130	-156.7697167	9.397616667	Macrofauna	Submitted
DY54IV-A5-BC16	20191130	-156.7697167	9.397616667	overlying water pH, DO, Eh; pH, DO, Eh in Sediment	Submitted
DY54IV-A5-BC17	20191201	-156.5843167	9.206233333	overlying water pH, DO, Eh; pH, DO, Eh in Sediment	Submitted
DY54IV-A5-BP01	20191203	-156.757	9.378	Phytoplankton	Submitted
DY54IV-A5-BP02	20191205	-155.558	9.451	Phytoplankton	Submitted
DY54IV-A5-BP03	20191206	-155.558	9.451	Phytoplankton	Submitted
DY54IV-A5-CTD01(200m)	20191128	-156.77	9.399	Hydrology, Chlorophyll	Submitted
DY54IV-A5-CTD02(200m)	20191206	-155.558	9.451	Hydrology, Chlorophyll	Submitted
DY54IV-A5-MC01	20191129	-156.77	9.399	Microplastic	Submitted
DY54IV-A5-MC01	20191129	-156.77	9.399	Meiofauna	Submitted
DY54IV-A5-MC02	20191129	-156.77	9.399	Meiofauna	Submitted

DY54IV-A5-MC03	20191205	-155.559	9.451	Meiofauna	Submitted
DY54IV-A5-TG01a	20191130	-156.770004	9.39877	In-situ geotechnical properties	Submitted
DY70-A5-GC02	20211119	-156.707179	9.080917	Major and trace elements(31), Particle size characteristics of sediment(31), Clay mineral(31), Organic carbon, Total nitrogen, 13C, 15N(31)	Submitted
DY70-A5-GC03	20211120	-156.788221	9.392917	Major and trace elements(37), Particle size characteristics of sediment(37), Clay mineral(37), Organic carbon, Total nitrogen, 13C, 15N(37)	Submitted
DY70I-A5-BC01	20211023	-156.5925943	9.384644	Sediment types, Particle size characteristics of sediment, Clay mineral, Organic carbon, Total nitrogen, 13C, 15N, Major and trace chemical composition	Submitted
DY70I-A5-BC02	20211023	-156.59177	9.3526	Sediment types, Particle size characteristics of sediment, Clay mineral, Organic carbon, Total nitrogen, 13C, 15N, Major and trace chemical composition	Submitted
DY70I-A5-BC02	20211023	-156.59177	9.3526	Macrofauna	Submitted
DY70I-A5-BC03	20211023	-156.5904882	9.323303167	Sediment types, Particle size characteristics of sediment, Clay mineral, Organic carbon, Total nitrogen, 13C, 15N, Major and trace chemical composition	Submitted
DY70I-A5-BC04	20211024	-156.623769	9.32345	Sediment types, Particle size characteristics of sediment, Clay mineral, Organic carbon, Total nitrogen, 13C, 15N, Major and trace chemical composition	Submitted
DY70I-A5-BC04	20211024	-156.623769	9.32345	Macrofauna	Submitted
DY70I-A5-BC05	20211024	-156.6234387	9.352372167	Sediment types, Particle size characteristics of sediment, Clay mineral, Organic carbon, Total nitrogen, 13C, 15N, Major and trace chemical composition	Submitted
DY70I-A5-BC06	20211025	-156.6239173	9.384092333	Sediment types, Particle size characteristics of sediment, Clay mineral, Organic carbon, Total nitrogen, 13C, 15N, Major and trace chemical composition	Submitted
DY70I-A5-BC07	20211025	-156.6567397	9.383648167	Sediment types, Particle size characteristics of sediment, Clay mineral, Organic carbon, Total nitrogen, 13C, 15N, Major and trace chemical composition	Submitted
DY70I-A5-BC07	20211025	-156.6567397	9.383648167	Nodule fauna	Submitted

DY70I-A5-BC08a	20211026	-156.6570237	9.353222333	Sediment types, Particle size characteristics of sediment, Clay mineral, Organic carbon, Total nitrogen, 13C, 15N, Major and trace chemical composition	Submitted
DY70I-A5-BC09	20211026	-156.6562892	9.324442167	Sediment types, Particle size characteristics of sediment, Clay mineral, Organic carbon, Total nitrogen, 13C, 15N, Major and trace chemical composition	Submitted
DY70I-A5-BC10	20211104	-156.5344992	9.381856833	Sediment types, Particle size characteristics of sediment, Clay mineral, Organic carbon, Total nitrogen, 13C, 15N, Major and trace chemical composition	Submitted
DY70I-A5-BC11	20211104	-156.5334638	9.321247333	Sediment types, Particle size characteristics of sediment, Clay mineral, Organic carbon, Total nitrogen, 13C, 15N, Major and trace chemical composition	Submitted
DY70I-A5-BC11	20211104	-156.5334638	9.321247333	Nodule fauna	Submitted
DY70I-A5-BC12	20211105	-156.5939313	9.260753333	Sediment types, Particle size characteristics of sediment, Clay mineral, Organic carbon, Total nitrogen, 13C, 15N, Major and trace chemical composition	Submitted
DY70I-A5-BC12	20211105	-156.5939313	9.260753333	Nodule fauna	Submitted
DY70I-A5-BC13	20211105	-156.6885303	9.323651333	Sediment types, Particle size characteristics of sediment, Clay mineral, Organic carbon, Total nitrogen, 13C, 15N, Major and trace chemical composition	Submitted
DY70I-A5-BC13	20211105	-156.6885303	9.323651333	Nodule fauna	Submitted
DY70I-A5-BC14	20211106	-156.6886107	9.352893833	Sediment types, Particle size characteristics of sediment, Clay mineral, Organic carbon, Total nitrogen, 13C, 15N, Major and trace chemical composition	Submitted
DY70I-A5-BC15	20211106	-156.6890678	9.384267833	Sediment types, Particle size characteristics of sediment, Clay mineral, Organic carbon, Total nitrogen, 13C, 15N, Major and trace chemical composition	Submitted
DY70I-A5-BC16	20211107	-156.7169785	9.383414833	Sediment types, Particle size characteristics of sediment, Clay mineral, Organic carbon, Total nitrogen, 13C, 15N, Major and trace chemical composition	Submitted
DY70I-A5-BC17	20211107	-156.716031	9.354129833	Sediment types, Particle size characteristics of sediment, Clay mineral, Organic carbon, Total nitrogen, 13C, 15N, Major and trace chemical composition	Submitted

DY70I-A5-BC18	20211107	-156.7173278	9.323373	Sediment types, Particle size characteristics of sediment, Clay mineral, Organic carbon, Total nitrogen, 13C, 15N, Major and trace chemical composition	Submitted
DY70I-A5-BC19	20211108	-156.7968152	9.319911167	Sediment types, Particle size characteristics of sediment, Clay mineral, Organic carbon, Total nitrogen, 13C, 15N, Major and trace chemical composition	Submitted
DY70I-A5-BC20	20211108	-156.8442673	9.321343333	Sediment types, Particle size characteristics of sediment, Clay mineral, Organic carbon, Total nitrogen, 13C, 15N, Major and trace chemical composition	Submitted
DY70I-A5-BC21	20211108	-156.847908	9.3811385	Sediment types, Particle size characteristics of sediment, Clay mineral, Organic carbon, Total nitrogen, 13C, 15N, Major and trace chemical composition	Submitted
DY70I-A5-BC22a	20211109	-156.7899232	9.381835	Sediment types, Particle size characteristics of sediment, Clay mineral, Organic carbon, Total nitrogen, 13C, 15N, Major and trace chemical composition	Submitted
DY70I-A5-BC23	20211109	-156.8462558	9.443334667	Sediment types, Particle size characteristics of sediment, Clay mineral, Organic carbon, Total nitrogen, 13C, 15N, Major and trace chemical composition	Submitted
DY70I-A5-BC24	20211113	-156.7082265	9.073180833	Sediment types, Particle size characteristics of sediment, Clay mineral, Organic carbon, Total nitrogen, 13C, 15N, Major and trace chemical composition	Submitted
DY70I-A5-BC25	20211113	-156.6452067	9.194344333	Sediment types, Particle size characteristics of sediment, Clay mineral, Organic carbon, Total nitrogen, 13C, 15N, Major and trace chemical composition	Submitted
DY70I-A5-BC26	20211114	-156.5948517	9.445955	Sediment types, Particle size characteristics of sediment, Clay mineral, Organic carbon, Total nitrogen, 13C, 15N, Major and trace chemical composition	Submitted
DY70I-A5-BC27	20211116	-156.5302	9.197656167	Sediment types, Particle size characteristics of sediment, Clay mineral, Organic carbon, Total nitrogen, 13C, 15N, Major and trace chemical composition	Submitted
DY70I-A5-BC28a	20211117	-156.4646465	9.195292333	Sediment types, Particle size characteristics of sediment, Clay mineral, Organic carbon, Total nitrogen, 13C, 15N, Major and trace chemical composition	Submitted

DY70I-A5-BC28a	20211117	-156.4646465	9.195292333	Nodule fauna	Submitted
DY70I-A5-BC29	20211118	-156.4017817	9.131127333	Sediment types, Particle size characteristics of sediment, Clay mineral, Organic carbon, Total nitrogen, 13C, 15N, Major and trace chemical composition	Submitted
DY70I-A5-BC30	20211118	-156.4642543	9.130193	Sediment types, Particle size characteristics of sediment, Clay mineral, Organic carbon, Total nitrogen, 13C, 15N, Major and trace chemical composition	Submitted
DY70I-A5-BC31	20211118	-156.5294467	9.1340785	Sediment types, Particle size characteristics of sediment, Clay mineral, Organic carbon, Total nitrogen, 13C, 15N, Major and trace chemical composition	Submitted
DY70I-A5-BC32	20211119	-156.590648	9.132582167	Sediment types, Particle size characteristics of sediment, Clay mineral, Organic carbon, Total nitrogen, 13C, 15N, Major and trace chemical composition	Submitted
DY70I-A5-BC33	20211119	-156.657558	9.131703	Sediment types, Particle size characteristics of sediment, Clay mineral, Organic carbon, Total nitrogen, 13C, 15N, Major and trace chemical composition	Submitted
DY70I-A5-BC34	20211120	-156.7880703	9.447041167	Sediment types, Particle size characteristics of sediment, Clay mineral, Organic carbon, Total nitrogen, 13C, 15N, Major and trace chemical composition	Submitted
DY70I-A5-BC35	20211121	-156.6594275	9.4472015	Sediment types, Particle size characteristics of sediment, Clay mineral, Organic carbon, Total nitrogen, 13C, 15N, Major and trace chemical composition	Submitted
DY70I-A5-BP01	20211115	-156.594421	9.349461	Phytoplankton	Submitted
DY70I-A5-BP02	20211115	-156.59077	9.351587	Phytoplankton	Submitted
DY70I-A5-BP03	20211115	-156.627561	9.324299	Phytoplankton	Submitted
DY70I-A5-BP04	20211115	-156.629223	9.328913	Phytoplankton	Submitted
DY70I-A5-CTD01-200	20211024	-156.624322	9.322963	Chlorophyll, DO, Reactive phosphate, Nitrite, Nitrate, Silicate, Ammonium, pH, Hydrology, TSM, POC	Submitted
DY70I-A5-CTD01-Q	20211024	-156.623834	9.323536	Hydrology	Submitted
DY70I-A5-CTD02-200	20211110	-156.76987	9.396628	Chlorophyll, DO, Reactive phosphate, Nitrite, Nitrate, Silicate, Ammonium, pH, Hydrology, TSM, POC	Submitted

DY70I-A5-CTD02-Q	20211110	-156.768547	9.411589	DO, Reactive phosphate, Nitrite, Nitrate, Silicate, Ammonium, pH, Hydrology, TSM, POC	Submitted
DY70I-A5-CTD03-Q	20211110	-156.624372	9.325829	DO, Reactive phosphate, Nitrite, Nitrate, Silicate, Ammonium, pH, Hydrology, TSM, POC	Submitted
DY70I-A5-Lander01	20211120	-156.77555	9.374333	Lander	Submitted
DY70I-A5-Lander02	20211130	-156.623769	9.32345	Lander	Submitted
DY70I-A5-MC01	20211113	-156.62467	9.323213	Meiofauna Chlorophyll in Sediment, Microorganisms	Submitted
DY70I-A5-MC02	20211114	-156.624449	9.323363	Meiofauna, Chlorophyll in Sediment	Submitted
DY70I-A5-MC03	20211114	-156.59185	9.353407	Meiofauna, Chlorophyll in Sediment	Submitted
DY70I-A5-MC04	20211115	-156.591647	9.352721	Meiofauna, Chlorophyll in Sediment	Submitted
DY70I-A5-MN01	20211115	-156.59296	9.352947	Zooplankton	Submitted
DY70I-A5-MN02	20211115	-156.62544	9.323855	Zooplankton	Submitted
DY70I-A5-TG01	20211027	-156.591826	9.3534	In-situ geotechnical properties	Submitted
DY70I-A5-TG02	20211027	-156.656285	9.353827	In-situ geotechnical properties	Submitted
DY70I-A5-TG03a	20211028	-156.716853	9.353408	In-situ geotechnical properties	Submitted
DY70I-A5-TG04	20211028	-156.788869	9.381476	In-situ geotechnical properties	Submitted
DY70I-A5-TG05	20211029	-156.645422	9.194786	In-situ geotechnical properties	Submitted
DY70I-A5-TG06	20211029	-156.590774	9.13553	In-situ geotechnical properties	Submitted
DY70I-A5-TG07	20211104	-156.414452	9.384685	In-situ geotechnical properties	Submitted
DY70I-A5-TG08	20211111	-156.495239	9.379422	In-situ geotechnical properties	Submitted
DY70I-A5-TG09	20211111	-156.465046	9.195499	In-situ geotechnical properties	Submitted
DY70I-A5-TG10	20211112	-156.526931	9.006414	In-situ geotechnical properties	Submitted
DY70I-A5-TG11	20211027	-156.707692	9.073583	In-situ geotechnical properties	Submitted
DY70II-A5-BC36	20211125	-156.8132492	9.1977725	Sediment types, Particle size characteristics of sediment, Clay mineral, Organic carbon, Total nitrogen, 13C, 15N, Major and trace chemical composition	Submitted

DY70II-A5-BC37	20211125	-156.8297287	9.1385695	Sediment types, Particle size characteristics of sediment, Clay mineral, Organic carbon, Total nitrogen, 13C, 15N, Major and trace chemical composition	Submitted
DY70II-A5-BC38	20211125	-156.8411723	9.066289	Sediment types, Particle size characteristics of sediment, Clay mineral, Organic carbon, Total nitrogen, 13C, 15N, Major and trace chemical composition	Submitted
DY70II-A5-BC39	20211126	-156.8411217	9.000916667	Sediment types, Particle size characteristics of sediment, Clay mineral, Organic carbon, Total nitrogen, 13C, 15N, Major and trace chemical composition	Submitted
DY70II-A5-BC40	20211126	-156.7767557	9.006617667	Sediment types, Particle size characteristics of sediment, Clay mineral, Organic carbon, Total nitrogen, 13C, 15N, Major and trace chemical composition	Submitted
DY70II-A5-BC41	20211127	-156.6563897	9.001109333	Sediment types, Particle size characteristics of sediment, Clay mineral, Organic carbon, Total nitrogen, 13C, 15N, Major and trace chemical composition	Submitted
DY70II-A5-BC42	20211127	-156.530642	9.007055333	Sediment types, Particle size characteristics of sediment, Clay mineral, Organic carbon, Total nitrogen, 13C, 15N, Major and trace chemical composition	Submitted
DY70II-A5-BC43	20211127	-156.531172	8.951277333	Sediment types, Particle size characteristics of sediment, Clay mineral, Organic carbon, Total nitrogen, 13C, 15N, Major and trace chemical composition	Submitted
DY70II-A5-BC44	20211128	-156.470313	8.948818833	Sediment types, Particle size characteristics of sediment, Clay mineral, Organic carbon, Total nitrogen, 13C, 15N, Major and trace chemical composition	Submitted
DY70II-A5-BC45	20211128	-156.4001413	8.947262	Sediment types, Particle size characteristics of sediment, Clay mineral, Organic carbon, Total nitrogen, 13C, 15N, Major and trace chemical composition	Submitted
DY70II-A5-BC46	20211128	-156.4001913	9.0030945	Sediment types, Particle size characteristics of sediment, Clay mineral, Organic carbon, Total nitrogen, 13C, 15N, Major and trace chemical composition	Submitted
DY70II-A5-BC47	20211211	-156.5342447	9.4471925	Sediment types, Particle size characteristics of sediment, Clay mineral, Organic carbon, Total nitrogen, 13C, 15N, Major and trace chemical composition	Submitted

DY70II-A5-BC48	20211211	-156.4676332	9.448344833	Sediment types, Particle size characteristics of sediment, Clay mineral, Organic carbon, Total nitrogen, 13C, 15N, Major and trace chemical composition	Submitted
DY70II-A5-BC49	20211211	-156.4065747	9.447611	Sediment types, Particle size characteristics of sediment, Clay mineral, Organic carbon, Total nitrogen, 13C, 15N, Major and trace chemical composition	Submitted
DY70II-A5-BC50	20211212	-156.4657513	9.260197	Sediment types, Particle size characteristics of sediment, Clay mineral, Organic carbon, Total nitrogen, 13C, 15N, Major and trace chemical composition	Submitted
DY70II-A5-BC51	20211212	-156.4665085	9.3200655	Sediment types, Particle size characteristics of sediment, Clay mineral, Organic carbon, Total nitrogen, 13C, 15N, Major and trace chemical composition	Submitted
DY70II-A5-BC52	20211213	-156.4012943	9.323144167	Sediment types, Particle size characteristics of sediment, Clay mineral, Organic carbon, Total nitrogen, 13C, 15N, Major and trace chemical composition	Submitted
DY70II-A5-BC53	20211213	-156.334972	9.321787167	Sediment types, Particle size characteristics of sediment, Clay mineral, Organic carbon, Total nitrogen, 13C, 15N, Major and trace chemical composition	Submitted
DY70II-A5-BC54	20211213	-156.27655	9.316785833	Sediment types, Particle size characteristics of sediment, Clay mineral, Organic carbon, Total nitrogen, 13C, 15N, Major and trace chemical composition	Submitted
DY70II-A5-BC55	20211214	-156.2107242	9.4515355	Sediment types, Particle size characteristics of sediment, Clay mineral, Organic carbon, Total nitrogen, 13C, 15N, Major and trace chemical composition	Submitted
DY70II-A5-BC56	20211214	-156.2797788	9.448636333	Sediment types, Particle size characteristics of sediment, Clay mineral, Organic carbon, Total nitrogen, 13C, 15N, Major and trace chemical composition	Submitted
DY70II-A5-BC57	20211214	-156.3993683	9.070066	Sediment types, Particle size characteristics of sediment, Clay mineral, Organic carbon, Total nitrogen, 13C, 15N, Major and trace chemical composition	Submitted
DY70II-A5-BC58	20211215	-156.4629167	9.070570167	Sediment types, Particle size characteristics of sediment, Clay mineral, Organic carbon, Total nitrogen, 13C, 15N, Major and trace chemical composition	Submitted

DY70II-A5-BC59	20211215	-156.527309	9.0699725	Sediment types, Particle size characteristics of sediment, Clay mineral, Organic carbon, Total nitrogen, 13C, 15N, Major and trace chemical composition	Submitted
DY70II-A5-BC60	20211215	-156.5876193	9.0716745	Sediment types, Particle size characteristics of sediment, Clay mineral, Organic carbon, Total nitrogen, 13C, 15N, Major and trace chemical composition	Submitted
DY70II-A5-BC61	20211216	-156.649201	9.0718575	Sediment types, Particle size characteristics of sediment, Clay mineral, Organic carbon, Total nitrogen, 13C, 15N, Major and trace chemical composition	Submitted
DY70II-A5-BC62	20211216	-156.7825043	9.0667145	Sediment types, Particle size characteristics of sediment, Clay mineral, Organic carbon, Total nitrogen, 13C, 15N, Major and trace chemical composition	Submitted
DY70II-A5-BC63	20211216	-156.7822737	9.137587167	Sediment types, Particle size characteristics of sediment, Clay mineral, Organic carbon, Total nitrogen, 13C, 15N, Major and trace chemical composition	Submitted
DY70II-A5-BC64a	20211217	-156.721382	9.133013667	Sediment types, Particle size characteristics of sediment, Clay mineral, Organic carbon, Total nitrogen, 13C, 15N, Major and trace chemical composition	Submitted
DY70II-A5-BC65	20211218	-156.6173712	9.38435	Sediment types, Particle size characteristics of sediment, Clay mineral, Organic carbon, Total nitrogen, 13C, 15N, Major and trace chemical composition	Submitted
DY70II-A5-BC66	20211225	-156.7545767	9.322124833	Sediment types, Particle size characteristics of sediment, Clay mineral, Organic carbon, Total nitrogen, 13C, 15N, Major and trace chemical composition	Submitted
DY70II-A5-BC67	20211225	-156.8192005	9.321203	Sediment types, Particle size characteristics of sediment, Clay mineral, Organic carbon, Total nitrogen, 13C, 15N, Major and trace chemical composition	Submitted
DY70II-A5-BC68	20211226	-156.755576	9.362236833	Sediment types, Particle size characteristics of sediment, Clay mineral, Organic carbon, Total nitrogen, 13C, 15N, Major and trace chemical composition	Submitted
DY70II-A5-BC69	20211226	-156.7885393	9.351189667	Sediment types, Particle size characteristics of sediment, Clay mineral, Organic carbon, Total nitrogen, 13C, 15N, Major and trace chemical composition	Submitted

DY70II-A5-BC70	20211227	-156.8188635	9.38043	Sediment types, Particle size characteristics of sediment, Clay mineral, Organic carbon, Total nitrogen, 13C, 15N, Major and trace chemical composition	Submitted
DY70II-A5-BC71	20211227	-156.8186977	9.351473333	Sediment types, Particle size characteristics of sediment, Clay mineral, Organic carbon, Total nitrogen, 13C, 15N, Major and trace chemical composition	Submitted
DY70II-A5-BC72	20211227	-156.8460783	9.350812833	Sediment types, Particle size characteristics of sediment, Clay mineral, Organic carbon, Total nitrogen, 13C, 15N, Major and trace chemical composition	Submitted
DY70II-A5-MX01	20211225	-156.747517	9.430883	Mooring(Ocean current: 4, CTD: 3, ADCP: 1, Sedimentary flux: 2)	Submitted
DY70II-A5-TG12	20211124	-156.592314	9.35376	In-situ geotechnical properties	Submitted
DY70II-A5-TG13	20211124	-156.789623	9.38167	In-situ geotechnical properties	Submitted
DY70II-A5-TG14	20211130	-156.624369	9.383585	In-situ geotechnical properties	Submitted
DY70II-A5-TG15	20211228	-156.819667	9.32105	In-situ geotechnical properties	Submitted
DY73-A5-GC01	20221018	-156.84747	9.514537	Bioturbation	Submitted
DY73-A5-GC01	20221018	-156.84747	9.514537	210Pb(14), Major and trace elements(25), Particle size characteristics of sediment(25), Clay mineral(25), Organic carbon, Total nitrogen, 13C, 15N(25)	Submitted
DY73-A5-GC02	20221020	-156.586728	9.362625	210Pb(14), Major and trace elements(25), Particle size characteristics of sediment(25), Clay mineral(25), Organic carbon, Total nitrogen, 13C, 15N(25)	Submitted
DY73I-A5-BC01	20220901	-156.6604	9.577095	Sediment types, Particle size characteristics of sediment, Clay mineral, Organic carbon, Total nitrogen, 13C, 15N, Major and trace chemical composition	Submitted
DY73I-A5-BC02	20220901	-156.6001	9.5784633	Sediment types, Particle size characteristics of sediment, Clay mineral, Organic carbon, Total nitrogen, 13C, 15N, Major and trace chemical composition	Submitted
DY73I-A5-BC03	20220902	-156.5381	9.578345	Sediment types, Particle size characteristics of sediment, Clay mineral, Organic carbon, Total nitrogen, 13C, 15N, Major and trace chemical composition	Submitted
DY73I-A5-BC04	20220902	-156.5376	9.515465	Sediment types, Particle size characteristics of sediment, Clay mineral,	Submitted

				Organic carbon, Total nitrogen, 13C, 15N, Major and trace chemical composition	
DY73I-A5-BC05	20220902	-156.5962	9.5155483	Sediment types, Particle size characteristics of sediment, Clay mineral, Organic carbon, Total nitrogen, 13C, 15N, Major and trace chemical composition	Submitted
DY73I-A5-BC06	20220902	-156.6619	9.5156333	Sediment types, Particle size characteristics of sediment, Clay mineral, Organic carbon, Total nitrogen, 13C, 15N, Major and trace chemical composition	Submitted
DY73I-A5-BC07	20220910	-156.5326	9.3560783	Sediment types, Particle size characteristics of sediment, Clay mineral, Organic carbon, Total nitrogen, 13C, 15N, Major and trace chemical composition	Submitted
DY73I-A5-BC08	20220910	-156.5005	9.3568683	Sediment types, Particle size characteristics of sediment, Clay mineral, Organic carbon, Total nitrogen, 13C, 15N, Major and trace chemical composition	Submitted
DY73I-A5-BC09	20220912	-156.7176	9.3257517	Macrofauna	Submitted
DY73I-A5-BC10	20220913	-156.5649	9.3253017	Sediment types, Particle size characteristics of sediment, Clay mineral, Organic carbon, Total nitrogen, 13C, 15N, Major and trace chemical composition	Submitted
DY73I-A5-BC11	20220914	-156.5647	9.3565933	Sediment types, Particle size characteristics of sediment, Clay mineral, Organic carbon, Total nitrogen, 13C, 15N, Major and trace chemical composition	Submitted
DY73I-A5-BC12	20220913	-156.5647	9.3880017	Sediment types, Particle size characteristics of sediment, Clay mineral, Organic carbon, Total nitrogen, 13C, 15N, Major and trace chemical composition	Submitted
DY73I-A5-BC13	20220914	-156.868	9.3212233	Macrofauna	Submitted
DY73I-A5-BC14	20220915	-156.7252	9.513575	Sediment types, Particle size characteristics of sediment, Clay mineral, Organic carbon, Total nitrogen, 13C, 15N, Major and trace chemical composition	Submitted
DY73I-A5-BC15	20220916	-156.7854	9.5129117	Sediment types, Particle size characteristics of sediment, Clay mineral, Organic carbon, Total nitrogen, 13C, 15N, Major and trace chemical composition	Submitted
DY73I-A5-BC16	20220916	-156.7697	9.3967467	Macrofauna	Submitted

DY73I-A5-BC17	20220917	-156.4091	9.5796433	Sediment types, Particle size characteristics of sediment, Clay mineral, Organic carbon, Total nitrogen, 13C, 15N, Major and trace chemical composition	Submitted
DY73I-A5-BC18	20220917	-156.3427	9.5810467	Sediment types, Particle size characteristics of sediment, Clay mineral, Organic carbon, Total nitrogen, 13C, 15N, Major and trace chemical composition	Submitted
DY73I-A5-BC19	20220917	-156.2816	9.5817217	Sediment types, Particle size characteristics of sediment, Clay mineral, Organic carbon, Total nitrogen, 13C, 15N, Major and trace chemical composition	Submitted
DY73I-A5-BC20	20220917	-156.2825	9.5187717	Sediment types, Particle size characteristics of sediment, Clay mineral, Organic carbon, Total nitrogen, 13C, 15N, Major and trace chemical composition	Submitted
DY73I-A5-BC21	20220918	-156.342	9.5166783	Sediment types, Particle size characteristics of sediment, Clay mineral, Organic carbon, Total nitrogen, 13C, 15N, Major and trace chemical composition	Submitted
DY73I-A5-BC22	20220918	-156.3412	9.42197	Sediment types, Particle size characteristics of sediment, Clay mineral, Organic carbon, Total nitrogen, 13C, 15N, Major and trace chemical composition	Submitted
DY73I-A5-BC23	20220918	-156.3416	9.379375	Sediment types, Particle size characteristics of sediment, Clay mineral, Organic carbon, Total nitrogen, 13C, 15N, Major and trace chemical composition	Submitted
DY73I-A5-BC24	20220923	-156.623602	9.323367	Macrofauna	Submitted
DY73I-A5-BC25	20220923	-156.498497	9.327558	Macrofauna	Submitted
DY73I-A5-CTD01-Q	20220903	-156.769625	9.396762	Chlorophyll	Submitted
DY73I-A5-CTD02-Q	20220905	-156.62364	9.323263	Chlorophyll	Submitted
DY73I-A5-Lander01	20220905	-156.634247	9.317763	Scavengers, Biological trace elements, Mitochondrial DNA	Submitted
DY73I-A5-Lander02	20220916	-156.76625	9.398002	Scavengers, Biological trace elements, Mitochondrial DNA	Submitted
DY73I-A5-MC01	20220904	-156.671778	9.57747	Meiofauna, Chlorophyll in Sediment	Submitted
DY73I-A5-MC02	20220906	-156.769975	9.396112	Meiofauna, Chlorophyll in Sediment, Heavy metal in the pore water, Reactive phosphate, Nitrite, Nitrate, Silicate, Ammonium	Submitted

DY73I-A5-MC03	20220912	-156.717572	9.325738	Meiofauna, Chlorophyll in Sediment	Submitted
DY73I-A5-MC04	20220915	-156.868028	9.32122	Meiofauna, Chlorophyll in Sediment	Submitted
DY73I-A5-MC05	20220915	-156.655535	9.452777	Meiofauna, Chlorophyll in Sediment	Submitted
DY73I-A5-MC06	20220921	-156.625582	9.32217	Meiofauna, Chlorophyll in Sediment, Heavy metal in the pore water, Reactive phosphate, Nitrite, Nitrate, Silicate, Ammonium	Submitted
DY73I-A5-MC07	20220921	-156.498492	9.327575	Meiofauna, Chlorophyll in Sediment	Submitted
DY73I-A5-MC08	20220924	-155.680058	9.652047	Meiofauna, Chlorophyll in Sediment	Submitted
DY73I-A5-MX02	20220921	-156.625585	9.32282	Mooring(Ocean current: 2, CTD: 2)	Submitted
DY73I-A5-TG01	20220908	-156.739167	9.545522	In-situ geotechnical properties	Submitted
DY73I-A5-TG02	20220909	-156.53188	9.325503	In-situ geotechnical properties	Submitted
DY73I-A5-TG03	20220919	-156.789853	9.35076	In-situ geotechnical properties	Submitted
DY73I-A5-TG04	20220919	-156.532178	9.383167	In-situ geotechnical properties	Submitted
DY73I-A5-TG05	20220921	-156.498677	9.355697	In-situ geotechnical properties	Submitted
DY73I-A5-TG06	20220922	-156.43876	9.357338	In-situ geotechnical properties	Submitted
DY73I-A5-TG07	20220922	-156.481265	9.515533	In-situ geotechnical properties	Submitted
DY73I-A5-WTS01	20220905	-156.623667	9.323282	TSM, POC Isotope,	Submitted
DY73I-A5-WTS02	20220905	-156.769977	9.396103	TSM, POC Isotope,	Submitted
DY73II-A5-BC26	20221010	-156.4344	9.32353	Sediment types, Particle size characteristics of sediment, Clay mineral, Organic carbon, Total nitrogen, 13C, 15N, Major and trace chemical composition	Submitted
DY73II-A5-BC28	20221012	-156.4697	9.3574567	Sediment types, Particle size characteristics of sediment, Clay mineral, Organic carbon, Total nitrogen, 13C, 15N, Major and trace chemical composition	Submitted
DY73II-A5-BC29	20221012	-156.4417	9.3581	Sediment types, Particle size characteristics of sediment, Clay mineral, Organic carbon, Total nitrogen, 13C, 15N, Major and trace chemical composition	Submitted
DY73II-A5-BC30	20221013	-156.4429	9.3840433	Sediment types, Particle size characteristics of sediment, Clay mineral, Organic carbon, Total nitrogen, 13C, 15N, Major and trace chemical	Submitted

				composition	
DY73II-A5-BC31	20221013	-156.4696	9.3805767	Sediment types, Particle size characteristics of sediment, Clay mineral, Organic carbon, Total nitrogen, 13C, 15N, Major and trace chemical composition	Submitted
DY73II-A5-BC32	20221014	-156.7253	9.5772433	Sediment types, Particle size characteristics of sediment, Clay mineral, Organic carbon, Total nitrogen, 13C, 15N, Major and trace chemical composition	Submitted
DY73II-A5-BC33	20221014	-156.7886	9.5749833	Sediment types, Particle size characteristics of sediment, Clay mineral, Organic carbon, Total nitrogen, 13C, 15N, Major and trace chemical composition	Submitted
DY73II-A5-BC34	20221015	-156.8438	9.56972	Sediment types, Particle size characteristics of sediment, Clay mineral, Organic carbon, Total nitrogen, 13C, 15N, Major and trace chemical composition	Submitted
DY73II-A5-BC35	20221017	-156.8475	9.5144517	Sediment types, Particle size characteristics of sediment, Clay mineral, Organic carbon, Total nitrogen, 13C, 15N, Major and trace chemical composition	Submitted
DY73II-A5-MC09	20221009	-155.1627517	9.655376667	Meiofauna, Chlorophyll in Sediment	Submitted
DY73II-A5-TG08	20221013	-156.60005	9.578565	In-situ geotechnical properties	Submitted
DY79I-A5-BC14	20230917	-156.0241	9.51953	pH, DO, Eh in Sediment	Submit in 2025.3
DY79I-A5-BVP01	20231030	upper line: -156.871865 lower line: -156.799688	upper line: 9.391363 lower line: 9.389448	Megafauna, Nodule coverage	Submit in 2025.3
DY79I-A5-BVP02	20231031-20231101	upper line: -156.877778666667 lower line: -156.688968	upper line: 9.37309 lower line: 9.37206	Megafauna, Nodule coverage	Submit in 2025.3

DY79I-A5-BVP03	20231101-20231102	upper line: -156.700198 lower line: -156.517377	upper line: 9.350732 lower line: 9.35156433333333	Megafauna, Nodule coverage	Submit in 2025.3
DY79I-A5-BVP04	20231102-20231103	upper line: -156.700504 lower line: -156.511836	upper line: 9.326965 lower line: 9.325966	Megafauna, Nodule coverage	Submit in 2025.3
DY79I-A5-CTD01-200m	20230828	-156.76953	9.397228333	Hydrology, DO, pH, Reactive phosphate, Nitrite, Nitrate, Silicate, Ammonium, Chlorophyll	Submit in 2025.3
DY79I-A5-CTD02-Q	20230828	-156.76952	9.397223333	Hydrology, DO, pH, Reactive phosphate, Nitrite, Nitrate, Silicate, Ammonium, Chlorophyll	Submit in 2025.3
DY79I-A5-CTD03-200m	20230901	-156.6947683	9.352626667	Hydrology, DO, pH, Reactive phosphate, Nitrite, Nitrate, Silicate, Ammonium, Chlorophyll	Submit in 2025.3
DY79I-A5-CTD04-200m	20230905	-156.6233383	9.323058333	Hydrology, DO, pH, Reactive phosphate, Nitrite, Nitrate, Silicate, Ammonium, Chlorophyll	Submit in 2025.3
DY79I-A5-CTD05-Q	20230908	-156.620715	9.333008333	Hydrology, DO, pH, Reactive phosphate, Nitrite, Nitrate, Silicate, Ammonium, Chlorophyll	Submit in 2025.3
DY79I-A5-CTD06-Q	20230911	-156.6946967	9.3534	Hydrology, DO, pH, Reactive phosphate, Nitrite, Nitrate, Silicate, Ammonium, Chlorophyll	Submit in 2025.3
DY79I-A5-CTD07-200m	20230930	-155.5209667	9.529448333	Hydrology, DO, pH, Reactive phosphate, Nitrite, Nitrate, Silicate, Ammonium, Chlorophyll	Submit in 2025.3
DY79I-A5-CTD08-Q	20230930	-155.514325	9.526068333	Hydrology, DO, pH, Reactive phosphate, Nitrite, Nitrate, Silicate, Ammonium, Chlorophyll	Submit in 2025.3
DY79I-A5-Lander01	20230911	-156.5585417	9.318683333	Ocean current, Noise	Submit in 2025.3
DY79I-A5-MC02a	20230904	-156.76965	9.396681667	pH, DO, Eh in Sediment	Submit in 2025.3
DY79I-A5-MX01	20230908	-156.6397833	9.297251667	Mooring(Ocean current:3, CTD:5)	Submit in 2025.3
DY79I-A5-TG01	20230913	-156.620927	9.620927	In-situ geotechnical properties	Submit in 2025.3

DY79II-A5-Lander02	20231020	-156.6092917	9.339468333	Scavengers, Biological trace elements, Mitochondrial DNA	Submit in 2025.3
DY79II-A5-MX02	20231020	-156.6049567	9.308566667	Mooring(Not Recovered)	Submit in 2025.3
DY79II-A5-TG02	20231109	-155.292582	9.292582	In-situ geotechnical properties	Submit in 2025.3

Table 2 Plan for the environmental survey mission of the China Minmetals Corporation cruise in 2024

Field	Content	Method	No. of Station
Environmental Survey	Long-term physical oceanographic characteristics and sediment flux	Mooring	2
	Temperature and Salinity profiles Chemistry Chlorophyll *a* eDNA	CTD	3
	Scavenger	Lander	1
	Benthos	Multicorer	8
		Box corer	8
		AUV(optical)	80 km
	Geotechnical properties testing	In-situ geomechanics tester	2
	Plankton	Multinet	4
	Ocean noise	Hydrophone	1
	Short-term physical oceanographic characteristics	Lander	1
	Total		30